Chemical Alteration and Soil Provenance of Polar Desert Sediments from the McMurdo Dry Valleys, Antarctica: An Analog for Alteration Processes on Mars

Andrew B. Foerder

A thesis submitted in partial fulfillment
of the requirements for the degree of

Master of Science

University of Hawai‘i at Mānoa

2020

Reading Committee:

Peter Englert

Jeffrey Taylor

Neil Frazer

Program Authorized to Offer Degree:
Department of Earth and Planetary Sciences
University of Hawai‘i at Mānoa

Abstract

Chemical Alteration and Soil Provenance of Polar Desert Sediments from the McMurdo Dry Valleys, Antarctica: An Analog for Alteration Processes on Mars

Andrew B. Foerder

Chair of Supervisory Committee:

Professor Peter Englert

Hawai'i Institute of Geophysics and Planetology

The McMurdo Dry Valleys (MDV) of Antarctica are considered one of the best Earth-based environments for studying Mars on the basis of cold and dry surface conditions. It is through this analogy that investigations of potentially similar sub/surface processes have been established and researched. In an effort to determine type and degree of alteration processes across the past and present martian landscape, comprehensive elemental and mineralogical analyses were conducted on surface and core sediments across the MDV. Additionally, sediment provenance was investigated by analysis of Rare Earth Elements (REEs) and High Field Strength Elements (HFSEs) as a means to validate or refute alteration conclusions.

Physical alteration, manifesting as wind erosion, mass-wasting, sediment-mixing, and freeze-thaw processes dominate at the surface of the MDV, but under unique conditions, including hypersalinity and/or ample surface cover, chemical alteration can dominate. Chemical alteration in the MDV was found to manifest as core sediment ranges with clays, sulfates, carbonates, or standing hypersaline surface waters. Investigations of sediment provenance primarily bolstered alteration conclusions, exhibiting relative depletions of HFSEs in samples that experienced heavy chemical alteration.

Specific sites within the MDV are comparable to select Mars rover samples. Analysis of major elemental abundances, chemical alteration indices, and sulfite abundance show that the best analogy for the MDV to Mars is based on sulfate abundances, for which total sulfur and sulfite abundance can be a measure. Through this research we provide the means for further reconstruction of the martian paleoclimate and that of similar extraterrestrial environments.

TABLE OF CONTENTS

LIST OF FIGURES

Acknowledgments

The following deserve thanks for having helped and supported me in the writing of this thesis. I wish to thank Peter Englert, my advisor and thesis committee chair. Peter has spent many hours with me discussing this thesis, fielding questions, providing valuable guidance, and pushing me to reach higher. I would also like to thank my thesis committee for their time and support: Jeffrey Taylor and Neil Frazer. Additional thanks to Janice Bishop, for her vital assistance and sage advice in this research.

Finally, I would like to give a special thanks to my family (Sidney Bounds, Charles Foerder, Elizabeth Bounds, Daniel Johnson, Breanna Johnson, and Parker Johnson), and my partner Carly Paul for supporting me as I finished my master's degree.

CHAPTER 1: INTRODUCTION

1.1. OVERVIEW

The investigation of terrestrial environments that exhibit climatic or geologic similarities to extraterrestrial environments has been a useful tool in efforts to better understand potential past and/or present processes underway on planetary bodies outside of Earth. One such terrestrial environment is the McMurdo Dry Valley Region of Antarctica which has been used as an analog to Mars due to extremely cold and arid conditions exhibited by both. It is through the climatic similarities of these two environments that a window into what could be similar near-surface geologic processes has been opened. Such aspects of the valleys are investigated in this thesis in an effort to better understand Mars' past and present.

1.2. OBJECTIVE

The objective of this thesis is to investigate type and degree of sediment alteration, as well as sediment provenance in select, local-scale sites of the McMurdo Dry Valleys of Antarctica. The overall goal is to compare conclusions from this study to rock and soil data collected by martian rovers Spirit, Opportunity, and Curiosity, testing the efficacy of the valleys as an analog environment to the martian landscape, and aiding in the determination of potential short-term or long-term liquid-water-based chemical alteration on Mars. In doing this, we provide an important piece of the puzzle that is Mars' geochemical history, from which the scientific community could move closer to answering questions regarding the potential of life and habitability outside of Earth.

1.3. Thesis Outline

This research is presented in five main chapters, some of which will be submitted as publications in scientific journals. Chapter 1, the introductory chapter provides background information to familiarize the reader with the location of study and past research. Chapter 2 investigates type and degree of sediment alteration in the McMurdo Dry Valleys and introduces the Chemical Index of Alteration (Nesbitt and Young, 1982) and a modification for sulfate-rich sediments. Chapter 3 investigates sediment provenance to various rock formations, utilizing chemical, mineralogical, and spectral data. Chapter 4 compares microenvironment data to available martian rover data to test the efficacy of the localities, and the Dry Valley region, as suitable analogs for the martian landscape. The results sections in Chapters 2-4 individually detail each sample location and the soil cores taken there. Chapter 5, the concluding chapter, summarizes the main conclusions of chapters 2, 3, and 4, and explores possible avenues for future research. At the end of the thesis, appendices tabulate data not included in the main body of the thesis.

1.4. Regional Background

1.4.1. Location

The continent of Antarctica is a remote, desolate, and inhospitable landscape with an area of about 14.2 million km^2 that is largely composed of ice. Ice and snow-free regions compose less than 710,000 km^2 or 5 % of the area of the continent, with the ice-free "dry" valleys making up only 4,800 km^2 or 0.03 % (Harris, 1981). Proximity to McMurdo Station, a United States Antarctic research center on the south tip of Ross Island, has allowed for past and present study of the dry valleys—officially named the McMurdo Dry Valleys (MDV). The valleys are reached, camps established, and supplied by helicopter due to a rugged terrain inaccessible by foot. Due to extreme cold, high winds, and arid conditions, the majority of field work is conducted during the austral summer in the months of November, December, and January. The valleys are located at the

north end of the Transantarctic Mountains, and the south end of Victoria Land, approximately 90 km (Taylor Valley) to 120 km (Wright Valley) to the northwest. The valleys were likely cut by glaciers >4 million years ago, moving from east to west. In times since, the valleys have been reached by water from the Ross Sea, ice based in the Ross Sea, East Antarctic ice, and "alpine" ice from the mountain ranges bordering the valleys (Harris, 1981).

Figure 1. The continent of Antarctica and the McMurdo Dry Valleys (red circle), Source: Natural History Museum

1.4.2. Regions of Investigation

There are seven regions that are investigated in this thesis: 1) Don Juan Basin (DJB), 2) Don Quixote Basin (DQB), 3) VXE-6 Basin (VXB) (Harris, 1981), 4) the South Fork of Wright Valley (SF), 5) Prospect Mesa (PM), 6) Taylor Valley (TV), 7) Wright Valley (WV). Wright Valley includes Lakes Vanda (LVA) and Brownworth (LBR). Taylor Valley includes Lakes Fryxell (LFR) and Hoare (LHO). All are shown in Figure 2, below.

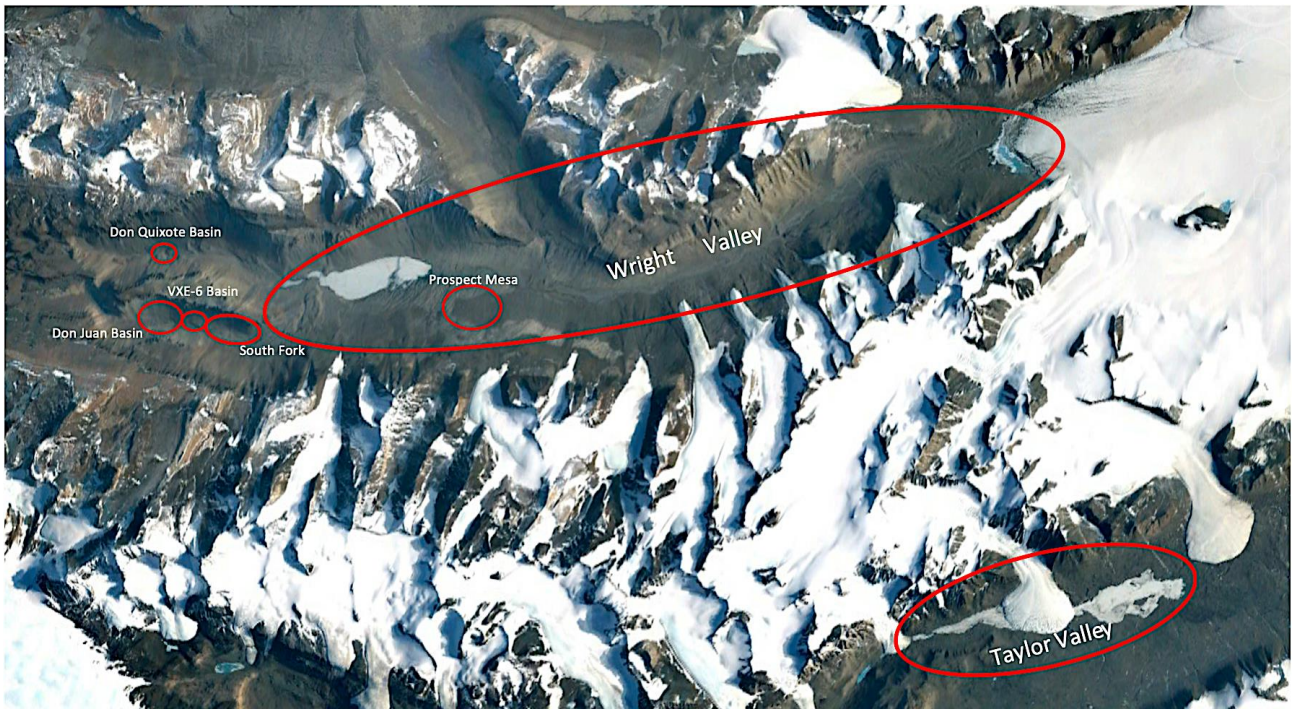

Figure 2. McMurdo Dry Valley regions of investigation

1.4.3. Climate

Climate plays a critical role in maintaining the valley's lack of ice. Mean annual precipitation, entirely as snow, is between 5 and 10 cm in valley bottoms (Thompson, 1971), while annual sublimation is at least 50 cm (Ragotzkie, 1964; Yusa, 1972; Anderton, 1976; Chinn, 1976).

In central Wright Valley, temperatures at lower elevations hover around -18 °C, with lows reaching -55 °C during winter, and highs reaching 10 °C for short periods of time in the late summer (Bull, 1966). Higher elevations, comparatively, are much colder, with temperatures rarely exceeding 0 °C above 1000 m. Ice and snow persist at these elevations in part due to the low average temperatures, but also due to decreased rates of sublimation as a result (Harris, 1981).

In Taylor Valley, mean annual temperatures average about -20 °C, with lows reaching -60 °C in winter, and highs reaching 10 °C in summer (Clow et al., 1988; Doran, 2002). Western Taylor Valley is typically warmer than eastern Taylor Valley by a few degrees (Fountain et al., 1999). Precipitation is limited to snowfall or windblown snow from katabatic winds (Fountain, 2010) and can be highly variable throughout the valley floor. Proximity to McMurdo Sound influences average snow accumulation; near the coast, average snow accumulation rates are approximately 70 mm/yr, but can be as high as 100 mm/yr some years; farther inland, average snow accumulation rates plummet to approximately 15 mm/yr near Canada Glacier, decreasing westward (Fountain et al., 2010).

1.4.4. GEOLOGY

Regional geology varies between the two valleys in which samples were taken. Wright Valley exhibits three major geologic residents: a basement complex made up of granitic plutons and microdiorite-granodiorite dykes of the Wright Intrusives that were eventually peneplained and overlain by a thick sequence (4,000 ft) of Beacon Sandstone deposited from Devonian to mid-Mesozoic times, and, lastly, Ferrar Dolerite sill and dyke intrusion (McKelvey, 1962).

Taylor Valley, specifically the lower end (77° 37’ S, 163° 00’ E), exhibits Bonney Pluton, a flow aligned quartz-monzodiorite with mafic-microgranite enclaves, extending from east Taylor Glacier to the southern lobe of Seuss Glacier. From here, continuing eastward, Biotite orthogneiss, a quartz-biotite-plagioclase-Kspar gneiss of granitic

composition, extends to the Ross Sea (Peterson and Marsh, 2008). Soils in the McMurdo Dry Valleys, according to the World Reference Base for Soil Resources classification system, are classified as Gelisols (Staff, 2010). Gelisols are soils that have permafrost within 100 cm of the soil surface.

1.4.5. Ground Water

As a result of the hyper arid and frigid environment, prevalence of liquid water is limited. The primary form of water transportation is therefore assumed to be glacial. However, it has now been shown that with the necessary thermal and chemical conditions, liquid water does occur at a local level; hypersaline lakes and ponds being the best examples. These lakes and ponds can range in size from 100 m^2 to 2-3 km^2 with compositions rich in Na and Cl, or Ca, Mg, and Cl. (Harris, 1981). Common surficial soluble salts of the region are calcite, thenardite, halite, and gypsum (Nishiyama and Kurasawa, 1975; Nishihyama, 1978, 1979). Anhydrite is reported in select localities in this thesis. The origin of these salts is still debated, hypotheses being: 1) sequestration from persistent seawater (Yamagata et al., 1976; Matsubaya et al., 1979), 2) saline snow/and or aerosols from the Ross Sea (Dort and Dort, 1970; Torii and Yamagata, 1981), 3) bedrock alteration (Oberts, 1973; Jones and Faure, 1978), and 4) an unknown combination of all the above (Nakai et al., 1975; Claridge and Campbell, 1977; Torii and Yamagata, 1977). The McMurdo Dry Valleys are also reported to exhibit brines throughout the region (Harris, 1981), but it is those of Lake Vanda and Don Juan Pond in Wright Valley that are most intriguing. Bottom waters of Lake Vanda exhibit Ca dominated brine, followed by Mg, and NaCl; Don Juan Pond exhibits Ca dominated brine followed by NaCl (Harris, 1981).

Toner (2012), reports soluble salt accumulations in Taylor Valley to be controlled by soil age, distance from the sea (McMurdo Sound), leaching, soil texture, cation exchange, and past glacial and lacustrine events. It is possible that similar processes operate in Wright Valley.

1.4.6. Chemical Alteration

In an environment so cold and dry, and therefore unfavorable to chemical alteration, peculiar brines in tandem with the precipitation of a collection of salts, in and around ponds and lakes, begin to form a different, more complex picture of alteration process in the valleys—one possibly of greater chemical alteration than previously thought. It is for these same reasons—extreme cold and aridity—that the McMurdo Dry Valleys Region, and specific locations therein, have been proposed as a viable analog environment for potential chemical alteration processes operating on Mars.

1.5. Research Sites

1.5.1. Microenvironments

In this thesis, "microenvironments" are defined as cores and sample sites from specified regions of Wright and Taylor Valleys. Thirteen cores are investigated: Three in Don Juan Basin, one in Don Quixote Basin, one in the South Fork region of Wright Valley, one in VXE-6 Basin, one at Prospect Mesa, and six at Lake Hoare. The cores in DJB, DQB, VXB, SF, and PM were taken to the depth of the permafrost. Of the six cores at LH, four are from oxic zones and two from anoxic zones of the lake. Twenty-three surface (SS) and edge (E) samples from LV, LB, and LF are also investigated. Below, a more detailed look is taken into each region and the microenvironments therein. Ponds 2 and 3, as defined by Harris, 1981, of the South Fork region, and Cores 20 and 41 of DQB, are not discussed in this paper but available data on the two is presented in Appendix G, Tables 40 and 41. Principal wind directions are reported by Nylen et al. (2004) who conclude that summer wind directions are predominantly down-valley (easterly), making aeolian sedimentation from westerly sources a possibility. Each microenvironment is discussed in detail below.

1.5.2. Don Juan Basin Cores: 2074, 33, 39

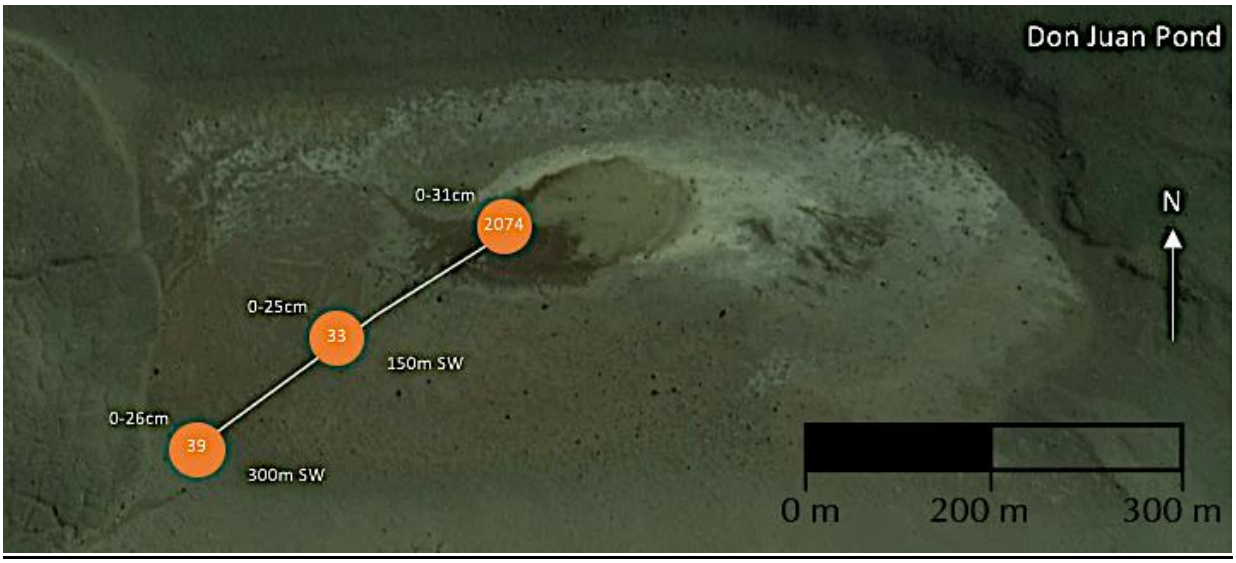

Figure 3. Sample sites of Don Juan Basin: core 2074, 33, and 39

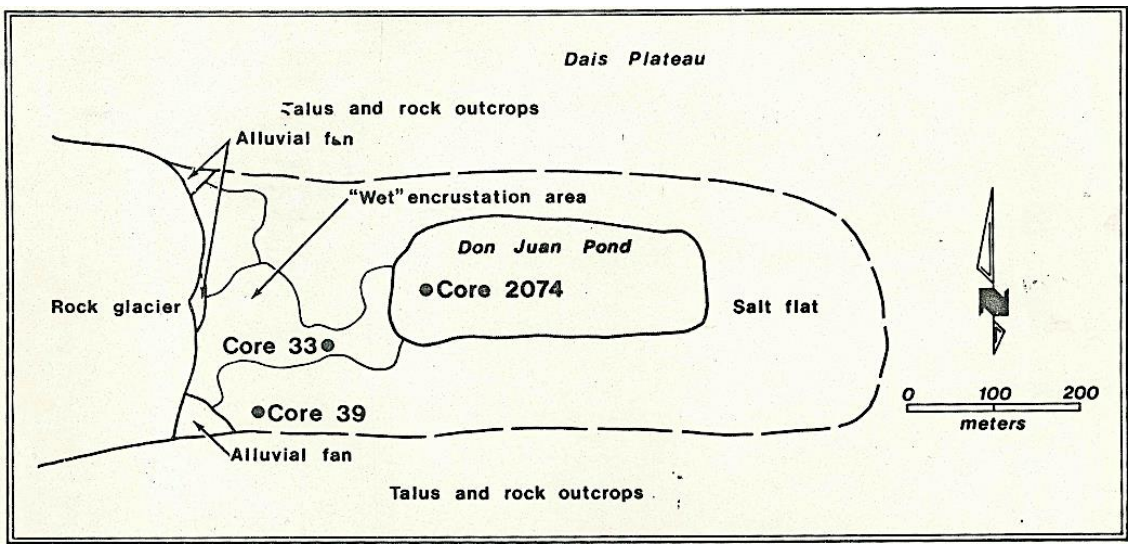

Figure 4. Original field drawing of Don Juan Pond, Don Juan Basin, Source: E.K. Gibson

Don Juan Basin floor is 117 m above Mean Seawater Level (MSL) with plateaus to the north and south rising above 1000 m. The basin floor has an eastward 200 m acclivity to the South Fork entrance (Harris, 1981). The basin floor is dominated by Ferrar Dolerite, while the plateaus to the north and south are primarily granitic Gneiss (Peterson and Marsh, 2008).

Don Juan Pond is the primary focus of Don Juan Basin. The pond is the second most saline body of water on Earth (Pérez and Chebude, 2017), and was discovered in 1961 (Meyer et al., 1962). Webb and McKelvey were the first to traverse the basin, in 1957-58. Not finding the pond, variance of spatial coverage of the unfrozen brine throughout the year is suggested (Harris, 1981). A "bathtub ring" of salt encrustation surrounds the pond. The pond and basin contain significantly elevated levels of calcium in the form of antarcticite ($CaCl_2 + 6H_2O$) (Torii et al., 1977), gypsum ($CaSO_4$) , and halite (NaCl) (Oberts, 1973). There are several schools of thought regarding the source of Don Juan Pond: 1) direct precipitation (snow); 2) stream input from the western lobe; 3) upwelling of a deep groundwater dolerite aquifer; and 4) active layer transport atop the permafrost table within the colluvium end of the pond (Dickson et al., 2013; Harris, 1981).

The first—direct precipitation via snow—is unlikely, as snow precipitation produces only between 5 and 10 g/cm^2 annually (Harris and Cartwright, 1979). Furthermore, while snowfall is capable of introducing salt into the pond, there is no reason for snow-deposited salts to be predominantly $CaCl_2$ (Lyons et al., 2003).

The second—stream input from the western lobe (Hassinger et al., 1983; Morgan et al., 2008)—is unlikely, as while there is evidence of drainage into the pond occurring in a small network of incised channels, several investigations involving ionic analyses of water in the stream show that the water is depleted in Ca^{2+} and Cl^-, excluding it from being a candidate for the $CaCl_2$ in the pond.

The third—upwelling of a deep groundwater aquifer—is a still-debated hypothesis. It can explain both a source of water that maintains the pond, and a source of $CaCl_2$ that comes from aqueous interaction with an underlying dolerite deposit (Harris, 1981).

Electrical depth soundings (McGinnis et al., 1971; McGinnis, 1973) and seismic profiles (McGinnis, 1973) have shown that the terrain beneath the pond is unfrozen to a depth of ~30 m, sloping westward to ~60 m. The geologic sequence was interpreted to be unfrozen basement rock superposed by wet lacustrine deposits directly beneath the pond (McGinnis, 1973). Through the Dry Valley Drilling Project (DVDP), samples of water showed that subsurface water beneath the pond was enriched in $CaCl_2$ with a contrast from surface weight percent that can be explained by evaporative concentration of the salts. This hypothesis is favored by Cartwright and Harris (1981). Additionally, Toner (2012) reports the amount of $CaCl_2$ that can be produced by exchange reactions to be consistent with estimated amounts of $CaCl_2$ in groundwaters beneath Don Juan Pond. This suggests that cation exchange reactions can explain the Ca and Cl-enriched composition of Don Juan Pond and other brines in the Dry Valleys.

Last is active layer transport atop the permafrost table within the colluvium end of the pond. At the surface this is seen as water tracks (Cartwright and Harris, 1981; Hastings et al., 1989; McNamara et al., 1999; Head et al., 2007; Levy et al., 2011)—areas of high soil moisture that act as downslope paths for saline liquids on top of the permafrost table. Additionally, the liquids have been found to be enriched in Ca^{2+} which bolster this hypothesis.

Don Juan Pond's behavior is dependent on that of other pieces of the system. Occasional freshwater streams serve as significant sources of volumes of water, believed to be the product of melting frozen ground (Harris and Cartwright, 1981), as well as Recurring Slope Lineae (RSL) (Dickson et al., 2013). Additionally, and likely the primary source of the annual water supply to the pond, there is discharge of saline groundwater from a dolerite aquifer to the surface (Harris, 1981).

Three cores are investigated in Don Juan Basin: 2074 (JB1124-26), 33 (JB1129-33), and 39 (JB1134-38) as seen in Figure 3 above. Core 2074 is situated in the center of Don Juan Pond, and core 33 and 39 are 150 and 300 m to the southwest. Each of the cores from Don Juan Basin is discussed in detail in the Results section.

1.5.3. Don Quixote Basin: Core 35

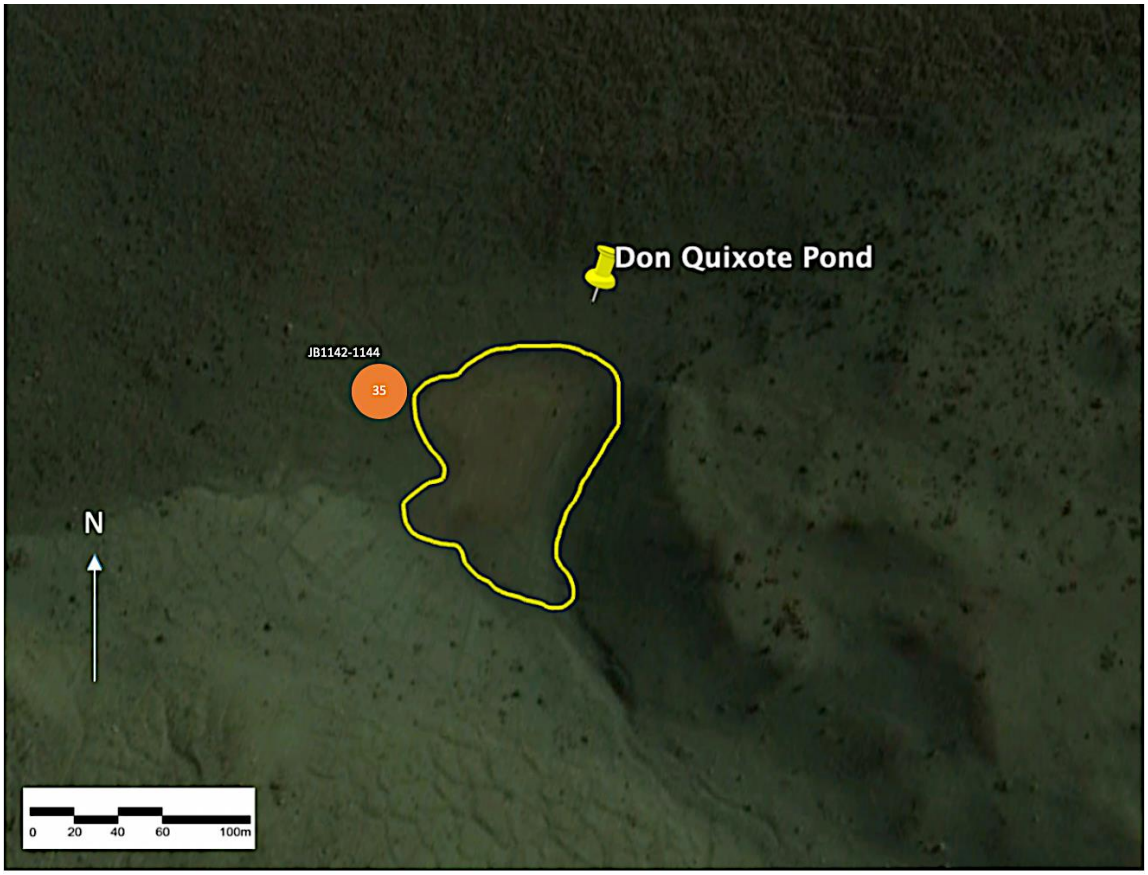

Figure 5. Core 35 sample site at Don Quixote Pond

Don Quixote Basin is just north of Don Juan Basin and the Dais Plateau, in the western end of Upper Wright Valley. Don Quixote Basin is the site of Don Quixote Pond and Core 35 (JB1142-45), sitting at approximately 100 m above Mean Seawater Level, surrounded by valley walls up to 2500 m high (Harris, 1981).

DQP is bounded by Biotite orthogneiss to the north, east, and south, and by undifferentiated Granitoids to the west. The basin floor is primarily composed of Ferrar Dolerite (Peterson and Marsh, 2008). The formation of DQP serves as a unique representation of terrestrial weathering, accumulation, and distribution of calcium, chlorine, and sulfate (Harris and Cartwright, 1981; Torii and Yamagata, 1981). Its brine

is seasonally frozen (Harris and Cartwright, 1981). In the field season of 1979-1980, E.K. Gibson collected samples from the surface of DQB and as depth profiles (Gibson et al., 1983).

1.5.4. VXE-6 Basin: Core 42

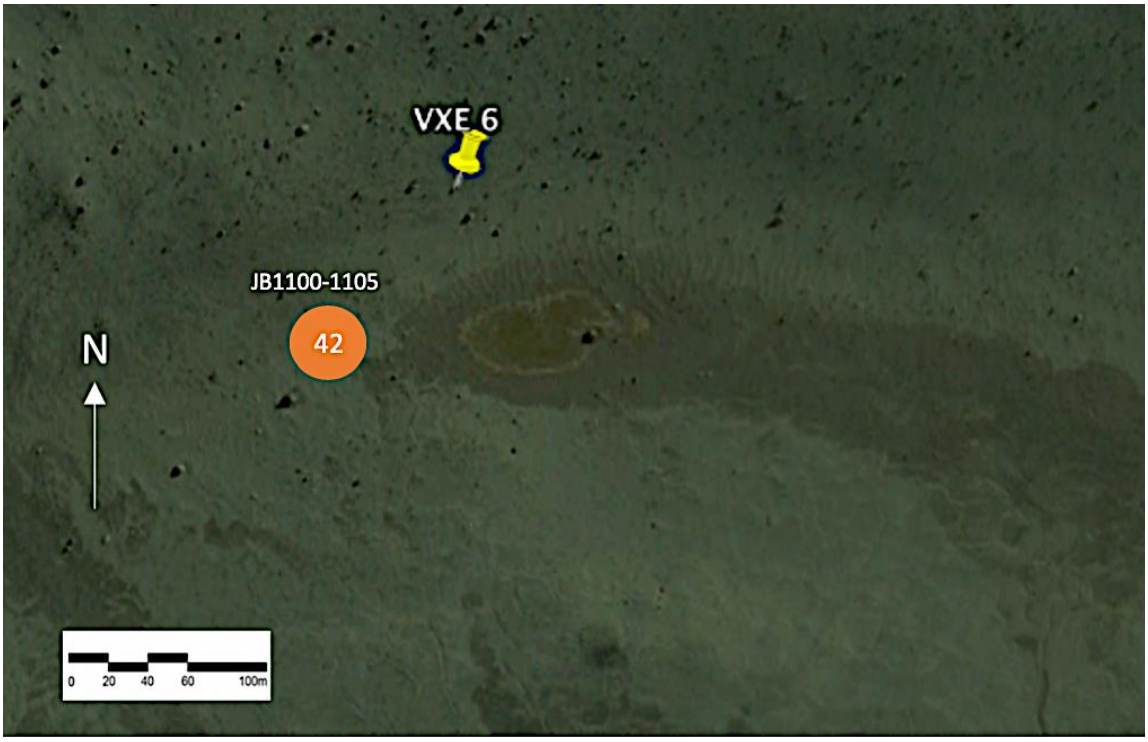

Figure 6. Core 42 sample site of VXE-6 Basin.

VXE-6 Basin is located approximately 2 km to the east of Don Juan Pond. Within VXE-6 Basin, the microenvironment of interest is Core 42 (JB1100-05) which was taken approximately 15 meters to the west of VXE-6 Pond. The pond is found at the center and topographically lowest point in VXB which is separated from DJB by a low divide. It is fed by glacial meltwaters (Harris, 1981). VXB is bounded to the north by a plateau of Biotite orthogneiss, and outcrops of Metagabbro Diorite, and to the south by Granitic

Gneiss. The basin floor is composed primarily of Ferrar Dolerite (Peterson and Marsh, 2008).

1.5.5. Core 52

Figure 7. Core 52 sample site in the South Fork of Wright Valley.

The South Fork region is located approximately 3 km east of Don Juan Pond, DJB. The region contains three ponds (Gibson, 1980): 1 (east SF), 2 (middle SF), and 3 (west SF), however geochemical analysis in this paper is limited to soil samples JB1107-1110 taken from Core 52, close to Pond 1. The soil trench was dug to a depth of 20 cm at which point permafrost is met. The sample site is bounded by Biotite Orthogneiss and

Metagabbro Diorite to the north, and Granitic Gneiss to the south (which will collectively be referred to as Granitoid). A small outcrop of the Bonney Pluton sits at the east end of the Dais Plateau, just north of the north of South Fork Basin (Peterson and Marsh, 2008). Pond 1 is a seasonally frozen body, and is supplied by localized shallow groundwaters (Harris, 1981).

1.5.6. Prospect Mesa: core 72

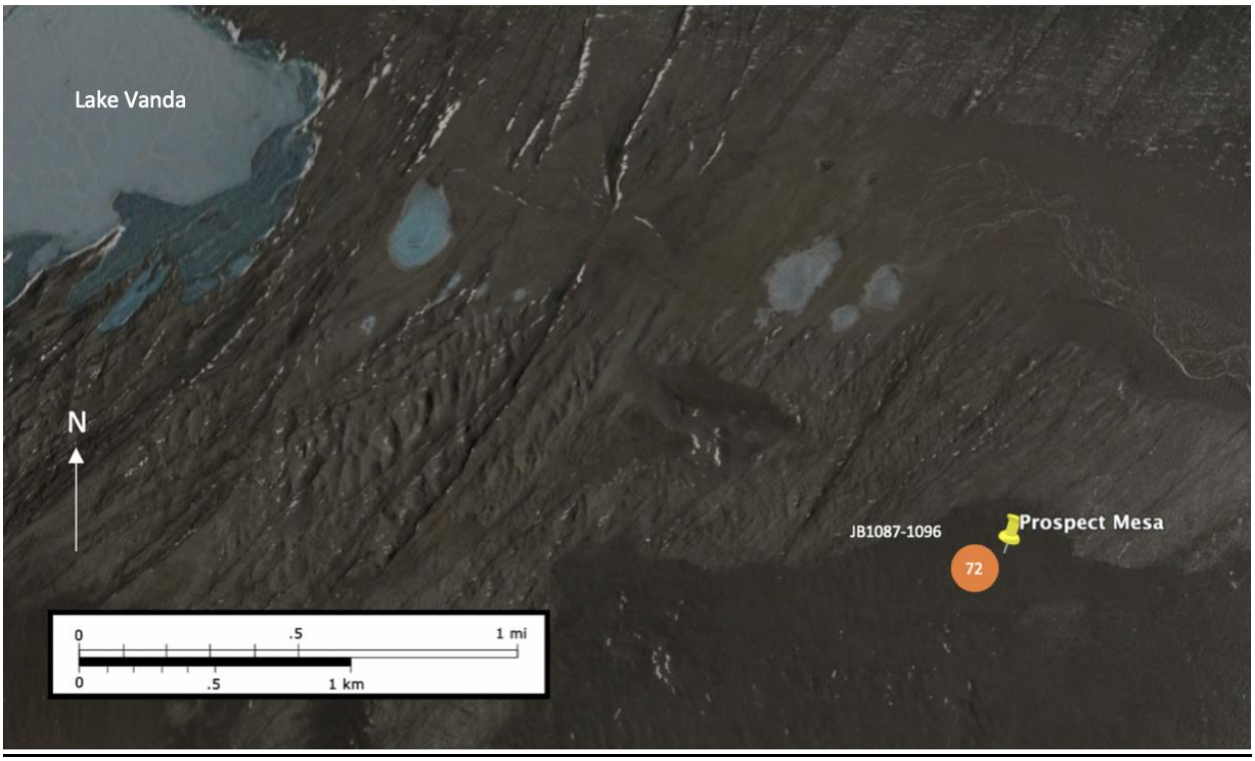

Figure 8. Core 72 sample site, Prospect Mesa.

The Prospect Mesa Formation is located on the southern side of Wright Valley, approximately 3 km southeast of Lake Vanda (Figure 8). The microenvironment of interest in this region is Core 72 (JB1087-96) taken in 1980 by Everett Gibson to a depth of 80 cm. Geochemical analysis was completed for the whole core, including ~45 cm of soil above permafrost depth. Core 72 sits in the middle of a large swath of the Bonney

Pluton with the Valhalla Pluton to the east (Peterson and Marsh, 2008). Felsic and mafic dikes are reported to the northeast of Lake Vanda (Allibone et al., 1993a). These formations are the source rocks, based solely on location, that most likely belong to Core 72 at Prospect Mesa.

1.5.7. Lake Fryxell

Lake Fryxell is located in lower Taylor Valley with Canada Glacier directly to the west and Commonwealth Glacier to the east. It is the site of samples JB650-JB660 (LFR-1 – LFR-10). JB650 and JB656-JB660 are all lake surface sediment samples. JB651-JB655 are edge sediment samples. Samples were collected in the summer of 2004. Lake Fryxell likely has one major source rock: Undifferentiated Gneiss or Biotite Orthogneiss. However, Brownworth Pluton is reported to the northeast, and Bonney Pluton to the southwest; those two possible source rocks could be influencing the composition of sediments (Peterson and Marsh, 2008).

1.5.8. Lake Vanda

Lake Vanda is located in Wright Valley, Antarctica, and is the site of samples JB661-669 (LVA-1 – LVA-9). JB661-664 and JB669 are all sediment samples collected from the edge of Lake Vanda. JB665-668 are all sediment samples that were collected from the surface of the lake. Samples were collected in the summer of 2004 (Bishop et al., 2014). Lake Vanda is bounded on all sides by the Bonney Pluton, and to the north and south by Ferrar Dolerite (Peterson and Marsh, 2008). Allibone et al. (1993a) base their conclusions on locations of plutons after the removal of surficial Ferrar Dolerite. Felsic and mafic dikes are to the northeast are also reported.

1.5.9. Lake Brownworth

Lake Brownworth is located in east Wright Valley, directly west of Wright Lower Glacier, and is the site of samples JB670-673 (LBR-1 – LBR-4). JB670-672 are all sediments

samples collected from the surface of Lake Brownworth, and JB673 is the sole edge sediment sample. Samples were collected in the summer of 2004 (Bishop et al., 2014). The Onyx River notably extends from the west side of Lake Brownworth, meanders through Wright Valley, and reaches Lake Vanda—approximately 27 km to the west. Sediment transport over this distance by the Onyx river needs to be taken into account. Lake Brownworth likely has one major source rock: the Brownworth Pluton, a coarse-grained, homogenous granite and quartz monzonite (Peterson and Marsh, 2008). As noted above, Ferrar Dolerite is removed to expose the surface below (Allibone et al., 1993a)

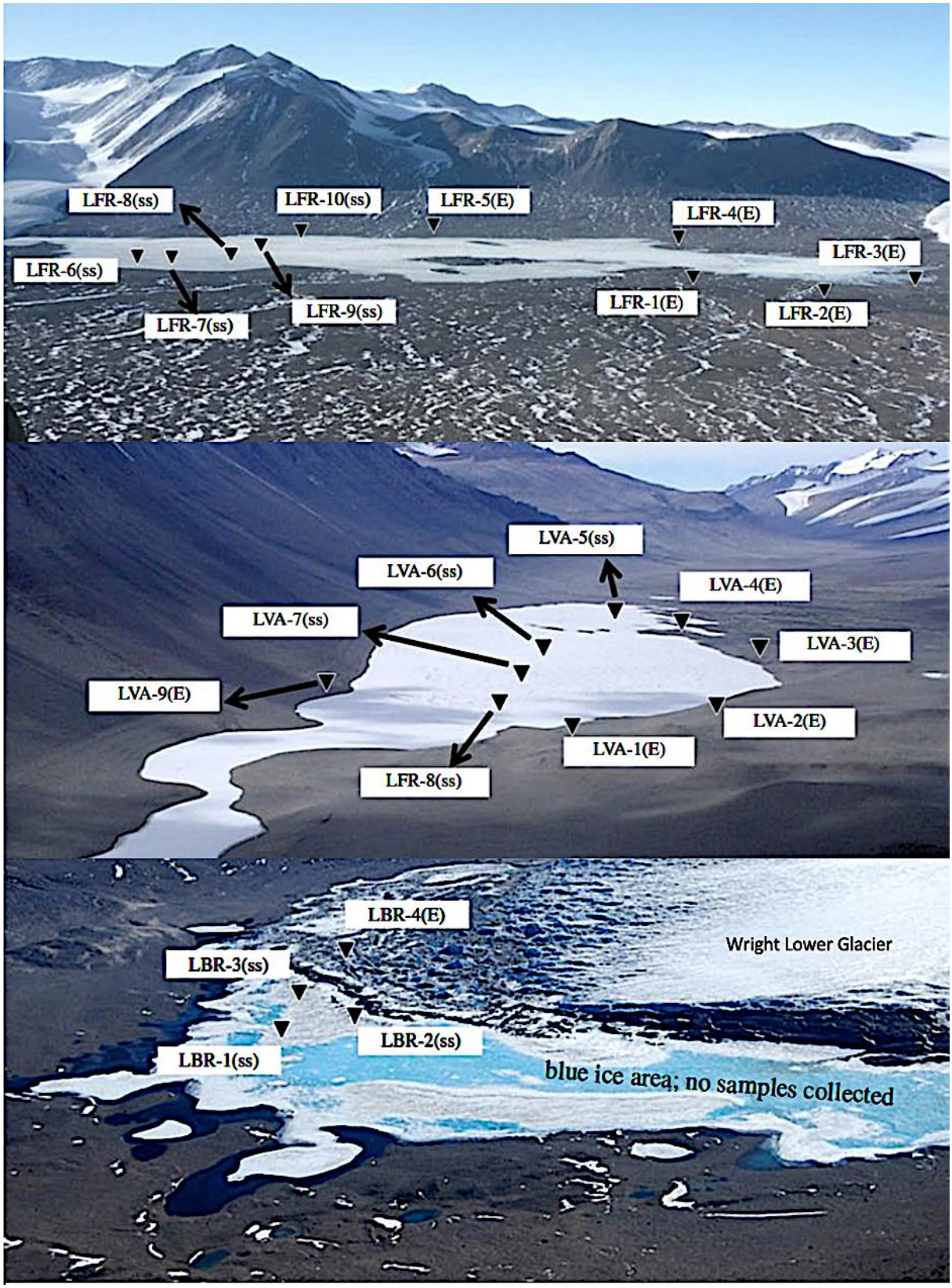

Figure 9. Sample sites of Lake Fryxell (top), Vanda (middle) and Brownworth (bottom). Source: Bishop et al. (2014)

1.5.10. LAKE HOARE

Lake Hoare is approximately 1 km wide and 4 km long with a maximum depth of 34 m (Nedell et al., 1987). The lake is perennially covered by > 3 m of ice and snow (Wharton et al., 1992; Craig et al., 1992) and the temperature of the water is -0.3 ± 1.0°C (Wharton et al., 1993). The lake water is stratified into oxic (beneath ice to 27 m depth) and anoxic (below 27 m) regions (Wharton et al. 1986, 1987; Craig et al., 1992).

Cores A-D, E, and H are all located in the northeast corner of the lake. Cores A-B, E, and D are approximately 130 m and 190 m from the shoreline. Cores C and H are approximately 300 m from the shoreline. Cores A, B, E, and D were collected from oxic zones, while cores C and H were collected from anoxic zones. Each core was taken to a different depth, and is discussed below. Sediments were collected from dive holes (essentially cores) during the 1979-80, 80-81, and 81-82 austral summers (Nedell et al., 1987).

Lake Hoare likely has one major source rock: Undifferentiated Gneiss or Biotite Orthogneiss. However, two nearby potential source rocks and could be influencing the data (Peterson and Marsh, 2008).

Minor amounts of cobble sloughed off the face of Canada glacier, which extends between Lakes Hoare and Fryxell, are intermixed with sand, believed to be of aeolian origin, on the eastern shoreline of Lake Hoare. During the summer, several small streams flow from the 15-20 m high glacial terminus onto the sand bank. As the streams flow, they cut through the sandbanks and form small deltas at the lake margin, introducing the possibility of sediment deposition into Lake Hoare by means of mass-wasting. The largest inflow stream exists on the western margin of the glacier. Smaller streams surrounding the lake begin to flow upon contact with direct sunlight (Nedell et al., 1987). Small outcrops of Ferrar Dolerite are reported to the northeast of Lake Hoare which connect to the regional swath of Undifferentiated Gneiss or Biotite Orthogneiss (Peterson and Marsh, 2008).

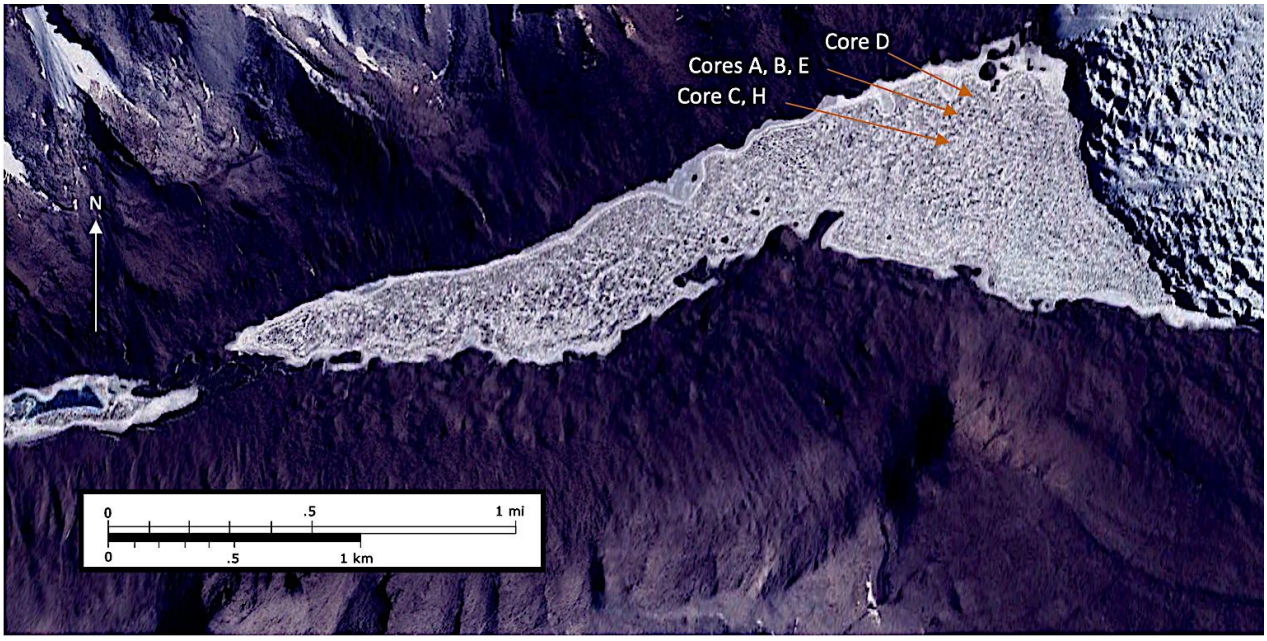

Figure 10. Lake Hoare sample sites.

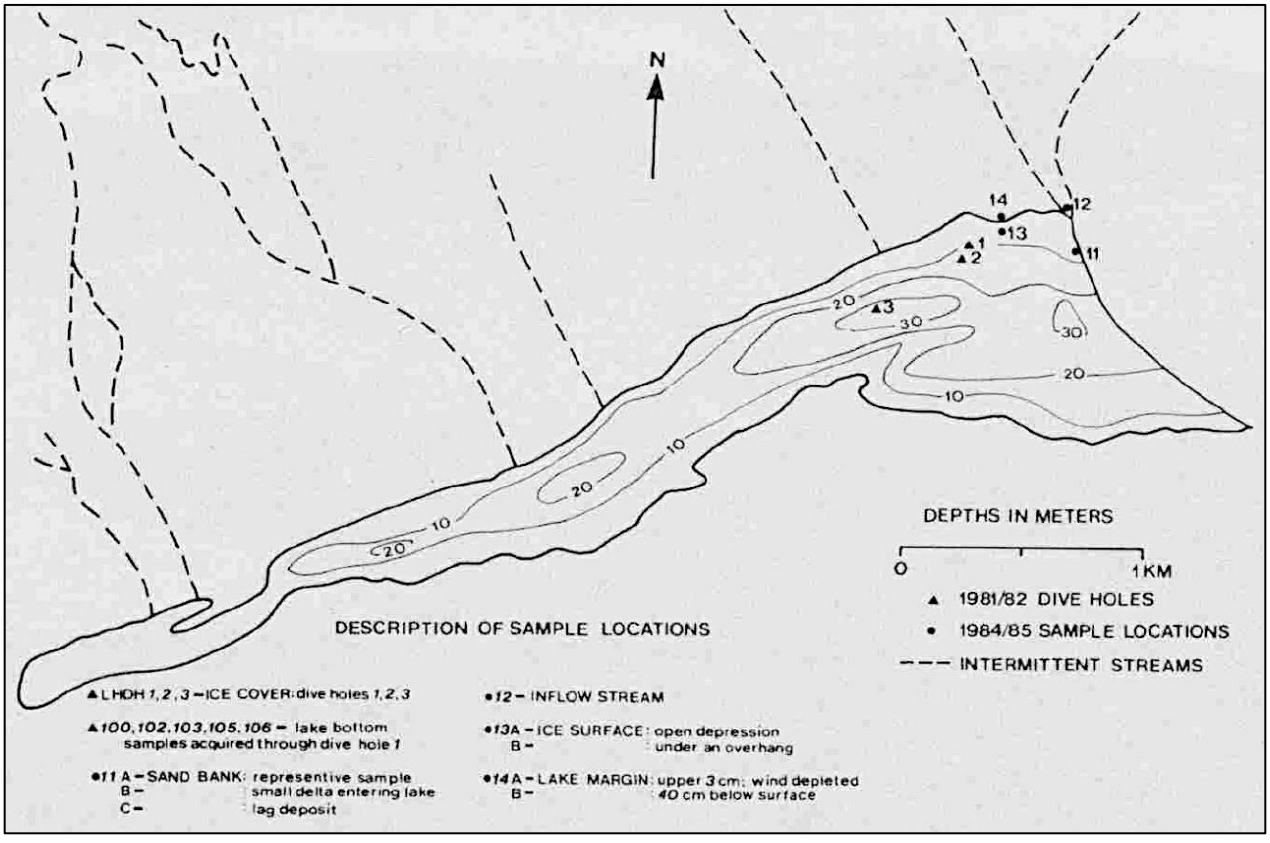

Figure 11. Bathymetric map of Lake Hoare showing sample locations and their descriptions. Source: Nedell et al. (1987)

The image above, from Nedell et al. (1987) shows locations of intermittent streams and their proximity to dive holes and sample locations. Notably, there is an intermittent stream that terminates approximately 250 m north from the cluster of dive holes, strengthening the possibility of sediment deposition into Lake Hoare by means of mass-wasting.

CHAPTER 2: TYPE AND DEGREE OF SEDIMENT ALTERATION IN THE MCMURDO DRY VALLEYS

2.1. ABSTRACT

Investigation of alteration signatures in sediment samples from microenvironments in the McMurdo Dry Valleys was done with the purpose of applying these data to Mars in order to determine if there are similar chemical alteration indicators rooted in martian rover data. Alteration signatures are determined through comprehensive elemental and mineralogical analysis and are organized into three modes of alteration: physical, chemical, and biological. Physical alteration, based on the frigid temperatures and the extremely dry nature of valleys, appears to dominate. Chemical alteration is suggested to be operating on a secondary scale, and biological alteration, due to the extreme conditions, is suggested to be operating on a tertiary scale. Analysis shows surface sediment formation is dominated by physical alteration; chemical alteration begins to occur as a relatively ubiquitous layer, a few centimeters below the surface, in nearly all core samples, while select lake bottom sediments experience biological alteration. Identifying the type and degree of alteration in sediment samples offers insight into

alteration processes occurring in the McMurdo Dry Valleys and supports understanding alteration in the frigid and dry conditions of Mars.

2.2. INTRODUCTION

2.2.1. BACKGROUND

The McMurdo Dry Valleys (MDV) region is the Earth's coldest and driest desert; the mean annual air temperatures range from -25 to -20 °C and the mean annual precipitation, in the form of snowfall, is 15 g/cm^2/yr (Bull, 1966; Thompson et al., 1971). The region is desolate and liquid water is scarce. It is for these reasons that the region is frequently used as a terrestrial analog to Mars.

Investigations of chemical and mineralogical alteration of valley sediments have found more extensive physical alteration than chemical alteration. This is not to say that chemical alteration is not occurring, and possibly more so than previously thought. The aim of this study is to conduct a comprehensive elemental and mineralogical analysis of sediments to determine the extent of chemical alteration in the McMurdo Dry Valleys. Because valley conditions are not conducive to chemical alteration, special focus is given to microenvironments exhibiting data different from expected abundances and patterns. Once interpreted, we seek to apply our data to that collected by the martian rovers. In doing this, we test the efficacy of select localities in the McMurdo Dry Valley Region as terrestrial analogs to the martian landscape. Data and results from Chapters 2 and 3 is applied to Mars rover data in Chapter 4.

2.2.2. CHARACTERIZING SEDIMENT ALTERATION

Determination of type and extent of sediment alteration is the primary objective of Chapter 2. The principal approach taken here is through the analysis of major, minor, and trace (rare earth elements included) element abundances and mineralogical composition of samples from microenvironments. A specific, quantitative method to

evaluate alteration that uses major element abundances is the Chemical Index of Alteration (CIA). The CIA is used to assess the effects of physical versus chemical alteration in pedogenesis. It reflects the proportions of primary and secondary minerals in bulk sample, providing a means to order samples (Krissek and Kyle, 2000; Sheldon and Tabor, 2009; Li and Yang, 2010; Nesbitt and Young, 1982). Additionally, the CIA can be used as a means to assess degree and process of alteration (Nesbitt and Young, 1982; Fedo et al., 1995) by the comparison of sample to source rock. The CIA is based on the mobility of major elements Al, Ca, Na, and K. Fresh basalts have a CIA range of 30-45; fresh granites and granodiorites have a CIA range of 45-55; feldspars, 50; illite, 75-90; and kaolinite, 100. (Nesbitt and Young, 1982; Fedo at al., 1995). The equation defining the CIA (Nesbitt and Young, 1982) is outlined below:

CIA = 100 x Al_2O_3 / (Al_2O_3 + CaO* + Na_2O + K_2O) (molar basis)

where the sample abundance of each oxide is divided by the molecular weight of each oxide. CaO* is the amount of CaO in in the silicate fraction of the samples.

Also discussed is the possibility of salts, primarily Calcium and Potassium sulfates, creating a dilution effect that can, if in great enough abundance, significantly influence the CIA. In order to determine the undiluted CIA value, we modify the CIA equation by assuming that all SO_3 is present as $CaSO_4$, K_2SO_4, or Na_2SO_4. To do this, the following steps are taken:

1. Convert CaO %, K_2O %, Na_2O % to mole fraction

2. Multiply oxide mols by the molecular weight of each in its sulfate form to attain % sulfate: (Ca), (K_2), (Na_2) SO_4

3. Subtract (Ca), (K_2), (Na_2) SO_4 % from each oxide's original % abundance

4. Insert new value of oxide % into CIA equation to determine undiluted CIA value

Note: If after subtracting (Ca), (K_2), (Na_2) SO_4 % from each oxide's original % abundance, the value returned is negative, the oxide is assumed to be completely consumed by SO_3 to form the oxide's sulfate form. In this instance, CaO, K_2O, and Na_2O are inserted into the CIA equation as "0".

In addition to sulfate salts, there is one unique case with carbonate salts that requires a slightly different approach when using a modified Chemical Index of Alteration. Many samples from Lake Hoare contain calcite (e.g. Bishop et al., 1996). For this study samples with abundances of CaO greater than 5 % were assumed to contain calcite. In order then to modify the CIA, 5 % is subtracted from the total measured CaO, and any remainder is assumed to be calcite. From here, the above steps regarding sulfates are followed.

Degree and process of alteration is also assessed through the analysis and comparison of select elements and elemental ratios that are diagnostic of particular source rocks. Ti, Zr, and Rare Earth Elements, due to their high field strengths, are more immobile than elements such as K and Ca. REE patterns have also been used to determine sediment provenance because basic rocks contain low Light REE/High REE (LREE/HREE) ratios and no Eu anomalies, whereas more silicic rocks usually contain higher LREE/HREE ratios and negative Eu anomalies (Cullers and Graf, 1983). Based on this, certain REE patterns and abundances can be used to infer degree/type of alteration (Nesbitt and Markovics, 1997).

2.3. METHODS

2.3.1. STUDY SITES

There are nine different study sites, microenvironments within Wright and Taylor Valleys, that are shown below. Cores 2074, 33, and 39 are all located in Don Juan Basin, Core 42 in VXE-6 Basin (Harris, 1981), Core 52 in the South Fork Region, Core 35 in Don Quixote Basin, and Cores A-E, and H at Lake Hoare. Lakes Fryxell, Vanda, and Brownworth microenvironments consist of 23 lake surface and edge samples. Detailed descriptions of the sites and the overall geologic context are given in Chapter 1.

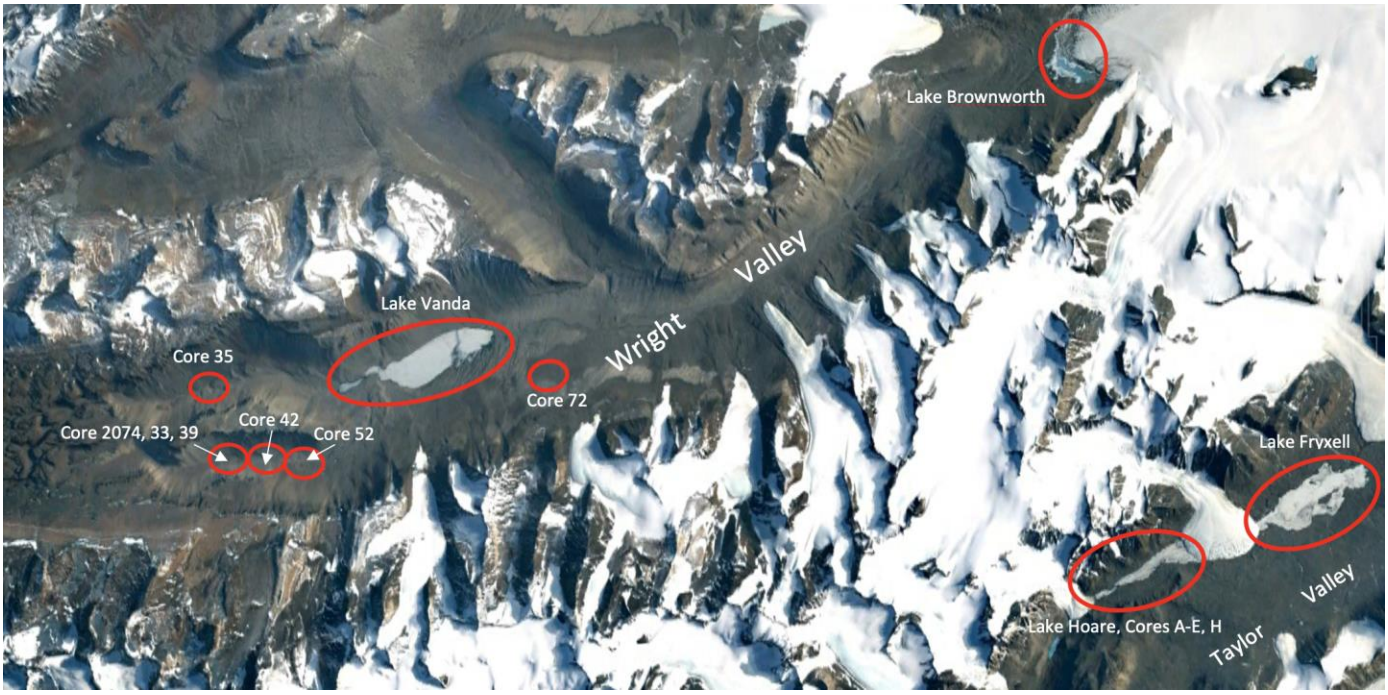

Figure 12. Study sites of the McMurdo Dry Valleys.

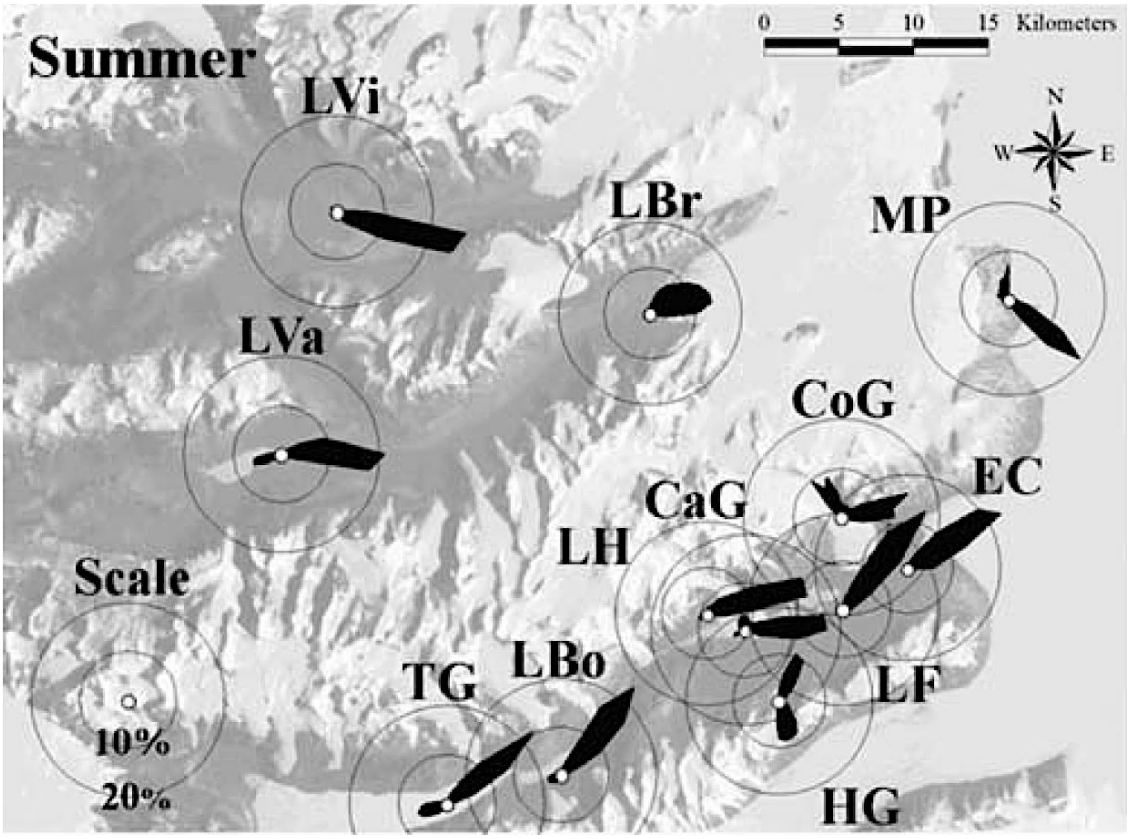

Figure 13, Summer wind directions of the McMurdo Dry Valleys, Antarctica. Source: Nylen et al. (2004).

Principal summer wind directions, as reported by Nylen et al. (2004), are seen in Figure 13 above. Summer wind directions are predominantly down-valley (to the east), making aeolian sedimentation from western sources a possibility as well.

2.3.3. Sampling and Analytical Methods

Sediment samples from seven cores taken in 1980 from Wright Valley (Gibson, 1980), and 23 surface/edge sediment samples from Lakes Fryxell, Vanda, and Brownworth were taken in 2004 (Bishop et al., 2014) are analyzed in this chapter. Each core was taken to the depth of the permafrost (permanently frozen ground) which varies from core to core. Six Lake Hoare samples were collected from cores taken in three different dive holes: DH-1, DH-2, and DH-4, as described by Nedell et al. (1987).

For Cores 2074, 33, 39, 35, 42, 52, 72, and all samples from Lakes Fryxell, Vanda, and Brownworth, major, minor, and trace elements were measured in the 125 µm size

fraction of the ground samples by ACME Laboratories of the Bureau Veritas in Vancouver, B.C., Canada via X-ray fluorescence (XRF). Additional minor and trace element abundances, including those of the rare earth elements, were measured by instrumental neutron activation analysis (INAA) at the Department of Lithospheric Research, University of Vienna, Austria. The details of this method are described by Koeberl and co-workers (Koeberl, 1993, Mader and Koeberl, 2009). Rare Earth Elements (REE) are normalized to Solar System averages per Masuda et al. (1973) and Taylor and McLennan (1985). Figure 14, below, displays Solar System atomic abundances normalized to Si = 10^6. Visible near-infrared (VNIR) spectra were measured from 0.35-2.5 µm at the SETI Institute with an ASD Spectrometer under ambient conditions relative to Spectralon. Additional reflectance spectra were measured at the Reflectance Experiment Laboratory (RELAB) at Brown University. These spectra are composites prepared from bidirectional VNIR spectra measured from 0.3-2.5 µm under ambient conditions relative to halon that were connected near 1.2 µm to Fourier Transform Infrared (FTIR) data collected from a Nicolet spectrometer in a biconical configuration under a H_2O- and CO_2-purged environment relative to a rough gold standards (e.g., Bishop et al., 1996, 2001, 2003, 2013, 2014).

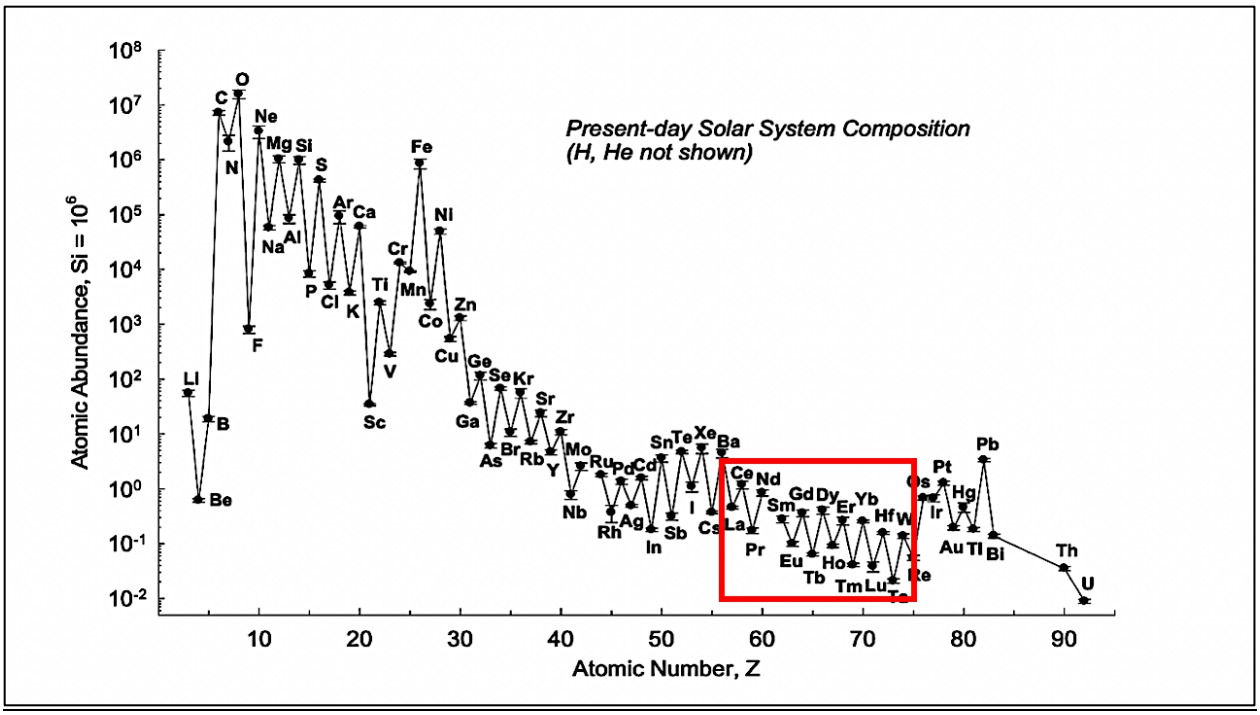

Figure 14. Rare Earth Elements analyzed in this thesis (red box), normalized to solar system averages. Source: Lodders (2010).

Mineralogical analysis, for all samples was conducted with the Terra-166 XRD (X-ray Diffraction)/XRF instrument on particulates less than 125 μm size fraction of each sample. Core 42 XRD measurements, in addition to the Terra-166 XRD/XRF instrument, were done using a Bruker D8 Advance with a LYNXEYE XE detector, at the University of Hawai'i at Mānoa.

Core 72 XRD quantitative measurements, in addition to the Terra-166 XRD/XRF instrument, were measured for "prepared powders" of evaporites from the bulk samples using a Picker Diffractometer. Some XRD analysis was also done by N. Guven at Texas Tech University (Gibson, 1983).

"Total Salts", occasionally referred to in core analysis, is defined as the sum % of all salts as measured by XRD in the sample, which include halite, thenardite, anhydrite, and gypsum.

Raman spectroscopy was applied to selected surface and edge samples from Lake Fryxell, Vanda, and Brownworth, measuring several spots on sediment grains for each sample in order to characterize as many minerals present as possible. Confocal Raman microscopy (Dieing et al., 2011) was used in order to view the surface of the mineral grains at the specific sites where spectra were collected (Bishop et al., 2014). Lake Hoare XRD measurements were performed on pressed powders with a Philips PW 1710 diffractometer.

For select microenvironment samples, water soluble cations and anions were measured by either ion selective electrode or ion chromatography techniques (Small et al., 1975; Gibson et al., 1983).

2.4. RESULTS

2.4.1. CORE 2074

Core 2074 is situated near the middle of DJP and has three samples ranging from the surface to a depth of 10 cm with permafrost at 31 cm. Core 2074 surface sample, JB1126, is primarily salt and is therefore not discussed. The relative depletion in what are generally seen as immobile elements suggest that sediments in Core 2074 have experienced chemical alteration. Depletion of the most soluble, more mobile ions, such as Na, Ca, K, is expected as there is a lack of source rock remaining in which the most soluble ions would be highest. Major elemental analysis is pending.

2.4.1.1. Elements: Minor and Rare Earth

U, Th, Ba, and Sr measurements of Core 2074 are unusual when compared to cores 33 and 39, exhibiting significantly lower abundances, as are diagnostic elemental ratios K/Th (0.61-0.67), and oxide ratio Al_2O_3/TiO_2. Interestingly, though, there is U enrichment in the top 2 cm (3.03 ppm) that is approximately twice the abundance of Cores 33 (1.45 ppm) and 39 (1.14 ppm) at their corresponding depths. The U/Th ratio at Core 2074 for 2 cm is 0.95, Core 33 is 0.27, and Core 39 is 0.21.

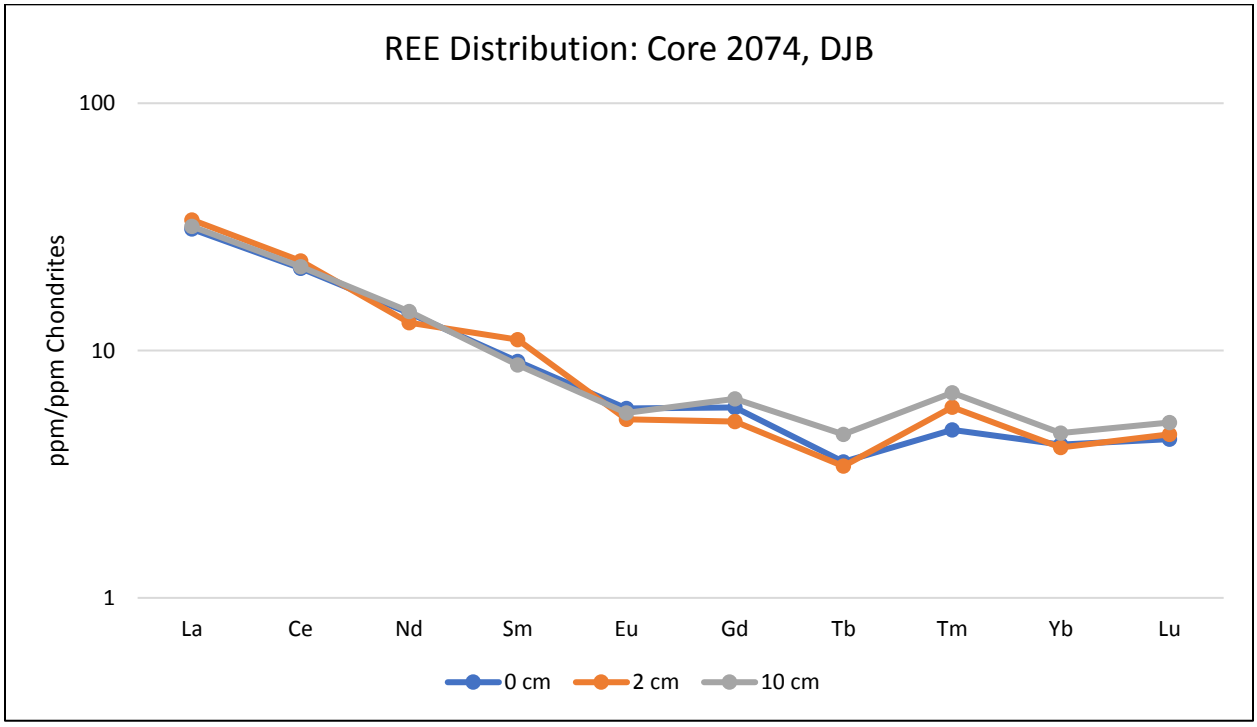

Figure 15. Rare Earth Element distribution of Core 2074, Don Juan Basin.

Rare Earth Elements at core 2074 show a similar trend, but general depletion compared to other microenvironments. All core 2074 samples exhibit a negative Eu anomaly which is typically attributed to CaO and Na_2O depletion which in turn could be due to plagioclase weathering (Nyakairu and Koeberl, 2001). Additionally, all samples exhibit a negative Tb anomaly. REE abundances also provide diagnostic information for degree

of chemical alteration because of their relative immobility and insolubility. The depletion in REE abundances corroborates depletion in other trace elements as well as major elements, strongly suggesting active chemical alteration at Core 2074.

2.4.1.2. MINERALOGY: XRD, SPECTRA

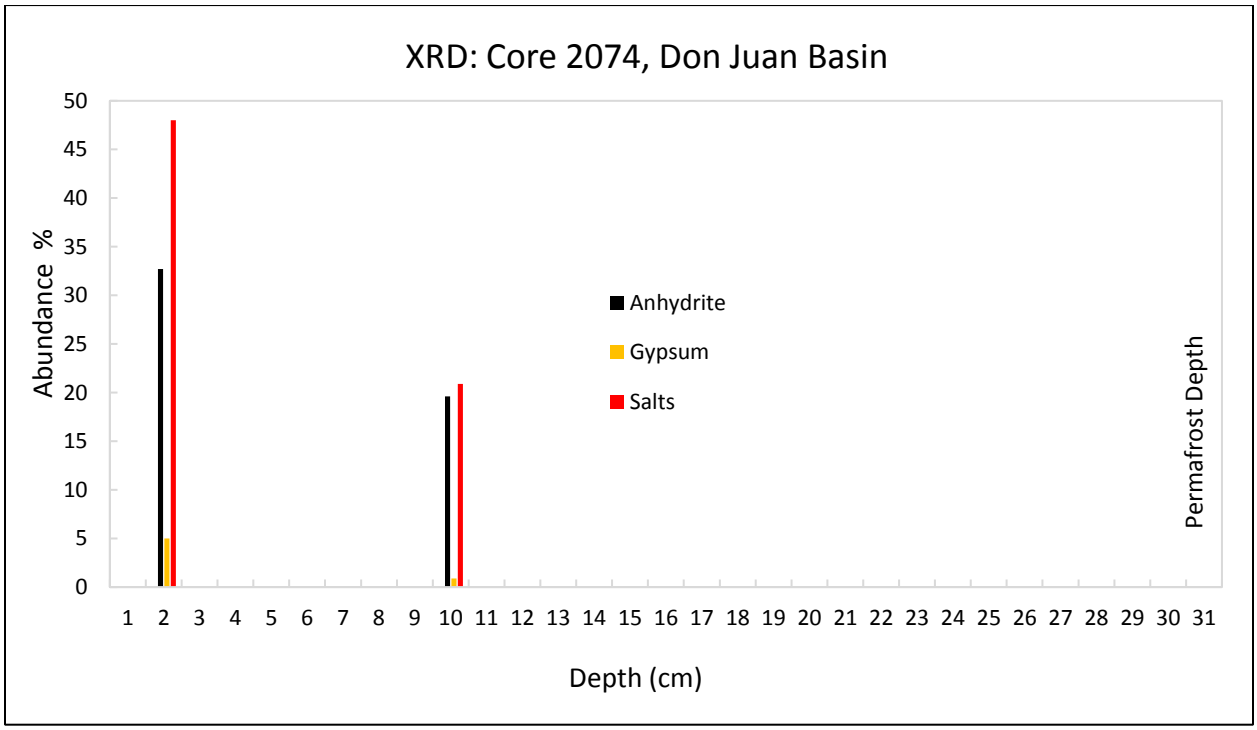

Figure 16. Mineralogical analysis of Core 2074, Don Juan Basin.

Nearly all depth profile and surface samples of Don Juan Basin show sulfates, including thenardite, anhydrite, bassanite, and gypsum. Gypsum and anhydrite are the dominant sulfates. Preliminary XRD analysis of JB1124 (top 2 cm) shows gypsum (4 %), anhydrite

(32 %), and salts (36 %). JB1125 (upper 10 cm) exhibits basanite (0.4 %), gypsum (0.9 %), anhydrite (19.6 %), and salt (24 %) (Figure 16, above). Core 2074 exhibits the highest sulfate abundances in Don Juan Basin, with anhydrite distinctly dominating.

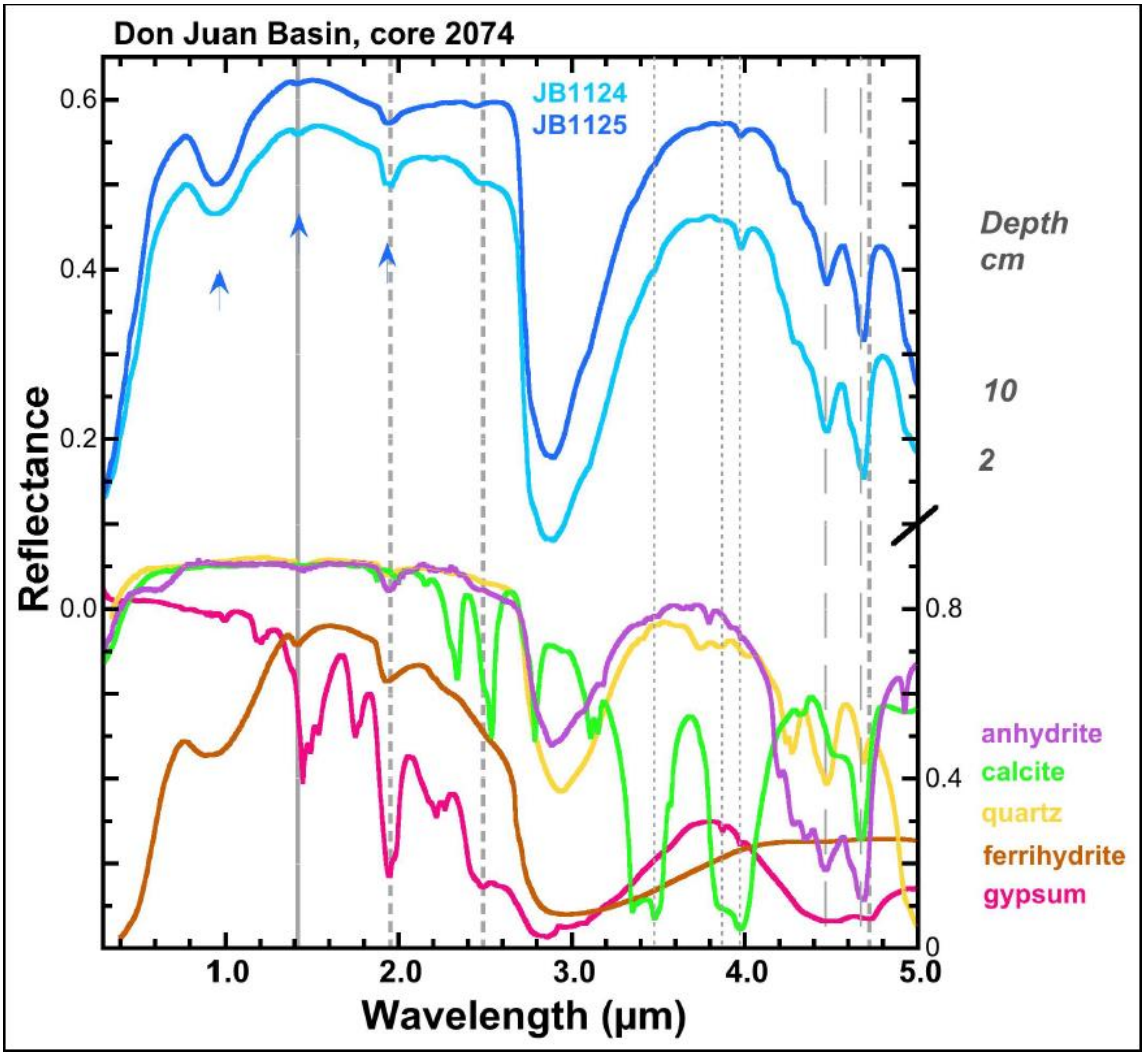

Figure 17. Spectral analysis of Core 2074, Don Juan Basin.

Spectra from Core 2074 (Englert et al., 2017) confirm the presence of quartz and gypsum and the high abundance of anhydrite. Also shown is the presence of calcite and

hydrated ferric oxide. The presence of evaporites infers the existence, past or present, of an aqueous solution, which is suggestive of chemical weathering.

2.4.1.3. Special Analyses: Anions

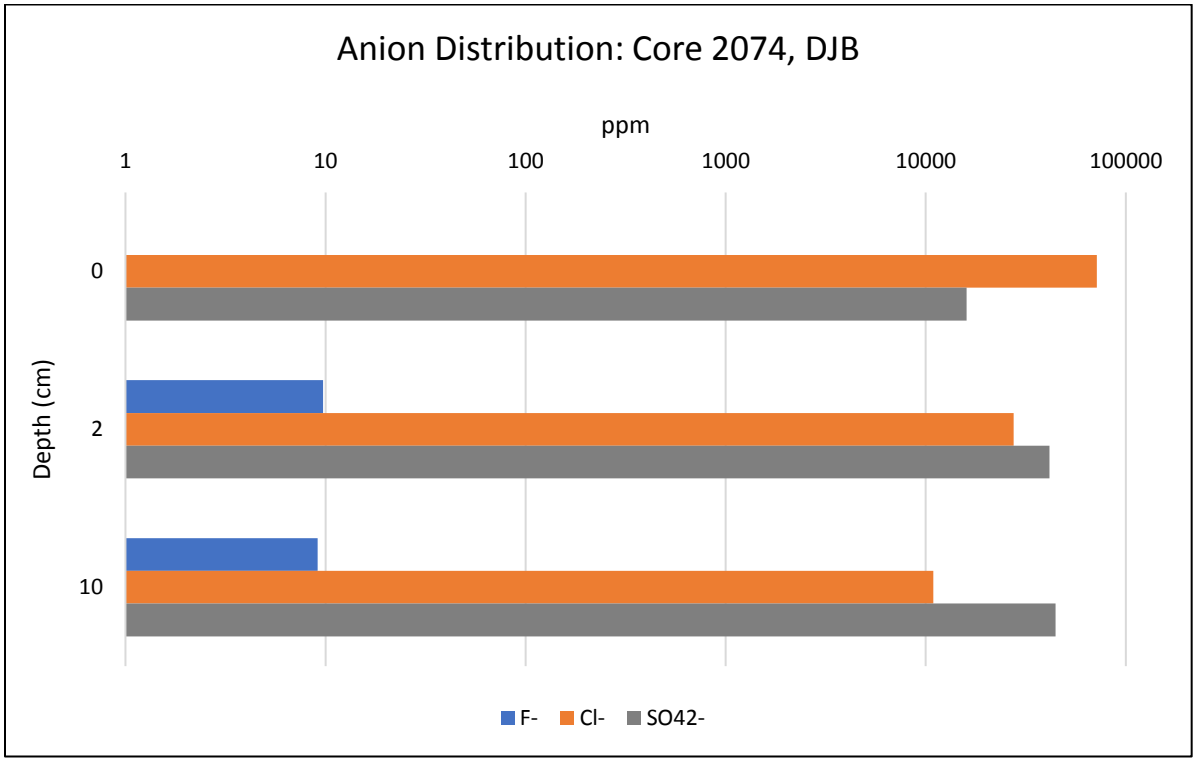

Figure 18. Soluble anion distribution of Core 2074, Don Juan Basin.

Soluble anion distribution throughout Core 2074 shows SO_4^{2-} abundance increasing with depth, Cl^- abundance decreasing with depth, and F^- remaining relatively stable. The Cl^- pattern could be due to a combination of surficial influx of Cl^- in the form of a $CaCl_2$ brine and $CaCl_2$-enriched waters existing in a subsurface dolerite aquifer that become concentrated, through evaporation, at the surface (Dickson et al., 2013). The pattern

could be due to a well-formed salt layer, likely of gypsum or anhydrite, that is also observed in Cores 33 and 39 (Gibson, 1980).

2.4.2. Core 33

Core 33 is situated approximately 150 m SW of core 2074, in the path of a "wet" encrustation (Figure 4) that meets with the west edge of the pond, understood to be a water source for DJP (Dickson et al., 2013). The core has five samples ranging from surface to 20 cm depth with permafrost at 25 cm.

2.4.2.1. Elements: Major, Minor, and Rare Earth

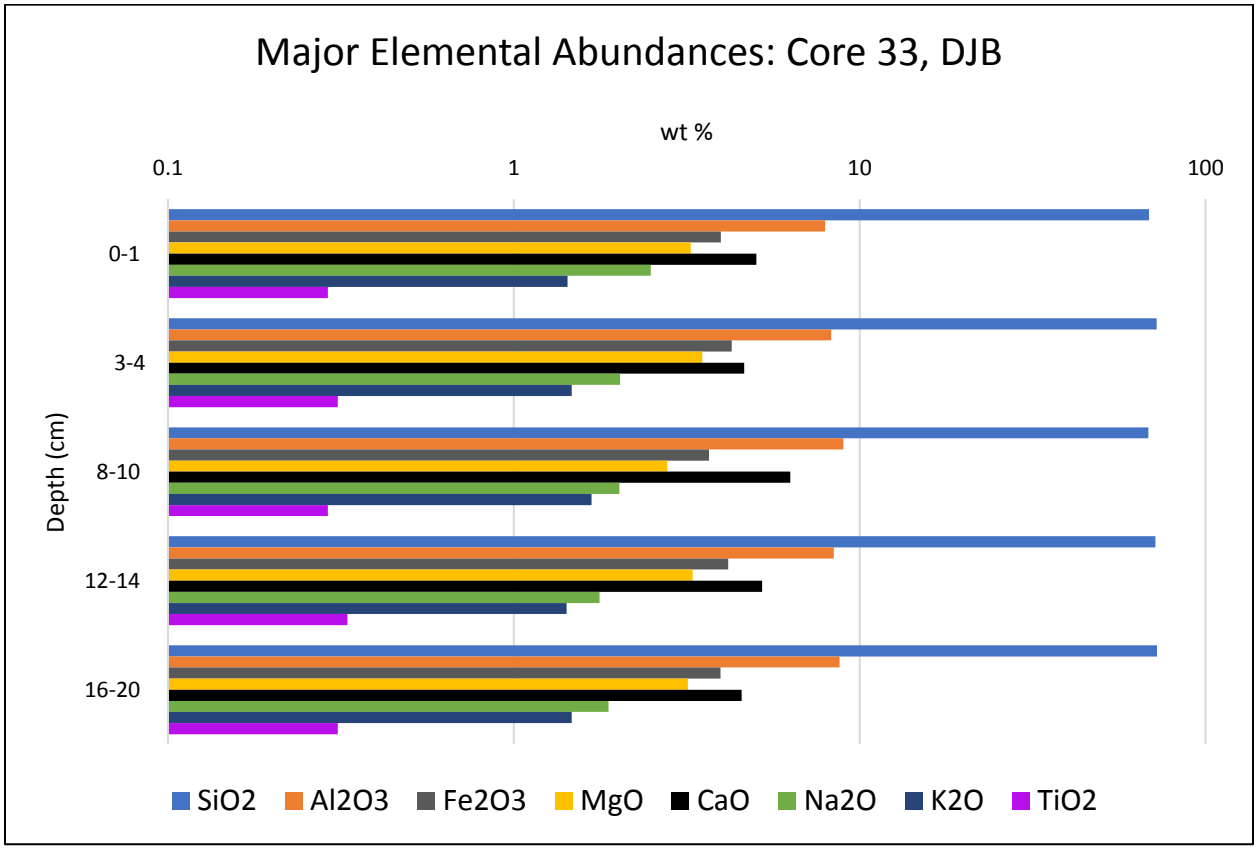

Figure 19. Major element distribution, Core 33, Don Juan Basin.

Major elemental analysis at Core 33 shows little variation in abundance throughout the soil profile. Na and K, however, are enriched compared to Core 2074, suggesting there is still source rock remaining. Th and Ba enrichment compared to Core 2074 supports this theory and strongly suggests chemical alteration is occurring to a lesser degree than at Core 2074. The highest abundances of major elements and oxides are seen between 4-10 cm. K/Th values range from 0.56 (JB1133, 16-20 cm) to 0.86 (JB1132, 12-14 cm). JB1133 and JB1130 (0.67, 3-4 cm) are below and inside the range of K/Th values (0.61-0.67) in Core 2074. This could suggest enhanced alteration at these depths in Core 33.

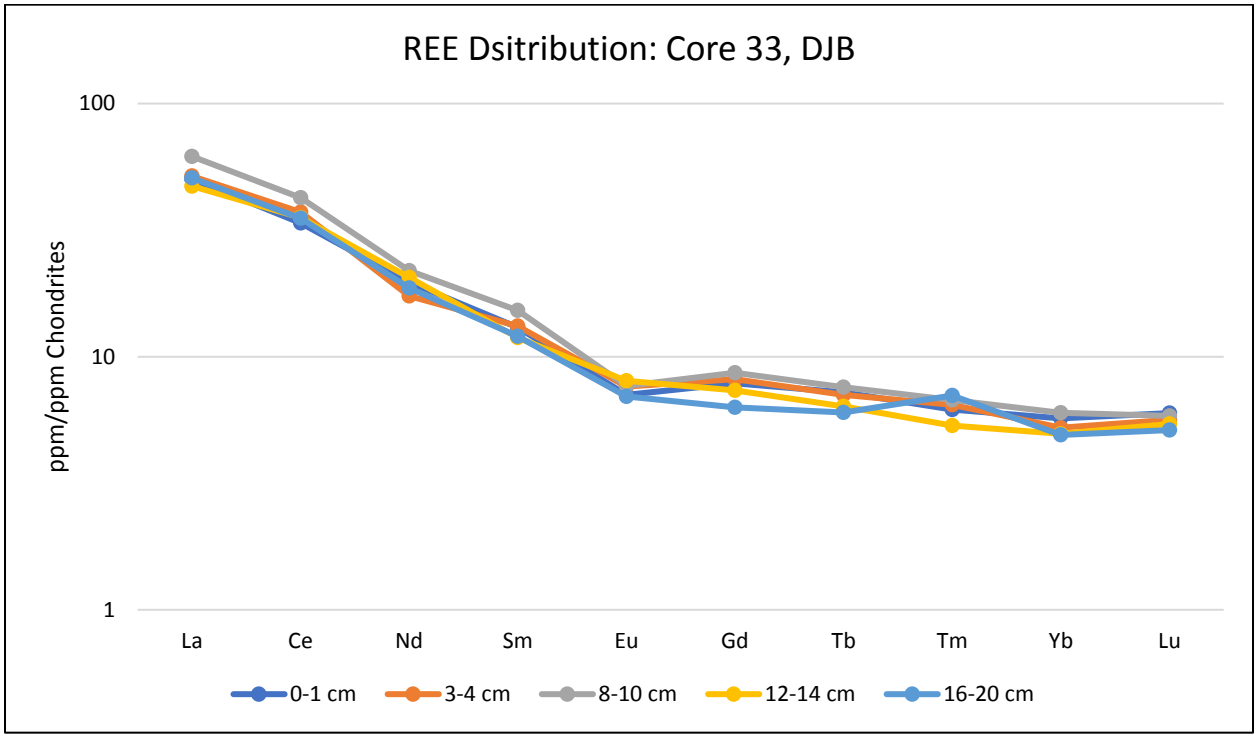

Figure 20. Rare Earth Element distribution, Core 33, Don Juan Basin.

Rare Earth Element analysis shows a pattern similar to that of other samples but with different abundances. A negative Eu anomaly is exhibited in all samples except for JB1132 (12-14 cm), and a positive Tm anomaly is exhibited in JB1133 (16-20 cm). A negative Eu anomaly is typically associated with CaO and Na_2O depletion, occasionally

as a result of plagioclase weathering (Nyakairu, Koeberl, 2001). REE abundance is highest between 3-4 and 8-10 cm. This is also seen in the major elements. Based on abundance of major and trace (REE included) elements, physical alteration is favored throughout the core, with chemical alteration possibly occurring in the 4-10 cm range.

2.4.2.2. Mineralogy: XRD, Spectra

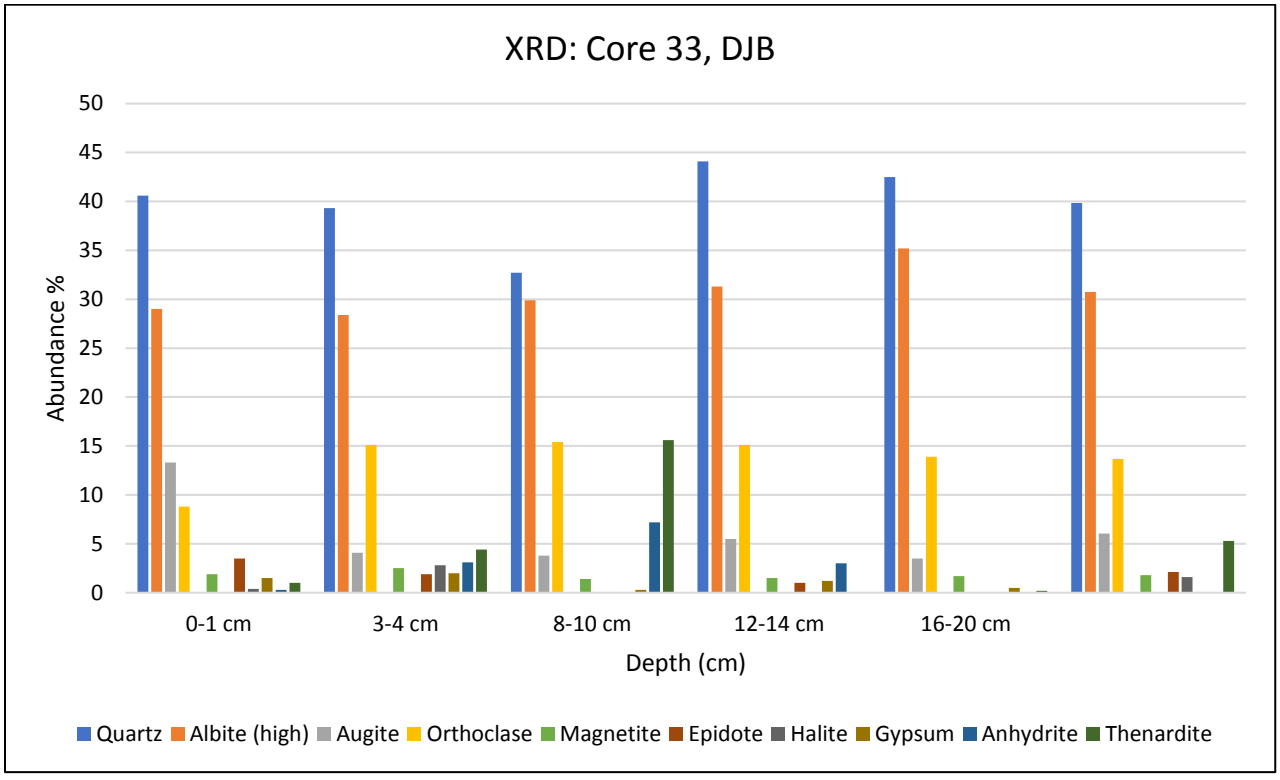

Figure 21. Mineralogical analysis of Core 33, Don Juan Basin.

XRD analysis of Core 33 shows relatively consistent abundances of quartz and albite in all but the 3-10 cm depth range. This range, notably, exhibits the highest total salts: 14.2 % in JB1130 (3-4 cm) and 23.1 % in JB1130 (8-10 cm), corroborating the observation by Gibson, 1980. JB1130 exhibits the highest abundances of halite (2.8 %), the second highest abundance of thenardite (4.4 %) and anhydrite (3.1 %), the lowest abundances of albite (28.4 %) and the second lowest abundance of quartz (39.3 %). JB1131 exhibits the highest abundance of thenardite (15.6 %) and anhydrite (7.2 %), the lowest abundance of quartz (32.7 %) and the second lowest abundance of albite (29.9 %). The albite and quartz depletions in JB1130 and JB1131 are paralleled by the two highest abundances of orthoclase (15.1 and 15.4 %) in the soil profile. The relative depletions in quartz and albite could simply be due to salt enrichment and dilution, changing ratios of the bulk sample, however, relative REE enrichment in JB1131 could suggest active alteration is occurring.

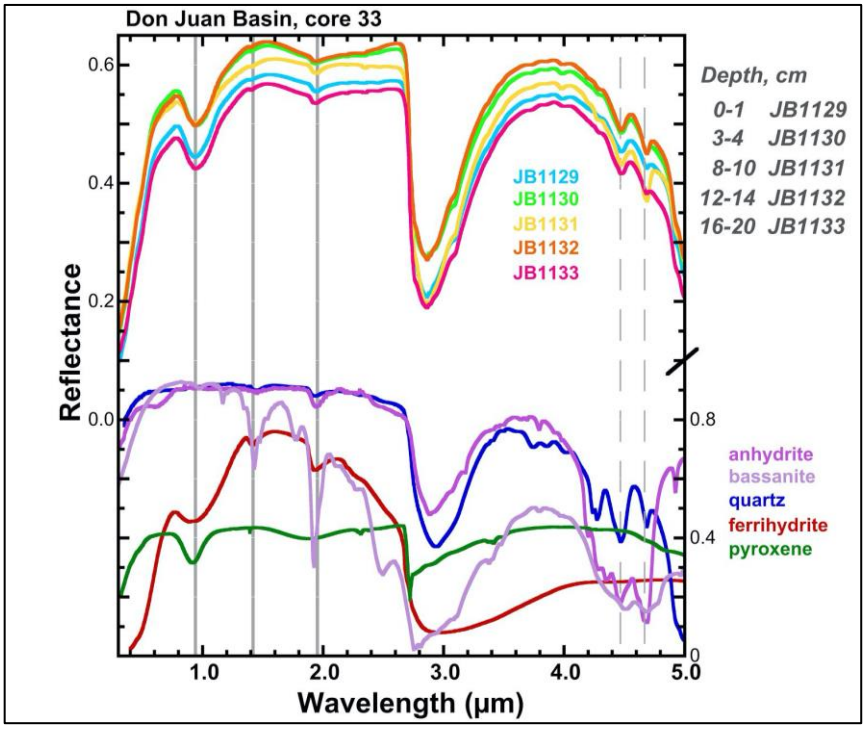

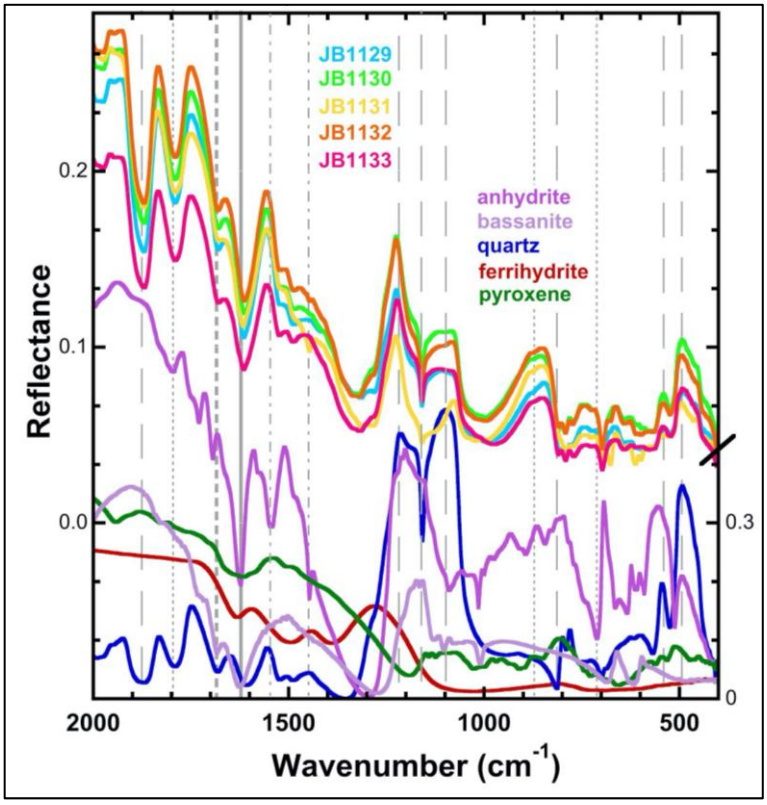

Figure 22. Spectral analyses of Core 33, Don Juan Basin

Spectral analysis (e.g. Lane and Bishop, 2019; Bishop, 2019) of Core 33 shows a strong band near 2.9-3.0 µm due to bound water, Si-O stretching vibrations near 1090 and 1215 cm^{-} (~8.3 and 9.2 µm) due to quartz as well as overtones and combinations near 4-5 µm due to quartz, and broad Fe bands near 1 and 2 µm due to pyroxene. Weak bands near 1.39, 1.93, and 2.19 µm are attributed to poorly crystalline aluminosilicates similar to allophane. Additional weak bands near 2.35 and 2.45 µm are due to OH bands in mica (e.g. biotite) or actinolites (e.g. tremolite) that are likely part of the primary material, as discussed in Bishop et al. (2013) for other MDV sediments. Minor amounts of poorly crystalline ferric oxide-bearing components (e.g. ferrihydrite) are also present in the upper layers, which might account for deeper water bands and shifts in the ~1 µm band towards lower wavelengths.

2.4.2.3. Special Analyses: Anions, CIA

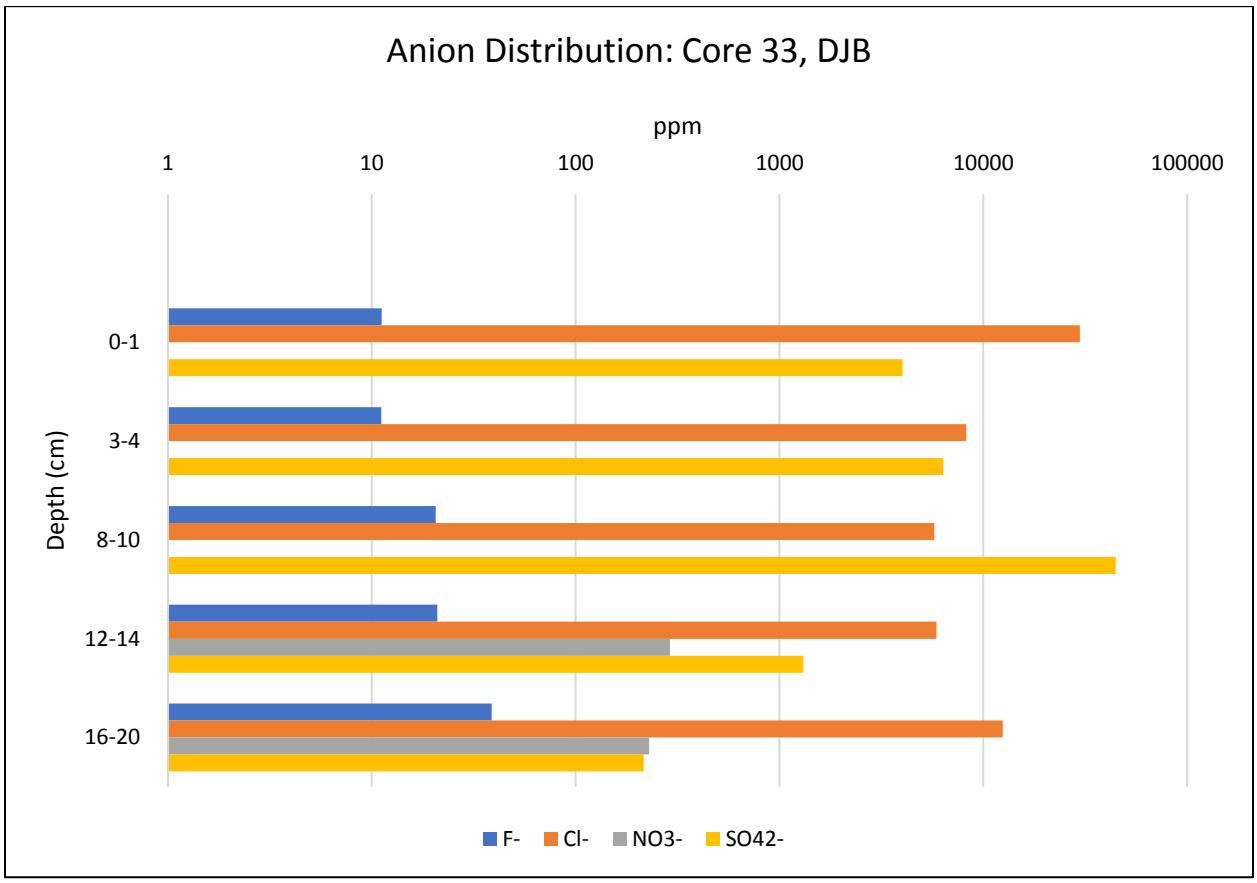

Figure 23. Soluble anions of Core 33, Don Juan Basin.

Soluble anion distribution in Core 33 shows an increase in F^- with depth, and an increase in SO_4^{2-} with depth until 10 cm. The SO_4^{2-} enrichment (44.5 x 10^3 ppm) in JB1131 (8-10 cm) is corroborated by the highest reported anhydrite in the soil profile. Based on XRD, spectral, and anion analyses, gypsum is likely not present. Not enough data exists on NO_3^-, and Cl^- is too variable to draw firm conclusions as to the cause of their distribution in Core 33.

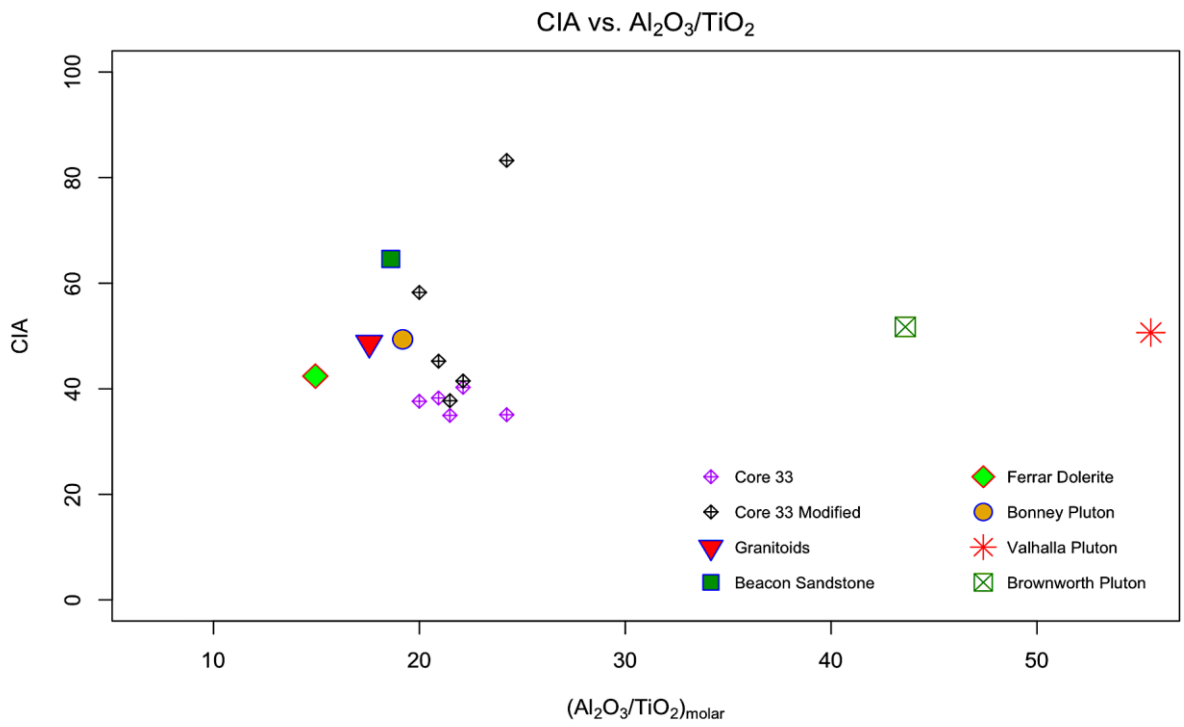

Figure 24. Core 33 unmodified and modified CIA values and regional source rock CIA values

The Chemical Index of Alteration values at Core 33 range from 34-40, in the range of fresh basalts (Nesbitt and Young, 1982) and in line with regional geology (Peterson and Marsh, 2008). The lowest CIA value, 34, corresponds to JB1129 (0-1 cm) and the highest value, 40, corresponds to JB1133 (16-20 cm). JB1129 (0-1 cm) exhibits relative Na_2O enrichment which could be due to the solution responsible for the "wet" encrustation effectively lowering the CIA by dilution. NaCl surface salts could be reducing the CIA, too, through a similar dilution process. The two highest CIA values (38 and 40) belong to the two samples (JB1130 and JB1133) that are most depleted in CaO, which is likely due to depletion in Ca-sulfates relative to other Core 33 samples.

Analysis of modified CIA values at Core 33, to account for dilution by salt, shows significant variation in 3 of 5 samples. JB1131 (8-10 cm) shows the greatest modification, 35 → 83, due to its highest reported total salts (primarily thenardite and anhydrite). JB1132 (12-14 cm) shows the next highest modification, 37 → 58, reporting

low total salts which is likely an inaccurate measurement. Lastly, JB1130 (3-4 cm) reports a significant modification, 38 → 45, likely due to its relatively high total salts. Separately, JB1129 (0-1 cm), the surface sample, reports a very slight modification, 35 → 38, likely due to its minor abundance of sulfates. The range of modified CIA values is 38 – 83, in the range of granodiorites to potassic granites (Fedo et al., 1995). This is supported by regional and local geology.

Based on information discussed, the most likely picture for Core 33 is one dominated by physical alteration in the surface sample and bottom sample, likely manifesting as sediment mixing and freeze-thaw processes. Because the surface sample reports a minor abundance of gypsum, chemical alteration is likely operating at a very low level and under particular conditions, possibly when the reported “wet encrustation” is most intense. Chemical alteration is likely operating between 4 and 12-14 cm, manifesting as a sulfate layer, in the 4-8 cm depth range (JB1130 and JB1131), that tapers off to JB1132 (12-14 cm).

2.4.3. Core 39

Core 39 is situated approximately 120 m SW of core 33 near the base of an alluvial fan and outside of the path of "wet" encrustation (Figure 4). The core has five samples ranging from surface to 16 cm depth.

2.4.3.1. Elements: Major, Minor, and Rare Earth

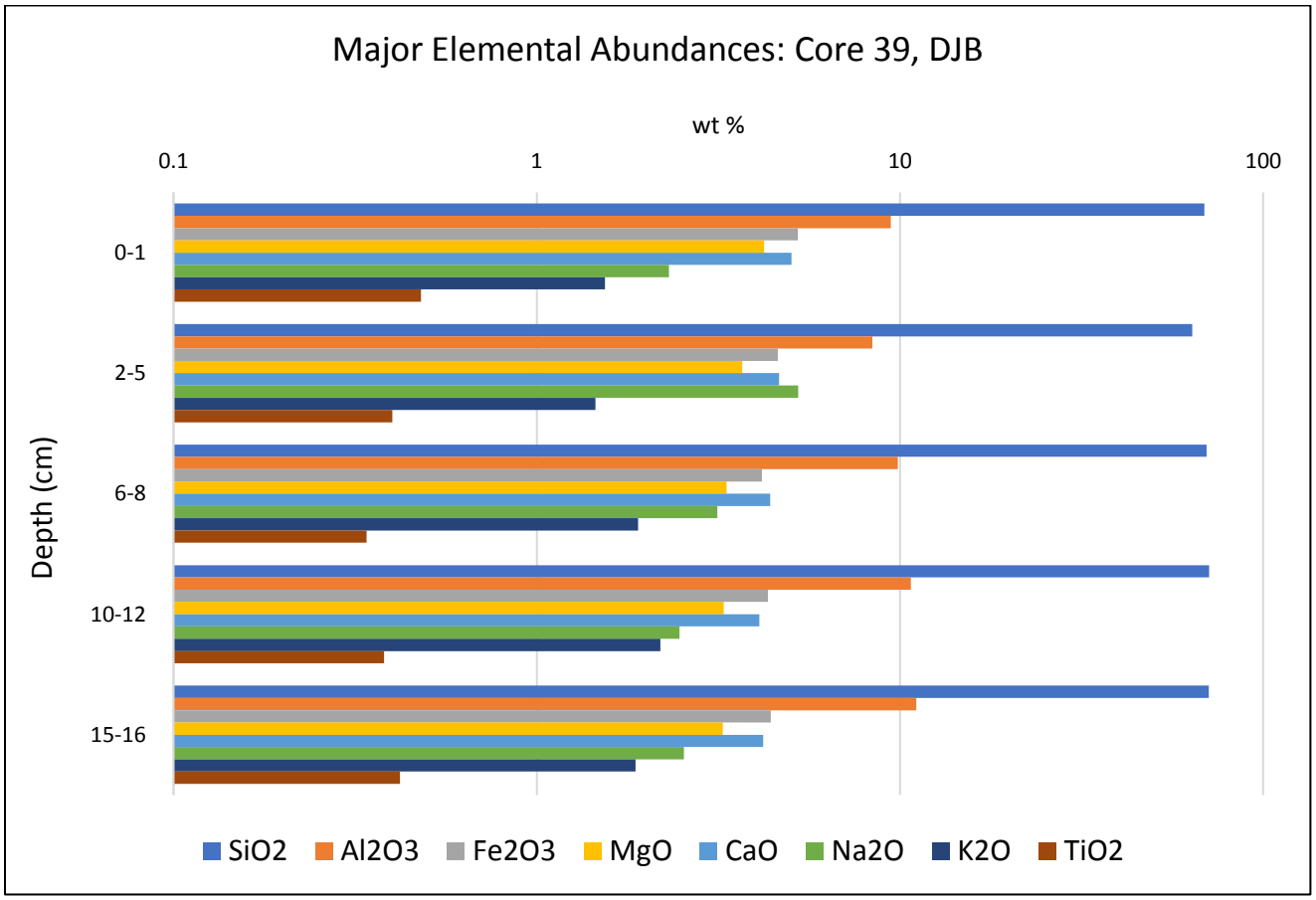

Figure 25. Major element distribution, Core 39, Don Juan Basin.

Major elemental analysis of Core 39 shows relative enrichment in major ions Na and K as compared to Core 2074, suggesting more source rock in the sediments, and a lesser degree of alteration. There is little variation in oxide abundance throughout the soil profile. Anomalous cases are seen in the first two samples, to a depth of 5 cm. Relative

CaO enrichment (5.03 %) in JB1134 (top 1 cm), and Na_2O enrichment (5.25 %) in JB1135 (2-5 cm) are the only notable differences from the other sample abundances. K/Th values range from 0.82 (JB1134, top 1 cm) to 0.86 (JB1138, 15-16 cm), significantly above the range of values (0.61-0.67) in Core 2074. This could suggest a lower degree of alteration in Core 39, as could the limited variation across samples. Core 39 has the second highest U/Th, K/Th, and Al/Ti ratio of the samples, suggesting that is has experienced a lower degree of chemical alteration than core 2074 but higher than Core 33. Core 39 is not in the path of any liquid water, though, and is therefore a likely candidate for sediment mixing between multiple sources.

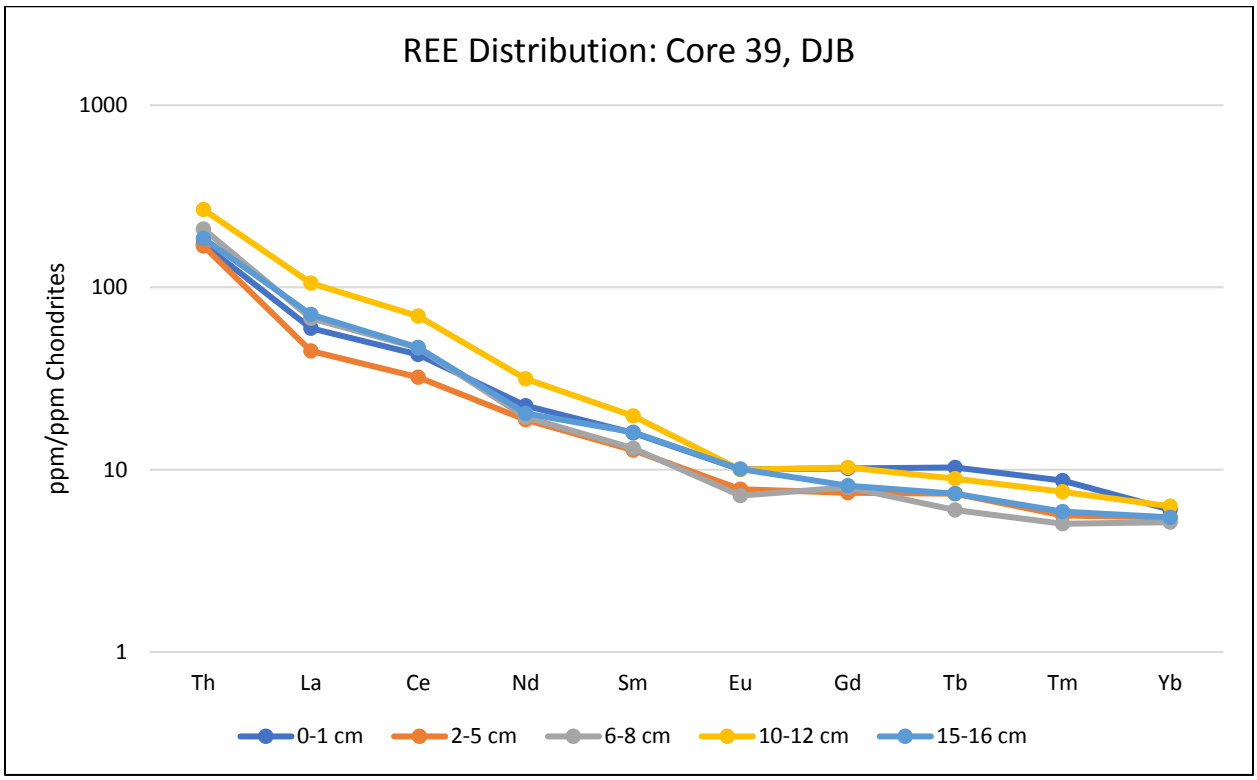

Figure 26. Rare Earth Element distribution, Core 39, Don Juan Basin.

Rare Earth Element analysis shows significant variation across samples. JB1135 (2-5 cm) exhibits the lowest values and JB1137 (10-12 cm) the highest. La ranges from 44-105

ppm/ppm chondrite; Ce from 32-69 ppm/ppm chondrite; and Nd ranges from 18-31 ppm/ppm chondrite. Abundances in these elements increase steadily from JB1135 (2-5 cm), through JB1136 (6-8 cm), peaking at JB1137 (10-12 cm), and decreasing in JB1138 (15-16 cm). JB1135 (2-5 cm) and JB1136 (6-8 cm), however, show relative depletions in nearly all elements, particularly Sm, Eu, and Gd. Sediment mixing in the alluvial fan, near Core 39, could be the reason for the chemical inconsistencies in the top 8-10 cm. Conversely, continuous cycling of REEs from a leaching zone near the surface to deeper parts of soil profiles could create an enriched REE reservoir in the subsurface (Nesbitt and Markovics, 1997). JB1137 (10-12 cm), a sample heavily enriched in REEs, could bolster the case for such a process. This would then suggest that chemical alteration is occurring near the surface and is cycling REEs downwards to depths where physical alteration dominates.

2.4.3.2. Mineralogy: XRD, Spectra

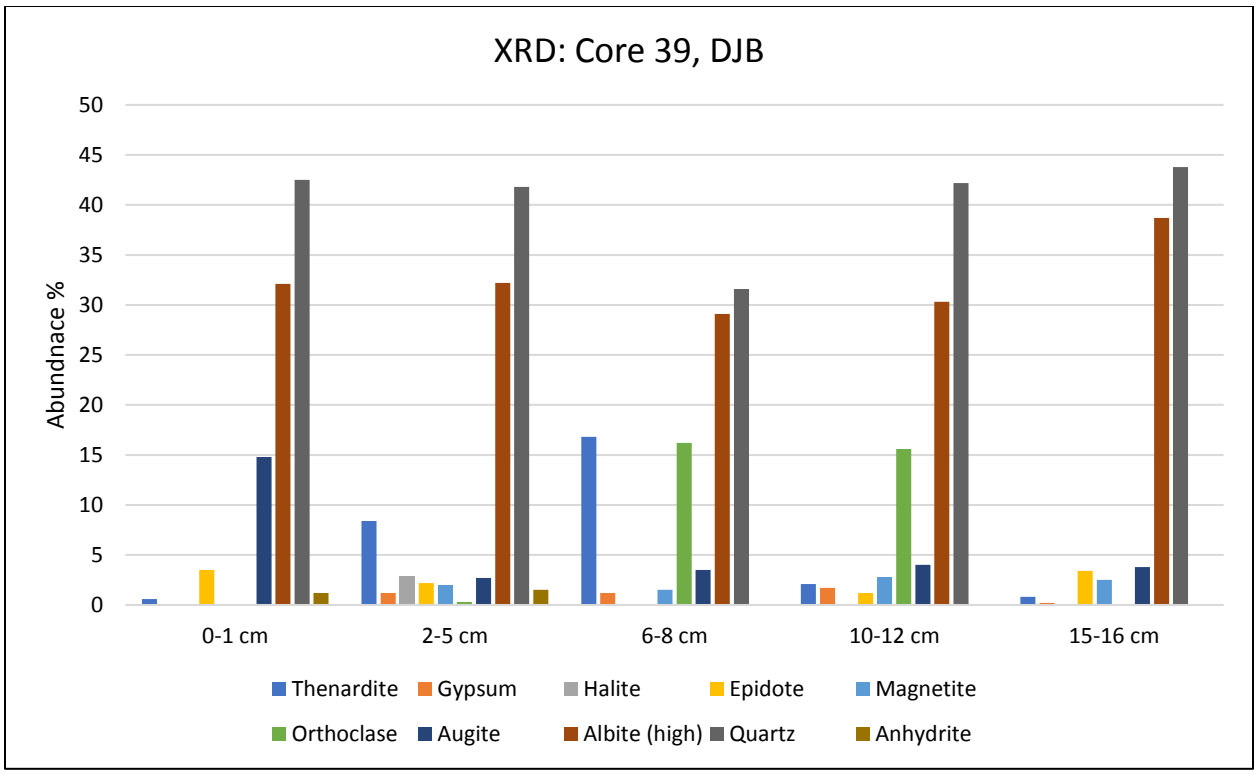

Figure 27. Mineralogical analysis of Core 39, Don Juan Basin.

XRD analysis of Core 39 shows the greatest abundance of total salts between samples JB1135 (2-5 cm) and JB1136 (6-8 cm) with values of 16.2 % and 18 %, corroborating the hypothesis of a salt layer in this depth range made by Gibson (1980). Thenardite is the dominant salt in these two samples (8.4 % and 16.8 %). The highest abundance of epidote (3.5 %) is found in the surface sample, JB1134 (top 1 cm), closely followed by the deepest sample taken (JB1138, 15-16 cm) with 3.4 %. The highest abundance of gypsum (1.7 %) is recorded in JB1137 (10-12 cm), and JB1135 (2-5 cm) reports the highest abundance of anhydrite (1.5 %) and halite (2.9 %). Quartz exhibits relative depletions in JB1135 (2-5 cm) and JB1136 (6-8 cm), likely due to a dilution effect from the high salt content. Quartz abundance is consistent in all other samples. Albite is enriched (42 %) in JB1138 (15-16 cm), augite is enriched (14.8 %) in JB1134 (top 1 cm),

and orthoclase is enriched (16.2 % and 15.6 %) in JB1136 (6-8 cm) and JB1137 (10-12 cm). JB1135 (2-5 cm) and JB1136 (6-8 cm) exhibit the two highest Na_2O values (5.25 % and 3.14 %) which corroborate the highest abundances of thenardite in the soil profile. JB1134 (top 1 cm) exhibits the highest CaO value (5.03 %), corroborating the highest abundance of epidote.

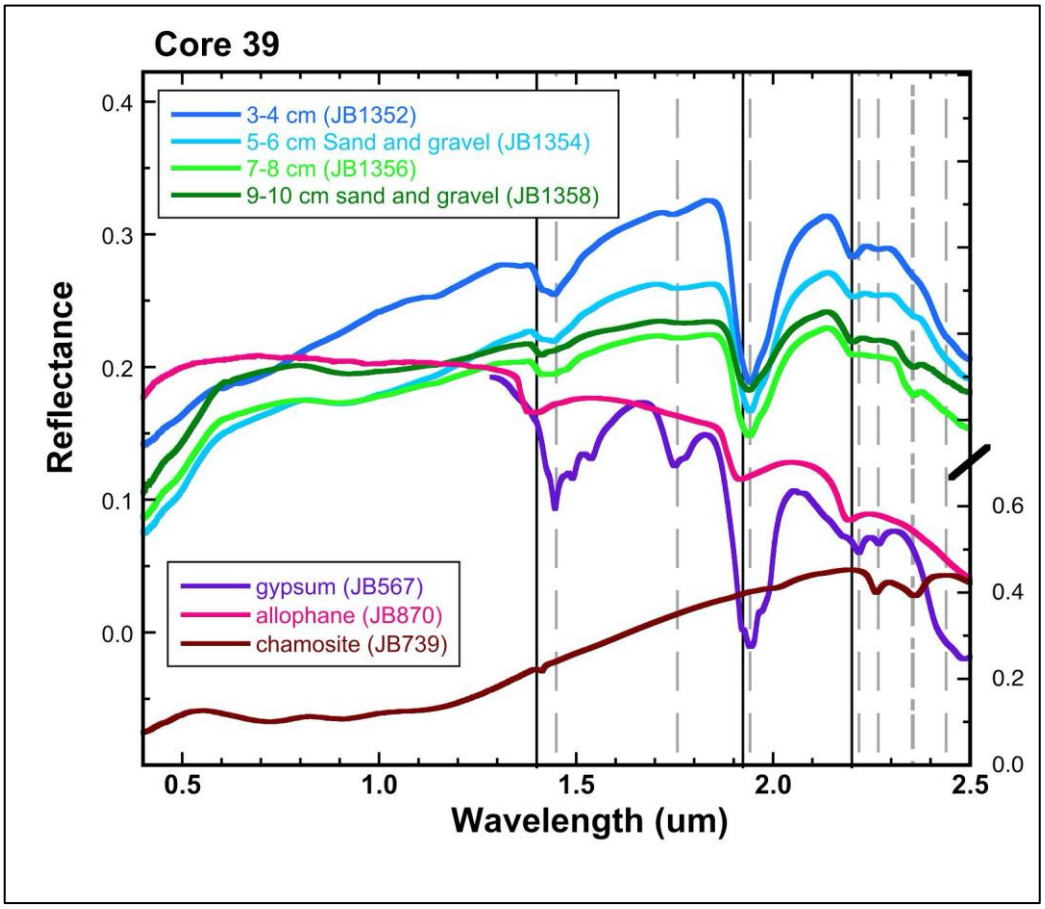

Figure 28. Spectral analysis of Core 39, Don Juan Basin.

Spectral analysis for Core 39 (Patel at al., 2015) was conducted on different samples (JB1352-1358) than those discussed above (JB1134-1138); however, the mineralogy is likely similar. The primary minerals exhibited are quartz, feldspar, and pyroxene. Spectral bands characteristic of gypsum near 1.45, 1.76, 1.94, 2.22, and 2.26 µm

(Bishop, 2019) and are strongest in the upper sediments (3-4 cm and 5-6 cm). Bands near 1.39, 1.93, and 2.19 µm are attributed to poorly crystallized aluminosilicates similar to allophane and are strongest in the lower sediments. The presence of allophane instead of crystalline clay minerals indicates limited soil maturity (Patel et al., 2015). Core 42, at VXE-6 Pond, also displays allophane in approximately the same depth range, and chemical alteration was concluded to be the cause. An additional band near 2.36 µm is due to an OH combination band in chlorite that is most consistent with Fe-rich chamosite (Bishop, 2019) that is a high-temperature phyllosilicate and likely part of the primary material, rather than an alteration phase. Spectral features due to quartz and feldspar are not detected in this spectral region but these minerals are detected by XRD.

2.4.3.3. Special Analyses: Anions, CIA

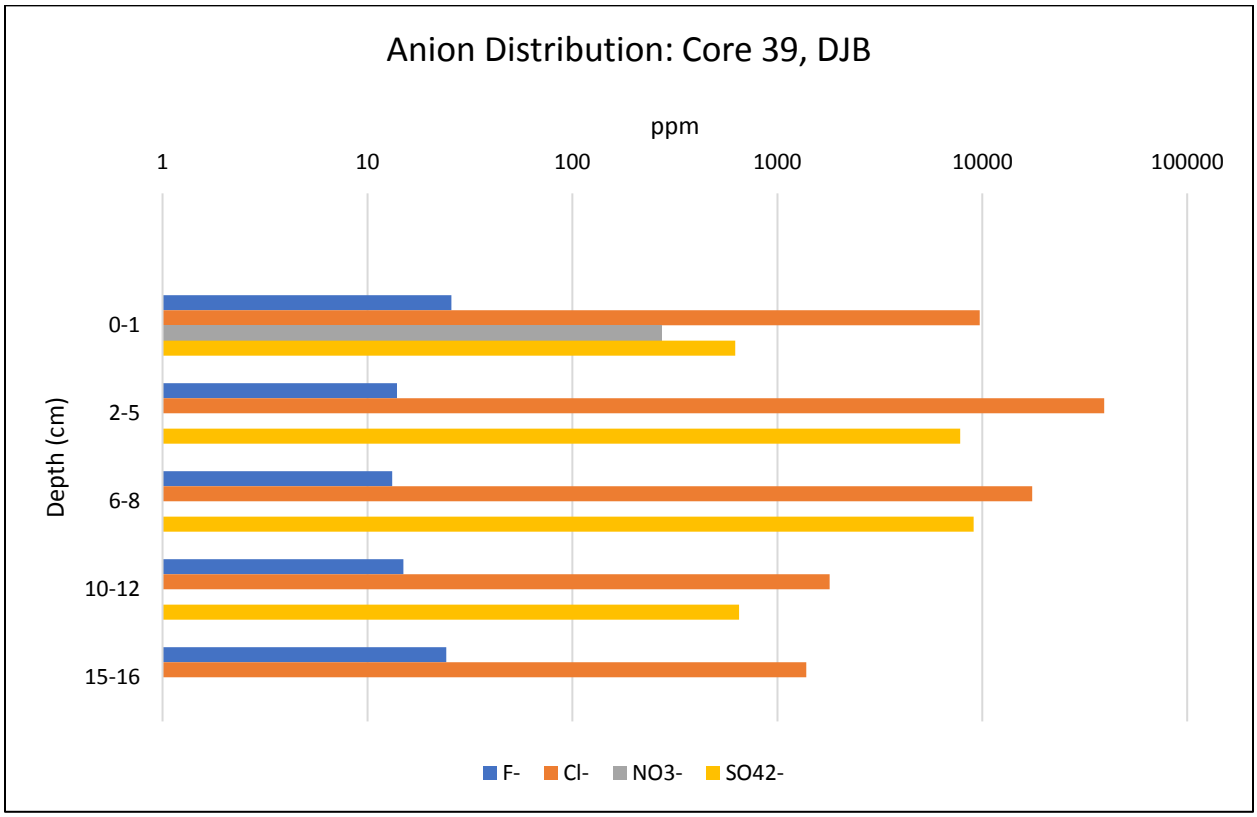

Figure 29. Soluble anion distribution of core 39, Don Juan Basin.

Soluble anion distribution throughout Core 39 shows peaks in Cl^- and in the 5-8 cm depth range that correlate with observations by Patel et al., 2015 of clay and sulfate mineralogy. Burton et al (2019) and Foerder et al. (2020) note major and trace (REEs included) element enrichment in Core 42 of VXB, paired with mineralogically diagnostic spectra, and suggest a chemically altered clay-rich layer. Major and trace element enrichment is seen in JB1137 (10-12 cm) of Core 39 along with spectra diagnostic of a clay-rich layer similar to that of Core 42. JB1138 (15-16 cm) shows a drastic depletion in REE abundance in comparison to JB1137 (10-12 cm) just above it, suggesting the clay-rich layer to be closer to JB1136 (6-8 cm) than to JB1138 (15-16 cm). This hypothesis would also corroborate mineralogical observations made in the 5-8 cm range. NO_3^- data is too limited, and F^- shows no significant variations to draw any conclusions on their abundance patterns.

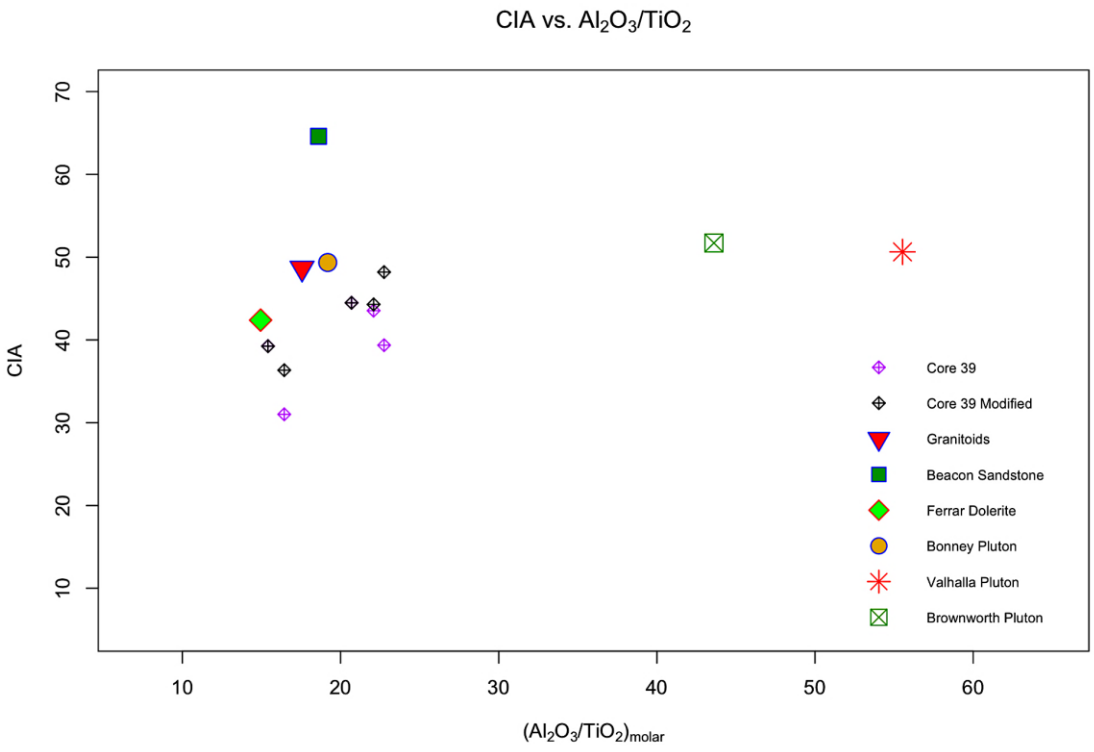

Figure 30. Core 39 unmodified and modified CIA values and regional source rock CIA values.

The Chemical Index of Alteration at Core 39 ranges from 31-44, in the range of fresh basalts (Nesbitt and Young, 1982; Fedo et al., 1995) and in line with regional geology

(Peterson and Marsh, 2008). The lowest value, 31, corresponds to JB1135 (2-5 cm) and the highest value, 44, corresponds to JB1138 (15-16 cm). A noteworthy drop in CIA value—from 39 to 31—from JB1134 to JB1135 (1 to 5 cm depth) is likely due to a Na_2O enrichment in JB1135 that could in turn be due to sediment mixing.

Analysis of modified CIA values at Core 39, to account for dilution by salt, shows slight modification. Terra XRD analysis shows that all samples exhibit relatively low abundances of gypsum and/or anhydrite, two minerals responsible for the skewed CIAs at other microenvironments, but it is thenardite enrichment in JB1135 and JB1136 that yields the greatest, though relatively insignificant, modification: 31 → 36 and 39 → 48. The range of modified CIA values is 39 – 48, in the range of fresh basalts and fresh granites and granodiorites (Nesbitt and Young, 1982; Fedo et al., 1995).

Based on information discussed, the most likely picture for Core 39 is physical alteration at the surface, manifesting as sediment mixing, with chemical alteration operating most notably in the depth range of 5-8 cm, which manifests as a layer of primarily thenardite, and secondarily gypsum, as well as allophane, a clay. Gypsum is shown to extend to JB1137 (10-12 cm) but in a much lesser abundance than JB1135 (2-5 cm) and JB1136 (6-8 cm). A layer of relative REE enrichment in JB1137 (10-12 cm) supports chemical alteration higher in the soil profile that is cycling REEs downwards from the zone of leaching (Nesbitt and Markovics, 1997). Physical alteration, likely manifesting as freeze-thaw processes, looks to resume dominance in JB1138 (15-16 cm).

2.4.4. CORE 35

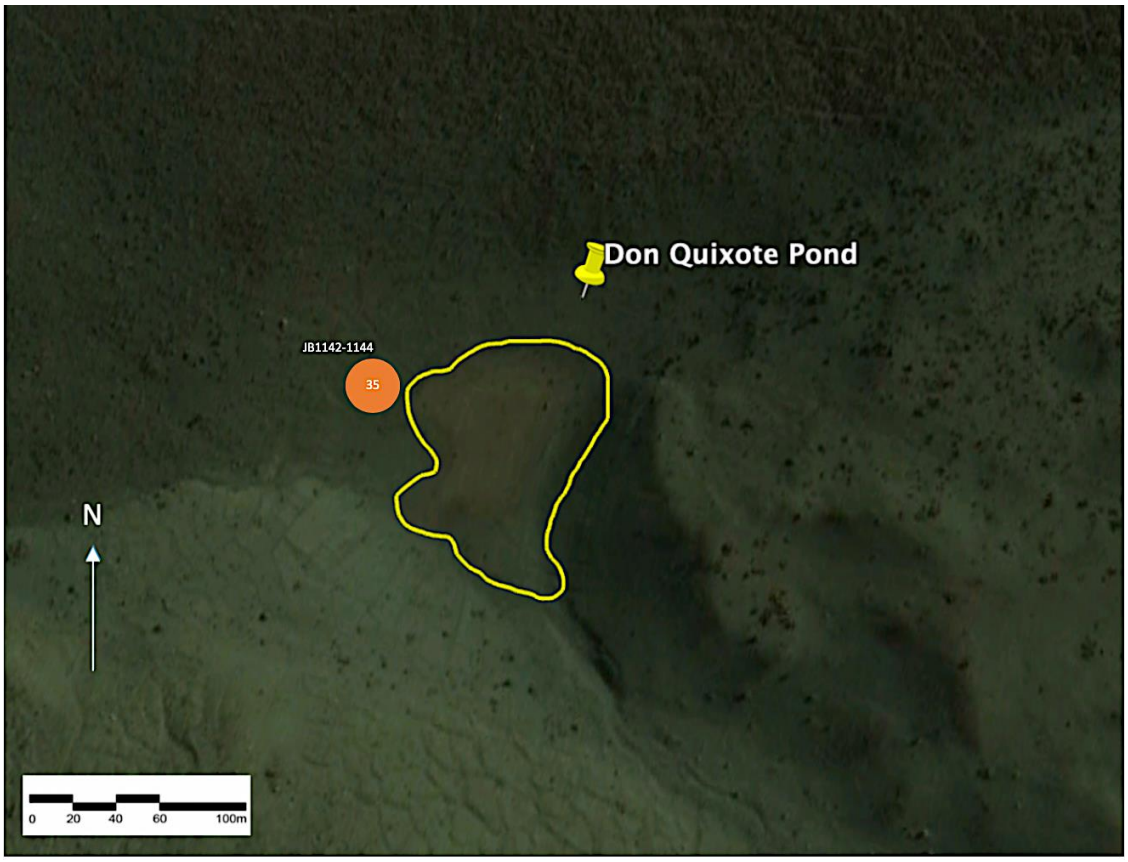

Figure 31. Core 35 sample site, Don Quixote Basin.

Don Quixote Basin is just north of Don Juan Basin and the Dais Plateau, in the western end of Upper Wright Valley. The basin contains Don Quixote Pond and the microenvironment of interest, Core 35, sitting at approximately 100 m above mean aeawater level, surrounded by valley walls up to 2500 m high. The formation of DQP serves as a unique representation of terrestrial weathering, accumulation, and distribution of calcium, chlorine, and sulfate (Harris and Cartwright, 1981; Torii and Yamagata, 1981). Its brine is seasonally frozen (Harris and Cartwright, 1981). In the field season of 1979-1980, E.K. Gibson collected samples from the surface and as depth

profiles (Gibson et al., 1983). Two additional cores, 20 and 41, were taken near DQP and are discussed by Englert et al., 2017.

2.4.4.1. Elements: Rare Earth

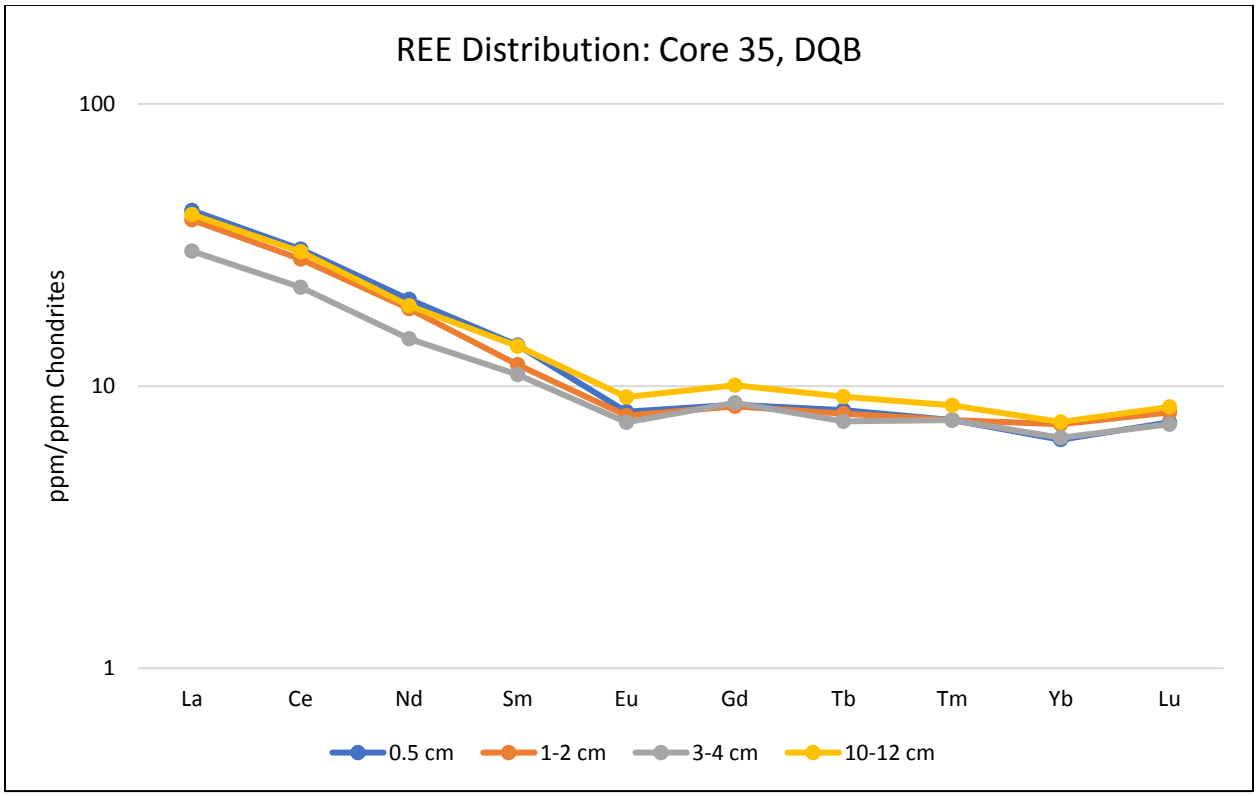

Figure 32. Rare Earth Element distribution, Core 35, Don Quixote Basin.

Rare Earth Element patterns (Figure 32) in Core 35 are similar to those of other cores (Figure 14), but differ in abundance, showing general depletion in all REEs as compared to other cores, except for Core 2074. Little is noteworthy about the core, except for the consistent negative Eu anomaly in all samples. Per Koeberl and Nyakairu (2001), negative Eu anomalies are associated with depletion in Na and Ca which is seen at Core 35, particularly in JB1143 - JB1144 (1-4 cm). Major elemental analysis is pending.

2.4.4.2 Mineralogy: XRD, Spectra

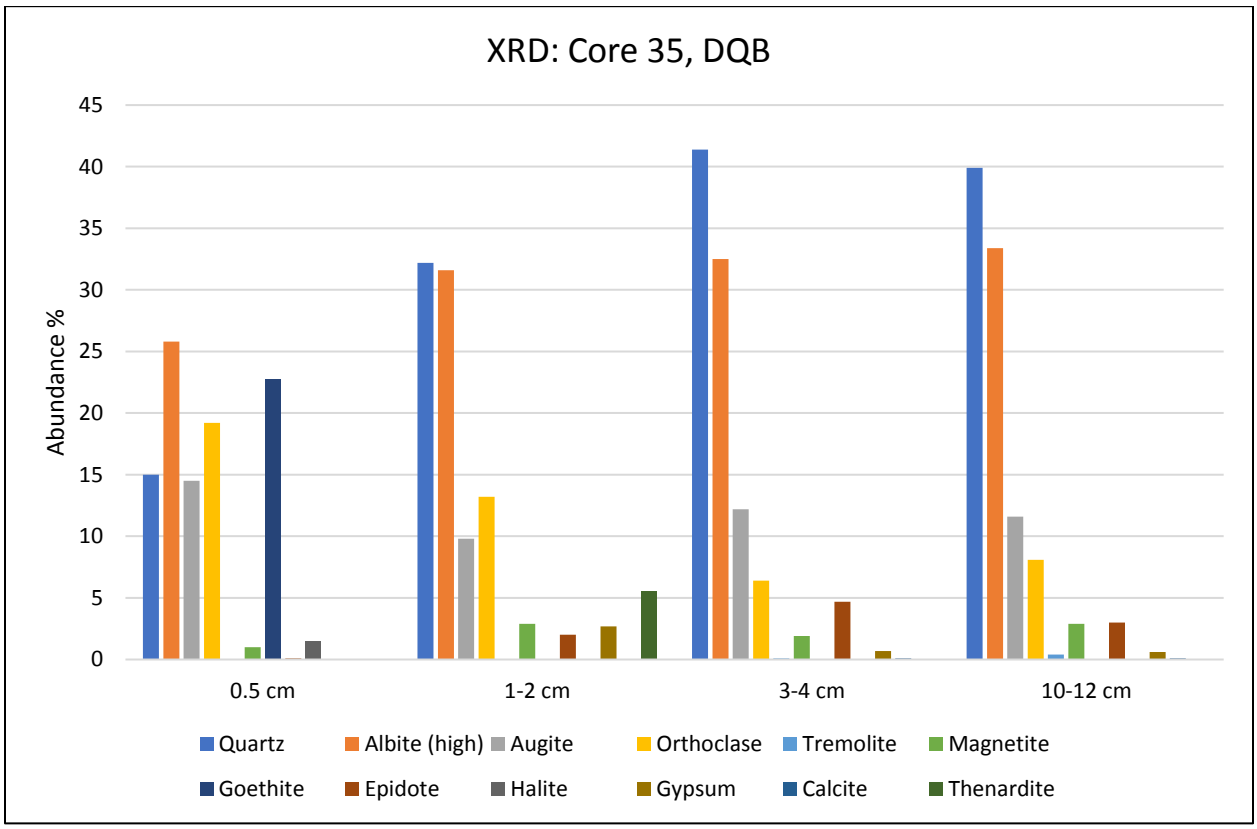

Figure 33. Mineralogical analysis of Core 35, Don Quixote Basin.

Compared to other microenvironments, XRD analysis of Core 35 sediments shows heavy quartz depletion (15 %) and moderate depletion of albite (25.8 %) in JB1142 (surface sample). JB1142 shows relative enrichments in augite (14.5 %) and orthoclase (19.2 %) while the opposite is seen in all other samples. JB1142 (top 0.5 cm) is the only sample with halite recorded (1.5 %). JJB1143 (1-2 cm) exhibits the highest abundance of gypsum (2.7 %), thenardite (5.6 %), and total salts (8.6 %). Anhydrite exists in most samples but in trace (< 0.4 %) abundances.

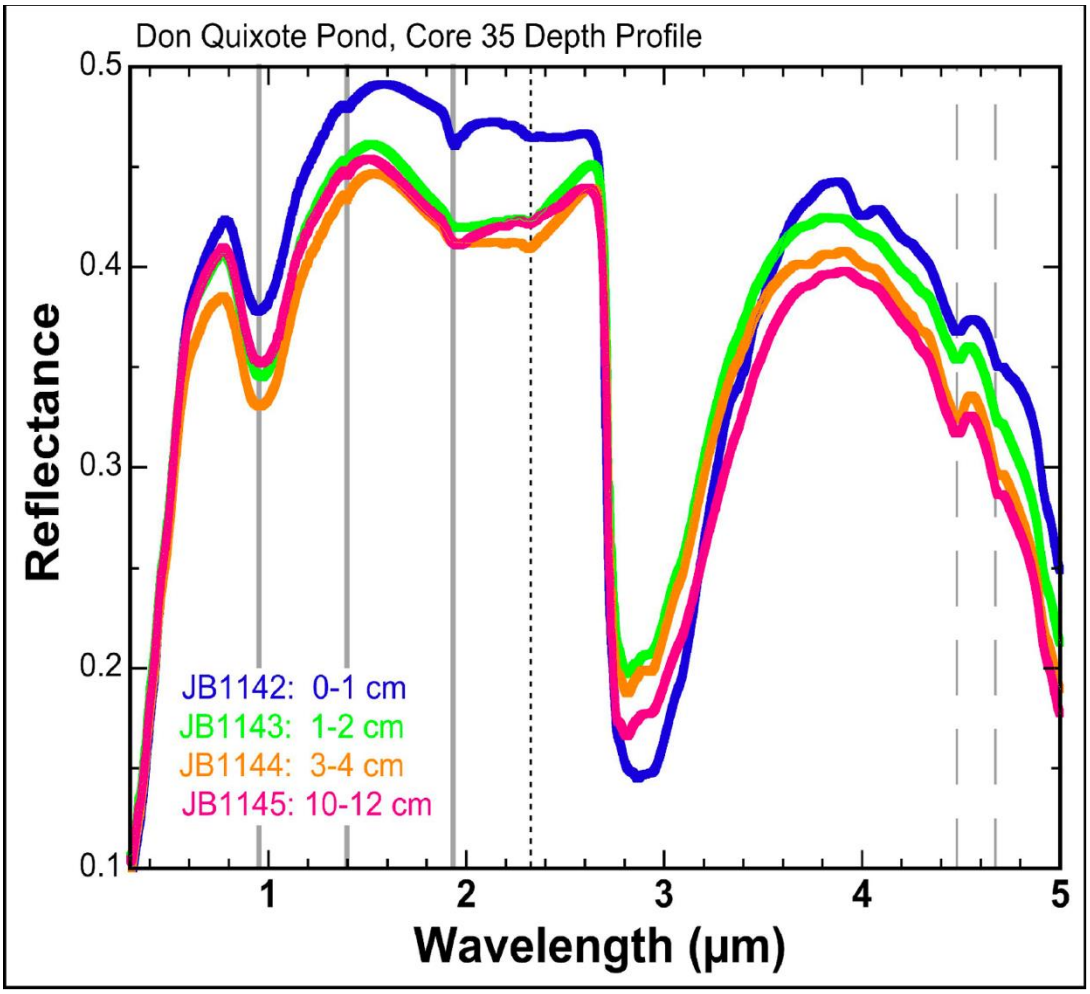

Figure 34. Spectral analysis of Core 35, Don Quixote Basin.

Spectra from soils near Core 35, Don Quixote Pond, show the presence of gypsum, calcite, and Al-rich phyllosilicates. Mineralogical differences vary with depth, including variations in abundances of quartz, pyroxene, and hydrated components. Dashed lines near 4.5 and 4.7 μm denote anhydrite bands, and the line at 0.98 μm is due to Fe^{2+} pyroxene. At 1.4, 1.9, and 2.35 μm, weak bands are consistent with Fe/Mg-phyllosilicates (Englert et al., 2013).

Based on available analyses, Core 35 at Don Quixote Pond is likely dominated by chemical alteration. Salts, primarily Ca and Na-sulfates, present in all samples support

this conclusion, with enrichment occurring in the 1-2 cm depth range. Physical alteration is likely operating on a secondary scale.

2.4.5. CORE 42

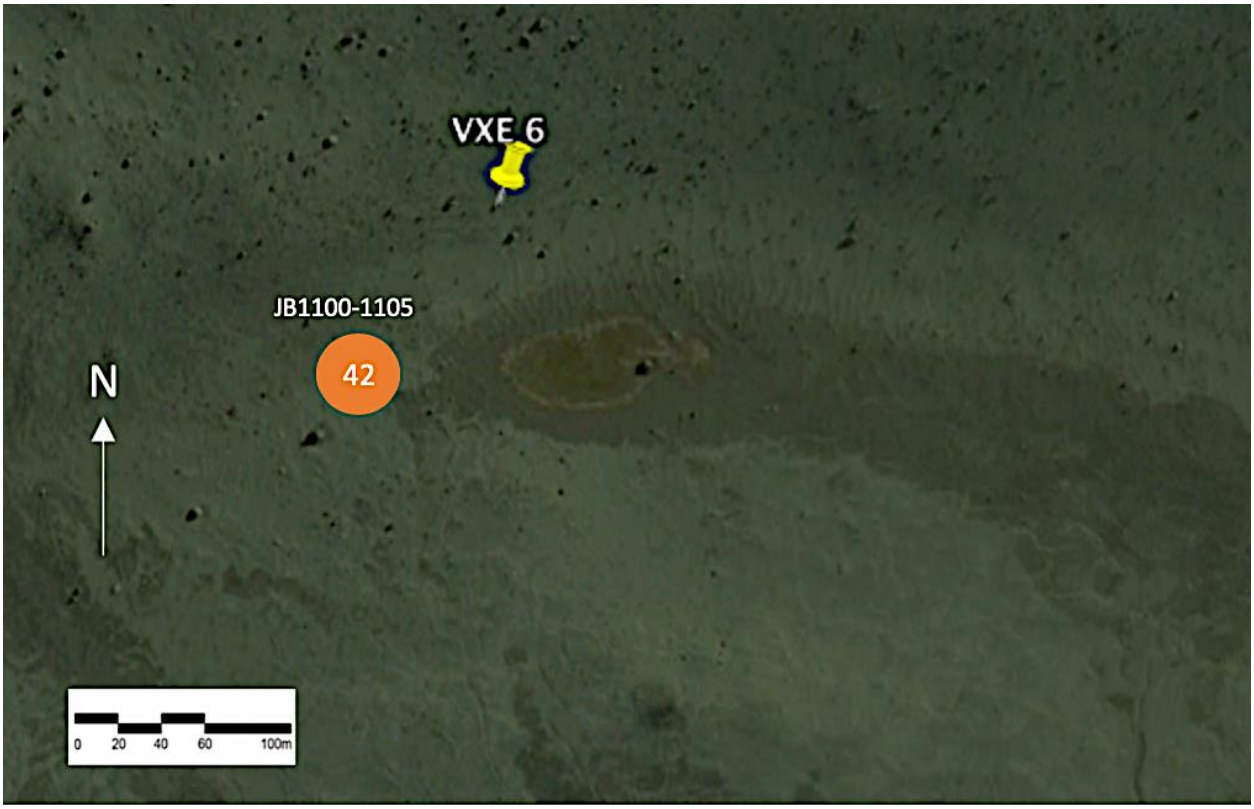

Figure 35. Core 42 sample site, VXE-6 Basin.

VXE-6 Basin is located approximately 2 km to the east of Don Juan Pond. Within VXE-6 Basin, the microenvironment of interest is Core 42 which was taken approximately 15 m to the west of VXE-6 Pond. The pond is found at the center and topographically lowest point in VXB which is separated from DJB by a low divide. It is fed by glacial meltwaters (Harris, 1981).

2.4.5.1. Elements: Major, Minor, and Rare Earth

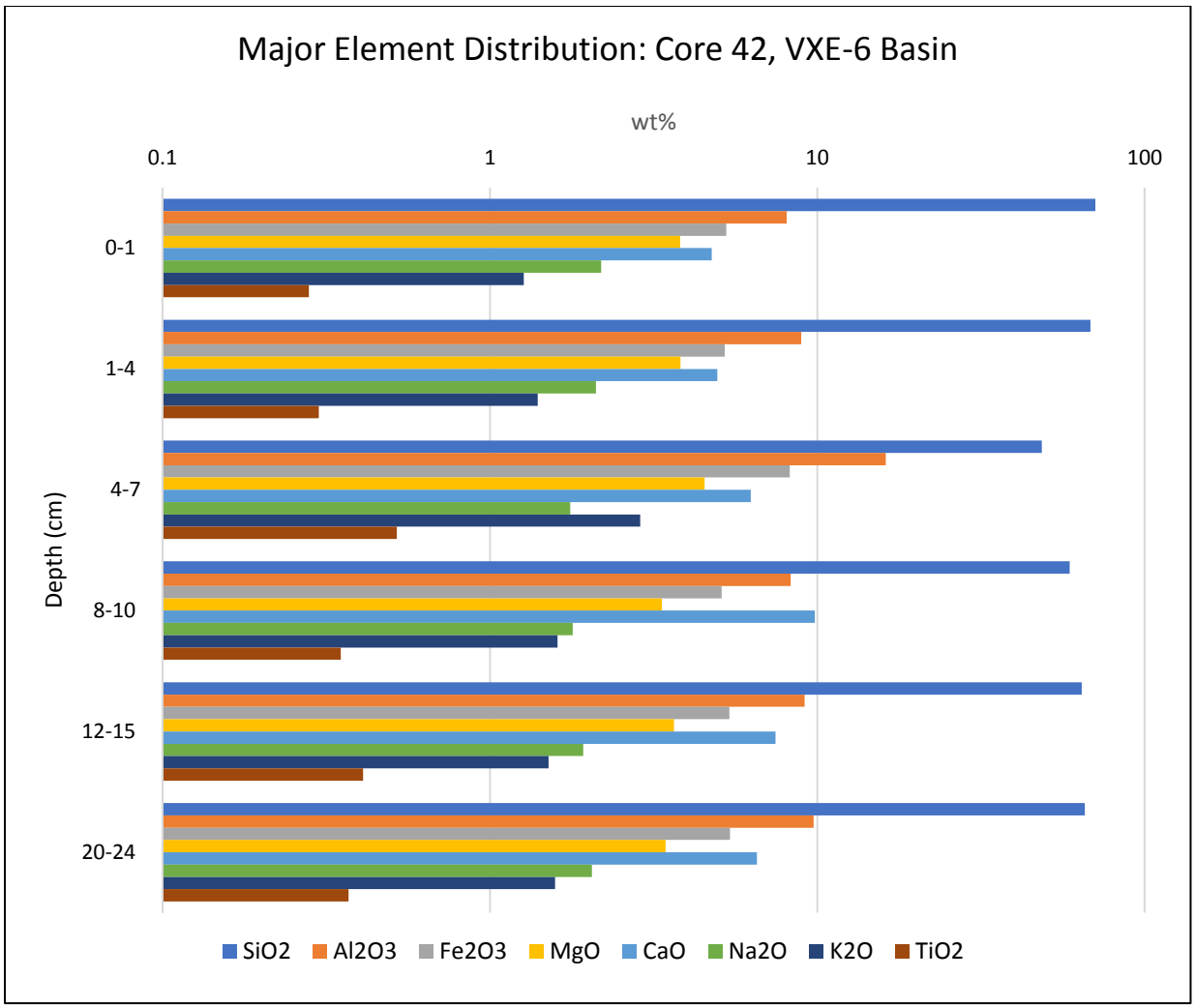

Figure 36. Major element distribution, Core 42, VXE-6 Basin.

Major elemental analysis of Core 42 shows variability in soluble ions Na^+ and K^+, though in significantly higher abundances than Core 2074. This suggests a lower degree of weathering and a comparably higher proportion of source rock(s) to be in Core 42. Notably, there is a relatively high abundance (2.28 %) of K, in JB1102 (4-7 cm). Major oxide abundances throughout the soil profile are relatively consistent, except for an anomaly in JB1102 (4-7 cm). JB1102 (4-7 cm) exhibits significant depletion in only SiO_2 (48.5 %), and enrichment in nearly all other major oxides. JB1103 (8-10 cm) displays

similar characteristics to JB1102 (4-7 cm), but not to the same degree. K/Th values range from 0.60 (JB1105, 20-24 cm) to 1.17 (JB1100, 0-1 cm). JB1105 and JB1102 (0.63, 4-7 cm) place near and in the range of Core 2074 K/Th values (0.61-0.67). This could suggest enhanced alteration at these depths in Core 42.

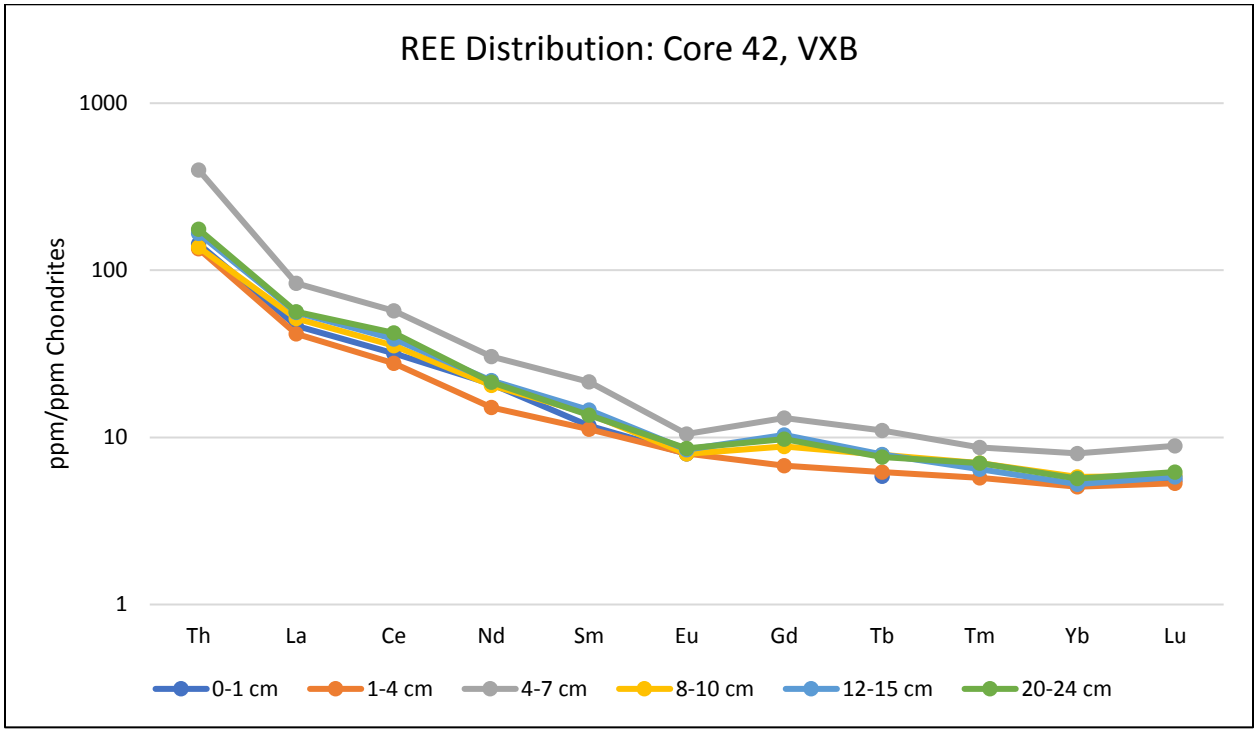

Figure 37. Rare earth element distribution, Core 42, VXE-6 Basin.

Rare Earth Element analysis for samples at 1 cm, 10 cm, 15 cm, and 24 cm depth exhibit similar REE abundance trends, while samples at 4 cm and 7 cm depth show comparatively low (4 cm) and high (7 cm) REE abundances, with the sample at 4cm not experiencing a negative Eu anomaly, which is likely due to Na_2O enrichment (Nyakairu and Koeberl, 2001). A horizon of elevated elemental abundance in the 4-7 cm depth range suggests a clay layer undergoing active alteration (Burton et al., 2019). Elevated REE abundance in the 4-7 cm depth range corroborates these findings. The clay layer could potentially extend close to 10 cm depth because relatively elevated abundances

of major oxides are displayed. However, elevated REE abundances are not seen at this depth.

2.4.5.2. Mineralogy: XRD, Spectra

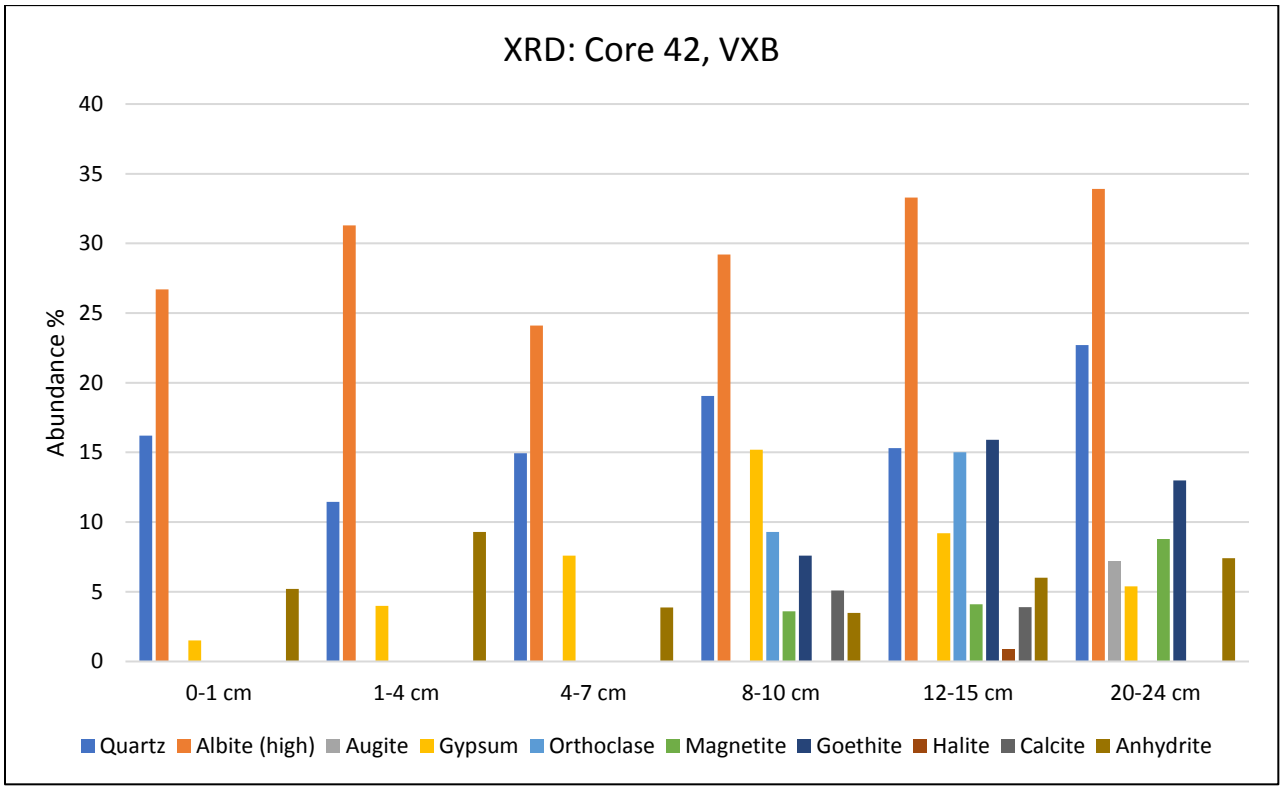

Figure 38. Mineralogical analysis of Core 42, VXE-6 Basin.

Terra XRD analysis of Core 42 shows highest total salts in JB1104 (12-15 cm), at 35.9 %, closely followed by JB1103 (10-12 cm), at 31.4 %. JB1105 (20-24 cm) still exhibits relatively elevated total salts but is significantly lower (25.8 %). This could suggest a salt horizon around 12cm. Notably, there is a significant presence of anhydrite, as compared to other microenvironments, in Core 42—particularly in JB1101 (1-4 cm), at 9.3 %. JB1101 (1-4 cm), in addition to the highest reported anhydrite, exhibits the lowest quartz abundance (11.45 %) of the profile. JB1102 (4-7 cm) exhibits the lowest albite

abundance (24.1 %) and the second lowest quartz abundance (14.95 %). Qualitative XRD results from the Bruker D8 Advance (LYNXEYE XE detector) instrument support the results of the Terra-166.

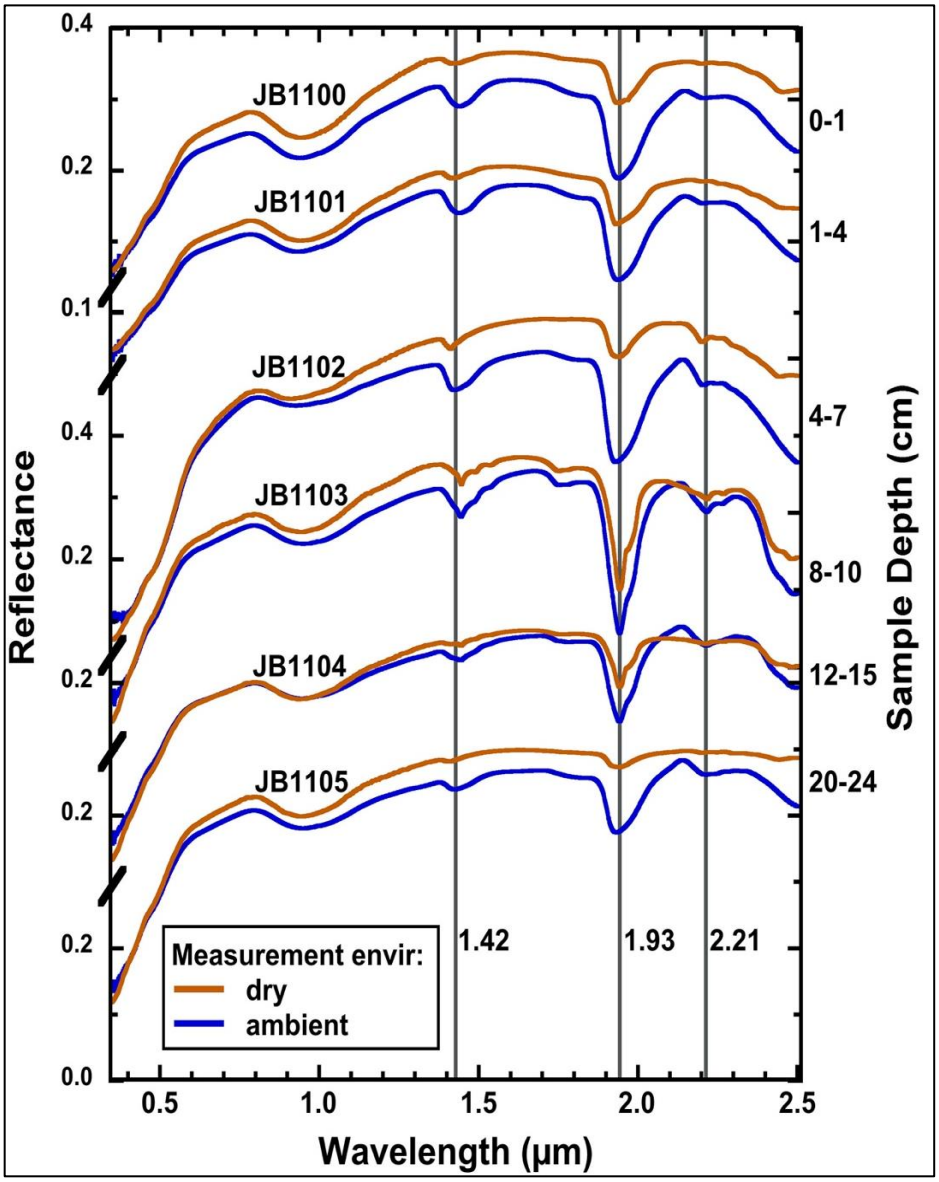

Figure 39. Spectral analysis of Core 42, VXE-6 Basin.

Spectral analysis of Core 42, VXE-6 Pond, displays mineralogically diagnostic absorption bands. A broad band near 1µm indicates Fe^{2+} which suggests the presence of pyroxene in all samples. Broad bands near 1.43, 1.93, and 2.20 µm in samples JB1100 (0-1 cm), JB1101 (1-4 cm), and JB1105 (20-24 cm) are characteristic of poorly crystalline aluminosilicates such as allophane or hydrated NaCl. JB1102 (4-7 cm) displays clearer characteristics for aluminosilicates, strengthening a hypothesis of a clay horizon undergoing active alteration in this depth range (Burton et al., 2019). JB1103 (8-10 cm) and JB1104 (12-15 cm) exhibit bands highly characteristic of gypsum, suggesting a horizon mixed with aluminosilicates and gypsum beneath the clay-dominated horizon just above.

2.4.5.3. Special Analysis: Anions, CIA

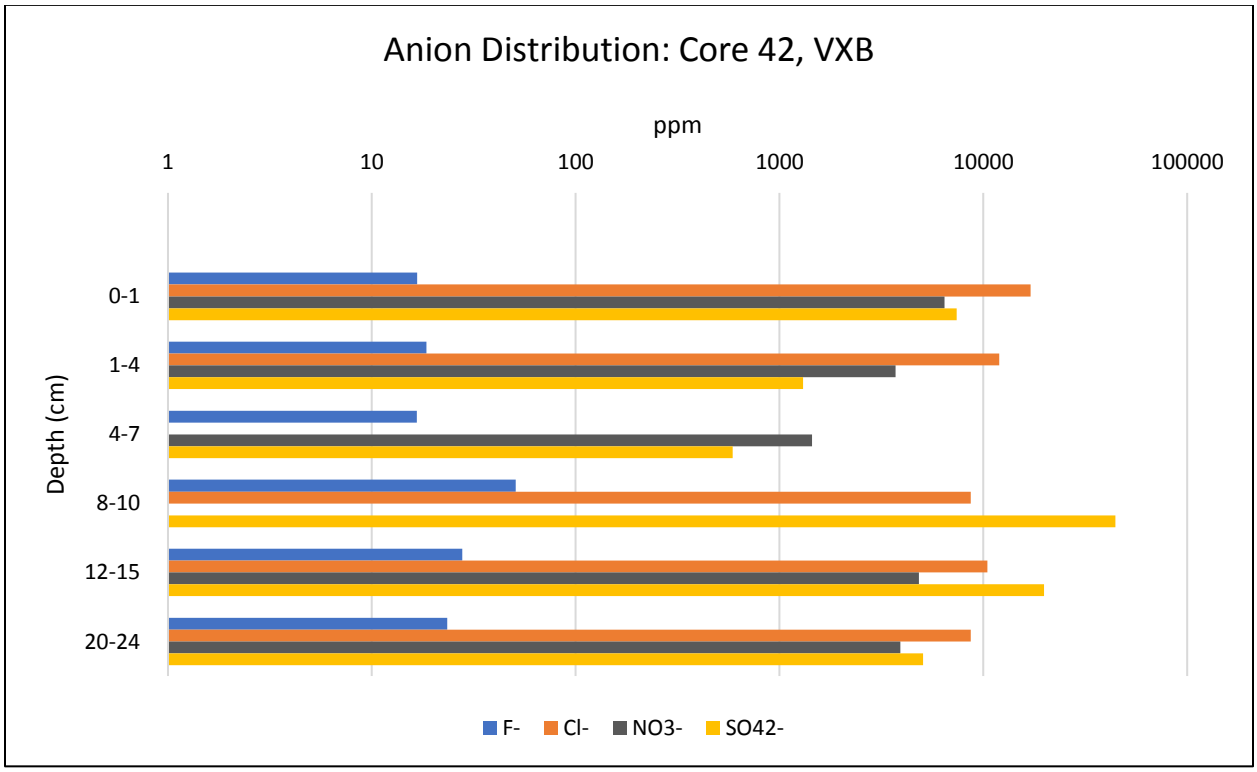

Figure 40. Soluble anion distribution at Core 42, VXE-6 Basin.

Soluble anion distribution in Core 42, VXB, shows decreasing abundance in all anions in the top 7 cm, particularly in the 4-7 cm range, followed by significant increasing abundance from 7-10 cm, particularly in F^- (16.65 to 50.75 ppm) and (590 to 44 x 10^3 ppm). This observation is in line with those made for XRD and spectral data which noted enrichment in gypsum at this depth. The distinct anion depletion in the 4-7 cm depth range corroborates an actively altering clay layer proposed by Burton et al. (2019) sitting atop a layer of gypsum.

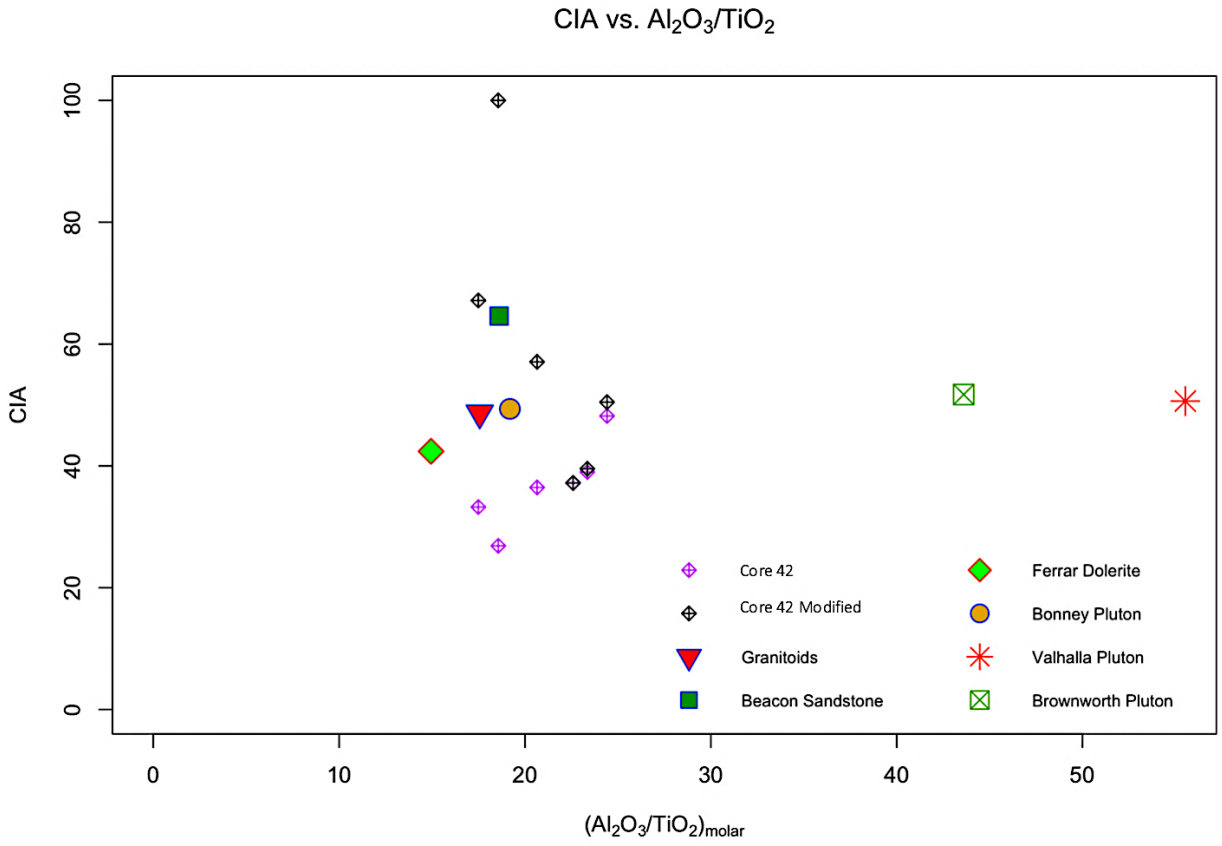

Figure 41. Core 42 unmodified and modified CIA values and regional source rock CIA values.

Chemical Index of Alteration values in Core 42 range from 26-48, in the CIA range for fresh basalts and entering the range of fresh granites and granodiorites (Nesbitt and Young, 1982), in line with regional geology (Peterson and Marsh, 2008). The lowest CIA value, 26, is exhibited in JB1103 (8-10 cm). JB1103 (8-10 cm) also reports the highest

total salts, primarily in the form of sulfates, which could be causing a dilution effect, pushing the sample's CIA value down. The highest CIA value, 48, is exhibited just above in JB1103 (4-7 cm), supporting the hypothesis of active chemical alteration occurring in this sample.

Analysis of modified CIA values at Core 42, to account for dilution by salt, begins to show variation from unmodified values in JB1102 (48 → 50) followed by the greatest modification, in JB1103 (27 → 100, 8-10 cm), JB1104 (33 → 67, 12-15 cm), JB1105 (36 → 57, 20-24 cm). The minor adjustment in JB1102 is expected because the 4-7 cm depth range reports a clay horizon rather than a salt horizon. This is why the following sample, JB1103, which reports the highest abundance of gypsum and total salts, reports the greatest modification. JB1104 (12-15 cm) reports the second highest abundance of gypsum and total salts and, as expected, the second greatest modification. The modified CIA values fall in the range of granites to authigenic K-feldspar (Fedo et al., 1995), consistent with regional and local geology.

Based on these analyses, a likely picture for Core 42 is one dominated by physical alteration in the top approximately 4 cm, manifesting as sediment mixing from source rock formations. From approximately 4-10 cm, is a layer of chemically altering clay sitting atop a layer enriched in gypsum that may taper to JB1104 (12-15 cm) and be cycling downwards to JB1105 (20-24 cm) by freeze-thaw processes (physical alteration).

2.4.6. CORE 52

Figure 42. Core 52 sample site, Wright Valley South Fork.

The South Fork region is located approximately 3 km east of Don Juan Pond, DJB. The region contains three ponds: 1 (east SF), 2 (middle SF), and 3 (west SF) (Gibson, 1980), however geochemical analysis in this paper is limited to sediment samples JB1107-1110 (0-20 cm) taken from Core 52, close to Pond 1. The soil trench was dug to a depth of 20 cm at which point permafrost is met. Pond 1 is a temporal, frozen body, and is supplied by localized shallow groundwaters (Harris, 1981).

2.4.6.1. Elements: Major, Minor, and Rare Earth

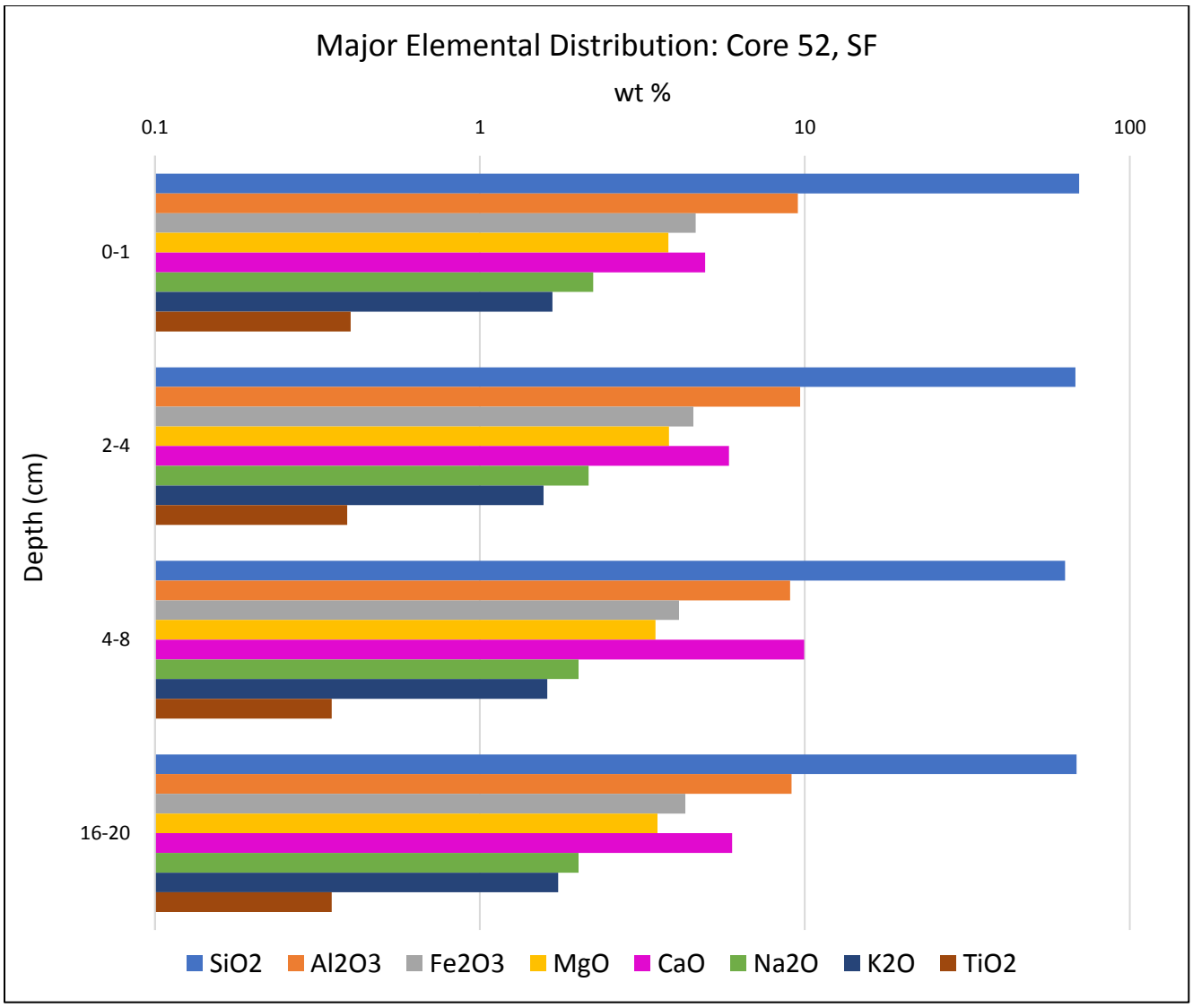

Figure 43. Major element distribution, Core 52, South Fork.

Major element analysis of the soil trench at Pond 1, South Fork, shows consistent oxide abundances for every sample except for JB1109 (4-8 cm) that exhibits a CaO enrichment (9.95 %) and slight SiO_2 depletion. K/Th values range from 0.87 in JB1110 (16-20 cm) and 0.97 in JB1108 (2-4 cm), significantly higher than those in Core 2074 (0.61-0.67).

This may indicate a lower degree of alteration in the soils near Core 52 than in Core 2074.

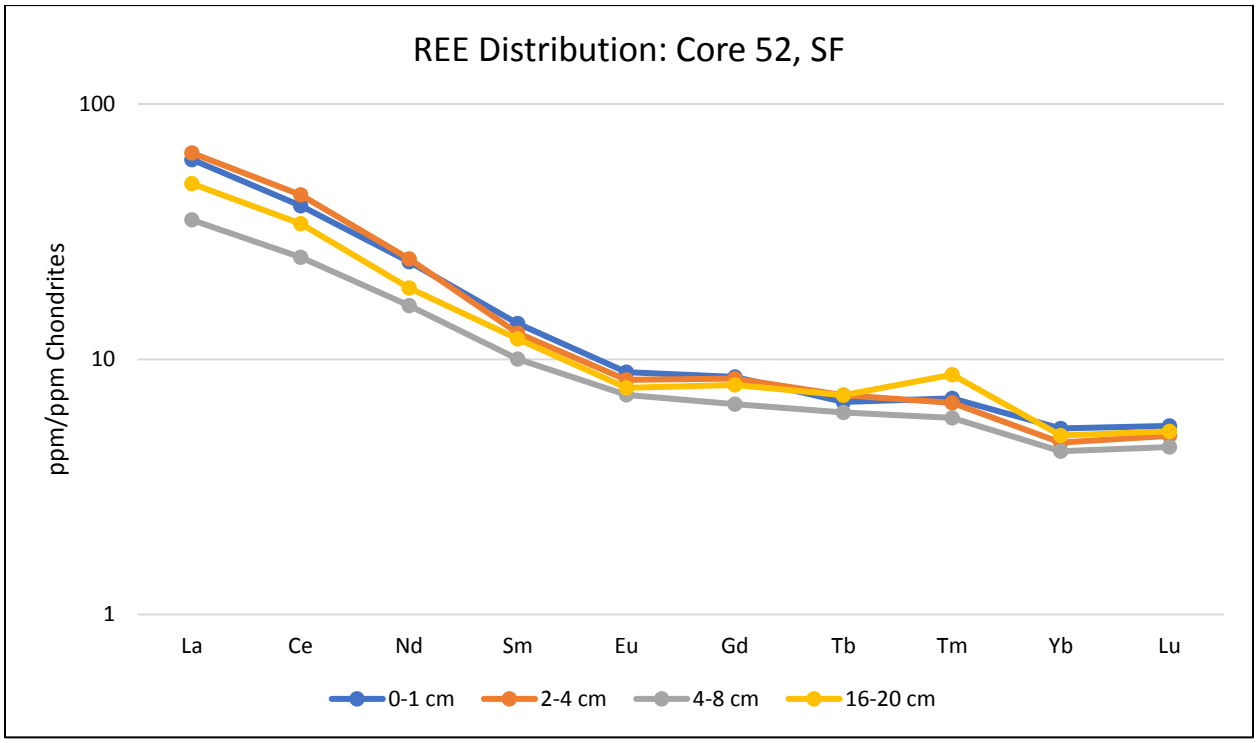

Figure 44. Rare Earth Element distribution of Core 52, South Fork.

Rare Earth Element analysis shows a significant drop in La, Ce and Nd, from JB1107 (0-1 cm) and JB1108 (2-4 cm) to JB1109 (4-8 cm). All samples, except for JB1109 (4-8 cm), exhibit a negative Eu anomaly. JB1109 (4-8 cm) exhibits the lowest Na_2O abundance, but the highest CaO abundance—an enrichment, relative to other samples—which is likely the reason for no Eu anomaly (Nyakairu and Koeberl, 2001). The low total REE abundance in JB1109 (4-8 cm) is likely due to a dilution effect caused by CaO and SO_3^- enrichment that manifests as gypsum (see XRD below). Additionally, JB1110 (16-20 cm) exhibits a positive Tm anomaly.

2.4.6.2. Mineralogy: XRD, Spectra

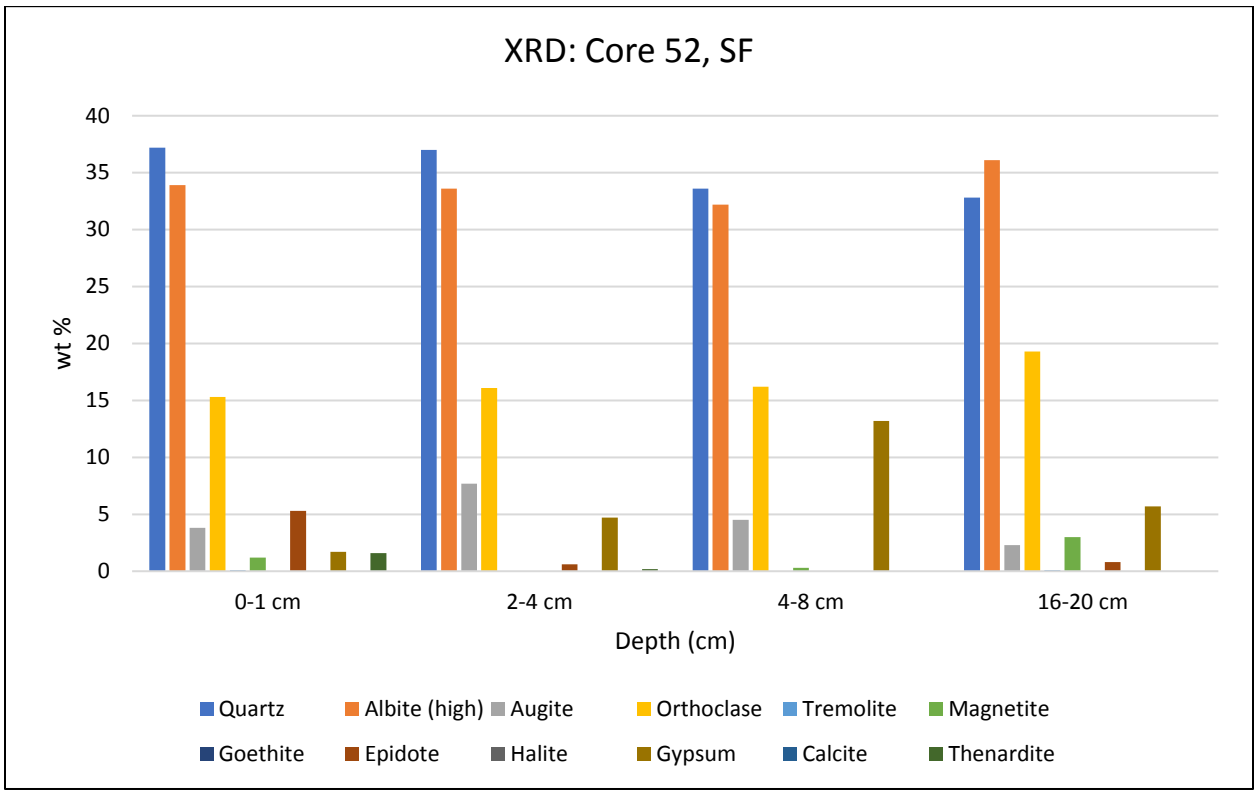

Figure 45. Mineralogical analysis of Core 52, South Fork.

XRD analysis shows quartz depletion in JB1109 and JB1110 (33.6 and 32.8 %), augite enrichment in JB1108 (2-4 cm), and significant gypsum enrichment (13.2 %) in JB1109 (4-8 cm). Gypsum enrichment corroborates CaO enrichment at this depth. Gypsum also exists in a lesser (5.7 %) but still notable abundance in JB1110 (16-20 cm), suggesting gypsum deposits taper off with increasing depth from JB1109 (4-8 cm).

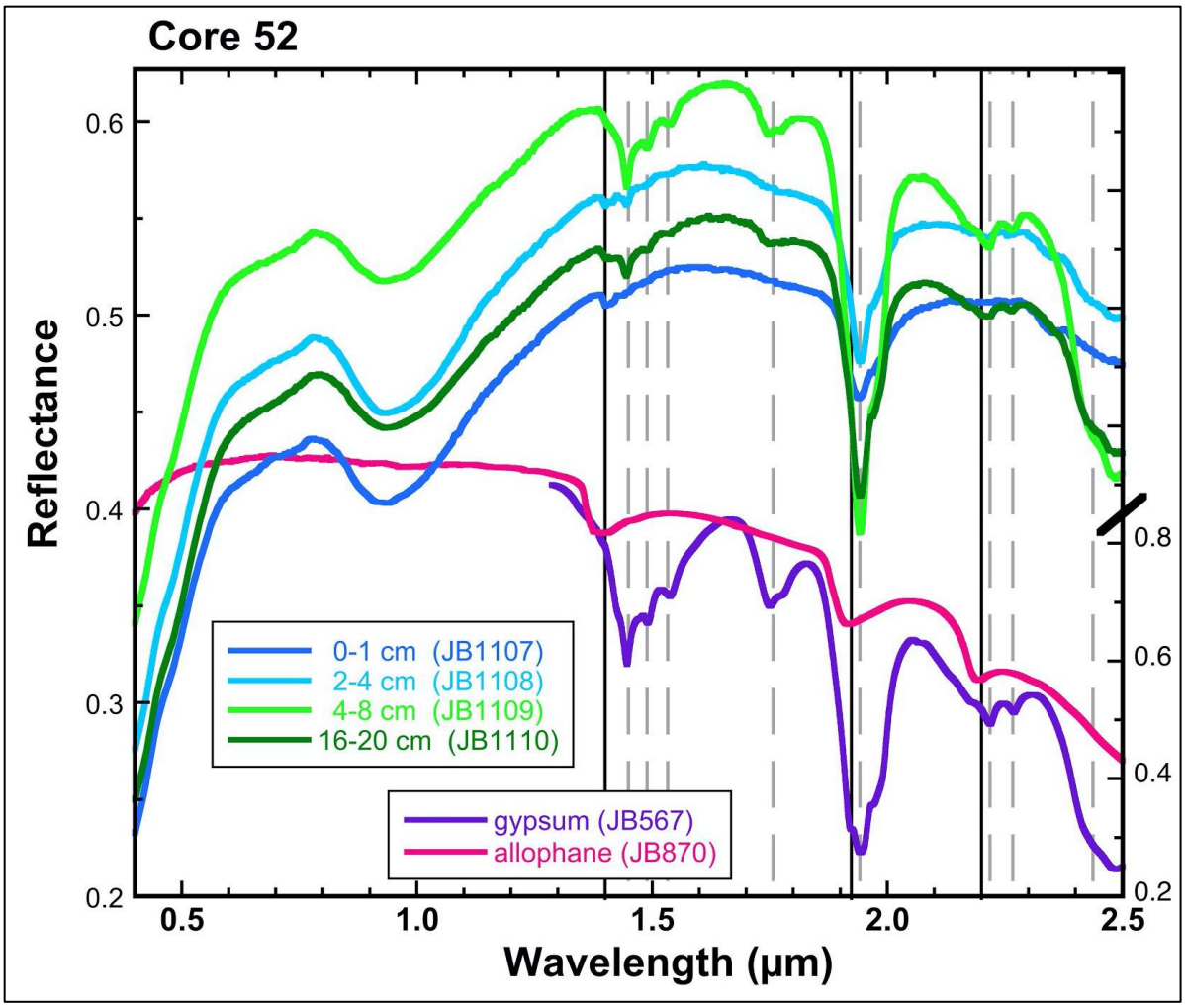

Figure 46. Spectral analysis of Core 52, South Fork.

Figure 46 exhibits features due to gypsum in all samples below 2 cm. These features are strongest in JB1109 (4-8 cm) where the characteristic triplet at 1.45-1.53 µm is observed, as well as bands at 1.76, 1.94, and a doublet at 2.22 and 2.26 µm. mineral (Bishop, personal communication, 2020). The upper samples contain hydrated amorphous material similar to allophane and all spectra include an Fe band near 0.93 µm that is characteristic of Fe^{3+} in ferrihydrite, a hydrated amorphous ferric oxide-bearing mineral (e.g. Bishop and Murad, 2002).

2.4.6.3. Special Analysis: Anions, CIA

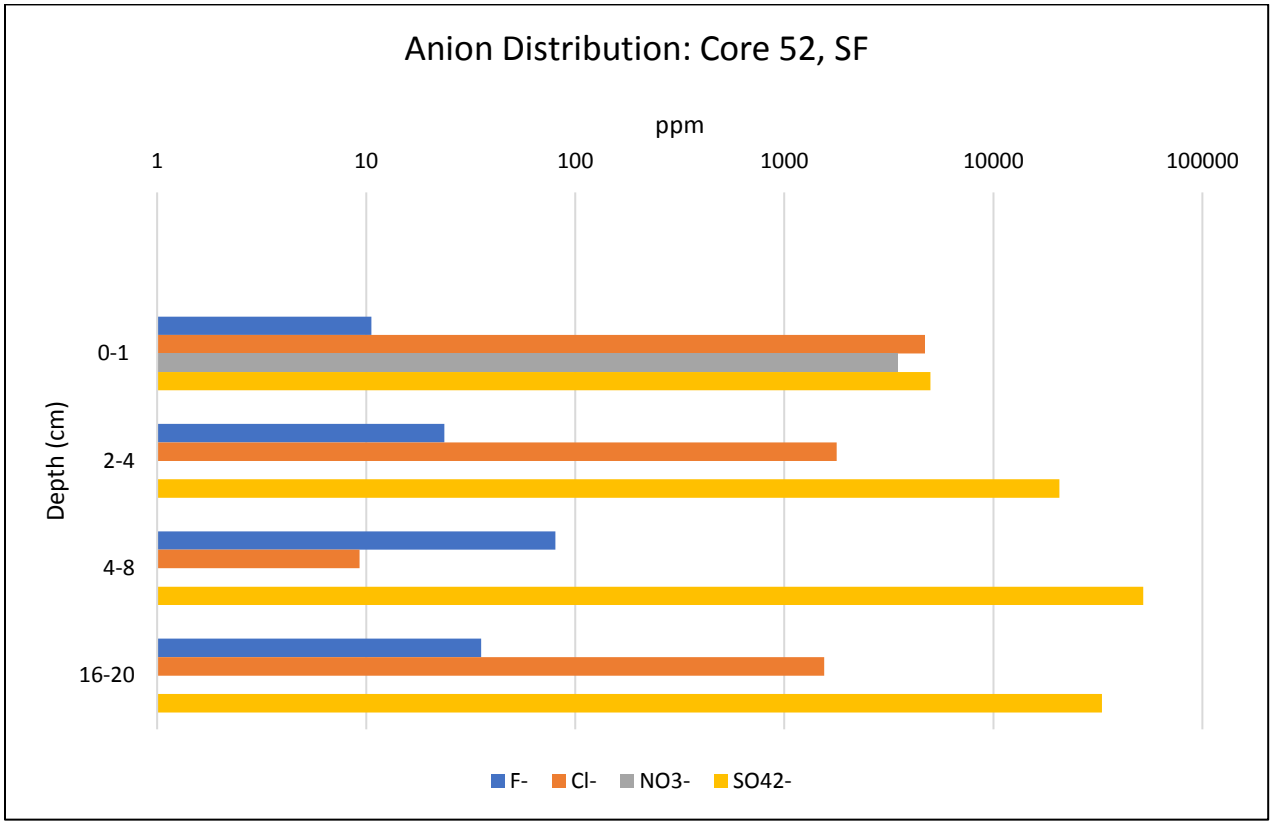

Figure 47. Soluble anion distribution of Core 52, South Fork.

Abundance is at its greatest (52 x 10^3 ppm) in JB1109 (4-8 cm) and at its second greatest (33 x 10^3 ppm) in JB1110 (16-20 cm), bolstering the theory of gypsum enrichment at 8 cm that tapers off with depth. Additionally, Cl^- exhibits its lowest abundance, and F^- its highest, in JB1109 (4-8 cm).

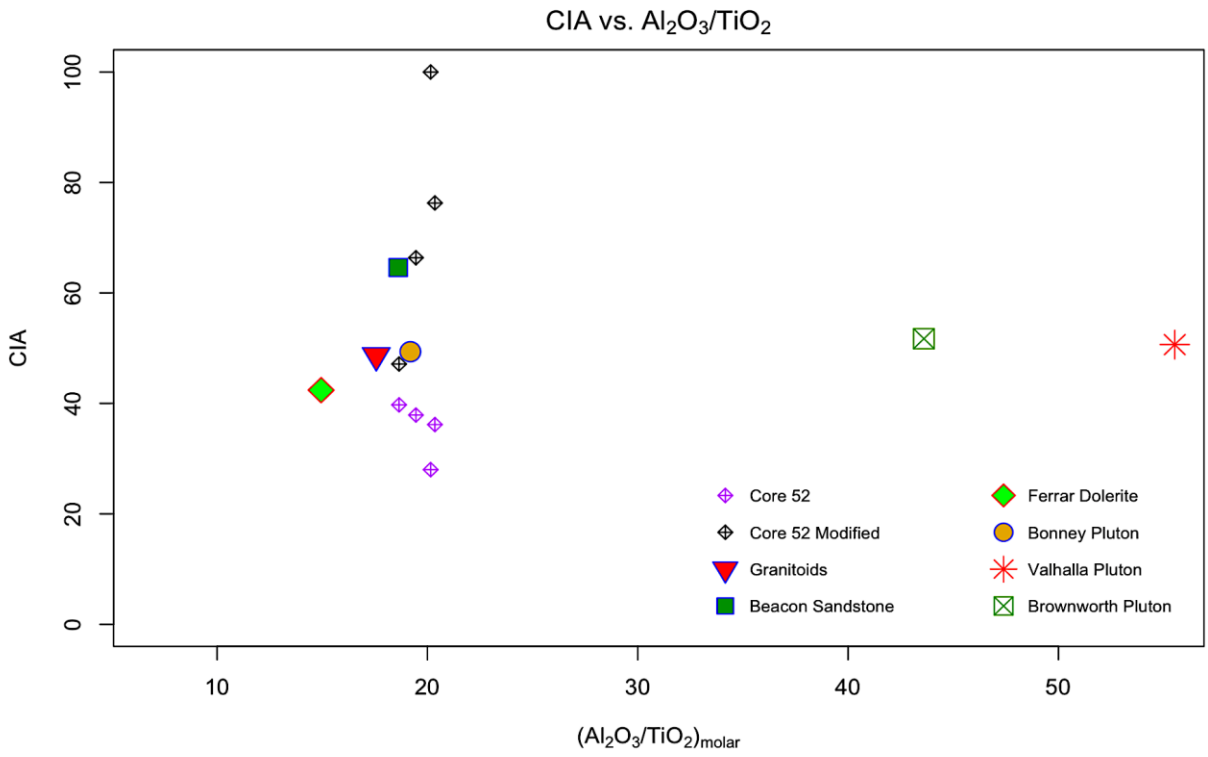

Figure 48. Core 52 modified and unmodified CIA values and regional source rock CIA values.

Chemical Index of Alteration values in the soil trench at Pond 1 range from 28-39, in the range of fresh basalts, as proposed by Nesbitt and Young, 1982, and in line with regional geology (Peterson and Marsh, 2008). The lowest value, 28, is seen in JB1109 (4-8 cm), and the highest, 39, is seen in JB1107 (0-1 cm). Ca-sulfate relative enrichment in JB1109 (4-8 cm) is likely the reason for the lower CIA value, while JB1107 exhibits relative Ca-sulfate depletion, which is likely the reason for the higher CIA value. With higher CIA values and practically unchanged $(Al_2O_3/TiO_2)_{molar}$ values—in comparison to those of the soil trench—the case for the soil trench being dominated by chemical alteration is weak. A possible reason for this, as is the case in other microenvironments, is sediment mixing between the Ferrar Dolerite and Granitoids.

Analysis of modified CIA values at Core 52, to account for dilution by salt, shows significant variation from unmodified CIA values. After modification, JB1109 (4-8 cm)

reports a CIA value of 100—completely altered—yet there are igneous minerals present. This demonstrates the utility of the CIA, though it may not be appropriate for soils. JB1109 (4-8 cm) reports as a “white layer” in visual examination prior to spectral analysis, and XRD confirms it to be gypsum. JB1108 (2-4 cm) and JB1110 (16-20 cm) are both significantly modified from their original CIA values to gypsum: 38 → 66 and 36 → 76.

Based on this information, the most likely picture for Core 52 at Pond 1, is one dominated by physical alteration in the top 2 cm, manifesting as sediment mixing. Chemical alteration is likely operating most between 4-12 cm, manifesting as the precipitation of gypsum primarily in the 4-8 cm range, possibly tapering off around 12-14 cm. Gypsum being cycled downwards could be a reason for relatively high CIA values as far down as 16-20 cm. Core 52 is therefore a good example of chemical alteration in the McMurdo Dry Valleys.

2.4.7. CORE 72

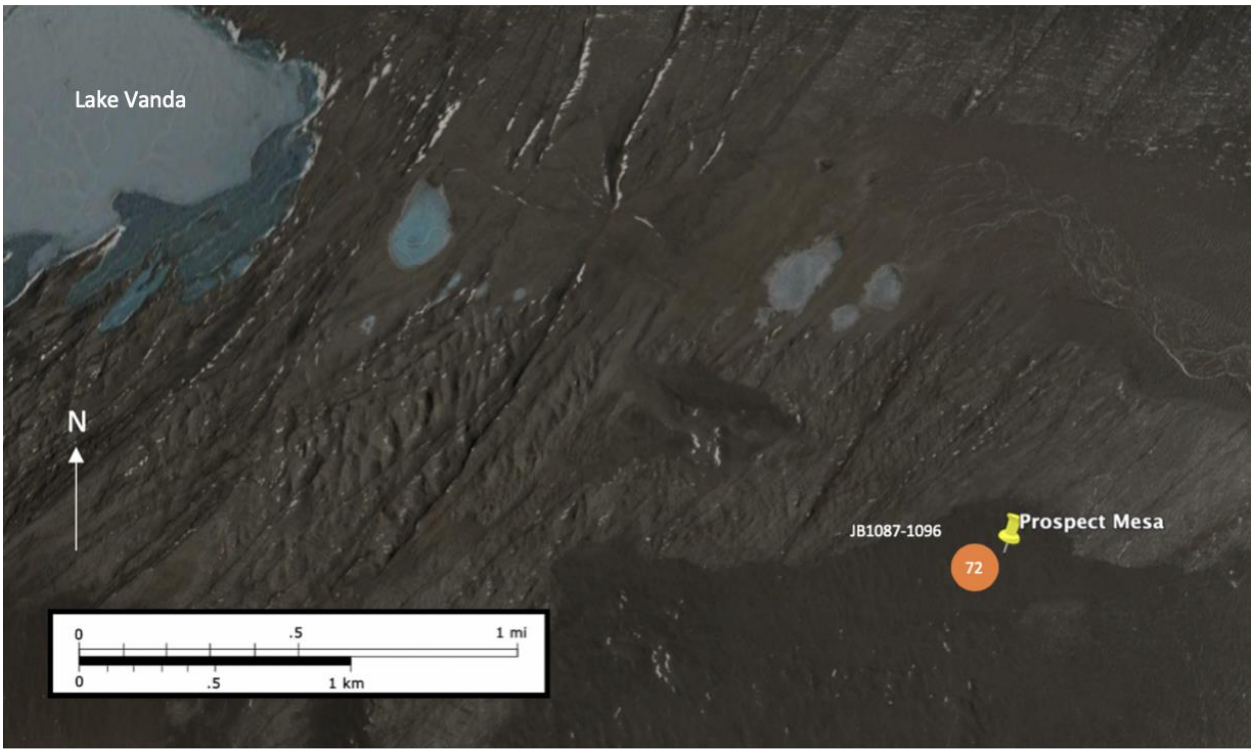

Figure 49. Core 72 sample site, Prospect Mesa. Lake Vanda is approximately 2.5 km to the northwest.

The Prospect Mesa Formation is located on the southern side of Wright Valley, approximately 3 km southeast of Lake Vanda (Figure 49, above). The microenvironment of interest in this region is Core 72 taken in 1980 by Everett Gibson to a depth of 80 cm. Geochemical analysis was completed for the whole core, including ~45 cm of soil above permafrost depth of which are discussed here.

2.4.7.1. Elements: Major and Rare Earth

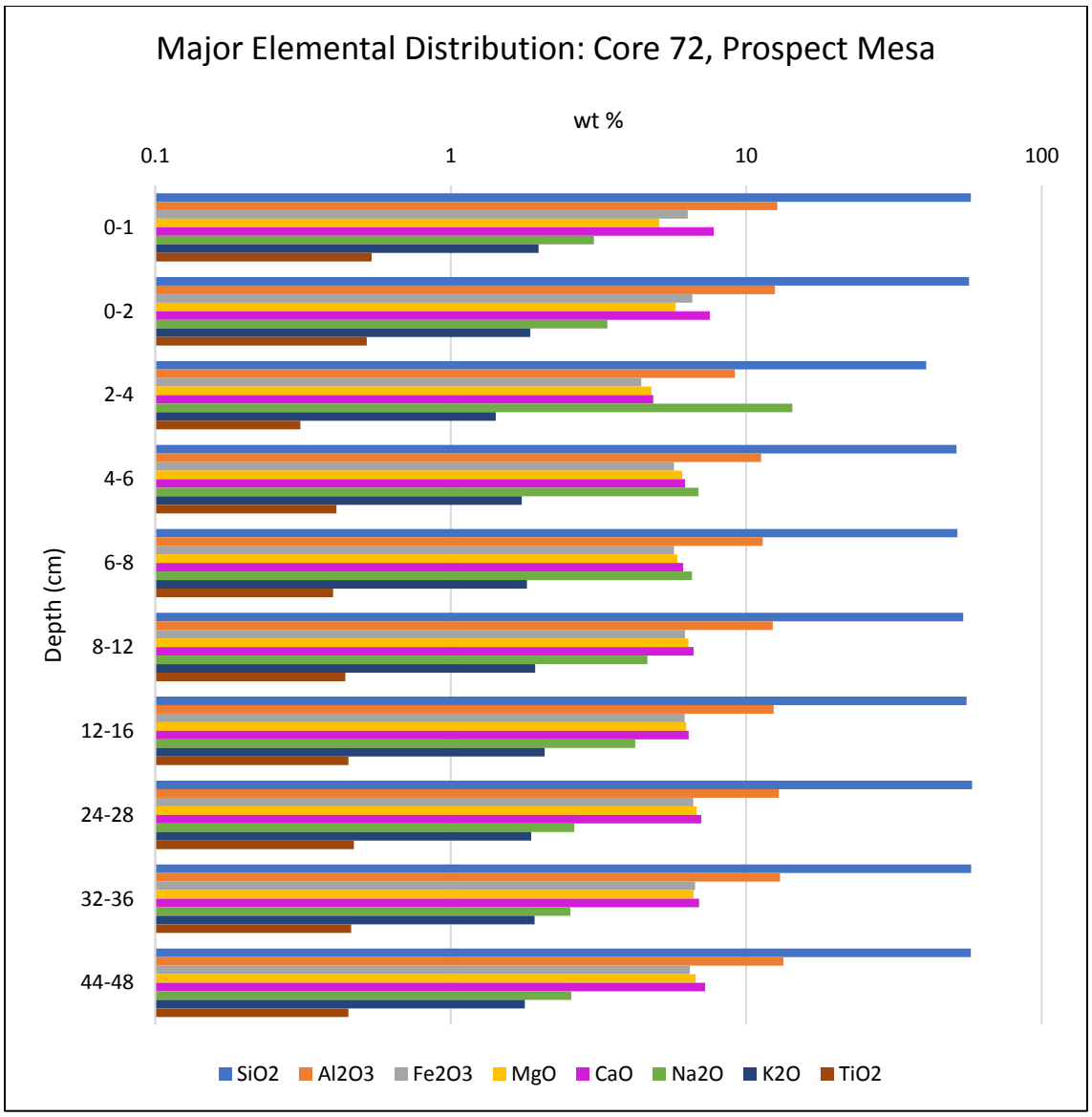

Figure 50. Major element distribution of Core 72, Prospect Mesa.

Major element analysis from Core 72 shows little variation with depth nor do the oxide ratios TiO_2/Al_2O_3 (~0.3), K_2O/Al_2O_3 (~1.4), and Al_2O_3/TiO_2 (~2.2) (not pictured). The one exception is JB1089 (2-4 cm) in which all elements and oxides—except for Na_2O— are depleted (11.95 and 14.32 %) in relation to the sample average.

K/Th values range from 0.63 (JB1090, 4-6 cm) to 1.63 (JB1091, 6-8 cm), within the range and significantly above the K/Th values of Core 2074 (0.61-0.67). This could suggest enhanced alteration in the 4-6 cm depth range followed by just the opposite in the 6-8 cm range of Core 72. Some variation exists in FeO/Al_2O_3 (~4.5), reflecting slight differences in abundances of ferromagnesian minerals, potassium feldspar, and plagioclase. Variations in the ratio of MgO/Al_2O_3 (~5) above the permafrost layer, at approximately 45 cm, are believed to be caused by the weathering of ferromagnesian minerals, which increases in degree towards the surface (Gibson et al., 1983).

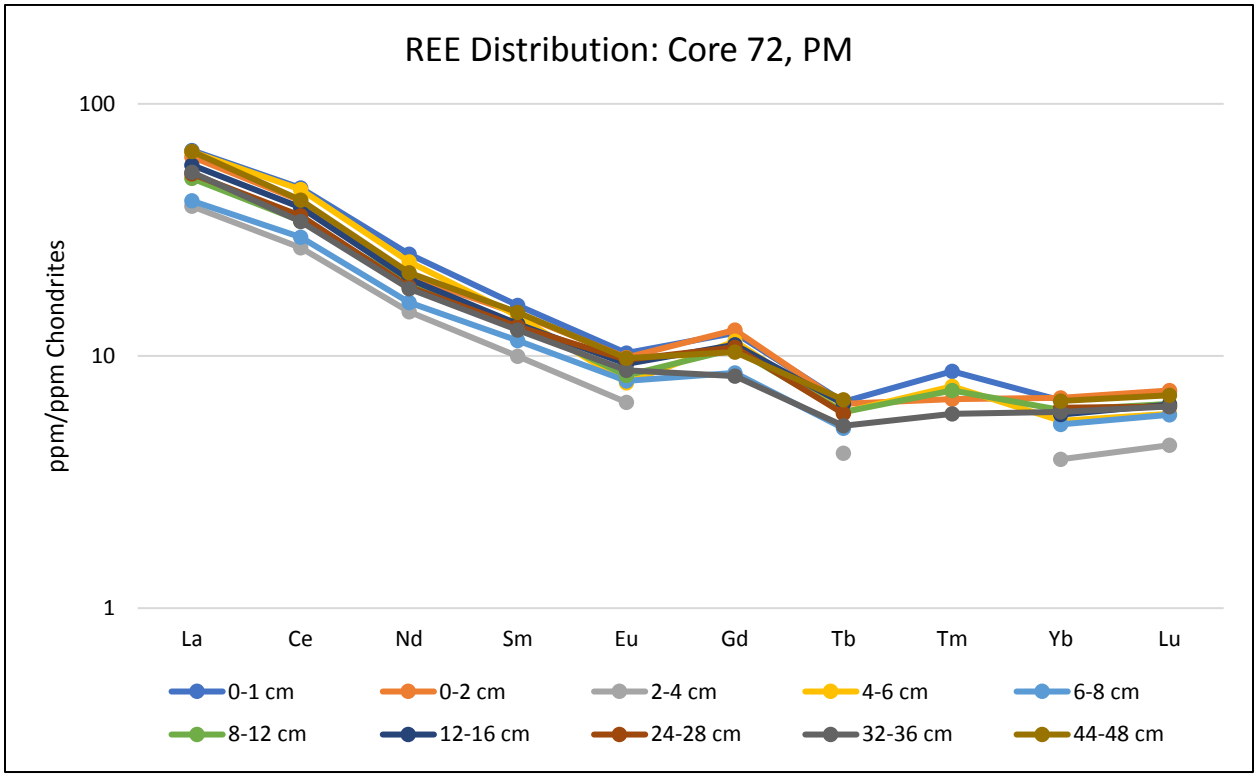

Figure 51. Rare Earth Element distribution of Core 72, Prospect Mesa.

Rare Earth Element patterns follow a similar trend to that of other microenvironments but are different in abundance. The majority of Core 72 samples exhibit negative Eu anomalies, attributed to depletion in CaO and Na_2O (Nyakairu and Koeberl, 2001) Significant relative depletions in all REEs are seen in JB1089 (2-4 cm) and JB1091 (6-8

cm). These depletions are paralleled by the highest reported total salts. Highest REE abundance is exhibited in JB1087 (surface sample), followed closely by JB1090. The highest REE abundances in Core 72 parallel the lowest K/Th ratio and total salt abundances.

2.4.7.2. MINERALOGY: XRD

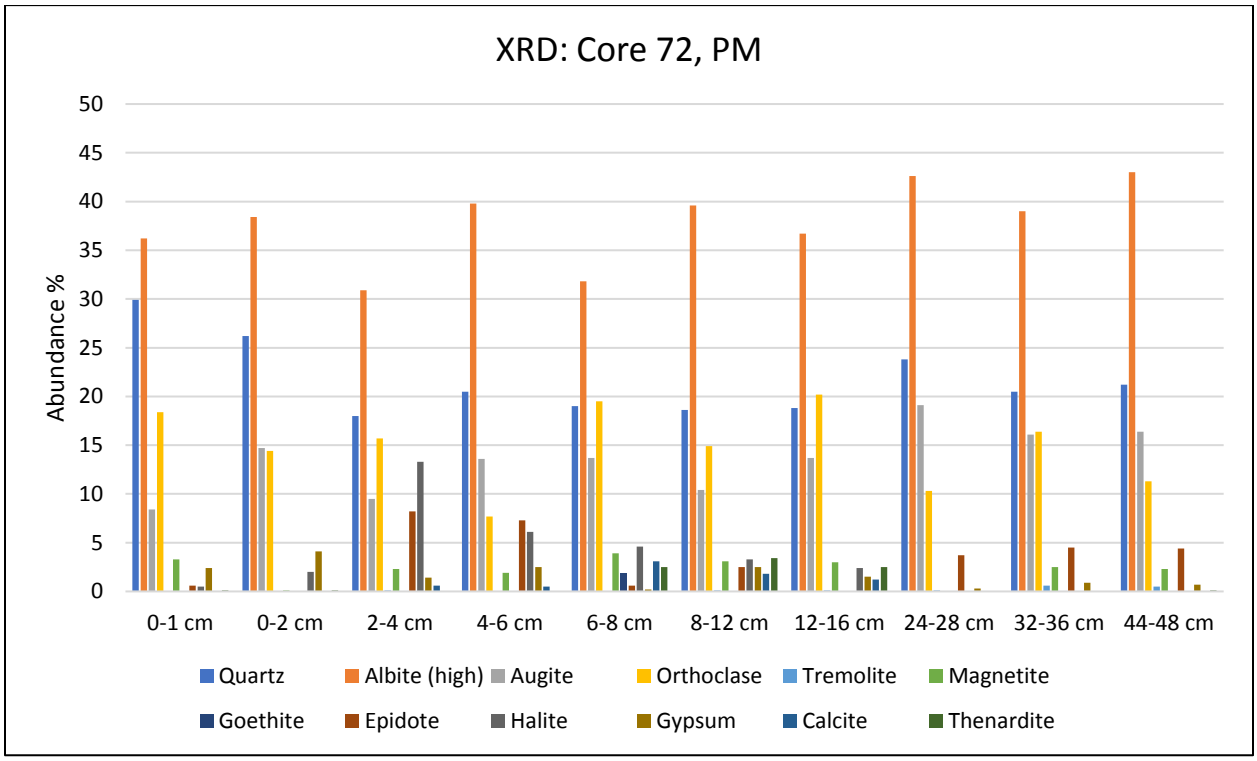

Figure 52. Mineralogical analysis of Core 72, Prospect Mesa.

XRD analysis of Core 72 at Prospect Mesa shows the existence of major minerals quartz, augite, albite, orthoclase, halite, and gypsum. Quartz exists in greatest abundance (29.9 %) in JB1087 (surface sample), and at lowest abundances (18 and 18.6 %) in JB1089 and JB1092 (2-4 and 8-12 cm). JB1089 (2-4 cm) also exhibits the highest total salts (15.3 %). The relatively high abundance of halite in JB1089 (2-4 cm) is corroborated by the highest reported Na and Cl^- (shown below in Anions) in the core. The lowest recorded halite

value is 0.5 % in JB1087 (surface sample). JB1090-JB1092 (4-6, 6-8, 8-12 cm) also show relatively high total salts (9.1 %, 10.4 %, 11 %). Gypsum is highest (4.1 %) in JB1088 (0-2 cm) and in the depth range of surface to 6 cm. Gypsum is lowest (0.2 %) in JB1091 (6-8 cm). Augite is highest (19.1 %) in JB1094 (24-28 cm) and lowest in JB1087 (surface sample). Orthoclase is highest (20.2 %) in JB1093 (12-16 cm) and lowest (7.7 %) in JB1090 (4-6 cm).

2.4.7.3. Special Analysis: Anions, CIA

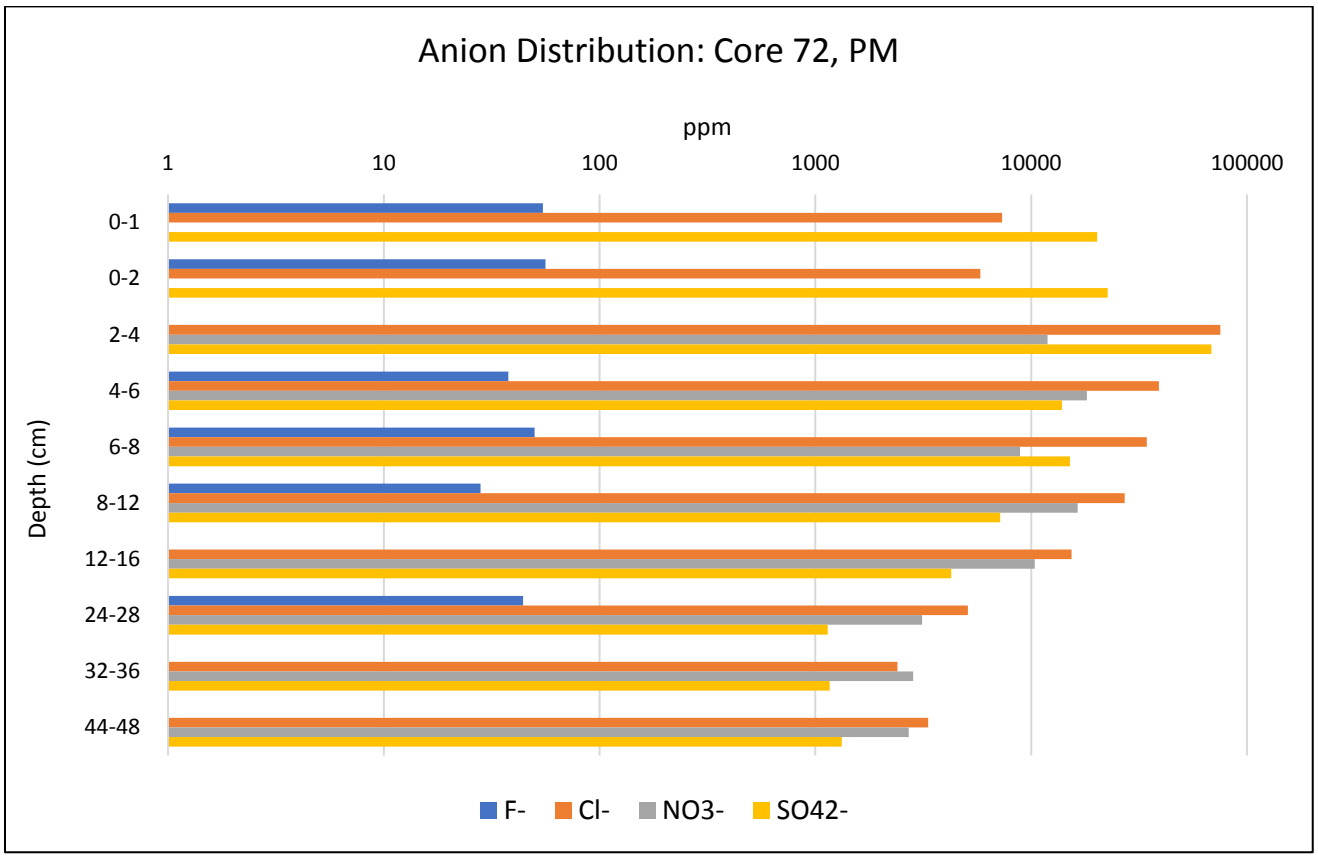

Figure 53. Soluble anion distribution of Core 72, Prospect Mesa.

Soluble anion analysis of Core 72 at Prospect Mesa shows relative Cl^-, NO_3^-, and enrichment between JB1089 and JB1093 (4-16 cm). JB1089 (2-4 cm) exhibits the greatest Cl^- and abundance (75,342 ppm), and JB1090 (4-6 cm) exhibits the greatest

NO_3^- abundance (18,149 ppm). The high abundance of Cl^- in JB1089 corroborates the high abundance of halite found in the sample with XRD analysis. The highest abundance of Cl^- (68,412 ppm) is in JB1089, yet the highest abundance of gypsum occurs in the sample just above, at 2cm, in which the highest abundance of Na and Na_2O exists, presenting a puzzling picture. Thenardite is shown to be the dominant Na-sulfate in the Dry Valleys, which would explain enriched Na_2O in JB1089. This, however, is a hypothesis because it would need to be confirmed from more data in the sample.

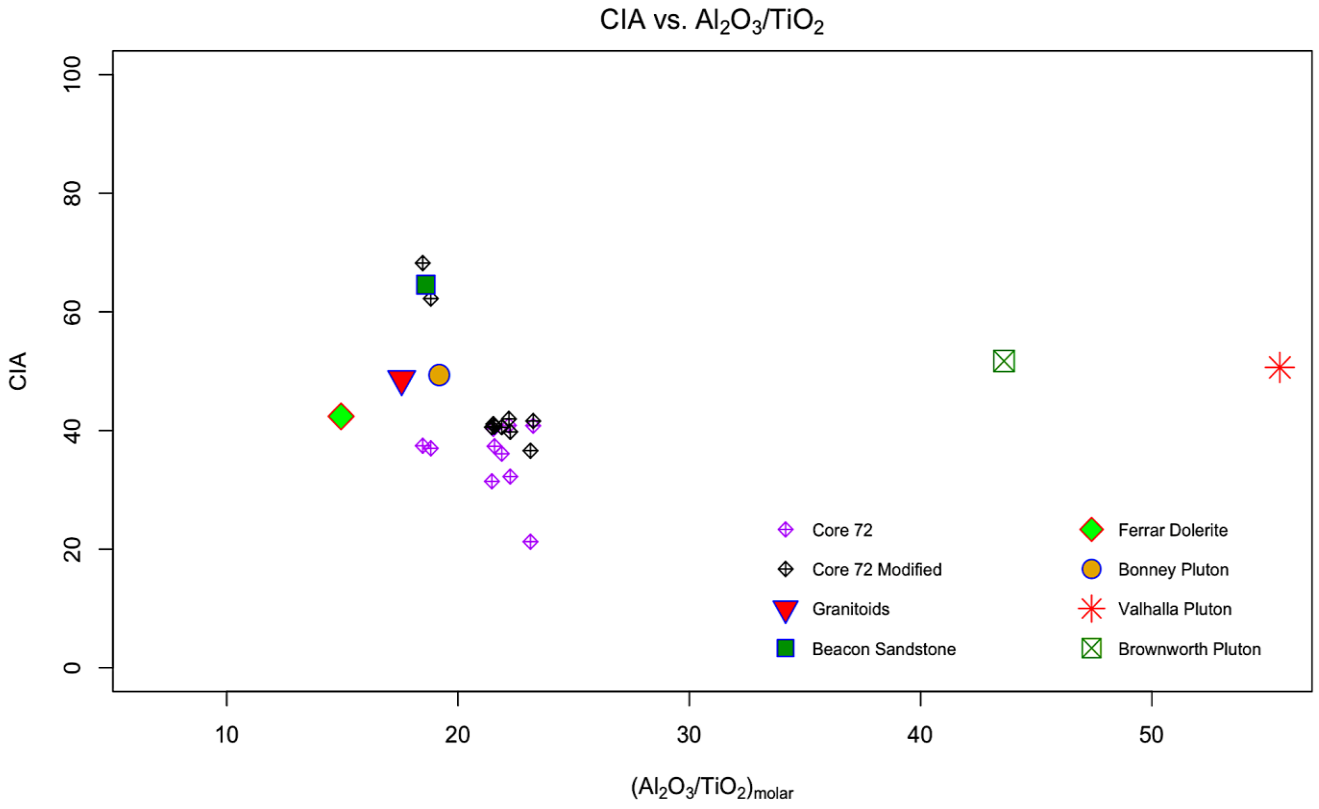

Figure 54. Core 72 modified and unmodified CIA values and regional source rock CIA values.

Chemical Index of Alteration values at Core 72 range from 21 to 41, with all but one sample outside the range of 31 - 41. The single, anomalous sample, JB1089 (2-4 cm), is enriched in Na_2O (14.32 %), likely manifesting as NaCl, and is the presumed reason for the low CIA value. With JB1089 (2-4 cm) set apart from all other samples, the CIA values

place in the range of fresh basalts as proposed by Nesbitt and Young, 1982, and in line with regional geology (Peterson and Marsh, 2008). Significant REE depletion in samples JB1089 (2-4 cm) and JB1091 (6-8 cm) is likely caused by dilution from high salt content, suggesting chemical alteration in this depth range.

Analysis of modified CIA values at Core 72, to account for dilution by salt, shows significant variation in samples JB1087 (0-1 cm) and JB1088 (0-2 cm). JB1087 (surface sample) reports a CIA value of 68, and JB1088 (0-2 cm), 62. The two samples exhibit the two highest abundances of gypsum, suggesting that water must have been present at the time of precipitation. Oddly, a salt-rich layer reported in JB1089 (2-4 cm) (Gibson et al., 1983), confirmed to be halite, does not show as drastic a CIA modification as the gypsum-rich samples above.

Based on this information, Core 72 is likely dominated by physical alteration, with chemical alteration, manifesting as a salt-rich horizon, between 2-4 cm—possibly extending to 6 cm— operating on a secondary scale. Gypsum at the surface serves as evidence of previously aqueous sediment and supports chemical alteration at and near the surface.

2.4.8. LAKE VANDA

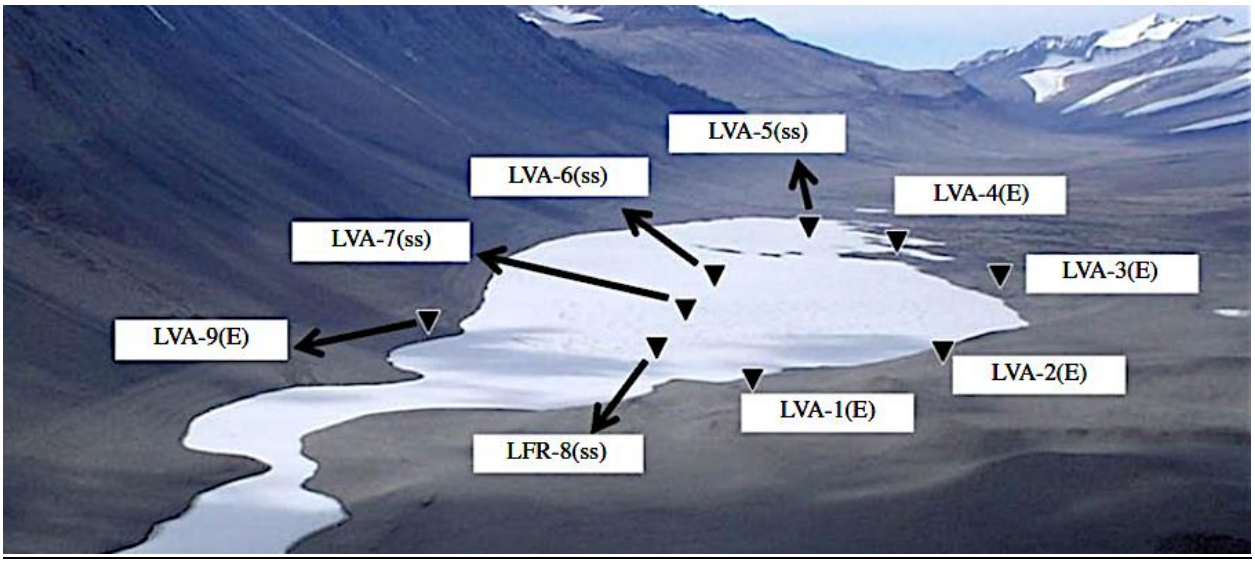

Figure 55. Lake Vanda sample sites, Source, Bishop et al., 2014

Lake Vanda is located in Wright Valley, Antarctica, and is the site of samples JB661-669 (LVA-1 – LVA-9). JB661-664 and JB669 are all sediment samples collected from the edge of Lake Vanda. JB665-668 are all sediment samples that were collected from the surface of the lake. Summer wind directions are predominantly down-valley (easterly) making aeolian sedimentation from westerly sources a possibility (Nylen et al., 2004). Samples were collected in the summer of 2004.

2.4.8.1. Elements: Major, Minor, and Rare Earth

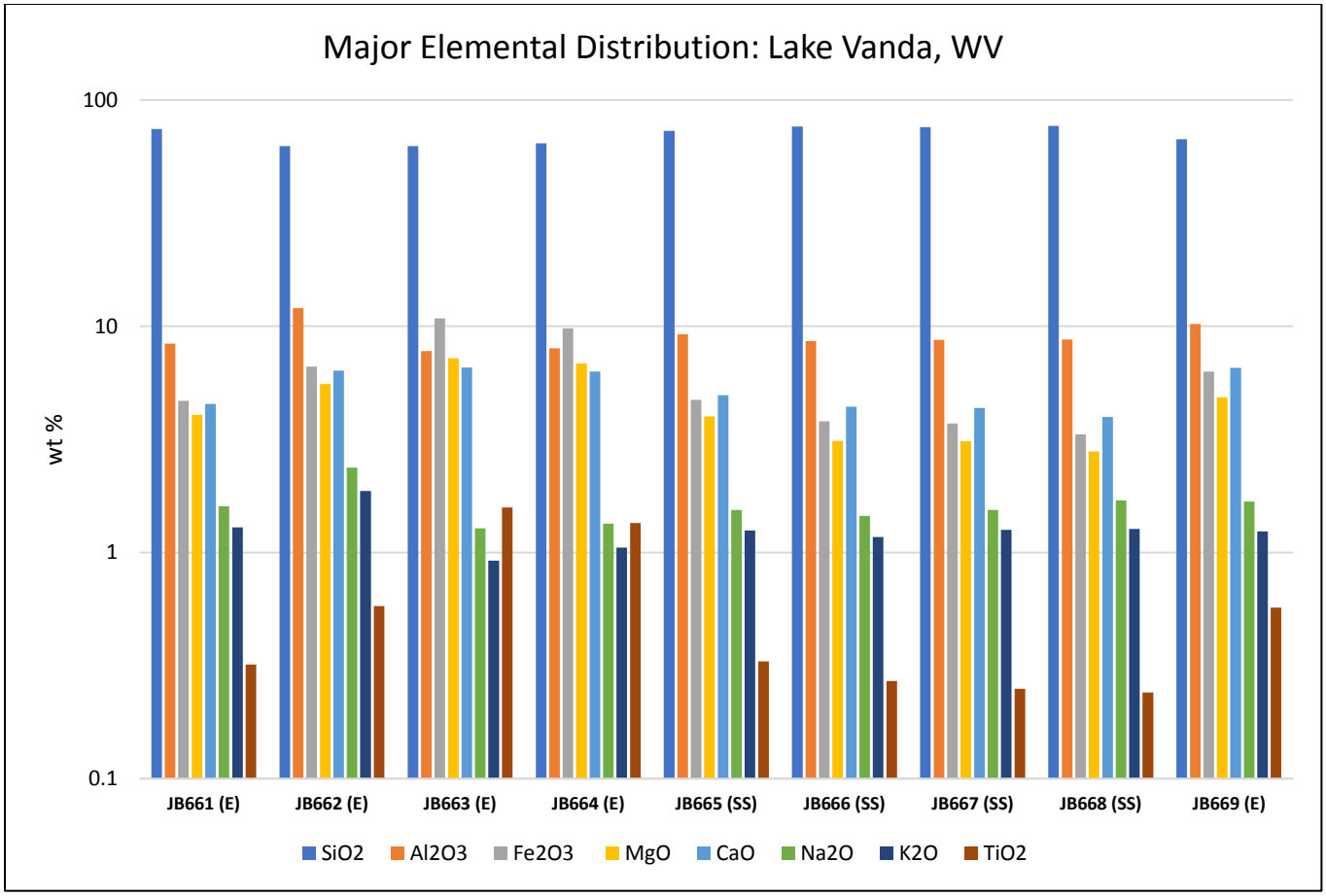

Figure 56, Major element distribution at Lake Vanda, Wright Valley, surface and edge samples.

Major element analyses of Lake Vanda surface and edge samples show similar trends and abundances for all oxides except for TiO_2, CaO, and Fe_2O_3. The difference is likely due to the sample type: Surface vs. Edge. The majority of the surface samples show relative depletion in each of the aforementioned compounds, while the majority of the edge samples show relative enrichment. However, surface samples exhibit higher SiO_2 content than do the edge samples.

K/Th values span a significant range: 0.18 (JB663, edge) to 0.67 (JB661, edge), well below and inside the range of K/Th values at Core 2074 (0.61-0.67). This suggests alteration could be occurring at Lake Vanda.

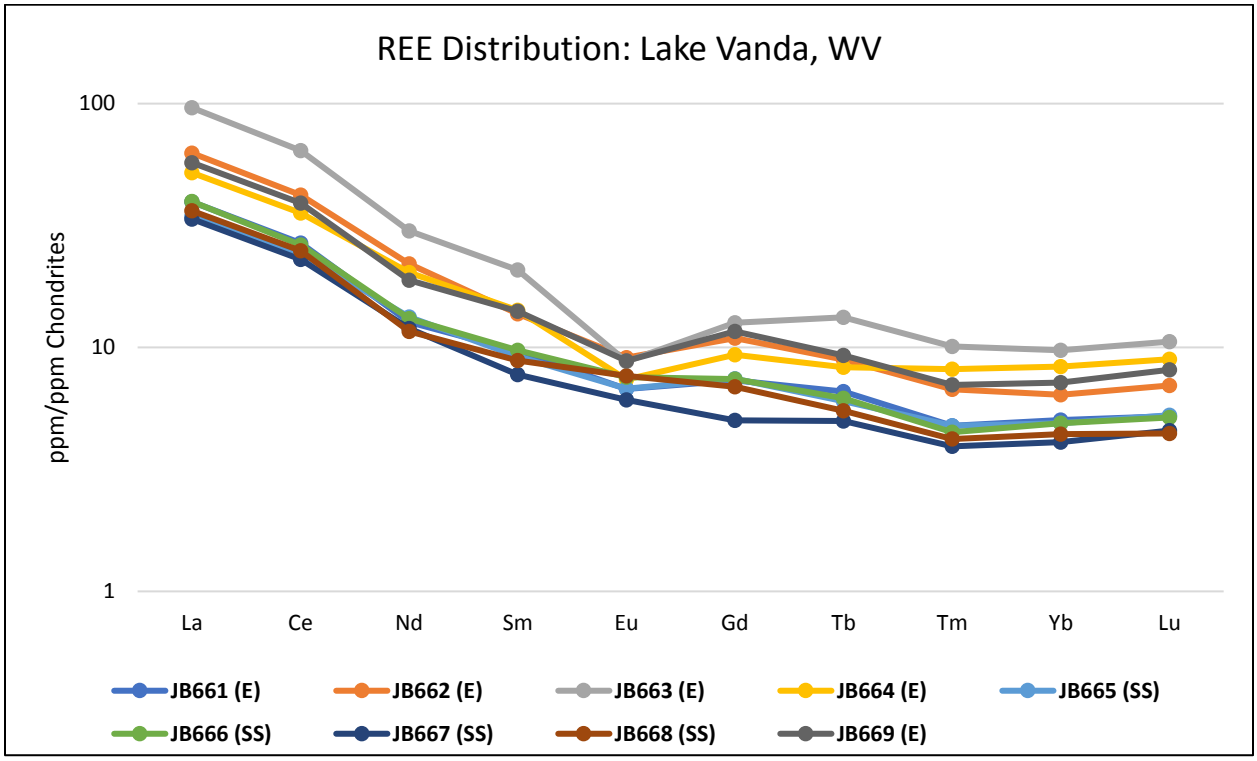

Figure 57. Rare Earth Element distribution at Lake Vanda, Wright Valley, surface and edge samples.

Similar patterns of depletion are seen for the REEs La, Ce, and Nd in all surface samples, while most edge samples exhibit enrichment. JB663 (edge) exhibits the highest REE abundances of all samples, and JB667 (SS) exhibits the lowest. Negative Eu anomalies, attributed to depletion in CaO and Na_2O (Nyakairu and Koeberl, 2001), are seen in all samples except for JB665 (SS), JB667 (SS), and JB668 (SS).

2.4.8.2. MINERALOGY: XRD, REFLECTANCE, RAMAN

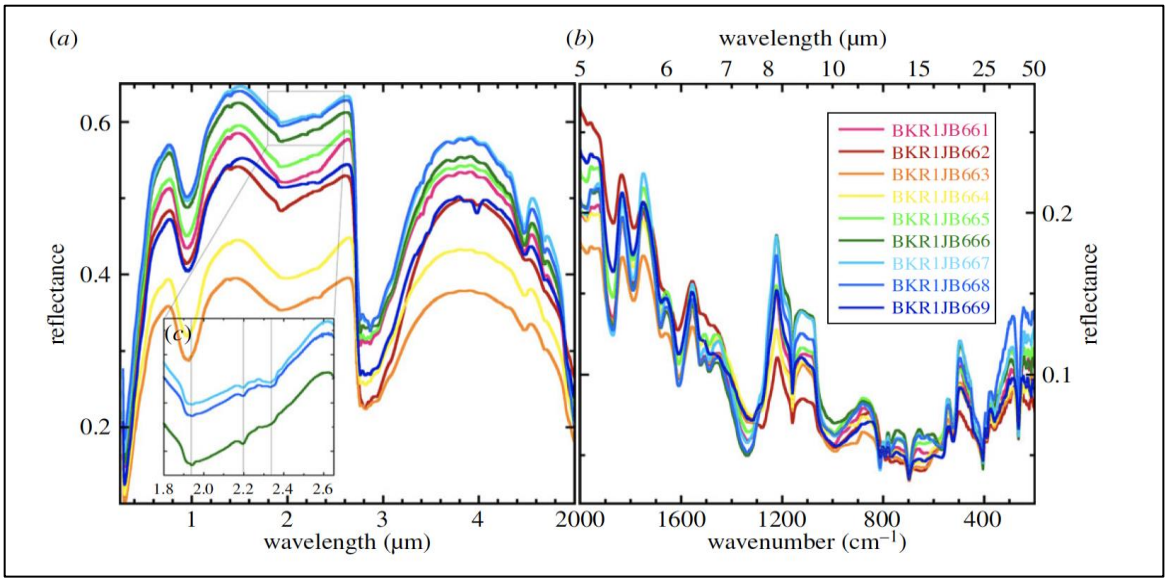

Figure 58. Reflectance spectra of the <125 μm size fraction of Lake Vanda samples. (a) VNIR spectra from 0.35 to 5 μm showing features owing to pyroxene, carbonate and aluminosilicates. (b) Mid-IR spectra from 5 to 50 μm showing features owing to quartz, feldspar, pyroxene and carbonate. (c) NIR inset from 1.8 to 2.5 μm showing a broad H_2O band centred at 1.94 μm and OH features at 2.19, 2.25 and 2.34 μm (Bishop et al., 2014).

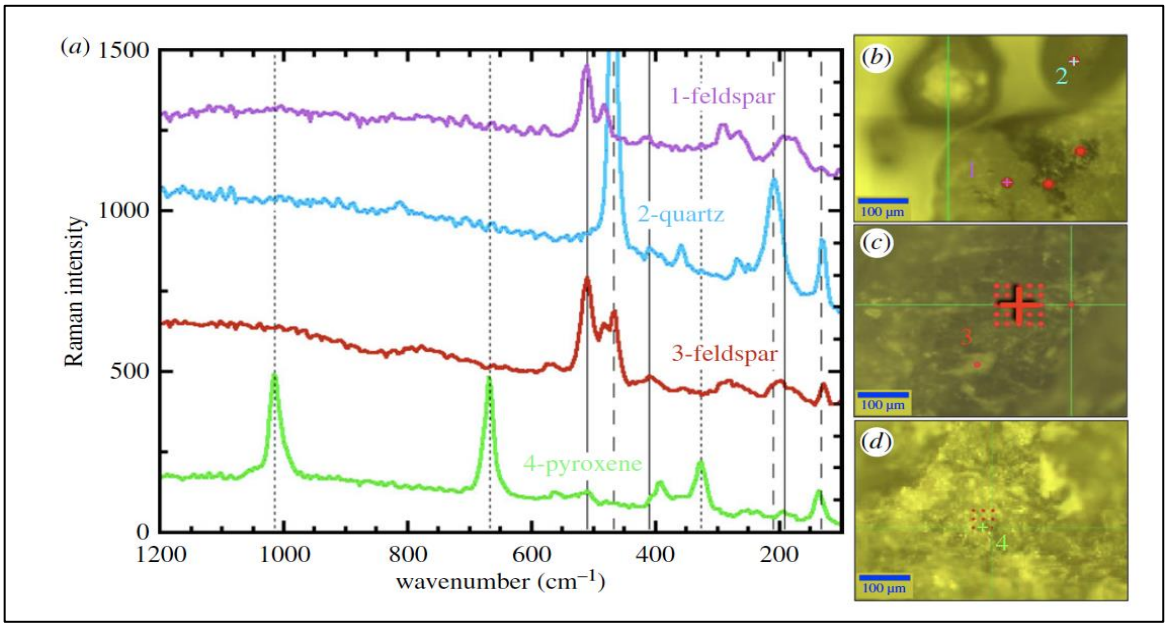

Figure 59. (a) Raman spectra of mineral grains in sample 9 from Lake Vanda (JB669), (b) image of grains 1 and 2, (c) image of grain 3, and (d) image of grain 4. Spectra are offset for clarity and lines mark key features in Raman spectra (Bishop et al., 2014).

Mineralogy was determined using data from a Terra XRD instrument, Raman spectroscopy, and visible-infrared reflectance spectra. Lake Vanda has the highest abundances of quartz and lowest of feldspar for which Raman spectra are consistent with albite and Na and Ca-rich feldspars. Quartz content in lake surface samples is higher than those on the edge, while the augite content is higher in edge samples than those on the lake surface. Spectral analysis shows VNIR spectra from 0.35 to 5 μm features owing to pyroxene, carbonate and aluminosilicates such as allophane. Allophane is an indicator of immature volcanic soils (Wada, 1987). Mid-IR spectra from 5 to 50 μm show features owing to quartz, feldspar, pyroxene and carbonate. The NIR inset from 1.8 to 2.5 μm shows a broad H_2O band centered at 1.94 μm and OH features at 2.19, 2.25 and 2.34 μm (Bishop et al., 2014).

2.4.8.3. Special Analysis: CIA

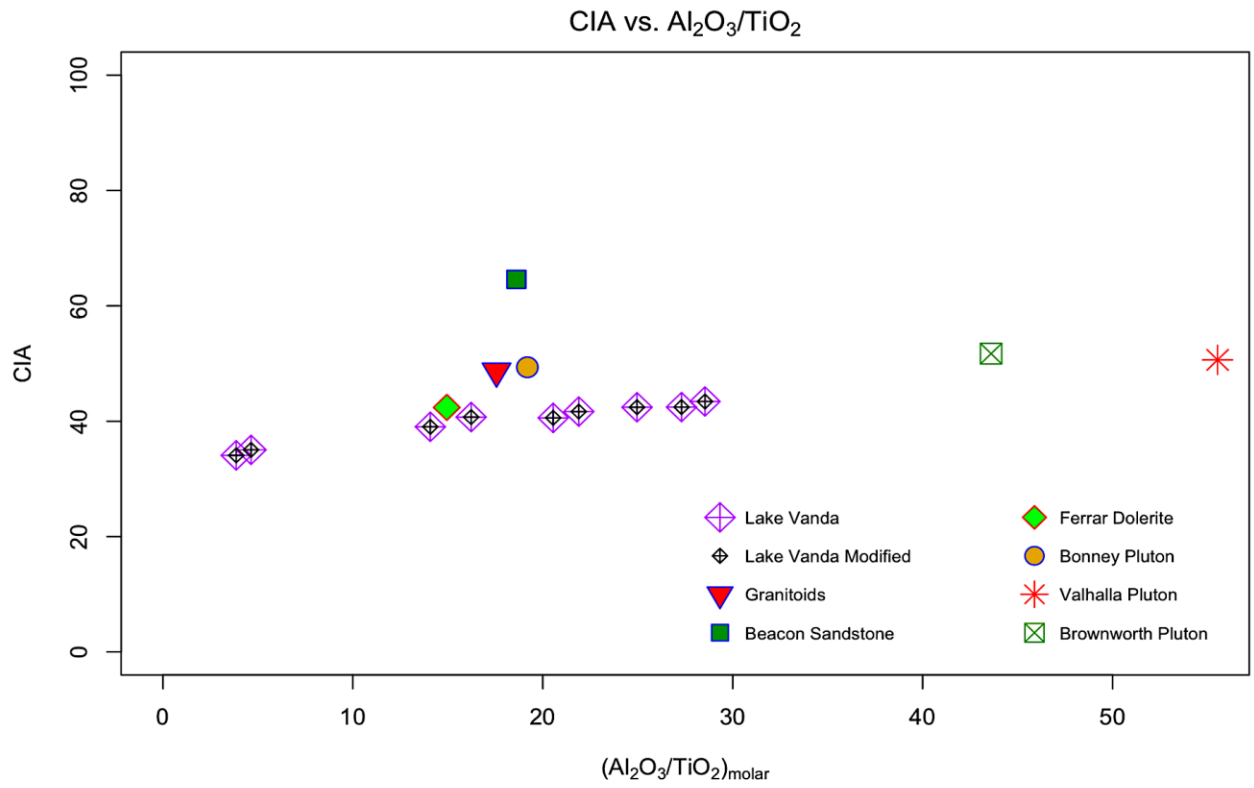

Figure 60. Lake Vanda modified and unmodified CIA values and regional source rock CIA values.

Chemical Index of Alteration values at Lake Vanda range from 34-43 at Lake Vanda which are in the range of relatively fresh basalts, per Nesbitt and Young (1982) and in line with regional geology (Peterson and Marsh, 2008). The presence of allophane corroborates this conclusion. In tandem with K/Th and Al/Ti ratios, the CIA values indicate that there is little chemical alteration on the *surface and edge* of Lake Vanda, thus suggesting the lake is dominated by physical alteration.

Analysis of modified CIA values at Lake Vanda, to account for dilution by salt, shows practically identical values to unmodified CIA values. This supports physical alteration dominance *at the surface*. Because only lake surface and edge samples were analyzed,

the picture is not complete. Analysis of sediment samples from beneath the surface, as in Lake Hoare, would provide a more comprehensive conclusion.

2.4.9. LAKE BROWNWORTH

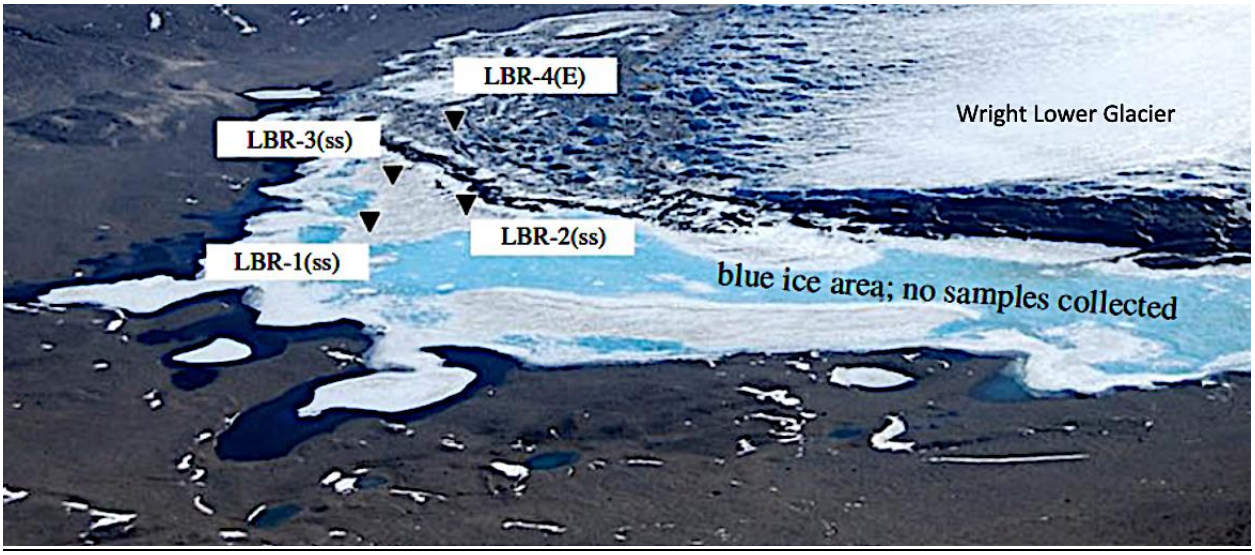

Figure 61. Lake Brownworth sample sites, Source: Bishop et al., 2014.

Lake Brownworth is located in east Wright Valley, directly west of Wright Lower Glacier, and is the site of samples JB670-673 (LBR-1 – LBR-4). JB670-672 are all sediments samples collected from surface of Lake Brownworth, and JB673 is the sole edge sediment sample. Principal summer wind directions, as reported by Nylen et al. (2004), are easterly making aeolian sedimentation from westerly sources a possibility. Samples were collected in the summer of 2004.

2.4.9.1. Elements: Major, Minor, and Rare Earth

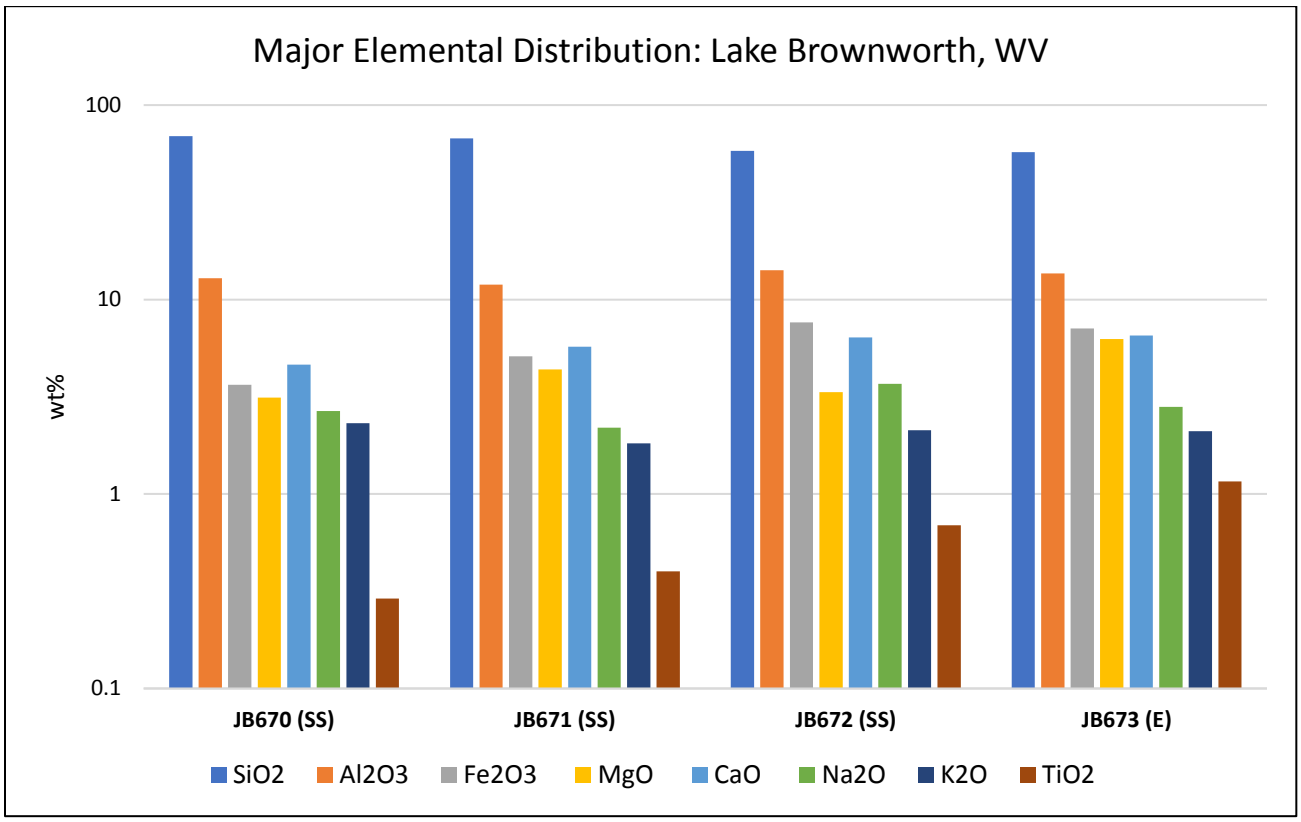

Figure 62. Major element distribution at Lake Brownworth, Wright Valley, surface and edge samples.

Major element analysis of samples at Lake Brownworth shows comparable trends and abundances for all oxides in surface samples, with the sole edge sample serving as the anomaly, exhibiting relatively high abundances of TiO_2, MgO, and Fe_2O_3. K/Th values range from 0.73 (JB670, SS) to 1.75 (JB672, SS), outside of the range of K/Th values at Core 2074 (0.61-0.67) and very different from those at Lake Vanda (0.18-0.67). Notably, Lake Brownworth has only four samples, but a large range of K/Th values.

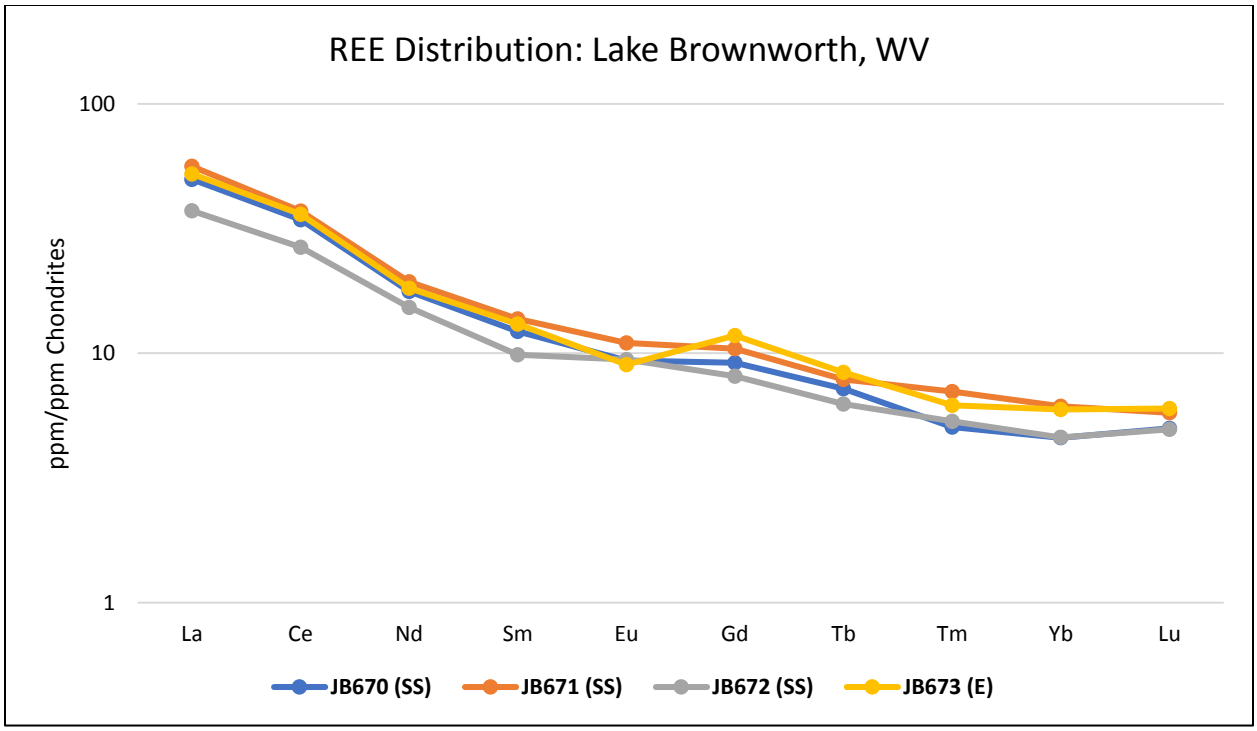

Figure 63, Rare Earth Element distribution at Lake Brownworth, Wright Valley, surface and edge samples.

Rare Earth Elements follow a similar pattern to other microenvironments but differ in abundance. All samples, except for surface sample JB672 (LBR-3), have similar REE values. JB672 exhibits notable depletions in La (37.27 ppm/ppm chondrite), Ce (26.58 ppm/ppm chondrite), and Nd (15.26 ppm/ppm Chondrite). JB672 (SS) also exhibits the lowest U (0.64 ppm) and Th (3.95 ppm) values for Lake Brownworth samples. Edge sample JB673 (LBR-4) exhibits a negative Eu anomaly that can be explained by relative Na^{+} depletion (1.61 %).

2.4.9.2. MINERALOGY: XRD, REFLECTANCE, RAMAN

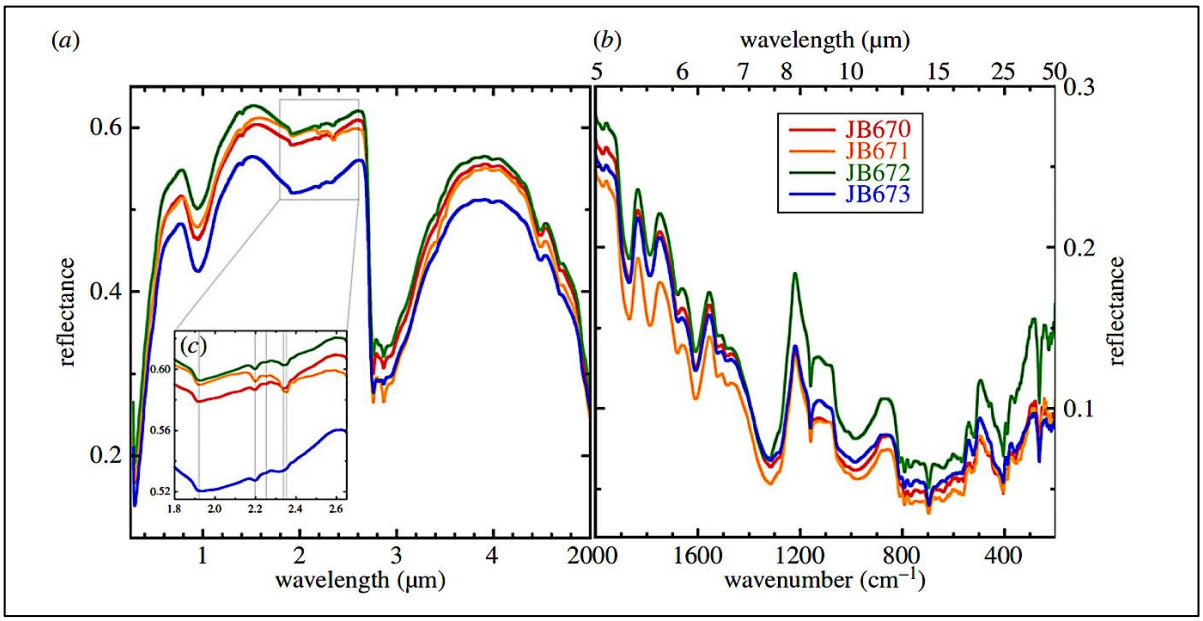

Figure 64, Reflectance spectra of the <125 μm size fraction of Lake Brownworth samples. (a) VNIR spectra from 0.35 to 5 μm showing features owing to pyroxene and aluminosilicates. (b) Mid-IR spectra from 5 to 50 μm showing features owing to quartz, feldspar and pyroxene. (c) NIR insert from 1.8 to 2.5 μm showing a very broad H_2O band centred at 1.92 μm with a shoulder extending past 2.1 μm and OH features at 2.19, 2.25 and 2.34 μm (Bishop et al., 2014).

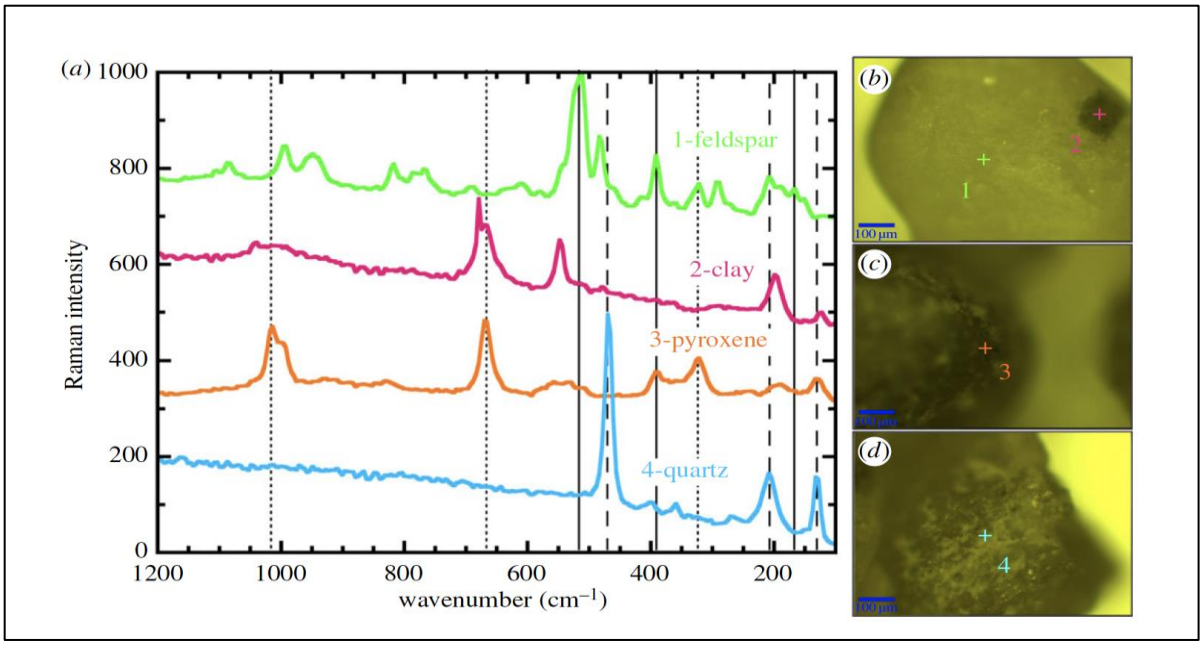

Figure 65, (a) Raman spectra of mineral grains in sample 2 from Lake Brownworth (JB671), (b) image of grains 1–2, (c) image of grain 3 and (d) image of grain 4. Spectra are offset for clarity and lines mark key features in Raman spectra (Bishop et al., 2014).

Terra XRD analysis of Lake Brownworth samples show sediments rich in albite and Na/Ca-rich feldspars. The average quartz value of these sample is lower than those of Lake Vanda, but higher than those of Lake Fryxell. The 2.34 μm band is generally owing to Fe^{2+}– OH species and is strongest in JB671 but is present in all four LBR samples. VNIR spectra from 0.35 to 5 μm show features owing to pyroxene and aluminosilicates. Mid-IR spectra from 5 to 50 μm show features owing to quartz, feldspar and pyroxene. NIR insert from 1.8 to 2.5 μm show a very broad H_2O band centered at 1.92 μm with a shoulder extending past 2.1 μm and OH features at 2.19, 2.25 and 2.34 μm. Raman spectra are consistent with minor amounts of chlorite in all LBR samples (Bishop et al., 2014).

2.4.9.3. Special Analysis: CIA

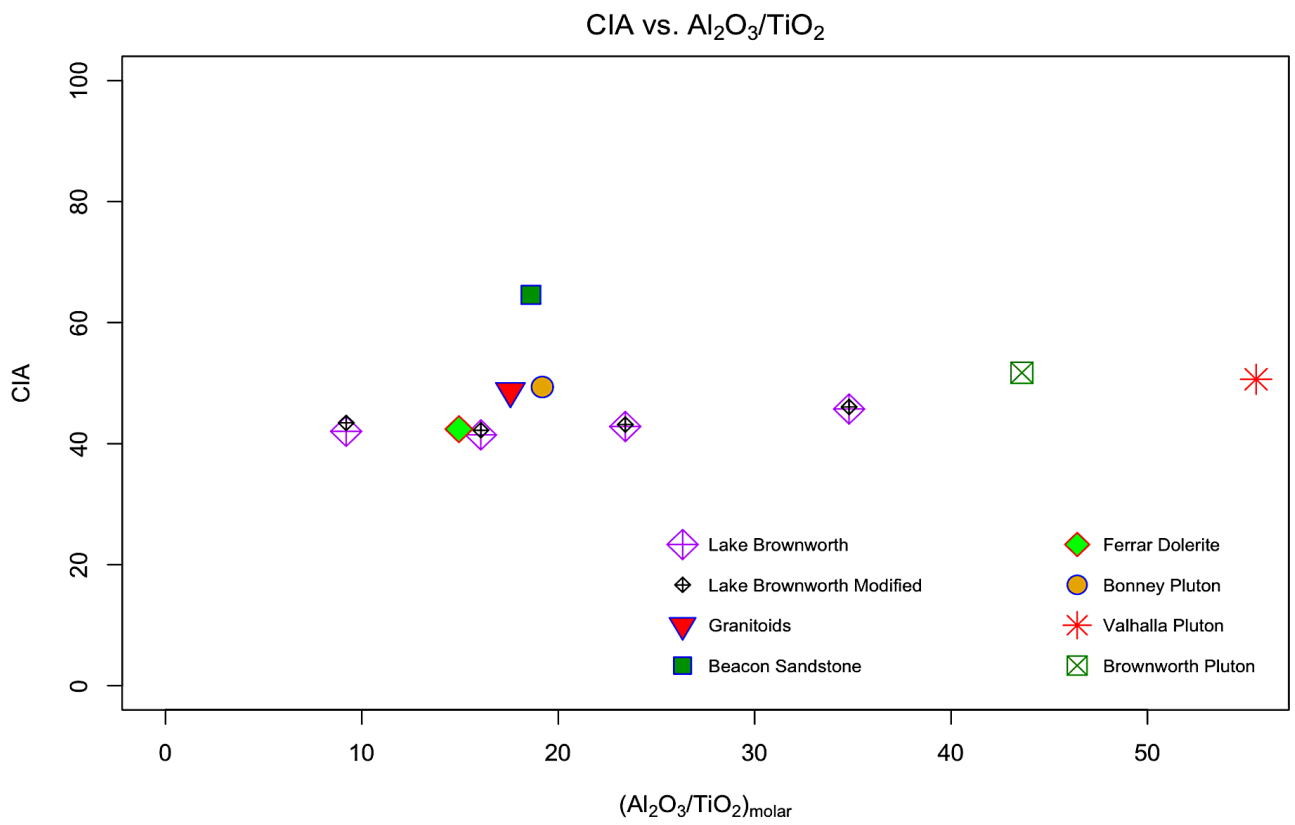

Figure 66. Lake Brownworth modified and unmodified CIA values and regional source rock CIA values.

Chemical Index of Alteration values of Lake Brownworth samples range from 41-45, in the range of fresh basalts as proposed by Nesbitt and Young, 1982, and in line with regional geology (Peterson and Marsh, 2008). In the figure above, CIA values exhibit high consistency, yet a significant $(Al_2O_3/TiO_2)_{molar}$ range. This could be due to multiple sediment sources with varying $(Al_2O_3/TiO_2)_{molar}$ values, supporting physical alteration as the dominant weathering process at the surface of Lake Brownworth.

Analysis of modified CIA values at Lake Brownworth, to account for dilution by salt, shows values practically identical to unmodified CIA values. This supports physical alteration dominance *at the surface*. Because only four lake surface and edge samples

were analyzed, the picture is not complete. Analysis of sediment samples from beneath the surface, as in Lake Hoare, would provide a more comprehensive conclusion.

2.4.10. LAKE FRYXELL

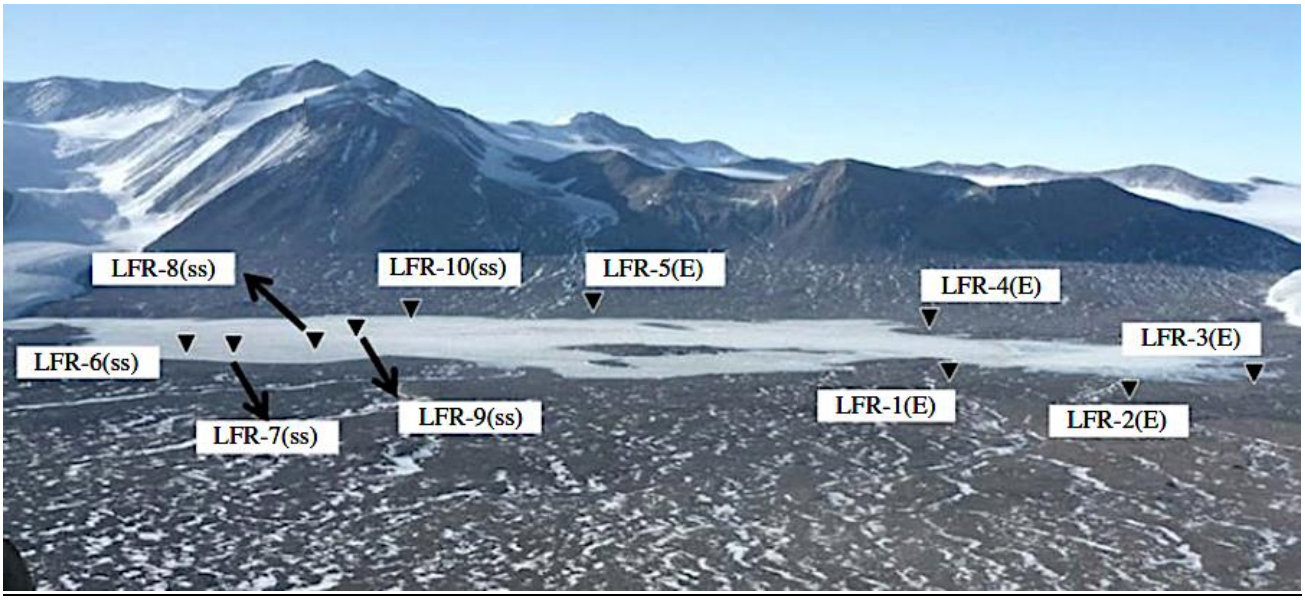

Figure 67, Lake Fryxell sample sites, Taylor Valley. Source: Bishop et al., 2014.

Lake Fryxell is located in lower Taylor Valley with Canada Glacier directly to the west and Commonwealth Glacier to the east. It is the site of samples JB650-JB660 (LFR-A – LFR-10). JB650 and JB656 – JB660 are all lake surface sediment samples. JB651 – JB655 are edge sediment samples. Samples were collected in the summer of 2004. Summer wind directions are predominantly down-valley (easterly), making aeolian sedimentation from westerly sources a possibility as well.

2.4.10.1. Elements: Major, Minor, and Rare Earth

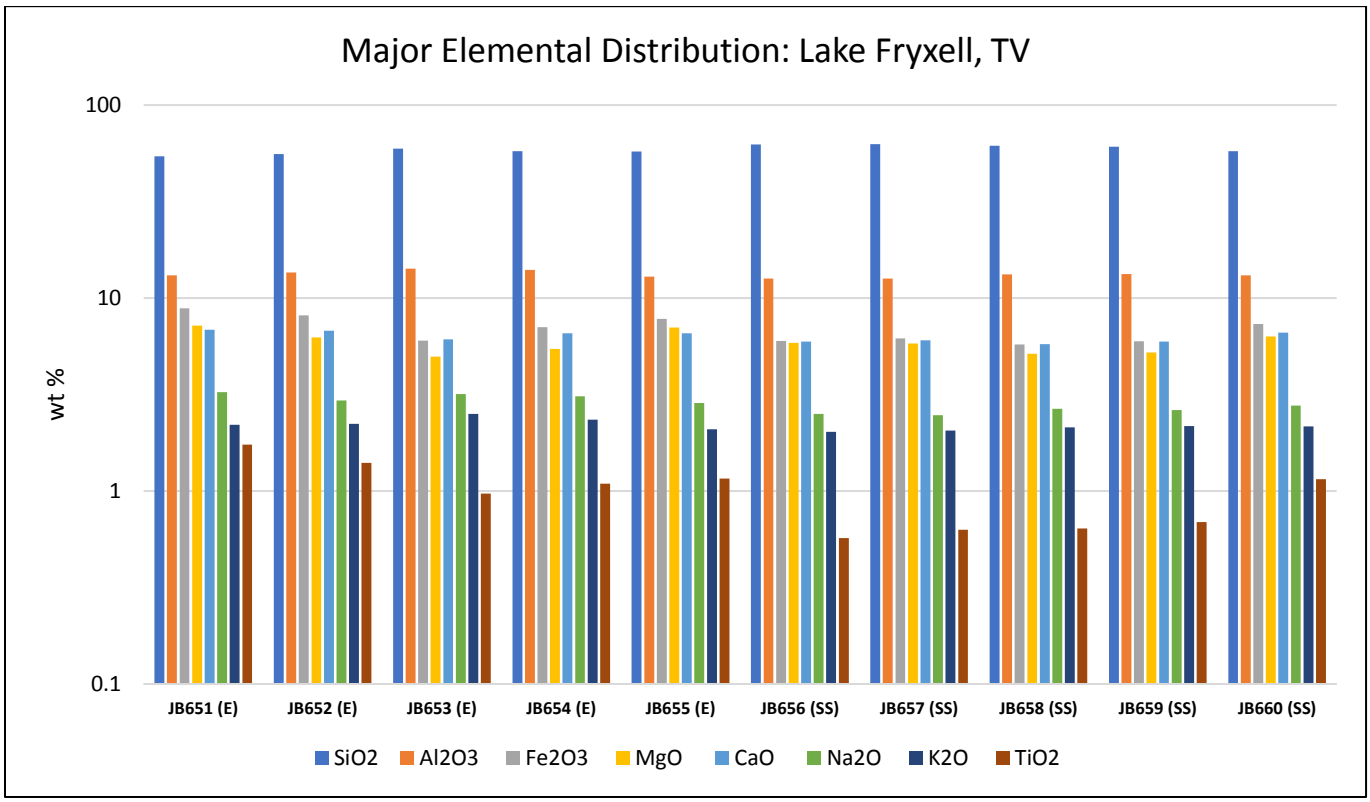

Figure 68. Major element distribution at Lake Fryxell, Taylor Valley, surface and edge samples.

Major elemental analysis of samples from Lake Fryxell show, on average, higher Na^+ and K^+ in edge than surface samples. With a greater proportion of major ions, this suggests a greater proportion of source rock remaining in edge samples. All samples are relatively enriched in TiO_2 except for surface sample JB650 (0.76 %). K/Th values range from 0.63 (JB660, SS) to 1.15 (JB656, surface sample). Only JB660 falls in the range of K/Th values of Core 2074 (0.61-0.67). K/Th values for Lake Fryxell samples exhibit higher K/Th values than Lake Vanda, but lower than Lake Brownworth.

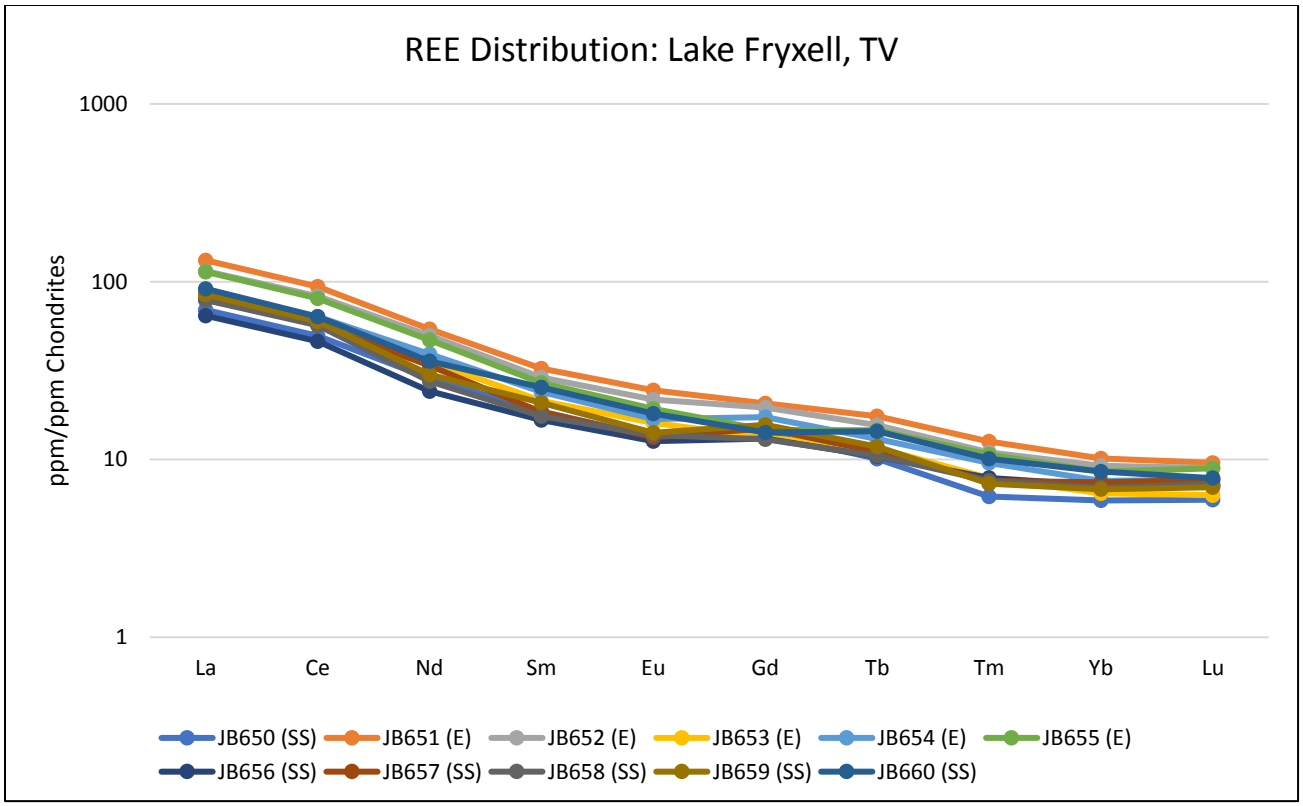

Figure 69. Rare Earth Element distribution of Lake Fryxell, Taylor Valley, surface and edge samples.

Rare Earth Element analysis shows highest REE enrichment in all edge samples as compared to surface samples. Edge samples JB651, JB652, and JB655 display relatively high abundances of La (120 ppm/ppm chondrite, avg), Ce (85 ppm/ppm chondrite, avg), Nd (50 ppm/ppm chondrite, avg), Sm (29 ppm/ppm chondrite, avg), and Eu (21 ppm/ppm chondrite, avg), while edge samples JB653 and JB654 display significantly lower abundances, particularly JB650 (all REEs). Surface samples JB657 – JB660 display relatively high abundances of La (83 ppm/ppm chondrite, avg) and Ce (59 ppm/ppm chondrite, avg), while surface sample JB656 displays significantly lower abundances.

2.4.10.2. MINERALOGY: XRD, REFLECTANCE, RAMAN

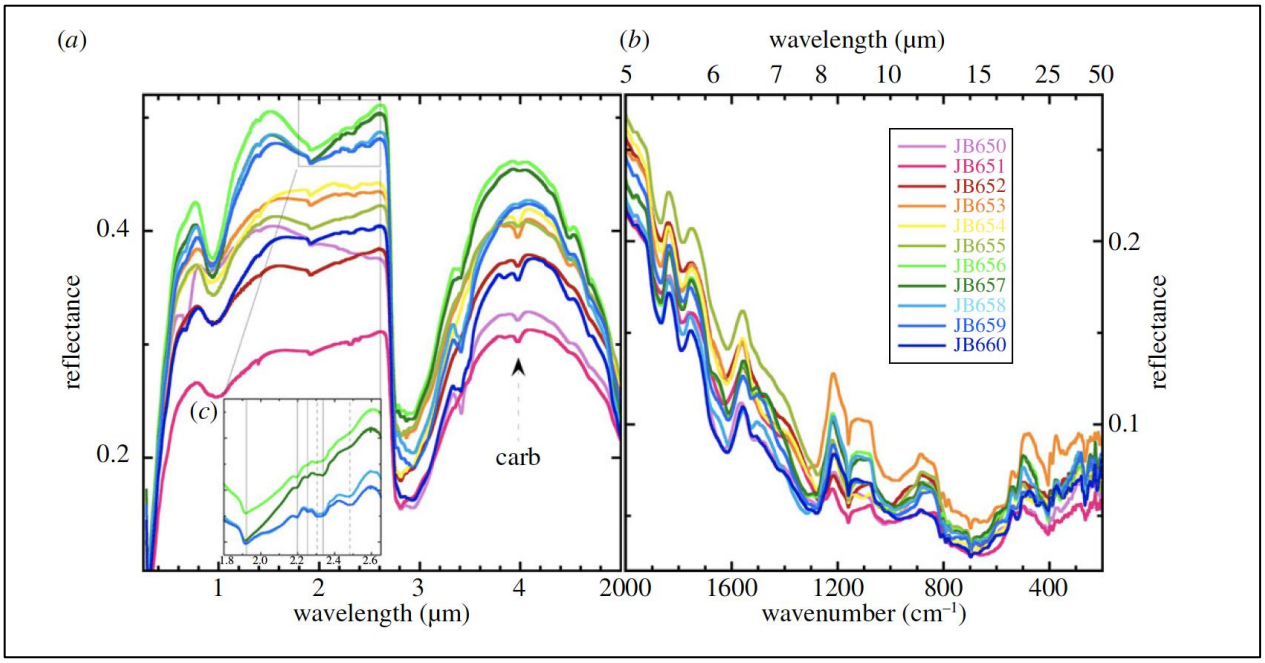

Figure 70. Reflectance spectra of the <125 μm size fraction of Lake Fryxell samples. (a) VNIR spectra from 0.35 to 5 μm showing features owing to pyroxene, carbonate and aluminosilicates. (b) Mid-IR spectra from 5 to 50 μm showing features owing to quartz, feldspar, pyroxene and carbonate. (c) NIR inset from 1.8 to 2.5 μm showing a H_2O band at 1.92 μm, OH features at 2.19, 2.25 and 2.34 μm, and carbonate bands near 2.3 and 2.5 μm (Bishop et al., 2014).

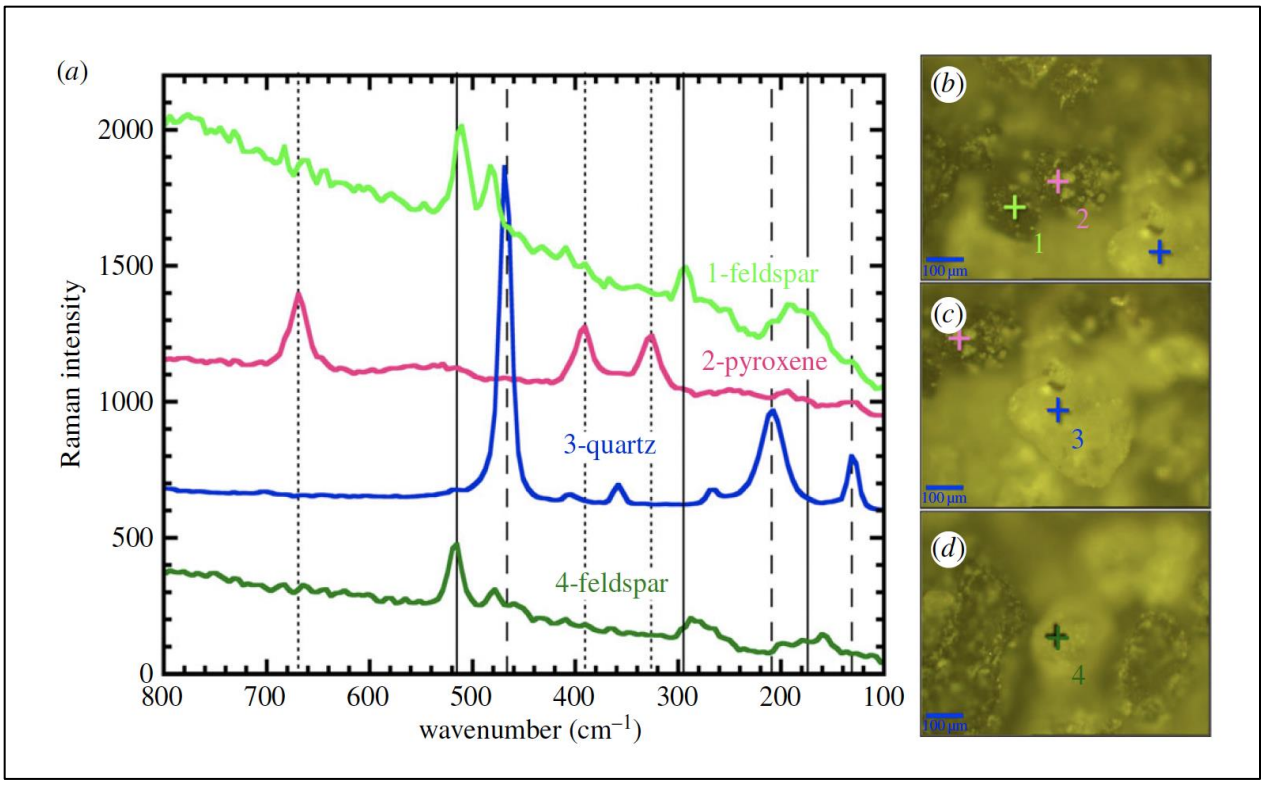

Figure 71. (a) Raman spectra of mineral grains in sample 1 from Lake Fryxell (JB651), (b) image of grains 1–3, (c) image of grains 2–3 and (d) image of grain 4. Spectra are offset for clarity and lines mark key features in Raman spectra (Bishop et al., 2014).

Terra XRD analysis shows sediments at Lake Fryxell are dominated by feldspar—namely albite—and experience the lowest quartz content of all the lakes. Samples collected at the surface of Lake Fryxell tend to have higher quartz content than those on the edge. VNIR spectra from 0.35-5 µm show features owing to Fe^{2+} – rich pyroxene, carbonate, and aluminosilicates. Mid-IR spectra from 5 to 50 µm show features owing to quartz, feldspar, Fe^{2+} – rich pyroxene and carbonate. NIR inset from 1.8-2.5 µm show an H_2O band at 1.92 µm, OH features at 2.19, 2.25 and 2.34 µm, and carbonate bands near 2.3 and 2.5 µm. Samples JB650-JB654 and JB660 exhibit spectra diagnostic of calcite. Samples JB650, and JB656-JB660 exhibit significant organic carbon components collected from the top of the lake ice. Raman spectra from grain 4 (Panel d in Figure 71, above) are consistent with trace amounts of Sanidine (K-feldspar) along with Na/Ca-rich feldspar (Bishop et al., 2014).

2.4.10.3. Special Analysis: CIA

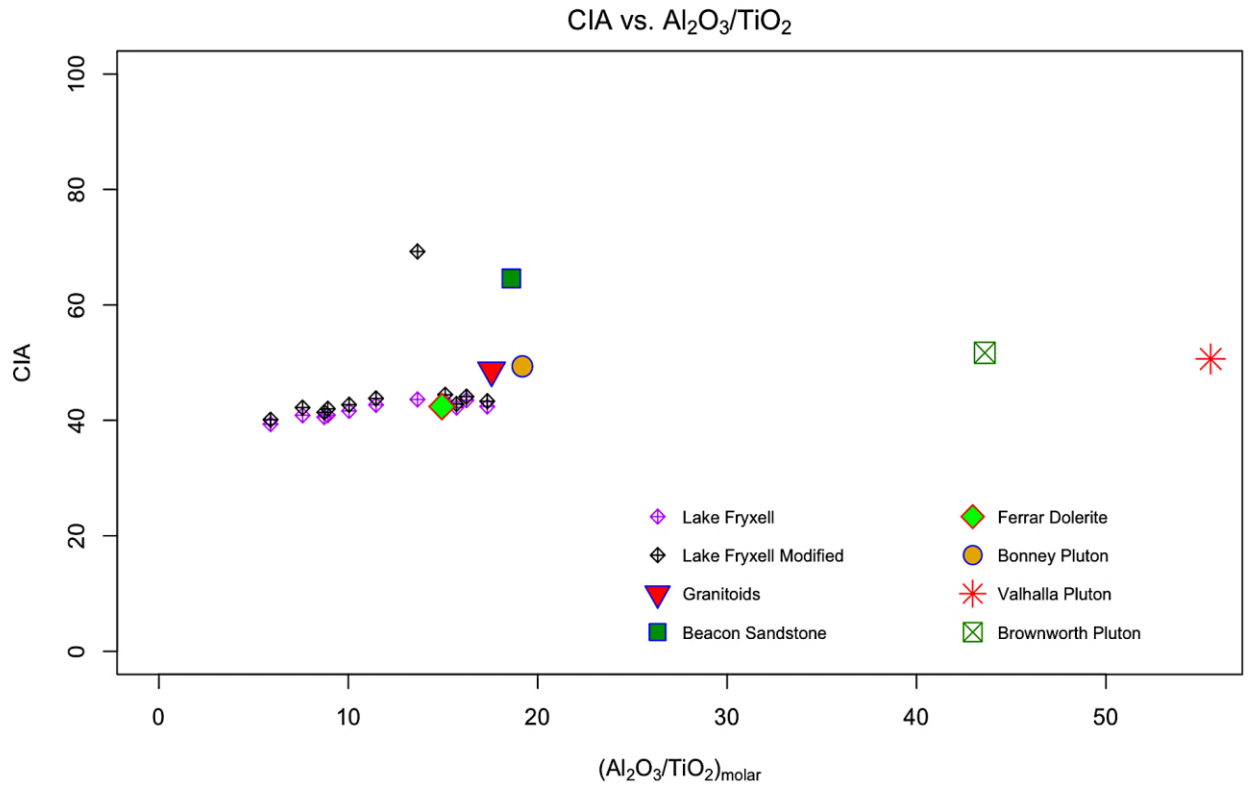

Figure 72. Lake Fryxell modified and unmodified CIA values and regional source rock CIA values.

Chemical Index of Alteration values at Lake Fryxell range from 39-43, in the range of fresh basalts, and near the range of fresh granites and granodiorites, as proposed by Nesbitt and Young (1982). In the above figure, CIA values exhibit high consistency while $(Al_2O_3/TiO_2)_{molar}$ exhibit significant variation due to a large range of TiO_2 abundances as compared to other lake and core samples. This weakens the argument for chemical alteration dominance at Lake Fryxell and strengthens physical.

Analysis of modified CIA values, to account for dilution by salt, shows similarity in all samples except for JB650 that reports a CIA value of 69, nearly in the range of charnockite (Fedo et al., 1995), a granofels that contains orthopyroxene, quartz, and feldspar. Because all other samples exhibit low CIA values and little variation, and all

samples were taken at the surface, JB650 is likely a good candidate for sediment mixing between source rocks with high levels of major elemental abundances.

Because only lake surface and edge samples were analyzed, the picture is not complete. Analysis of sediment samples from beneath the surface, as in Lake Hoare, would provide a more comprehensive conclusion.

2.4.11. Lake Hoare: Cores A-D, E, H

Taylor Valley sits to the southeast and runs approximately parallel to Wright Valley. The location of interest, microenvironments therein, is Lake Hoare, which is approximately 1 km wide and 4 km long with a maximum depth of 34 m (Nedell et al., 1987). Cores, A-D, E, and H are all located in the northeast corner of the lake.

Sediment mixing between cobbles and sand as well as summertime streamflow termination on the eastern shoreline is reported by Nedell et al. (1987). In addition, easterly aeolian sediment transport is also a likely contributing factor to sediment composition at Lake Hoare.

2.4.11.1. Core A, Elements: Major, Minor, and Rare Earth

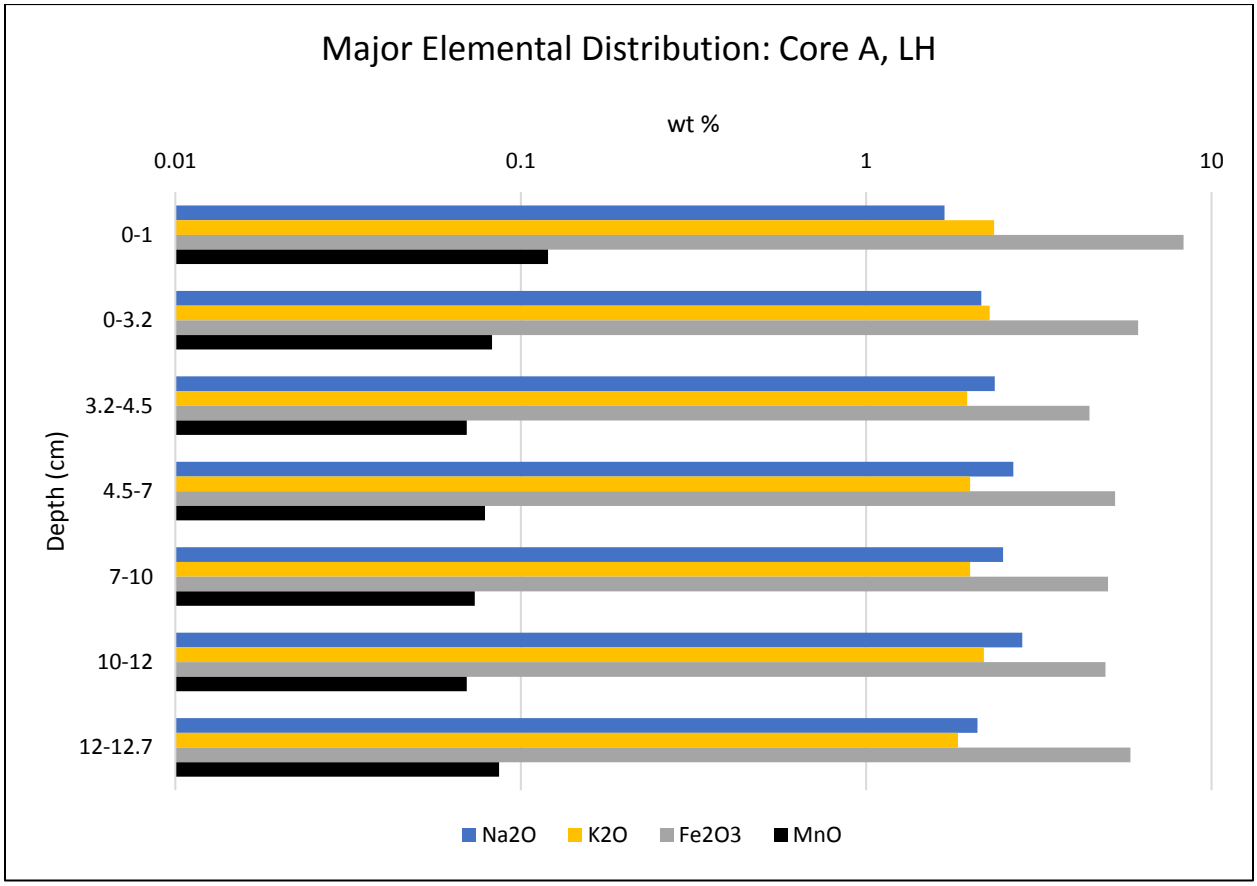

Figure 73. Major element distribution of Core A, Lake Hoare, Taylor Valley.

Major elemental analysis is limited to INAA measurements, consisting of only Na, K, Fe, and Mn, and their oxidized states, shown in the above plot. Analysis of Core A shows a relatively increasing abundance of Na with depth and decreasing K and Fe abundance with depth. Fe is the most abundant element of those that are measure, and Fe_2O_3 is the most abundant Fe-oxide. Fe is in greatest abundance (5.81 %) in A-1 (0-1 cm) and lowest abundance (3.1 %) in A-3 (3.2-4.5 cm). K/Th values range from 0.94 (A-1, 0-1 cm) to 1.84 (A-5, 7-10 cm), significantly above the K/Th values of Core 2074 (0.61-0.67) suggesting a comparatively lower degree of alteration.

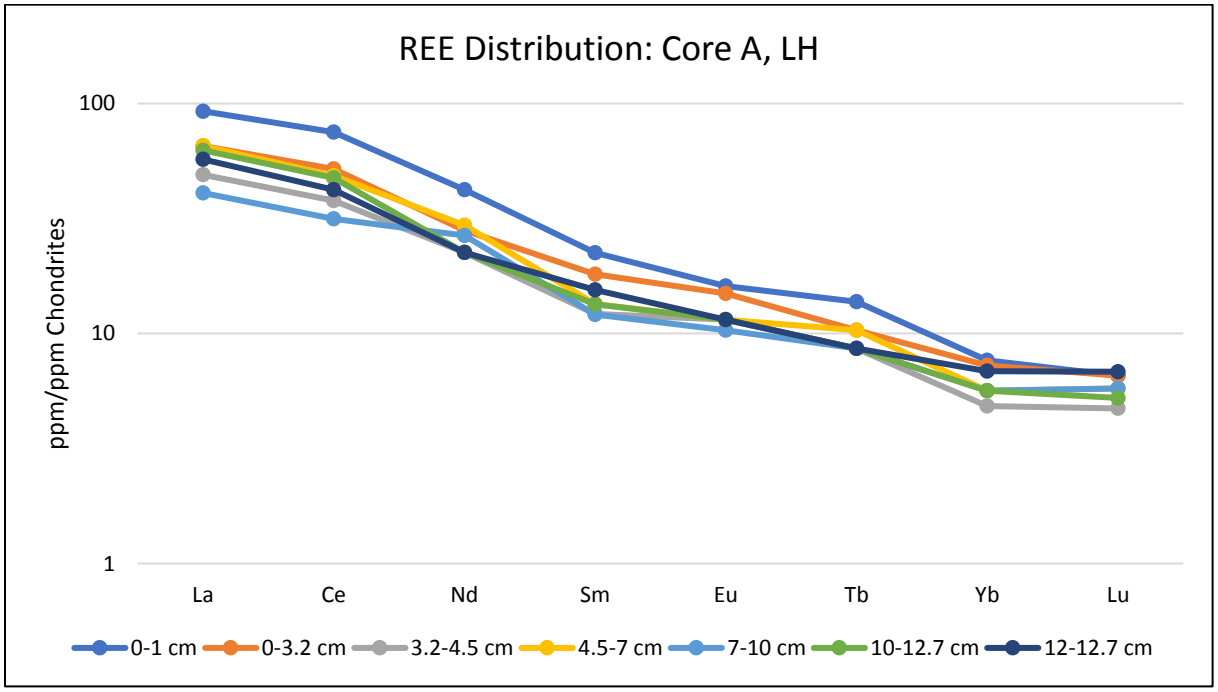

Figure 74. Rare Earth Element distribution, Core A, Lake Hoare, Taylor Valley.

Rare Earth Element analysis shows REE surface enrichment, followed by significant variability through the rest of the core. Negative Eu anomalies are not displayed. Core A is located in DH-2, the same as Core B (Bishop et al., 1996). Core B, as is discussed below, is taken to a depth of 20 cm, and exhibits a relative REE surface enrichment and a massive enrichment at 20 cm. Core A exhibits a REE surface enrichment, relative to

microenvironments, but is only taken to 12 cm depth. Because they are both from the same dive hole, and exhibit similar REE surface enrichment, it is reasonable to infer a similar enrichment feature in Core A had it been taken to the approximate depth of Core B. Continuous cycling of REEs from a leaching zone near the surface to deeper parts of soil profiles could create an enriched REE reservoir in the subsurface as is seen in Core B. Zr and Th, High Field Strength Elements, and La, are elements that can be used to measure alteration (Nesbitt and Markovics, 1997), and exhibit depletion in A-3 (3.2-4.5 cm) relative to other samples. Similarly, depleted abundances of Zr and Th are exhibited in Core B, strengthening the likelihood of like processes occurring in each core. Processes that could be responsible for these patterns could be surficial chemical alteration and subsurface physical alteration, cycling REEs downwards, or dilution from high salt abundance— Bishop et al. (1996) reports calcite in many of Core B samples, including the depth at which strongest REE depletion is exhibited in Core A. Based on the information discussed, the most likely picture for Core A is one dominated by physical alteration at the surface, manifesting as sediment mixing from glacial and aeolian transport as well as mass-wasting, with chemical alteration manifesting as the precipitation of calcite, operating on a secondary scale.

2.4.12.1. Core B, Elements: Major, Minor, and Rare Earth

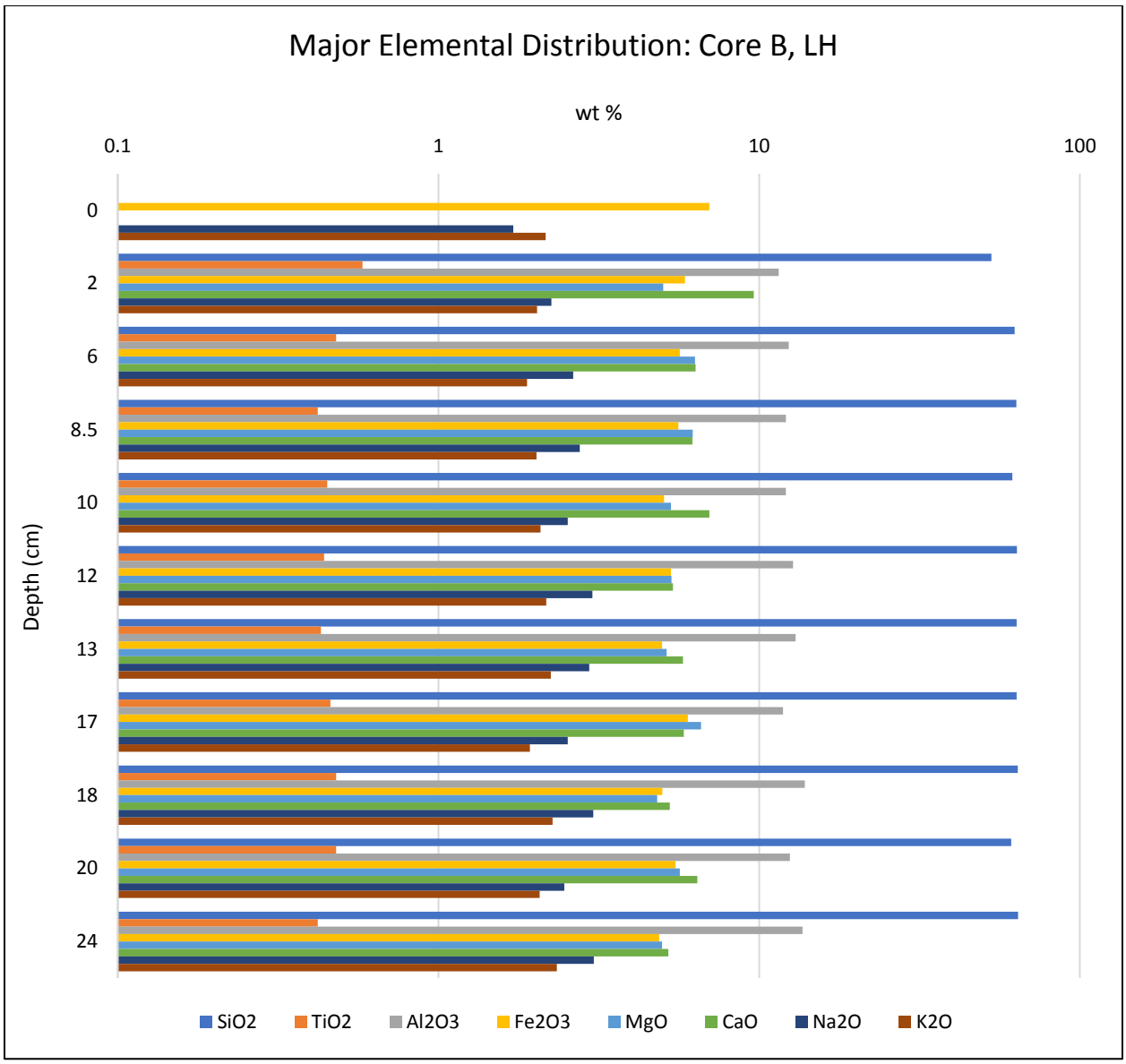

Figure 75. Major element distribution, Core B, Lake Hoare, Taylor Valley.

Major elemental analysis of Core B at Lake Hoare shows relative consistency of oxides in all samples *after* B-2a (2 cm), in which the lowest SiO_2 value (52.98 %), and highest CaO and TiO_2 values (9.63 % and 0.58 %) are exhibited. Carbon abundance is highest

(8.35 %) in B-9 (18 cm), which stands alone, while B-4 – B-6 (8.5-12 cm) exhibit the most consistently elevated abundances (6.49 – 7.3 %).

Samples relatively rich in C exhibit the lowest K/U and Th/U ratios. Variations in the abundance of Sc, Rb, Cs, Th, Sr, Zr, Hf, U, Cr, Zn, and Co are generally paralleled by the presence of organic materials and Carbonates. Organic-rich samples show relatively elevated abundances of the aforementioned elements, while Carbonate-rich samples show relatively depleted abundances. (Bishop et al., 1996).

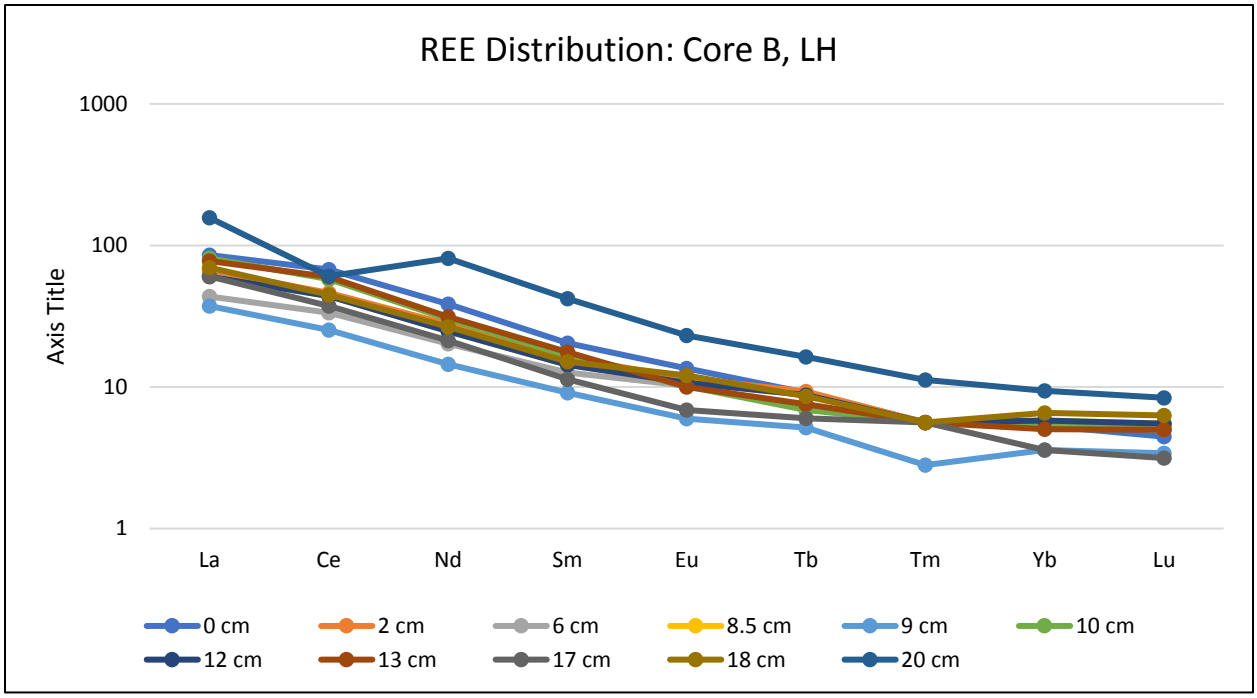

Figure 76. Rare Earth Element distribution, Core B, Lake Hoare, Taylor Valley.

Rare Earth Element analysis shows REE abundances are highest in Core B samples. Relative REE enrichment is seen in B-1a (surface) and B-2a, followed by significant variability down to B-11 (20 cm) at which point a massive enrichment in La, Nd, Sm, Eu, and Tb is seen. Continuous cycling of REEs from a leaching zone near the surface to deeper parts of soil profiles could create an enriched REE reservoir in the subsurface

(Nesbitt and Markovics, 1997). The same process is proposed for Core A. B-11 also experiences a negative Ce anomaly that could be due to oxidation to Ce (IV).

2.4.12.2. Core B, Mineralogy: XRD, Reflectance Spectra

Quantitative mineralogical measurements were not possible for Lake Hoare Cores A-D because of the small amount of sample available, the complex nature of the multicomponent sediments, and the destructive nature of XRF techniques (Bishop et al., 1996).

XRD analysis of cores A-D shows the primary composition of all sediments to consist of quartz, pyroxene, and feldspar. Both orthoclase and plagioclase forms of feldspar were identified. Many Core B samples (B-2a, 3a, 3b, 3c, 3d, 3e, 3f, 5a, 5b, and 7a) contain major abundances of carbonate. Carbonate abundances were especially notable for inorganic C, and primarily present in the form of calcite. Most samples contain secondary abundances of mica, chlorite, and amphibole. Samples B-1a, B-1, B-4, B-5, and B-10a, carbonate is also a secondary component. Low clay diffraction content of the samples made determination of clay silicates difficult. Slight amounts (less than a few vol %) of illite, smectite, and possibly vermiculite were found in many of the samples (Bishop et al., 1996). Spectra for Core B are shown and discussed below.

Spectral analysis (Figure 83, at the end of Core D) exhibits broad spectral bands near 1 and 2 µm indicating the presence of pyroxene in most samples (B-2, B-3d, B-4 to 9, B-10a, B-10, and B-11). Relatively broad features near 1.4, 1.9, and 2.5 µm are due to bound or adsorbed water, and are seen in B-1a, B-1, B-2a, B-3 (a-f), B-5a, B-5b, and B-7a. B-1 exhibits a narrow spectral feature near 0.7µm that is due to pigmenting agents such as chlorophyll and carotene in organic materials. Spectral features near 3.5 µm are consistent with carbonates and organic components, and are observed strongly in B-1a, B-3 (a-f), B-5a, B-5b, B-7a, and B-10a. Very strong carbonate features are observed in B-3 (a-d, f), B-5a, B-5b, B-7a, and B-10a. The carbonate features suggest the presence of calcite in many samples, including B-1a, B-2a, B-2, B-3 (all), B-5a, B-5b, B-5, B-7a, and B-

7 (Bishop et al., 1996). The presence of carbonate and calcite supports the case for chemical alteration near the surface.

2.4.12.3. Core B, Special Analysis: CIA

Chemical Index of Alteration values for Core B at Lake Hoare range from 32-44, in the range of fresh basalts, and nearly in the range of fresh granites and granodiorites as proposed by Nesbitt and Young, 1982. The lowest value, 32, is seen in B-2a (top 2 cm) which also exhibits the highest CaO abundance (9.63 %) — likely the reason for the low CIA value, and a case for a dilution effect from high salt abundance.

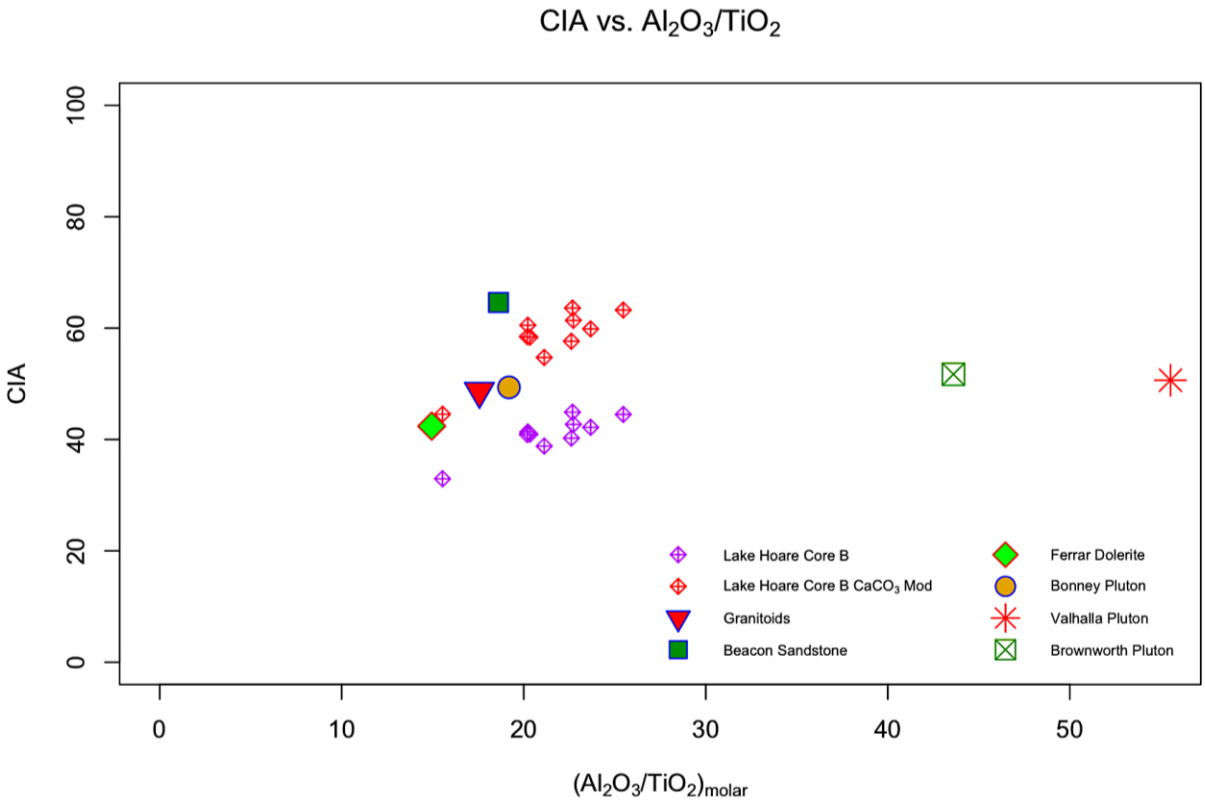

Figure 77. Modified and unmodified CIA values of Core B, Lake Hoare, and regional source rock CIA values.

With B-2a (CIA of 32) set apart as an anomaly, the CIA range is 38-44 (as seen above) and is suggestive of minimal chemical alteration. The likely picture is one of surficial

chemical weathering combined with surficial and subsurface physical alteration that manifests as sediment mixing between source rocks, and freeze-thaw processes.

Analysis of modified CIA values, to account for dilution by calcite, reports a new range of 44-63, at the high end of fresh basalt and well in the range of fresh granites and A-type granites (Nesbitt and Young, 1982; Fedo et al., 1995). Adjusted for calcite dilution, the new range, except for B-2a, is limited and averages 60— approximately 20 points higher than the unmodified CIA average (40). The new range favors subsurface chemical alteration manifesting as calcite precipitation. The values are still low enough, though, that physical alteration likely plays a significant role.

2.4.13.1. Core C, Elements: Major, Minor, and Rare Earth

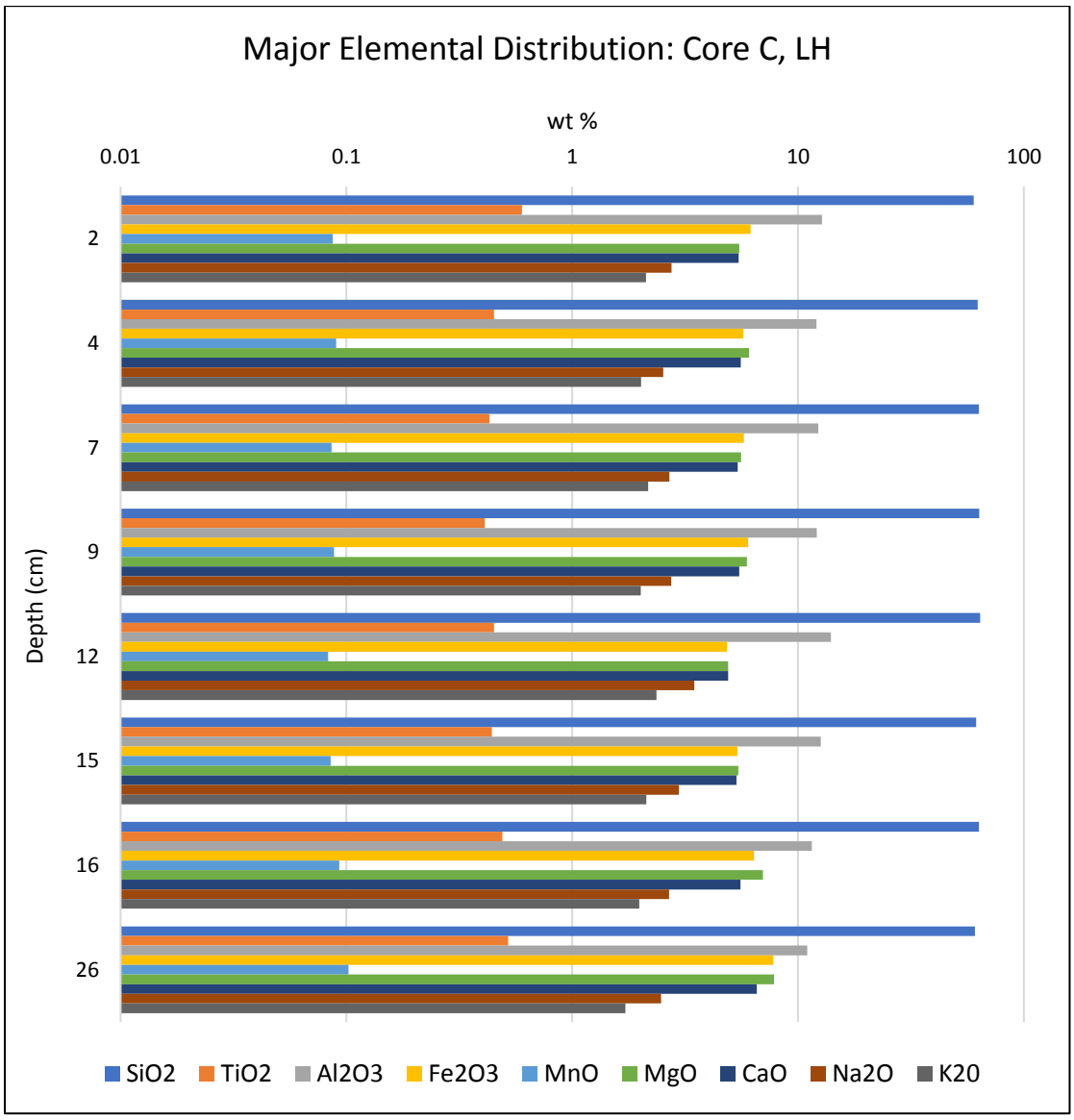

Figure 78. Major element distribution, Core C, Lake Hoare, Taylor Valley.

Major elemental analysis for Core C at Lake Hoare shows little variation across all samples. The lowest SiO_2 value (59.99 %) is reported in C-1 (1-2 cm) and the highest (63.96) in C-5 (11-12 cm). C-10 (24-26 cm) exhibits the highest Cr (289 ppm) and MgO (7.82 %) abundances while C-5 has the lowest of both elements (161 ppm, 4.9 %). C-5

also exhibits the highest Al_2O_3 abundance (14 %), and lowest Fe_2O_3 and CaO abundances (4.84 % and 4.9 %).

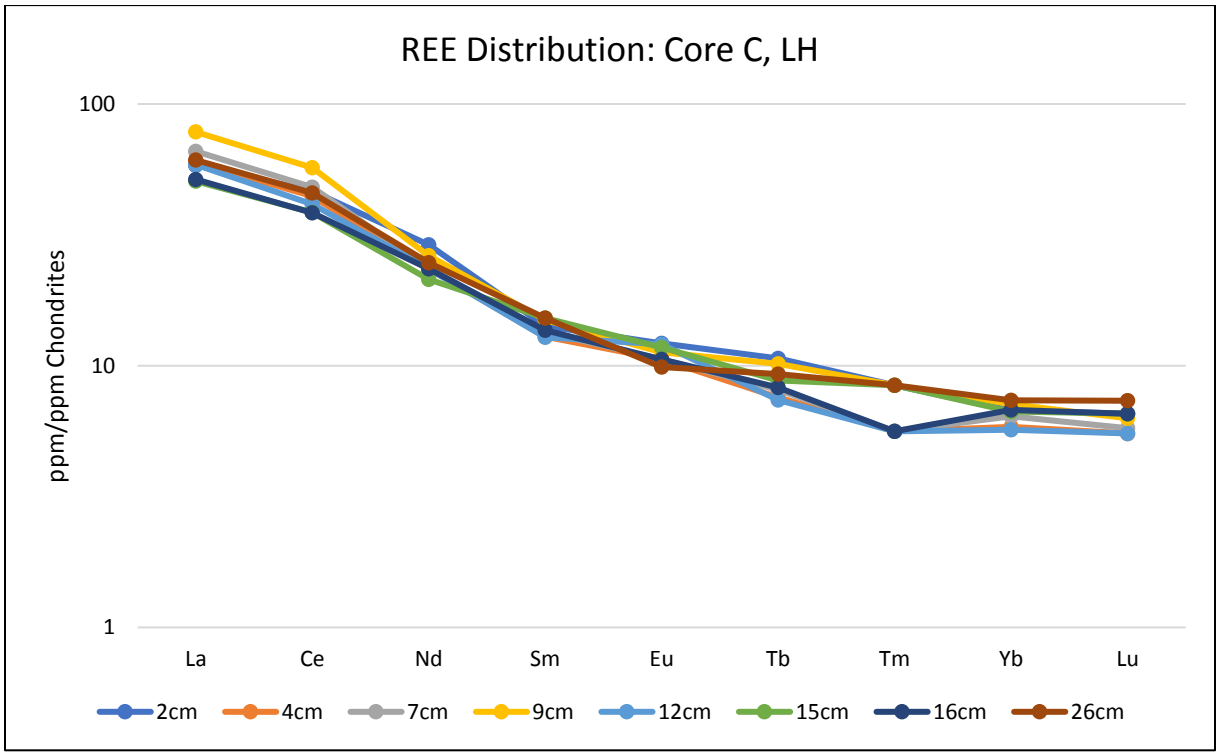

Figure 79. Rare Rarth Element distribution, Core C, Lake Hoare, Taylor Valley.

Rare Earth Elemental analysis shows REE enrichment in C-4b (8-9 cm) of La (78 ppm/ppm chondrite) and Ce (57 ppm/ppm chondrite). C-6c (14-15 cm) exhibits the lowest abundances of La (50 ppm/ppm chondrite) and Ce (38 ppm/ppm chondrite). C-5, for which MgO, MnO, and Fe_2O_3 is lowest but major ions, Na and K, is highest, also exhibits the lowest Sc, Cr, and Th abundances.

2.4.13.2. Core C, Mineralogy: XRD, Spectra

Refer to 2.4.12.2 for Core C XRD analysis.

Spectral analysis for Core C (Figure 83, at the end of Core D) shows the presence of pyroxene and structural OH, characteristic of clays and other aluminosilicates, in all samples. Pigmenting agents such as chlorophyll and carotene are measured in C-1, C-2c, and C-6c. The Christiansen feature in the spectra is consistent with the presence of quartz and feldspar. Quartz is spectrally dominant in samples C-2c, C-3, C-4b, C-7a, and C-10. feldspar is spectrally dominant in C-1, C-5, and C-6c (Bishop et al., 1996).

Core 42, from VXB, exhibits allophane, a poorly crystalline proto-clay, in the range of 4-7 cm, and is seen in tandem with REE enrichment. Chemical alteration is inferred to be occurring in this range by Burton et al., 2019. Characteristics of clays are seen in all samples of Core C from Lake Hoare, and REE-enrichment is seen in the range of 6-9 cm. It is possible then that a case similar to that of Core 42 is true for Core C.

2.4.13.3. Core C, Special Analysis: CIA

Chemical Index of Alteration values for Core C at Lake Hoare (Figure 82, below) range from 38-45, on the far end of the fresh basalt spectrum and approaching fresh granites and granodiorites (Nesbitt and Young, 1982).

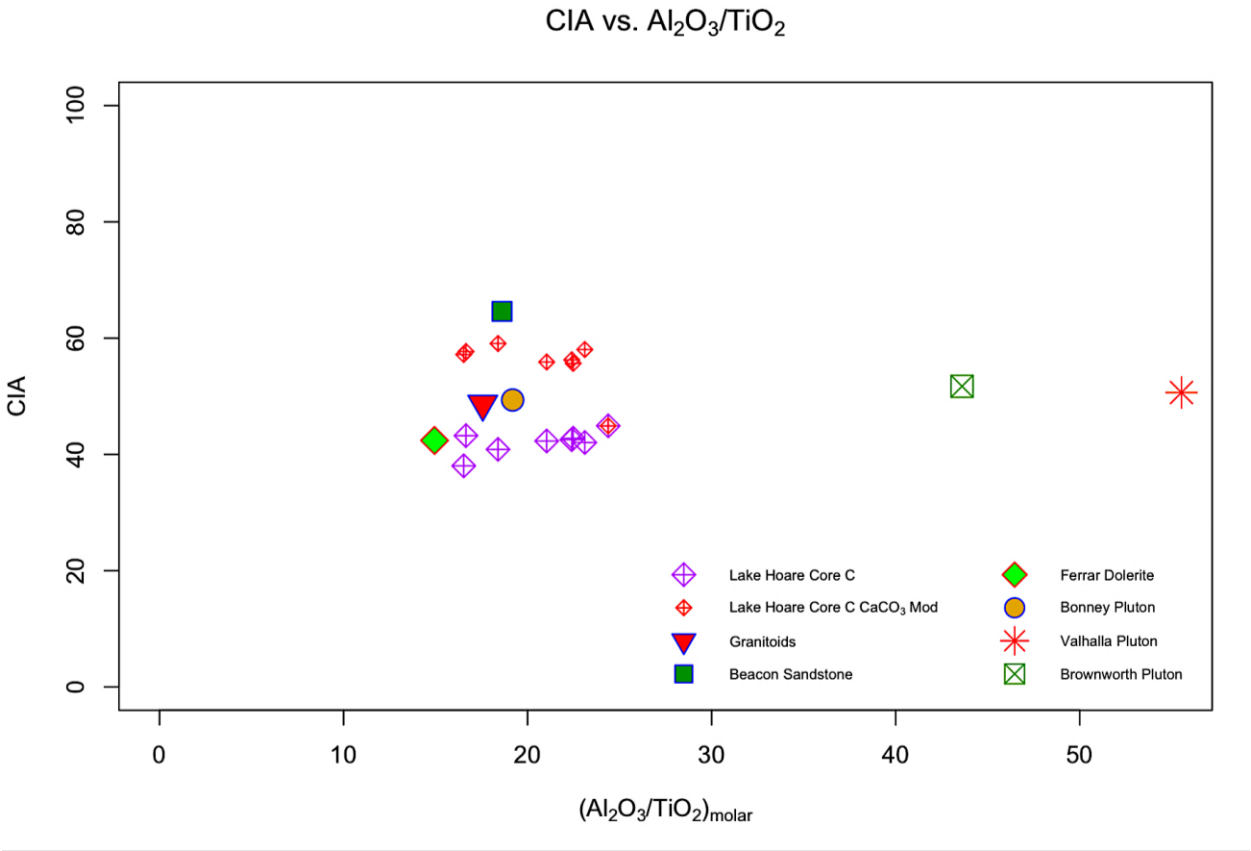

Figure 80. Modified and unmodified CIA vaues of Core C, Lake Hoare, and regional source rock CIA values.

Analysis of modified CIA values, to account for dilution by calcite, reports a new range of 44 – 59, at the high end of fresh basalts and well into the range of fresh granites and granodiorites (Nesbitt and Young, 1982; Fedo et al., 1995). Adjusted, the new range is limited and averages 55— approximately 13 points higher than the unmodified CIA average (42).

Based on information discussed, Core C is likely evenly subject to chemical alteration and physical alteration, manifesting as calcite precipitation and aluminosilicate clays, and sediment-mixing from local source rocks.

2.4.14.1. Core D, Elements: Major, Minor, and Rare Earth

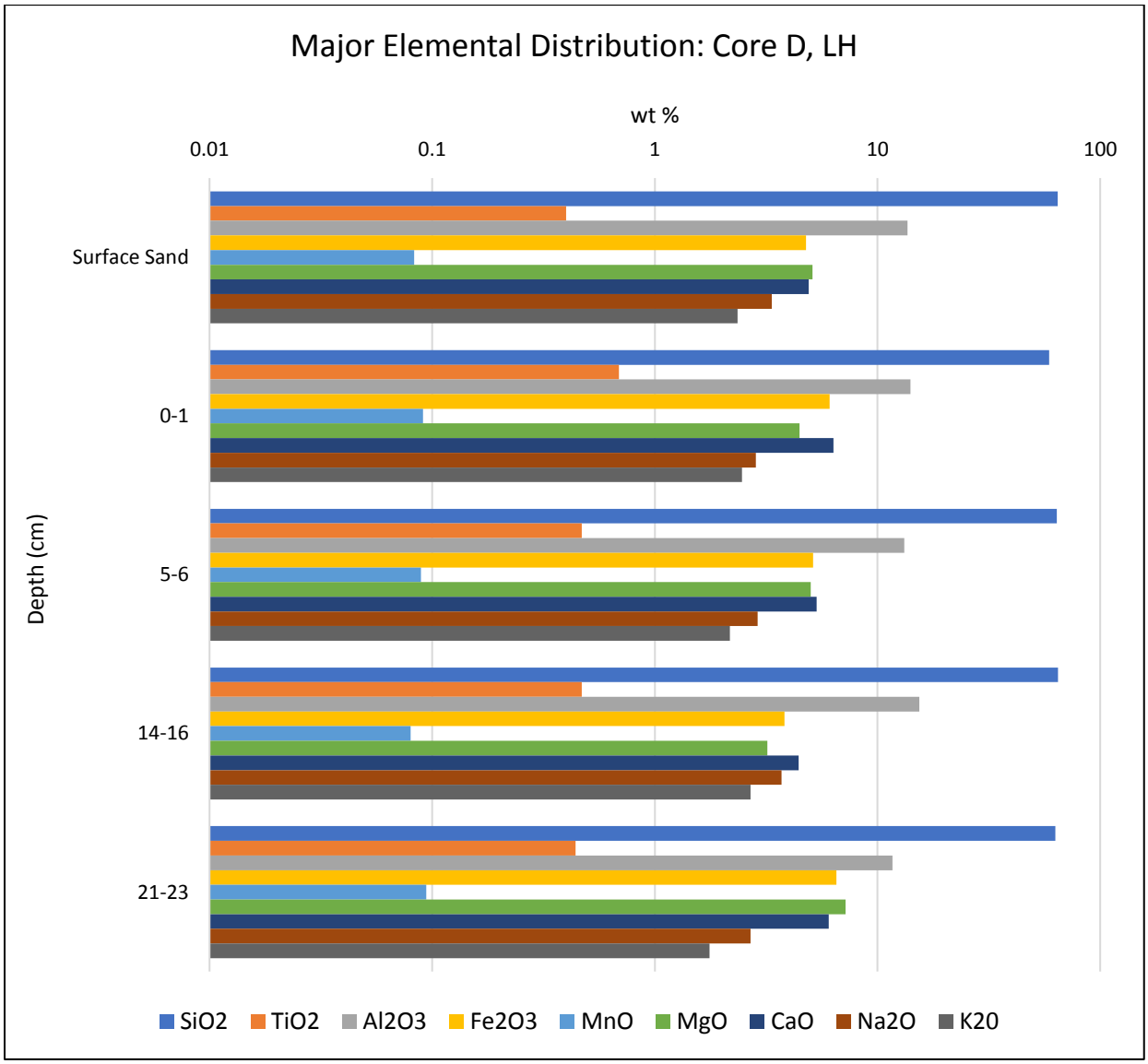

Figure 81. Major element distribution of Core D, Lake Hoare, Taylor Valley.

Major elemental analysis of Core D shows limited variation. Notable exceptions are in D-1 (0-1 cm), including the highest measured TiO_2 (0.69 %) and CaO (6.34 %) abundances, and the lowest SiO_2 abundance (59 %). The highest SiO_2 abundance (64.58 %) is in D-4 (14-16 cm). The high abundance of CaO near the surface could be due to surface salts which could suggest chemical alteration processes. D-4 also exhibits the highest abundances of Na_2O (3.71 %), K_2O (2.69 %), and Al_2O_3 (15.39 %). Core D displays a similar pattern to Core C in that D-5 (21-23 cm) has the highest Cr and Mg abundances, while D-4 (14-16 cm) has the lowest. Elevated abundances of Cr and Mg suggests an increased pyroxene content in these samples (Bishop et al., 1996).

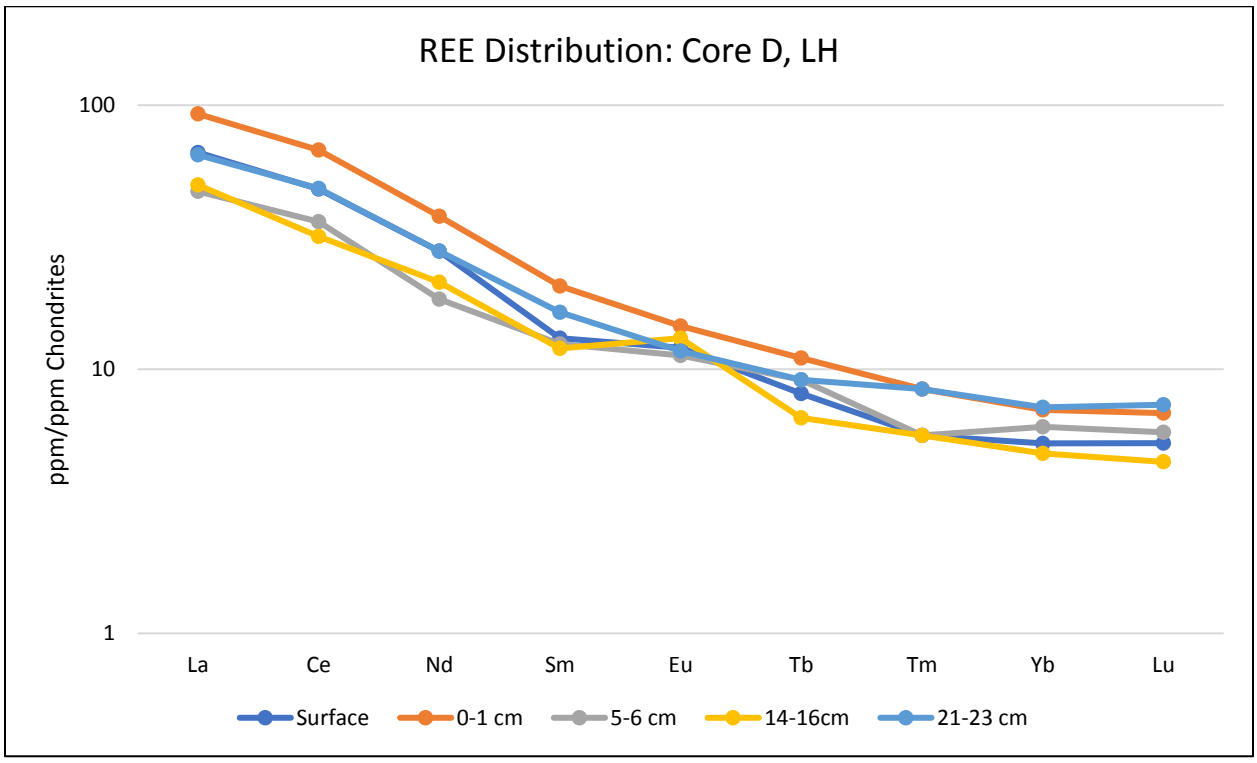

Figure 82. Rare Earth Element distribution, Core D, Lake Hoare, Taylor Valley.

Rare Earth Element analysis shows significant variation across Core D. D-1 (0-1 cm) exhibits the highest relative abundances of La (92 ppm/ppm chondrite), Ce (67 ppm/ppm chondrite), Nd (38 ppm/ppm chondrite), and Sm (20 ppm/ppm chondrite).

D-4 (14-16 cm) exhibits a positive Eu anomaly. Eu anomalies typically parallel CaO and Na_2O enrichments/depletions, occasionally as a result of plagioclase weathering (Nyakairu and Koeberl, 2001), and D-4 experiences an enrichment in Na_2O (3.71 %).

2.4.14.2. Core D, Mineralogy: XRD, Reflectance Spectra

Refer to 2.4.12.2 for Core D XRD analysis.

Spectral analysis of Core D (Figure 83, below) shows a strong presence of pyroxene in D-5 (21-23 cm), and a weak presence of pigmenting agents such as chlorophyll and carotene in D-1 (0-1 cm). D-1, D-2 (5-6 cm), and D-4 exhibit relatively broad features due to bound or adsorbed water that are characteristic of aluminosilicates. Confirming this, all Core D samples exhibit spectral features characteristic of structural OH found in clays. The relatively strong Christiansen feature seen in D-1, D-2, and D-3 is diagnostic of quartz, while the feature seen in D-4 is diagnostic of feldspar (Bishop et al., 1996).

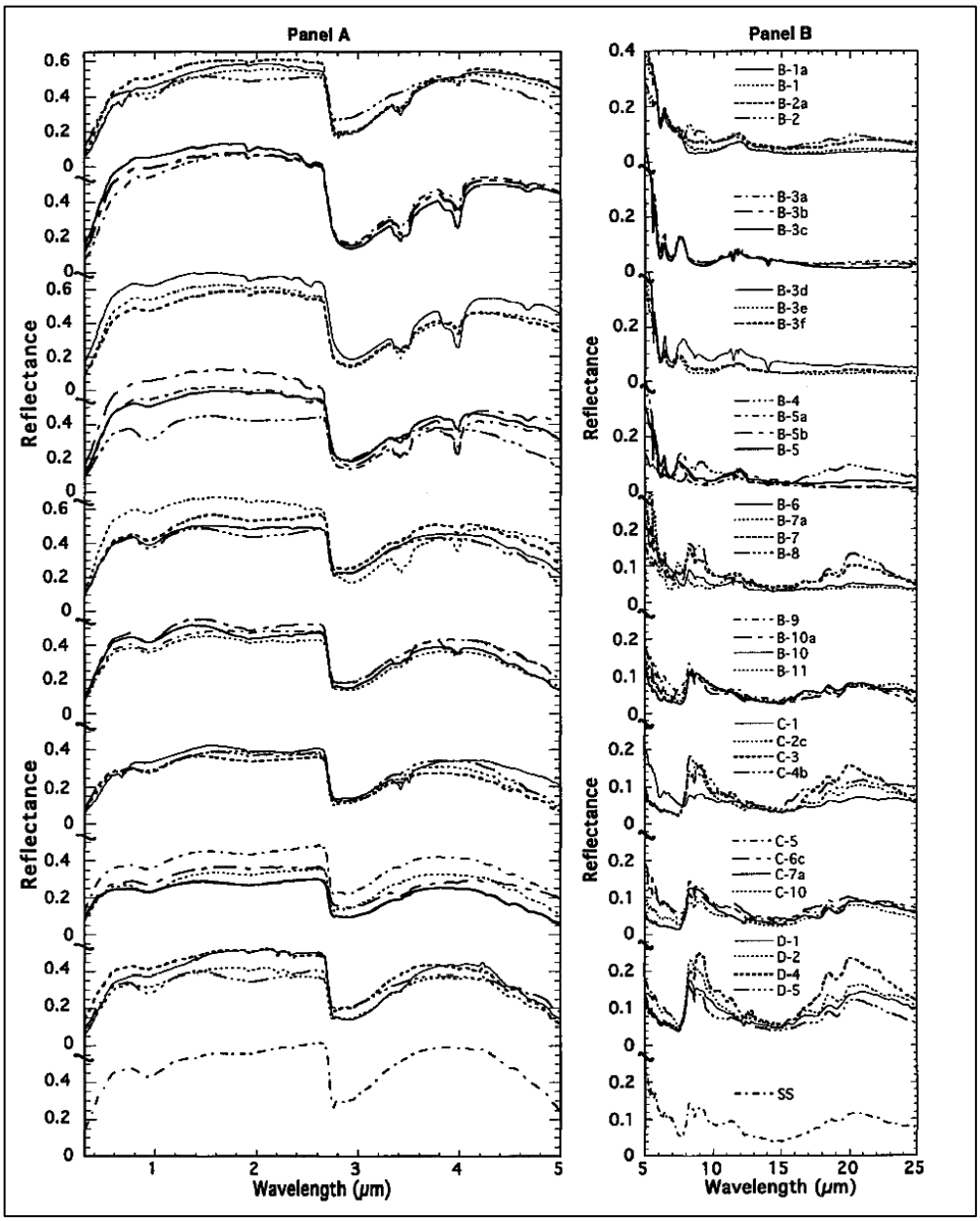

Figure 83. Reflectance spectra from 0.3 to 25 μm for Lake Hoare samples from cores B, C, and D ground to approx. <125 μm particle size. The spectra are offset in groups and labeled in Panel B. This figure is subdivided to allow better illustration of the spectra: Panel A includes spectra in the range of 0.3-5 μm and Panel B includes spectra in the range 5-25 μm. These reflectance values were measured relative to Halon and corrected to give absolute reflectance (Bishop et al., 1996).

2.4.14.3. CORE D, SPECIAL ANALYSIS: CIA

Chemical Index of Alteration values for Core D at Lake Hoare range from 40-47, on the far end of the fresh basalt spectrum and in the range of fresh granites and granodiorites

(Nesbitt and Young, 1982). The highest CIA value, 47, is exhibited in D-4 (14-16 cm), while the lowest CIA value, 40, is exhibited in D-5 (21-23 cm). The presence of aluminosilicates in D-4 paired with the highest-reported CIA value could be reason to believe a horizon of active alteration exists in the 14-16 cm range, as in Core 42 at VXB. However, as *is seen* in Core 42, D-4 does not exhibit elemental enrichment in this depth range.

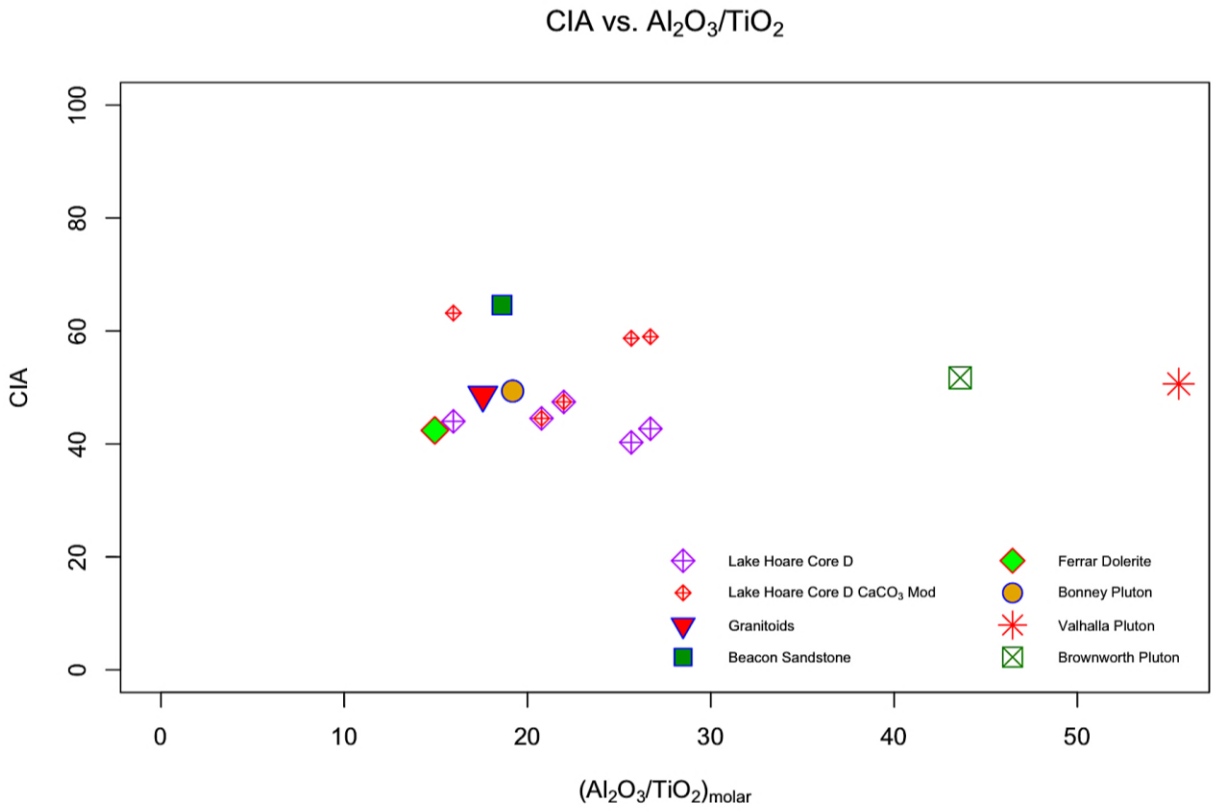

Figure 84. Modified and unmodified CIA values of Core D, Lake Hoare, and regional source rock CIA values.

Core D is located both closest to the shoreline, for which coarse and poorly sorted material is reported, and near the east end of the lake, for which sand, believed to be of aeolian origin, is reported. Termination of an intermittent stream just north (~130 m), and another to the east (~190 m), of the sample site (Nedell et al., 1987) supports

the sediment-mixing theory. With this in mind, Core D could be the best example of sediment mixing at Lake Hoare.

Analysis of modified CIA values, to account for dilution by calcite, reports a new range of 44-63, at the high end of fresh basalts and into the range of A-type granites (Nesbitt and Young, 1982; Fedo et al., 1995). Adjusted, the new range is not limited, showing relative variation from sample to sample and averaging 54. This is 11 points higher than the unmodified CIA average (44) and is the lowest reported difference between modified and unmodified average CIA values. Additionally, 54 is the lowest average modified CIA value among the Lake Hoare cores. Core D reports the lowest C % of Lake Hoare cores and no prominent spectral bands diagnostic of carbonates but does report strong spectral bands diagnostic of aluminosilicates.

Based on location, it is likely that Core D at Lake Hoare is experiencing sediment-mixing, however, relatively high CIA values corresponding to the samples with aluminosilicates support chemical alteration. It is therefore likely that Core D at Lake Hoare is evenly subject to physical and chemical alteration.

2.4.15.1. Core E, Elements: Major

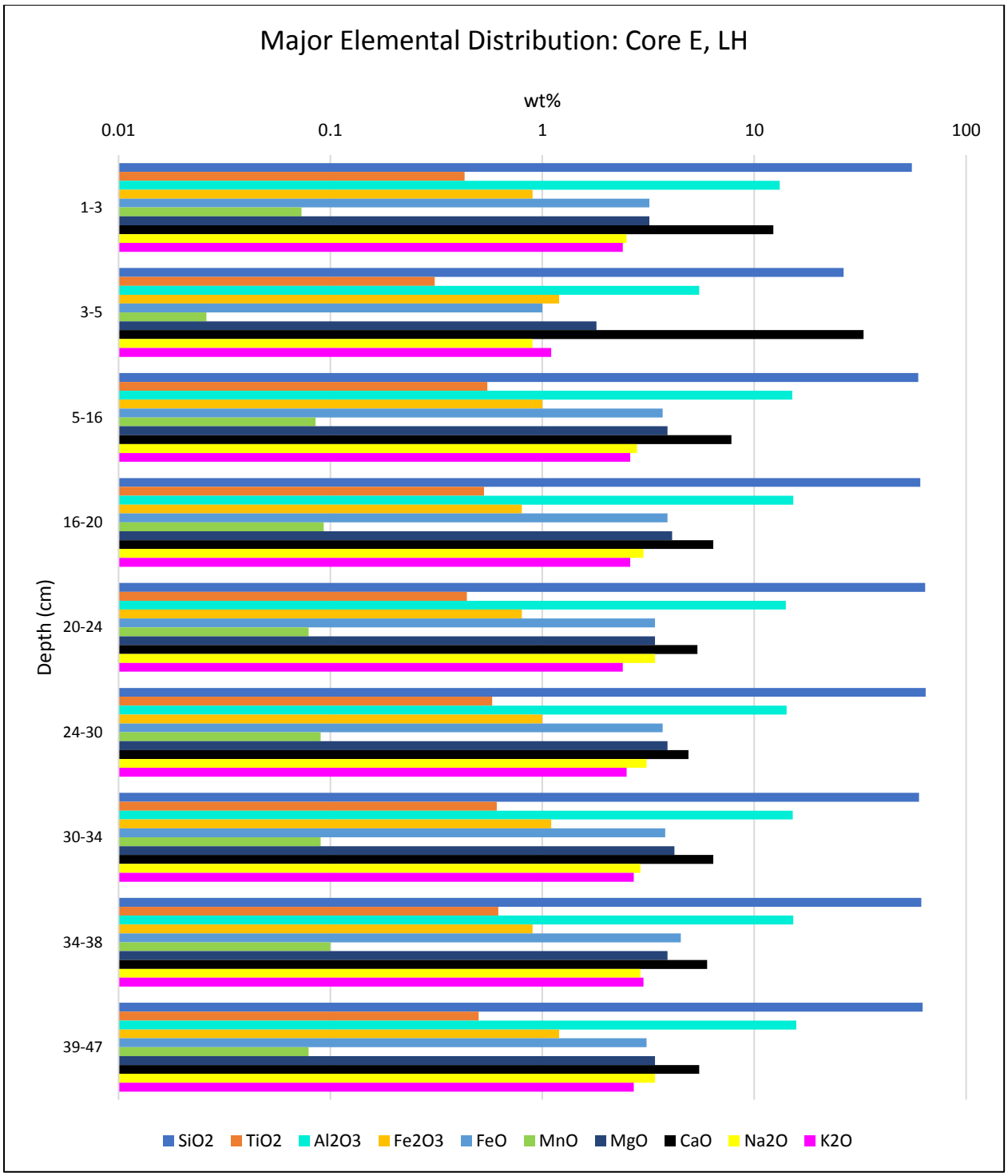

Figure 85. Major element distribution, Core E, Lake Hoare, Taylor Valley.

Major Elemental analysis of Core E at Lake Hoare shows very little oxide variation in all but one sample: E-3 (3-5 cm). E-3 exhibits heavily depleted SiO_2 (26.4 %), and heavily enriched CaO (32.8 %). E-2 (1-2 cm), while not nearly as enriched as E-3, exhibits a much higher CaO abundance (12.3 %) than all other samples. SiO_2 abundance in E-2 is similar to other samples. Al_2O_3, K_2O, and CaO abundances in Core E appear to follow FeO and Fe_2O_3 abundances, with slight depletions in E-6 (20-24 cm) and E-9 (34-38 cm). Except for E-3, SiO_2 abundance is inversely related to Al_2O_3, K_2O, and CaO abundance. Na_2O and MgO, except in E-6 (20-24 cm) for which abundances are the same, are inversely related. In general, Fe content is lower, while Al and Si is higher, in Core E, as compared to Core H. Al_2O_3/TiO_2 values are higher in Core E than Core H, while the opposite is true for S abundances, and minor elements Cr, Ni, and V are lower in Core E than Core H (Bishop et al., 2001).

2.4.15.2. Core E Mineralogy: XRD, Reflectance Spectra

XRD analysis of Core E at Lake Hoare shows mineral dominance of plagioclase, K-feldspar, quartz, and pyroxene—similar to the mineralogy of surface sediments from the Antarctic Dry Valleys reported by Gibson, 1983. Pyroxene is particularly difficult to identify due to high plagioclase abundance and XRD peaks that mask those of pyroxene. Secondary abundances of mica, amphibole, and chlorite are present throughout Core E. Sample E-3 reports the highest abundance of calcite and is not reported elsewhere in the core (Bishop et al., 2001).

Spectral analysis (Figure 88, below, with Core H) confirms the presence of pyroxene in all samples and specifies it as Fe-rich. Additionally, all samples exhibit a strong water band near 3 μm. This feature is stronger in spectra containing organic or calcite features. High abundances of calcite in E-2 and E-3 are confirmed by spectral features at approximately 3.4 and 4 μm. Evidence for calcite is also seen in E-6 (20-24 cm) and E-8

(30-34 cm). The "calcite mat layers" in Core E are believed to be associated with organisms (Bishop et al., 2001).

2.4.15.3. Core E Special Analysis: CIA

Chemical Index of Alteration values for Core E at Lake Hoare range from 8 – 46. The lowest value, 8, is exhibited in E-3 (3-5 cm) and is likely due to heavy CaO enrichment which exists as calcite, likely causing a strong dilution effect. Sample E-2 exhibits a relatively enhanced CaO abundance as well, thus, further analysis of samples based on the CIA was done apart from E-2 and E-3, making the range of values 41 – 46. This amended CIA range locates in the far end of the fresh basalt range and in fresh granites and granodiorites range (Nesbitt and Young, 1982). Based on information discussed, sediment mixing between source rocks is possible, occurring between basaltic and granitic sources.

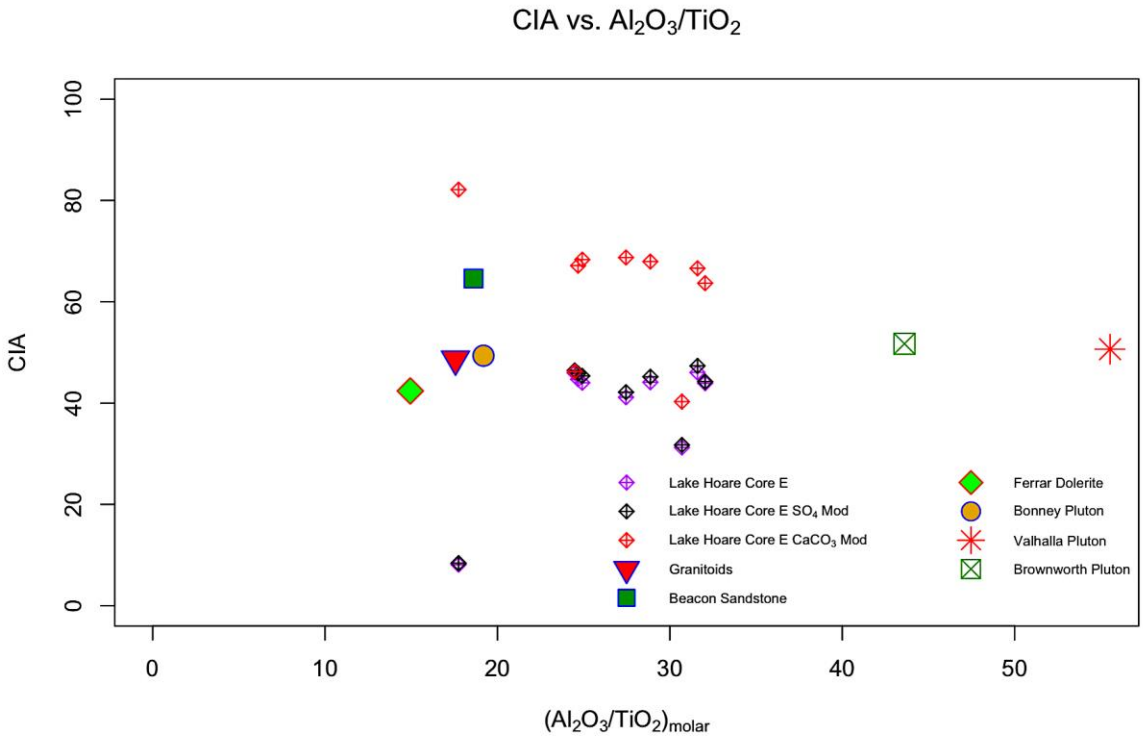

Figure 86. Modified and unmodified CIA values of Core E, Lake Hoare, and regional source rock CIA values.

Analysis of modified CIA values to account for dilution by calcite—including samples E-2 and E-3— reports a new range of 40 – 82. This wide range is likely due to Core E being relatively enriched, some samples massively so, in calcite. Adjusted, the new range is variable, exhibiting two values diagnostic of fresh basalt with the majority diagnostic of A-type granites, and a single sample diagnostic of potassic granite (Nesbitt and Young, 1982; Fedo et al., 1995). The average of the new range is 63, the second highest of Lake Hoare cores, 25 points higher than the unmodified average CIA value, and near the average CIA value of Beacon Sandstone (62). Beacon Sandstone, though, is not reported in the region's geology (Peterson and Marsh, 2008), and Core E at Lake Hoare is strong candidate for *biologic alteration* manifesting as the precipitation of the calcite mat layers (Bishop et al., 2001). Rare Earth Elemental analysis, if it were available, would provide an additional gauge on type and degree of alteration.

2.4.16.1. Core H Elements: Major

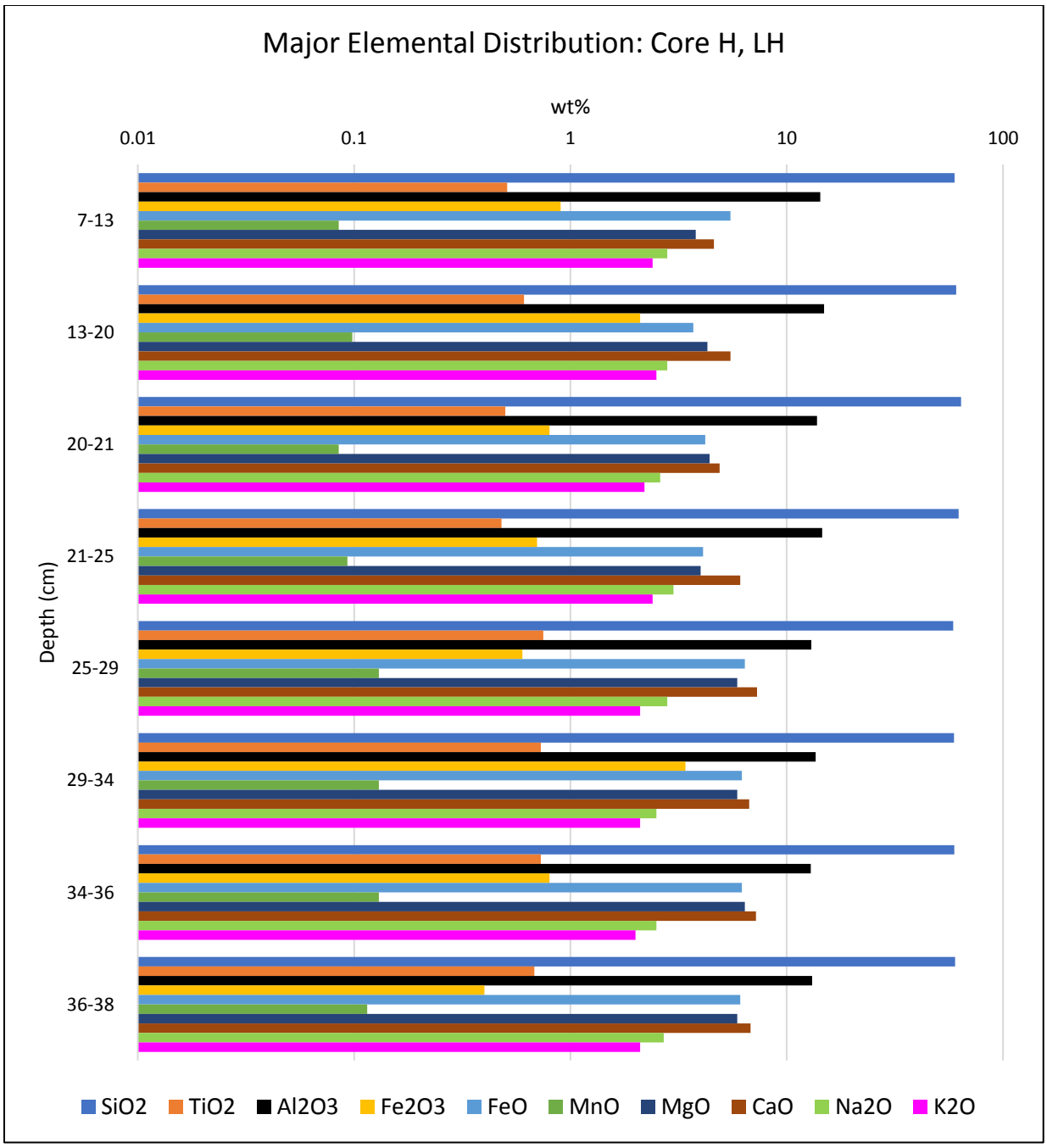

Figure 87. Major elemental distribution, Core H, Lake Hoare, Taylor Valley.

Major elemental analysis of Core H shows relative consistency in abundances of major oxides across the soil profile. However, changes in chemistry are seen at approximately

15-21 cm, near 32 cm, and near 36 cm. Abundances of SiO_2 decrease, while those of Al_2O_3 increase, below 25 cm.

Generally, though, SiO_2 and Al_2O_3 abundances are lower for Core H than Core E. MgO and CaO also increase below 25 cm. A relative change of Fe^{2+} and Fe^{3+} occurs near 15 cm and is accompanied by minor changes in other elements. The elevated Fe^{3+} abundance near 15 cm could be due to redox changes during sedimentation and/or biological activity. The increased Fe^{3+} abundance at 15 cm is paralleled by higher Fe-rich pyroxene abundances as compared to other sediment layers, suggesting a variation over time in lake water iron concentrations. Relative increases in SiO_2, Al_2O_3, K_2O, and Na_2O, (36 cm), and decreases in Fe^{3+}, MgO, and CaO from H-9 (34-36 cm) to H-10 (36-38 cm) are observed in tandem with a small increase in pyrite in H-10. Minor elements Cr, Ni, and V have higher abundances in Core H than Core E, but not in the case of Sr. Depleted $\delta^{34}S$, possibly associated with increased pyrite abundance, is also reported. The ratio of organic C to insoluble S content exhibits its highest values in H-1 (0-3 cm), H-5 (20-21 cm), and H-10. These layers may indicate areas of higher bacterial reduction in sediments (Bishop et al., 2001).

2.4.16.2. Core H Mineralogy: XRD, Spectra

XRD analysis of Core H at Lake Hoare shows elevated abundances of quartz, and the new presence of pyrite using Mössbauer spectroscopy (Bishop et al., 2001) and Raman spectroscopy (Bishop et al., 2003), which is believed to be associated with micro-organisms. Secondary abundances of mica, amphibole, and chlorite are present (Bishop et al., 2001). Spectral analysis (Figure 88, below) shows pyroxene present in all samples, particularly characteristic of Fe-rich pyroxene. Also observed for all samples is a strong water band near 3 μm. This feature is stronger in spectra containing organic or calcite features. Samples H-3 (7-13 cm), H-4 (13-20 cm), and H-5 (20-21 cm) exhibit sharp chlorophyll bands at 0.67 μm. These spectra also exhibit C-H stretching bands near 3.4 μm, while the lower layers contain calcite features (Bishop et al., 2001).

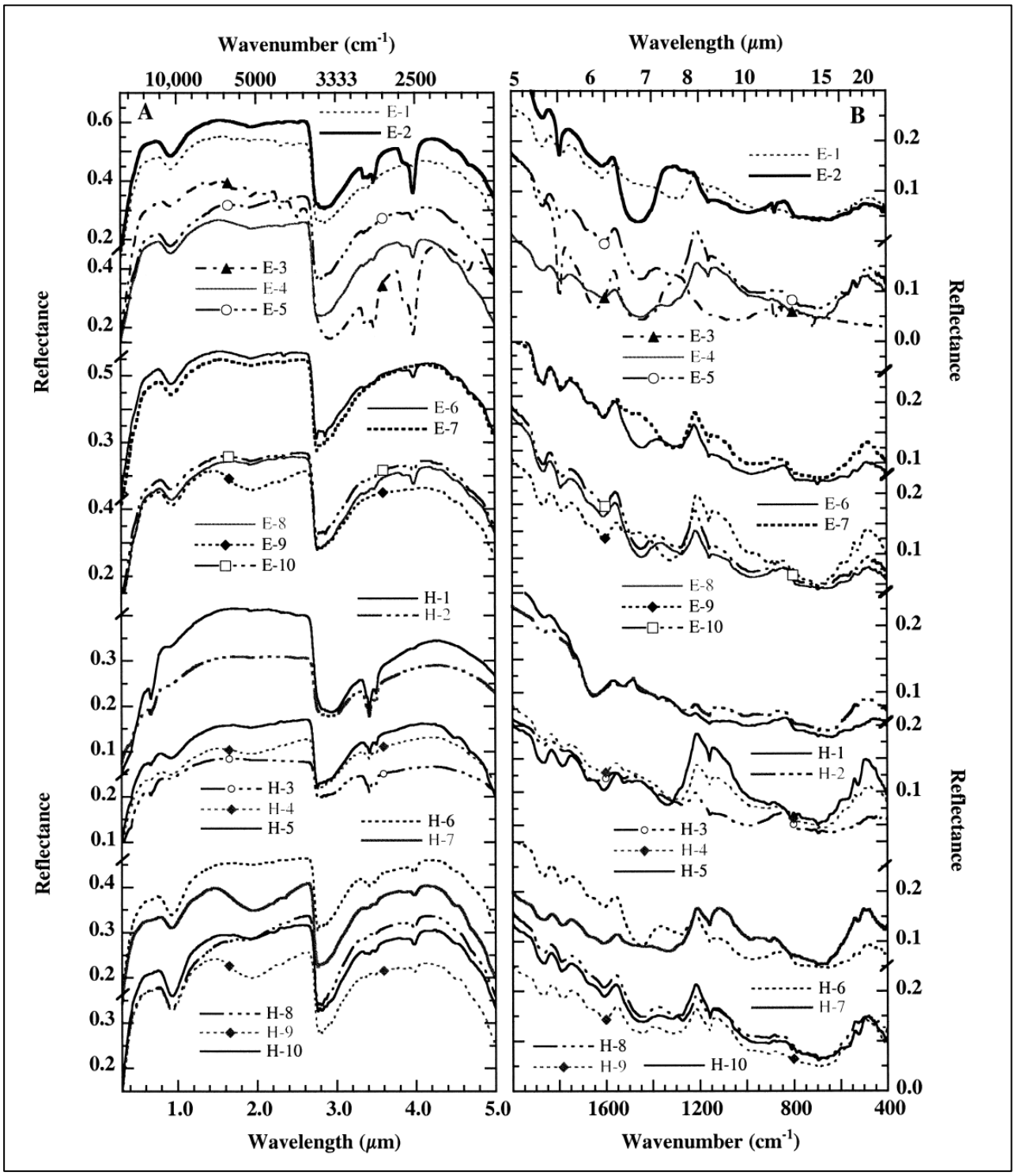

Figure 88. Reflectance spectra from 0.3 to 25 mm of sediments from the oxic and anoxic regions of Lake Hoare. The visible to near-infrared region is shown in terms of wavelength (A) and the mid-infrared region is shown in terms of wavenumber (B) to facilitate visualization of the spectral features (Bishop et al., 2001).

2.4.16.3. Core H Special Analysis: CIA

Chemical Index of Alteration values for Core H at Lake Hoare range from 39-47, at the far end of the fresh basalt range and in the fresh granites and granodiorites range, per Nesbitt and Young (1982). Core H notably exhibits the highest average CIA (43) and the lowest average Al_2O_3/TiO_2 ratio (22) of all Lake Hoare cores, weakening the argument for physical alteration.

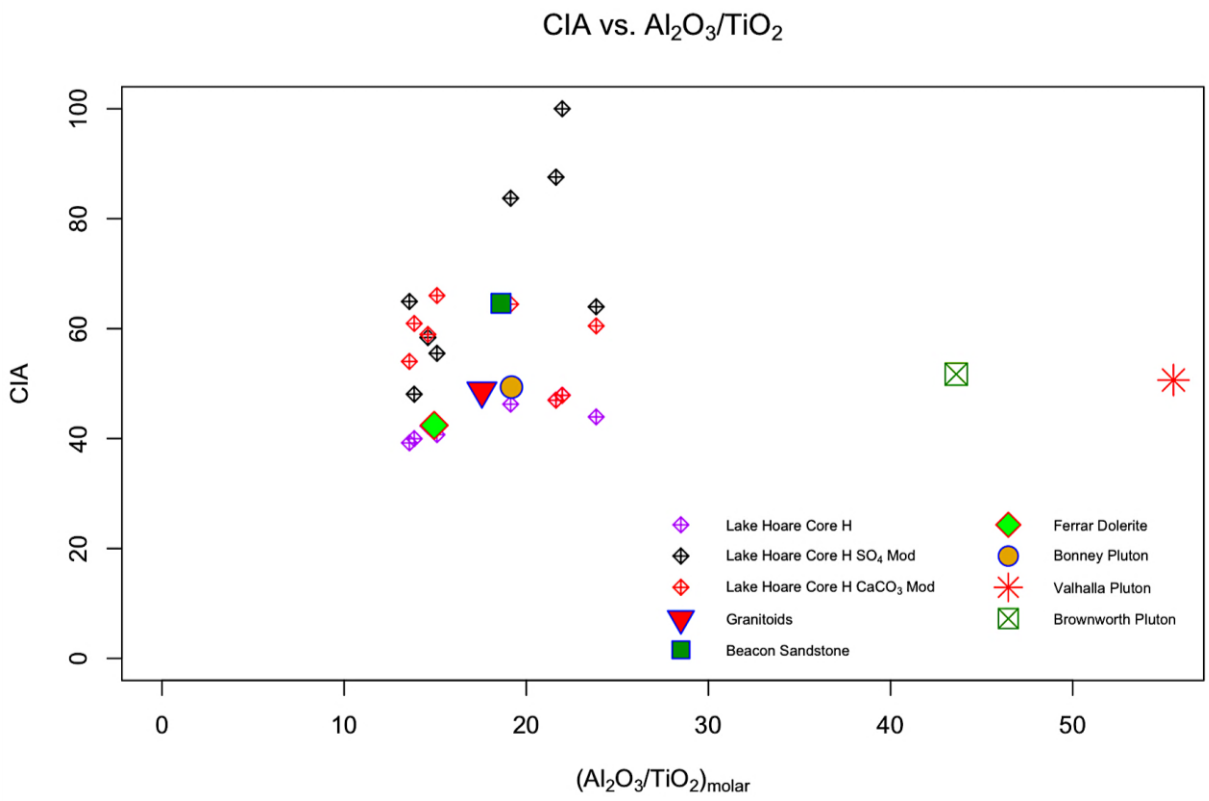

Figure 89. Modified and unmodified CIA values of Core H, Lake Hoare, Taylor Valley.

Analysis of modified CIA values, to account for calcite dilution, reports a new range of 47 – 66. Core H's new range is much smaller than Core E's due to relative calcite depletion. The Core H average CIA value (57), though, is still significantly higher than the unmodified average CIA value (43), suggesting calcite still plays a noteworthy role in skewing the CIA. Parts of the current anoxic region that were in an oxic zone at the

time of sediment deposition or mixing of oxic and anoxic waters could explain the lesser but still-reported calcite abundances (Bishop et al., 2001).

As it stands, the most likely picture for Core H is primarily biological alteration by what would be sulfanogens that are responsible for depleted $\delta^{34}S$, and the presence of pyrite. Physical alteration is likely operating on a secondary scale, manifesting as sediment-mixing between source rocks that could be entering the system through mass-wasting processes on slopes to the north of Lake Hoare. Intermittent fluvial transport from the north, as well as aeolian transport from the west are also potential sediment deposition processes. Mixing between oxic and anoxic waters would also be considered a form of physical alteration.

2.5. Discussion and Implications

2.5.1. Discussion

Analysis of different sediment samples, from cores and lake surfaces/edges across the McMurdo Dry Valleys region, shows physical alteration to dominate, existing primarily as sediment mixing at a surficial level. Sediment mixing is likely due to various factors including: 1) Mass-wasting between regional rock formations, 2) aeolian transport, 3) sediment transport by the Onyx river which can lead to 4) glacial transport to lakes in the south. Analysis of samples from Lakes Fryxell, Vanda, and Brownworth indicate that physical alteration dominates at the surface. Microenvironment surface samples from Prospect Mesa, Lake Hoare, and those in Upper Wright Valley exhibit similar alteration signatures. This is likely the result of environmental conditions unfavorable to standing water which is critical to chemical alteration. This confirms long-standing conceptions of alteration in this cold and dry region. However, in our investigation, we show chemical alteration to be more pervasive than previously thought.

In unique cases, hypersaline waters, the best example being Core 2074 in the middle of Don Juan Pond, permit water to remain stable and chemical alteration at the surface. Beneath the surface, chemical alteration enters the picture, rather ubiquitously, at a depth of 4-5 cm and extends, tapering off in some cases, to 10-12 cm, at which point physical alteration returns as what are hypothesized to be freeze-thaw processes. Layers of elemental enrichment and, in some cases, depletion, beneath the depth that surficial physical alteration can extend are strong signs of chemical alteration. Mineralogical analyses show that chemical alteration primarily manifests as layers of salt—namely gypsum, thenardite—or clays—namely allophane. Chemical alteration is likely permitted between 4-12 cm because it is beyond the reach of the cold and dry conditions on the surface.

Of our samples, biological alteration exists only in lake bottom sediments at Lake Hoare, manifesting as biomineralization of sulfur into pyrite (Bishop et al., 2001) by what would be sulfanogens.

2.5.2. IMPLICATIONS

Our results show that in extremely cold and dry environments surficial chemical alteration is possible under specific conditions— in the case of our research, in hypersaline waters as in Don Juan Pond. Additionally, we show, through analysis of cores taken in Upper Wright Valley, that chemical alteration can occur beneath sufficient sediment cover, 4-5 cm by our analysis, so as to exist beyond the reach of the harsh surface conditions. Our findings indicate that chemical alteration in these two scenarios typically manifests as salts, primarily sulfates such as gypsum, thenardite, and anhydrite. Traces of halite are found at the surface of various samples.

Sulfur abundances of Dry Valley sediments are similar to those at the two Viking sites. Martian soils that were identified as duricrust (Clark et al., 1981) were enriched in total sulfur as compared to other soils. This enrichment has been suggested to represent evaporites deposited at a time when the planet was enriched in fluids. The Dry Valley

soils that are enriched in evaporites have sulfur abundances similar to those found on Mars (Gibson, 1983). This similarity suggests that a fraction of the sulfur present in the martian regolith may have an evaporite origin (Clark and Van Hart, 1981). Additional orbital observations as well as exploration by landers and rovers have reported widespread Ca-sulfate minerals, with the most striking example displayed at the dune field of Olympia Undae (Langevin et al., 2005).

Bishop 2014 uses normalized K/Th ratios and the CIA to evaluate relationships between MDV sediments, and sediments and rocks from Gusev Crater (Spirit rover) and Meridiani (Opportunity rover), coming to the conclusion of physical alteration dominance across the regions of investigation. However, the martian data are highly dependent on sulfur content, and can skew the CIA when it combines with major elements of the CIA to form sulfates. We propose now that the relationship between MDV and martian sediments, collected by all three rovers, be evaluated through the lens of comprehensive elemental and mineralogical analysis with particular focus on sulfates. In doing this, we test the efficacy of the MDV region as a suitable terrestrial analog to Mars, potentially allowing for the reconstruction of Mars' geochemical history.

CHAPTER 3: SEDIMENT PROVENANCE AND ALTERATION IN THE MCMURDO DRY VALLEYS

3.1. ABSTRACT

Investigation and determination of sediment provenance in the McMurdo Dry Valleys was performed, as in Chapter 2, to better understand and corroborate type and degree of alteration in this polar desert environment. Due to their immobility during alteration processes, sediment provenance is primarily evaluated through the analysis of Rare Earth Element and High Field Strength Element abundances measured in MDV sediments and compared to source rocks. Major elements are analyzed in a secondary capacity due to their higher mobility during alteration processes. By investigating sediment provenance through these lenses, we test methods of provenance determination and the results of Chapter 2, which reports physical alteration to dominate at the surface to a depth of approximately 3-4 cm and beneath a depth of approximately 12-14 cm to the depth of the permafrost. Chemical alteration operates in between this range and biological alteration operates only at one location in lake bottom sediments. Analysis indicates a Granitoid Basement Complex is present in all samples, suggesting ubiquity across the valleys, as well as distinct geologic formations specific to the location. Moving forward, we look to combine findings from this chapter and Chapter 2 and apply these data to Mars rover data to further test the efficacy of the McMurdo Dry Valleys as a suitable analog to Mars.

3.2. INTRODUCTION

3.2.1. BACKGROUND

The McMurdo Dry Valleys (MDV) region are the Earth's coldest and driest desert; the mean annual air temperatures range from -25 to -20 °C and the mean annual precipitation, strictly in the form of snowfall, is 15 g/cm^2/yr (Bull, 1966; Thompson et

al., 1971). The region is desolate and liquid water is scarce. It is for these reasons that the region is frequently used as a terrestrial analog to Mars.

It is valuable to have an understanding of the degree to which the composition of sediment has been altered away from the original source material(s), and by which processes, in order to have a clear picture of past and present geochemical conditions in an environment. Investigation of sediment provenance in the McMurdo Dry Valleys was done with the purpose of applying these data to that of Chapter 2 in order to validate or refute the conclusion of chemical alteration in the MDV.

3.2.2. Source Rocks

In order to make conclusions on sediment provenance, geochemical analysis of sediment's "source rocks" must be factored in. There are a handful of different source rocks that are discussed herein, of which differ from region to region. The source rock possibilities for the North Fork, South Fork, Don Juan Basin, and VXE-6 Basin are Ferrar Dolerite, Beacon Sandstone, and Granitoids (gneissic). The source rock possibilities for Lake Vanda and Prospect Mesa are Ferrar Dolerite, Bonney Pluton, and Valhalla Pluton with prominent swarms of coincident mafic and felsic porphyry dikes immediately east of Lake Vanda (Allibone et al., 1993a). Lake Brownworth has one major source rock possibility, the Brownworth Pluton, and Lakes Fryxell and Hoare have one major Granitoid source—the same seen in DJB, DQB, the NF, and SF (Peterson and Marsh, 2008).

Available major and trace (REEs and HFSEs included) elemental data of the Granitoids (Palmer, 1987, 1990; Ellery, 1989), Beacon Sandstone (Roser, Korsch, and Pyne, unpubl. data), Ferrar Dolerite (Grapes et al., 1989; Morrison, 1995), Bonney Pluton (granitic), Brownworth Pluton (granitic), and Valhalla Pluton (granitic) (Allibone et al., 1993a; Peterson and Marsh, 2008) are compared to that of the microenvironments in attempt to determine sediment provenance and degree/type of alteration.

3.2.3. Characterizing Sediment Provenance

We characterize sediment provenance primarily through the analysis of High Field Strength Elements (HSFEs) and Rare Earth Elements (REEs), and secondarily through major elements. HFSEs consist of Zr, Hf, Nb, Ta, Ti, and occasionally Th. There are 17 Rare Earth Elements; 15 of which are known as "Lanthanides", the other two being Yttrium and Scandium. These two element groups have a particular utility to geologists due to their relative immobility during alteration processes and can therefore be used to trace sediment provenance.

HFSEs have been used for some time as tracers to classify igneous rocks and their tectonic settings (Pearce and Cann, 1973), and to distinguish source rocks from their altered sediments (Finlow-Bates and Stumpfl, 1981; Hickmott and Spear, 1992). Ratios of HSFEs to another, Zr/Ti, for example, can be diagnostic of source material(s) (Nesbitt and Markovics, 1997). There is evidence, however, that under unique conditions they can be fairly mobile (Jiang et al., 2005).

REEs can also be used to trace sediment provenance (Nesbitt and Markovics, 1997) due to their relatively small ionic radii which is responsible for their immobility. What's more, ratios of REEs/HFSEs can be utilized. Notably, Nesbitt and Markovics (1997) report La/Ti to increase more than 100 % and the heavy REE/Ti ratios by more than over 200 % from fresh rock to the most weathered in situ samples, therefore it is important to consider this when concluding sediment provenance.

The Chemical Index of Alteration (CIA) (Nesbitt and Young, 1982) is used here as an additional means to corroborate the findings from the REE, HFSE, and major elemental analysis. The CIA is evaluated for our samples both as it was originally formulated and modified in Chapter 2 to account for salt dilution.

3.3. METHODS

3.3.1. STUDY SITES

Study sites investigated for sediment provenance in Chapter 3 are the same as those investigated for type and degree of alteration in Chapter 2; There are ten different study sites, microenvironments within, that are shown below. Cores 2074, 33, and 39 are all located in Don Juan Basin, Core 42 in VXE-6 Basin (Harris, 1981), Core 52 in the South Fork Region, Core 35 in

Don Quixote Basin, and Cores A-E, and H at Lake Hoare. Lakes Fryxell, Vanda, and Brownworth are composed of 23 lake surface and edge samples.

3.3.2. SAMPLING AND ANALYTICAL METHODS

Sampling and analytical methods are described in Chapters 2.3.

3.4. RESULTS

3.4.1. CORE 2074

Core 2074 is situated in the middle of hypersaline Don Juan Pond and has three microenvironments ranging from the surface to a depth of 10 cm with permafrost at 31 cm. JB1126, the surface sample, is not analyzed because it is primarily salt.

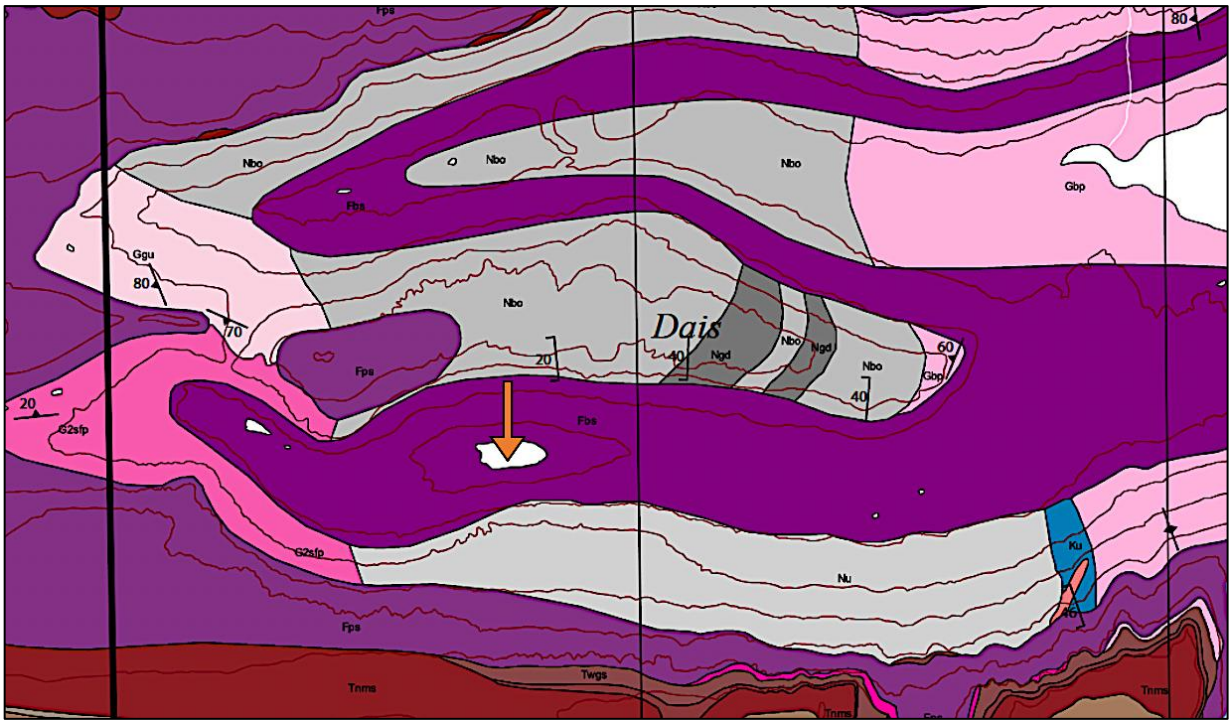

Figure 90. Regional geology of Core 2074, Don Juan Basin (Peterson and Marsh, 2008).Ferrar Dolerite (purple), bounded by Undifferentiated Gneiss (light gray) to the south and the same, with the addition of a small Ferrar Dolerite outcrop to the north, and the South Fork Pluton (pink) to the west, at the base of the Labyrinth (purple extending from left of image).

3.4.1.1. Rare Earth Elements

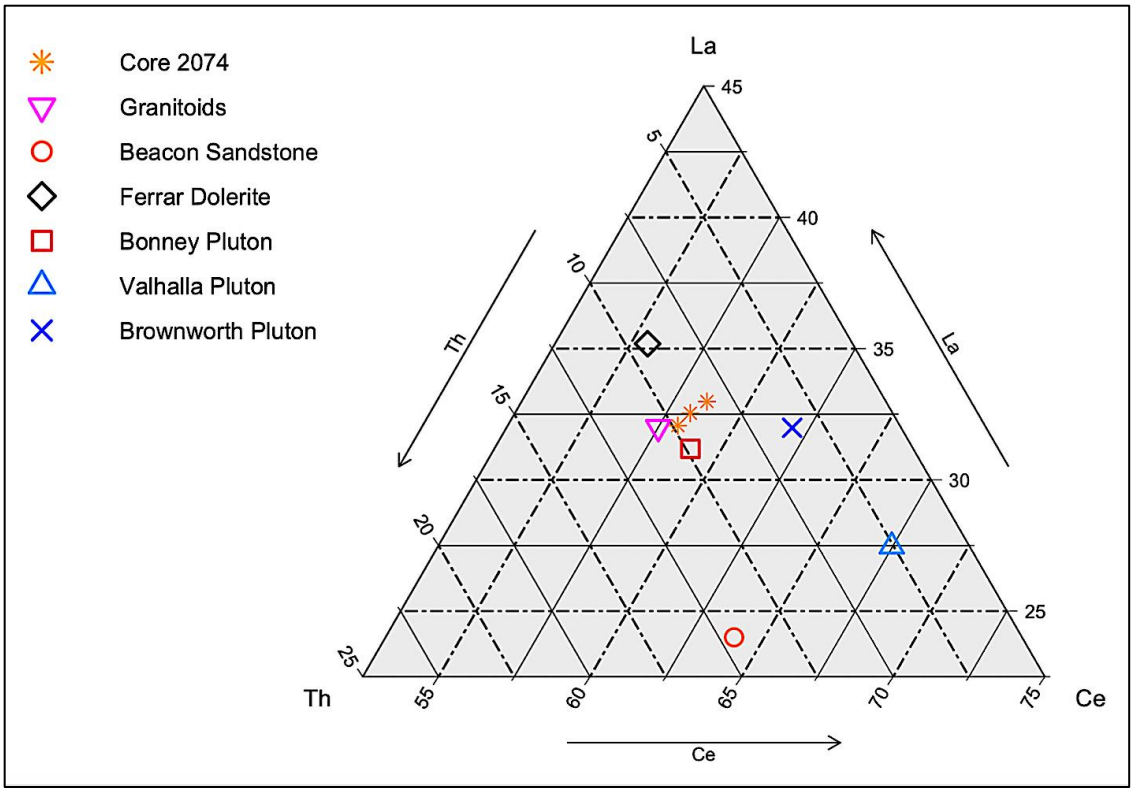

Figure 91. Th, La, Ce abundance of Core 2074, Don Juan Basin, and regional source rocks.

Figure 91 shows the relative abundances of Th, La, and Ce of samples from Core 2074, and source rocks. All samples exhibit similar abundances of each element, of which best align with average abundances of Granitoids. Additionally, Core 2074 exhibits the lowest abundances of Th, La, and Ce of all microenvironments in this study. This is likely due to being located in the middle of hypersaline Don Juan Pond which reports high abundances of anhydrite and gypsum. Depletion of REE abundances strongly suggests active chemical alteration at Core 2074. Because abundance of REEs can increase by more than over 200 % from fresh rock to the most weathered in situ samples (Nesbitt and Markovics, 1997), abundance of REEs such as La and Ce can give a slightly skewed picture of sediment provenance. To check the validity of conclusions made from REEs, HFSEs are utilized due to their greater immobility.

3.4.2. CORE 33

Core 33 is situated approximately 150 m SW of core 2074, in the path of a "wet" encrustation (Figure 4) that meets with the west edge of the pond, understood to be a water source for DJP (Dickson et al., 2013). The core has five samples ranging from surface to 16 cm depth with permafrost at 25 cm. It is important to consider that the "wet" encrustation from the west could potentially be entraining sediments from the South Fork Pluton and depositing them, downslope, at Core 33.

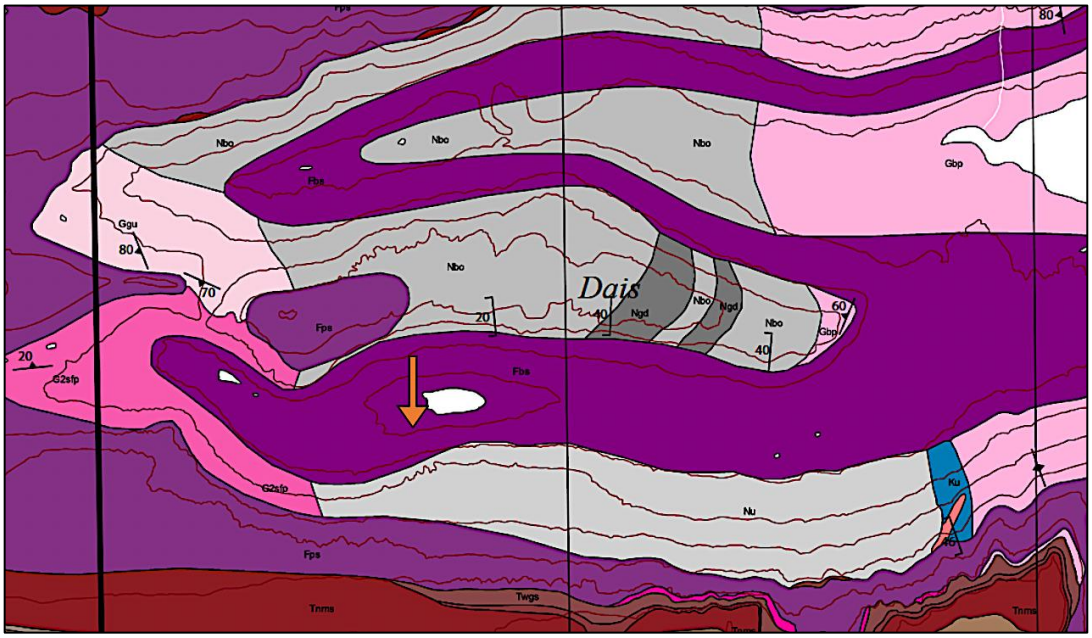

Figure 92. Regional geology of Core 33, Don Juan Basin (Peterson and Marsh, 2008). Ferrar Dolerite (purple), bounded by Undifferentiated Gneiss (light gray) to the south and the same, with the addition of a small Ferrar Dolerite outcrop to the north, and the South Fork Pluton (pink) to the west, at the base of the Labyrinth (purple extending from left of image).

3.4.2.1. Rare Earth Elements

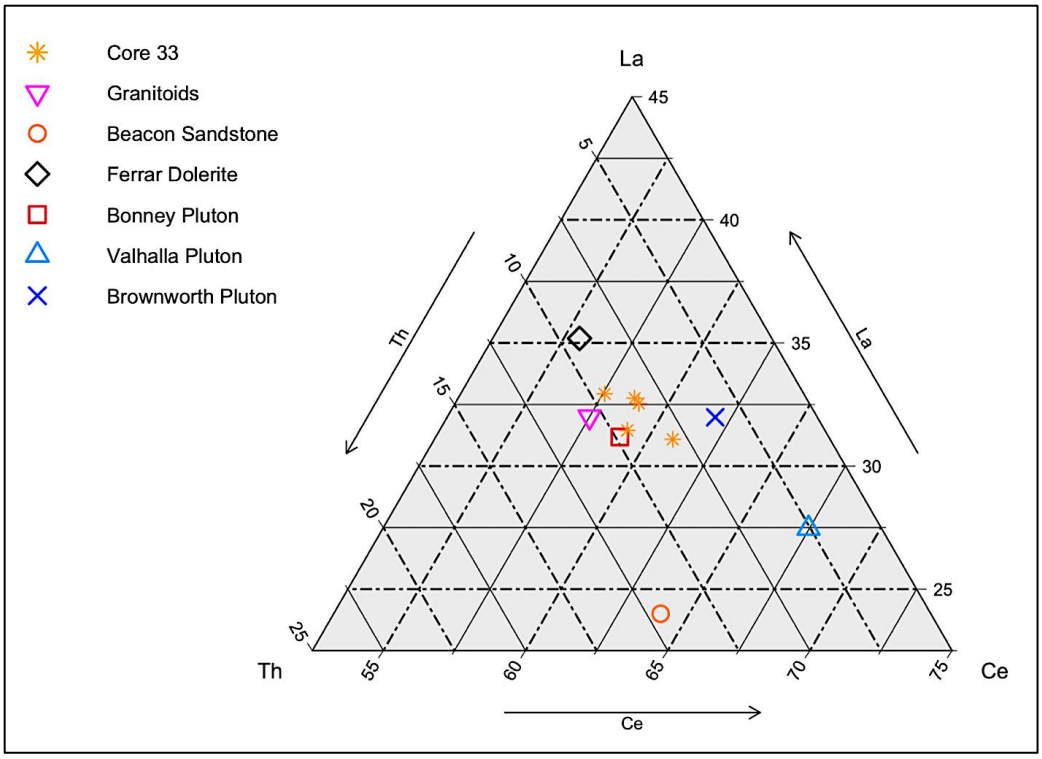

Figure 93. Th, La, Ce abundance of Core 33, Don Juan Basin, and regional source rocks.

Figure 93 shows the relative abundances of Th, La, and Ce of samples from Core 33, and source rocks. Variation in abundances of these elements is seen across the soil profile with the highest abundances exhibited in sample JB1131 (8-10 cm). Based on Th, La, and Ce abundances, Core 33 sediments best match Granitoids and Bonney Pluton. Similarity to Bonney Pluton abundances is unexpected due to the formation being nearly 7 km away (Peterson and Marsh, 2008). However, South Fork Pluton exists a couple hundred meters to the west of Core 33 suggesting the possibility of elemental similarity in pluton formations across the MDV region. To check the validity of conclusions made from REEs, HFSEs are utilized due to their greater immobility.

3.4.2.2. High Field Strength Elements

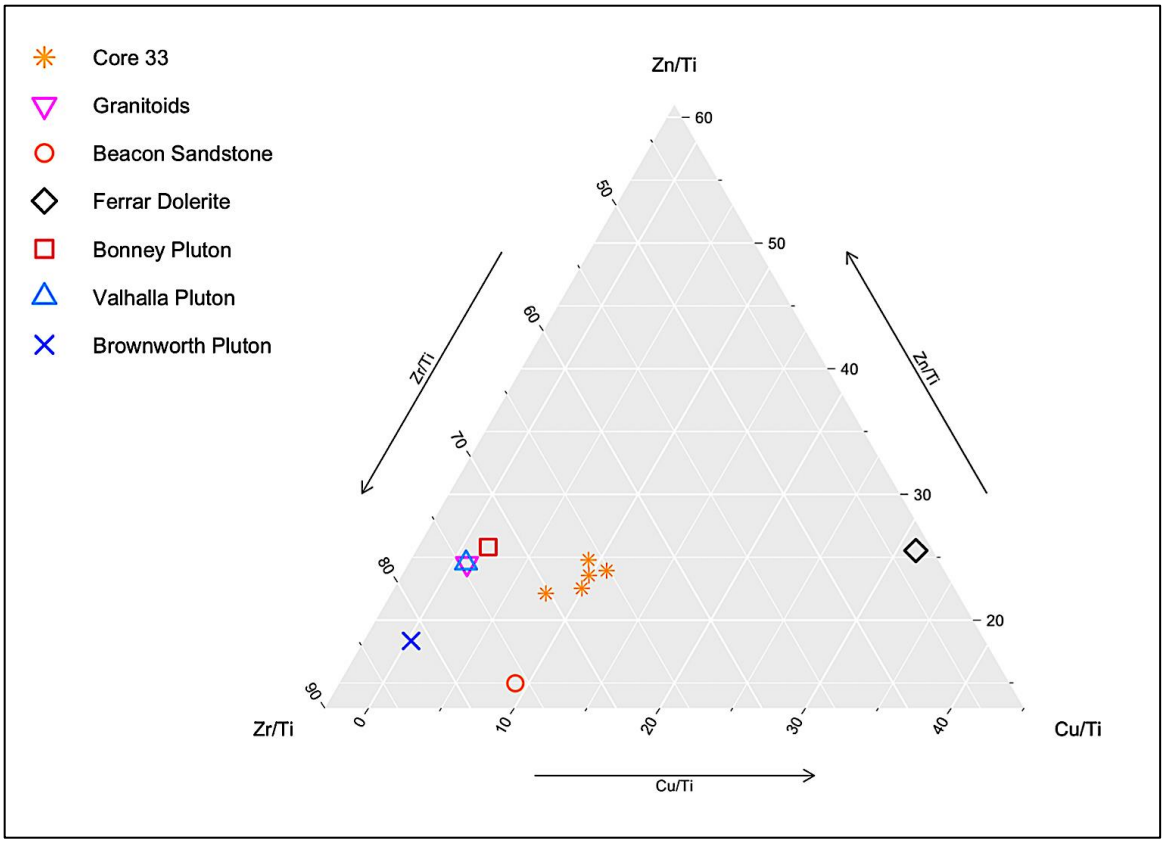

Figure 94. High Field Strength Element ratios Zr/Ti, Zn/Ti, and Cu/Ti of Core 33, Don Juan Basin, and regional source rocks.

Figure 94, above, shows relative abundances of Zr/Ti, Zn/Ti, and Cu/Ti in Core 33 samples. Samples show minimal variation in Zr/Ti abundance suggesting a low degree of chemical alteration. Samples plot most similarly to Granitoids and pluton formations Bonney and Valhalla. These findings corroborate those from Rare Earth Analysis and further pushes the case for Granitoid/South Fork Pluton provenance, bolstering the case for elemental similarity in pluton formations across the MDV region. Importantly, the average abundances of Zr/Ti, Zn/Ti, and Cu/Ti in Granitoids, Ferrar Dolerite, and Bonney Pluton are all very similar, therefore further investigation is required. Major elemental analysis is discussed below. While HFSE elements are very durable and

immobile in alteration processes, unique conditions can mobilize them (Jiang et al., 2005). Core 33 is a reasonable candidate for a high enough degree of chemical alteration to carry out such a process.

3.4.2.3. Major Elements

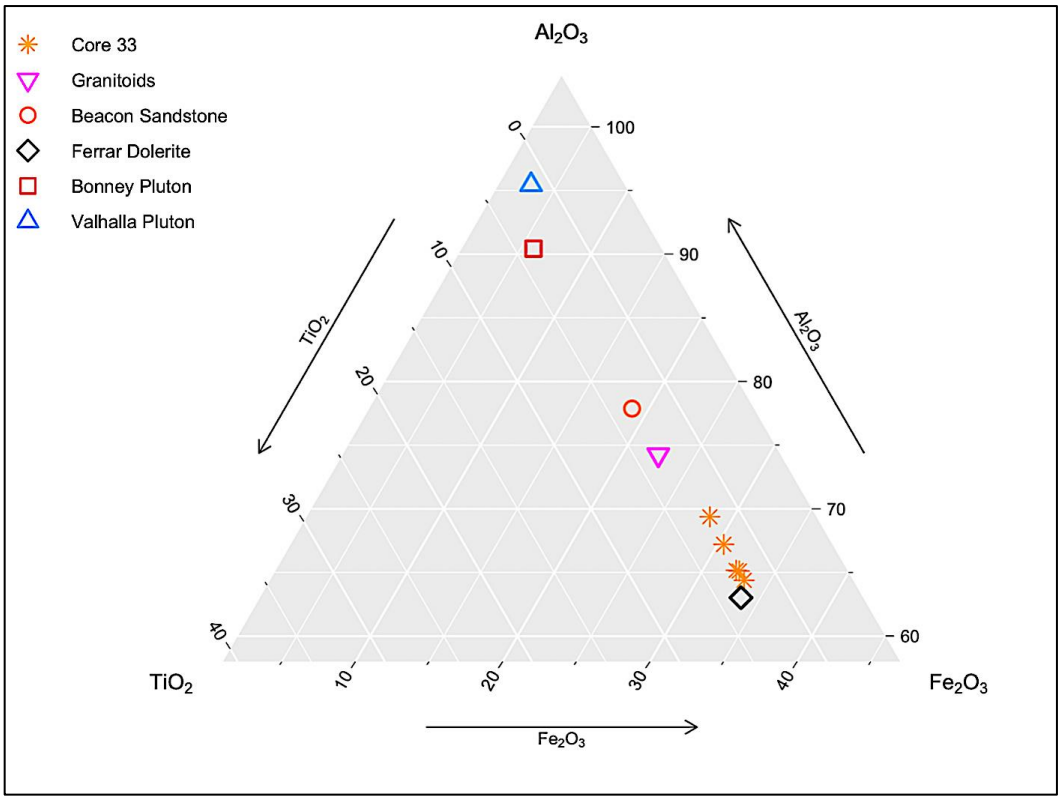

Figure 95. TiO_2, Al_2O_3, Fe_2O_3 abundance of Core 33, Don Juan Basin, and regional source rocks.

Major elemental analysis of oxides TiO_2, Al_2O_3, and Fe_2O_3 of Core 33 samples shows greatest similarity to Ferrar Dolerite with a trend toward Granitoids. These findings, though they do not align with those from REE and HFSE analysis, make sense—particularly the trend toward Granitoids. TiO_2 and Fe_2O_3 are relatively enriched in Ferrar Dolerite and less so in Granitoids, possibly suggesting alteration away from Ferrar dolerite—which is ubiquitous across Don Juan Basin floor (Peterson and Marsh, 2008)—

towards Granitoids, which exists as a “basement” component in the region (Harris, 1981).

3.4.2.4. CIA

Unmodified Chemical Index of Alteration values average about 37, in the range of fresh basalts, (Nesbitt and Young, 1982; Fedo et al., 1995) and just below the average CIA of the Ferrar Dolerite: 42 (based on data from Grapes et al., 1989; Morrison, 1995). Based on this, the most likely provenance for Core 33 sediments is Ferrar Dolerite.

Modified Chemical Index of Alteration values, corrected for salt dilution, average about 53, in the range of Fresh granites and granodiorites (Nesbitt and Young, 1982; Fedo et al., 1995) and just above the average CIA of Granitoids (48), and plutons Bonney (49), Valhalla (51), Brownworth (52) (based on data from Allibone et al., 1993a). According to modified CIA values and location, the most likely provenance for Core 33 sediments is Granitoids.

3.4.2.5. Provenance Conclusion

Based on information discussed above, Core 33 sediment data best aligns with source rocks Granitoids, Ferrar Dolerite, and plutons Bonney and Valhalla. This conclusion, however, is geographically puzzling as Bonney and Valhalla Pluton are both found nearly 7 km to the east of Core 33 in central Wright Valley. The South Fork Pluton, however, is found just a couple hundred meters upslope to the west of Core 33 (Peterson and Marsh, 2008). Dickson et al., 2013 reports a small network of 1-2 m wide channels that drain into Don Juan Basin, forming the possibility of aqueously-transported sediment from the South Fork Pluton. Therefore, we propose Core 33 sediment provenance, based on elemental analyses in tandem with a spatial understanding of regional

geologic formations, to primarily be Ferrar Dolerite and Granitoids, with South Fork Pluton present in a secondary capacity.

3.4.3. CORE 39

Core 39 is situated approximately 120 m SW of core 33 near the base of an alluvial fan and **outside** of the "wet" encrustation path. Harris (1981) identifies ledge rock to the north and south of the as Ferrar Dolerite and Granitoids. These observations are corroborated and built upon by Peterson and Marsh (2008). Notably, Core 39 is located near the base of an alluvial fan (Figure 4) and is therefore hypothesized to be subject to sediment-mixing between the aforementioned rocks.

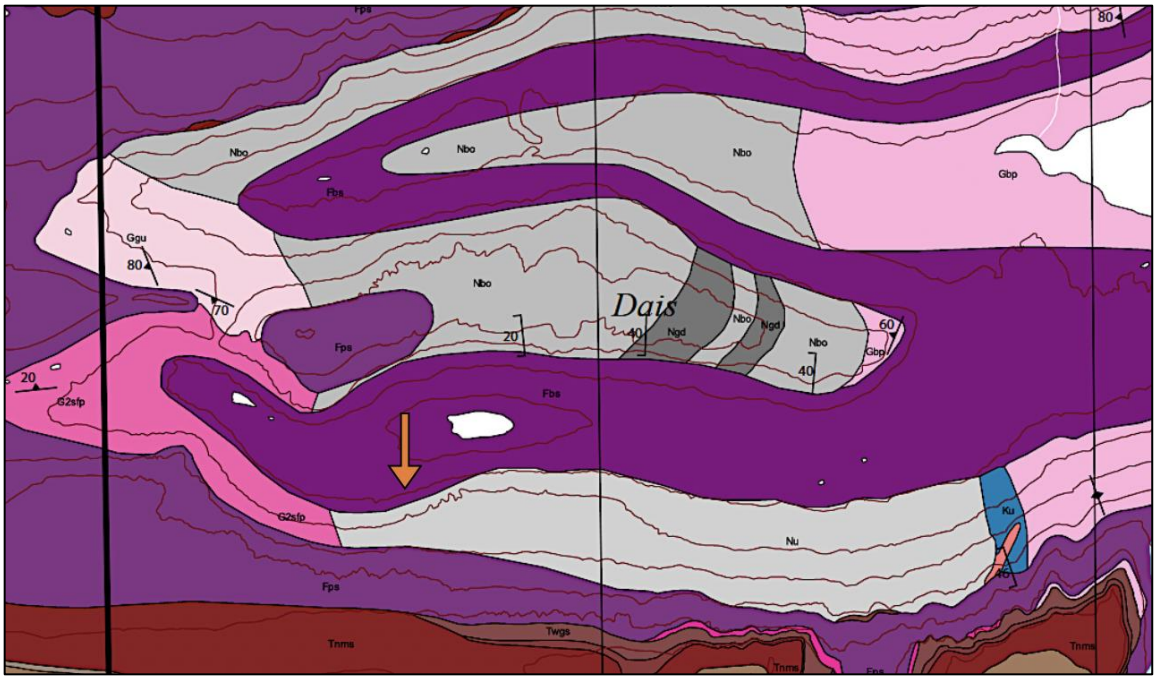

Figure 96. Regional geology of Core 39, Don Juan Basin (Peterson and Marsh, 2008). Ferrar Dolerite (purple), bounded by Undifferentiated Gneiss (light gray) to the south and the same, with the addition of a small Ferrar Dolerite outcrop, to the north.

3.4.3.1 Rare Earth Elements

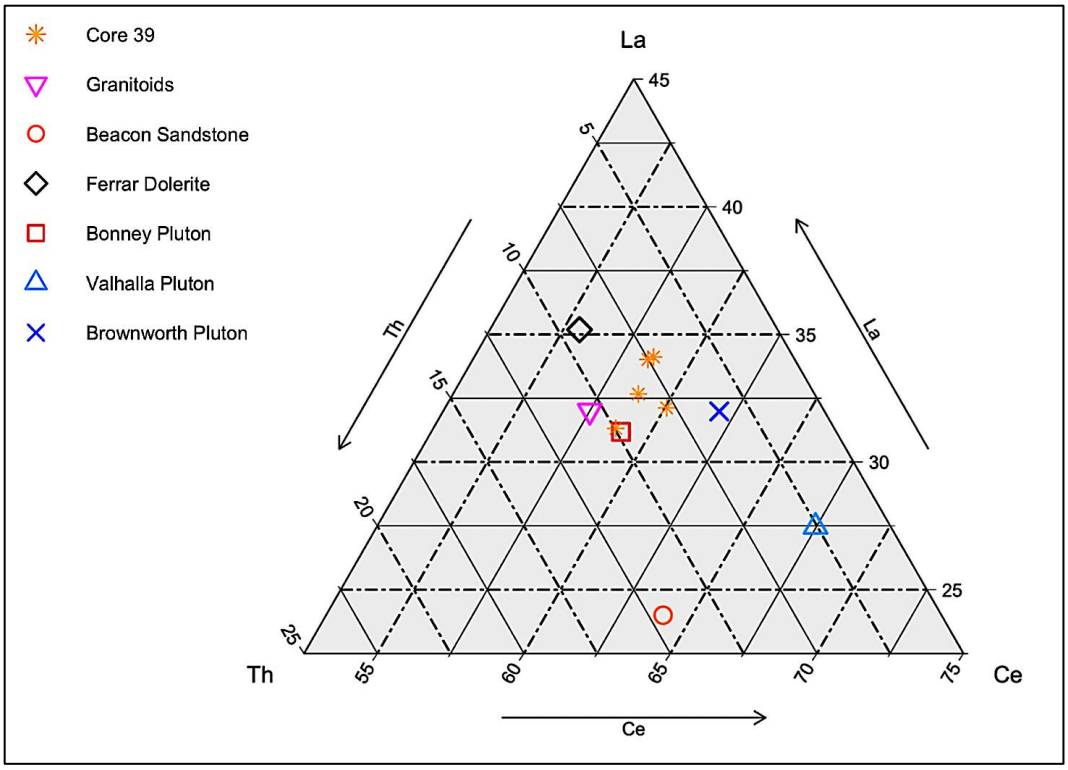

Figure 97. Th, La, Ce abundance of Core 39, Don Juan Basin, and regional source rocks.

Figure 97 shows the relative abundances of Th, La, and Ce of samples from Core 33, and source rocks. There is a low degree of sample grouping, and variation from sample to sample. Samples exhibit Th, La, and Ce abundances most similar to Bonney Pluton and Granitoids, and look to be trending toward Ferrar Dolerite. As is discussed in for Core 33, similarity to Bonney Pluton abundances is unexpected due to the formation being nearly 7 km away (Peterson and Marsh, 2008), but South Fork Pluton, which exists a couple hundred meters west of Core 33 and could bear elemental similarity is a possible candidate. HFSEs are analyzed for REE validity.

3.4.3.2. High Field Strength Elements

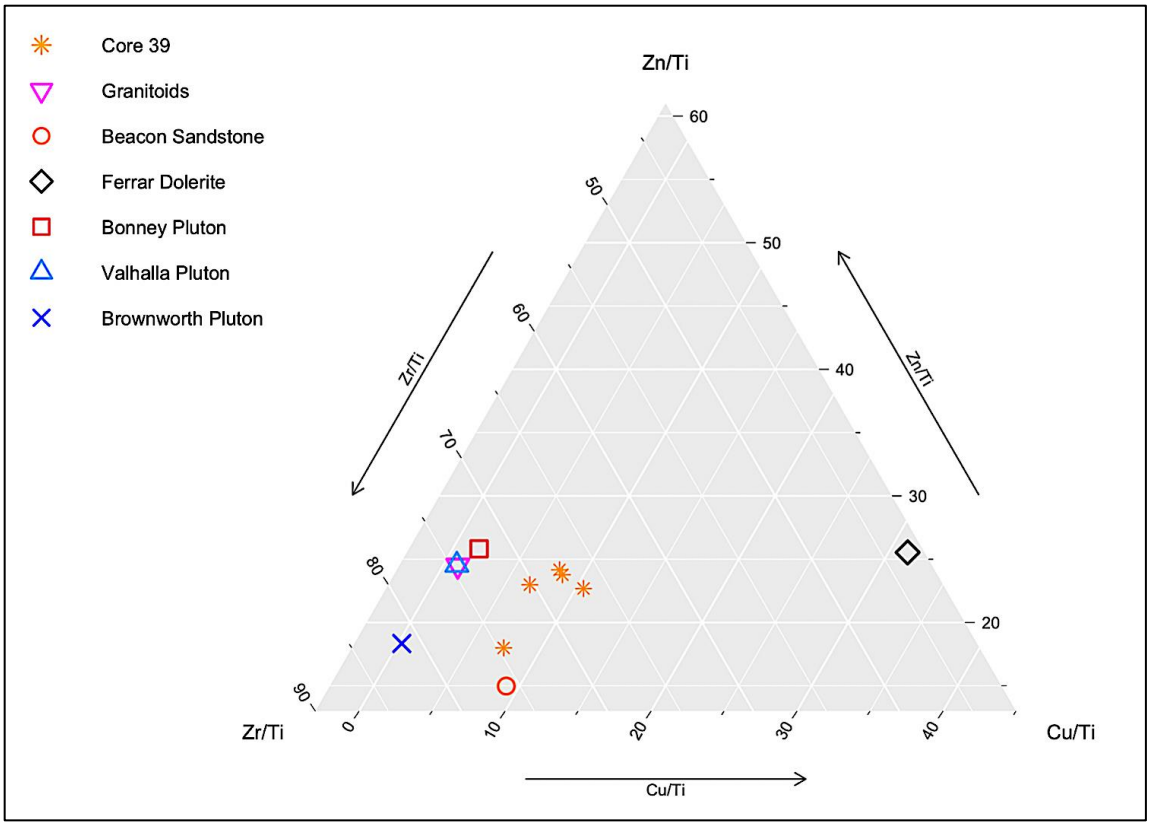

Figure 98. High Field Strength Element ratios Zr/Ti, Zn/Ti, and Cu/Ti of Core 33, Don Juan Basin, and regional source rocks.

Figure 98 shows relative abundances of Zr/Ti, Zn/Ti, and Cu/Ti in Core 33 samples. Samples show slight variation in Zr/Ti, the most immobile HFSE ratio (Nesbitt and Markovics, 1997) suggesting chemical alteration is occurring at a low degree. Samples plot most similarly to Granitoids, Beacon Sandstone, and plutons Bonney and Valhalla. These findings, except for Beacon Sandstone, corroborate those from REE analysis and further push the case for Granitoid/South Fork Pluton provenance, supporting the theory of elemental similarity in pluton formations across the MDV region. While HFSE elements are very durable and immobile in alteration processes, unique conditions can mobilize them (Jiang et al., 2005). Core 39 is a reasonable candidate for a high enough

degree of chemical alteration to carry out such a process. Physical alteration is also a strong possibility for this core. Major elemental analysis is discussed below.

3.4.3.3. Major Elements

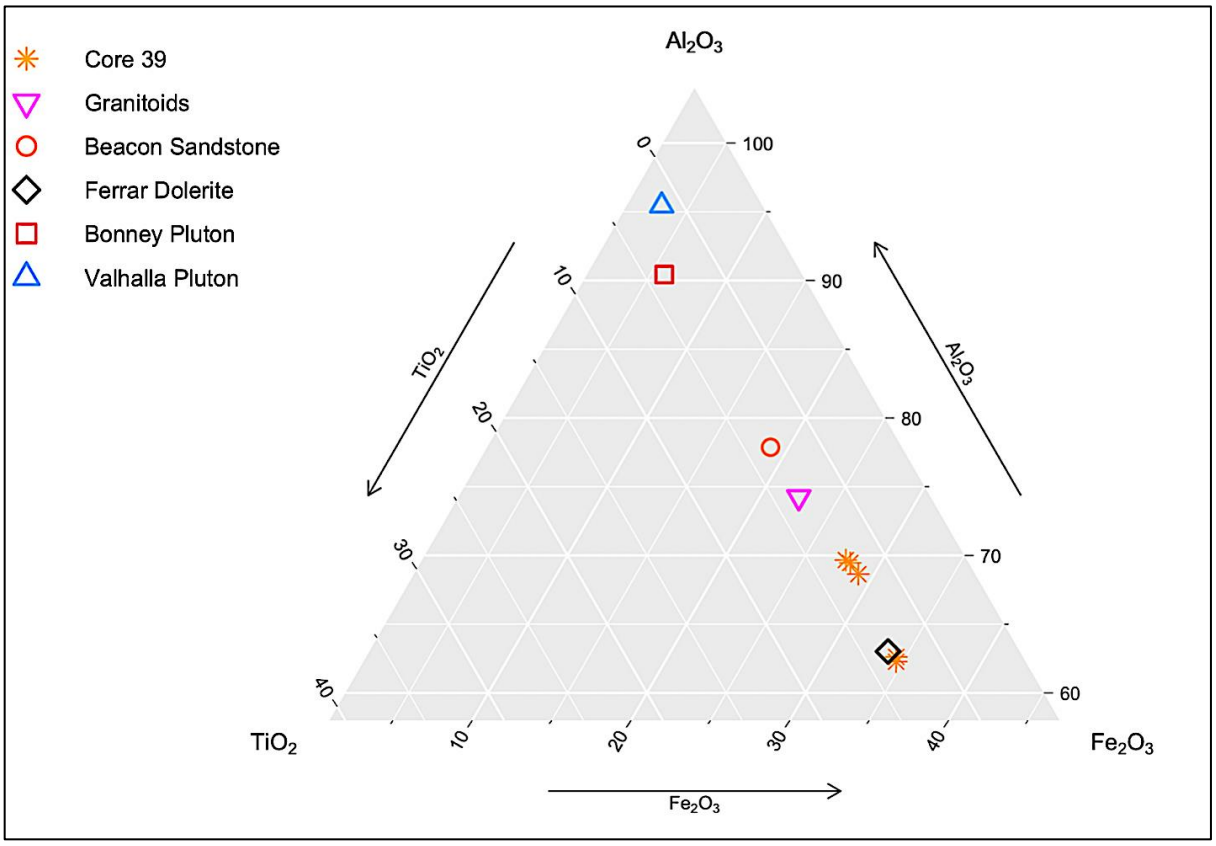

Figure 99. TiO_2, Al_2O_3, Fe_2O_3 abundance of Core 39, Don Juan Basin, and regional source rocks.

Major elemental analysis of oxides TiO_2, Al_2O_3, and Fe_2O_3 of Core 39 shows greatest variation in Al_2O_3 and Fe_2O_3, exhibiting similar abundances to Ferrar Dolerite and trending towards Granitoids. These findings, though they do not align with those from REE and HFSE analysis, make sense— particularly the trend toward Granitoids. TiO_2 and Fe_2O_3 are relatively enriched in Ferrar Dolerite and less so in Granitoids, possibly suggesting alteration away from Ferrar dolerite—which is ubiquitous across Don Juan

Basin floor (Peterson and Marsh, 2008)—towards Granitoids, which exists as a "basement" component in the region (Harris, 1981).

3.4.3.4. CIA

Unmodified Chemical Index of Alteration values average about 40, in the range of fresh basalts (Nesbitt and Young, 1982; Fedo et al., 1995) and just below the average CIA of the Ferrar Dolerite: 42 (based on data from Grapes et al., 1989; Morrison, 1995). Based on this, the most likely provenance for Core 33 sediments is Ferrar Dolerite.

Modified Chemical Index of Alteration values, corrected for salt dilution, average about 57, in the range of granites to A-type granites (Fedo et al., 1995). This value is significantly higher than all source rocks except for Beacon Sandstone, which, as shown in the HFSE analysis, is favored in one sample. According to CIA values and location, the most likely provenance for Core 33 sediments is primarily Granitoids and Ferrar Dolerite. These higher CIA values indicate the occurrence of chemical weathering in sediments of Core 39.

3.4.3.4. PROVENANCE CONCLUSION

Based on information discussed above, Core 39 sediment data best aligns with source rocks Granitoids, Ferrar Dolerite, and Bonney Pluton. The conclusion of Bonney Pluton is unexpected because it is found nearly 7 km to the east of Core 39 in central Wright Valley. The South Fork Pluton, though, is found just a couple hundred meters upslope to the west of Core 33 (Peterson and Marsh, 2008). Due to the proximity of an alluvial fan to Core 39, mass-wasting of source rocks is very likely a contributing factor of the chemical composition of the core. If this is indeed the case, we propose Core 39 sediment provenance, based on elemental analyses in tandem with spatial understanding of regional geologic formations, to be primarily Ferrar Dolerite and Granitoids, with South Fork Pluton and Beacon Sandstone present in a secondary

capacity. Additionally, sediments, as indicated by the elevated modified CIA values, are likely undergoing chemical alteration in a secondary capacity.

3.4.4. CORE 35

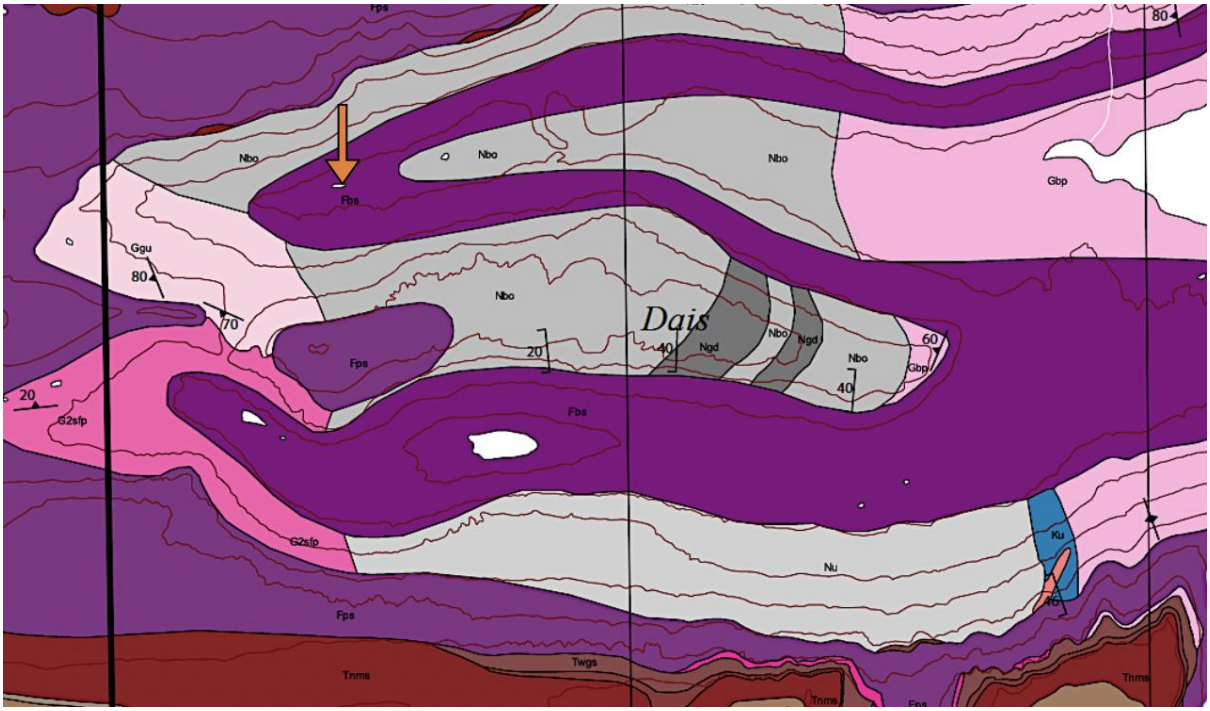

Figure 100. Regional geology of Core 35, Don Quixote Basin (Peterson and Marsh, 2008). Core 35 is bounded by Biotite orthogneiss (light gray) to the north, east, and south, and by undifferentiated Granitoids (light pink) to the west. The basin floor is primarily composed of Ferrar Dolerite (purple).

3.4.4.1. Rare Earth Elements

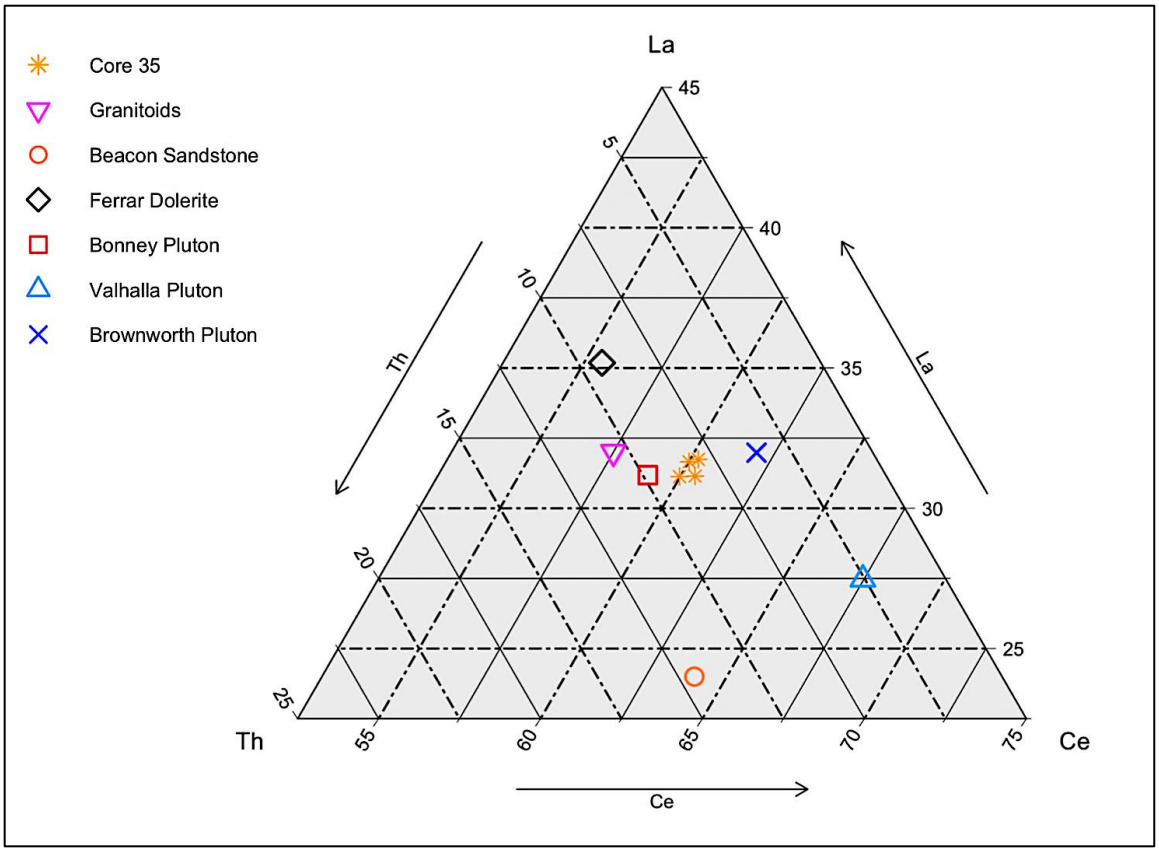

Figure 101. Th, La, Ce abundance of Core 35, Don Quixote Basin, and regional source rocks.

Figure 101 shows the relative abundances of Th, La, and Ce of samples from Core 35, and source rocks. Samples are grouped tightly and plot most similarly to Bonney Pluton and Granitoids. As is discussed above for Cores 33 and 39, similarity to Bonney Pluton abundances is unexpected due to the formation being nearly 7 km away (Peterson and Marsh, 2008). *Different* from Core 33 and 39, though, is that the South Fork Pluton, a likely sediment contributor to the two cores, is on the south side of the Dais Plateau and therefore an unlikely contributor to Core 35 sediment. Abundances of Th, La, and Ce in Core 35 are only slightly higher than those of Core 2074 which is located in the center of hypersaline Don Juan Pond, suggesting potentially similar processes at the two sites. Because abundance of REEs can increase by more than over 200 % from fresh rock

to the most weathered in situ samples (Nesbitt and Markovics, 1997), HFSEs are used to validate REE conclusions.

3.4.4.2 Provenance Conclusion

Core 35 data is limited and thus an accurate conclusion is not possible. However, based solely on available data and regional geologic descriptions (Peterson and Marsh, 2008), the most likely source for Core 35 is Ferrar Dolerite and Granitoids. Additional data and analysis is pending.

3.4.5. CORE 42

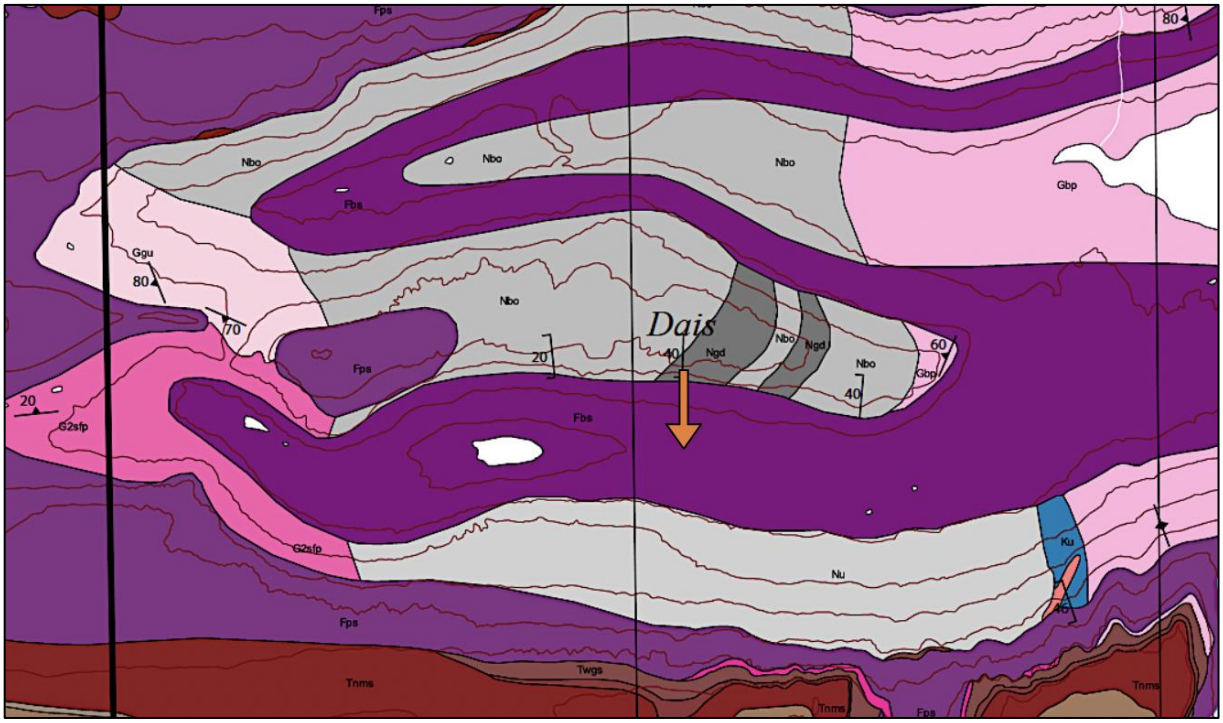

Figure 102. Regional geology of Core 42, VXE-6 Basin (Peterson and Marsh, 2008). VXE-6 Basin is bounded to the north by a plateau of Biotite orthogneiss (medium gray), and outcrops of Metagabbro Diorite (dark gray), and to the south by Granitic Gneiss (light gray). The basin floor is composed primarily of Ferrar Dolerite (purple).

3.4.5.1. Rare Earth Elements

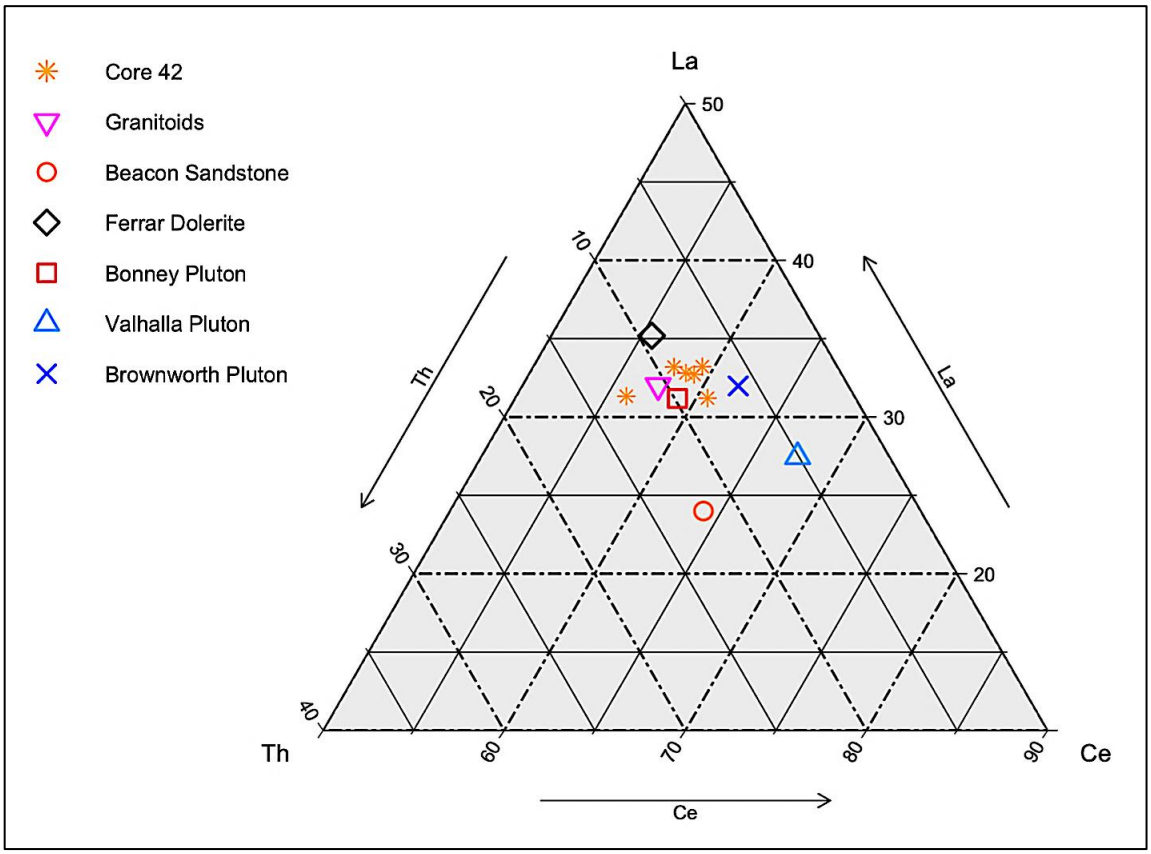

Figure 103. Th, La, Ce abundance of Core 42, VXE-6 Basin, and regional source rocks.

Figure 103 shows the relative abundances of Th, La, and Ce of samples from Core 42, and source rocks. All samples, except for one, are tightly grouped near source rocks Bonney Pluton and Granitoids, trending towards Ferrar Dolerite. REE abundance can increase by more than 200 % from fresh rock to the most weathered in situ samples (Nesbitt and Markovics, 1997), influencing the picture of sediment provenance. To check the validity of conclusions made from REEs, HFSEs are utilized due to their greater immobility.

As is discussed above for Cores 33 and 39, similarity to Bonney Pluton abundances is unexpected due to the formation being nearly 6 km away (Peterson and Marsh, 2008). The Bonney Pluton is shown to cover topographic lows across the majority of Central

Wright Valley, extending slightly into Upper Wright Valley, while the topographic highs, particularly the Dais Plateau, are primarily composed of gneissic plutonic rocks (Peterson and Marsh, 2008). Something to consider then is how far west the Bonney Pluton may extend *beneath* the Dais Plateau and influence the sediments of Core 42. However, due to the location of Core 42, Granitoids and Ferrar Dolerite are the favored source rocks.

3.4.5.2. High Field Strength Elements

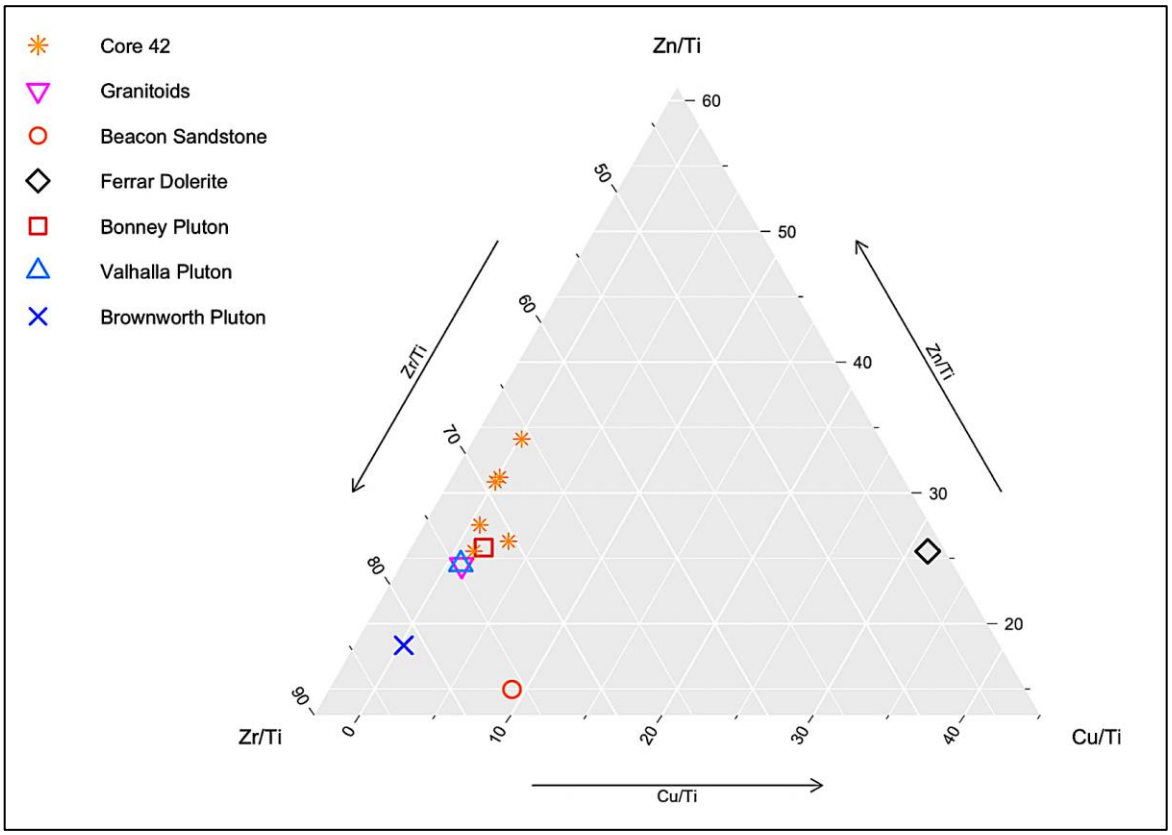

Figure 104. High Field Strength Element ratios Zr/Ti, Zn/Ti, and Cu/Ti of Core 42, VXE-6 Basin, and regional source rocks.

Figure 104 shows relative abundances of Zr/Ti, Zn/Ti, and Cu/Ti in Core 42 samples. Samples show significant variation in Zr/Ti, the most immobile HFSE ratio (Nesbitt and

Markovics, 1997) suggesting significant chemical alteration is occurring. Samples plot most similarly to Granitoids, and plutons Bonney and Valhalla. Similarity to Granitoids and Bonney Pluton corroborate the findings from REE analysis. Valhalla Pluton shows near identical abundances of Zr/Ti, Zn/Ti, and Cu/Ti to Granitoids however it exists 10+ km to the east making it unlikely a source rock to Core 42. While HFSE elements are very durable and immobile in alteration processes, unique conditions can mobilize them (Jiang et al., 2005). Core 42 at VXE-6 Pond is a good candidate for a high enough degree of chemical alteration to carry out such a process.

3.4.5.3. Major Elements

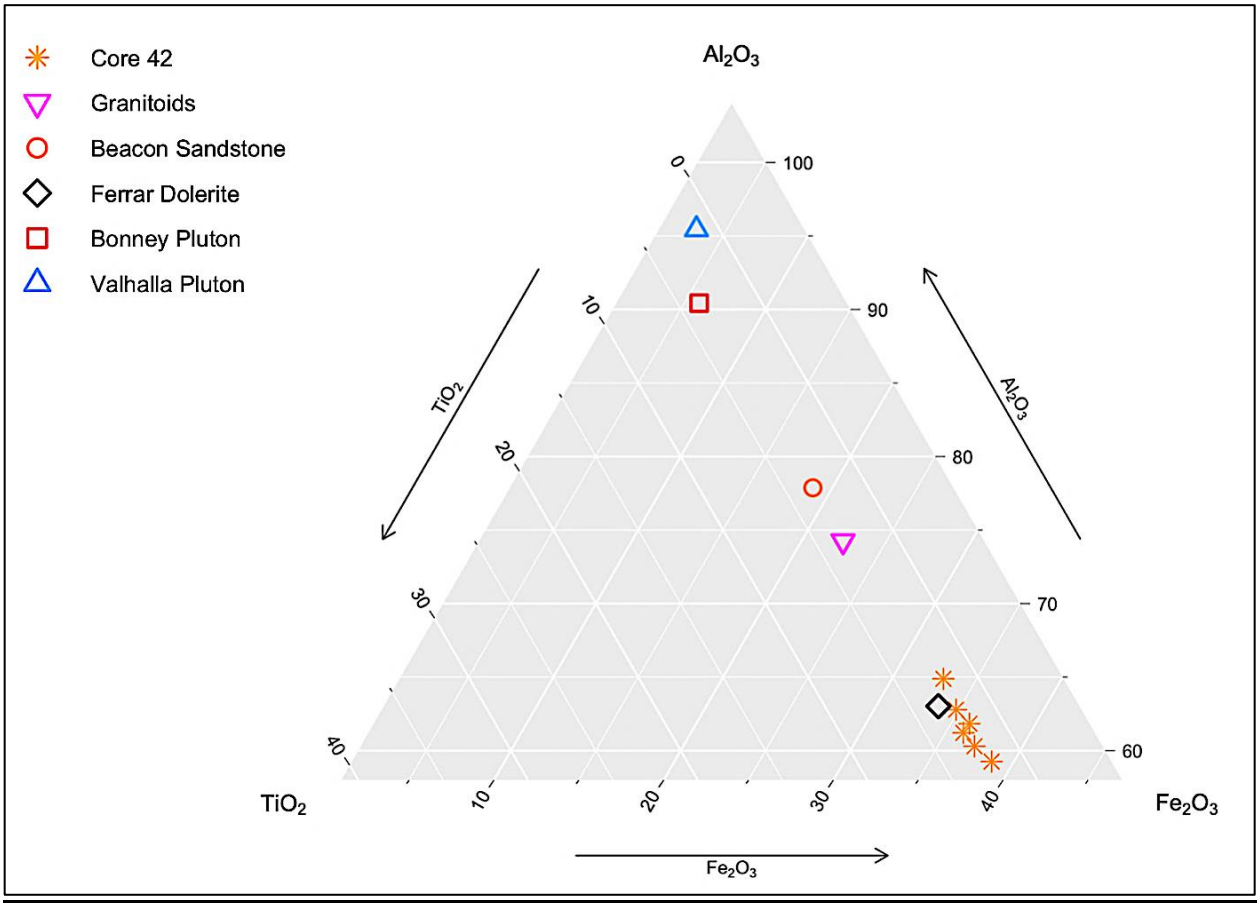

Figure 105. TiO_2, Al_2O_3, Fe_2O_3 abundance of Core 42, VXE-6 Basin, and regional source rocks.

Major elemental analysis of oxides TiO_2, Al_2O_3, and Fe_2O_3 of Core 42 samples shows variation primarily in abundance of Al_2O_3 and TiO_2, exhibiting greatest similarity to Ferrar Dolerite and trending away from all other source rocks. Ferrar Dolerite dominance makes sense as the source rock is ubiquitous across the basin floor (Peterson and Marsh, 2008).

3.4.5.4. CIA

Unmodified Chemical Index of Alteration values average about 37, in the range of fresh basalts (Nesbitt and Young, 1982; Fedo et al., 1995) and slightly below the average CIA of the Ferrar Dolerite: 42 (based on data from Grapes et al., 1989; Morrison, 1995). Based on this, the most likely provenance for Core 42 sediments is Ferrar Dolerite.

Modified Chemical Index of Alteration values, corrected for salt dilution, average about 58, in the range of granites to A-type granites (Fedo et al., 1995). This value is significantly higher than all source rocks except for Beacon Sandstone which is not shown near VXE-6 Basin (Harris, 1981). According to CIA values and location, the most likely provenance for Core 42 sediments is primarily Granitoids and Ferrar Dolerite that have been chemically altered.

3.4.5.5. Provenance Conclusion

Based on information discussed above, Core 42 sediment data best aligns with source rocks Granitoids, Ferrar Dolerite, and Bonney Pluton. This conclusion, however, is geographically puzzling as Bonney Pluton is found nearly 7 km to the east of Core 39 in central Wright Valley (Peterson and Marsh, 2008). The Bonney Pluton is shown to cover topographic lows across the majority of Central Wright Valley, extending slightly into Upper Wright Valley, while the topographic highs, particularly the Dais Plateau, are primarily composed of gneissic plutonic rocks (Peterson and Marsh, 2008). Something to consider then is how far west the Bonney Pluton may extend *beneath* the Dais Plateau and influence the sediments of Core 42. However, due to the location of Core

42, Granitoids and Ferrar Dolerite are the favored source rocks. Significant chemical alteration is likely occurring which could be responsible for REE and HFSE abundances similar to Bonney Pluton.

3.4.6. CORE 52

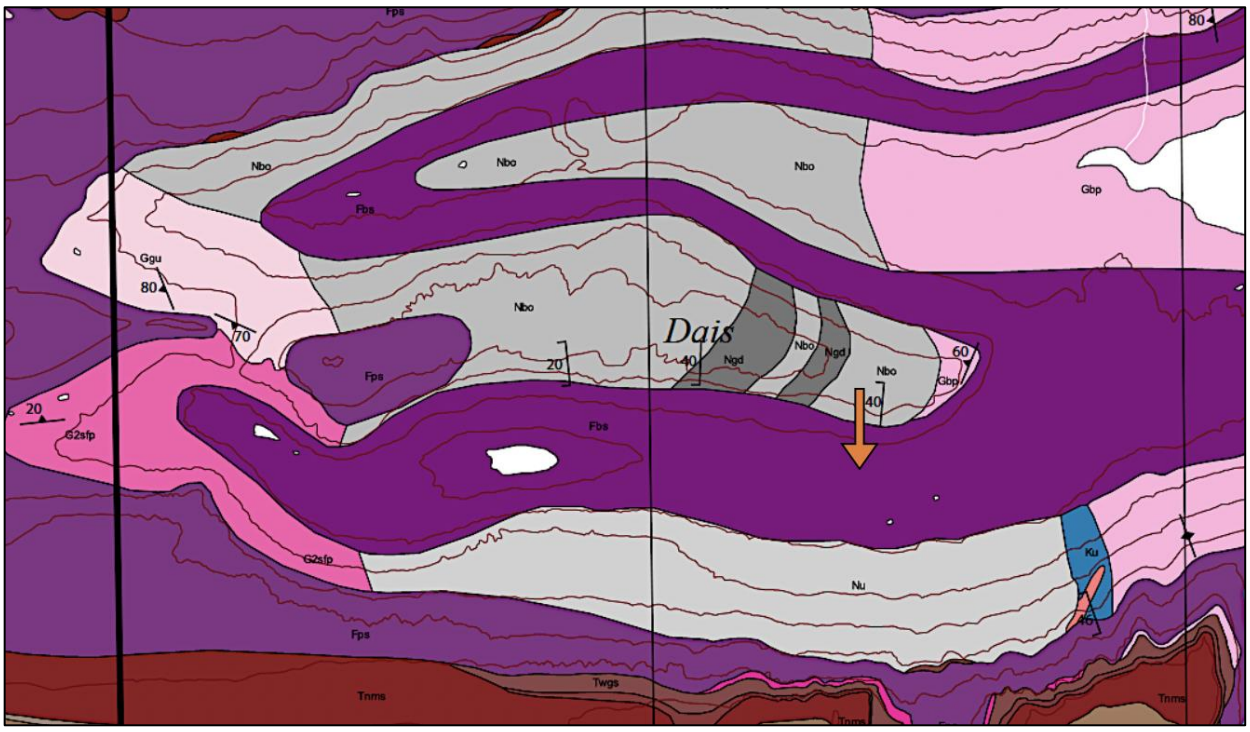

Figure 106. Regional geology of Core 52, South Fork (Peterson and Marsh, 2008). Core 52 is bound by Biotite Orthogneiss (medium gray) and Metagabbro Diorite (dark gray) to the north, and Granitic Gneiss (light gray) to the south. A small outcrop of the Bonney Pluton (medium pink) sits at the east end of the Dais Plateau, just north of the north of South Fork Basin. The basin floor is ubiquitously Ferrar Dolerite (purple).

3.4.6.1. Rare Earth Elements

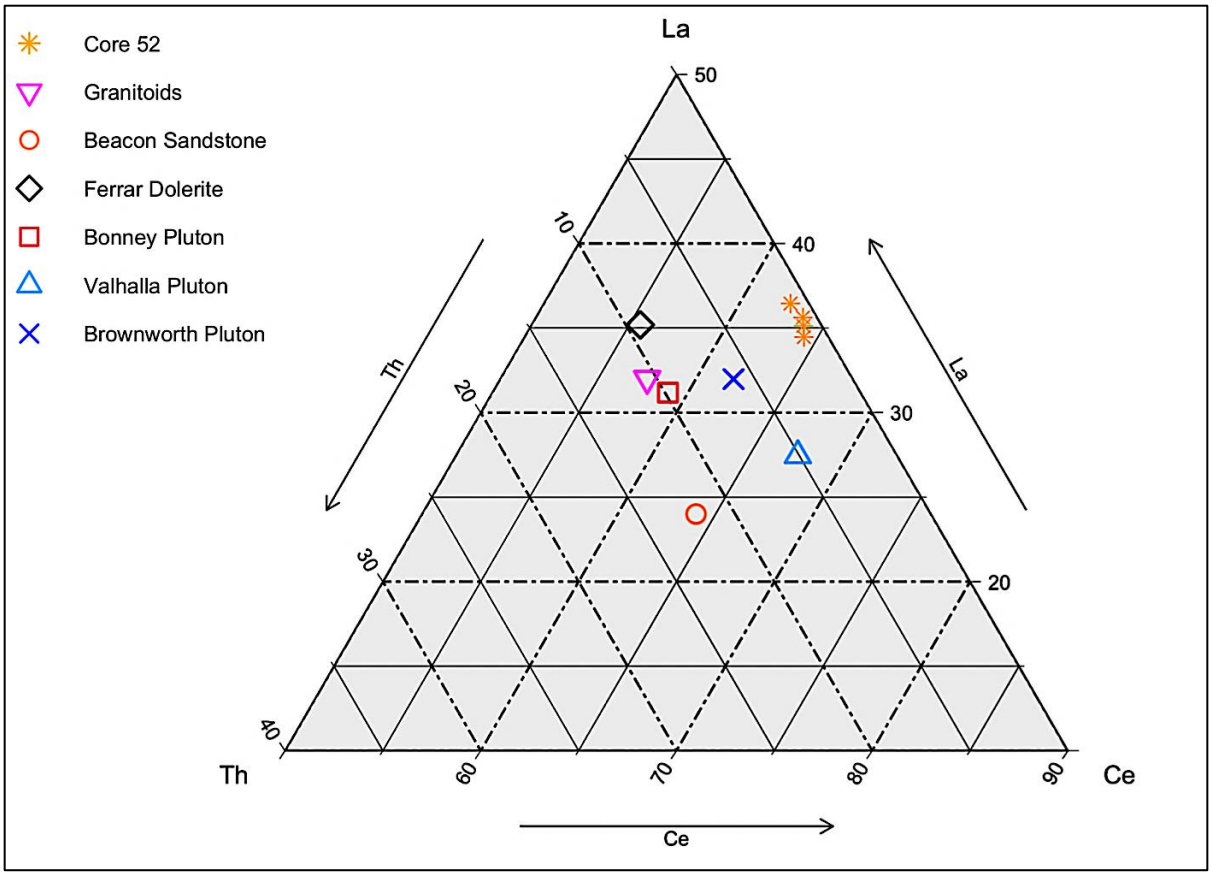

Figure 107. Th, La, Ce abundance of Core 52, South Fork, and regional source rocks.

Figure 107 shows the relative abundances of Th, La, and Ce of samples from Core 52, and source rocks. Samples are tightly grouped but very different in elemental abundance, likely due to the addition of local rock outcrops Bonney Pluton, and Metagabbro Diorite. Notably, all Core 52 samples exhibit enhanced Ce abundances, higher than any other microenvironment investigated. Ce abundances, though, could have significantly increased from source rock to sediment and be representing an inaccurate diagnosis of provenance. To check the validity of conclusions made from REEs, HFSEs are utilized due to their greater immobility.

3.4.6.2. High Field Strength Elements

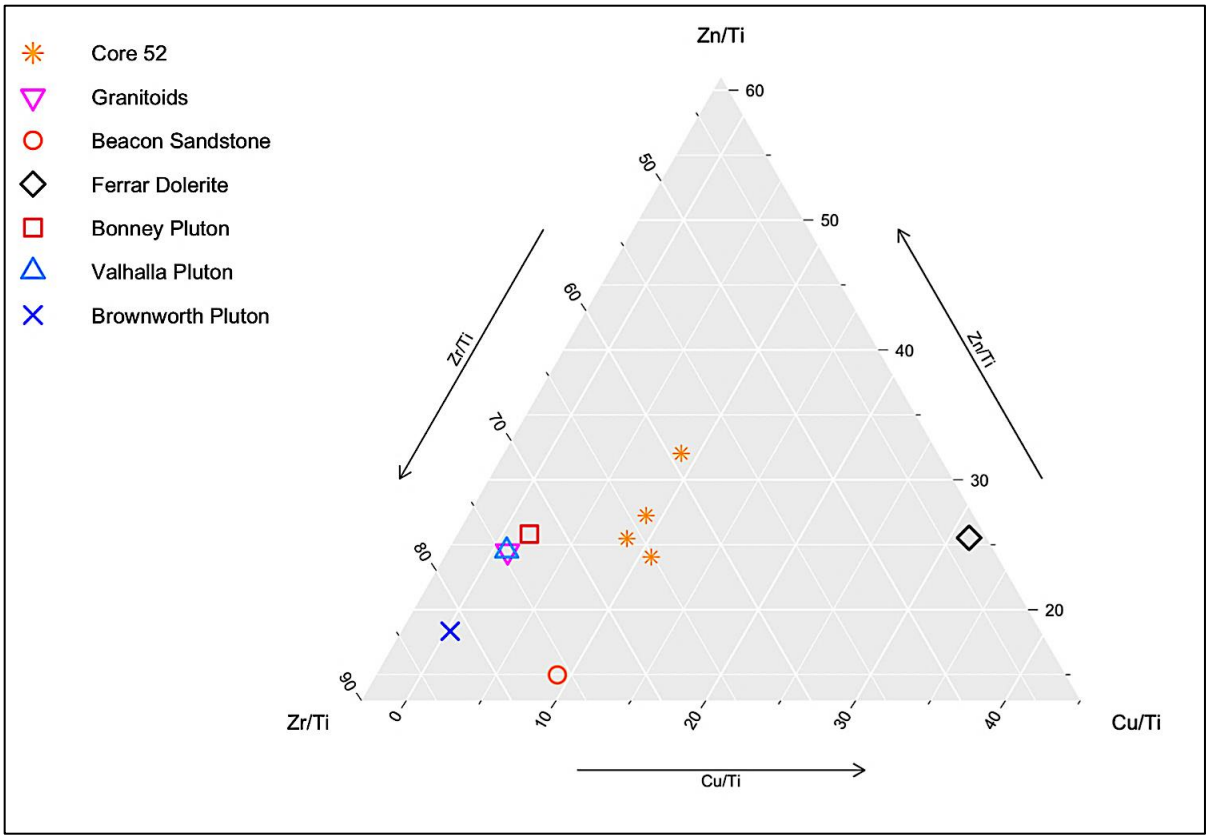

Figure 108. High Field Strength Element ratios Zr/Ti, Zn/Ti, and Cu/Ti of Core 52, South Fork, and regional source rocks.

Figure 108 shows relative abundances of Zr/Ti, Zn/Ti, and Cu/Ti in Core 52 samples. Samples exhibit similar elemental abundances to Cores 33 and 39 suggesting the possibility of similar processes operating at all sites. Based on the diagram, Core 52 sediments are most similar to Granitoids and Bonney Pluton, corroborating REE analysis. Valhalla Pluton and Granitoids exhibit similar Zr/Ti, Zn/Ti, and Cu/Ti abundances but Valhalla Pluton is far from Core 52 (Peterson and Marsh, 2008), ruling it out as a source rock. While HFSE elements are very durable and immobile in alteration processes, unique conditions can mobilize them (Jiang et al., 2005). Core 52 at Pond 1 is a good candidate for a high enough degree of chemical alteration to carry out such a process. Major elements are discussed below.

3.4.6.3. Major Elements

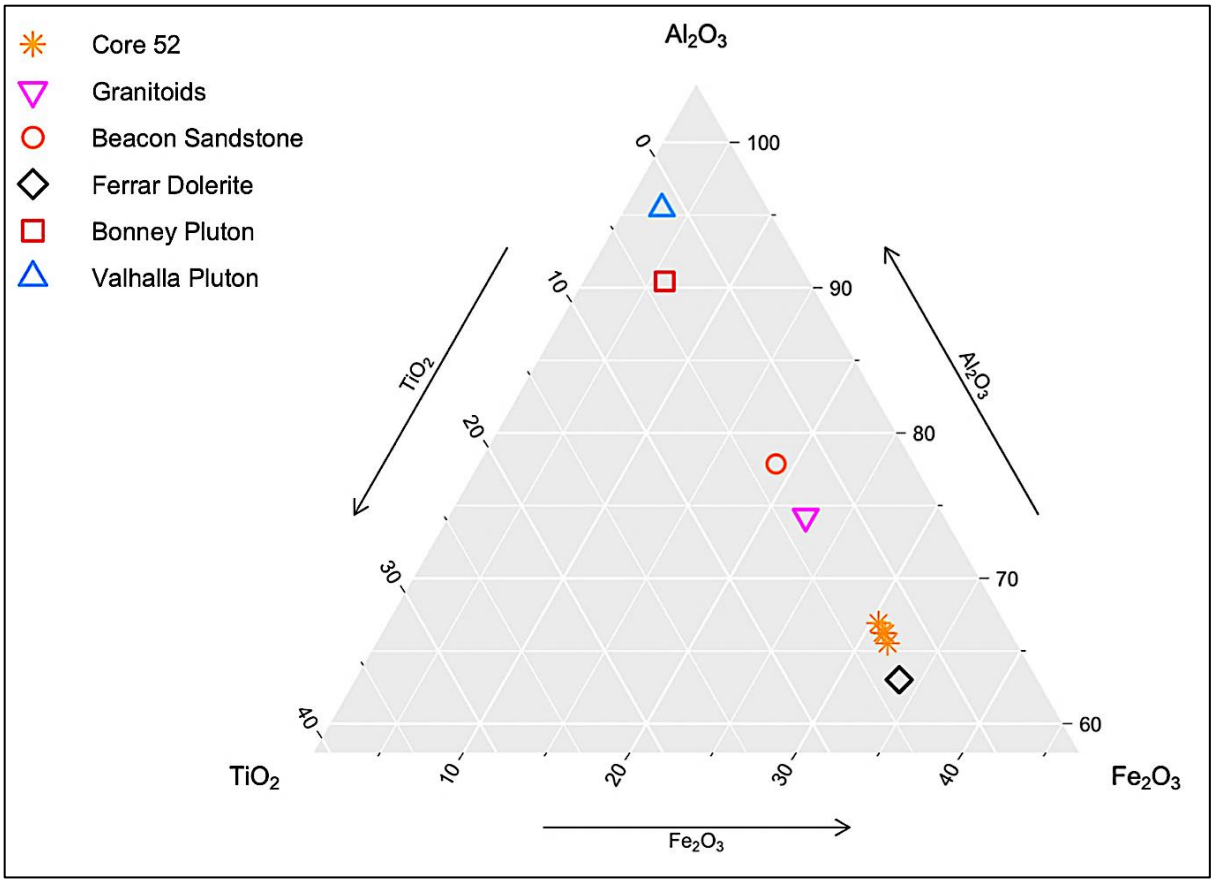

Figure 109. TiO_2, Al_2O_3, Fe_2O_3 abundance of Core 52, South Fork, and regional source rocks.

Major elemental analysis of oxides TiO_2, Al_2O_3, and Fe_2O_3 at Core 52 shows little variation among all three oxides. Samples bear greatest resemblance to Ferrar Dolerite and trend towards Granitoids. Though these findings do not align with those of REE and HFSE analysis, they are expected with the location: Ferrar Dolerite dominates the basin floor and Granitoids bind the basin to the north and south.

3.4.6.4. CIA

Unmodified Chemical Index of Alteration values average about 35, in the range of fresh basalts (Nesbitt and Young, 1982; Fedo et al., 1995) and slightly below the average CIA of the Ferrar Dolerite: 42 (based on data from Grapes et al., 1989; Morrison, 1995). Based on this, the most likely provenance for Core 52 sediments is Ferrar Dolerite.

Modified Chemical Index of Alteration values, corrected for salt dilution, average about 72, in the range of Charnockite (Fedo et al., 1995). According to CIA values and location, the most likely provenance for Core 52 sediments is primarily Granitoids and Ferrar Dolerite that have experienced heavy chemical alteration.

3.4.6.5. PROVENANCE CONCLUSION

Based on location and data discussed, Core 52 sediment data best align with source rocks Granitoids and Ferrar Dolerite. Granitoids, per modified CIA values, are likely present as charnockite, indicative of intermediate chemical alteration (Fedo et al., 1995). There is a possibility that the Bonney Pluton, whose presence is noted by REE and HFSE analysis and which exists at the east end of the Dais Plateau (Peterson and Marsh, 2008), could be extending beneath the Plateau farther *west* than previously thought.

3.4.7. CORE 72

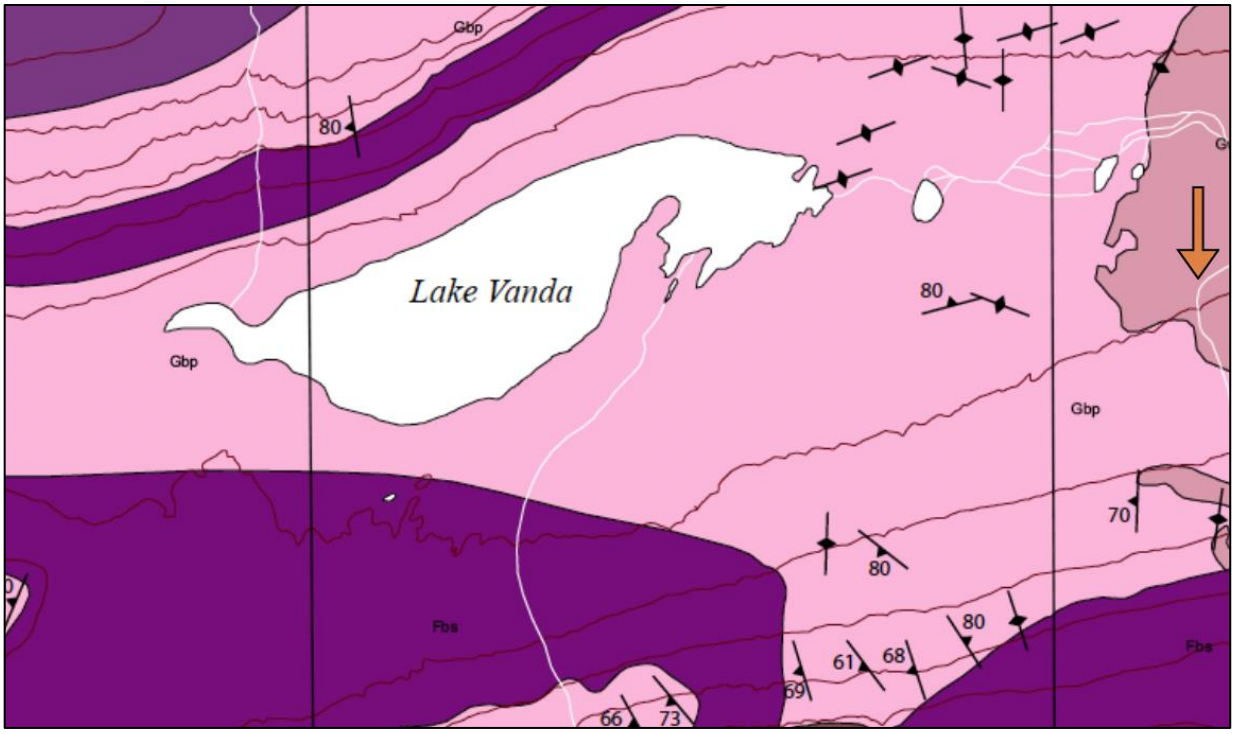

Figure 110. Regional geology of Core 72, Prospect Mesa (Peterson and Marsh, 2008). Core 72 sits in the middle of a large swath of the Bonney Pluton (light pink) with the Valhalla Pluton (medium pink) superimposed. Ferrar Dolerite (purple) exists to the north, west, and south (Peterson and Marsh, 2008). Felsic and mafic dikes are reported to the northeast of Lake Vanda (Allibone et al., 1993a).

3.4.7.1. Rare Earth Elements

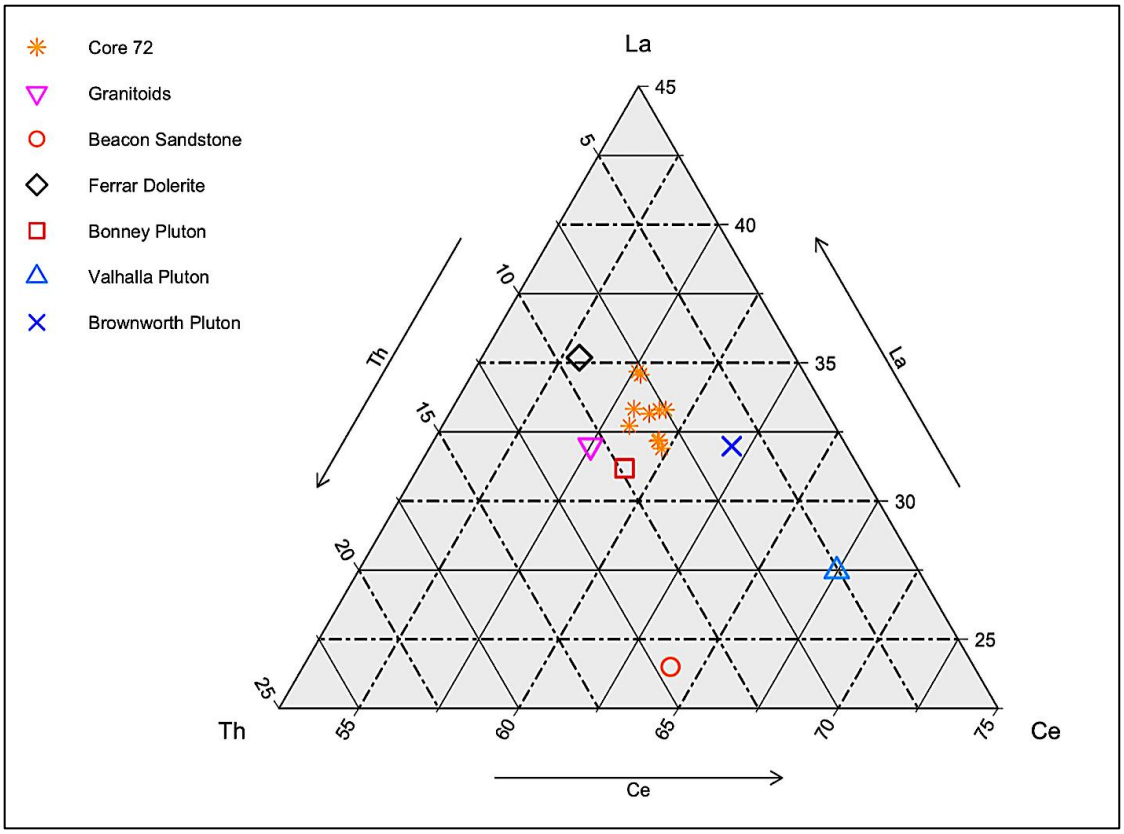

Figure 111. Th, La, Ce abundance of Core 72, Prospect Mesa, and regional source rocks.

Figure 111 shows the relative abundances of Th, La, and Ce of samples from Core 72, and source rocks. Variation is primarily seen in La and Th. Samples are relatively grouped and best match REE abundances of Bonney Pluton, Granitoids and Ferrar Dolerite. Based on the regional geology (Peterson and Marsh, 2008), these findings are expected.

3.4.7.2. High Field Strength Elements

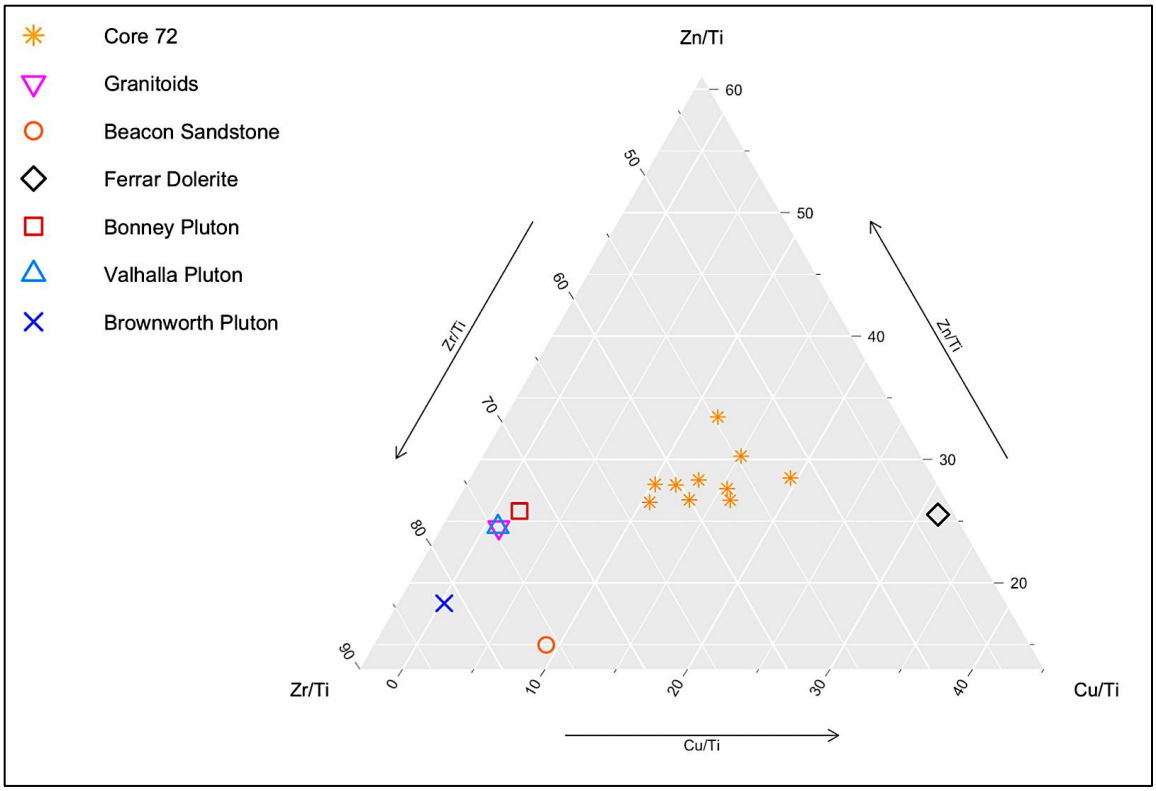

Figure 112. High Field Strength Element ratios Zr/Ti, Zn/Ti, and Cu/Ti of Core 72, Prospect Mesa, and regional source rocks.

Figure 112 shows relative abundances of Zr/Ti, Zn/Ti, and Cu/Ti in Core 72 samples. Samples show the greatest variation in Cu/Ti with a couple samples exhibiting elevated Zn/Ti, and depleted Zr/Ti. Core 72 samples sit in the middle of the diagram, halfway between plutons Bonney and Valhalla, and Granitoids and Ferrar Dolerite. Such findings are expected as all four of the aforementioned source rocks are reported in the region (Peterson and Marsh, 2008). Major elements are discussed below.

3.4.7.3. Major Elements

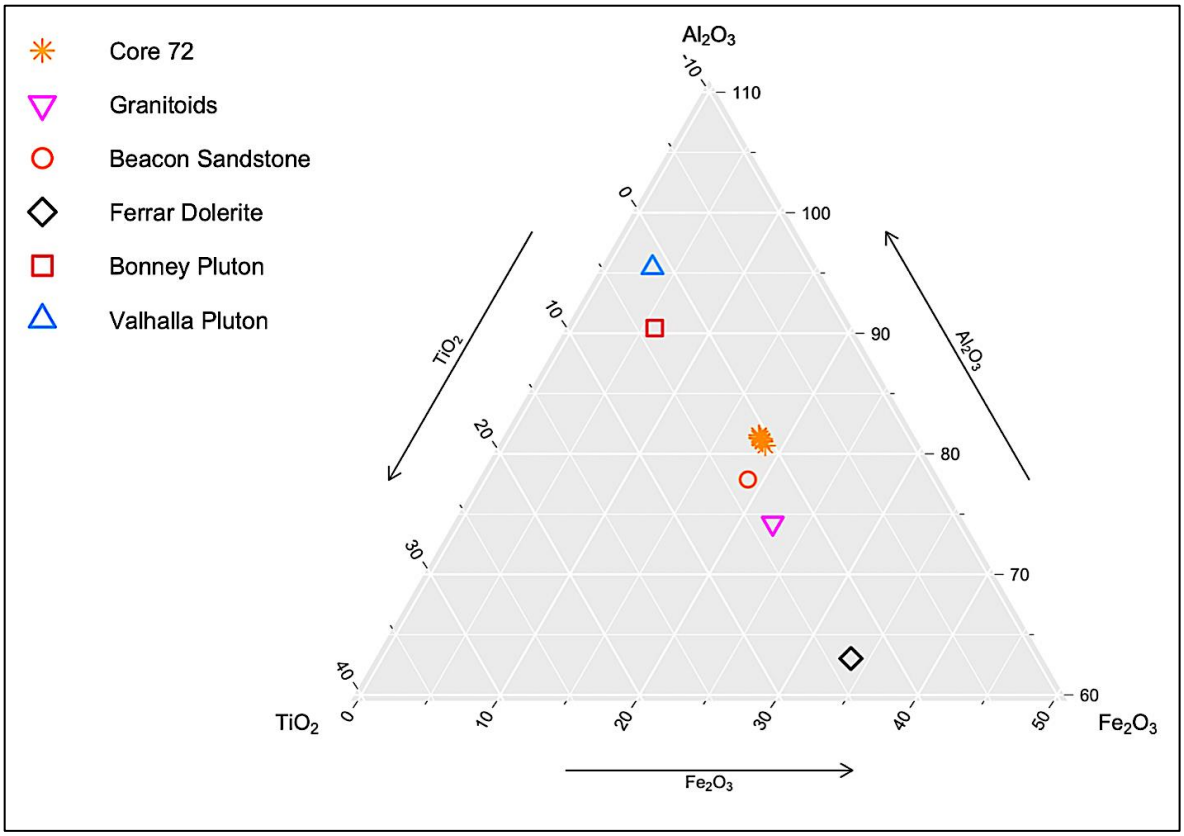

Figure 113. TiO_2, Al_2O_3, Fe_2O_3 abundance of Core 72, Prospect Mesa, and regional source rocks.

Major elemental analysis of oxides TiO_2, Al_2O_3, and Fe_2O_3 at Core 72 shows virtually no variation in abundance. Samples, as in REE and HFSE analysis, exist approximately halfway between the average abundances of plutons Bonney and Valhalla, Granitoids, and Ferrar Dolerite.

3.4.7.4. CIA

Unmodified Chemical Index of Alteration values average about 35, in the range of fresh basalts (Nesbitt and Young, 1982; Fedo et al., 1995) and slightly below the average CIA of the Ferrar Dolerite: 42 (based on data from Grapes et al., 1989; Morrison, 1995). Based on this, the most likely provenance for Core 72 sediments is Ferrar Dolerite.

Modified Chemical Index of Alteration values, corrected for salt dilution, average about 45, not much higher than the modified CIA values and still in the range of fresh basalts (Nesbitt and Young, 1982; Fedo et al., 1995).

3.4.7.5. Provenance Conclusion

Based on information discussed, the most likely provenance for Core 72 sediments is primarily Ferrar Dolerite that has experienced physical alteration by means of sediment mixing. Granitoids, and plutons Bonney and Valhalla are likely present as well, but in a secondary capacity. Overall, Core 72 does not seem to be experiencing significant chemical alteration. This conclusion corroborates that from Chapter 2— Core 72 is dominated by physical alteration.

3.4.8. LAKE VANDA

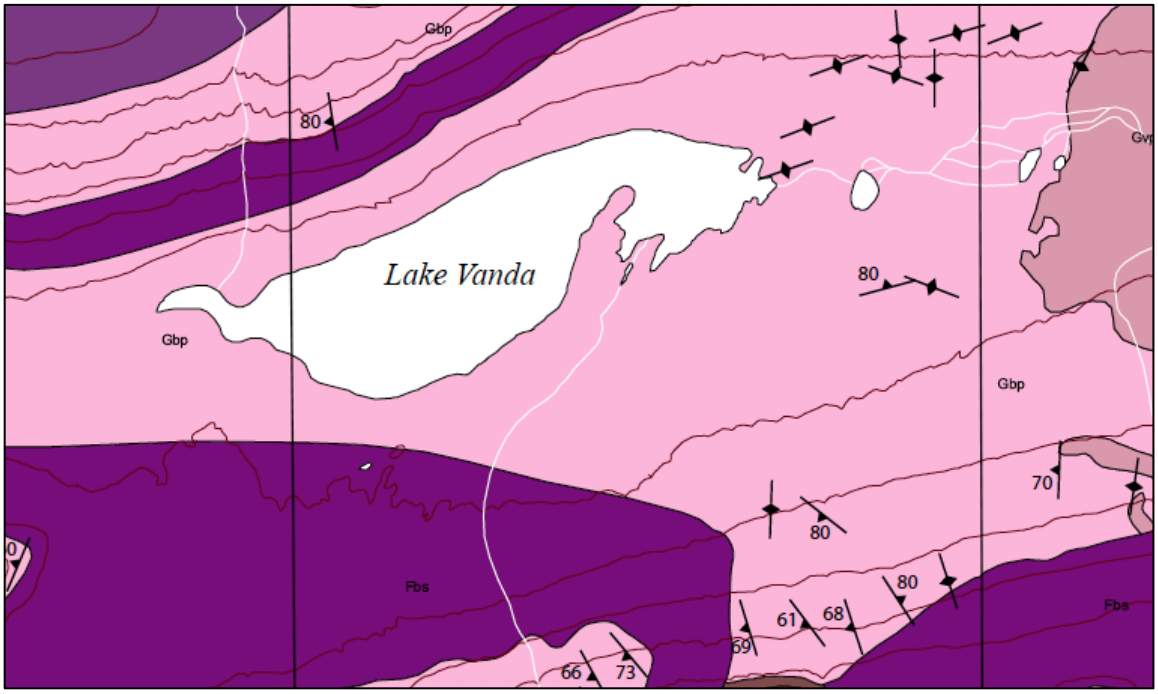

Figure 114. Regional geology of Lake Vanda, Wright Valley (Peterson and Marsh, 2008). Lake Vanda is bound on all sides by the Bonney Pluton (light pink), to the north and south by Ferrar Dolerite (purple), and Valhalla Pluton (medium pink) to the east. Felsic and mafic dikes are reported to the northeast (Allibone et al., 1993a).

3.4.8.1. Rare Earth Elements

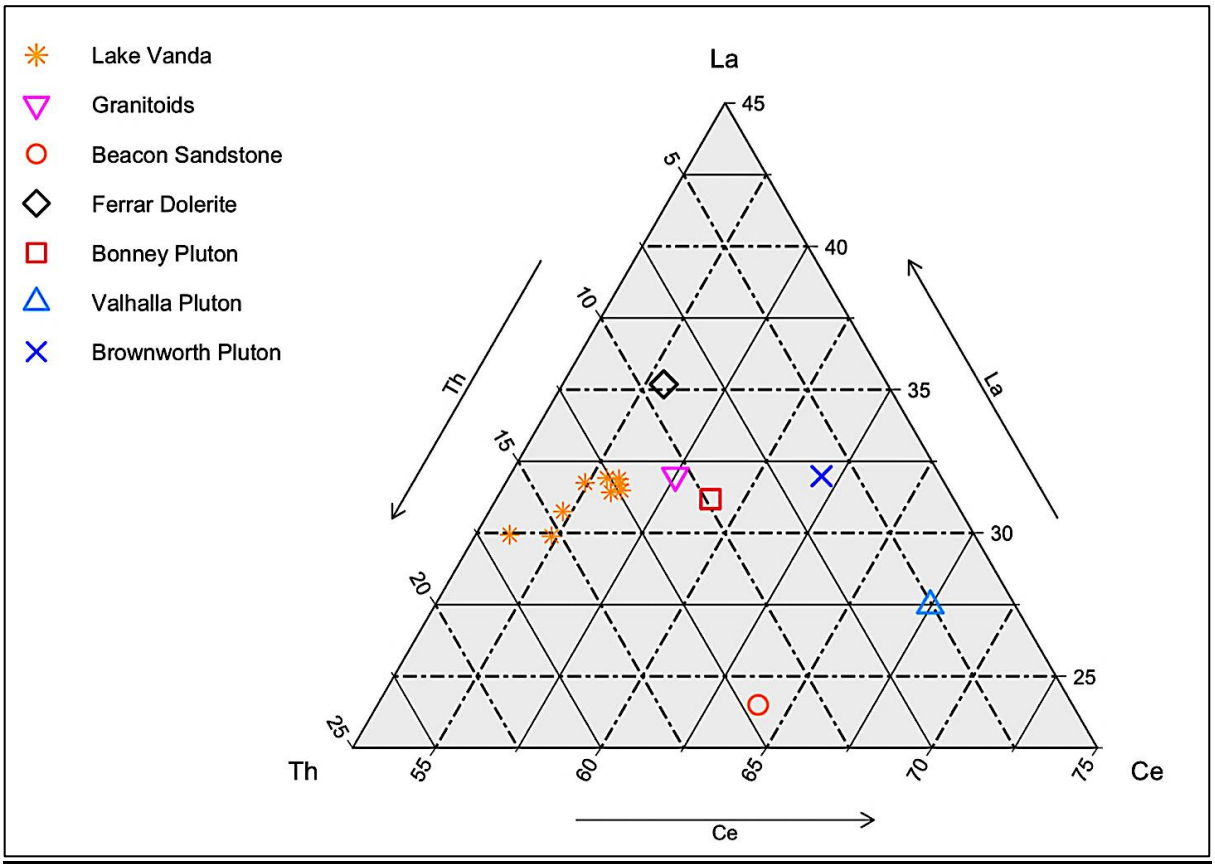

Figure 115. Th, La, Ce abundance at Lake Vanda, Wright Valley, and of regional source rocks.

Figure 115 shows the relative abundances of Th, La, and Ce of surface and edge samples from Lake Vanda, and source rocks. Variation is primarily seen in Th, however La and Ce exhibit notable variation as well. Lake Vanda sample abundances of Th, La, and Ce best align with Granitoids and Ferrar Dolerite. REE abundance diagnostic of Granitoids more so than Bonney Pluton is unexpected, but it is possible that fluvial transport by the Onyx River, which passes through a large swath of Biotite Orthogneiss and Hornblende-Biotite Orthogneiss (Peterson and Marsh, 2008) could be the reason for these results.

3.4.8.2. High Field Strength Elements

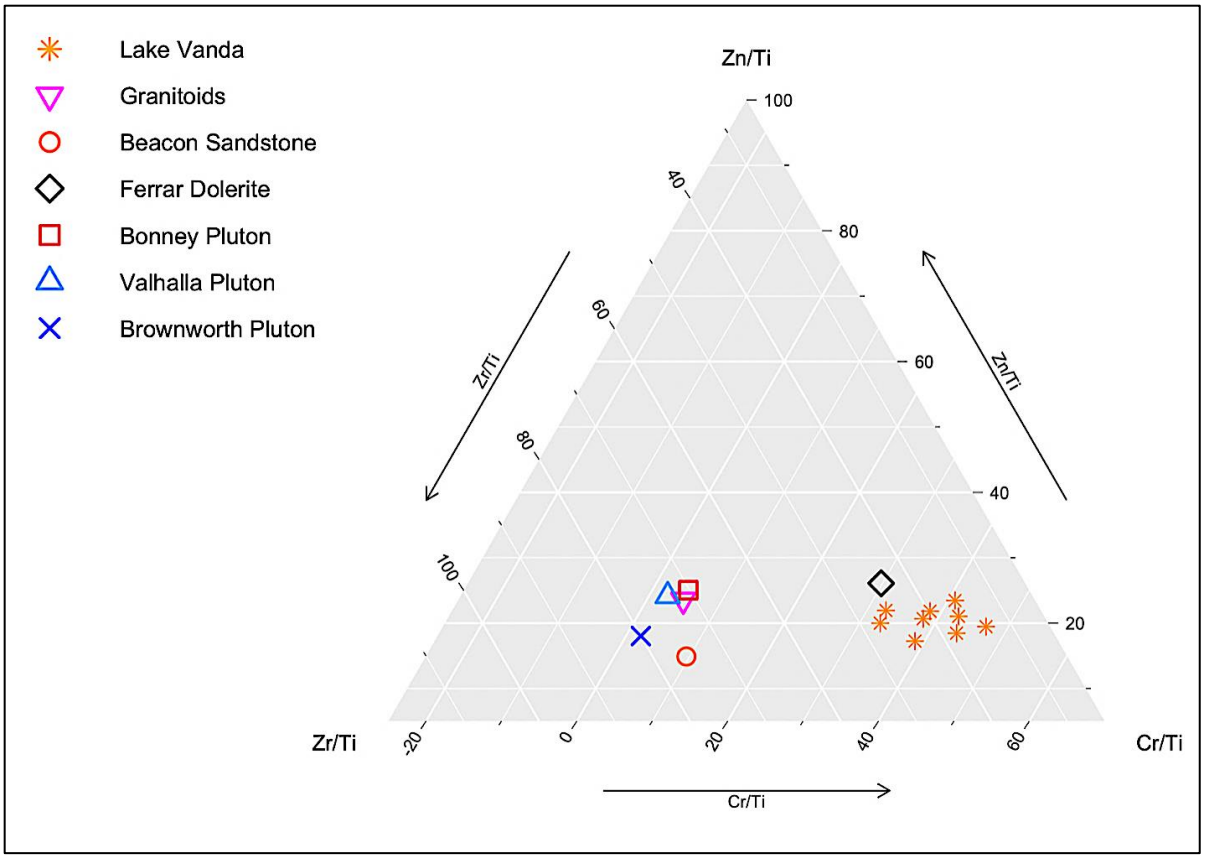

Figure 116. High Field Strength Element ratios Zr/Ti, Zn/Ti, and Cu/Ti at Lake Vanda, Wright Valley, and of regional source rocks.

Figure 116 shows relative abundances of Zr/Ti, Zn/Ti, and Cr/Ti in Lake Vanda surface and edge samples. Lake samples are well grouped and show variation primarily in abundances of Cr/Ti, the most mobile of the elemental ratios investigated here (Nesbitt and Markovics, 1997). Zr/Ti, Zn/Ti, and Cr/Ti abundances clearly align best with those of Ferrar Dolerite. It is possible that surficial Ferrar Dolerite, as noted by Allibone et al. (1993a), is responsible for such elemental favoritism. Aeolian and fluvial transport from Ferrar Dolerite outcrops to the north and west support this conclusion. Major elements are discussed below.

3.4.8.3. Major Elements

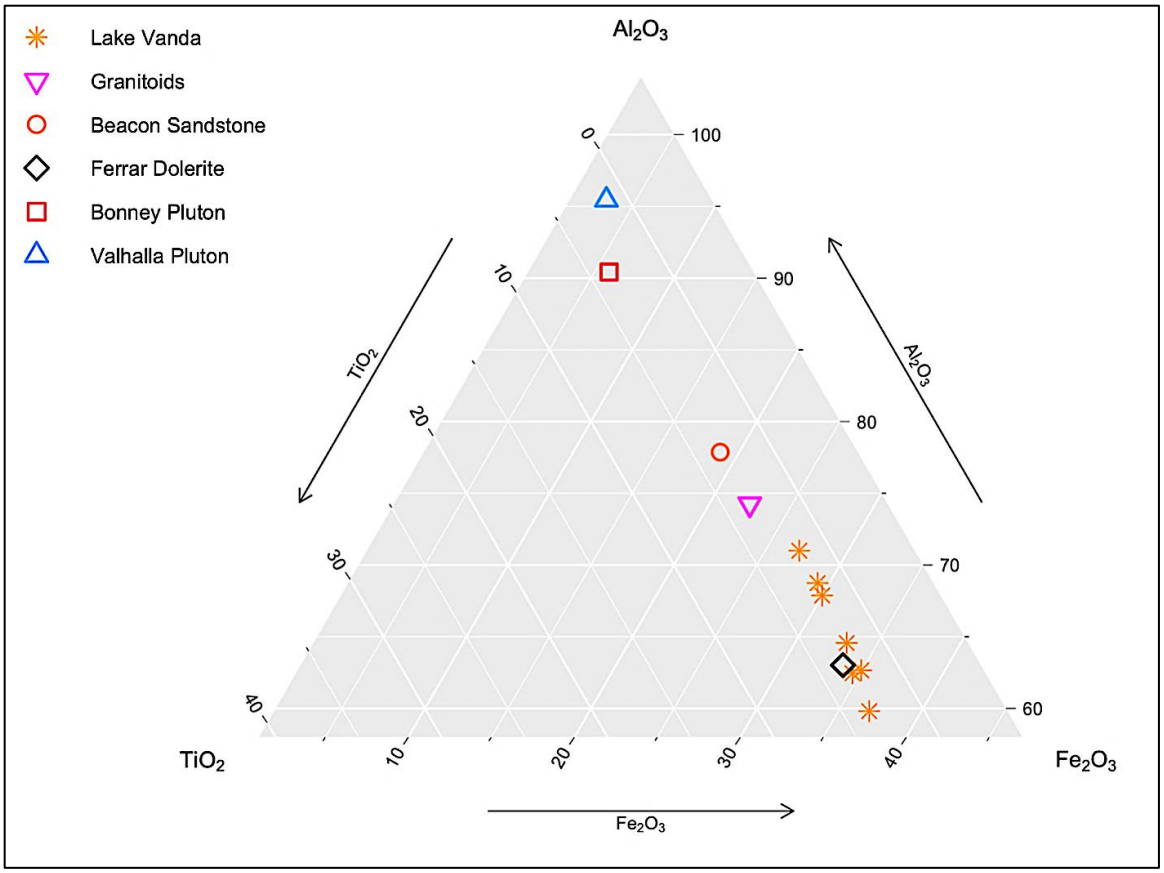

Figure 117. TiO_2, Al_2O_3, Fe_2O_3 abundance of Lake Vanda, Wright Valley, and of regional source rocks.

Major elemental analysis of surface and edge samples from Lake Vanda shows significant variation in Al_2O_3 and TiO_2 abundances. Sample elemental abundances best align with those of Ferrar Dolerite and trend towards Granitoids. These findings support those of REE and HFSE analysis. Ferrar Dolerite, and trends toward Granitoids could be due to Aeolian and fluvial transport from Ferrar Dolerite outcrops to the north and west, and Granitoid outcrops to the west and east.

3.4.8.4. CIA

Unmodified Chemical Index of Alteration values average about 40, in the range of fresh basalts (Nesbitt and Young, 1982; Fedo et al., 1995) and slightly below the average CIA

of the Ferrar Dolerite: 42 (based on data from Grapes et al., 1989; Morrison, 1995). Based on this, the most likely provenance for Lake Vanda sediments is Ferrar Dolerite.

Modified Chemical Index of Alteration values, corrected for salt dilution, average about 41, only slightly higher than the modified CIA values and still in the range of fresh basalts (Nesbitt and Young, 1982; Fedo et al., 1995). Because the average modified CIA value is nearly identical to the average unmodified value, surficial chemical alteration at Lake Vanda is not supported.

3.4.8.5. Provenance Conclusion

Based on information discussed, the most likely provenance for Lake Vanda is Ferrar Dolerite and Granitoids. This conclusion is supported by Bishop et al., 2014. Though these two source rocks do not dominate the region, their presence is supported by aeolian transport from the west, and fluvial transport from the north and east. Additionally, because the average modified CIA value is nearly identical to the average unmodified value, it is difficult to argue different source rocks provenance. For a more comprehensive analysis of the site, depth profiles (cores), as seen at sites to the west and at Lake Hoare, ought to be taken.

3.4.9. LAKE BROWNWORTH

Lake Brownworth is located in east Wright Valley, directly west of Wright Lower Glacier. Sediment samples were collected from the surface and edge of the lake. Principal summer wind directions, as reported by Nylen et al. (2004), are predominantly down-valley (easterly). Samples were collected in the summer of 2004, making aeolian transport a potential influencing factor of sediment deposition. Lake Brownworth likely has one major source rock: the Brownworth Pluton a coarse-grained, homogenous granite and quartz monzonite (Peterson and Marsh, 2008). Importantly, Allibone et al. (1993a), draws many of his conclusions of locations of plutons after Ferrar Dolerite being removed to expose the plutonic surface below. With Wright Lower Glacier directly to the east of Lake Brownworth, glacial transport of sediment from the east.

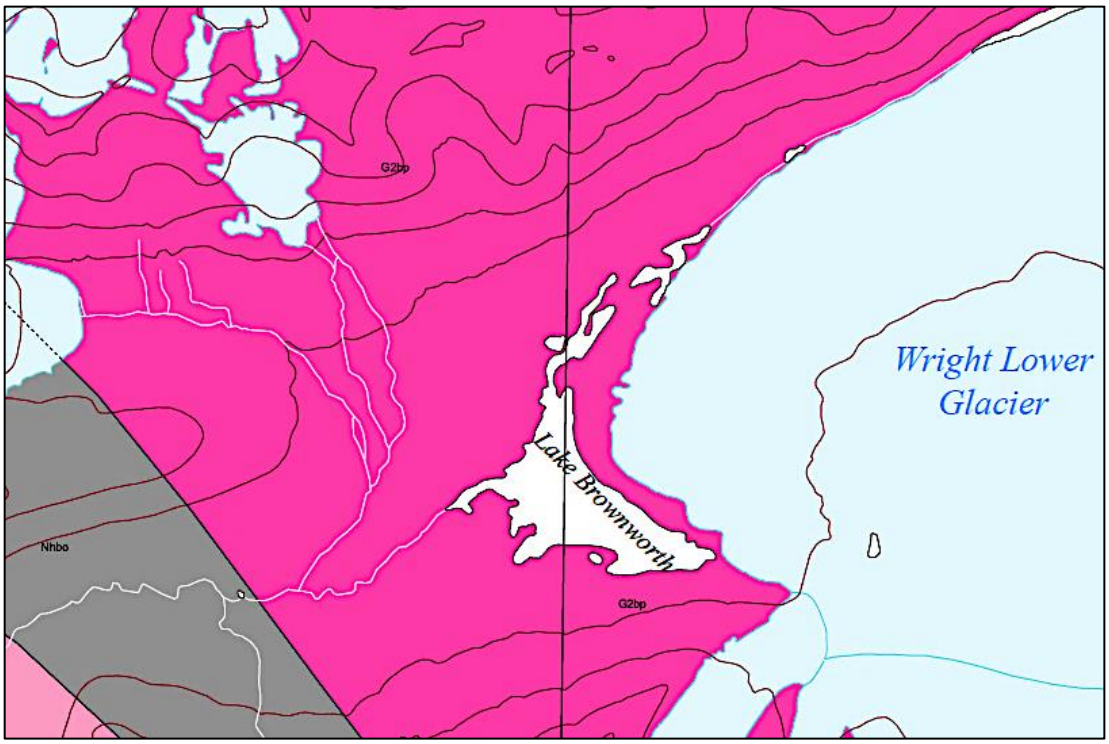

Figure 118. Regional geology of Lake Brownworth, Wright Valley (Peterson and Marsh, 2008). Brownworth Pluton (pink).

3.4.9.1. Rare Earth Elements

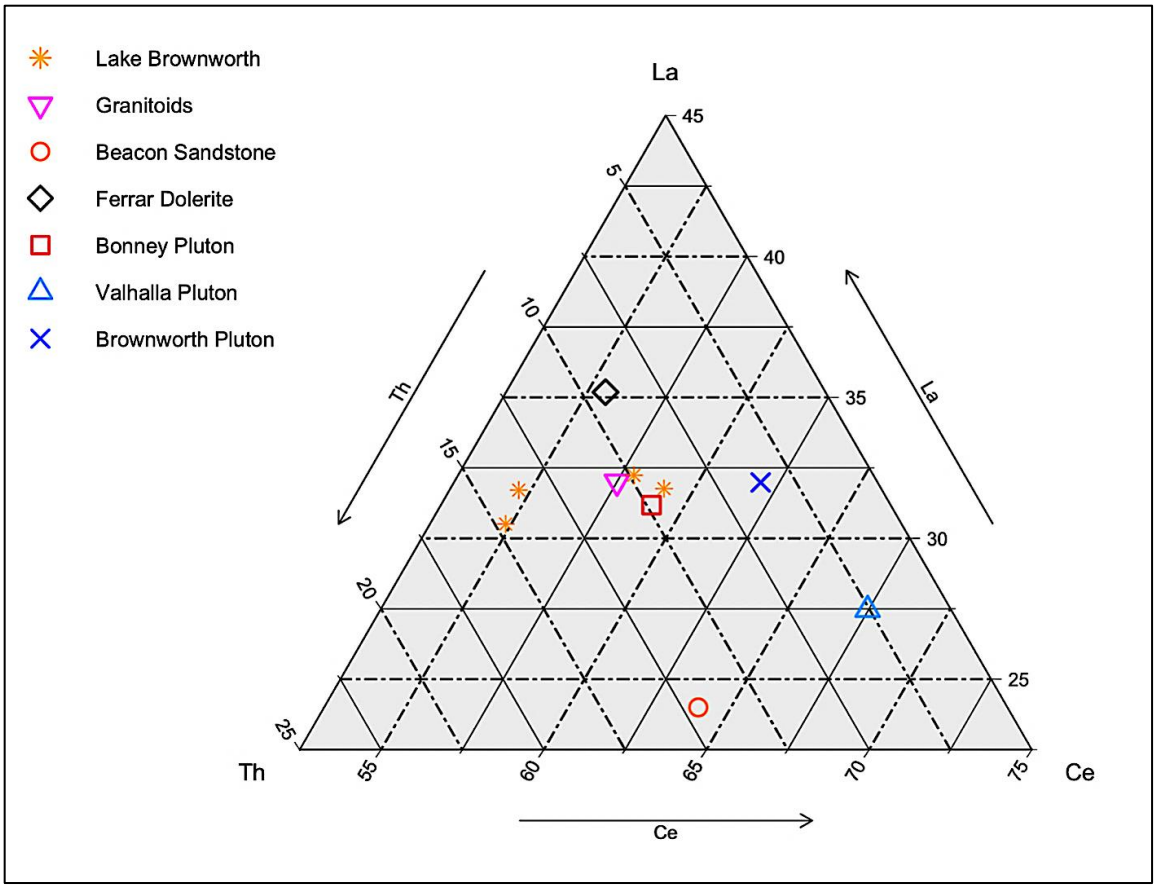

Figure 119. Th, La, Ce abundance at Lake Brownworth, Wright Valley, and of regional source rocks.

Figure 119 shows the relative abundances of Th, La, and Ce of surface and edge samples from Lake Brownworth, and source rocks. Samples exhibit significant Ce variation, and plot most similarly to Ferrar Dolerite, Granitoids, and Bonney Pluton. Ferrar Dolerite is reported to be extensive across the surface of the MDV (Allibone et al., 1993a), and Granitoids dominate western Wright Valley from which easterly aeolian transport can deposit sediments. Additionally, Granitoids are reported in small outcrops in and around Victoria Lower Glacier, Greenwood Glacier, and Wilson Piedmont Glacier—all of which connect with Lower Wright Glacier. Glacial transport of granitoid sediments is therefore a possibility as well.

3.4.9.2. High Field Strength Elements

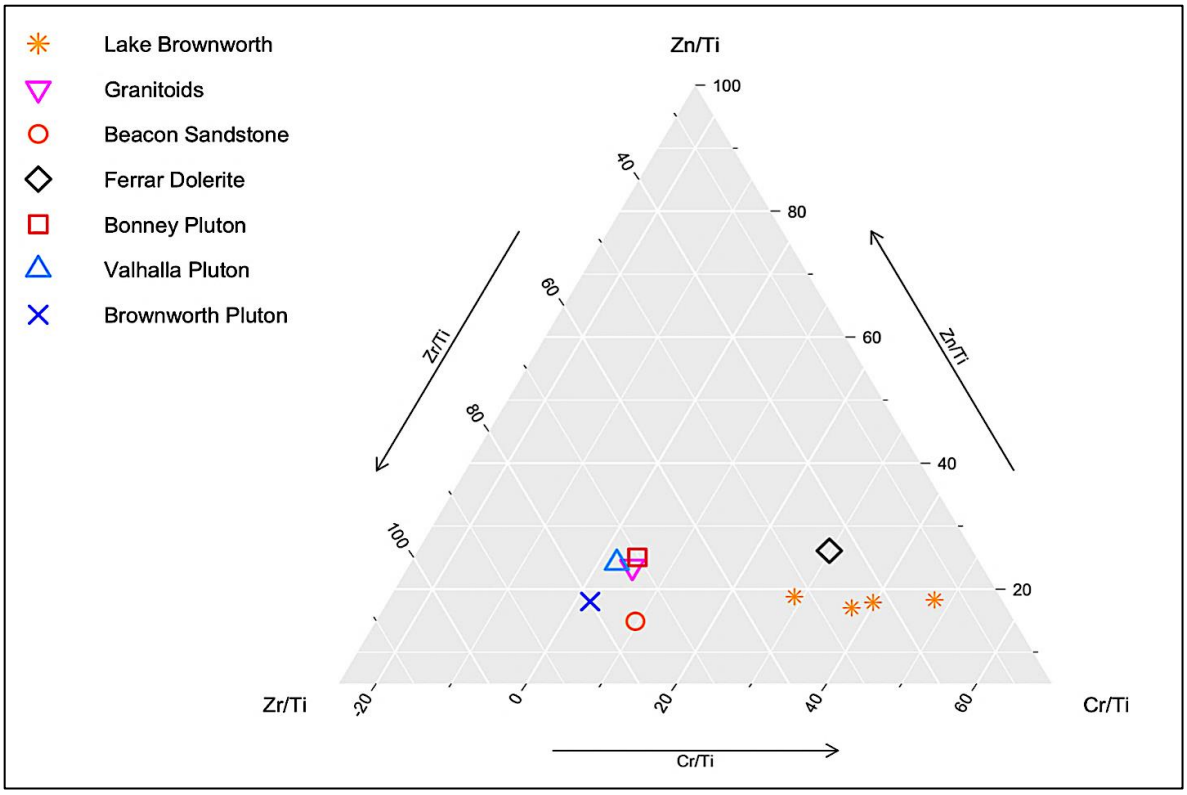

Figure 120. High Field Strength Element ratios Zr/Ti, Zn/Ti, and Cu/Ti at Lake Brownworth, Wright Valley, and of regional source rocks.

Figure 120 shows relative abundances of Zr/Ti, Zn/Ti, and Cr/Ti in Lake Brownworth surface and edge samples. Variation is seen almost exclusively in Cr/Ti abundances, the most mobile of the elemental ratios investigated here (Nesbitt and Markovics, 1997). Samples plot most similarly to elemental abundances of Ferrar Dolerite, supporting the findings from REE analysis. Major elements are discussed below.

3.4.9.3. Major Elements

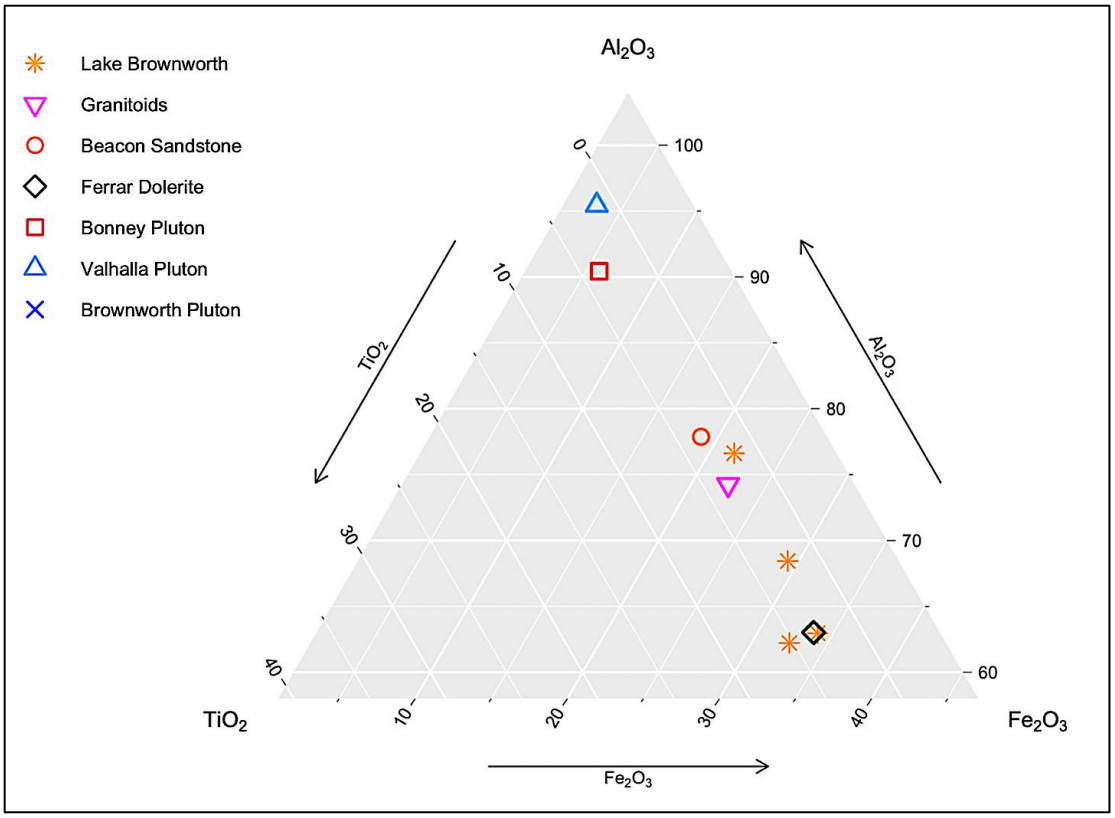

Figure 121. TiO_2, Al_2O_3, Fe_2O_3 abundance at Lake Brownworth, Wright Valley, and of regional source rocks.

Major elemental analysis of surface and edge samples from Lake Brownworth shows significant variation in Al_2O_3 and TiO_2 abundance. Samples plot most similarly to Ferrar Dolerite with a trend towards, and one sample highly diagnostic of, Granitoids. These findings combine and corroborate those of REE and HFSE analysis.

3.4.9.4. CIA

Unmodified Chemical Index of Alteration values average about 43, in the range of fresh basalts (Nesbitt and Young, 1982; Fedo et al., 1995) and slightly above the average CIA

of the Ferrar Dolerite: 42 (based on data from Grapes et al., 1989; Morrison, 1995). Based on this, the most likely provenance for Lake Vanda sediments is Ferrar Dolerite.

Modified Chemical Index of Alteration values, corrected for salt dilution, average about 43 as well. This is still in the range of fresh basalts (Nesbitt and Young, 1982; Fedo et al., 1995). Because the average modified CIA value is nearly identical to the average unmodified value, and *below* the lowest range of chemical alteration as proposed by Fedo et al., 1995, surficial chemical alteration at Lake Vanda is not supported and provenance is likely dominated by Ferrar Dolerite.

3.4.9.5. PROVENANCE CONCLUSION

Based on information discussed, the most likely provenance for Lake Brownworth surface and edge sediments is Ferrar Dolerite and Granitoids. This conclusion is supported by Bishop et al., 2014. Though the regional source rock should be Brownworth Pluton (Peterson and Marsh, 2008), because samples are all surficial (Allibone et al., 1993a), they are Ferrar Dolerite and Granitoids. Should cores be taken at Lake Brownworth, Brownworth Pluton would likely be sampled, and a potentially greater degree of chemical alteration would be observed.

3.4.10. LAKE FRYXELL

Lake Fryxell likely has one major source rock. Undifferentiated Gneiss OR Biotite Orthogneiss (gray in Figure 124, below). However, Brownworth Pluton is reported on either side of the two possible source rocks and could be influencing the data. Principal summer wind directions, as reported by Nylen et al. (2004), are predominantly down-valley (easterly), making aeolian sedimentation from westerly sources a possibility as well.

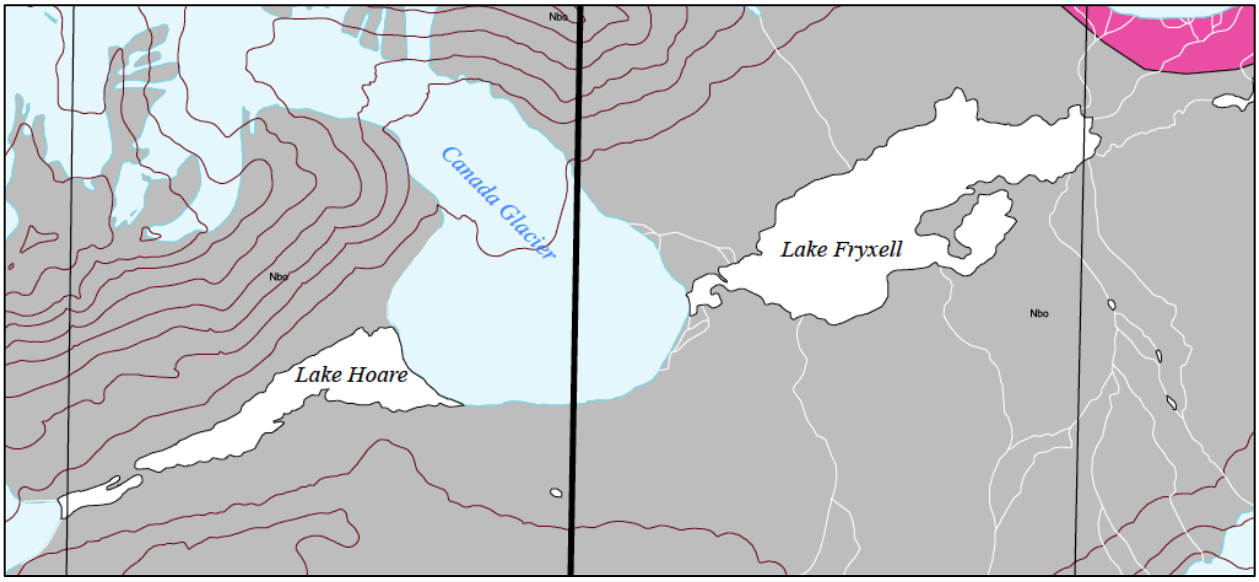

Figure 122. Regional geology of Lake Fryxell, Taylor Valley (Peterson and Marsh, 2008). Undifferentiated Gneiss or Biotite Orthogneiss (gray).

3.4.10.1. Rare Earth Elements

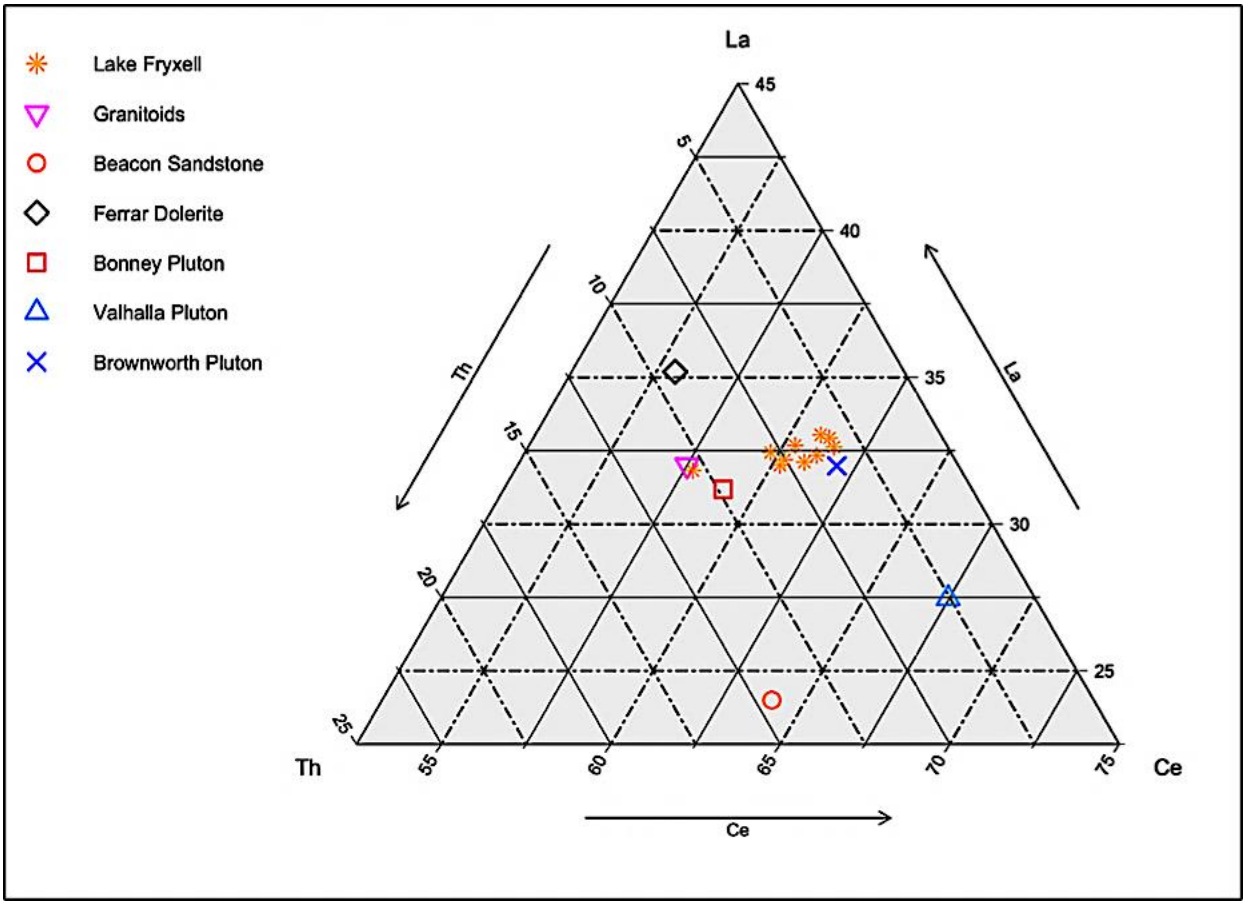

Figure 123. Th, La, Ce abundance at Lake Fryxell, Taylor Valley, and of regional source rocks.

Figure 123 shows the relative abundances of Th, La, and Ce of surface and edge samples from Lake Fryxell, and source rocks. Samples exhibit very little variation in all three elements except for one sample. All but one sample exhibit Th, La, and Ce abundances most similar to Brownworth Pluton. The single outlying sample is most similar to Granitoids. Elemental favoritism towards Brownworth Pluton, should it be accurate, supports the theory of southerly sediment transport from formations in the north via fluvial and glacial processes. Enhanced REE abundance from source rock to sediment is possible (Nesbitt and Markovics, 1997) making HFSE analysis critical.

3.4.10.2. High Field Strength Elements

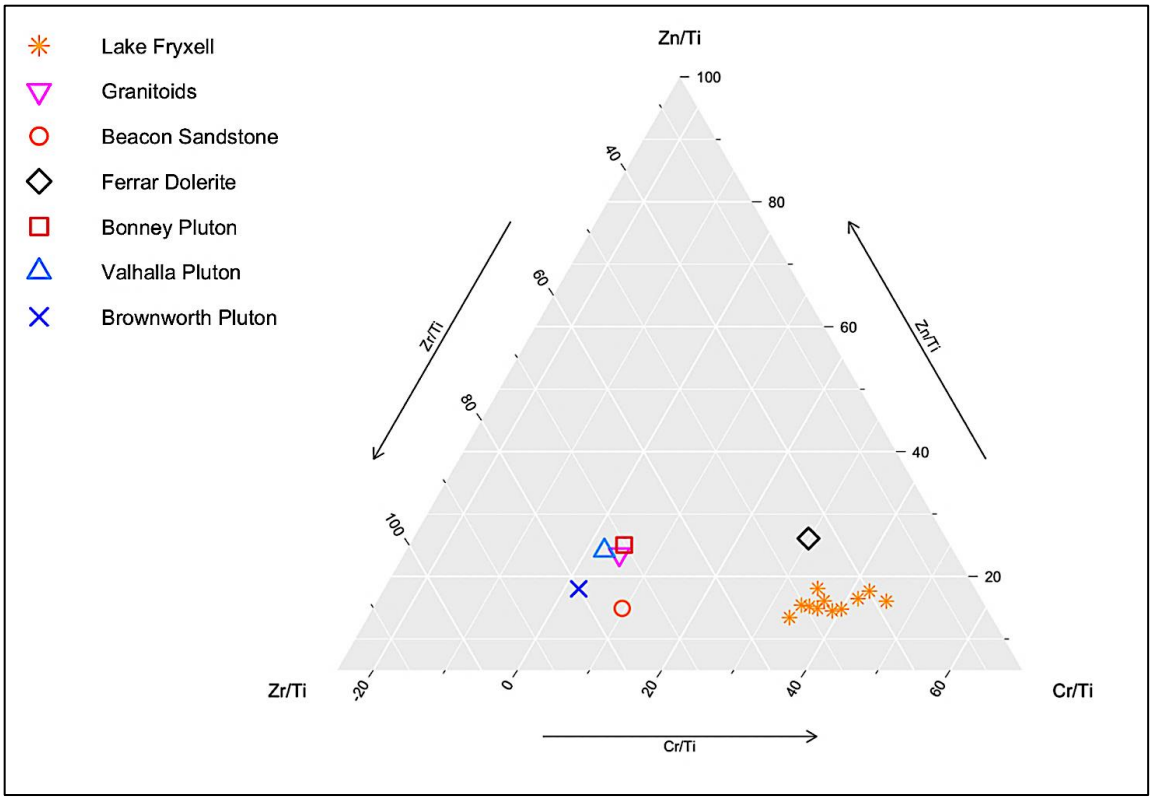

Figure 124. High Field Strength Element ratios Zr/Ti, Zn/Ti, and Cu/Ti at Lake Fryxell, Taylor Valley, and of regional source rocks.

Figure 124 shows relative abundances of Zr/Ti, Zn/Ti, and Cr/Ti in Lake Fryxell surface and edge samples. Variation is primarily seen in Cr/Ti abundances, the most mobile of the elemental ratios investigated here. Lake Fryxell samples exhibit greatest similarity to Ferrar Dolerite, disagreeing with the findings of REE analysis. Because HFSEs are less affected by alteration processes than REEs (Nesbitt and Markovics, 1997), the findings here are likely more accurate than those from REE analysis. Major elemental analysis is discussed below.

3.4.10.3. Major Elements

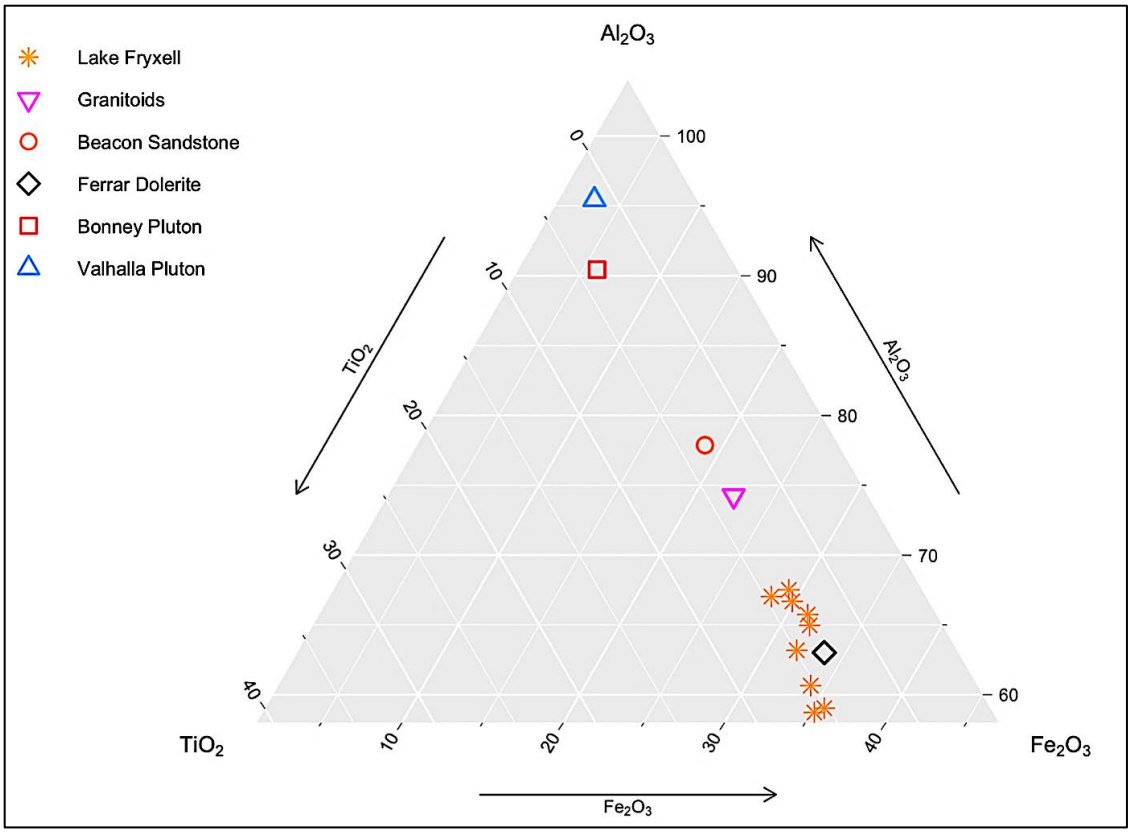

Figure 125. TiO_2, Al_2O_3, Fe_2O_3 abundance at Lake Fryxell, Taylor Valley, and of regional source rocks.

Major elemental analysis of surface and edge samples from Lake Fryxell shows relative Al_2O_3 and TiO_2 variation. Samples plot most similarly to Ferrar Dolerite, trending slightly towards Granitoids as well as away from all source rocks. These findings corroborate those of HFSE analysis and contradict those of REE analysis. Contradiction of REE analysis is likely due to the potential of REE abundance enhancement from source rock to sediment sample (Nesbitt and Markovics, 1997).

3.4.10.4. CIA

Unmodified Chemical Index of Alteration values average about 42, in the range of fresh basalts (Nesbitt and Young, 1982; Fedo et al., 1995) and the average CIA of the Ferrar Dolerite: 42 (based on data from Grapes et al., 1989; Morrison, 1995). Based on this, the most likely provenance for Lake Fryxell sediments is Ferrar Dolerite.

Modified Chemical Index of Alteration values, corrected for salt dilution, average about 45, still in the range of fresh basalts (Nesbitt and Young, 1982; Fedo et al., 1995). Because the average modified CIA value is so similar to the average unmodified value, and *below* the lowest range of chemical alteration as proposed by Fedo et al., 1995, surficial chemical alteration at Lake Vanda is not supported and provenance is likely dominated by Ferrar Dolerite.

3.4.10.5. Provenance Conclusion

Based on information discussed, the most likely provenance for Lake Fryxell surface and edge sediments is primarily Ferrar Dolerite and secondarily Granitoids. This conclusion is supported by Bishop et al., 2014. Though the regional source rock should be Undifferentiated Gneiss or Biotite Orthogneiss (Peterson and Marsh, 2008), because samples are all surficial (Allibone et al., 1993a), they are Ferrar Dolerite and Granitoids. Should cores be taken at Lake Fryxell, Brownworth Pluton could be sampled, and a potentially greater degree of chemical alteration would be observed.

3.4.11. LAKE HOARE (CORES B-E, H)

Lake Hoare likely has one major source rock. However, Brownworth Pluton is reported the south, and Bonney Pluton to the north, of the two possible source rocks, and could be influencing the data (Peterson and Marsh, 2008).

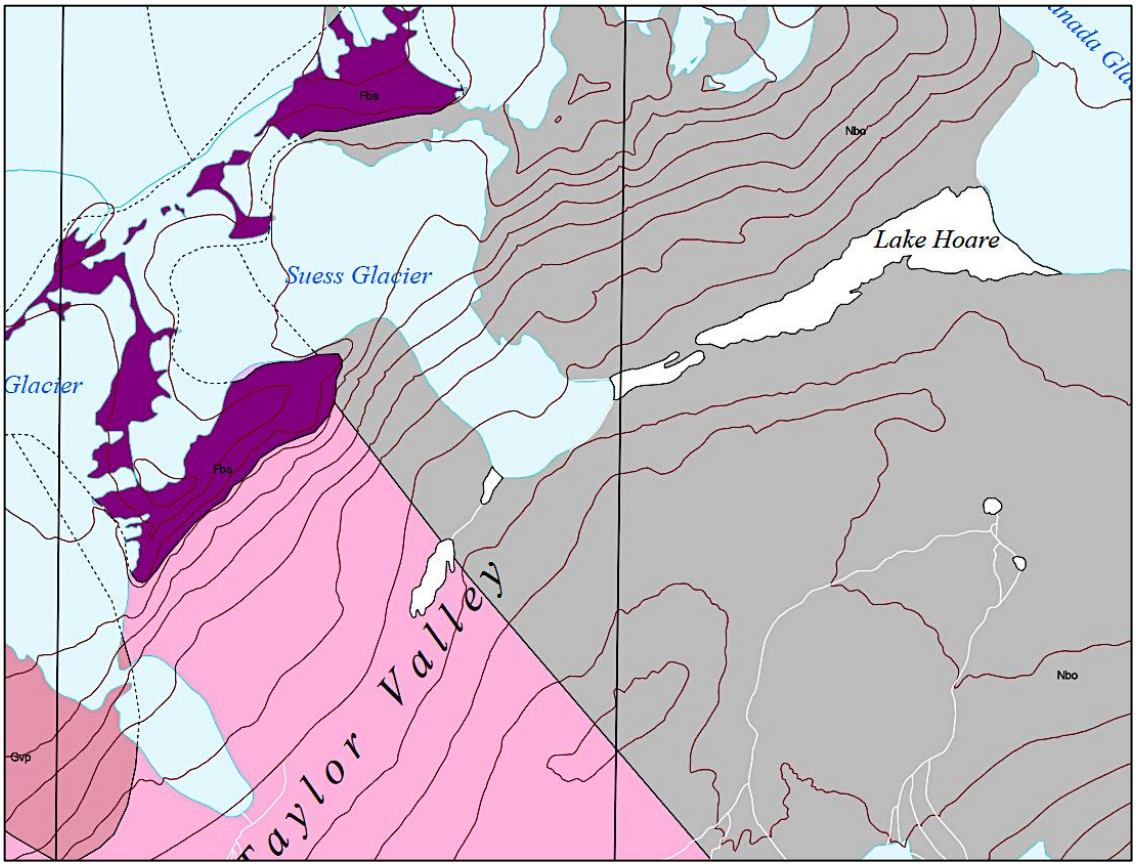

Figure 126. Regional geology of Lake Hoare, Taylor Valley (Peterson and Marsh, 2008). Undifferentiated Gneiss or Biotite Orthogneiss (gray). A small outcrop of Ferrar Dolerite (purple) exists to the northwest.

3.4.11.1. Core B, Rare Earth Elements

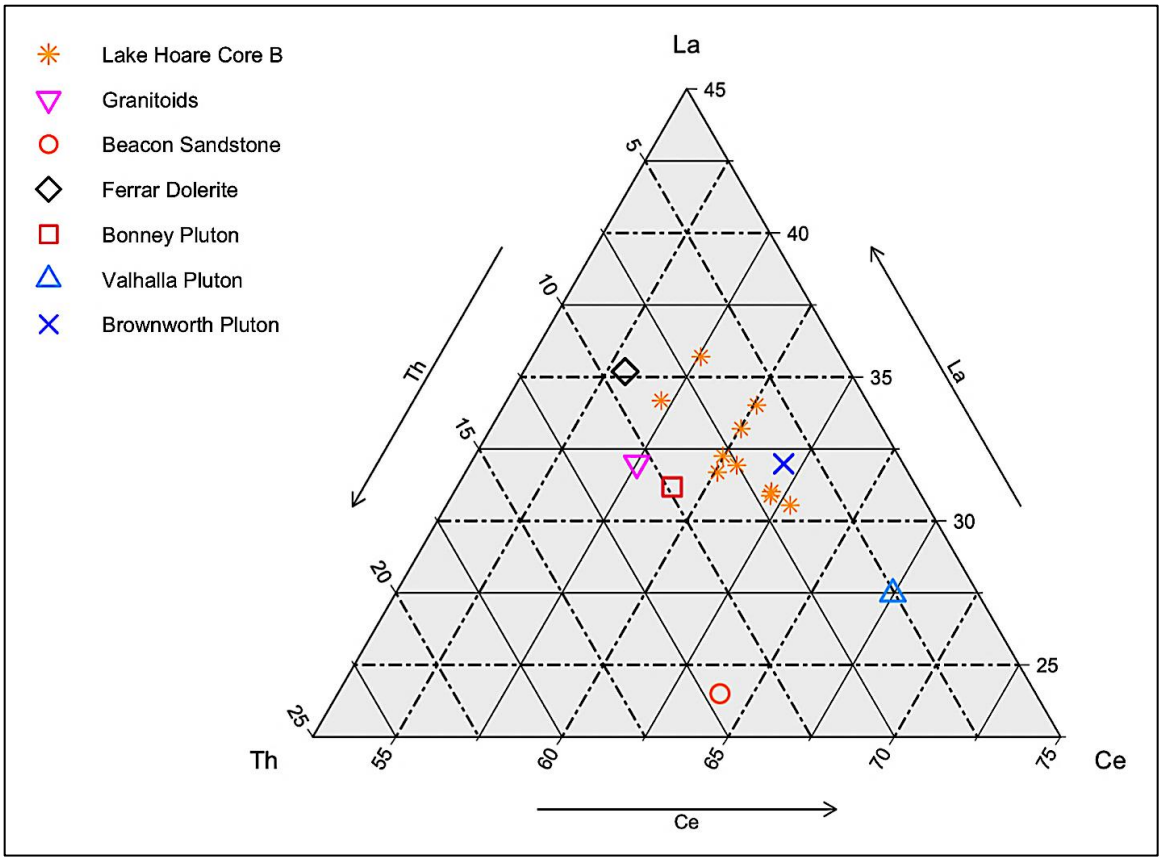

Figure 127. Th, La, Ce abundance of Core B at Lake Hoare, Taylor Valley, and regional source rocks.

Figure 127 shows the relative abundances of Th, La, and Ce of core samples from Core B at Lake Hoare, and source rocks. Samples exhibit significant variation in La and Th, and to a lesser degree, Ce. Samples exhibit elemental similarity primarily to Brownworth Pluton, and secondarily to Granitoids and Ferrar Dolerite. Because abundance of REEs can increase by more than 200 % from fresh rock to the most weathered in situ samples (Nesbitt and Markovics, 1997), abundance of REEs such as La and Ce can give a slightly skewed picture of sediment provenance. To check the validity of conclusions made from REEs, HFSEs are utilized due to their greater immobility.

3.4.11.2. Core B, High Field Strength Elements

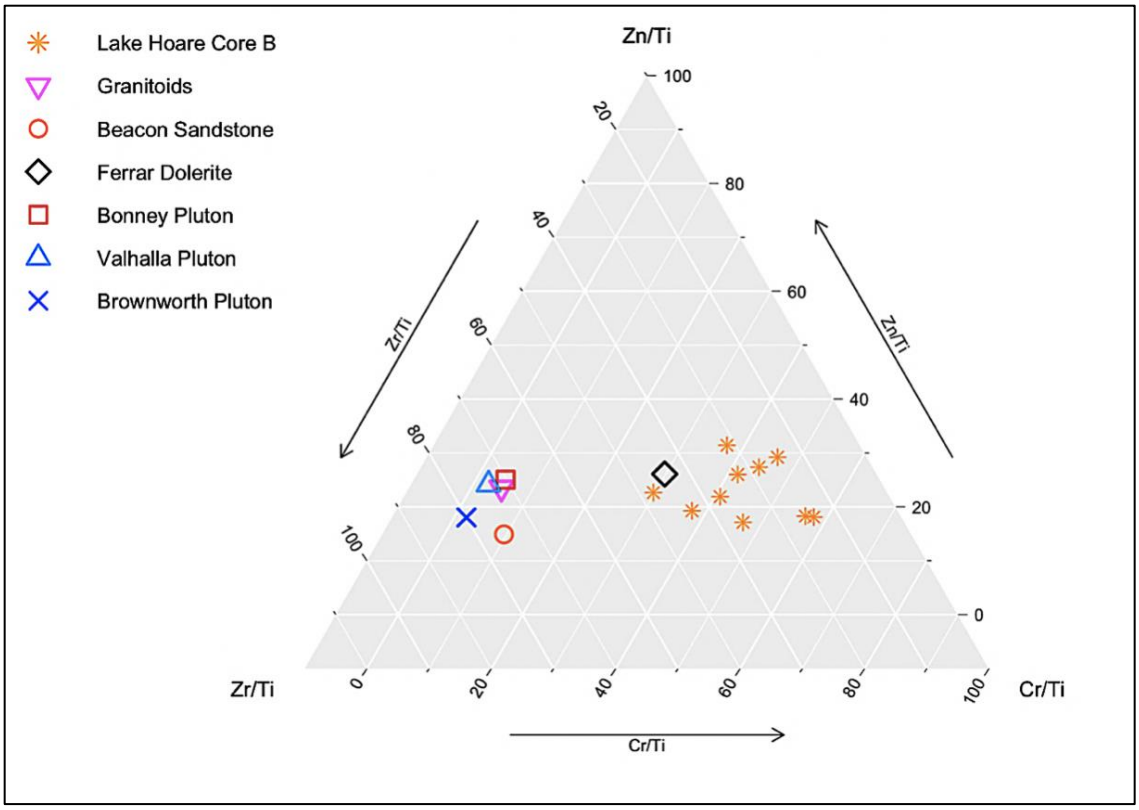

Figure 128. High Field Strength Element ratios Zr/Ti, Zn/Ti, and Cu/Ti of Core B, Lake Hoare, Taylor Valley, and regional source rocks.

Figure 128 shows relative abundances of Zr/Ti, Zn/Ti, and Cr/Ti at Lake Hoare, Core B. Variation is primarily seen in Cr/Ti abundances, the most mobile of the elemental ratios investigated here. Core B samples exhibit greatest similarity to Ferrar Dolerite, disagreeing with the REE analysis conclusion of Brownworth Pluton dominance. Because HFSEs are less affected by alteration processes than REEs (Nesbitt and Markovics, 1997), the findings here are likely more accurate than those from REE analysis. Major elemental analysis is discussed below.

3.4.11.3. Core B, Major Elements

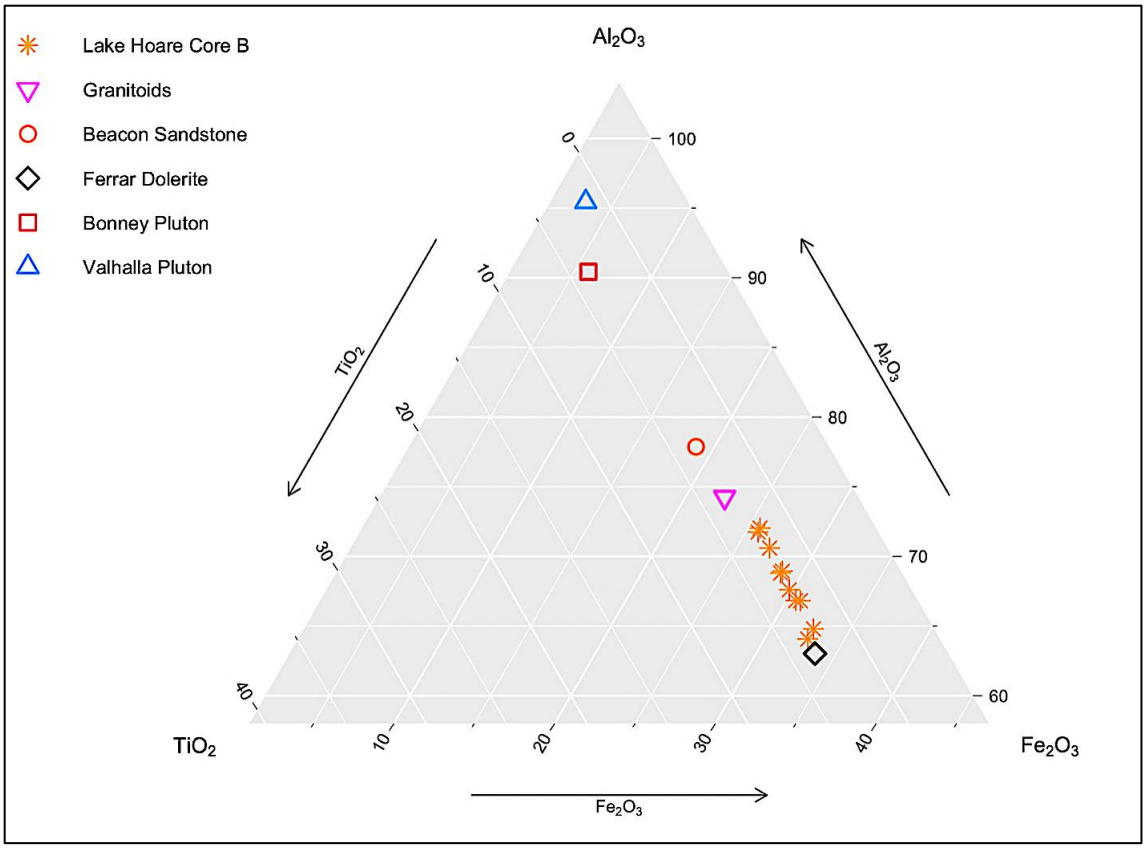

Figure 129. TiO_2, Al_2O_3, Fe_2O_3 abundance of Core B at Lake Hoare, Taylor Valley, and regional source rocks.

Major elemental analysis of samples from Core B at Lake Hoare shows significant variation in Al_2O_3 and TiO_2 abundance, and steady abundance in Fe_2O_3. Core B samples plot fairly evenly between Ferrar Dolerite and Granitoids.

3.4.11.4. Core B, CIA

Unmodified Chemical Index of Alteration values average about 41, in the range of fresh basalts (Nesbitt and Young, 1982; Fedo et al., 1995) and just below the average CIA of the Ferrar Dolerite: 42 (based on data from Grapes et al., 1989; Morrison, 1995). Based on this, the most likely provenance for Core B sediments is Ferrar Dolerite.

Modified CIA values for Lake Hoare, Core B, are adjusted for carbonate enrichment rather than sulfate. The same modification process for sulfates is used for carbonates. Modified Chemical Index of Alteration values, corrected for salt dilution, average about 58, in the range of granites to A-type granites (Nesbitt and Young, 1982; Fedo et al., 1995). The combination of unmodified and modified CIA values and their proposed corresponding source rocks aligns well with REE and HFSE analyses.

3.4.11.5. Core B, Provenance Conclusion

Based on information discussed, the most likely provenance for Core B at Lake Hoare is Ferrar Dolerite and Granitoids. This conclusion agrees with regional observations by Allibone et al. (1993a) and Peterson and Marsh (2008). Intermittent, seasonal streams (Nedell et al., 1987) and their proximity to dive holes, strengthens the possibility of sediment deposition into Lake Hoare by means of mass-wasting from source rocks to the north (Granitoids and Ferrar Dolerite) (Peterson and Marsh, 2008).

3.4.12.1. Core C, Rare Earth Elements

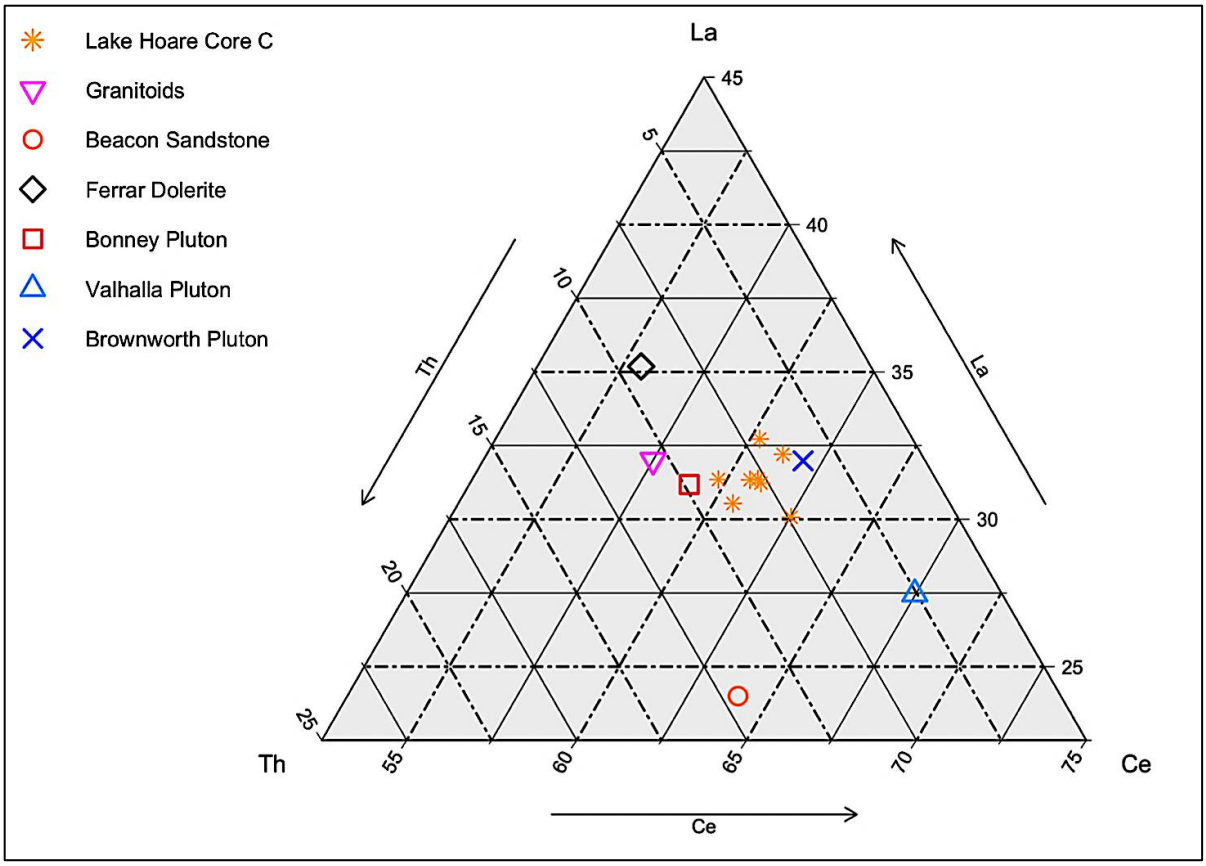

Figure 130. Th, La, Ce abundance of Core C at Lake Hoare, Taylor Valley, and regional source rocks.

Figure 130 shows the relative abundances of Th, La, and Ce of core samples from Core C at Lake Hoare, and source rocks. Samples exhibit some variation, less than Core B, and plot between Bonney and Brownworth Pluton. HFSEs are investigated to test REE conclusions.

3.4.12.2. Core C, High Field Strength Elements

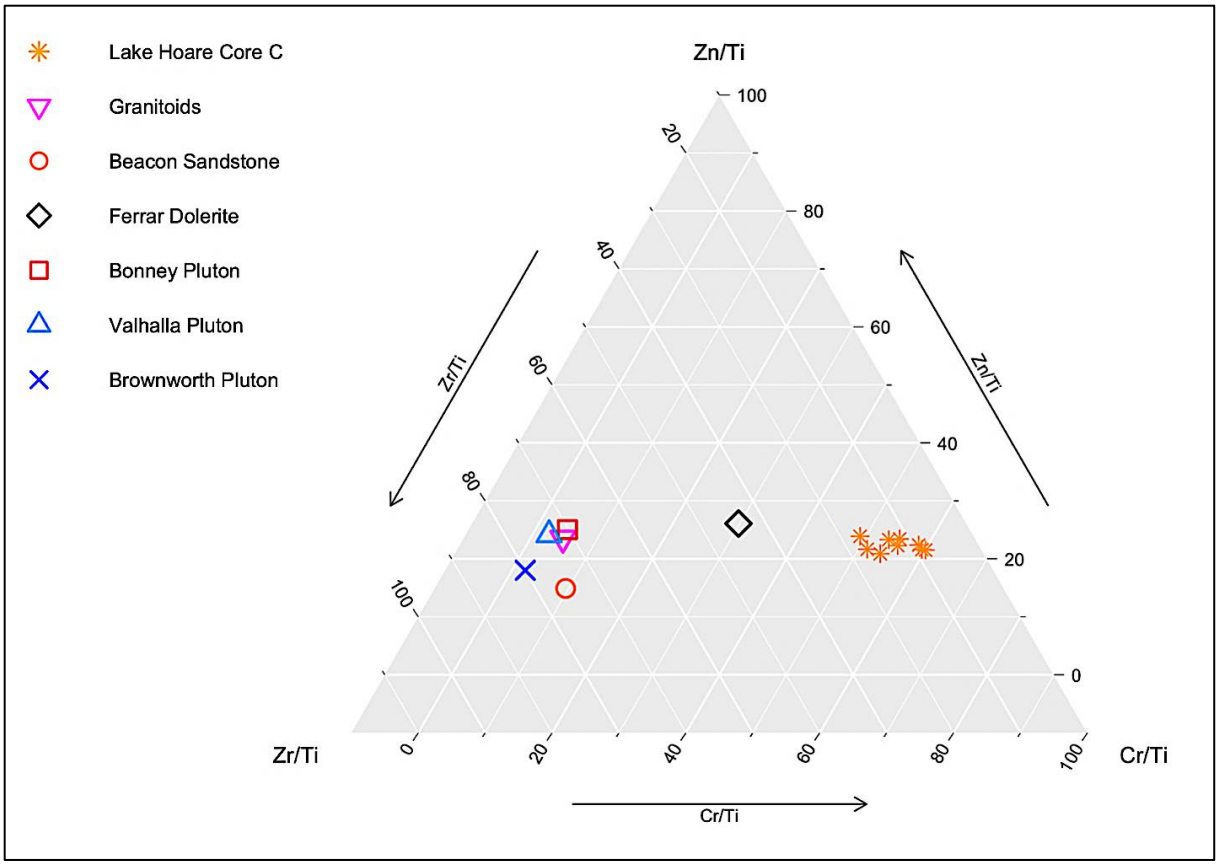

Figure 131. High Field Strength Element ratios Zr/Ti, Zn/Ti, and Cu/Ti of Core C, Lake Hoare, Taylor Valley, and regional source rocks.

Figure 131 shows relative abundances of Zr/Ti, Zn/Ti, and Cr/Ti in Core C at Lake Hoare. Samples almost exclusively exhibit variation in Cr/Ti abundances and group tightly. Core C samples plot most similarly to Ferrar Dolerite, though, they exhibit much higher Cr/Ti.

3.4.12.3. Core C, Major Elements

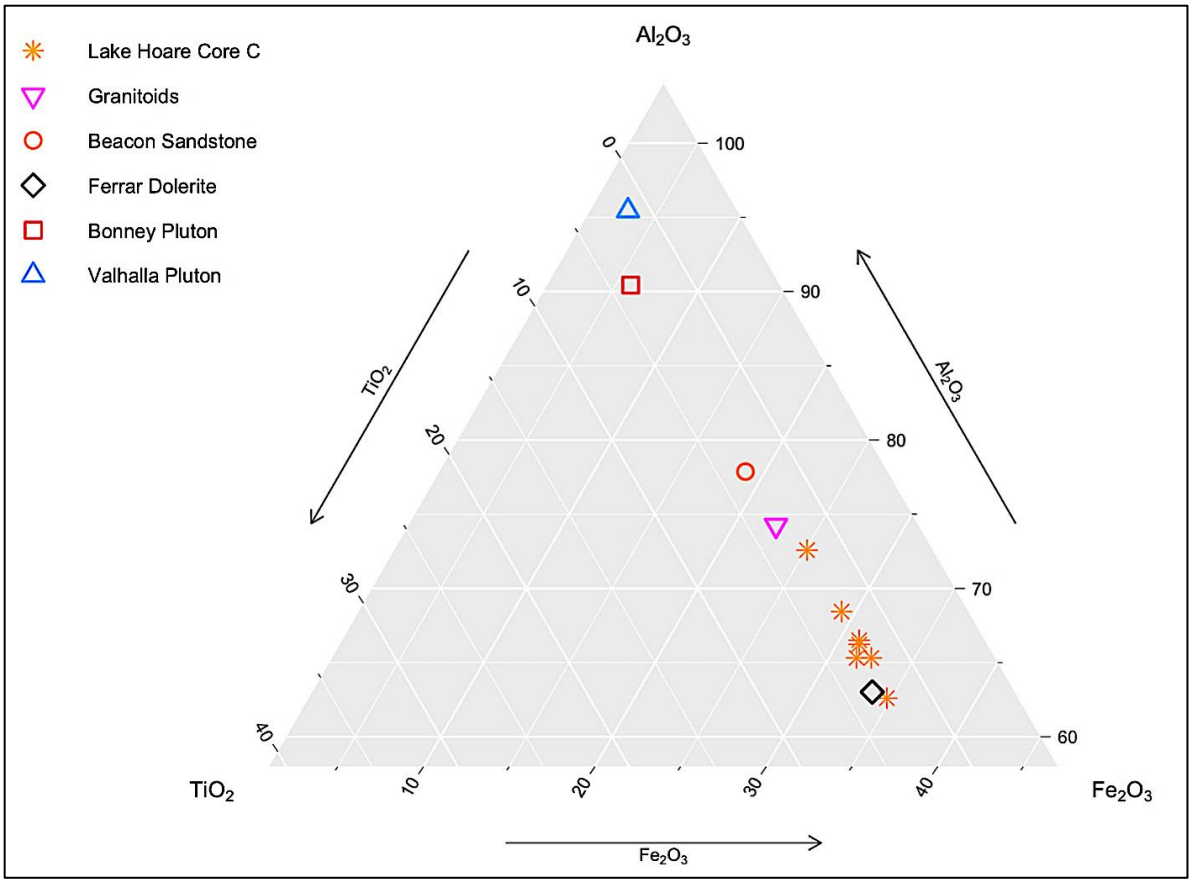

Figure 132. TiO_2, Al_2O_3, Fe_2O_3 abundance of Core C at Lake Hoare, Taylor Valley, and regional source rocks.

Figure 134 shows significant variation in Al_2O_3 and TiO_2 abundance, and relatively steady abundance in Fe_2O_3. Core C samples plot fairly evenly between Ferrar Dolerite and Granitoids, but favor Ferrar Dolerite. This conclusion supports HFSE analysis.

3.4.12.4. Core C, CIA

Unmodified Chemical Index of Alteration values average about 42, in the range of fresh basalts (Nesbitt and Young, 1982; Fedo et al., 1995) and the same average CIA value of the Ferrar Dolerite: 42 (based on data from Grapes et al., 1989; Morrison, 1995). Based

on the unmodified CIA, the most likely provenance for Core C sediments at Lake Hoare is Ferrar Dolerite.

Modified CIA values for Lake Hoare are adjusted for carbonate enrichment rather than sulfate. The same modification process for sulfates is used for carbonates. Modified Chemical Index of Alteration values, corrected for salt dilution, average about 53, in the range of granites to A-type Granites (Nesbitt and Young, 1982; Fedo et al., 1995). The combination of unmodified and modified CIA values and their proposed corresponding source rocks aligns well with HFSE and major elemental analyses.

3.4.12.5. Core C, Provenance Conclusion

Based on information discussed, the most likely provenance for Core C at Lake Hoare is Ferrar Dolerite and Granitoids. This conclusion agrees with regional observations by Allibone et al. (1993a) and Peterson and Marsh (2008).

3.4.13.1. Core D, Rare Earth Elements

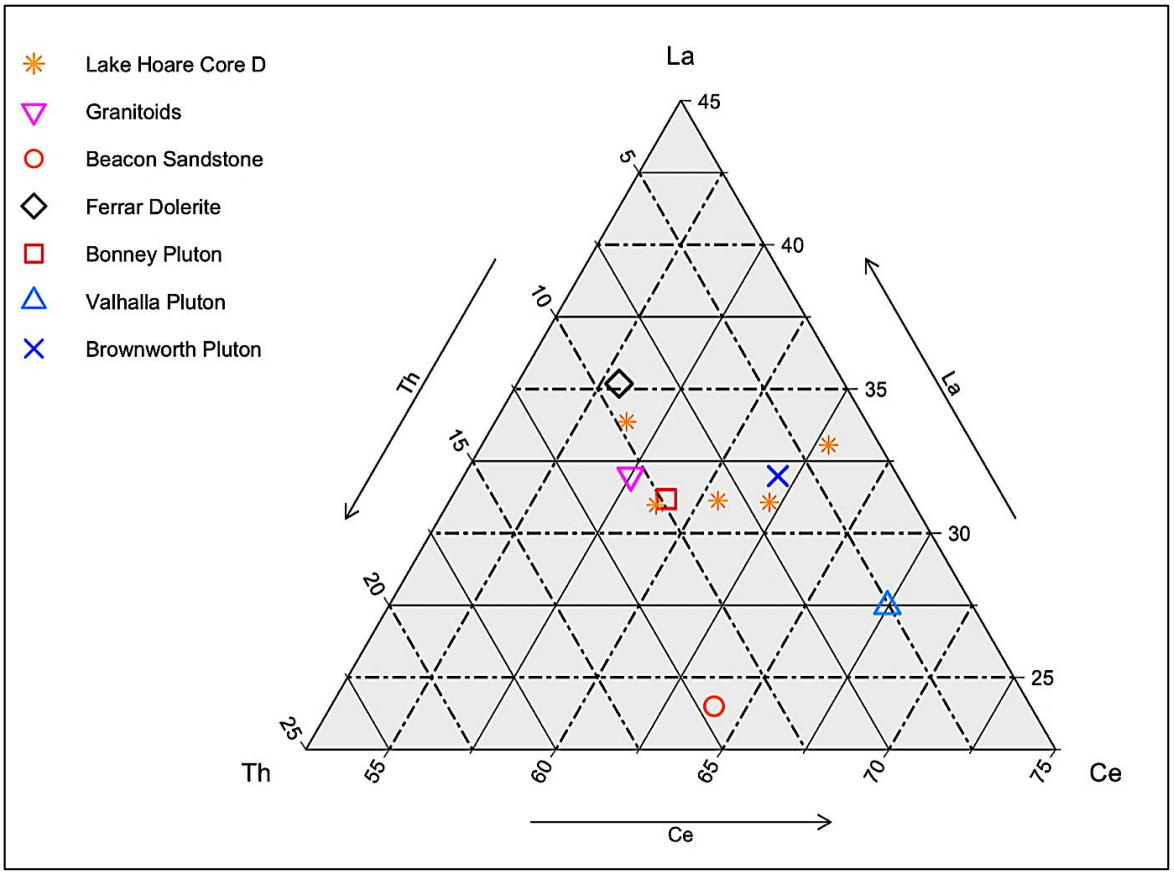

Figure 133. Th, La, Ce abundance of Core D at Lake Hoare, Taylor Valley, and regional source rocks.

Figure 133 shows the relative abundances of Th, La, and Ce of core samples from Core D at Lake Hoare, and source rocks. Samples exhibit significant variation, primarily in Ce abundance, and do not group well. Core D sample abundances exhibit similar elemental abundance to four different source rocks: Ferrar Dolerite, Granitoids, Bonney Pluton, and Brownworth Pluton. To check the validity of conclusions made from REEs, HFSEs are utilized due to their greater immobility.

3.4.13.2. Core D, High Field Strength Elements

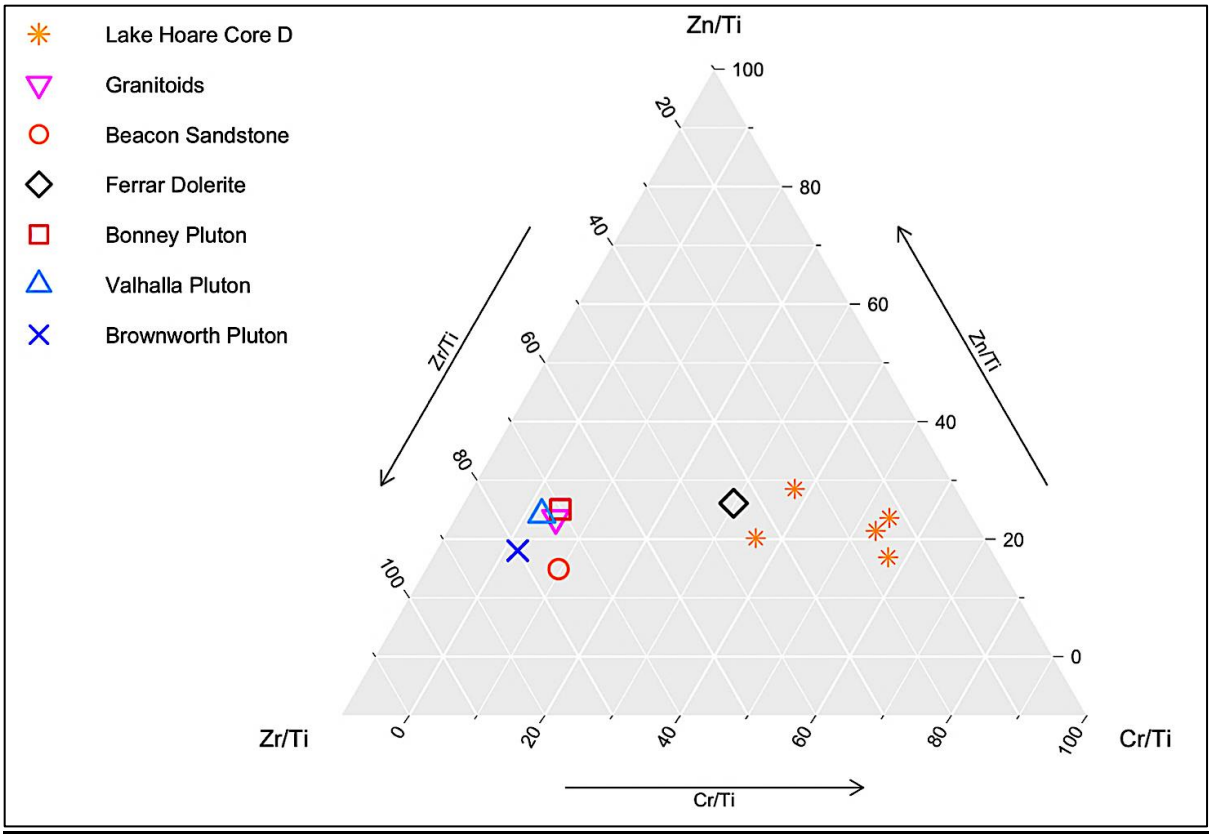

Figure 134. High Field Strength Element ratios Zr/Ti, Zn/Ti, and Cu/Ti of Core D, Lake Hoare, Taylor Valley, and regional source rocks.

Figure 134 shows relative abundances of Zr/Ti, Zn/Ti, and Cr/Ti in Core D at Lake Hoare. Samples exhibit variation primarily in Cr/Ti abundance, the most mobile of the elements investigated here (Nesbitt and Markovics, 1997). Sample abundances plot most similarly to Ferrar Dolerite, narrowing the findings from REE analysis to a single source, and supporting the possibility of REE abundance enhancement from source rock to weathered in situ samples. Major elements are discussed below.

3.4.13.3. Core D, Major Elements

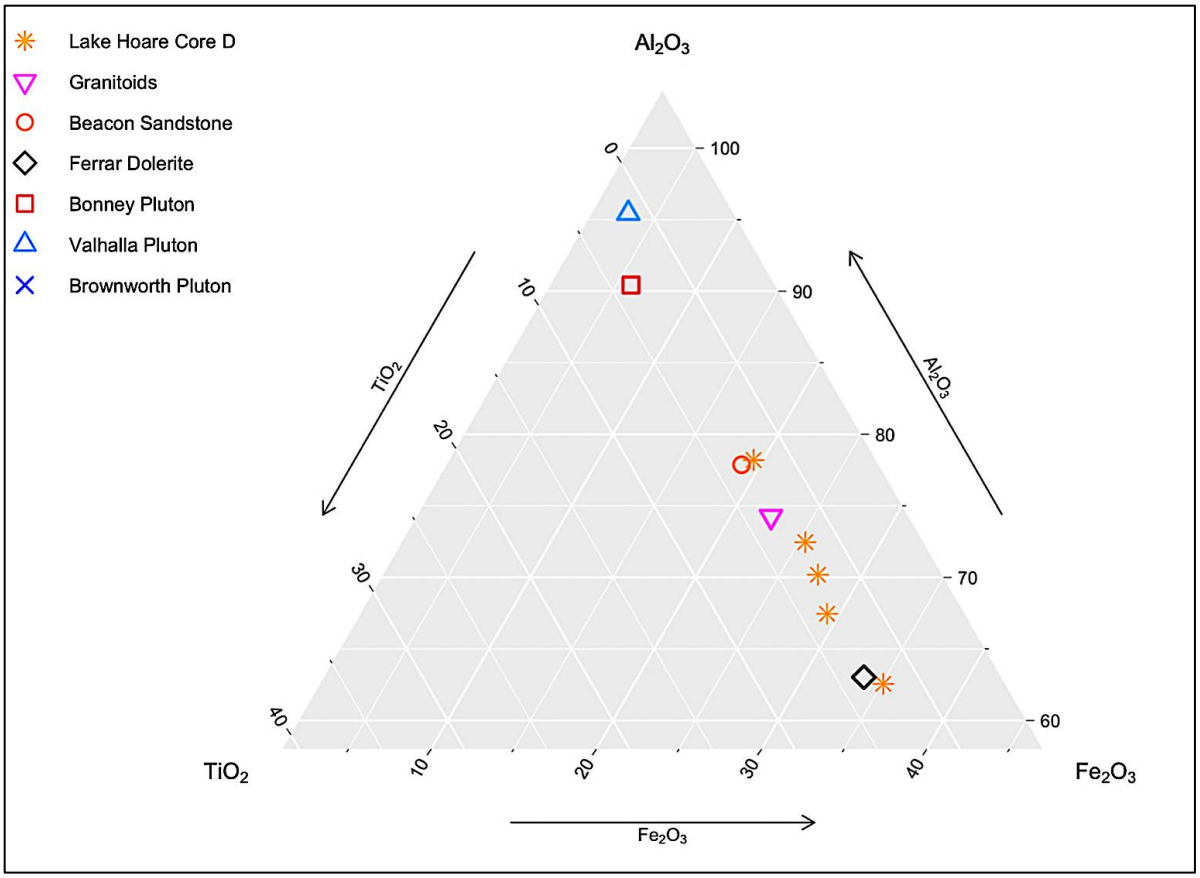

Figure 135. TiO_2, Al_2O_3, Fe_2O_3 abundance of Core D at Lake Hoare, Taylor Valley, and regional source rocks.

Major elemental analysis of samples from Core D at Lake Hoare shows significant variation in Al_2O_3 and TiO_2 abundance, and relatively steady abundance in Fe_2O_3. Samples plot primarily between Ferrar Dolerite and Granitoids with one sample favoring Beacon Sandstone. Major elemental analysis supports HFSE analysis.

3.4.13.4. Core D, CIA

Unmodified Chemical Index of Alteration values average about 44, in the range of fresh basalts (Nesbitt and Young, 1982; Fedo et al., 1995) and just above the average CIA value of the Ferrar Dolerite: 42 (based on data from Grapes et al., 1989; Morrison, 1995). Based on this, the most likely provenance for Core D sediments at Lake Hoare is Ferrar Dolerite.

Modified CIA values for Lake Hoare are adjusted for carbonate rather than sulfate enrichment. The same modification process for sulfates is used for carbonates. Modified Chemical Index of Alteration values, corrected for salt dilution, average about 55, in the range of granites to A-type Granites (Nesbitt and Young, 1982; Fedo et al., 1995). The combination of unmodified and modified CIA values, and their proposed corresponding source rocks aligns well with HFSE and major elemental analyses.

3.4.13.5. Core D, Provenance Conclusion

Based on information discussed, the most likely provenance for Core D at Lake Hoare is Ferrar Dolerite and Granitoids. This conclusion agrees with regional observations by Allibone et al. (1993a), Peterson and Marsh (2008) and nearby cores.

3.4.14.1. Core E, High Field Strength Elements

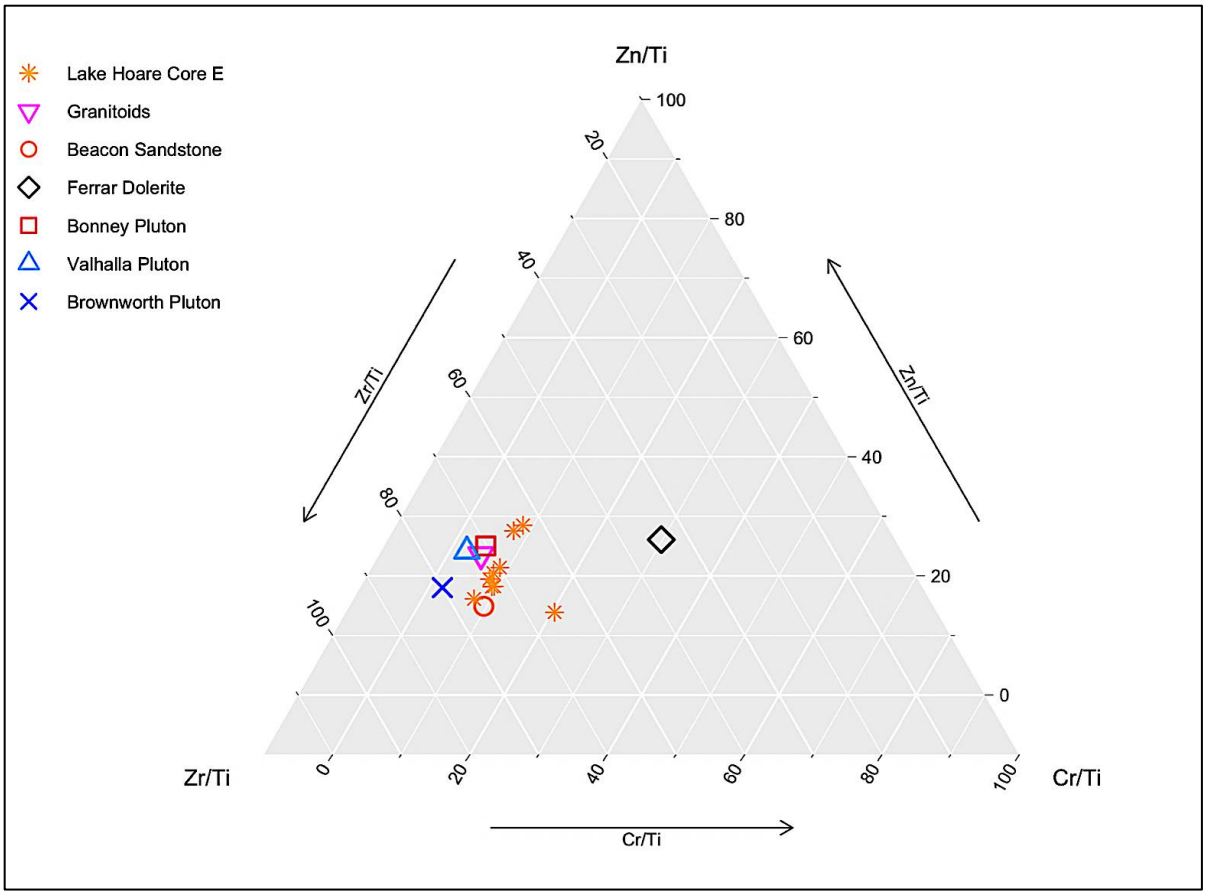

Figure 136. High Field Strength Element ratios Zr/Ti, Zn/Ti, and Cu/Ti of Core E, Lake Hoare, Taylor Valley, and regional source rocks.

Figure 136 shows relative abundances of Zr/Ti, Zn/Ti, and Cr/Ti in Core E at Lake Hoare. Samples exhibit variation primarily in Zr/Ti and Zn/Ti ratios, and relatively steady Cr/Ti ratios. This runs counter to HFSE findings from Cores B, C, and D. Core E samples plot most similarly to Granitoids, Beacon Sandstone, and plutons Bonney and Valhalla. Granitoids are expected based on regional geologic observations (Peterson and Marsh 2008), but plutons Bonney and Valhalla are not.

3.4.14.2. Core E, Major Elements

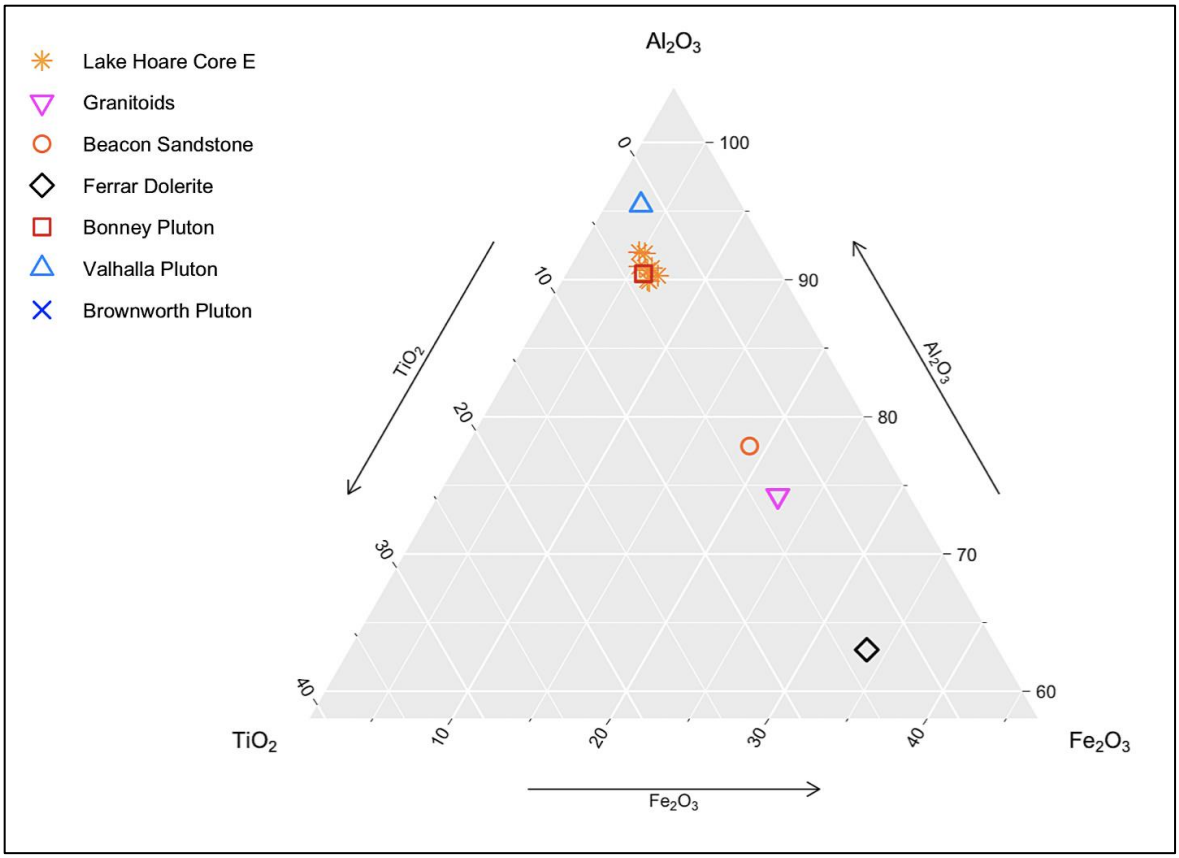

Figure 137. TiO_2, Al_2O_3, Fe_2O_3 abundance of Core E at Lake Hoare, Taylor Valley, and regional source rocks.

Figure 137 shows very little variation from sample to sample, grouping tightly near Bonney Pluton. These findings support the conclusion of Bonney Pluton from HFSE analysis, but not Granitoids or Valhalla Pluton.

3.4.14.3. Core E, CIA

Unmodified Chemical Index of Alteration values average about 38, in the range of fresh basalts (Nesbitt and Young, 1982; Fedo et al., 1995) and below the average CIA value of the Ferrar Dolerite: 42 (based on data from Grapes et al., 1989; Morrison, 1995). Based

on the unmodified CIA, the most likely provenance for Core E sediments at Lake Hoare is Ferrar Dolerite.

Modified CIA values for Lake Hoare are adjusted for carbonate and sulfate enrichment. The same modification process for sulfates is used for carbonates. sulfate modified CIA values average about 51, in the range of fresh granites and granodiorites (Nesbitt and Young, 1982). Plutons Bonney, Valhalla, and Brownworth all report average CIA values between 49 and 51 (based on data from Allibone et al., 1993a). Carbonate modified CIA values average about 63, in the range of A-type granites to charnockites (Nesbitt and Young, 1982; Fedo et al., 1995). Only Beacon Sandstone reports a similar CIA value (64).

The combination of unmodified and modified CIA values and their proposed corresponding source rocks aligns well with HFSE and major elemental analyses, favoring Bonney Pluton.

3.4.14.4. Core E, Provenance Conclusion

Based on information discussed, the most likely sediment provenance of Core E at Lake Hoare is Bonney Pluton. Surficially, this conclusion is not supported by regional geologic observations. Upon further investigation, a large swath of Bonney Pluton, approximately 3 km southwest of the west end of Lake Hoare, abruptly stops at a large swath of Undifferentiated Gneiss that saturates the region which also includes Lake Fryxell. The Undifferentiated Gneiss extends east all the way to the Ross Sea and up to Gneiss Point (77° 23’ S, 163° 42’ E) (Peterson and Marsh, 2008). It is possible that the large swath of Undifferentiated Gneiss was deposited on top of preexisting Bonney Pluton and that Core E (0-47 cm) embodies both Granitoids source rock and Bonney Pluton. It is also possible that Core E sediments have been chemically altered or subject to physical alteration processes such as freeze-thaw or sediment-mixing of multiple source rocks. Chemical alteration in supported by reports of relative calcite enrichment in Core E. If this is the case, lower CIA *source rocks*, Ferrar Dolerite and Granitoids, for example, would be favored.

3.4.15.1. Core H, High Field Strength Elements

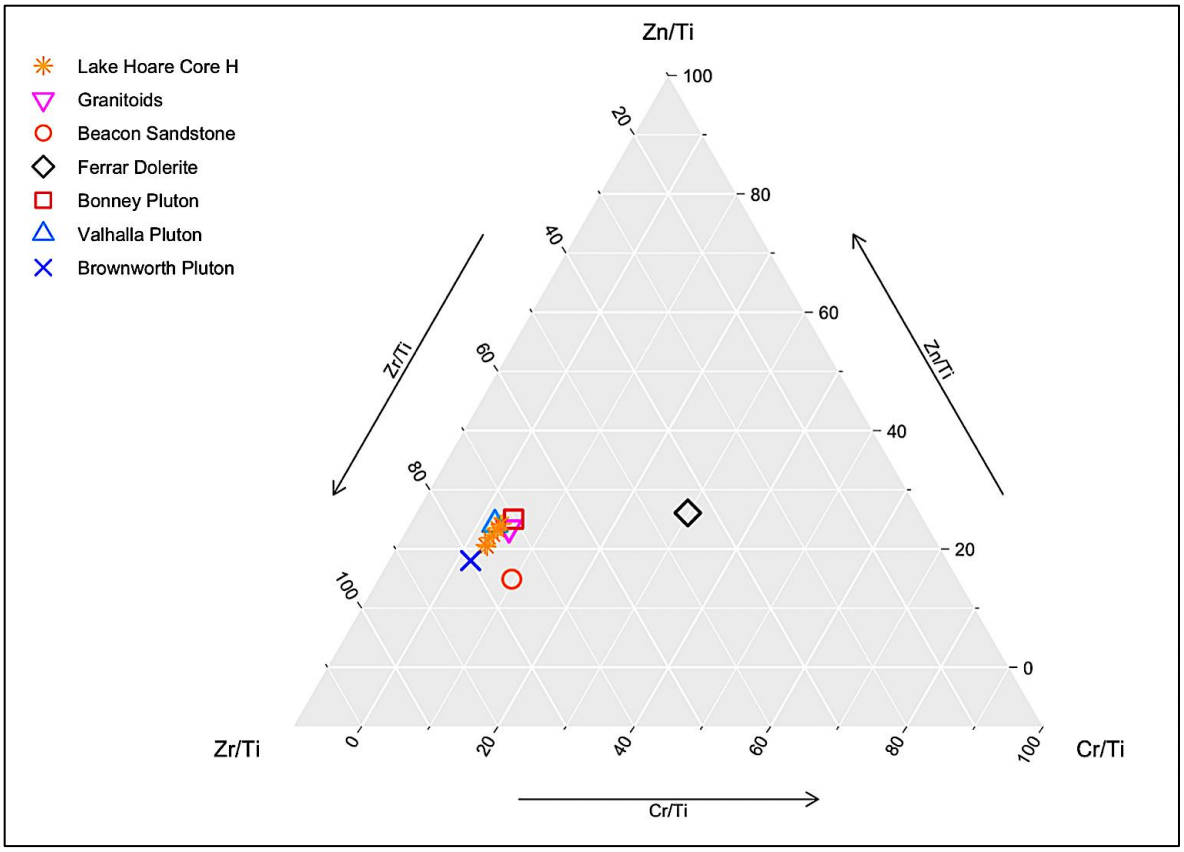

Figure 138. High Field Strength Element ratios Zr/Ti, Zn/Ti, and Cu/Ti of Core E, Lake Hoare, Taylor Valley, and regional source rocks.

Figure 138 shows relative abundances of Zr/Ti, Zn/Ti, and Cr/Ti in Core H at Lake Hoare. Samples are tightly grouped, more so than Core E, in the same location based on Zr/Ti, Zn/Ti, and Cr/Ti ratios. Core H samples plot most similarly to Granitoids, and plutons Bonney and Valhalla.

3.4.15.2. Core H, Major Elements

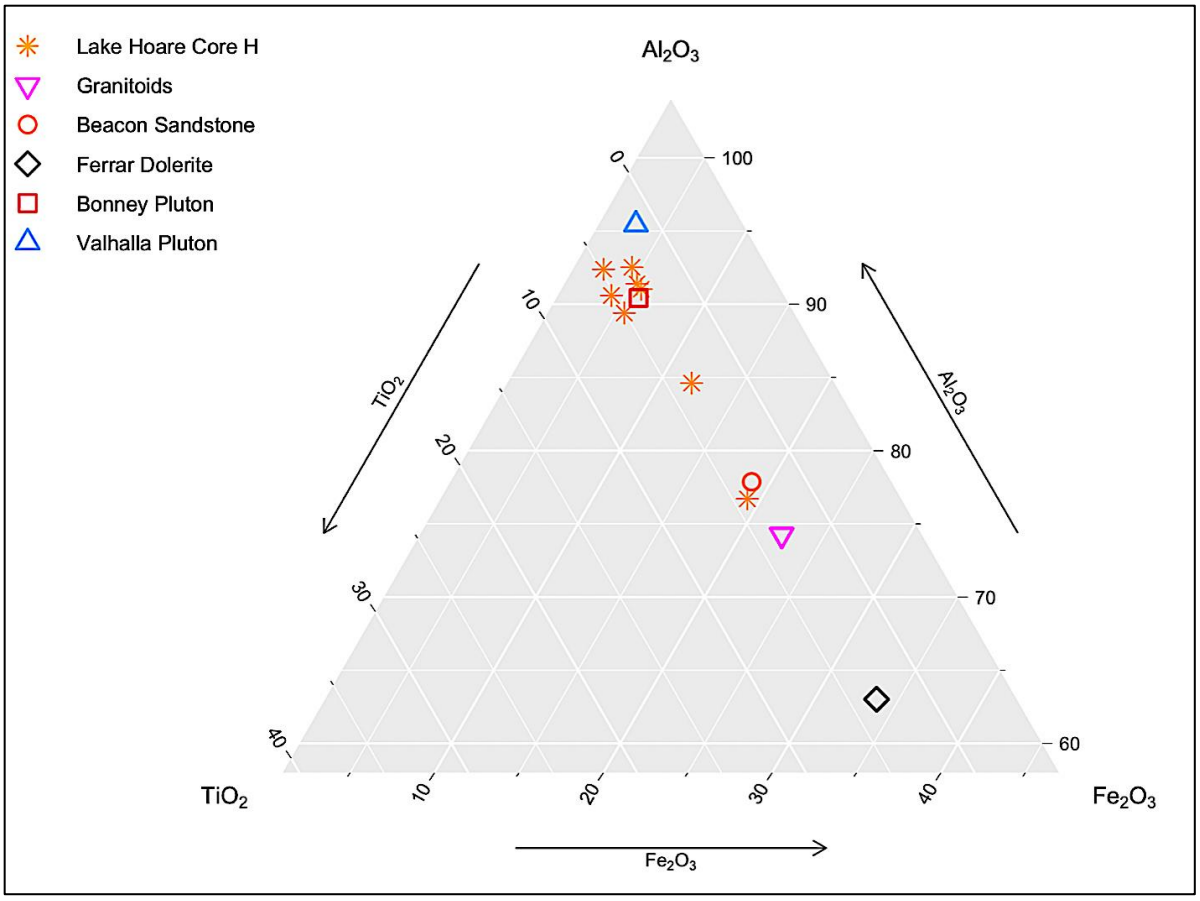

Figure 139. TiO_2, Al_2O_3, Fe_2O_3 abundance of Core H at Lake Hoare, Taylor Valley, and regional source rocks.

Major elemental analysis of samples from Core H at Lake Hoare shows significantly more variation than Core E. Where all Core E samples were tightly grouped, Core H samples exhibit variation primarily in Al_2O_3 and TiO_2 abundance. The majority of Core H sample group near Bonney Pluton elemental abundances with two samples trending towards Beacon Sandstone. These findings support those from HFSE analysis.

3.4.15.3. Core H, CIA

Unmodified Chemical Index of Alteration values average about 43, in the range of fresh basalts (Nesbitt and Young, 1982; Fedo et al., 1995) and just above the average CIA value of the Ferrar Dolerite: 42 (based on data from Grapes et al., 1989; Morrison, 1995). Based on the unmodified CIA, the most likely provenance for Core E sediments at Lake Hoare is Ferrar Dolerite.

Modified CIA values for Lake Hoare are adjusted for carbonate and sulfate enrichment. The same modification process for sulfates is used for carbonates. Sulfate modified CIA values average about 70, in the range of charnockites. Only Beacon Sandstone, though it is not reported in the area (Peterson and Marsh, 2008), reports a similar CIA value (64) (Roser and Pyne, 1989).

Carbonate modified CIA values average about 57, in the range of granites to A-type granites (Nesbitt and Young, 1982; Fedo et al., 1995). This value is about halfway between average CIA values of Beacon Sandstone and plutons Bonney, Valhalla, and Brownworth (based on data from Roser and Pyne , 1989; Allibone et al., 1993).

The combination of unmodified and modified CIA values and their proposed corresponding source rocks aligns well with HFSE and major elemental analyses, favoring Bonney Pluton and Granitoids *that have been altered.* Bishop et al. (2001) reports bacterial reduction of sulfur in sediments thus favoring *biological alteration in Core H*.

3.4.15.4. Core H, Provenance Conclusion

Based on information discussed, the most likely provenance for Core H sediments at Lake Hoare is Bonney Pluton and Granitoids. Surficially, Bonney Pluton is not supported by regional geologic observations (Peterson and Marsh, 2008), though, as discussed above, a large swath of Bonney Pluton, abruptly stops at a large swath of undifferentiated gneiss that saturates the region. The undifferentiated gneiss extends east all the way to the Ross Sea and up to Gneiss Point (Peterson and Marsh, 2008). It

is possible that the large swath of Undifferentiated Gneiss superimposes Bonney Pluton and that Core E (0-47 cm) is composed of both Granitoids and Bonney Pluton. It is likely, though, that Core H sediments have been biologically altered (Bishop et al., 2001) which would increase the CIA and favor Bonney Pluton provenance. If this is the case, lower CIA source rocks Ferrar Dolerite and Granitoids would be favored.

3.5. Discussion and Implications

3.5.1. Discussion

Analysis of different sediment samples, from core and lake surfaces/edges across the McMurdo Dry Valley region, shows sediment provenance to be dominated by Ferrar Dolerite and Granitoids. In most core samples, both chemical and physical alteration are probable. This is supported primarily by variation in HFSE elemental ratios— ratios that would go largely unchanged if chemical alteration were not occurring. Conversely, in most surface samples— primarily those at Lake Fryxell, Vanda, and Brownworth— physical alteration is probable, due to relatively steady HFSE elemental ratios. Major elemental analyses, namely of Al_2O_3, TiO_2, and Fe_2O_3, proved to be a reasonable method of provenance determination, frequently reporting similar findings to HFSE analyses.

Though Rare Earth Elements are fairly useful as sediment tracers, their tendency to increase in abundance by as much as 200 % from source rock to sediment (Nesbitt and Markovics, 1997) can cause inaccurate interpretation and conclusion of sediment provenance.

3.5.2. IMPLICATIONS

Our results support those of Chapter 2, showing that physical alteration, except in unique cases with hypersaline waters, dominates at the surface. In cores, chemical alteration occurs, again, except in unique cases with hypersaline waters, beneath a depth of approximately 3-4 cm, manifesting as differences in abundance of HFSE ratios and major element abundances from surface samples. Such is also seen beneath a depth of approximately 12-14 cm, in which physical alteration is also dominant. Importantly, these divergences manifest as data that favor provenances unsupported by regional geologic observations which bolster the findings of Chapter 2. Our findings also indicate that even for the most immobile elemental ratios, Zr/Ti, for example, a high enough degree of chemical alteration is capable of mobilizing them, corroborating the findings of Jiang et al. (2005).

The techniques for tracing sediment provenance discussed in this chapter, though limited, serve as suitable procedures for determining sediment provenance as well as validating degree and type of alteration. With this in mind, we propose the alteration results of Chapter 2, bolstered by those of Chapter 3, be applied to available Mars rover data to test the efficacy of the McMurdo Dry Valley Region as a suitable terrestrial analog to Mars.

CHAPTER 4: ALTERATION OF POLAR DESERT SEDIMENTS FROM THE MCMURDO DRY VALLEYS, ANTARCTICA: AN ANALOG FOR ALTERATION PROCESSES ON MARS

4.1. ABSTRACT

The McMurdo Dry Valley (MDV) Region of Antarctica is thought to be one of the best terrestrial analogs to Mars due to climatic similarity and is thus proposed to be subject to similar geologic alteration processes. Analysis and comparison of surface and core sediments from the MDV to samples collected and analyzed by martian rovers Spirit, Opportunity, and Curiosity was done in an effort to determine type and degree of alteration. For elemental analysis, MDV samples were studied using X-Ray Fluorescence and Instrumental Neutron Activation Analysis; martian samples were studied using the Alpha-Particle X-ray Spectrometer. In comparison of samples, particular focus is given to major elements and sulfates as measures of type and degree of alteration. Alteration processes are classified as either physical or chemical. Based solely on the frigid temperatures and extremely dry nature of the two environments, physical alteration is thought to dominate and chemical alteration is thought to be operating on a secondary scale.

Analysis shows there are locations within the MDV that are suitable analogs to select martian samples and therefore suggestive of similar alteration processes. Physical alteration still likely dominates on Mars, but chemical alteration likely operates at a greater degree than previously thought. The analogy in this chapter, between the MDV and Mars, is primarily based upon sulfate abundances which in turn are largely inferred from total sulfur, sulfite abundance, and corroborating scientific research. By comparing alteration signatures from these two locations, we test the efficacy of the MDV as a suitable terrestrial analog to Mars and potentially pave the way for a better historical account of the planet's geochemical history. With this, we expand the means to better

answer questions regarding past or present habitability on Mars and similar extraterrestrial bodies.

4.1. INTRODUCTION

The "analog approach" to planetary geology has been shown to have tremendous value, notably in lunar studies, affording researchers a look into the four natural spheres on Earth (geo-, bio-, hydro-, atmo-) that may be operating similarly on other planetary bodies. Terrestrial environments are never perfect copies of extraterrestrial environments, but some come close.

The McMurdo Dry Valley (MDV) Region of Antarctica has long been considered one of the closest terrestrial analogs to the martian environment due to climatic, surficial, and chemical similarities (Cameron et al., 1970; Horowitz and Cameron, 1972; Morris et al., 1972; Gibson, 1980, 1983). Because of this, many investigations of the region have been carried out in an attempt to better understand potentially similar geochemical processes that may be occurring on Mars (Gibson et al., 1983; Wharton et al., 1989; Bishop et al., 2013, 2014; Dickson et al., 2013).

Here we examine elemental data from core and surface samples taken in the cold and dry region of the McMurdo Dry Valleys in an effort to identify and interpret sediment alteration signatures and processes. Our overall goal is to apply these data to available data from martian rovers Spirit, Opportunity, and Curiosity to determine if there are indications of similar alteration processes rooted in current martian data. In doing this we further test the efficacy of the MDV as a suitable analog to Mars.

4.1.1. Characterizing sediment alteration

We characterize degree and type of sediment alteration through the analysis of major and minor elemental/oxide abundances from microenvironment samples. A specific, quantitative method that builds on this approach is the use of the Chemical Index of Alteration (Nesbitt and Young, 1982), and our CIA equation modified for salt dilution, primarily as sulfates, as is discussed in Chapter 2. In this chapter we compare unmodified and modified CIA values of MDV cores to Mars rover samples.

4.1.2. Sulfur

One of the main points of investigation in this chapter is sulfur and how it exists both similarly and dissimilarly in the MDV and martian environment. Sources of sulfur in both environments are believed to be atmospheric, but prior to such residence, sulfur provenances are thought to differ. Sulfur in MDV samples is largely held to originate in aerosols coming off of the Ross Sea/McMurdo Sound and combine with what little regional humidity exists, eventually forming sulfate minerals such as gypsum (Claridge and Campbell, 1968, 1977). Conversely, sulfur in rover samples is held to originate in the martian mantle and to have been transferred into the atmosphere during volcanic outgassing. The outgassed SO_2 is thought to have undergone photochemical conversion to H_2SO_4, forming surficial sulfate minerals (Farquhar et al., 2007). Though sources of sulfur in the MDV and on Mars are likely different, our analysis focuses on potentially similar surficial processes.

4.2. METHODS

4.2.1. STUDY SITES AND ANALYTICAL METHODS: MDV SAMPLES

All samples sites from Chapter 1.5, except for Lake Hoare Cores B-C, are investigated in this chapter. Refer to Chapter 2.3.3 for MDV sample analytical methods.

4.2.2.STUDY SITES AND ANALYTICAL METHODS: ROVER SAMPLES

In January 2004, martian rovers Spirit and Opportunity landed on opposite sides of the red planet; Spirit in Gusev Crater (14.6° S, 175.3° E); Opportunity in Meridiani Planum (0° latitude and longitude). Spirit remained in operation until March 2010, Opportunity until June 2018. During their lifetimes, each took thousands of measurements, yielding precious information on surface chemistry. In August 2012 the third rover discussed in this chapter, Curiosity, landed in the crater Gale (5.4° S, 137.8° E). It remains in operation at the time of writing this thesis.

All rovers sampled both rocks and soils. Soils were categorized as “Undisturbed”, “Disturbed”, “Fines”, “Clods” and “Trenched/Scuffed”. Rocks were categorized as “Undisturbed”, “RATted”, and “Brushed”. Prior to elemental analysis, many samples were “prepared” by the Rock Abrasion Tool (RAT) or the Dust Removal Tool (DRT). The RAT is a powerful grinder able to create a hole 45 mm in diameter and 5 mm deep into rocks on the martian surface and is exclusive to rovers Opportunity and Spirit. The RAT uses three electric motors to drive rotating, grinding teeth into the surface of a rock. Once a fresh surface is exposed, the abraded area can be investigated using the rover’s other science instruments. The DRT is exclusive to the Curiosity rover and uses wire brushes to clear a circular area 45 mm in diameter prior to additional scientific investigation.

For all three rovers, elemental chemistry was determined with the Alpha-Particle X-Ray Spectrometer (APXS). For the Curiosity rover, an improved version of the APXS that was attached to rovers Spirit and Opportunity was used. The APXS operates by making

contact with a sample, emitting several forms of radiation that come in contact and interact with the sample, and analyzing the chemical composition from the scattered alpha particles and fluorescent X-rays. The improved version utilizes, in addition to an Alpha-particle emitter, Particle-Induced X-ray Emission (PIXE) and X-ray Fluorescence (Rieder et al., 1997, 2003; Gellert et al., 2006).

4.3. RESULTS

4.3.1. CORE 33

4.3.1.1. MAJOR ELEMENTAL ANALYSIS

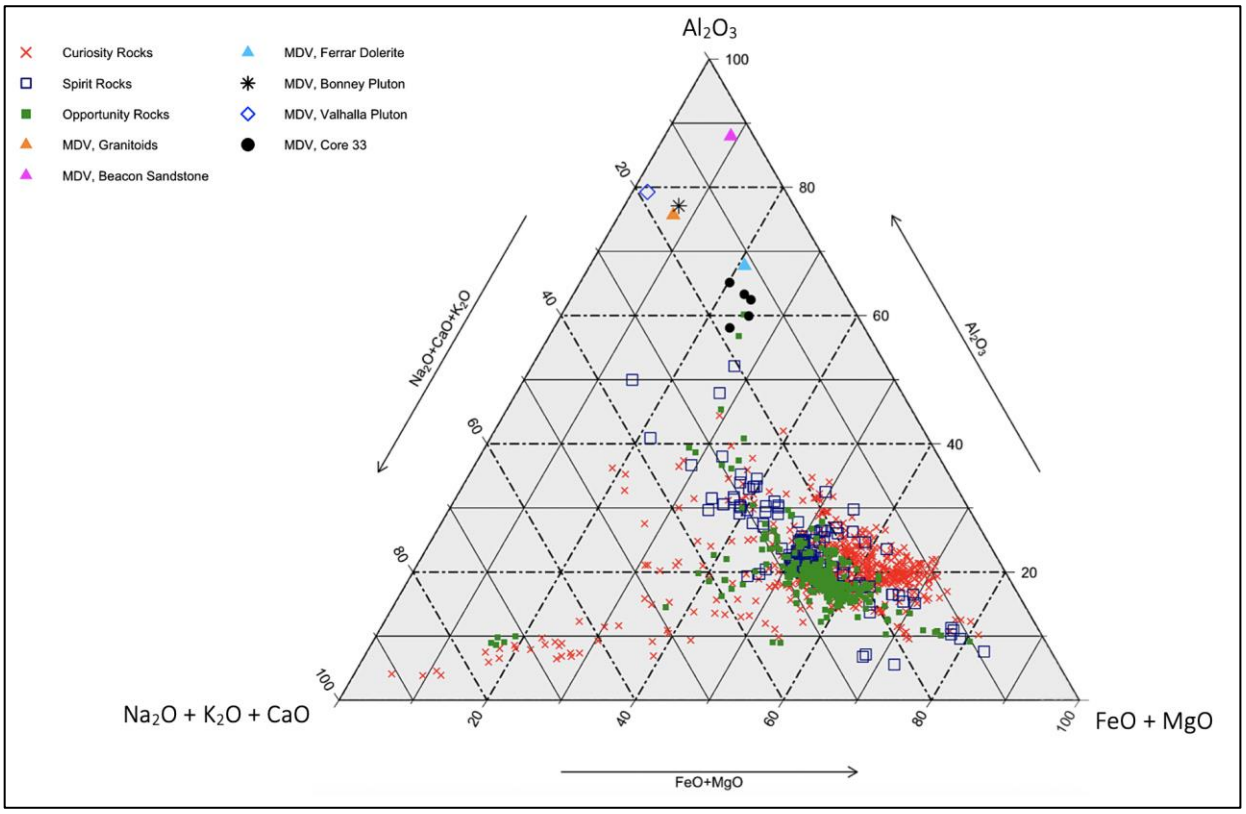

Figure 140. $Na_2O + K_2O + CaO$, Al_2O_3, and FeO + MgO abundances of all rover rocks, MDV source rocks (Brownworth Pluton not shown), and Core 33.

Major elemental analysis of Core 33, MDV source rocks, and all rover rock samples is shown in Figure 140. Core 33 FeO + MgO abundances are most in line with depleted, low-abundance (20-25 %) rover rocks. Core 33 $Na_2O + K_2O + CaO$ abundances best align with Curiosity Rocks, and Al_2O_3 abundances align poorly with all rover samples.

4.3.1.2. SPECIAL ANALYSIS: CIA

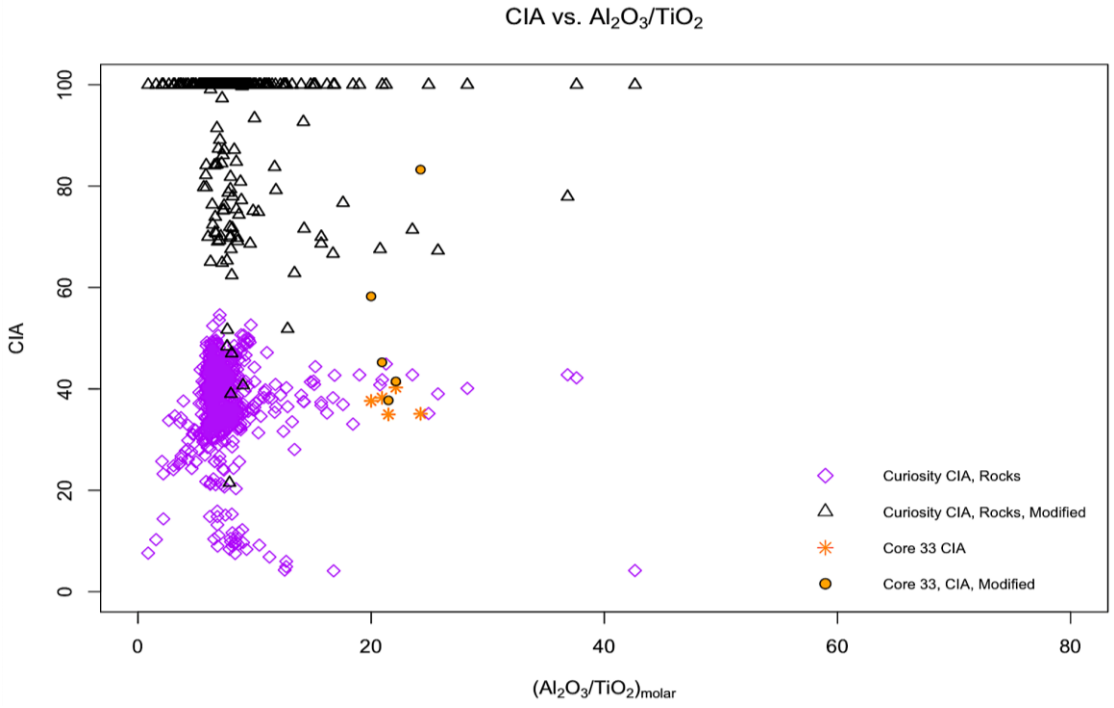

Figure 141. Modified and unmodified CIA values of Curiosity rover rocks and Core 33.

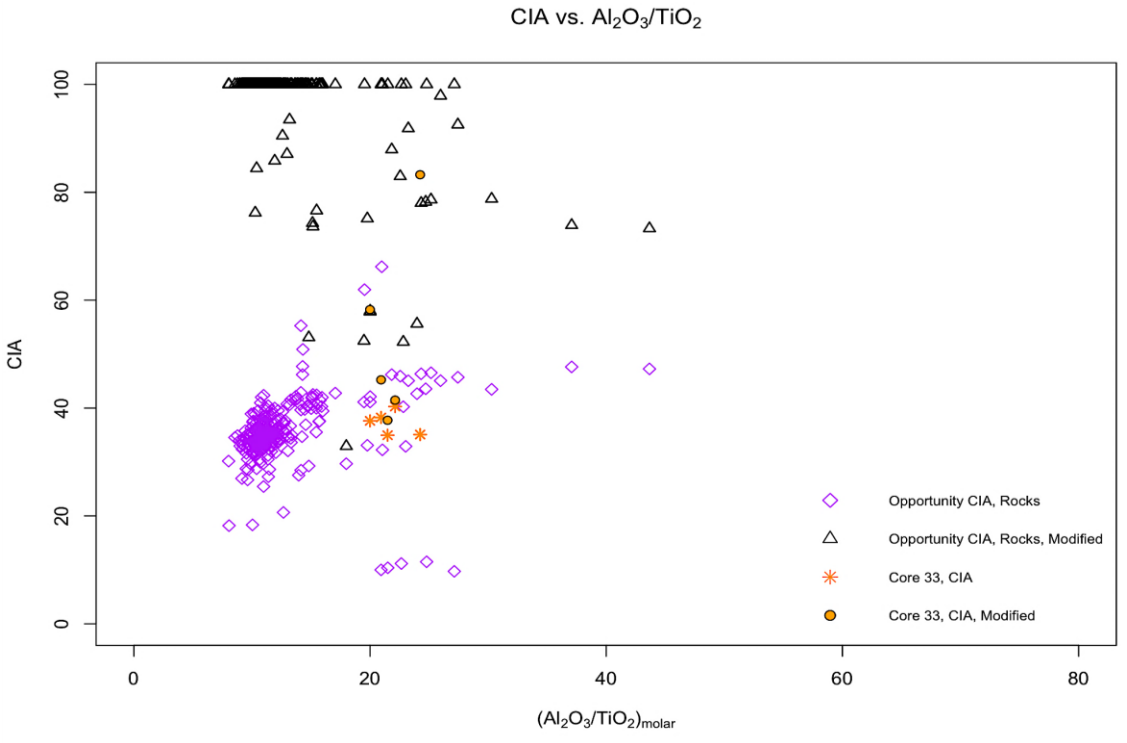

Figure 142. Modified and unmodified CIA values of Opportuinty rover rocks and Core 33.

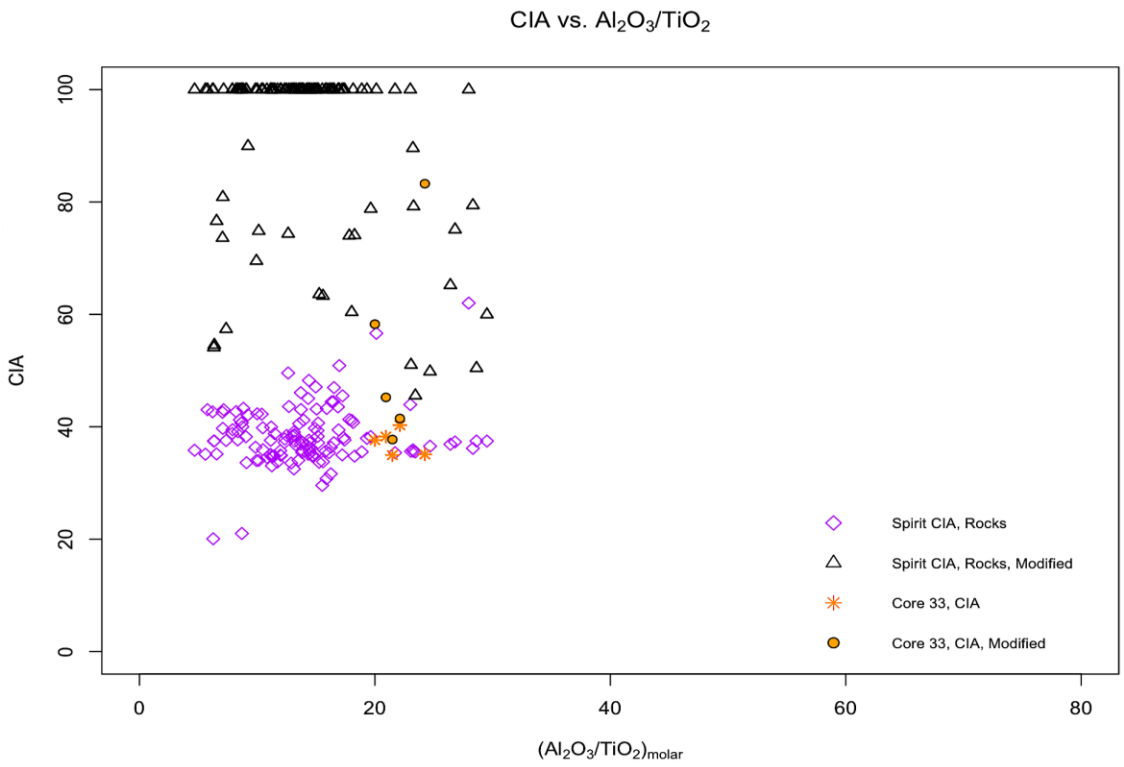

Figure 143. Modified and unmodified CIA values of Spirit rover rocks and Core 33.

Unmodified Chemical Index of Alteration values for Core 33 range from 34-40, in the range of fresh basalts (Nesbitt & Young, 1982) and in line with the regional geologic composition (Peterson and Marsh, 2008). Unmodified rover rock values range from 4, in Curiosity sample *Alvord_Mountain_raster2*, to 66 in Opportunity rock sample *Esperance6 RAT2*. This wide range includes a variety of corresponding geologic classifications (Nesbitt and Young, 1982; Fedo et al., 1995) and is likely due to salt dilution. Figures 141-143 show that *unmodified* Core 33 sample CIA values are relatively comparable to *unmodified* rover CIAs.

Modified Chemical Index of Alteration values, to correct for sulfate dilution, exhibit a significant increase for 3 of 5 Core 33 samples as do the majority of rover samples. In most cases the rover samples reach a value of 100— completely altered. This is likely due to the relative sulfate enrichment. But there are some samples that exhibit modified CIA values as low as 21, which are likely due to just the opposite— sulfate depletion. The plots above show that *modified* Core 33 sample CIA values are relatively

comparable to *modified* rover CIAs. Because of this, Core 33 sample(s) are considered suitable analogs to the martian landscape. The analogous *rover* samples are found in Appendix E .

4.3.1.3. SULFITE

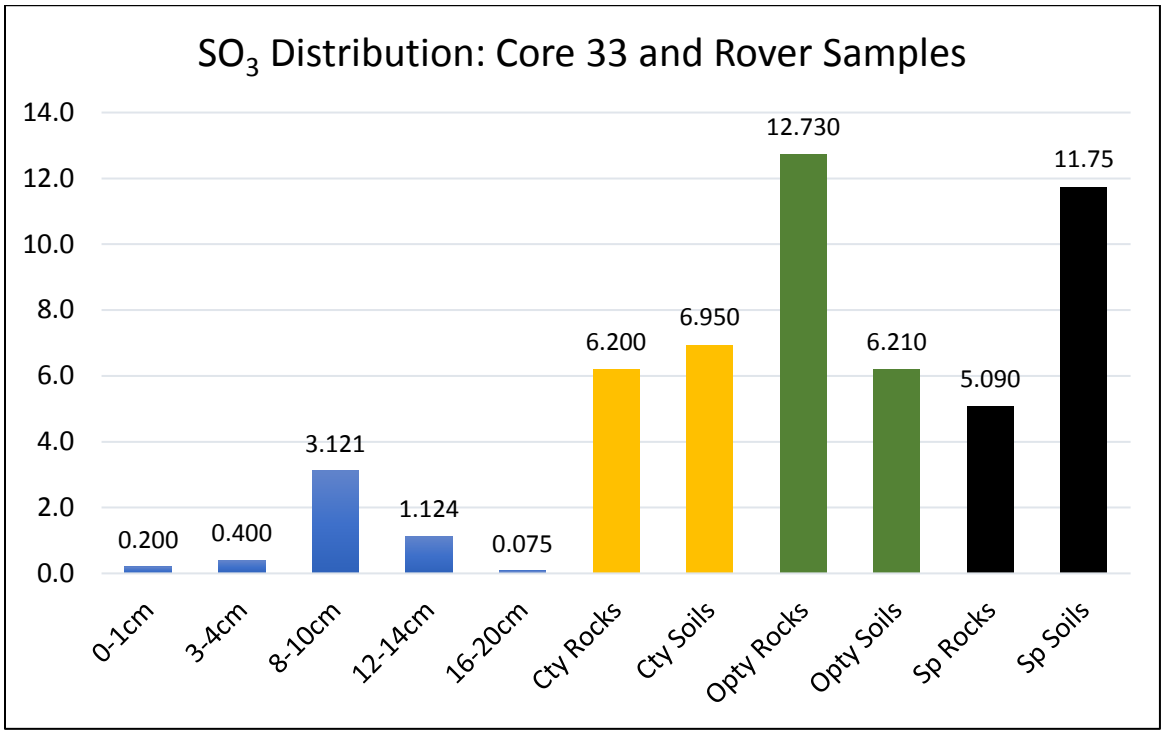

Figure 144. Sulfite abundance of Core 33 and all Mars rover rock and soil samples.

SO_3 analysis of Core 33 sediments and rover rocks/soils shows the 8-10 cm depth range of Core 33, though lower by approximately 3 %, to be the most comparable to rover samples, particularly Opportunity soils and Curiosity and Spirit rocks.

4.3.2. CORE 39

4.3.2.1. MAJOR ELEMENTAL ANALYSIS

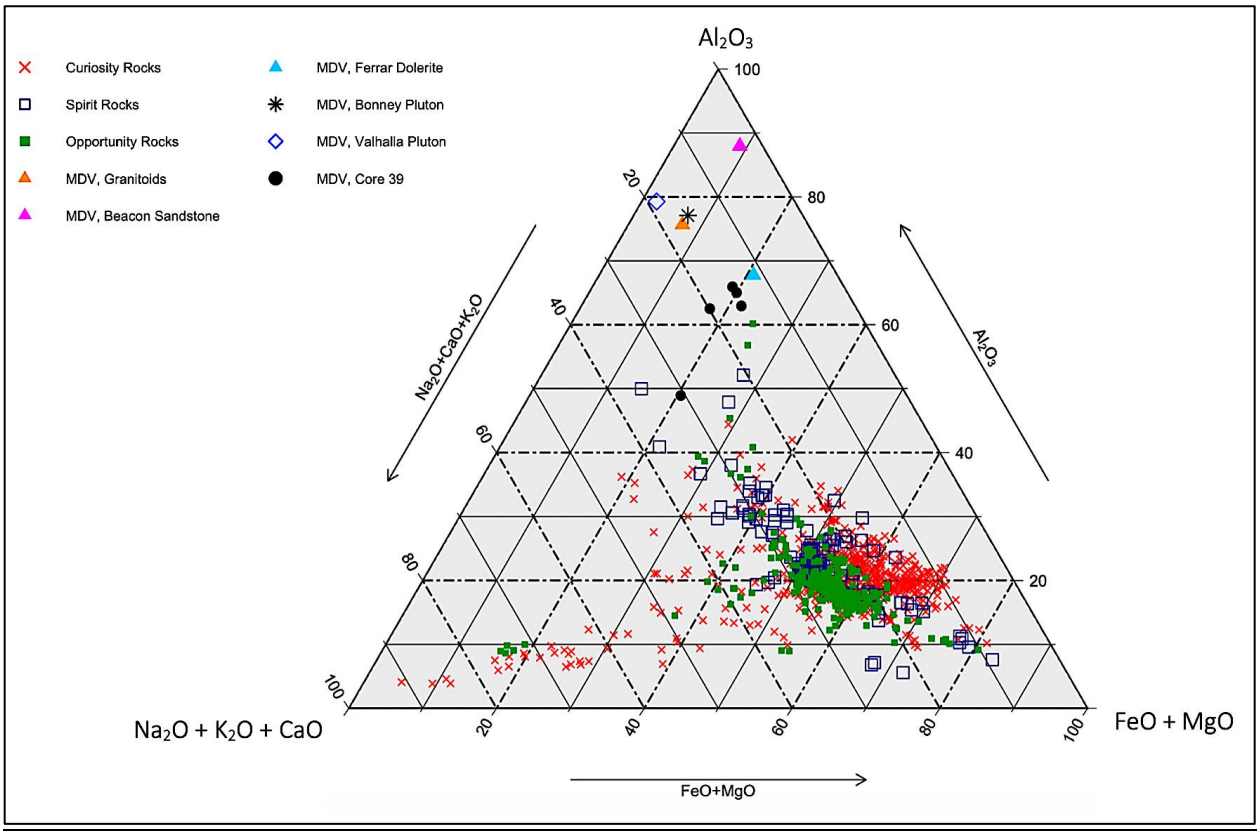

Figure 145. $Na_2O + K_2O + CaO$, Al_2O_3, and FeO + MgO abundances of all rover rocks, MDV source rocks (Brownworth Pluton not shown), and Core 39.

Major elemental analysis of Core 39, MDV source rocks, and all rover rock samples is shown in Figure 145. FeO + MgO abundances are in line with depleted, low-abundance (~20 %) rover rocks. Core 39 $Na_2O + K_2O + CaO$ relative abundances are in line with Curiosity and Spirit rocks. All samples, except for one, exhibit relative Al_2O_3 enrichment. The single anomalous, depleted sample is enriched in Na_2O relative to the other Core 39 samples.

4.3.2.2. SPECIAL ANALYSIS: CIA

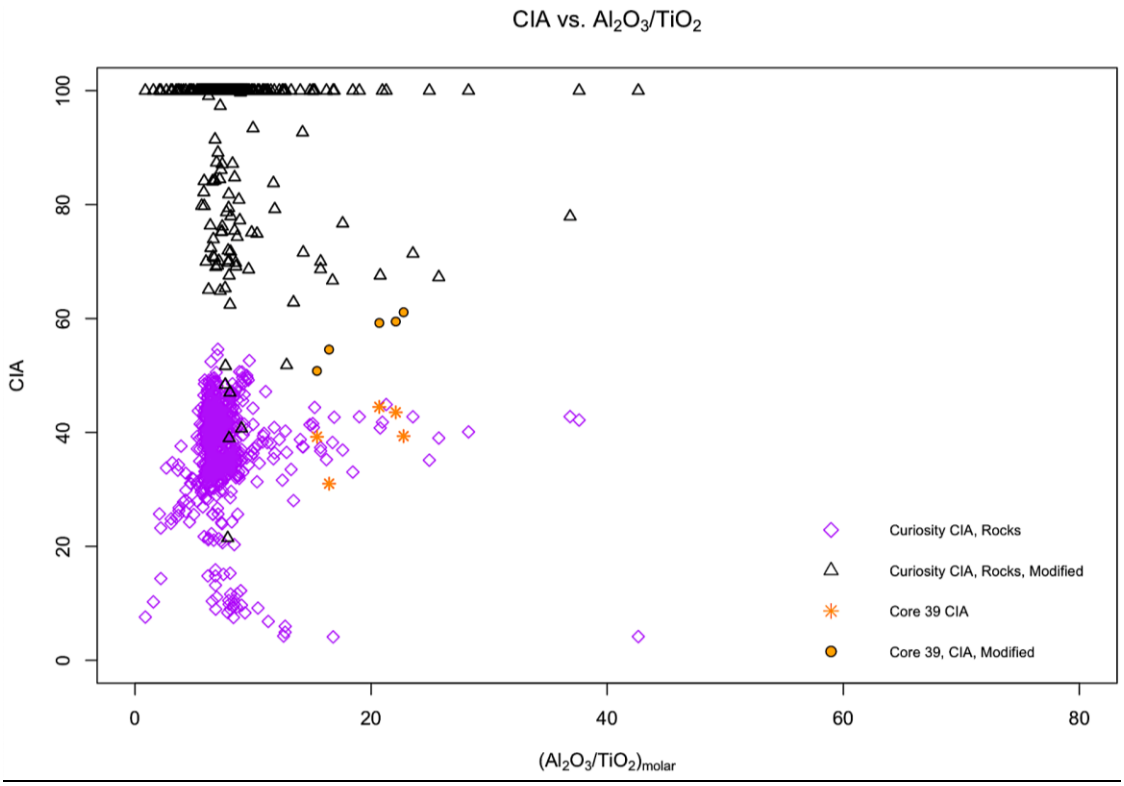

Figure 146. Modified and unmodified CIA values of Curiosity rover rocks and Core 39.

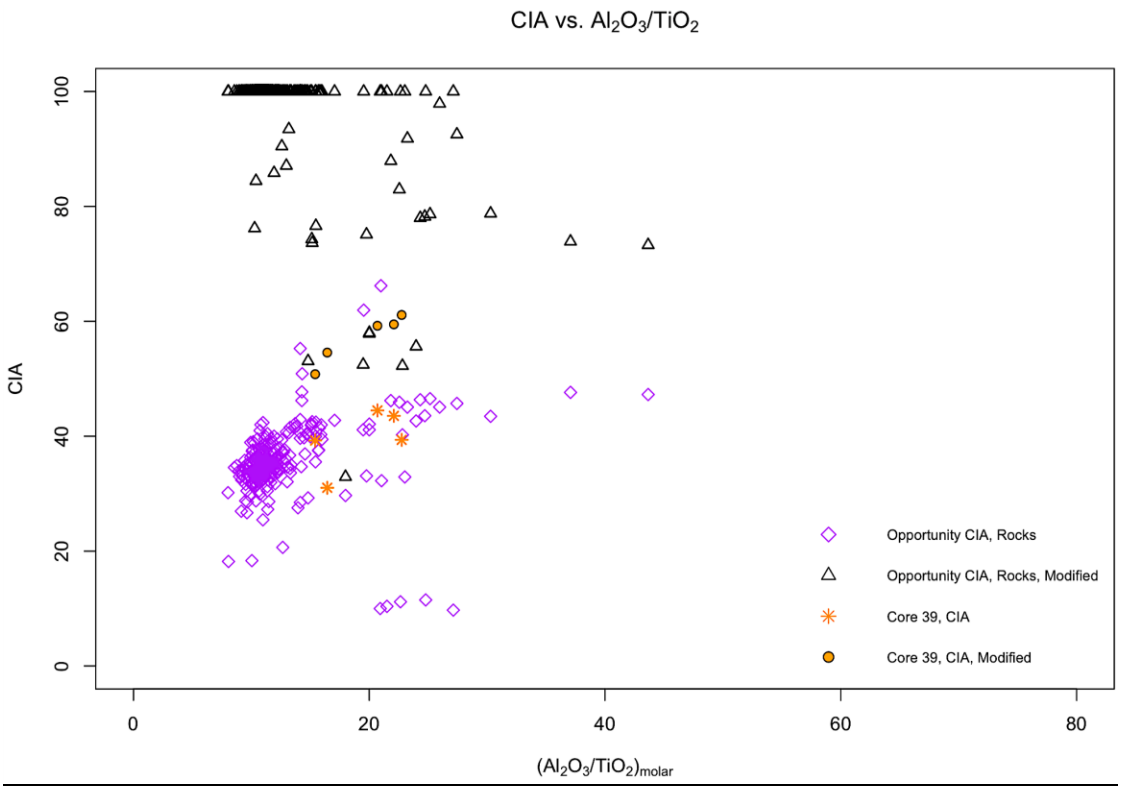

Figure 147. Modified and unmodified CIA values of Opportunity rover rocks and Core 39.

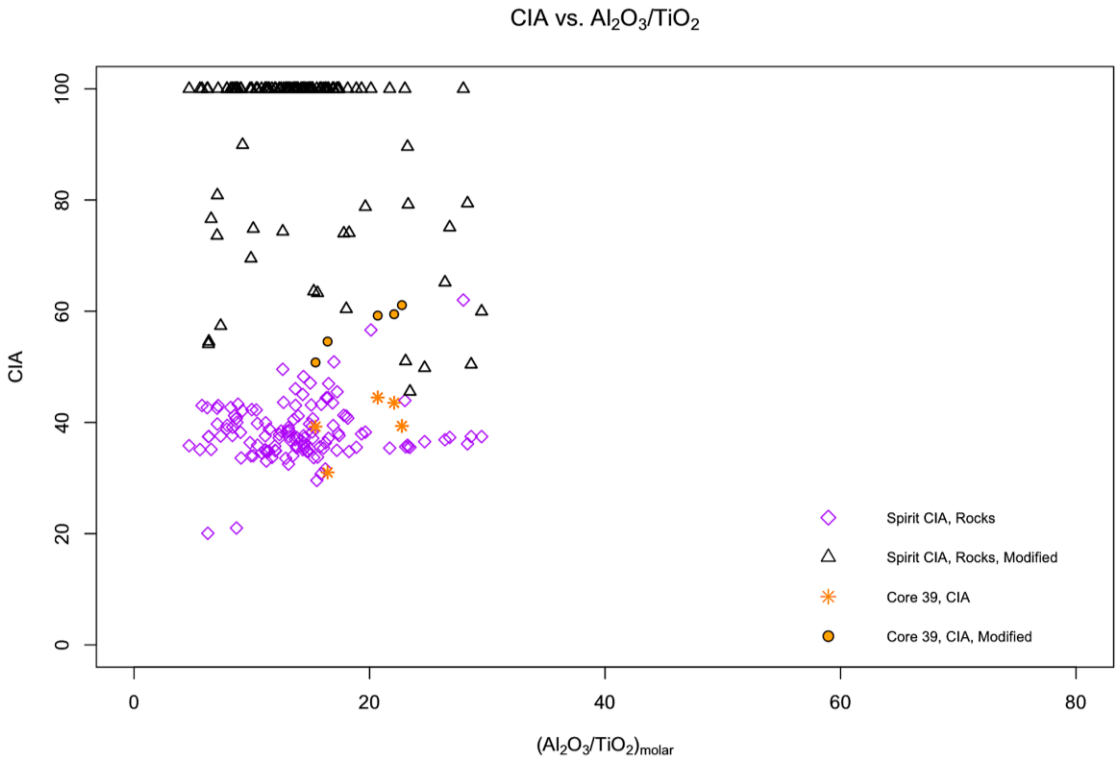

Figure 148. Modified and unmodified CIA values of Spirit rover rocks and Core 39.

Unmodified Chemical Index of Alteration values for Core 39 range from 31-44, in the range of fresh basalts (Nesbitt & Young, 1982) and in line with the regional geologic composition (Peterson and Marsh, 2008). Unmodified Mars rover samples exhibit a much wider range, possibly a sign of greater sulfate dilution. Figures 146-148 show that *unmodified* Core 39 sample CIA values are relatively comparable to rover *unmodified* CIAs.

Modified Chemical Index of Alteration values, to correct for sulfate dilution, exhibit a very slight increase in Core 39 samples, while the majority of rover samples exhibit large increases. In most cases the rover samples are completely altered, likely due to the relative sulfate enrichment. However, there are some samples that exhibit modified CIA values as low as 21, which are likely due to just the opposite— sulfate depletion. The minimal Core 39 CIA modification is likely due to the core's sediment mixing with aluminous source rocks because Core 39 samples, particularly JB1135 (2-5 cm) and JB1136 (6-8 cm), do indeed contain sulfates—primarily thenardite (Na_2SO_4). The plots above show that *modified* Core 39 sample CIA values are only slightly comparable to select Spirit and Opportunity *modified* CIAs. Because of this, select Core 39 sample(s) are considered analogous to the martian landscape. The analogous *rover* samples are found in Appendices E and F.

SO_3 at Core 39 is not compared to rovers due to negligible abundances.

4.3.3. CORE 42

4.3.3.1. MAJOR ELEMENTAL ANALYSIS

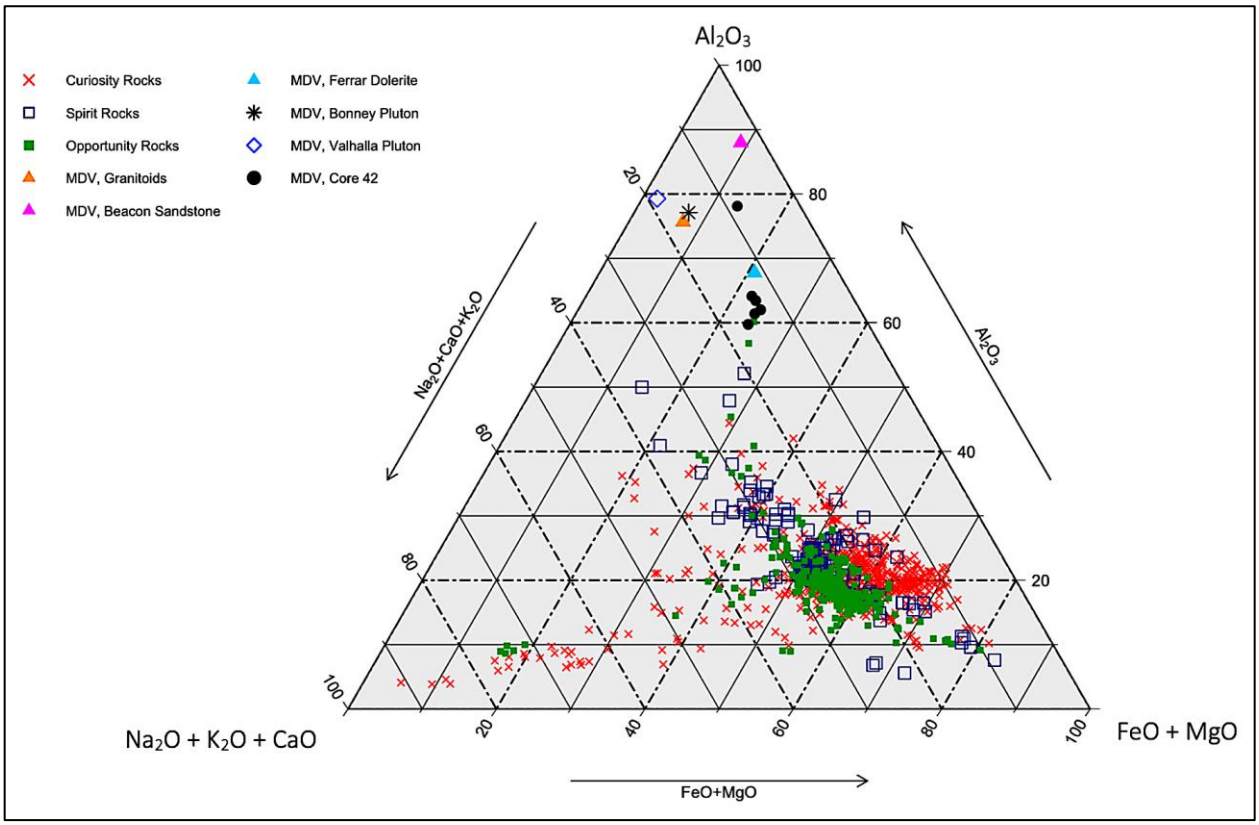

Figure 149. $Na_2O + K_2O + CaO$, Al_2O_3, and FeO + MgO abundances of all rover rocks, MDV source rocks (Brownworth Pluton not shown), and Core 42

Major elemental analysis of Core 42, MDV source rocks, and all rover rock samples is shown above. FeO + MgO Core 42 abundances best align with depleted, low-abundance (25 %) rover rocks, and show tight grouping except for a single sample that reports lower $Na_2O + K_2O + CaO$ abundances in tandem with lower FeO and MgO abundances. This same sample reports enhanced Al_2O_3 abundances. The anomalous Core 42 sample is JB1102 (4-7 cm) which exhibits aluminosilicate clays and enhanced major and minor

elemental abundances (Burton et al., 2020), corroborating the sample's position on the diagram above.

4.3.3.2. Special Analysis: CIA

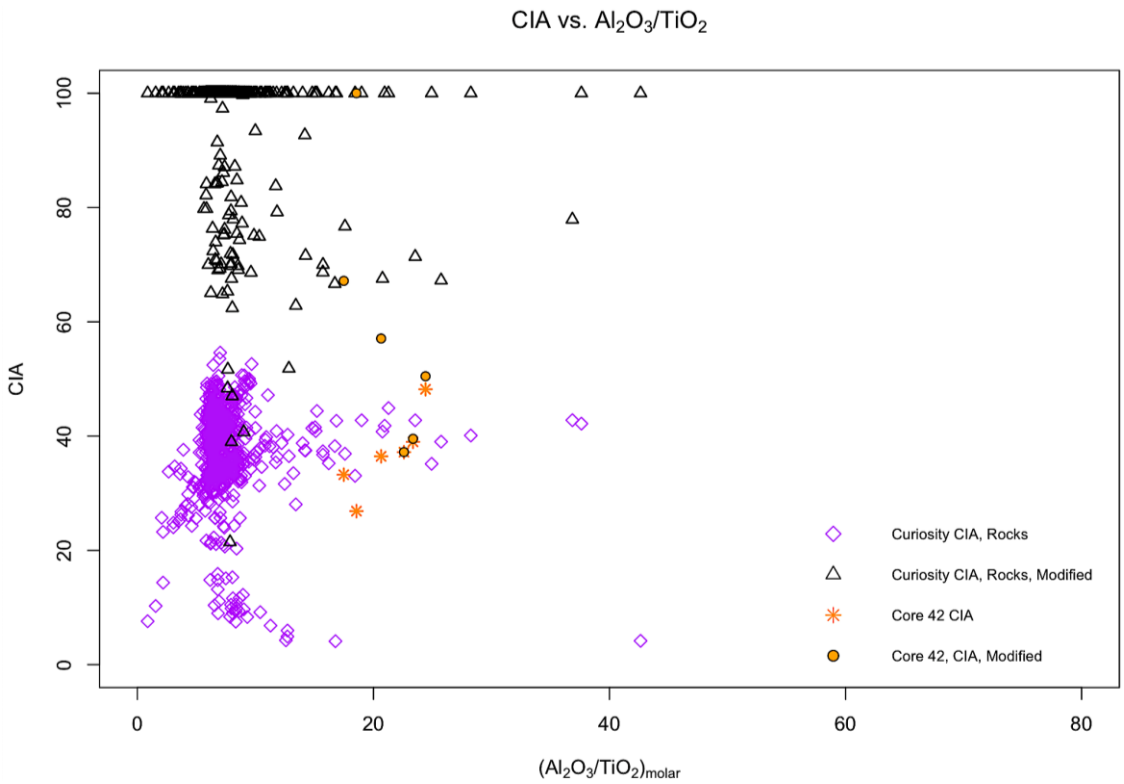

Figure 150. Modified and unmodified CIA values of Curiosity rover rocks and Core 42.

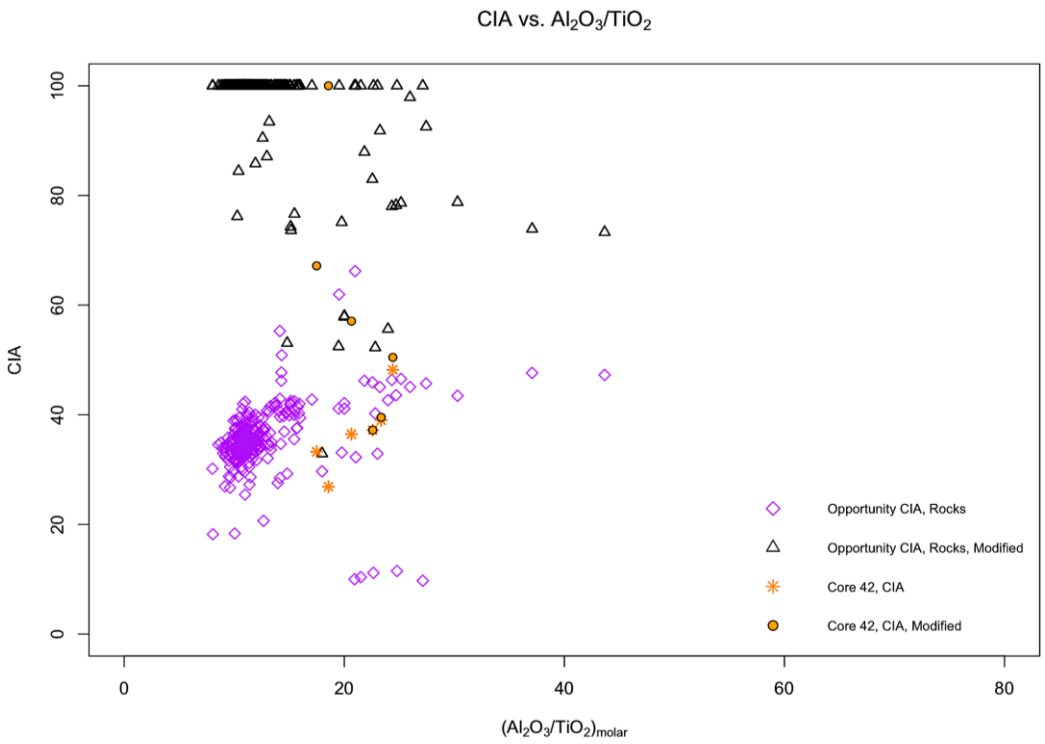

Figure 151. Modified and unmodified CIA values of Opportunity rover rocks and Core 42.

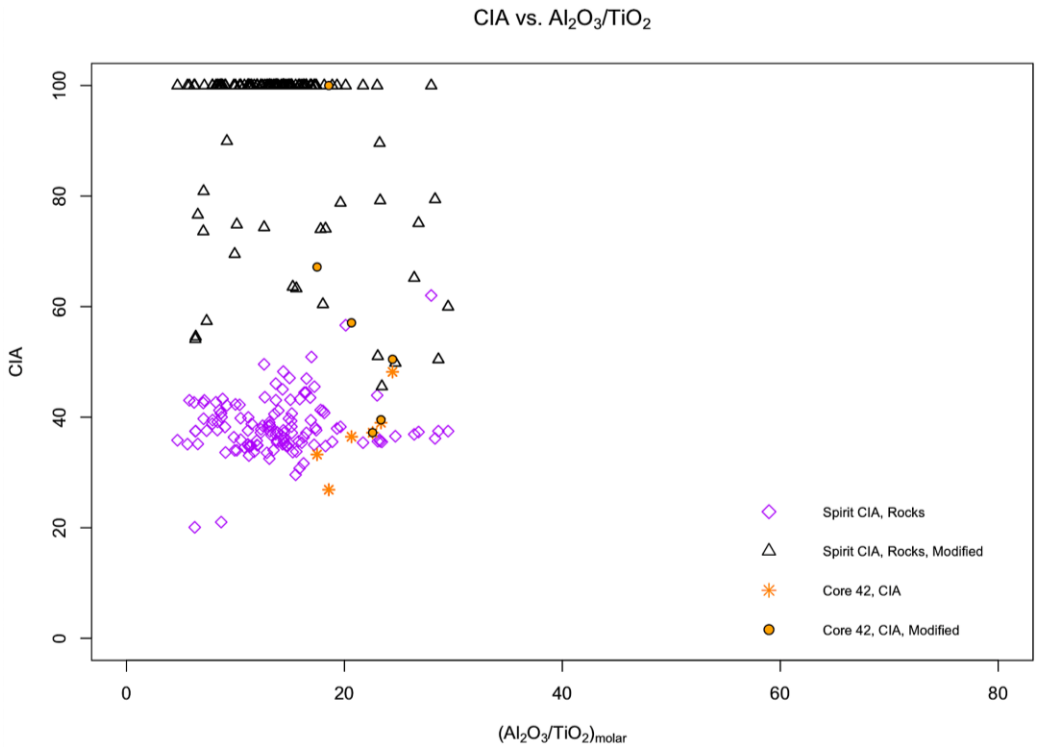

Figure 152. Modified and unmodified CIA values of Spirit rover rocks and Core 42.

Unmodified Chemical Index of Alteration values for Core 42 range from 26-48, in the range of fresh basalts, into fresh granites and granodiorites, (Nesbitt & Young, 1982) and in line with the regional geologic composition (Peterson and Marsh, 2008). Conversely, unmodified rover rock values report a wide range. Figures 150-152 show that *unmodified* Core 42 sample CIA values are comparable to select rover *unmodified* CIAs.

Modified Chemical Index of Alteration values exhibit both slight and massive increases in Core 42 samples, while the majority of rover samples exhibit large increases, likely a result of relative sulfate enrichment. The minimal Core 42 CIA modifications are likely due to the respective sample's sulfate depletion, while the substantial modifications— from 27 → 100 in JB1103 (8-10 cm), for example— are likely due to sulfate enrichment. As noted in Chapter 2, JB1103 (8-10 cm) reports massive gypsum ($CaSO_4$) enrichment thus corroborating the hypothesis of sulfate dilution. The plots above show that *modified* Core 42 sample CIA values are comparable to select rover *modified* CIAs. Because of this, specific sample(s) are considered suitable analogs to the martian landscape. The analogous *rover* samples are found in Appendices E and F.

4.3.3.3. SULFITE

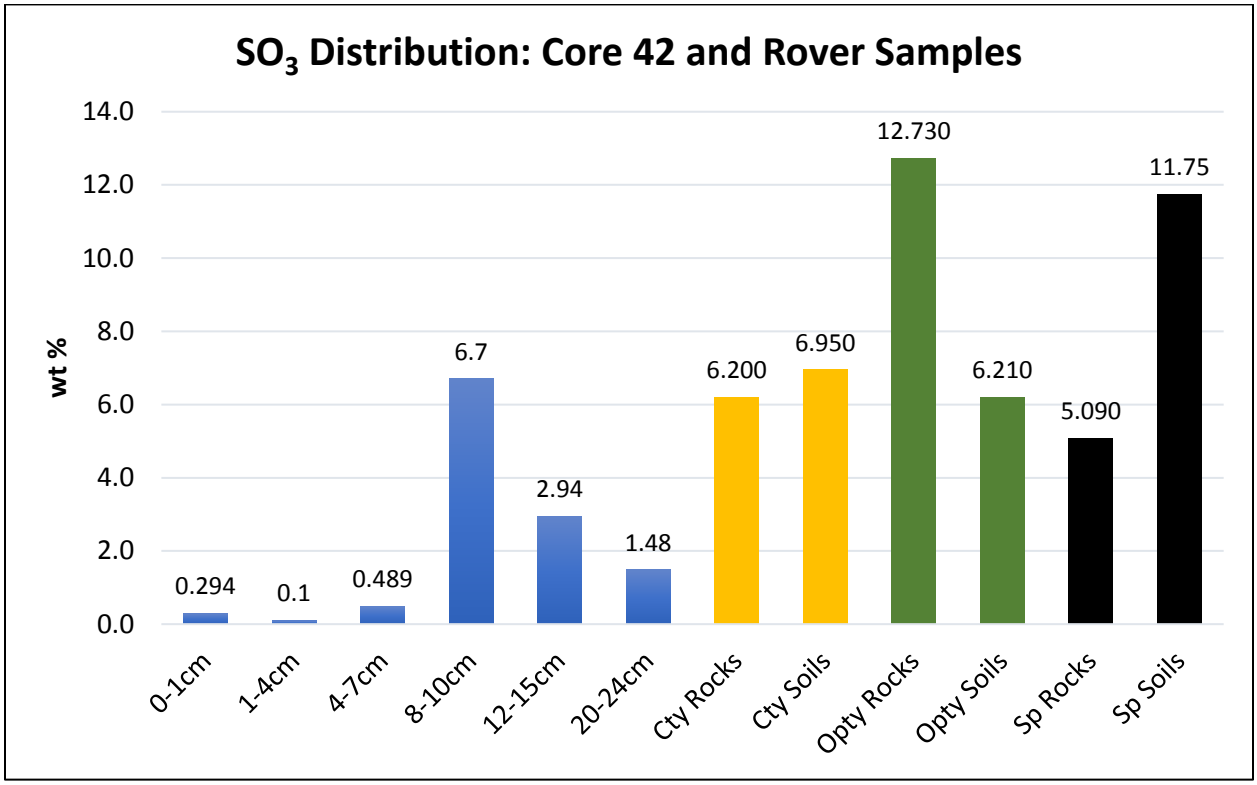

Figure 153. Sulfite abundance of Core 42 and all Mars rover rock and soil samples.

SO_3 analysis of Core 42 sediments and rover rocks/soils shows the 8-10 cm depth range, and slightly so 12-15 cm, to be most comparable to rover samples— particularly Curiosity rocks and soils. The still relatively high SO_3 abundances in the 12-15 cm depth range are likely due to a tapering off of sulfates (known to be gypsum) from the 8-10 cm depth range.

4.3.4. Core 52

4.3.4.1. Major Elemental Analysis

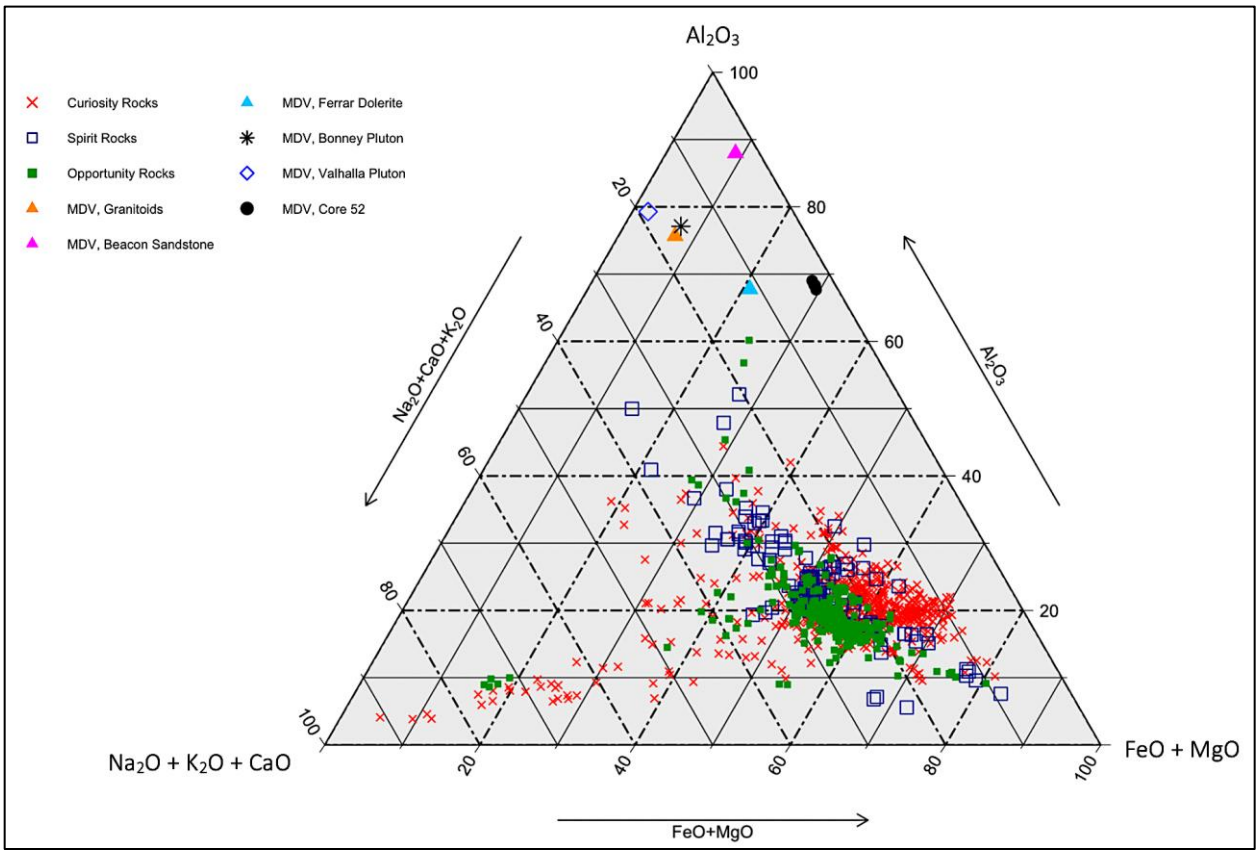

Figure 154. $Na_2O + K_2O + CaO$, Al_2O_3, and FeO + MgO abundances of all rover rocks, MDV source rocks (Brownworth Pluton not shown), and Core 52.

Figure 154 shows tight grouping of Core 52 samples, with FeO + MgO abundances aligning best with depleted, low-abundance (< 30 %) rover rocks. Core 52 $Na_2O + K_2O +$ CaO abundances are depleted compared to rover samples but align best with Spirit and Curiosity rocks. Core 52 Al_2O_3 abundances are enriched compared to all rover rock samples.

4.3.4.2. SPECIAL ANALYSIS: CIA

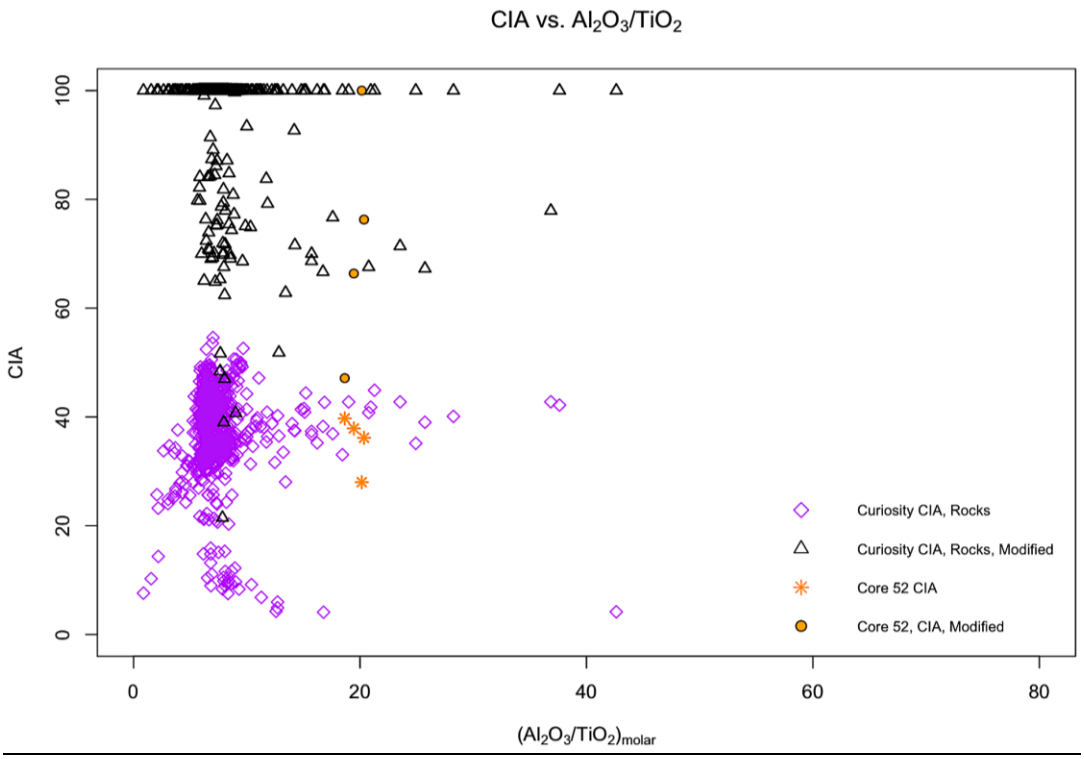

Figure 155. Modified and unmodified CIA values of Opportunity rover rocks and Core 52.

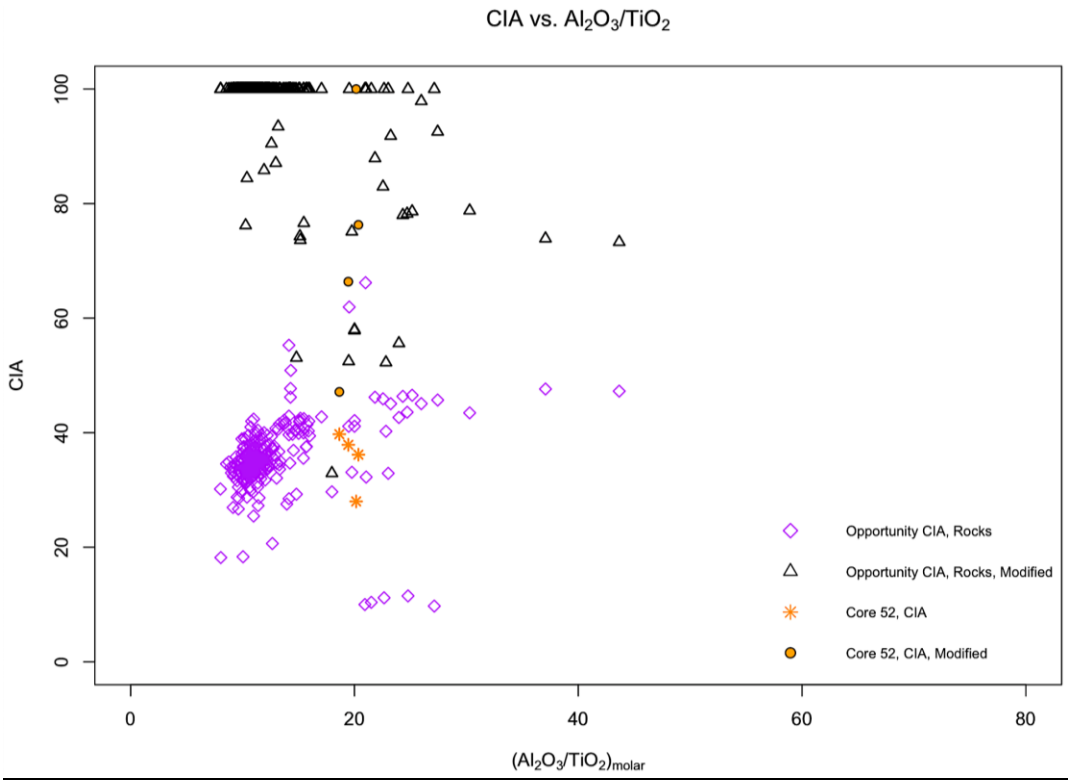

Figure 156. Modified and unmodified CIA values of Opportunity rover rocks and Core 52.

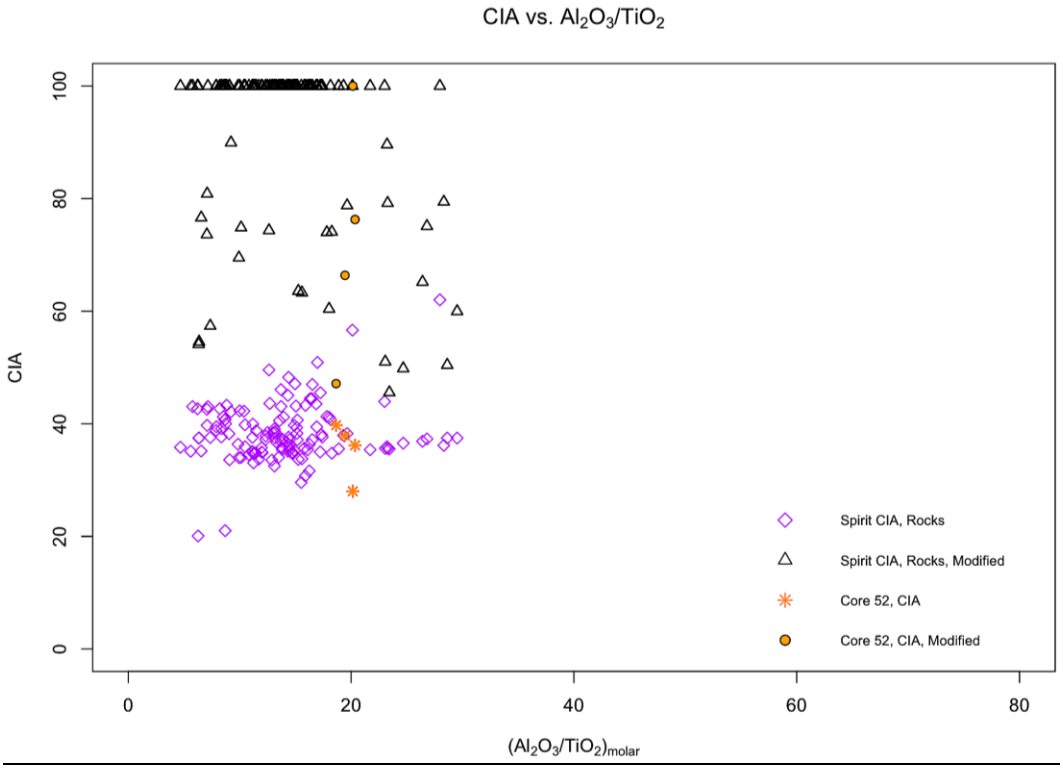

Figure 157. Modified and unmodified CIA values of Opportunity rover rocks and Core 52.

Unmodified Chemical Index of Alteration values for Core 52 range from 28-39, in the range of fresh basalts (Nesbitt & Young, 1982) and in line with the regional geologic composition (Peterson and Marsh, 2008). Figures 155-157, above, show that *unmodified* Core 52 sample CIA values are comparable to select rover *unmodified* CIAs.

Modified Chemical Index of Alteration values exhibit significant increases in Core 52 samples, while the majority of rover samples exhibit large increases. The smaller Core 52 CIA modifications are likely due to relative sulfate depletion, while the substantial modifications— 28 → 100 in JB1109 (4-8 cm), for example— are likely due to relative sulfate enrichment. As noted in Chapter 2, all Core 52 samples below 2 cm exhibit features due to gypsum (Bishop, personal communication, 2020), but JB1109 (4-8 cm) reports massive enrichment, corroborating the hypothesis of sulfate dilution. The majority of Mars rover samples exhibit completely altered (100) modified CIA values. The plots above show that *modified* Core 52 sample CIA values are also comparable to select rover *modified* CIAs. Because of this, specific Core 52 sample(s) are considered suitable analogs to the martian landscape. The analogous *rover* samples are found in Appendices E and F.

4.3.4.3. SULFITE

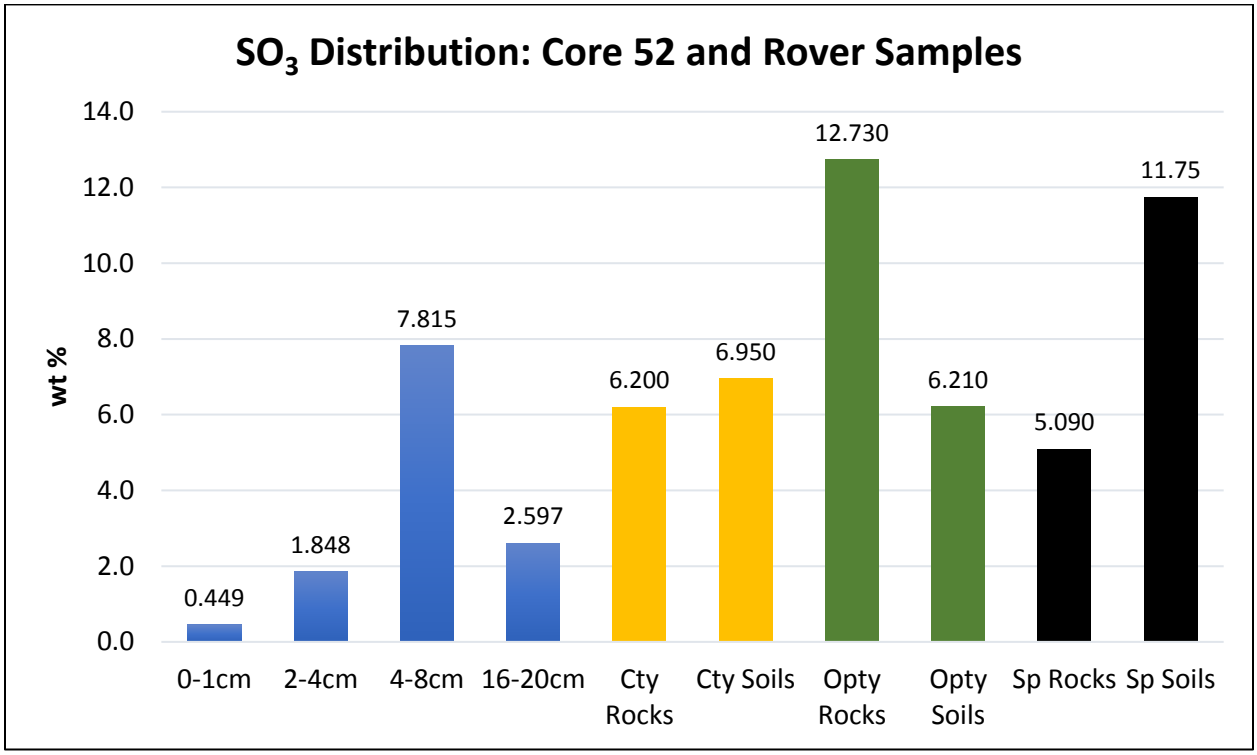

Figure 158. Sulfite abundance of Core 52 and all Mars rover rock and soil samples.

SO_3 analysis of Core 52 sediments and rover rocks/soils shows the 4-8 cm depth range, and slightly so 16-20 cm, to be most comparable to rover samples—particularly Curiosity rocks and soils and Opportunity soils, with a slight trend toward Spirit soils and Opportunity rocks.

4.3.5. Core 72

4.3.5.1. Major Elemental Analysis

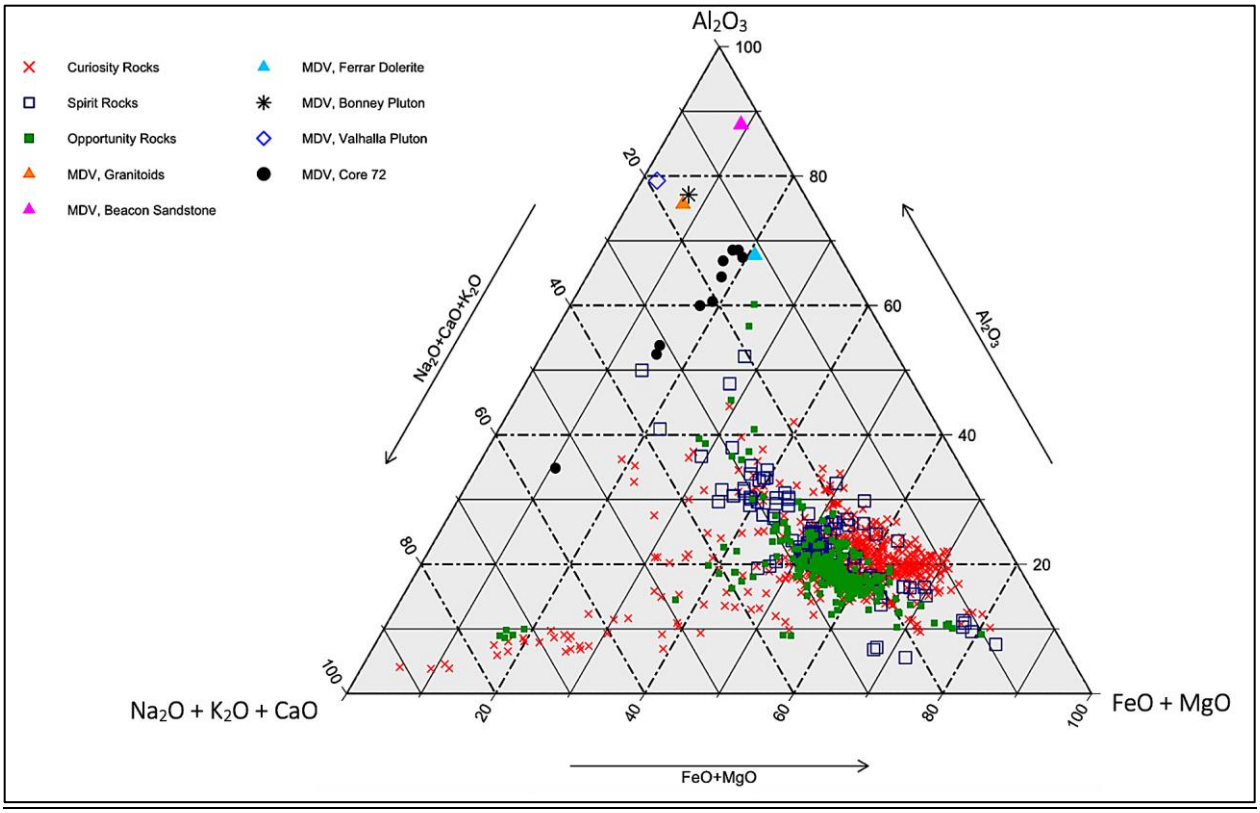

Figure 159. $Na_2O + K_2O + CaO$, Al_2O_3, and FeO + MgO abundances of all rover rocks, MDV source rocks (Brownworth Pluton not shown), and Core 72.

Major elemental analysis of Core 72, MDV source rocks, and all rover rock samples is shown above. Core 72 samples show significant variation, primarily in $Na_2O + K_2O + CaO$ and Al_2O_3 abundances. All Core 72 samples exhibit similar FeO + MgO abundances. Core 72 FeO + MgO abundances align poorly with all rover samples but spread relatively well across $Na_2O + K_2O + CaO$ abundances of all rovers. One sample, JB1089 (2-4 cm) exhibits enhanced in $Na_2O + K_2O + CaO$ levels, due to unusually high Na_2O levels that manifest as halite, per XRD analysis. However, anion analysis (Gibson et al., 1983) shows massive enrichment, making thenardite (Na_2SO_4) more likely to be present.

4.3.5.2. Special Analysis: CIA

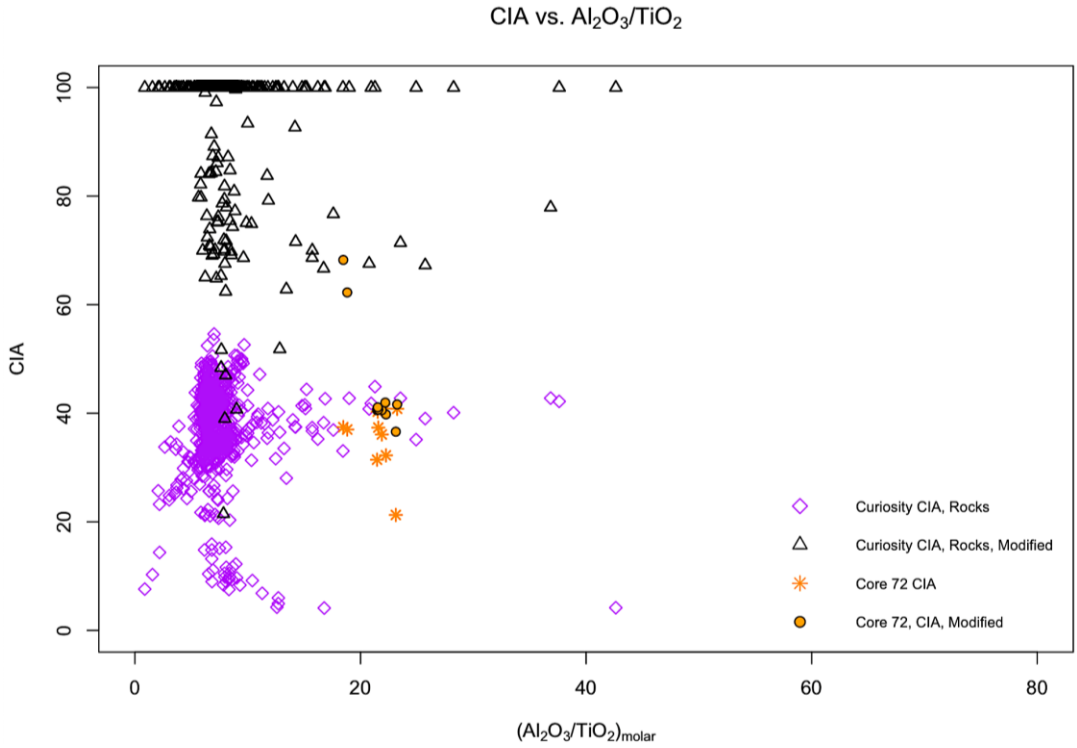

Figure 160. Modified and unmodified CIA values of Curiosity rover rocks and Core 72.

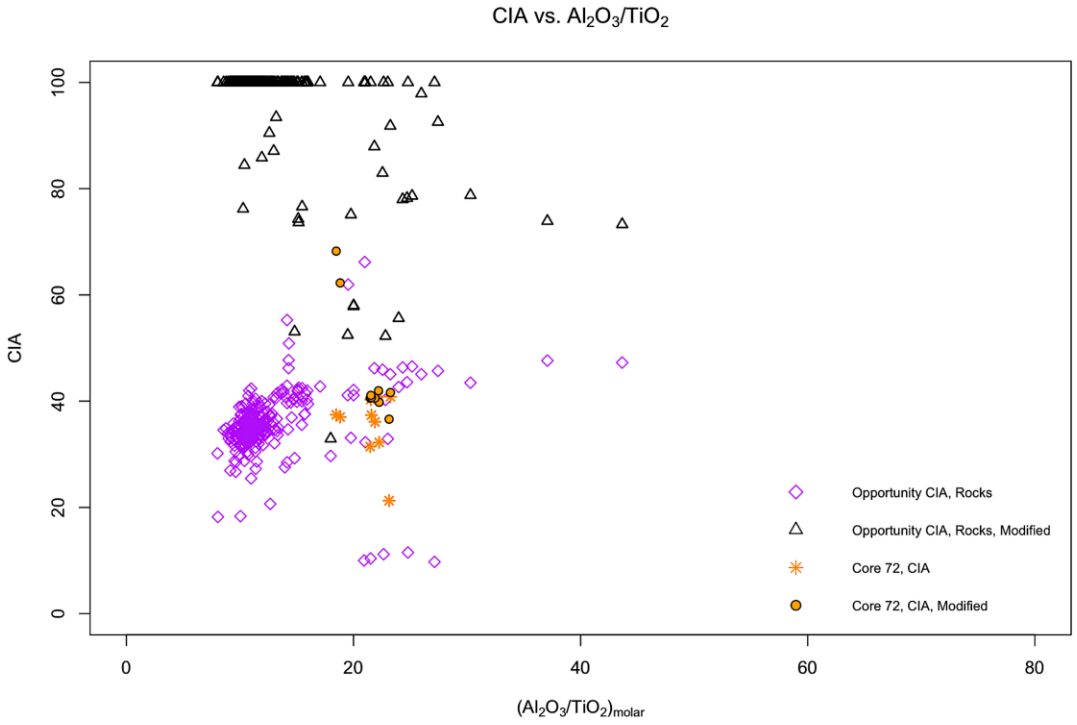

Figure 161. Modified and unmodified CIA values of Opportunity rover rocks and Core 72.

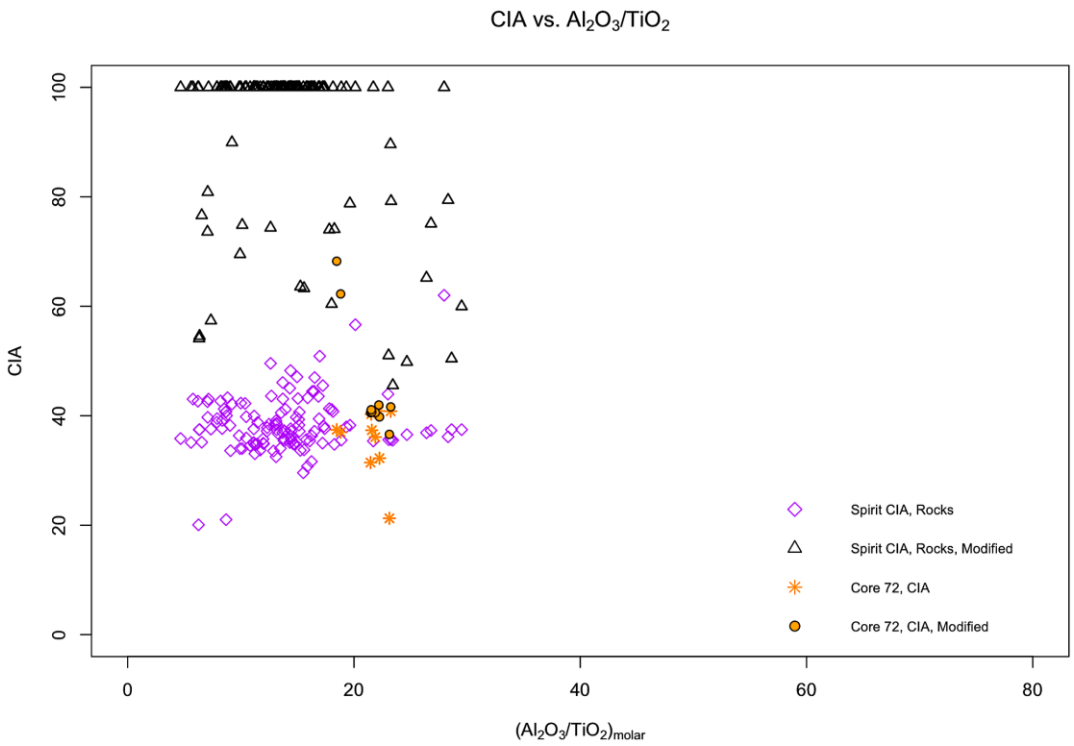

Figure 162. Modified and unmodified CIA values of Spirit rover rocks and Core 72.

Unmodified Chemical Index of Alteration values for Core 72 range from 21-41, in the range of fresh basalts (Nesbitt & Young, 1982) and in line with the regional geologic composition (Peterson and Marsh, 2008). The plots above show that *unmodified* Core 72 sample CIA values are comparable to very few *unmodified* rover CIAs.

Core 72 modified Chemical Index of Alteration values exhibit significant increases in select samples while the majority of rover samples exhibit large increases, in most cases reaching a value of 100— completely altered. The smaller Core 72 CIA modifications are likely due to the relative depletion of sulfates, while the substantial modifications— from 37 → 68 in JB1087 (0-1 cm), for example— are likely due to sulfate enrichment. As noted in Chapter 2, JB1088 (0-2 cm) and JB1089 (2-4 cm) report massive enrichment in what is believed to be thenardite (Na_2SO_4), corroborating the hypothesis of sulfate dilution. The plots above show that *modified* Core 72 sample CIA values are not

comparable to *modified* rover CIAs. Because of this, Core 72 is not considered a suitable analog to the martian landscape.

SO_3 at Core 72 is not compared to rovers due to negligible abundances.

4.3.6. Lake Fryxell

4.3.6.1. Major Elemental Analysis

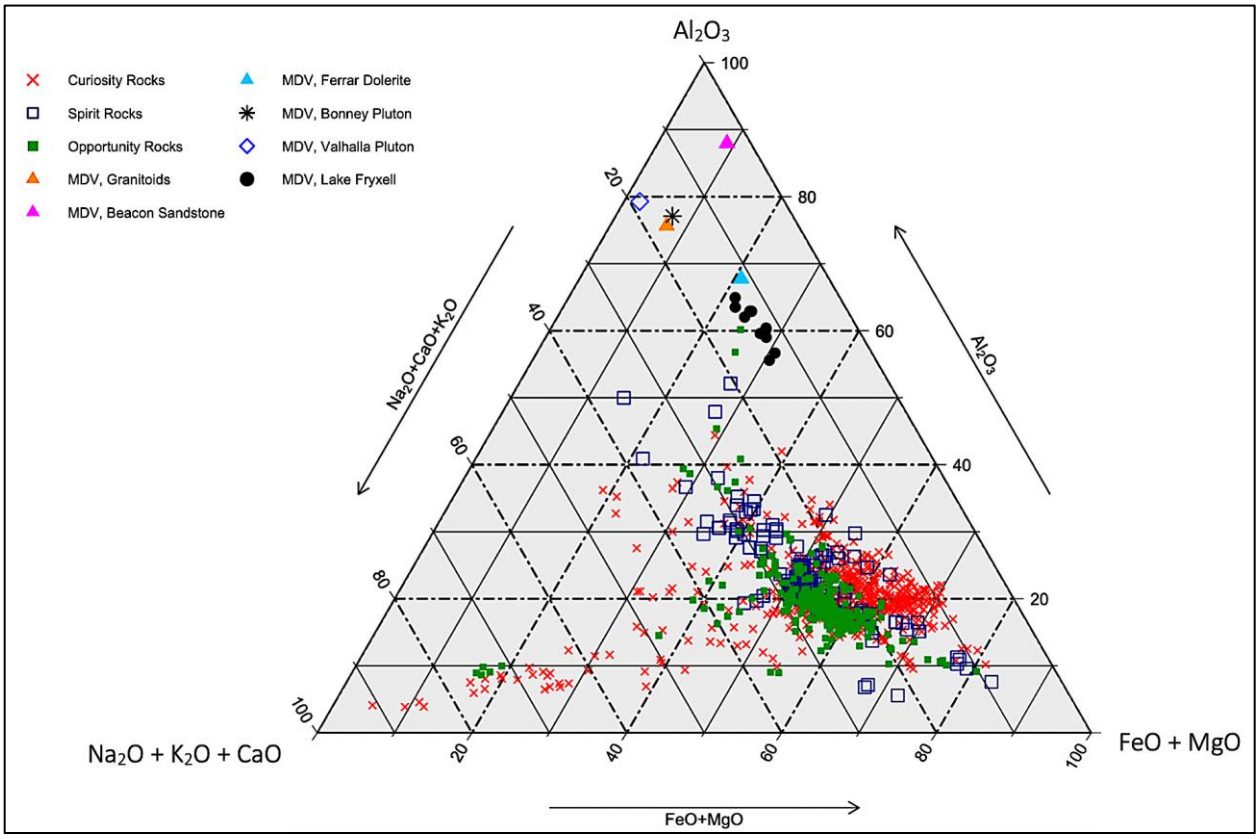

Figure 163. $Na_2O + K_2O + CaO$, Al_2O_3, and $FeO + MgO$ abundances of all rover rocks, MDV source rocks (Brownworth Pluton not shown), and Lake Fryxell edge and surface samples.

Major elemental analysis of Lake Fryxell surface and edge samples, MDV source rocks, and all rover rock samples is shown in Figure 163. Lake Fryxell samples exhibit similar Na_2O + K_2O + CaO abundance, aligning best with Curiosity rock samples. There is variation in FeO + MgO and Al_2O_3 abundances, but Al_2O_3 is, as is with all other MDV samples, significantly higher than martian samples.

4.3.6.2. SPECIAL ANALYSIS: CIA

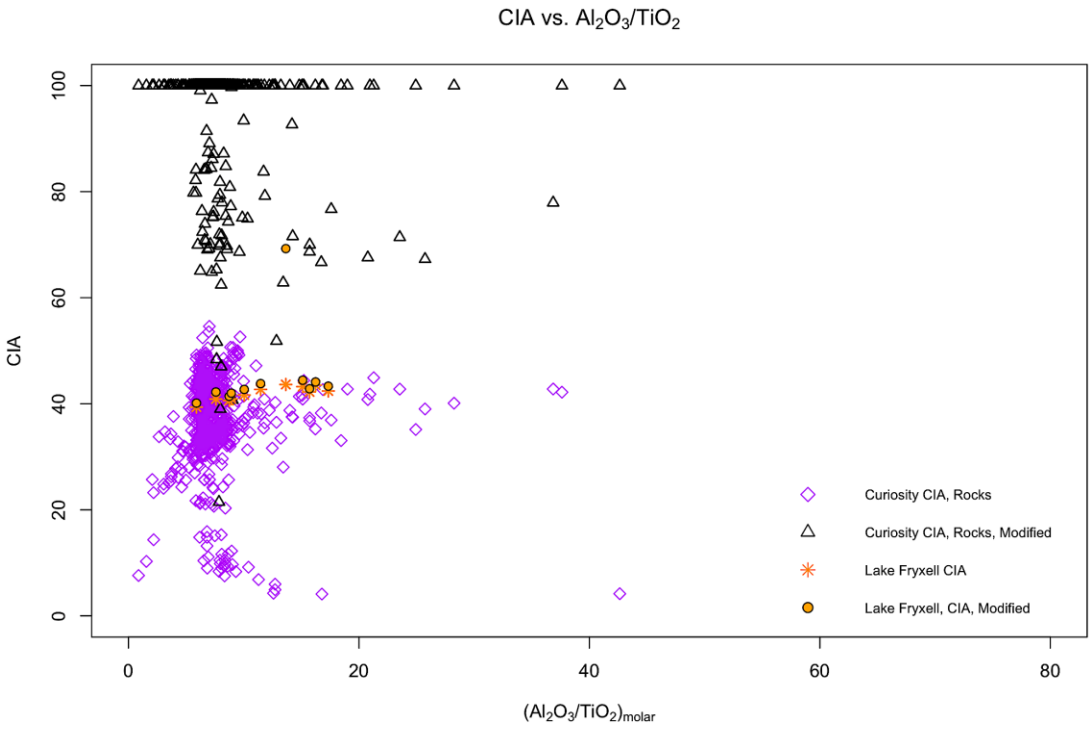

Figure 164. Modified and unmodified CIA values of Curiosity rover rocks and Lake Fryxell edge and surface samples

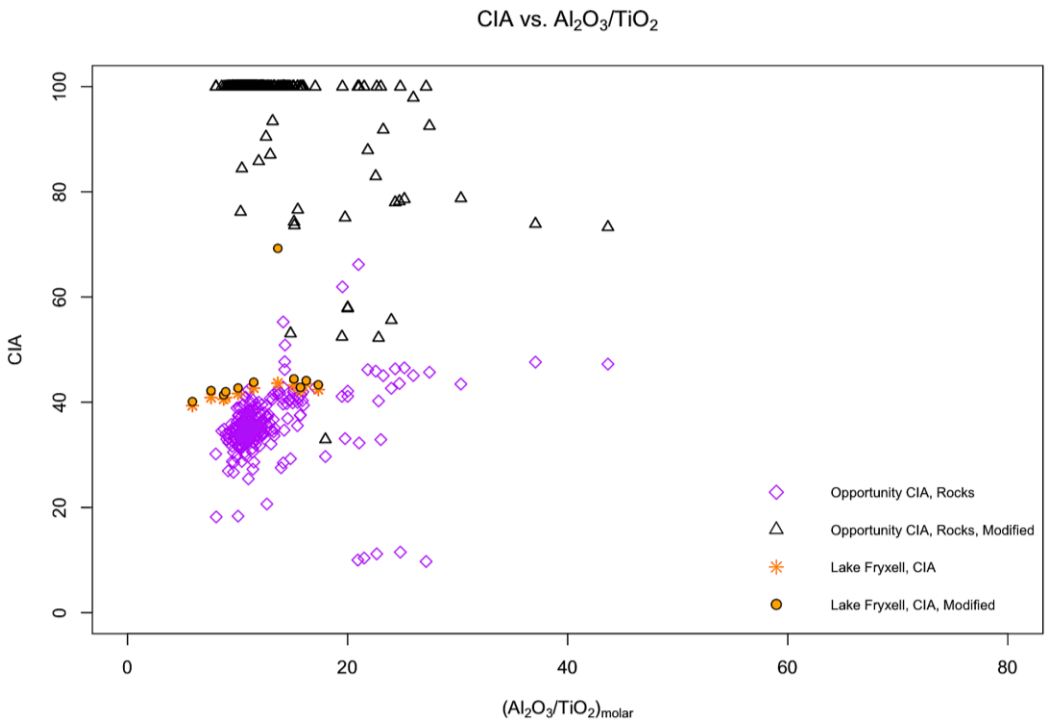

Figure 165. Modified and unmodified CIA values of Opportunity rover rocks and Lake Fryxell edge and surface samples.

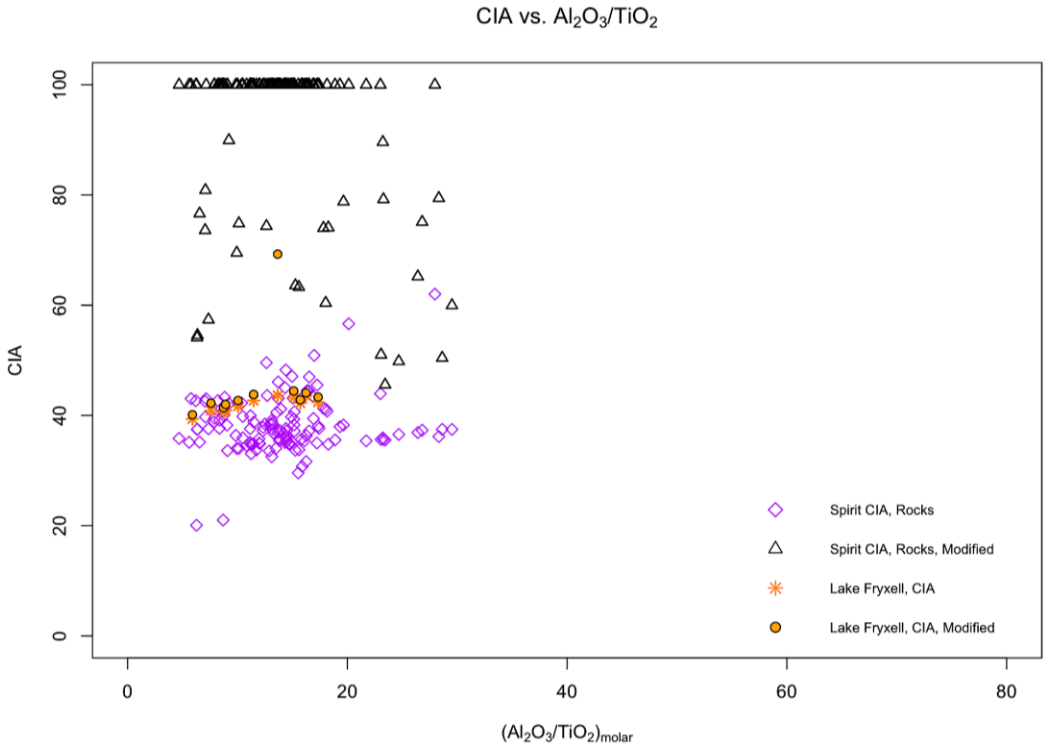

Figure 166. Modified and unmodified CIA values of Spirit rover rocks and Lake Fryxell edge and surface samples.

Unmodified Chemical Index of Alteration values for Lake Fryxell samples range from 40-43, in the range of fresh basalts, nearing granites and granodiorites, (Nesbitt & Young, 1982) and relatively in line with the regional geologic composition (Peterson and Marsh, 2008). Unmodified rover rock values exhibit a wide range and a significant number of corresponding geologic classifications (Nesbitt and Young, 1982; Fedo et al., 1995) likely do to sulfate dilution. The plots above show that *unmodified* Lake Fryxell sample CIA values are comparable to all *unmodified* rover bulk CIAs.

All Lake Fryxell modified CIA values, except for one, exhibit negligible increases. Conversely, the majority of rover samples exhibit large increases, likely a result of relative sulfate enrichment. The single Lake Fryxell sample that exhibits a significant CIA modification (43 → 69) is JB650, taken at the lake surface. With strong winds across the landscape (Doran et al., 2002), aeolian transport of sediments is probable and can potentially entrain and deposit sediments from other regions. The plots above show that *modified* Lake Fryxell sample CIA values are not comparable to all *modified* rover bulk CIAs. Because of this, the surface and edge of Lake Fryxell are not considered suitable analogs to the martian landscape. Cores will need to be taken at Lake Fryxell in order to properly conclude if it possesses similarities to the martian landscape.

SO_3 in Lake Fryxell surface and edge samples is not compared to rovers due to negligible abundances.

4.3.7. LAKE VANDA

4.3.7.1. MAJOR ELEMENTAL ANALYSIS

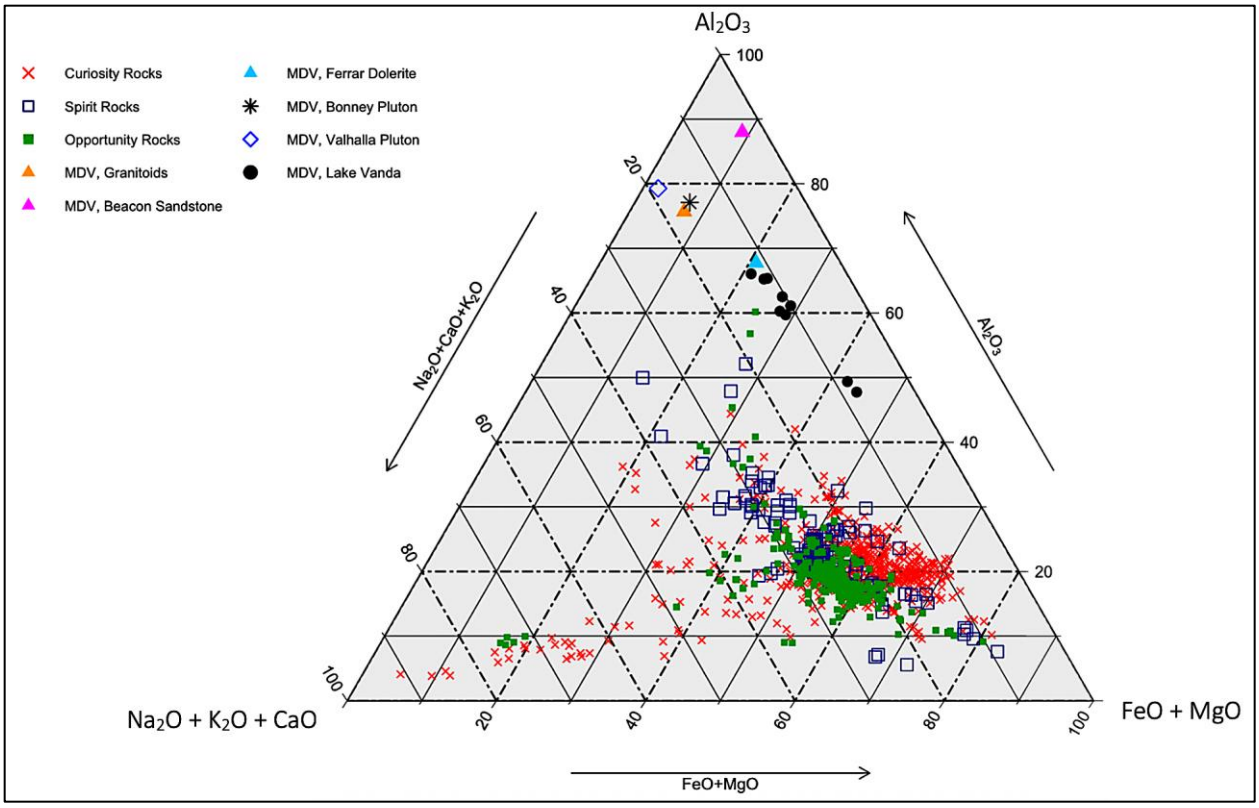

Figure 167. $Na_2O + K_2O + CaO$, Al_2O_3, and $FeO + MgO$ abundances of all rover rocks, MDV source rocks (Brownworth Pluton not shown), and Lake Vanda edge and surface samples.

A major element analysis of Lake Vanda surface and edge samples, MDV source rocks, and all rover rock samples is shown above. Lake Vanda samples exhibit varying FeO + MgO and Al_2O_3 abundances, with two samples, JB663 (edge) and JB664 (edge), plotting notably far from the main cluster. Lake Vanda $Na_2O + K_2O + CaO$ abundances show little variation. Based on this, Lake Vanda samples align best with select samples taken by all three rovers. Aeolian sediment transport from the west is likely an influencing factor in sample elemental composition.

4.3.7.2. SPECIAL ANALYSIS: CIA

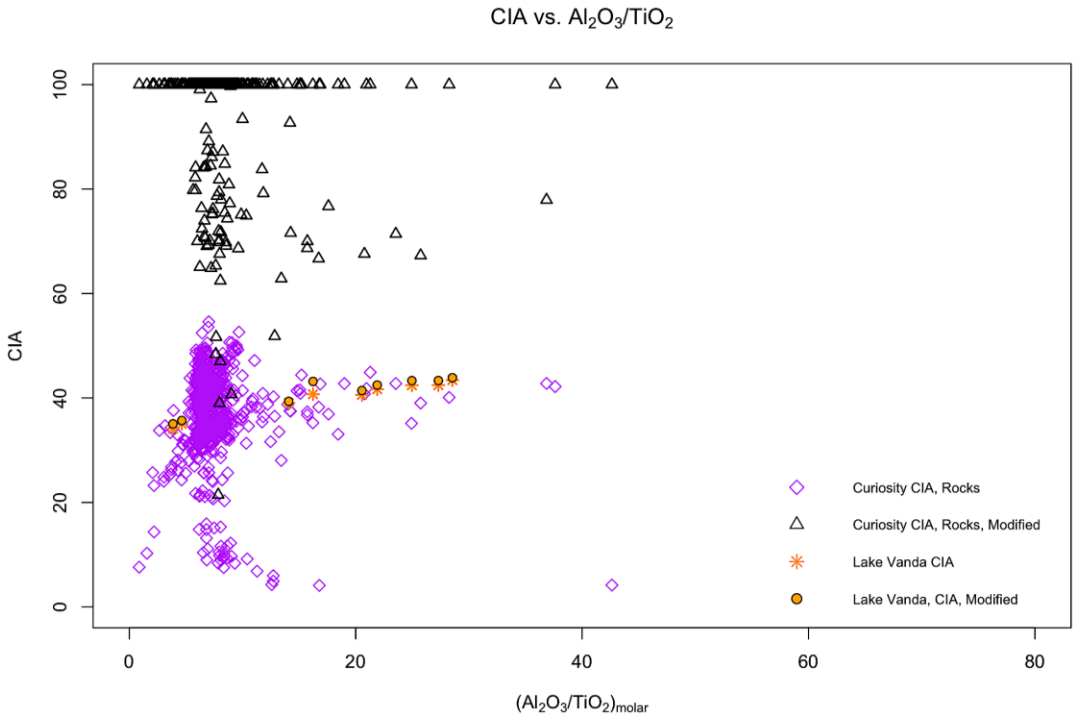

Figure 168. Modified and unmodified CIA values of Curiosity rover rocks and Lake Vanda edge and surface samples.

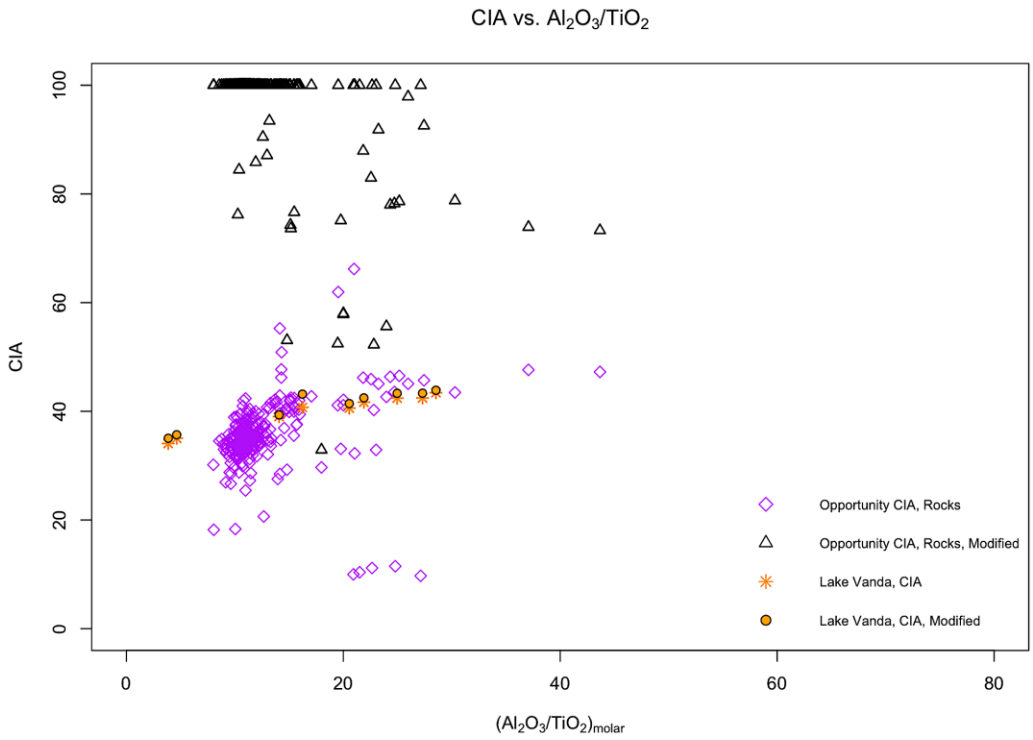

Figure 169. Modified and unmodified CIA values of Opportunity rover rocks and Lake Vanda edge and surface samples.

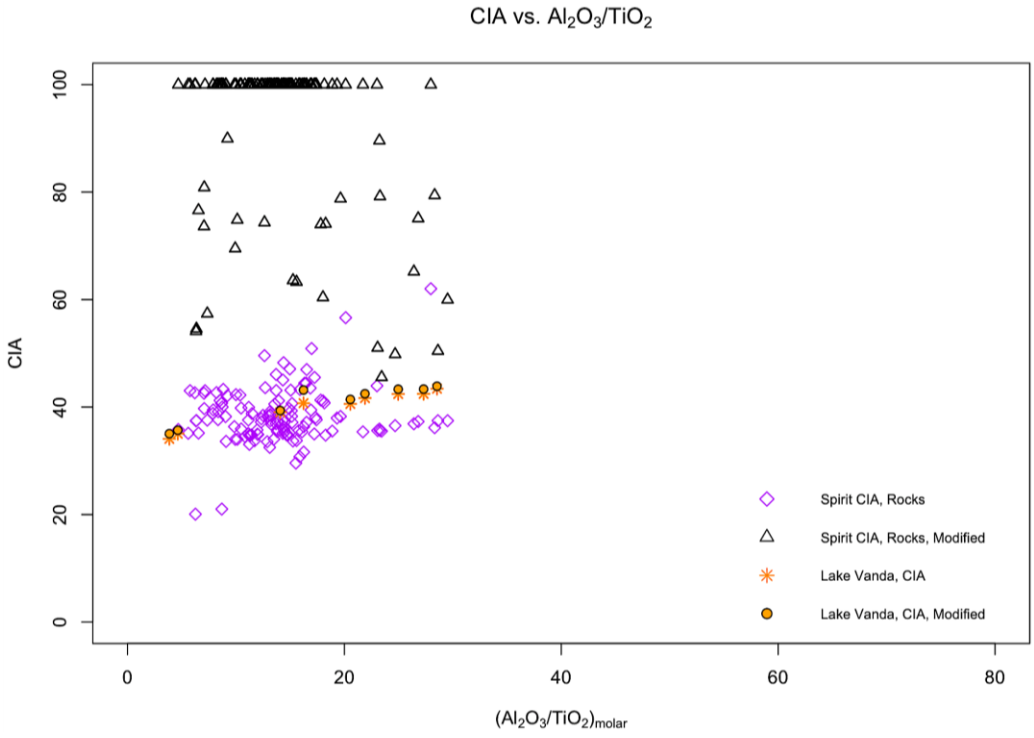

Figure 170. Modified and unmodified CIA values of Spirit rover rocks and Lake Vanda edge and surface samples.

Unmodified Chemical Index of Alteration values for Lake Vanda samples range from 35-43, in the range of fresh basalts, nearing granites and granodiorites, (Nesbitt & Young, 1982) and relatively in line with the regional geologic composition (Peterson and Marsh, 2008). Figures 168-170, above, show that *unmodified* Lake Vanda sample CIA values are relatively comparable to all *unmodified* rover bulk CIAs.

Modified CIA values exhibit negligible increases in Lake Vanda samples, likely due to a near absence of surface salts, while the majority of rover samples exhibit significant increases, likely due to the relative sulfate enrichment. Figures 168-170 show that *modified* Lake Vanda sample CIA values are not comparable to *modified* rover samples. Because of this, the surface and edge of Lake Vanda are not considered suitable analogs to the martian landscape. Cores will need to be taken at Lake Vanda in order to properly conclude if it possesses similarities to the martian landscape.

SO_3 in Lake Vanda surface and edge samples is not compared to rovers due to negligible abundances.

4.3.8. Lake Brownworth

4.3.8.1. Major elemental analysis

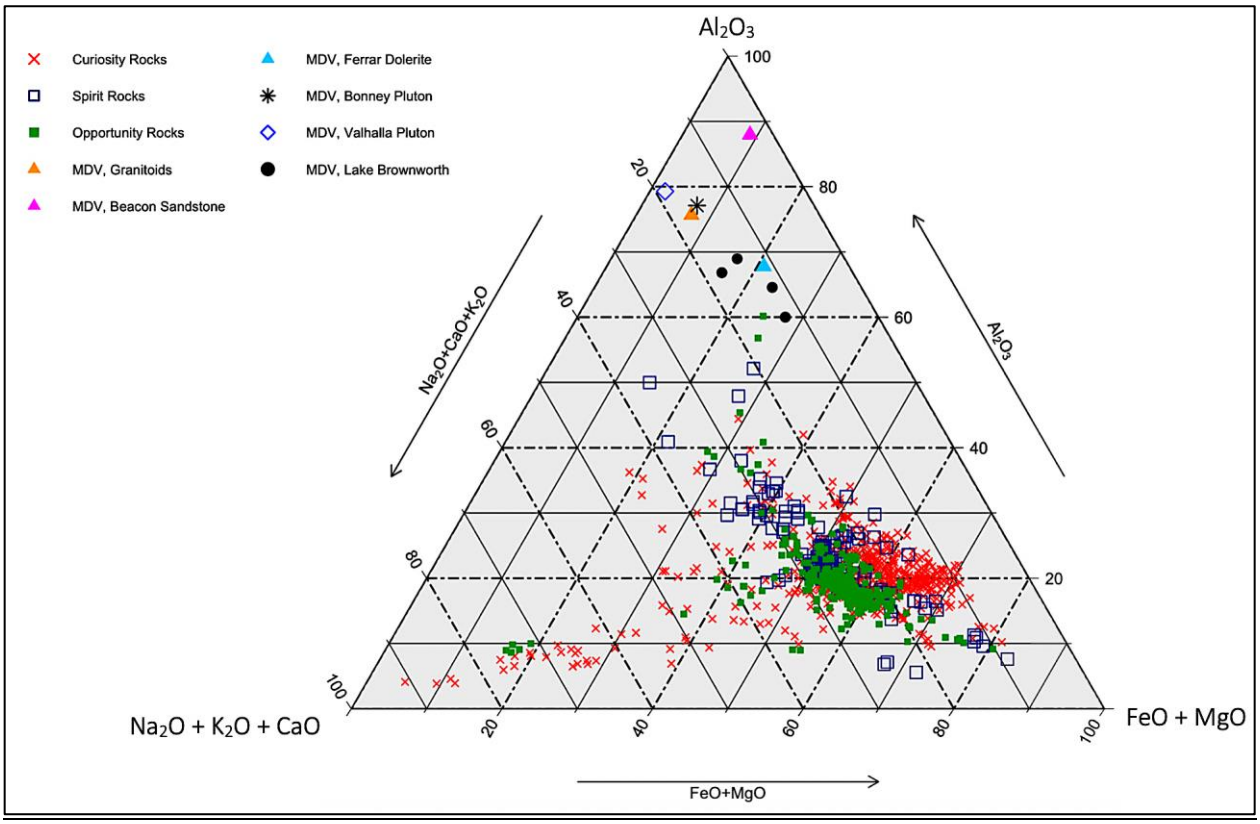

Figure 171. $Na_2O + K_2O + CaO$, Al_2O_3, and FeO + MgO abundances of all rover rocks, MDV source rocks (Brownworth Pluton not shown), and Lake Brownworth edge and surface samples.

Major elemental analysis of Lake Brownworth surface and edge samples, MDV source rocks, and all rover rock samples is shown in Figure 171, above. Lake Brownworth samples exhibit poor clustering with variation in all elements. FeO + MgO abundances align best with depleted, low-abundance (15-30 %) rover rocks and Al_2O_3 abundances are relatively enriched.

4.3.8.2. SPECIAL ANALYSIS: CIA

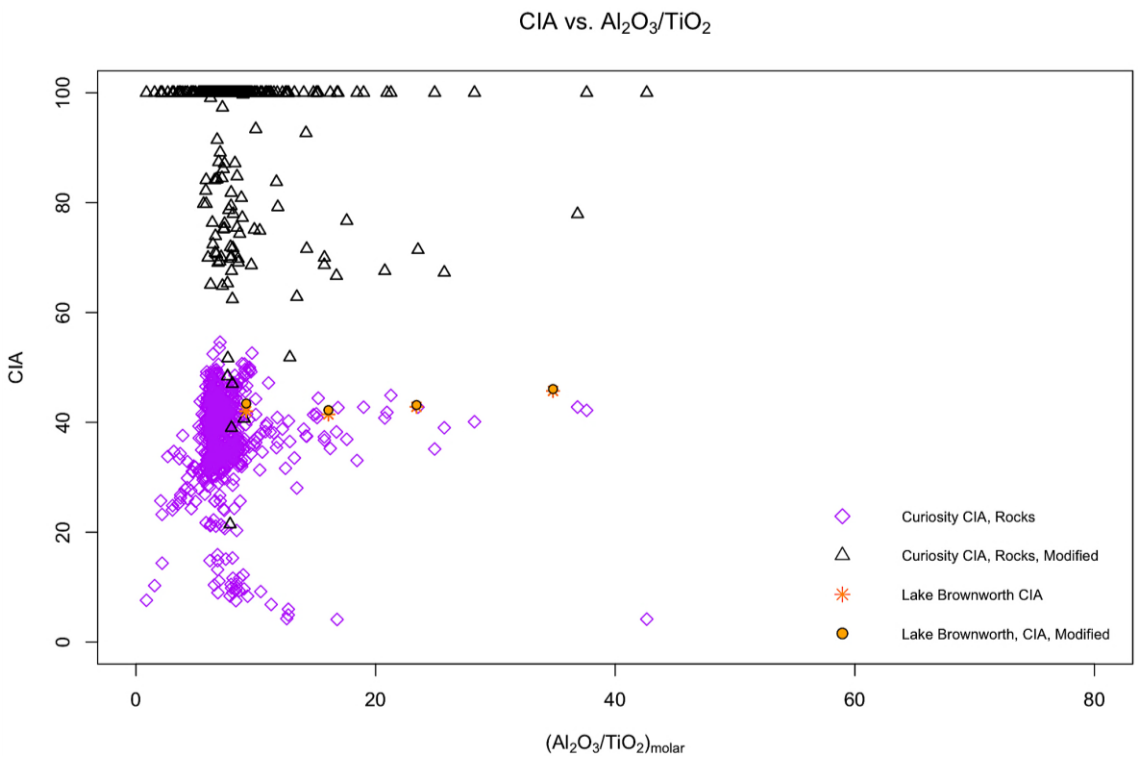

Figure 172. Modified and unmodified CIA values of Curiosity rover rocks and Lake Brownworth edge and surface samples.

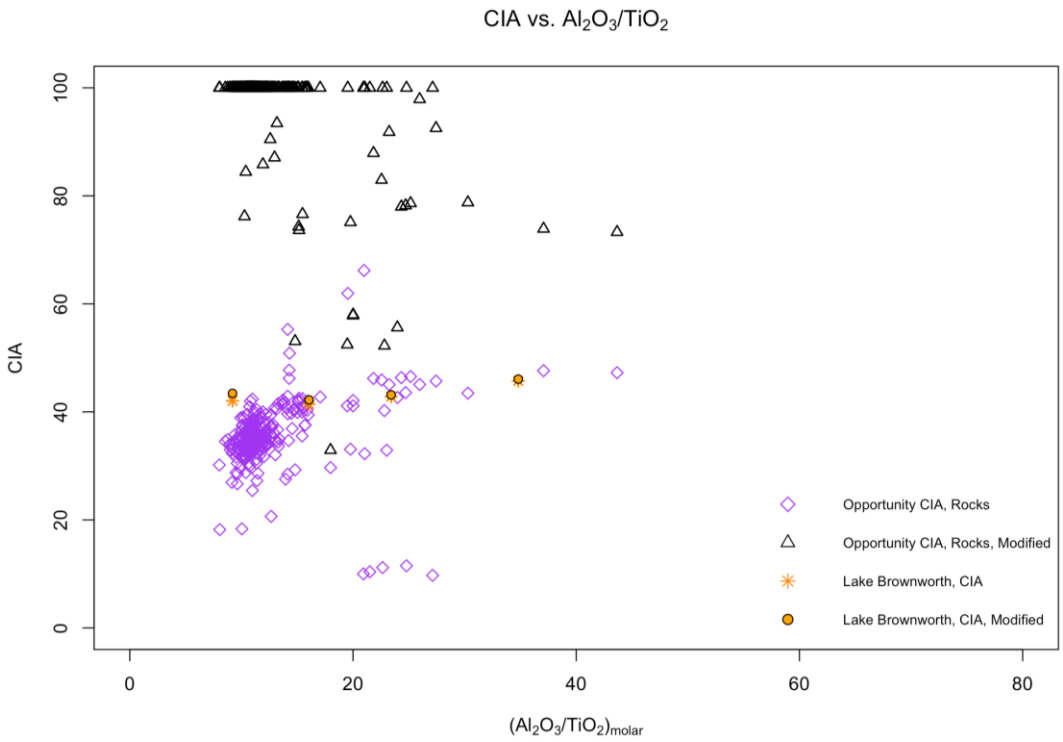

Figure 173. Modified and unmodified CIA values of Opportunity rover rocks and Lake Brownworth edge and surface samples.

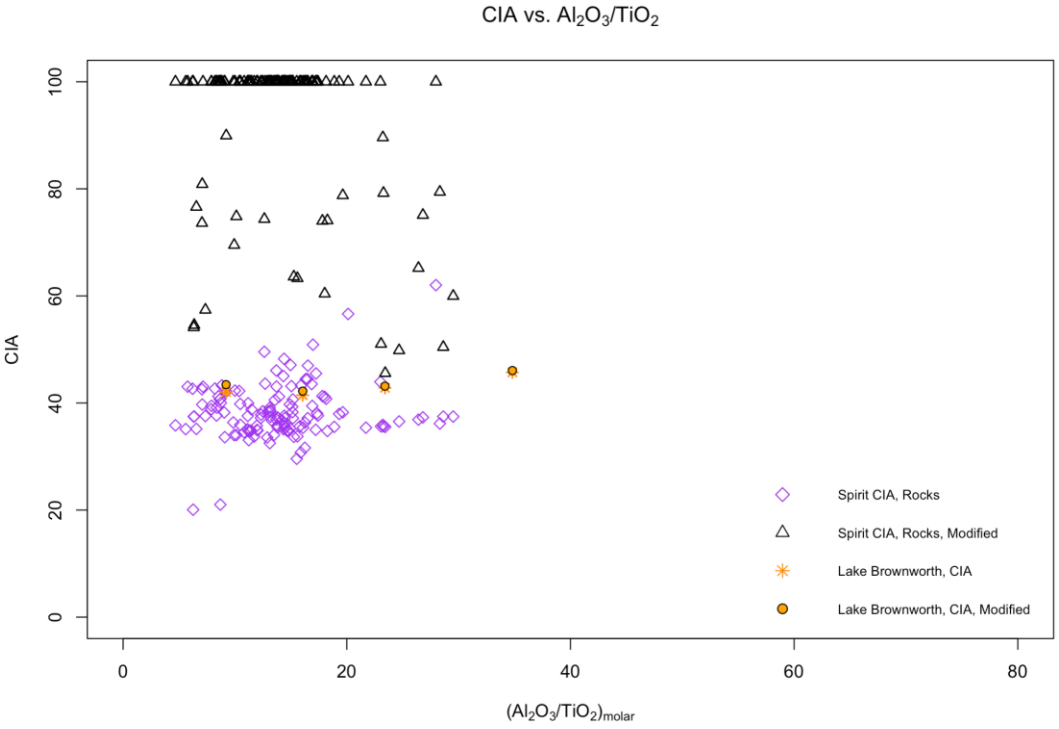

Figure 174. ***Modified and unmodified CIA values of Spirit rover rocks and Lake Brownworth edge and surface samples.***

Unmodified Chemical Index of Alteration values for Lake Brownworth samples range from 41-45, in the range of fresh basalts, nearing granites and granodiorites, (Nesbitt & Young, 1982) and relatively in line with the regional geologic composition (Peterson and Marsh, 2008). Unmodified rover rock values range from 4, in Curiosity sample *Alvord_Mountain_raster2*, to 66 in Opportunity rock sample *Esperance6 RAT2*. This wide range includes a significant number of corresponding geologic classifications (Nesbitt and Young, 1982; Fedo et al., 1995) and is likely due to salt dilution. Figures 172-174 show that two *unmodified* Lake Brownworth lake surface and edge sample CIA values are comparable to all *unmodified* rover bulk CIAs.

Modified Chemical Index of Alteration values exhibit negligible increases in Lake Brownworth samples, likely due to a near absence of surface salts. Figures 172-174, above, show that *modified* Lake Brownworth CIA values are not comparable to *modified* rover samples. Because of this, the surface and edge of Lake Brownworth are not considered suitable analogs to the martian landscape. Cores will need to be taken at Lake Brownworth in order to properly conclude if it possesses similarities to the martian landscape.

SO_3 in Lake Brownworth samples is not compared to rovers due to negligible abundances.

4.3.9. Lake Hoare: Cores E and H

4.3.9.1. Lake Hoare, Core E: Major Elemental Analysis

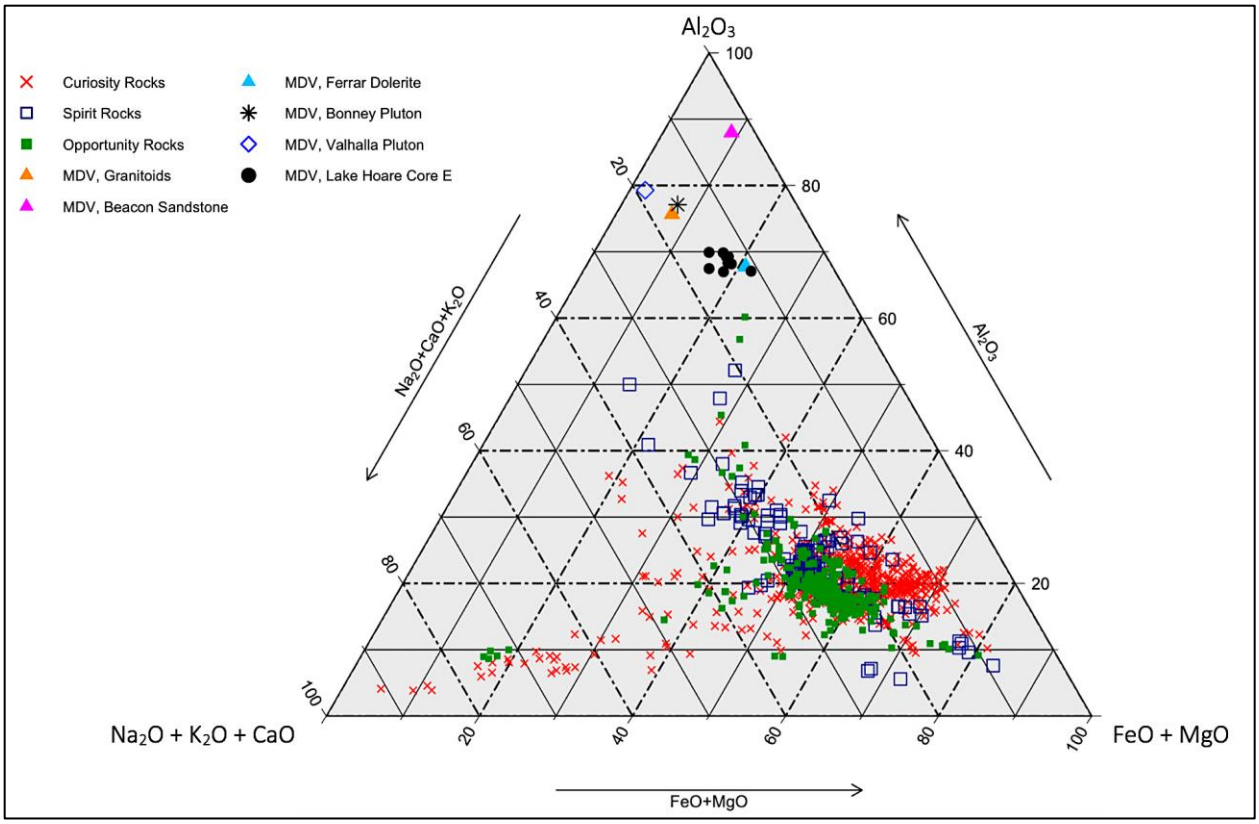

Figure 175. $Na_2O + K_2O + CaO$, Al_2O_3, and $FeO + MgO$ abundances of all rover rocks, MDV source rocks (Brownworth Pluton not shown), and Core E at Lake Hoare

Figure 174, above, shows major elemental analysis of Lake Hoare, Core E samples, MDV source rocks, and all rover rock samples. Core E samples exhibit good clustering, showing very little variation in any set of oxides. Core E $Na_2O + K_2O + CaO$ abundances best align with Curiosity and few Spirit samples; $FeO + MgO$ abundances best align with depleted, low-abundance (15-20 %) rover samples, and Al_2O_3 abundances exhibit enhanced abundances.

4.3.9.2. Lake Hoare, Core E, Special Analysis: CIA

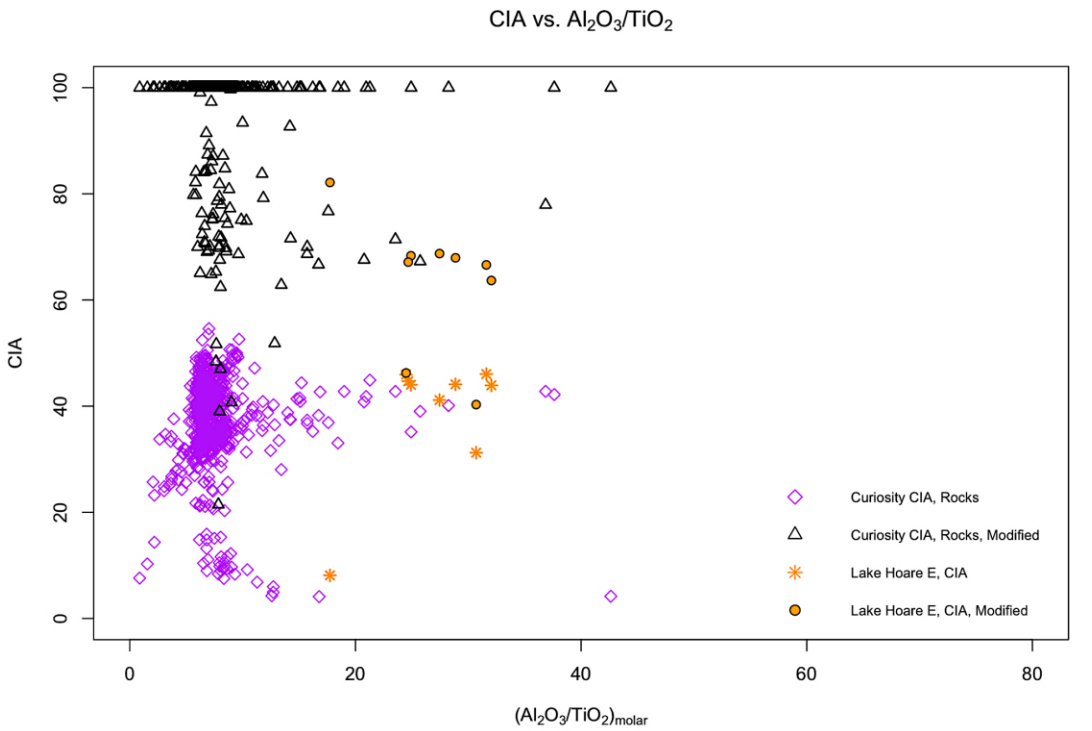

Figure 176. Modified and unmodified CIA values of Curiosity rover rocks and Core E at Lake Hoare.

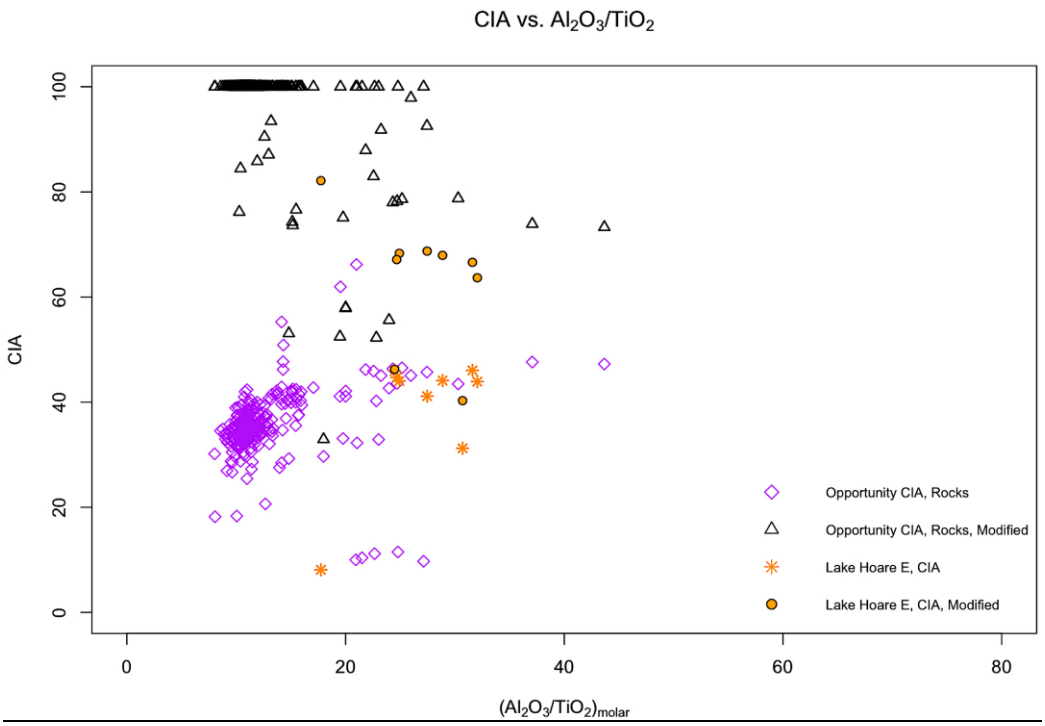

Figure 177. Modified and unmodified CIA values of Opportunity rover rocks and Core E at Lake Hoare.

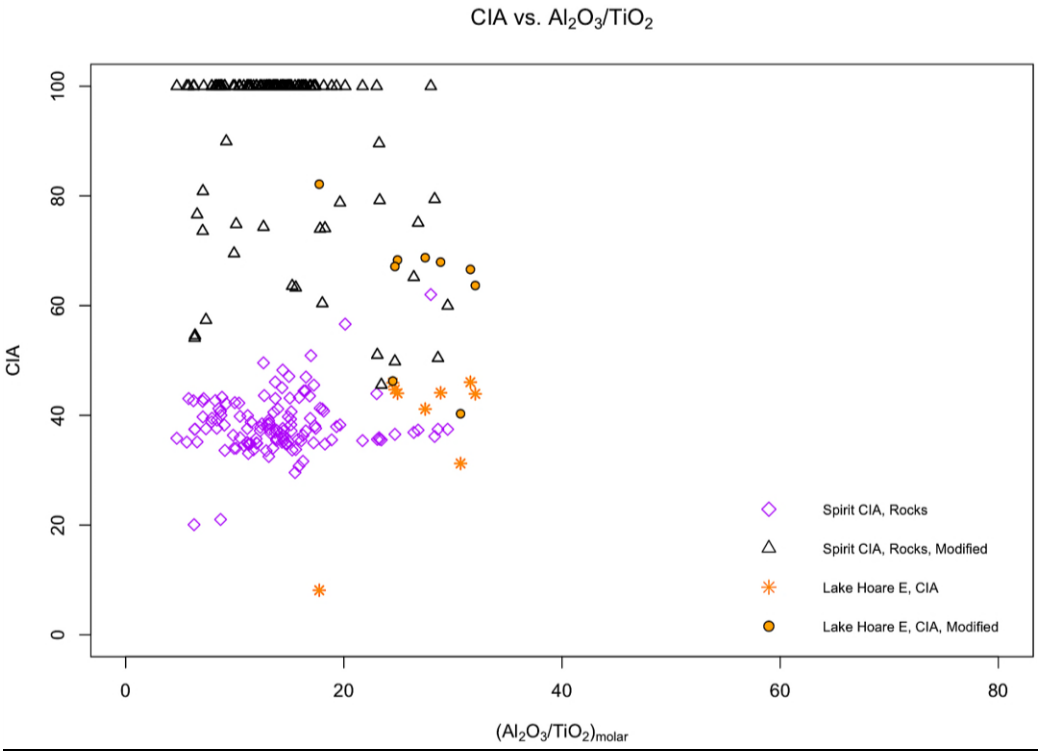

Figure 178. Modified and unmodified CIA values of Spirit rover rocks and Core E at Lake Hoare

Unmodified Chemical Index of Alteration values for Lake Hoare, Core E samples range from 8-46, well below the range of fresh basalts and into granites and granodiorites, (Nesbitt & Young, 1982) and relatively in line with the regional geologic composition (Peterson and Marsh, 2008). Figures 176-178 show that *unmodified* Core E CIA values are comparable to very few *unmodified* samples from each rover.

Modified CIA values exhibit negligible increases in Lake Hoare, Core E samples, likely due to relative SO_3 depletion. Calcite dilution, however, does occur and reports a modified CIA range of 40-82. This modified range is diagnostic of fresh basalts and granodiorites to potassic granites (Nesbitt and Young, 1982; Fedo et al., 1995). The plots above show that *modified* Core E CIA values are comparable to even fewer *modified* rover samples than the *unmodified* values. Because of this, Lake Hoare, Core E is not considered a suitable microenvironment analog to the martian landscape.

SO_3 in Lake Hoare, Core E samples is not compared to rovers due to negligible abundances.

4.3.9.3. Lake Hoare, Core H: Major Elemental Analysis

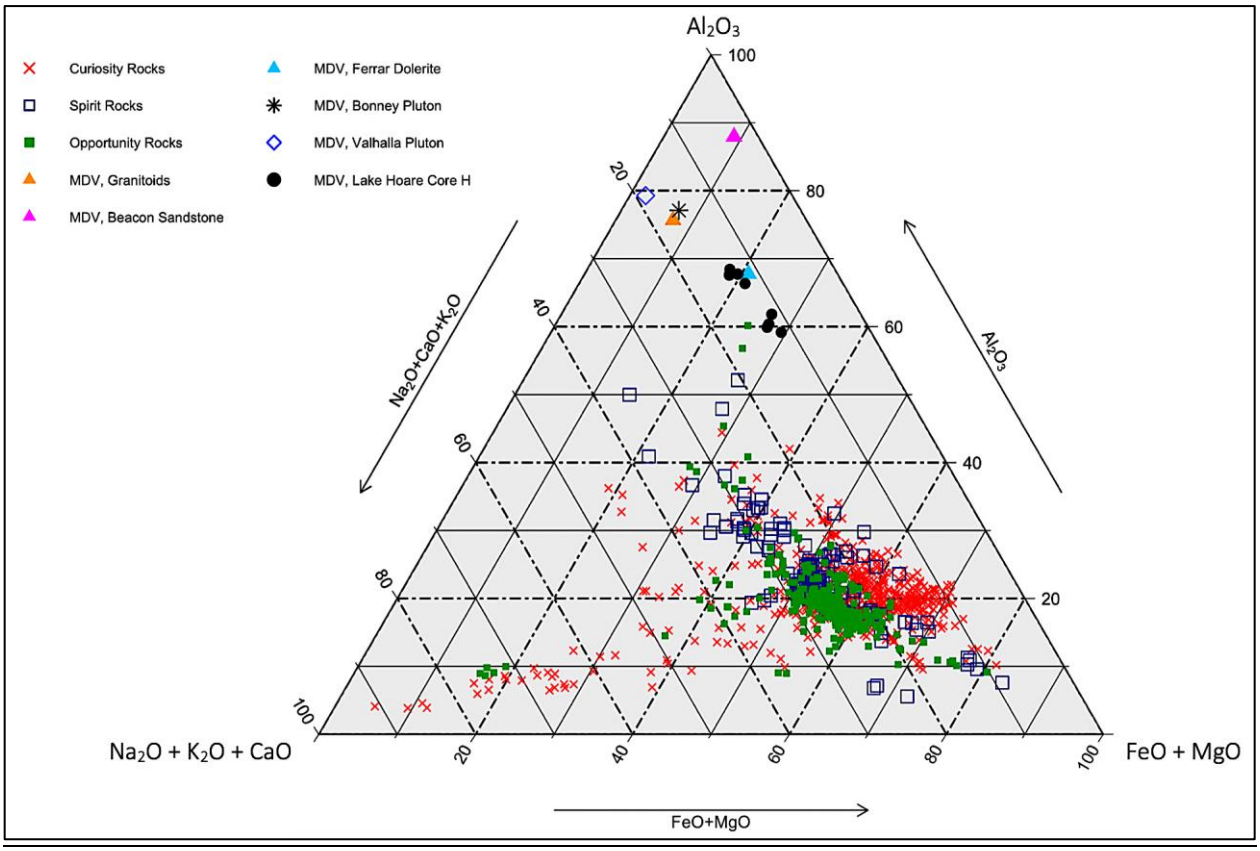

Figure 179. $Na_2O + K_2O + CaO$, Al_2O_3, and FeO + MgO abundances of all rover rocks, MDV source rocks (Brownworth Pluton not shown), and Core H at Lake Hoare.

Major elemental analysis of Lake Hoare, Core H samples, MDV source rocks, and all rover rock samples is shown above. Core H samples exhibit two well-clustered groups that are distinctly separate from one another. FeO + MgO abundance of each group exhibit little variation, with the lower abundance group aligning poorly with that of rover samples, while the higher abundance group aligns best with rover samples in the range of 35-40 %. All Core H samples exhibit very little $Na_2O + K_2O + CaO$ variation, aligning best with Curiosity samples, and Al_2O_3 abundances are relatively enriched.

4.3.9.4. Lake Hoare, Core H, Special Analysis: CIA

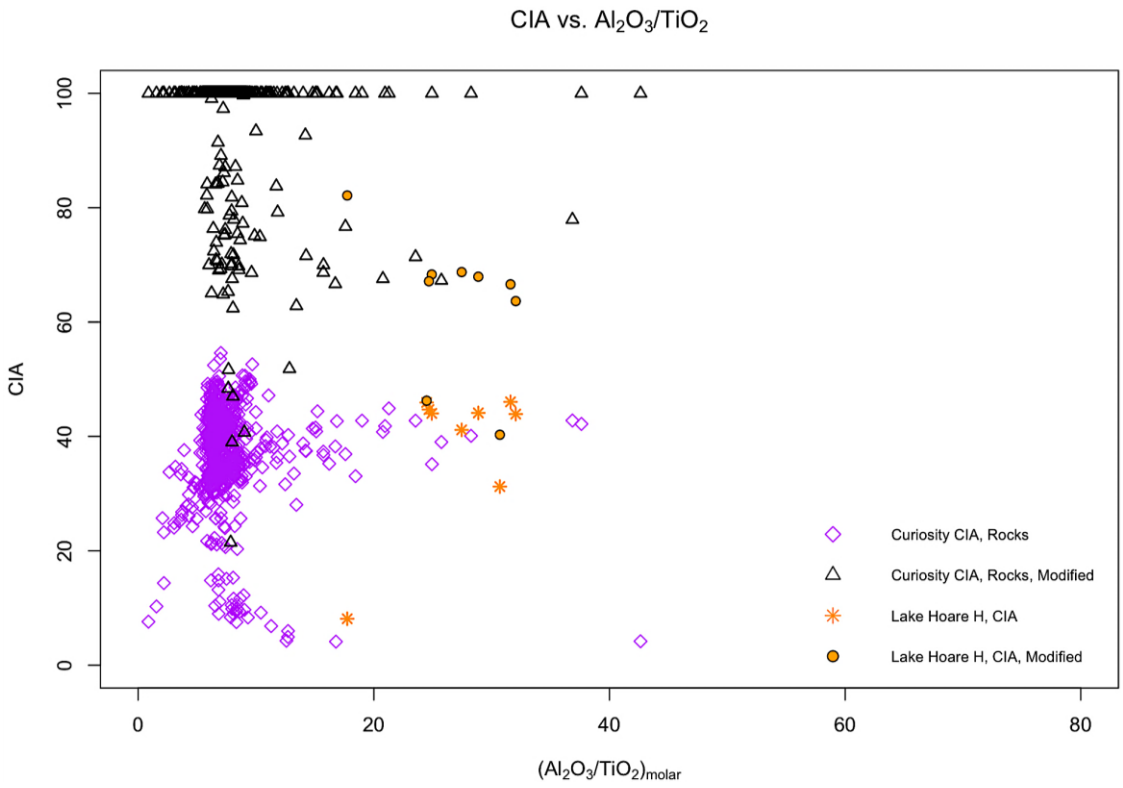

Figure 180. Modified and unmodified CIA values of Curiosity rover rocks and Core H at Lake Hoare.

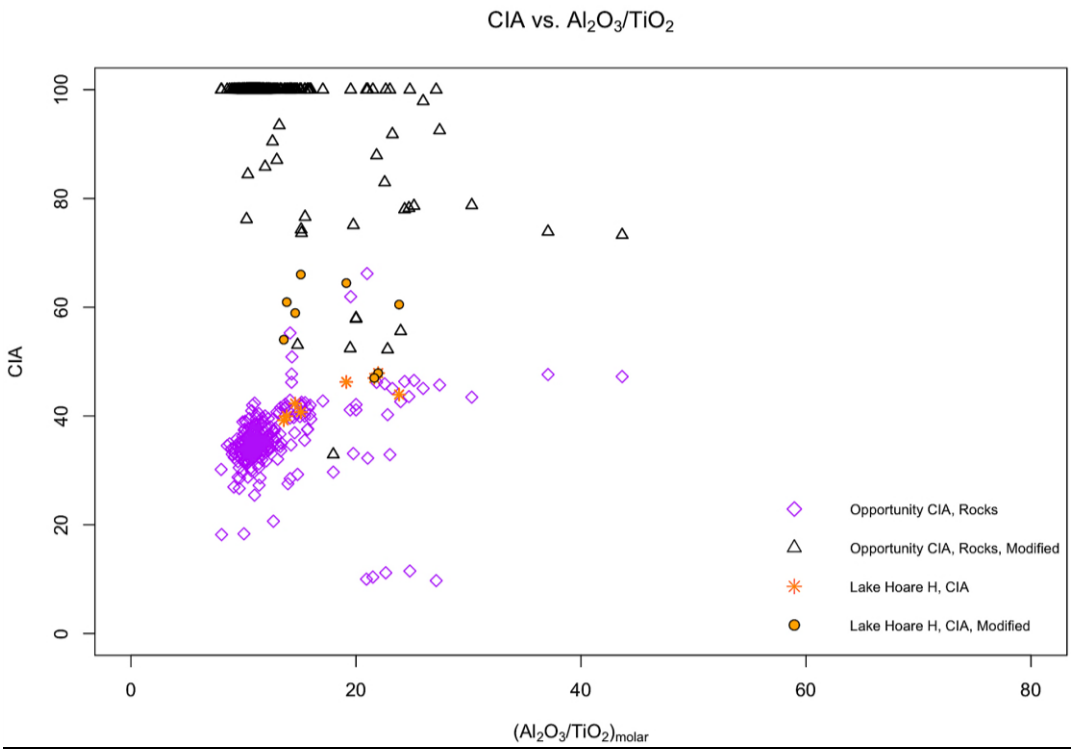

Figure 181. Modified and unmodified CIA values of Opportunity rover rocks and Core H at Lake Hoare.

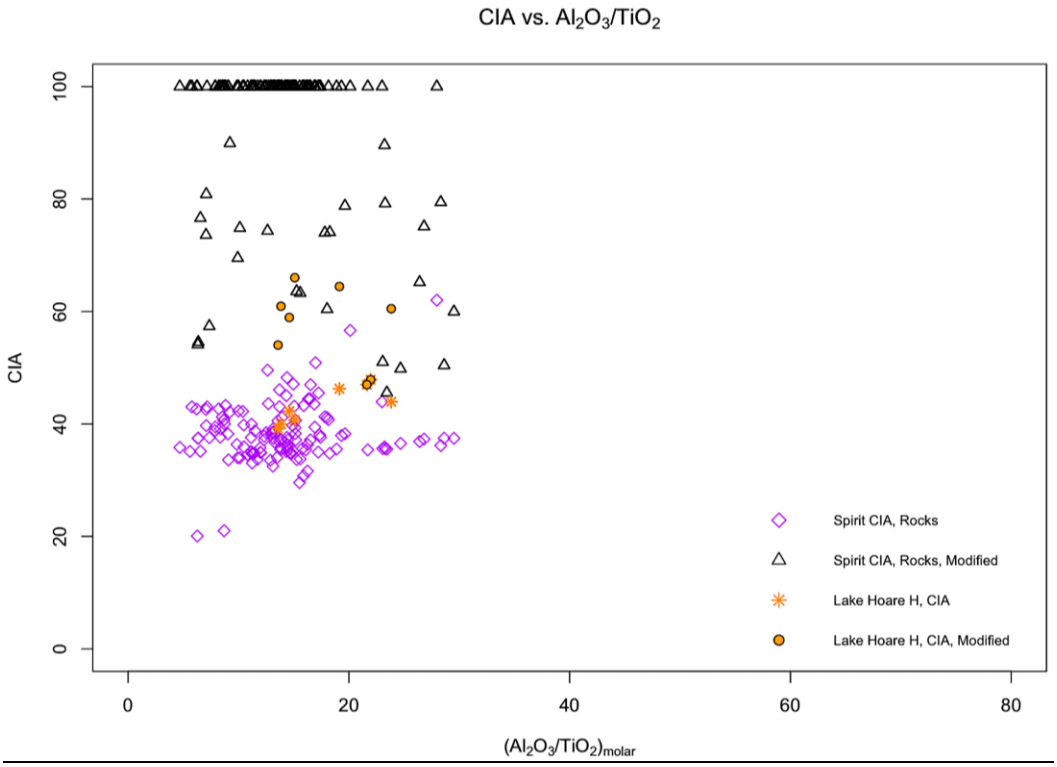

Figure 182. Modified and unmodified CIA values of Spirit rover rocks and Core H at Lake Hoare.

Unmodified Chemical Index of Alteration values for Lake Hoare, Core H samples range from 39-48, in the range of fresh basalts and into granites and granodiorites, (Nesbitt & Young, 1982; Fedo et al., 1995). Unmodified rover rock values range from 4, in Curiosity sample *Alvord_Mountain_raster2*, to 66 in Opportunity rock sample *Esperance6 RAT2*. This wide range includes a significant number of corresponding geologic classifications (Nesbitt and Young, 1982; Fedo et al., 1995) and is likely do to salt dilution. Figures 180-182, above, show that *unmodified* Core H CIA values are comparable to that of the majority of Spirit and Opportunity rover.

Modified Chemical Index of Alteration values, to correct for sulfate dilution, exhibit significant modifications, reporting a new range of 49-100. This range is diagnostic of fresh granites and granodiorites to authigenic K-feldspar (Nesbitt and Young, 1982; Fedo et al., 1995). The plots above show that *modified* Core H CIA values are no longer comparable to that of the majority of rovers Spirit and Opportunity. Instead, Core H samples are comparable to a select few *modified* rover samples. Because of this, specific Lake Hoare, Core H sample(s) are considered suitable analogs to the martian landscape. The analogous *rover* samples are found in Appendices E and F.

4.3.9.5. Lake Hoare Core H: Sulfite

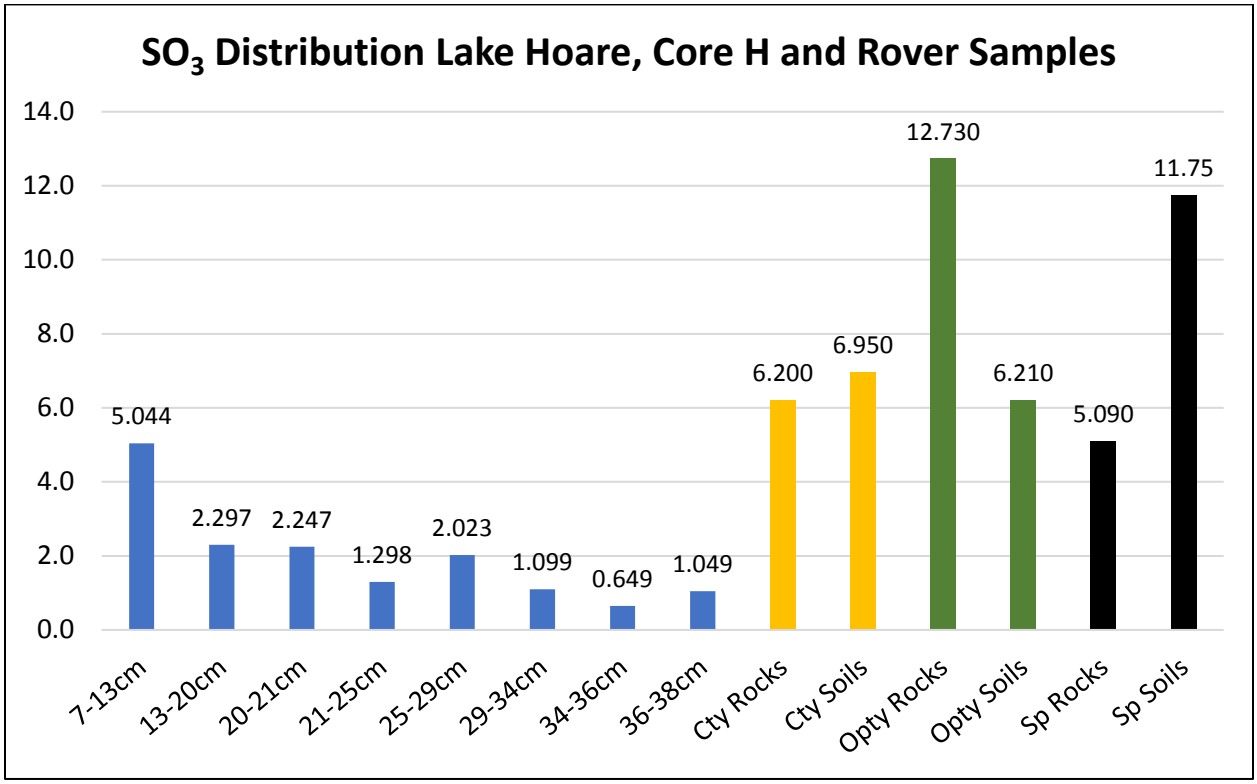

Figure 183. Sulfite abundance of Core H at Lake Hoare and all Mars rover rock and soil samples.

SO_3 analysis of Lake Hoare, Core H sediments and rover rocks/soils shows the 7-13 cm depth range to be the most comparable to rover samples, particularly Curiosity and Spirit rocks, and Opportunity soils. Beneath the 7-13 cm depth range, samples exhibit decreasing SO_3 abundance.

4.4. Discussion and Implications

4.4.1. Discussion

Analysis of different sediment samples from cores and lake surfaces/edges across the McMurdo Dry Valley Region, and their comparison to analyzed rock and soil samples taken by martian rovers Spirit, Opportunity, and Curiosity, shows there are MDV microenvironments that are suitable analogs to select martian samples. This, in turn, is suggestive of similar alteration processes in the two environments. The analogous MDV microenvironments include:

Core 33	8-10 cm
Core 42	4-10 cm
Core 52	4-8 cm
Lake Hoare, Core H	7-13 cm

Bishop et al., 2014, shows poor correlation between MOGRS, SNC meteorite and MDV lake surface samples based on K/Th vs K (ppm), and suggest the investigation of new elemental relationships that work well in analogs and can be applied to Mars elemental abundance databases. In this fourth chapter, we come to the conclusion that through the investigation of major elemental abundances, the CIA and our sulfate modification, and SO_3 abundance from the MDV—compared to that of martian rovers Spirit, Opportunity, and Curiosity— we can determine suitable analog microenvironments between Mars and the MDV (listed above). From this we infer that the alteration processes are operating in the analogous MDV microenvironments, as determined in Chapter 2, are operating as well at the locations of select Mars rover samples (Appendices E and F).

Core 2074 from Don Juan Basin and Core 35 from Don Quixote Basin were not considered in the results section due to a lack of elemental data. These cores, however, show promise as MDV microenvironment analogs to select Mars rover samples due to their reported elevated abundances of Ca-sulfates gypsum and anhydrite. Core 2074, in particular, reports heavy enrichment (~33 %) of anhydrite with much lower abundances of gypsum (~3 %). Core 35 reports much lower abundances of anhydrite (~0.3 %) and gypsum (~1.3 %) but reports significant levels of thenardite (5.6 %). These two cores need to be thoroughly investigated before they can be deemed suitable analog microenvironments to any Mars rover samples. Gypsum and anhydrite, however, have been found on the surface of Mars (Vaniman et al., 2018) and therefore make Core 2074 and 35 particularly intriguing MDV microenvironments.

4.4.2. IMPLICATIONS

Our results show that specific microenvironments within the McMurdo Dry Valley Region of Antarctica are analogous to select Mars rover samples. Through our analyses, we show that the best analogy for MDV microenvironments to Mars rover samples is based on sulfate abundances for which investigation of total sulfur and sulfite abundance can be a measure.

Importantly, the presence of gypsum on Mars is suggestive of evaporites deposited at a time when the planet had a greater abundance of fluids than it does currently.

With this information, multiple avenues of research can be expanded upon, including the incorporation of data from similar terrestrial analogs, such as the Atacama Desert (Azua-Bustos et al., 2019), that allow for further reconstruction of the martian paleoclimate and that of comparable extraterrestrial environments. In doing this we provide further means for answering questions of habitability outside of Earth.

CHAPTER 5: CONCLUSIONS AND FUTURE WORK

5.1. CONCLUSIONS

Elemental, spectral, and mineralogical analyses were conducted on surface and core sediments from the McMurdo Dry Valleys, Antarctica, in order to determine type and extent of alteration processes operating in this polar desert environment. Sediment provenance was investigated to bolster or refute any findings from the alteration investigation, and the information from both studies was applied to Mars rover data to test the McMurdo Dry Valleys as a suitable terrestrial analog to the martian landscape. The preliminary hypothesis of this thesis was that while chemical alteration is likely still operating on a secondary scale to physical, it is operating at a greater degree than previously thought. By extension, if this hypothesis is correct and analogies existed between the Dry Valleys and the martian landscape, alteration processes should be similar as well. Throughout this study, it was found that physical alteration remains the primary mode across the region, but that under particular conditions, such as hypersalinity, and/or sufficient surface cover, chemical alteration can dominate. Examples include core sediment ranges with clays, sulfates, carbonates, or standing hypersaline surface waters.

The Upper Wright Valley, basins Don Quixote, Don Juan, VXE-6, and the South Fork Region, contain cores with sediment ranges (typically 4-10 cm) relatively rich in allophane, gypsum, anhydrite, and thenardite. In Taylor Valley, Lake Hoare Cores B-E contain calcite; and Core H, in addition to pyrite, likely contains Ca-sulfates. Each of the aforementioned constituents is a product of chemical alteration and is therefore a sign of ongoing processes across the Dry Valley Region. Importantly, unless in the presence of hypersaline waters or brine, surface samples, as at Lake Fryxell, Vanda, and Brownworth, do not exhibit chemical alteration. This corroborates a theory of relative subsurface (~ 4+ cm) chemical alteration ubiquity across the region.

Application and comparison of MDV sediments to Mars rover samples suggests analogies between a select few MDV samples and a relatively long list of rover samples (Appendices E and F). Core 33 from 8-10 cm, Core 42 from 4-10 cm, Core 52 from 4-8 cm, and Lake Hoare, Core H, from 7-13 cm, bear resemblance—on the basis of major elemental abundances, the CIA and our sulfate modification, and SO_3 abundance—to select Mars rover samples. Many rover samples exhibit extremely high abundances of SO_3 (25+ %) and are deemed unsuitable comparators to our MDV samples due to no MDV samples exhibiting SO_3 abundances greater than 22 % (Core 2074).

Additionally, Rodrigue et al., 2020, by the method of K-means clustering, identifies five different "Metaclusters", diagnostic of different rock and soil samples taken by all three rovers. Within each "Metacluster" exist "Clusters" (subgroups) that apply another layer of specificity to the samples. In our list of suitable analog rover samples, we focus on "Metacluster S", defined as "Sulfur, acidic aqueous alteration", and specifically include all samples from "Cluster 4" that are defined as "Mars-typical rock, mudstone, or soil somewhat elevated in sulfur trioxide" and account for nearly 75 % of "Metacluster S" samples. The majority of such samples were taken by the rover Opportunity (Rodrigue et al., 2020).

The suitable analog rover samples are listed in Appendices E and F.

4.2. Future Work

The work here is unfinished and indicates areas that require future research. Major elemental and special analyses for Cores 2074 and 35 are necessary for a complete picture of MDV analog microenvironments. Mineralogy determined in this study, though available for all MDV sediment samples, remains an area that can be improved upon. The Terra-166 XRD/XRF instrument is quite capable, yet its accuracy is questionable. Its inaccuracies could be resolved by comparing its quantitative results to

qualitative results of a Bruker D8 Advance XRD instrument, as was done for Core 42 at VXE-6 Pond.

Lake Hoare is the only lake at which cores were taken to investigate alteration processes beneath the surface. For a complete picture of each location, Lakes Fryxell, Vanda, and Brownworth will need sediment cores taken as well. If their findings are similar to the cores at Lake Hoare or those in Upper Wright Valley, the case for regional subsurface chemical alteration ubiquity will be bolstered.

Upper Wright Valley, in addition to Don Juan Pond, VXE-6 Pond, and Pond 1, contains Ponds 2 and 3 (Harris, 1981). Unlike DJP, VXE-6, Pond, and Pond 1, though, Ponds 2 and 3 do not currently have enough data from which to conduct any comprehensive elemental analyses. It is very possible that these two ponds exhibit geochemical signatures and/or processes similar to those of the aforementioned ponds, and would therefore be valuable microenvironments to sample in order to gain a complete understanding of provenance and alteration across the region.

A second, more extensive geochemical analysis, as well as range of source rocks including Ferrar Dolerite, Basement Granitoid Complex, Beacon Sandstone, and plutons including Bonney, Valhalla, and Brownworth would allow for a more accurate gauge of type and degree of alteration occurring across the landscape.

The McMurdo Dry Valleys Region is one of many environments used as a terrestrial analog to Mars. For example, the Atacama Desert in Chile has been proposed and investigated as a viable analog to the martian landscape and the findings from our work here could supplement ongoing or completed research in the high Chilean desert. The more that is known about readily-accessible analog environments, the closer the scientific community will be to answering some of humanity's most compelling questions.

Bibliography

Allibone, A. H., Cox, S. C., Graham, I. J., Smellie, R. H., Johnstone, R. D., Ellery, S.G., Palmer, K. (1993a) Granitoids of the Dry Valleys area, southern Victoria Land, Antarctica: Plutons, field relationships, and isotopic dating, *New Zealand Journal of Geology and Geophysics*, 36:3, 281-297

Allibone, A. H., Cox, S. C., Smillie, R. H. (1993b) Granitoids of the Dry Valleys area, southern Victoria Land: Geochemistry and evolution along the early Paleozoic Antarctic Craton margin, *New Zealand Journal of Geology and Geophysics*, 36:3, 299-316

Anderton, P. H. (1976). Hydrological Research, Annual Report #37, Dry Valleys, Antarctica, 1973-74. Christchurch: New Zealand Ministry of Works and Development.

Bishop, J. L., Koeberl, C., Kralik, C., Froeschl, H., Englert, P. A. J., Andersen, D. H., Pieters, C. M., Wharton, R. A,. (1996). Reflectance spectroscopy and geochemical analyses of Lake Hoare sediments, Antarctica. *Geochim. Cosmochim. Acta*, 60, 765–785.

Bishop, J. L., Lougear, A., Newton, J., Doran, P. T., Froeschl, H., Trautwein, A. X., Körner. H., Koeberl, C., (2001). Mineralogical and geochemical analyses of Antarctic sediments: a reflectance and Mössbauer spectroscopy study with applications for remote sensing on Mars. *Geochim. Cosmochim. Acta,* 65, 2875–2897.

Bishop, J. L., Murad E. (2002) Spectroscopic and geochemical analyses of ferrihydrite from springs in Iceland and applications to Mars. Pp. 357-370 in: *Volcano-Ice Interactions on Earth and Mars* (J.L. Smellie & M.G. Chapman, editors). Geological Society, Special Publication No.202, London.

Bishop, J. L., Anglen B. L., Pratt L. M., Edwards H. G. M., Des Marais, D. J., Doran, P. T. (2003) A spectroscopy and isotope study of sediments from the Antarctic Dry Valleys as analogs for potential paleolakes on Mars. *International Journal of Astrobiology*, 2, 273-287.

Bishop, J. L. et al., (2013). Coordinated analyses of Antarctic sediments as Mars analog materials using reflectance spectroscopy and current flight-like instruments for CheMin, SAM and MOMA. *Icarus,* 224, 309–325

Bishop, J. L., Englert P. A. J., Patel, S., Tirsch, D., Roy, A. J., Koeberl, C., Böttger, U., Hanke, F., Jaumann, R. (2014) Mineralogical analyses of surface sediments in the Antarctic Dry Valleys: Coordinated analyses of Raman spectra, reflectance spectra and elemental abundances. Phil. Trans. R. Soc. A 372: 20140198.

Bishop, J. L. (2019) Chapter 4: Visible and near-infrared reflectance spectroscopy of geologic materials, in: Bishop, J. L., Bell III, J. F., Moersch, J. E. (Eds.), Remote Compositional Analysis: Techniques for Understanding Spectroscopy, Mineralogy, and Geochemistry of Planetary Surfaces. *Cambridge University Press*, Cambridge, UK, pp. 68-101.

Bull, C, (1966). Climatological observations in ice-free areas of southern Victoria Land, Antarctica: in *Antarctic Research Series*, 9, Amer. Geophys. Union, 177-194.

Burton, Z. F. M., et al., (2019). Salts and clays beneath surface sediments in Antarctica provide clues to weathering and geochemistry on Mars, Abstract, 50th Lunar and Planetary Science Conference.

Cameron, R. E., King, J., David, C. M., (1970). Microbiology, ecology, and microclimatology of soil sites in Dry Valleys of Southern Victoria Land, Antarctica. In Antarctic ecology, vol. 2 (ed. MW Holdgate), pp. 702–716. New York, NY: Academic Press.

Chinn, T., (1976). Hydrological Research Report, Dry Valleys, Antarctica, 1974-75. Christchurch: New Zealand Ministry of Works and Development.

Claridge, G. G. C., Campbell, I. B., (1968). Origin of nitrate deposits, *Nature*, 217, 428–430

Claridge, G. G. C., I. B. Campbell, (1977). The salts in Antarctic soils, their distribution and relationship to soil processes: *Soil Science*, 123, 6, 377-384.

Clark, B.C., Baird, A. K., Weldon, R. J., Tsusaki, D. M., Schnabel, L., Candelaria, M. P., (1982). Chemical composition of martian fines, *J. Geol. Res*., 87, 10059-10067.

Clark, B. C., D. C. Van Hart, (1980). The salts of Mars, *Icarus*, 45, 370-378.

Clow, G.D., McKay, C.P., Simmons, G.M., Jr., Wharton, R.A., Jr., (1988). Climatological observations and predicted sublimation rates at Lake Hoare, Antarctica. *Journal of Climate* 1, 715-728.

Craig H., Wharton R. A., Jr., McKay C. P. (1992) Oxygen supersaturation in ice-covered Antarctic lakes: Biological versus physical contributions. *Science*, 255, 318-321.

Cullers, R. L. and Graf, J. (1983). Rare earth elements in igneous rocks of the continental crust: intermediate and silicic rocks, ore petrogenesis. Rare-Earth Geochemistry (Henderson, P., ed.), 275–312, *Elsevier*, Amsterdam.

Dickson, J., Head, J., Levy, J., Marchant, D.R. (2013). Don Juan Pond, Antarctica: Near-surface $CaCl_2$-brine feeding Earth's most saline lake and implications for Mars. *Sci Rep*, 3**,** 1166.

Dieing, T., Hollricher, O., Toporski, J. (eds). (2011). Confocal Raman microscopy. Berlin, Germany: *Springer*.

Doran, P. M. (2002). Valley Floor Climate Observations from the McMurdo Dry Valleys, Antarctica, 1986-2000. *J. Geol. Res*, 107.

Dort, H., Jr. and D. S. Dort, (1970). Sodium sulfate deposits in Antarctica, *Modern Geology*1, 2, 97-117.

Ellery, S. G. (1989). Lower Wright geology. Unpublished M.Sc. thesis, lodged in the Library, University of Otago, New Zealand.

Englert, P. A. J., et al., (2013). Soils and weathering processes in the Antarctic Dry Valleys, Abstract, 44th Lunar Planetary Science Conference.

Farquhar J, Kima S. T., Masterson, A., (2007). Implications from sulfur isotopes of the Nakhla meteorite for the origin of sulfate on Mars. *Earth and Planetary Science Letters*, 264, 1-8

Fedo, C. M., Nesbitt, H. H., Young, G. M., (1995). Unraveling the effects of potassium metasomatism in sedimentary rocks and paleosols, with implications for paleo-weathering conditions and provenance. Geology 23, 921–924.

Finlow-Bates, T., Stumpfl, E. F., (1981). The behavior of so-called immobile elements in hydrothermally altered rocks associated with volcanogenic submarine-exhalative ore deposits. *Mineral. Deposita,* 16**,** 319–328.

Foerder, A. B., et al., (2020). Rare Earth Element abundances and chemical alteration in microenvironments of the McMurdo Dry Valleys, Abstract, 51st Lunar Planetary Science Conference.

Fountain, A. G., Lyons, H. B., Burkins, M. B., Dana, G.L., Doran, P. T., Lewis, K. J., McKnight, D. M., Moorhead, D. L., Parsons, A. N., Priscu, J. C., Wall, D. H., Robert, A. H. J., Virginia, R. A., (1999). Physical controls on the Taylor Valley ecosystem, Antarctica. *Bioscience*, 49, 961-971.

Fountain, A.G., Nylen, T. H., Monaghan, A., Basagic, H. J., Bromwich, D., (2010). Snow in the McMurdo Dry Valleys, Antarctica. *International Journal of Climatology*, 30, 633-642.

Franz H. B., King, P. L., Gaillard, F., (2018), Volatiles in the martian Crust, Ch. 6: Sulfur on Mars from the Atmosphere to the Core.

Gibson, E. K., Wentworth, S. J., and McKay, D. S., (1983). Chemical weathering and diagenesis of a cold desert soil from Wright Valley, Antarctica: An analog of martian weathering processes, J. Geophys. Res., 88 (S02), A912– A928.

Gibson, E. K., (1980). Salts from Chemically Weathered Soils in Wright Valley, Antarctica: A Geochemical Model for martian Regolith Formation, Manuscript.

Grapes, R., Gamble, J., Palmer, P., (1989). Basal dolerite boulders. In: Barrett P.J. (ed.), Antarctic Cenozoic history from CIROS-1 drillhole, McMurdo Sound. *DSIR Bulletin*, 245, 169-174

Harris, H. J. H. (1981). Hydrology and Hydrogeochemistry of the South Fork, Wright Valley, Southern Victoria Land, Antarctica. Doctoral Thesis, University of Illinois at Urbana-Champaign, Department of Geology.

Harris, H. J. H., Cartwright, K., Torii, T., (1979). Dynamic chemical equilibrium in a polar desert pond: A sensitive index of meteorological cycles. *Science* 204, 301–303.

Harris, H. J. H., Cartwright, K. (1981). Hydrogeology of the Dry Valley Region, Antarctica. In *Dry Valley Drilling Project*, L.D. McGinnis (Ed.).

Hassinger, J. M., Mayewski, P. A., (1983). Morphology and dynamics of the rock glaciers in Southern Victoria Land, Antarctica. *Arctic Alpine Res*. 15, 351–368.

Hastings, S. J., Luchessa, S. A., Oechel, H. C. & Tenhunen, J. D., (1989). Standing biomass and production in water drainages of the foothills of the Philip Smith Mountains, Alaska. Holarctic Ecology 12, 304–311.

Head, J. H., Marchant, D. R., Dickson, J. L., Levy, J. S. & Morgan, G. A., (2007). Slope streaks in the Antarctic Dry Valleys: Characteristics, candidate formation mechanisms, and implications for slope streak formation in the martian environment. Online Proc. of the 10th ISAES #177.

Hickmott, D., Spear, F.S., (1992). Major-and Trace-Element Zoning in Garnets from Calcareous Pelites in the NW Shelburne Falls Quadrangle, Massachusetts: Garnet Growth Histories in Retrograded Rocks. *Journal of Petrology*, 33, 5, 965–1005.

Horowitz, N. H., Cameron, R. E. S. H. J., (1972). Microbiology of the dry valleys of Antarctica. *Science*, 176, 242–245.

Jiang, S., Wang, R., Xu, Xi., Zhao, K., (2005). Mobility of high field strength elements (HFSE) in magmatic-, metamorphic-, and submarine-hydrothermal systems. *Physics and Chemistry of the Earth Parts A/B/C*, 1020-1029.

Jones, L. M., Faure, G., (1978). A study of strontium isotopes in lakes and surficial deposits of the ice-free valleys, southern Victoria Land, Antarctica. *Chemical Geology*, 22, 107-120.

Krissek L. A., Kyle, P. R. (2000). Geochemical indicators of weathering, Cenozoic paleoclimates, and provenance from fine-grained sediments in CRP-2/2A, Victoria Land Basin, Antarctica. *Terra Antarct*., 7, 589–597.

Koeberl, C., (1993). Instrumental neutron activation analysis of geochemical and cosmochemical samples: a fast and reliable method for small sample analysis. *J. Radioanal. Nucl. Chem*., 168, 47–60.

Langevin, H., Poulet, F., Bibring, J. P., Gondet, B., (2005). Sulfates in the north polar region of Mars detected by OMEGA/Mars Express. *Science*, 307, 5715, 1584-6.

Lane, M. D., Bishop, J. L., (2019). Chapter 3: Mid-infrared (thermal) emission and reflectance spectroscopy, in: Bishop, J.L., Bell III, J.F., Moersch, J.E. (Eds.), Remote Compositional Analysis: Techniques for Understanding Spectroscopy, Mineralogy, and Geochemistry of Planetary Surfaces. *Cambridge University Press,* Cambridge, UK, pp. 42-67.

Lee, H., Lim, H. S., Yoon, H. (2004). *Geochimica et Cosmochimica Act*., 68, 21, 4319-4333.

Lee, B. H. (1997). Meteorological Characteristics at King Sejong Station, Antarctica, 1988-1996. Korea Ocean Research and Development Institute.

Levy, J. S., Fountain, A. G., Gooseff, M. N., Welch, K. A., Lyons, H. B., (2011). Water tracks and permafrost in Taylor Valley, Antarctica: Extensive and shallow groundwater connectivity in a cold desert ecosystem. *GSA Bulletin,* 123, 2295–2311.

Li, C., Yang, S., (2010). Is chemical index of alteration (CIA) a reliable proxy for chemical weathering in global drainage basins? *Am. J. Sci*., 310, 111–127

Lyons, H. B., Welch, K. A., Fountain, A. G., Dana, G. L., Vaughn, B. H. & McKnight, D. M., (2003). Surface glaciochemistry of Taylor Valley, southern Victoria Land, Antarctica and its relationship to stream chemistry. *Hydrological Processes*, 17, 115–130.

Mader, D., Koeberl, C., (2009). Using instrumental neutron activation analysis for geochemical analyses of terrestrial impact structures: current analytical procedures at the University of Vienna gamma spectrometry laboratory. *Appl. Radiat. Isotopes*, 67, 2100–2103.

Masuda, A., Nakamura, N., Tanaka, T. (1973). Fine structures of mutually normalized rare-earth patterns of chondrites. *Geochim. Cosmochim. Acta*, 43, 1131 - 1140.

Matsubaya, O., H. Sakai, T. Torii, H. Burton, K. Terry, (1979). Antarctic saline lakes—stable isotopic ratios, chemical compositions and evolution. *Geochim. Cosmochim. Acta*., 43, 1, 7-25.

McGinnis, L. D., Jensen, T. E., (1971). Permafrost-hydrogeologic regimen in two ice-free valleys, Antarctica, from electrical depth sounding. Quaternary Research 1, 389–409.

McGinnis, L. D., Nakao, K. & Clark, C. C., (1973). Geophysical identification of frozen and unfrozen ground, Antarctica. 2nd Int. Conf. on Permafrost (N.A. Contribution), 136–146.

McKelvey, B. C. (1962). Geological investigations in southern Victoria land, Antarctica–Part 3–Geology of Wright Valley. *New Zealand Journal of Geology and Geophysics*, 5, 143-162.

McNamara, J. P., Kane, D. L., Hinzman, L. D., (1999). An analysis of an arctic channel network using a digital elevation model. *Geomorphology* 29, 339–353.

Meyer, G.H., Morrow, M.B., Wyss, O., Berg, T.E., Littlepage, J.L. (1962). Antarctica: the Microbiology of an unfrozen saline pond. *Science*, 138, 1103-1104.

Morgan, G. A., Head, J. H., Marchant, D. R., Dickson, J. L. & Levy, J. S., (2008). Interaction between gullies and lobate debris tongues on Mars and in the Antarctic Dry Valleys, Abstract, 39th Lunar Planetary Science Conference.

Morris, E. C., Mutch, T. A., Holt H. E., (1972). Atlas of geologic features in the dry valleys of South Victoria Land, Antarctica: possible analogs of martian surface features. USGS open-file report, 73-196. Reston, VA: *US Geological Survey.*

Morrison, A., Reay, A. (1995). Geochemistry of Ferrar Dolerite sills and dykes at Terra Cotta Mountain, south Victoria Land, Antarctica. *Antarctic Science*, 7, 1, 73-85.

Nakai, N., H. Wada, H. Kiuyosu, and M. Takimoto, 1975. Stable isotope studies on the origin and geological history of water and salts in the Lake Vanda area, Antarctica. *Geochemical Journal*, 9, 7- 24.

Nedell S. S., Andersen D. H., Squyres S. H., and Love F. G. (1987) Sedimentation in ice-covered Lake Hoare, Antarctica. *Sedimentology*, 34, 1093-1106.

Nesbitt, H. H., Young, G. M., (1982). Early Proterozoic climates and plate motions inferred from major element chemistry of lutites. *Nature* 299, 715–717

Nesbitt, H. H., Markovics, G., 1997. Weathering of granodioritic crust, long term storage of elements in weathering profiles, and petrogenesis of siliciclastic sediments. *Geochim. Cosmochim. Acta*., 61, 1653-1670.

Nishiyama, T. and H. Kurasawa, (1975). Distribution of evaporite minerals from Taylor Valley, Victoria Land, Antarctica: Dry Valley Drilling Project Bulletin, no. 6, Victoria Univ. of Wellington, N.Z., 22.

Nishiyama, T., (1978). Distribution and origin of evaporite minerals from Dry Valleys, Victoria Land, Antarctica: Dry Valley Drilling Project Seminar-Ill, Bulletin, no. 8, National Institute of Polar Research, Tokyo, 71.

——— (1979). Distribution and origin of evaporite minerals from Dry Valleys, Victoria Land: in Proceedings of the Seminar III on Dry Valley Drilling Project, 1978, T. Nagata (ed.), National Institute of Polar Research, Tokyo, 136-147.

Nyakairu, G. H. A., Koeberl, C., (2001). Mineralogical and chemical composition and distribution of rare earth elements in clay-rich sediments from central Uganda. *Geochemical Journal*, 35, 13-28.

Nylen, T. H., Fountain, A. G., Doran, P. T. (2004), Climatology of katabatic winds in the McMurdo dry valleys, southern Victoria Land, Antarctica. *J. Geophys. Res*., 109, D03114

Oberts, G. L., (1973). The chemistry and hydrogeology of dry valley lakes, Antarctica: M.S. Thesis, Northern Illinois Univ., DeKalb, 55 p.

Palmer, K., (1987). XRF analyses of granitoids and associated rocks from southern Victoria Land, Antarctica. Victoria University of Wellington Research School of Earth Sciences Geology Board of Studies publication 3.

Palmer, K., (1990). XRF analyses of granitoids and associated rocks, St Johns Range, south Victoria Land, Antarctica. Victoria University of Wellington Research School of Earth Sciences Geology Board of Studies publication 5.

Patel, S. N., et al., (2015). Coordinating Chemical and Mineralogical Analyses of Antarctic Dry Valley Sediments as Potential Analogs for Mars, Abstract, 46th Lunar and Planetary Science Conference.

Pearce, J. A., Cann, J. R., (1973). Tectonic setting of basic volcanic rocks determined using trace element analyses. *Earth and Planetary Science Letters*, 19, 2, 290-300.

Pérez, E., Chebude, H. Chemical Analysis of Gaet'ale, a Hypersaline Pond in Danakil Depression (Ethiopia): New Record for the Most Saline Water Body on Earth. *Aquat Geochem*, 23**,** 109–117 (2017)

Peterson, M.D., Marsh, B.D. (2008). Bedrock Geologic Map of the McMurdo Dry Valleys, Southern Victoria Land, Antarctica.

Ragotzkie, R. A. (1964). The Heat Balance of Two Antarctic Lakes. *Limnology and Oceanography*, 9, 3, 412-425.

Rodrigue, C. M., (2020). K-means Clustering and Mapping of all Four Mars Rovers' APXS Oxide and Element Relative Abundance Data, Abstract, 51st Lunar and Planetary Science Conference

Roser, B. P., Pyne, A.R., (1989). Whole rock geochemistry, in Antarctic Hannah, M.J., 1994. Eocene dinoflagellates from CIROS-1 drill hole, Cenozoic History from the CIROS-1 Drillhole, McMurdo Sound, McMurdo Sound, Terra Antarctica, 1, 371. Antarctica, 175–184, ed. Barrett, P. J., Department of Scientific Harwood, D. M., Barrett, P. J., Edwards, A.R., Rieck, H. J. & Webb, and Industrial Research Bulletin, 245, DSIR Publishing, Wellington.

Scott, R. F., The Voyage of the 'Discovery', C. Scribner's Sons, New York, 1905.

Sheldon, N. D., Tabor, N. J., (2009). Quantitative paleoenvironmental and paleoclimatic reconstruction using paleosols. *Earth-Sci. Rev*., 95, 1–52.

Small, H., Stevens, T. S., Bauman, H. C., (1975). Novel ion exchange chromatographic method using conductimetric detection. *Anal. Chern*., 47, 1801-1809.

Staff, S. S. (2010). Keys to Soil Taxonamy (11 ed.). Washington, D.C.: USDA-Natural Resources Conservation Service.

Taylor, S. R. and McLennan, S. M., (1985). The Continental Crust: Its Composition and Evolution. Blackwell Scientific Publ.

Taylor, G., et al., (2006). Variations in K/Th on Mars*. J. Geophys. Res*., 111, E03S06.

Thompson, D. C , R. M. F. Craig, A. M. Bromley, (1971). Climate and surface heat balance in an Antarctic dry valley: *N. Z. Jour. Sci*., 14, 2, 245-251.

Toner, J.D. (2012). Using Salt Accumulations and Luminescence Dating to Study the Glacial History of Taylor Valley, Antarctica, Doctoral Dissertation, University of Washington, Department of Earth and Space Sciences.

Torii, T., N. Yamagata, J. Ossaka, S. Murata, (1977). Salt balance in the Don Juan basin: *Antarctic Record (Jap.)*, 58, 116-130.

Torii, T., Yamagata, N., (1981): Limnological studies of saline lakes in the Dry Valleys. In McGinnis, L. D. (ed.), Dry Valley Drilling Project. *Antarctic Research Series*, 33. Washington, D.C.: American Geophysical Union, 141-160.

Wada, K., (1987). Minerals formed and mineral formation from volcanic ash by weathering. *Chem.Geol*. 60, 17-28.

Wentworth, S. J., Gibson, E. K., Velbel, M. A., McKay, D. S., (2005) Antarctic Dry Valleys and indigenous weathering in Mars meteorites: implications for water and life on Mars. *Icarus*, 174, 383–395.

Wharton R. A., Jr.. McKay C. P., Parker B. C., Simmons G. M., Jr. (1986) Oxygen budget of a perennially ice-covered Antarctic dry valley lake*. Limnol. Oceanogr*. 31, 437-443.

Wharton R. A., Jr., McKay C. P., Mancinelli R. L., Simmons G. M., Jr. (1987) Perennial N_2 supersaturation in an Antarctic lake. *Nature* 325, 343-345.

Wharton, R. A., McKay C. P., Mancinelli R. L., Simmons G. M., Jr., (1989). Early martian environments: the Antarctic lake. *Adv. Space Res*. 9, 147–153

Wharton R. A., Jr., McKay C. P., Clow G. D., Andersen, D. T., Simmons G. M., Jr.,Love F. G. (1992) Changes in ice cover thickness and lake level of Lake Hoare, Antarctica: Implications for local climatic change. *J. Geophys. Res.* 97, 3503- 3513.

Wharton R. A., Jr., Lyons H. B., and Des Marais D. 3. (1993) Stable isotopic biogeochemistry of carbon and nitrogen in a perennially ice-covered Antarctic lake. *Chem. Geol*. (Isotope Geosci. Section) 107, 159-172.

Yamagata, N., T. Torii, S. Murata, K. Watanuki (1967). Report of the Japanese summer parties in Dry Valleys, Victoria Land, 1963-65: 7 - Chemical composition of pond waters in Ross Island with reference to those in Ongul Islands. *Antarctic Record (Jap.)*, 29, 2368-2375.

Yoo, C. M., Choe, M. H., Jo, H. R., Kim, H., Kim, K. H. (2001). Volcaniclastic sedimentation of the Sejong Formation (Late Paleo-cene-Eocene), Barton Peninsula, King George Island, Antarctica. *Ocean Polar Res.* 23, 97–107.

Yusa, H., (1972). The re-evaluation of heat balance in Lake Vanda, Victoria Land, (Jap.): in Contributions, Geophysical Institute, Kyoto University, 12, 87-100.

APPENDIX A, COMPLETE DATASET MCMURDO DRY VALLEY SAMPLES: ELEMENTAL ABUNDANCES

TABLE 1. ELEMENTAL ABUNDANCES. CORE 2074 (JB1124-1126) AND CORE 35 (JB1142-2245).

	JB1126	JB1124	JB1125
Depth (cm)	0	2	10
elements (ppm)			
Na %	0.80	0.77	0.78
K %	0.66	0.61	0.58
Sc	14.90	13.64	17.07
Cr	126.83	82.09	114.38
Fe %	2.40	2.41	2.81
Co	14.55	13.28	16.86
Ni	33.34	37.19	46.11
Zn	40.28	37.38	41.13

	JB1142	JB1143	JB1144	JB1145
Depth (cm)	0–0.5	1–2	3–4	10–12
elements (ppm)				
Na %	1.85	1.23	1.23	1.40
K %	1.04	0.89	0.82	1.19
Sc	23.6	34	29.3	33.3
Cr	113	181	144	174
Fe %	4.42	5.69	4.94	5.57
Co	24.3	34.4	29.4	33.9
Ni	45	65	53	76
Zn	63	81	87	76

Ga	4.83	1.95	5.41	**Ga**	6.74	4.87	9.34	10.4
As	<1.0	0.51	<0.8	**As**	0.67	0.38	0.47	<1.1
Se	<1.6	<1.7	<1.8	**Se**	<1.5	<3.2	<2	<2.2
Br	0.29	6.17	2.73	**Br**	2.8	<0.7	<0.7	<0.8
Rb	28.50	26.92	32.27	**Rb**	45.9	36.8	33.6	44.3
Sr	43.63	148.55	82.80	**Sr**	134	124	74	105
Zr	107.65	166.30	91.18	**Zr**	149	99	130	148
Sb	<0.2	<0.2	0.06	**Sb**	<0.2	<0.2	<0.2	<0.2
Cs	0.77	0.98	1.01	**Cs**	1.32	1.13	1.01	1.42
Ba	122.93	127.20	130.53	**Ba**	237	153	128	203
La	11.37	12.39	11.65	**La**	15.4	14.2	11.0	14.9
Ce	20.61	22.03	20.88	**Ce**	29.2	27	21.4	28.7
Nd	10.09	9.21	10.23	**Nd**	14.4	13.3	10.5	13.7
Sm	2.09	2.56	2.02	**Sm**	3.22	2.75	2.53	3.2
Eu	0.51	0.46	0.49	**Eu**	0.71	0.68	0.65	0.8
Gd	1.80	1.58	1.95	**Gd**	2.63	2.6	2.67	3.08
Tb	0.30	0.29	0.39	**Tb**	0.48	0.46	0.44	0.53
Tm	0.17	0.21	0.24	**Tm**	0.27	0.27	0.27	0.30
Yb	1.03	1.01	1.15	**Yb**	1.60	1.82	1.63	1.85
Lu	0.17	0.17	0.19	**Lu**	0.28	0.31	0.28	0.32
Hf	2.15	3.42	2.55	**Hf**	2.46	2.62	2.37	2.81
Ta	0.23	0.31	0.25	**Ta**	0.43	0.32	0.37	0.40
W	0	0	0	**W**	<3.2	<2.6	<3.1	<3.7
Ir (ppb)	<1.9	<1.8	<2	**Ir (ppb)**	<1.3	<1.9	0.40	<1.9
Au (ppb)	1.09	<1.4	<1.1	**Au (ppb)**	<1.8	<2.2	<1.6	<1.9
Th	3.48	3.15	3.28	**Th**	3.88	3.75	2.98	4.25
U	1.60	3.02	1.23	**U**	3.02	0.45	0.67	0.94

TABLE 2. ELEMENTAL ABUNDANCES. CORE 33 (JB1129-JB133) AND CORE 39 (JB1134-JB1138).

	JB1129	JB1130	JB1131	JB1132	JB1133		JB1134	JB1135	JB1136	JB1137	JB1138
Depth (cm)	0-1	3-4	8-10	12-14	16-20	Depth (cm)	0-1	2-5	6-8	10-12	15-16
elements (ppm)						elements (ppm)					
SiO_2 %	68.69	72.25	68.39	71.64	72.50	**SiO_2 %**	68.87	63.81	69.90	70.97	70.83
Al_2O_3 %	7.95	8.28	8.97	8.42	8.75	**Al_2O_3 %**	9.44	8.39	9.87	10.71	11.09
Fe_2O_3 %	3.97	4.27	3.67	4.17	3.96	**Fe_2O_3 %**	5.24	4.61	4.17	4.33	4.41
MgO %	3.57	3.84	3.30	3.75	3.56	**MgO %**	4.71	4.15	3.75	3.90	3.97
CaO %	3.25	3.51	2.78	3.29	3.19	**CaO %**	4.23	3.68	3.33	3.27	3.25
Na_2O %	5.03	4.64	6.30	5.23	4.56	**Na_2O %**	5.03	4.65	4.39	4.10	4.20
K_2O %	2.49	2.03	2.02	1.77	1.88	**K_2O %**	2.31	5.25	3.14	2.47	2.54
TiO_2 %	1.43	1.47	1.68	1.42	1.47	**TiO_2 %**	1.54	1.45	1.90	2.19	1.87
P_2O_5 %	0.29	0.31	0.29	0.33	0.31	**P_2O_5 %**	0.48	0.40	0.34	0.38	0.42
MnO %	0.05	0.06	0.06	0.07	0.06	**MnO %**	0.12	0.08	0.07	0.09	0.10

Cr_2O_3 %	0.07	0.08	0.07	0.09	0.08	**Cr_2O_3 %**	0.10	0.09	0.08	0.08	0.08
SiO_2 %	0.02	0.02	0.01	0.02	0.02	**SiO_2 %**	0.02	0.02	0.02	0.02	0.02
SO_3 %	0.20	0.40	3.12	1.12	0.07	**SO_3 %**	n.d.	0.47	0.55	0.05	n.d.
$CaSO_4$ %	0.34	0.68	5.31	1.91	0.13	**$CaSO_4$ %**	n.d.	0.81	0.93	0.08	n.d.
Na_2SO_4 %	0.35	0.71	5.54	1.99	0.13	**Na_2SO_4 %**	n.d.	0.84	0.97	0.09	n.d.
K_2SO_4 %	0.43	0.87	6.79	2.45	0.16	**K_2SO_4 %**	n.d.	1.03	1.20	0.11	n.d.
Cu	19.00	22.00	16.00	21.00	21.00	**Cu**	21.00	25.00	17.00	17.00	24.00
Co	16.79	17.41	13.32	16.03	14.73	**Co**	21.09	18.04	14.41	16.59	15.55
Ni	52.50	51.80	44.44	36.54	35.97	**Ni**	57.02	52.34	33.89	53.27	42.47
Zn	51.14	50.15	46.48	50.17	46.22	**Zn**	62.25	53.83	47.32	58.30	58.31
Ga	20.81	8.85	7.41	8.08	17.07	**Ga**	8.68	20.65	11.54	17.13	42.31
As	<1.8	<1.3	<1.3	<1.2	0.26	**As**	<1.3	<2	<1.5	<1.8	0.59
Se	<1.8	<1.7	<1.6	<1.2	<1.5	**Se**	<2.3	<1.8	<1.5	<1.8	<2.7
Br	1.81	1.45	2.11	1.61	2.19	**Br**	<1.1	<1.4	<1.1	<1.3	0.15
Rb	51.38	52.82	64.04	49.03	43.91	**Rb**	55.64	53.89	54.91	79.49	63.59
Sr	130.29	95.60	123.23	109.40	92.35	**Sr**	124.49	88.80	86.74	115.15	154.10
Zr	136.20	150.50	147.65	141.86	125.89	**Zr**	174.43	158.52	134.76	178.39	241.80
Sb	<0.2	<0.2	<0.2	<0.2	<0.2	**Sb**	<0.2	<0.3	<0.2	<0.2	0.08
Cs	1.23	1.16	1.70	1.90	1.83	**Cs**	1.37	1.13	1.07	1.47	1.69
Ba	220.20	245.45	234.63	204.93	195.02	**Ba**	262.16	219.44	211.32	301.28	365.23
La	50.33	51.68	61.85	47.19	50.78	**La**	59.70	44.74	67.70	105.74	70.98
Ce	33.74	37.25	42.51	35.44	35.29	**Ce**	42.81	32.17	46.75	69.67	46.79
Nd	19.68	17.39	21.86	20.59	18.69	**Nd**	22.47	18.78	19.41	31.50	20.42
Sm	13.06	13.19	15.22	11.91	12.04	**Sm**	15.93	12.82	13.11	19.72	16.04
Eu	7.07	7.62	7.65	8.02	6.97	**Eu**	10.05	7.83	7.22	9.99	10.10
Gd	7.85	8.14	8.63	7.35	6.31	**Gd**	10.16	7.48	8.01	10.29	8.18
Tb	7.23	7.06	7.57	6.37	6.02	**Tb**	10.29	7.40	6.02	8.95	7.40

Tm	6.18	6.46	6.74	5.34	7.02	**Tm**	8.71	5.62	5.06	7.58	5.90
Yb	5.71	5.24	6.00	4.96	4.91	**Yb**	6.04	5.48	5.16	6.30	5.48
Lu	5.99	5.63	5.84	5.43	5.13	**Lu**	6.53	6.06	5.36	6.45	5.39
Hf	3.41	3.06	3.25	2.94	2.79	**Hf**	3.56	3.38	2.98	4.31	3.89
Ta	0.44	0.42	0.45	0.42	0.47	**Ta**	0.63	0.41	0.39	0.62	0.52
W	0.00	0.00	0.00	0.00	0.00	**W**	0.00	0.00	0.00	0.00	0.00
Ir (ppb)	<2.1	<2	<1.9	<1.4	<1.8	**Ir (ppb)**	<2.5	<2.1	<1.8	<2.1	<2
Au (ppb)	0.41	<1.7	<1.7	<1.6	<1.4	**Au (ppb)**	<1.7	<2	<1.5	<1.7	0.44
Th	5.33	5.70	5.92	4.47	4.87	**Th**	5.33	5.22	6.47	8.27	5.75
U	1.45	1.46	1.77	1.12	1.19	**U**	1.14	1.02	1.09	1.64	1.48

TABLE 3. ELEMENTAL ABUNDANCES. CORE 42 (JB1100-1105) AND CORE 52 (JB1107-1110).

	JB1100	JB1101	JB1102	JB1103	JB1104	JB1105		JB1107	JB1108	JB1109	JB1110
Depth (cm)	0-1	1-4	4-7	8-10	12-15	20-24		0-1	2-4	4-8	16-20
elements (ppm)							elements (ppm)				
SiO_2 %	70.80	68.30	48.50	59.10	64.30	65.70	**SiO_2 %**	69.88	68.02	63.18	68.61
Al_2O_3 %	8.07	8.94	16.20	8.29	9.15	9.75	**Al_2O_3 %**	9.52	9.68	9.00	9.09
Fe_2O_3 %	5.27	5.22	8.25	5.11	5.39	5.41	**Fe_2O_3 %**	4.61	4.54	4.10	4.29
MgO %	4.74	4.70	7.42	4.60	4.85	4.87	**MgO %**	4.15	4.09	3.69	3.86
CaO %	3.81	3.82	4.53	3.35	3.65	3.44	**CaO %**	3.80	3.82	3.47	3.52
Na_2O %	4.76	4.95	6.27	9.83	7.46	6.55	**Na_2O %**	4.93	5.84	9.95	5.97
K_2O %	2.19	2.11	1.76	1.79	1.93	2.05	**K_2O %**	2.23	2.16	2.01	2.01

TiO_2 %	1.27	1.40	2.88	1.61	1.51	1.58	**TiO_2 %**	1.67	1.57	1.61	1.74
P_2O_5 %	0.28	0.30	0.52	0.35	0.41	0.37	**P_2O_5 %**	0.40	0.39	0.35	0.35
MnO %	0.05	0.06	0.16	0.06	0.08	0.10	**MnO %**	0.08	0.07	0.06	0.06
Cr_2O_3 %	0.09	0.08	0.10	0.08	0.09	0.09	**Cr_2O_3 %**	0.08	0.08	0.08	0.08
SiO_2 %	0.02	0.02	0.01	0.02	0.02	0.02	**SiO_2 %**	0.02	0.02	0.02	0.02
SO_3 %	0.29	0.10	0.49	6.70	2.94	1.48	**SO_3 %**	0.45	1.85	7.82	2.60
$CaSO_4$ %	0.00	0.17	0.83	11.39	5.00	2.52	**$CaSO_4$ %**	0.76	3.14	13.29	4.42
Na_2SO_4 %	0.52	0.18	0.87	11.89	5.22	2.63	**Na_2SO_4 %**	0.80	3.28	13.87	4.61
K_2SO_4 %	0.64	0.22	1.06	14.58	6.40	3.22	**K_2SO_4 %**	0.98	4.02	17.01	5.65
Cu	0.294	0.1	0.489	6.7	2.94	1.48	**Cu**	26	18	16	15
Co	19.12	18.61	28.79	17.87	16.87	18.01	**Co**	17.9	16.6	14.8	17.5
Ni	70.15	71.28	63.53	43.95	66.35	61.56	**Ni**	39	36	45	37
Zn	53.07	55.39	100.15	55.11	58.25	60.30	**Zn**	58	54	49	54
Ga	44.12	18.62	24.49	40.32	14.49	42.78	**Ga**	13	16	4	15
As	<1.5	<1.7	1.33	<1.2	<0.9	<1.1	**Sr**	290	305	365	295
Se	<2.0	<2.1	<2.5	1.49	<2.1	<2.3	**Br**	<1.5	<1.5	<1.2	<1.4
Br	<0.9	<1.1	0.26	0.30	<0.6	<0.7	**Rb**	54.6	57.3	47.8	56.5
Rb	45.65	51.43	115.78	47.82	52.87	48.67	**Sr**	252	318	395	319
Sr	286.53	295.72	372.93	274.26	257.44	238.03	**Zr**	157	140	115	100
Zr	116.81	124.11	192.94	147.75	166.89	157.13	**Sb**	<0.2	<0.2	<0.2	<0.2
Sb	<0.1	<0.2	0.12	<0.2	<0.2	<0.1	**Cs**	1.27	1.28	1.21	1.22
Cs	1.09	1.30	4.68	1.08	1.24	1.21	**Ba**	276	264	283	264
Ba	231.67	258.90	281.44	202.06	235.16	190.42	**La**	22.2	23.6	12.9	17.9
La	17.05	15.26	30.65	18.92	20.58	20.78	**Ce**	38.2	42.2	24.0	32.6
Ce	30.47	26.57	54.88	33.81	37.19	40.36	**Nd**	17.1	17.6	11.5	13.5
Nd	14.81	10.76	21.69	14.54	15.55	15.20	**Sm**	3.19	2.92	2.32	2.77

Sm	2.71	2.59	4.97	3.20	3.38	3.14	**Eu**	0.78	0.72	0.63	0.67
Eu	0.69	0.70	0.91	0.69	0.73	0.75	**Gd**	2.61	2.57	2.04	2.43
Gd	<1.1	2.07	3.99	2.70	3.17	2.99	**Tb**	0.4	0.42	0.36	0.42
Tb	0.34	0.36	0.64	0.46	0.46	0.44	**Tm**	0.25	0.24	0.21	0.31
Tm	0.27	0.20	0.31	0.25	0.23	0.25	**Yb**	1.33	1.17	1.08	1.25
Yb	1.27	1.26	1.99	1.44	1.30	1.41	**Lu**	0.21	0.19	0.17	0.2
Lu	0.21	0.20	0.34	0.22	0.22	0.24	**Hf**	3.26	2.98	2.56	3.26
Hf	2.67	2.60	2.98	2.87	3.35	3.22	**Ta**	0.58	0.48	0.47	0.48
Ta	0.35	0.44	1.13	0.72	0.78	0.82	**W**	0.0	0.0	0.0	0.0
W	<4.7	<4.7	0.85	<3.6	<2.5	<3.4	**Ir (ppb)**	<2.3	<2.1	<1.9	<1.9
Ir (ppb)	<2.2	<2.3	<1.8	<1.5	<1.5	<1.6	**Au (ppb)**	<1.4	<1.3	<1.4	<1.3
Au (ppb)	<1.8	<2.9	<1.9	<1.5	0.57	<1.4	**Th**	5.53	5.00	4.00	5.74
Th	4.45	4.15	12.32	4.25	5.13	5.44	**U**	0.64	0.97	1.17	1.18
U	0.72	1.29	3.42	1.40	1.11	1.20					

TABLE 4. ELEMENTAL ABUNDANCES. CORE 72.

Data from Gibson et al., 1983.

	JB1087	JB1088	JB1089	JB1090	JB1091	JB1092	JB1093	JB1094	JB1095	JB1096
Depth (cm)	0-1	0-2	2-4	4-6	6-8	8-12	12-16	24-28	32-36	44-48
elements (ppm)										
SiO_2 %	57.52	56.76	40.61	51.49	51.83	54.25	55.70	58.15	57.72	57.61
Al_2O_3 %	12.73	12.49	9.15	11.23	11.36	12.29	12.39	12.91	13.03	13.35
Fe_2O_3 %	6.34	6.57	4.41	5.70	5.69	6.21	6.19	6.62	6.71	6.45
MgO %	5.70	5.91	3.97	5.13	5.12	5.59	5.57	5.96	6.04	5.80
CaO %	5.08	5.77	4.77	6.08	5.84	6.37	6.27	6.79	6.64	6.74
Na_2O %	7.76	7.52	4.84	6.20	6.12	6.63	6.38	7.04	6.93	7.27

K_2O %	3.05	3.39	14.32	6.89	6.56	4.63	4.21	2.62	2.54	2.56
TiO_2 %	1.98	1.86	1.42	1.74	1.81	1.93	2.08	1.87	1.92	1.78
P_2O_5 %	0.54	0.52	0.31	0.41	0.40	0.44	0.45	0.47	0.46	0.45
MnO %	0.09	0.08	0.05	0.06	0.06	0.06	0.07	0.06	0.07	0.07
Cr_2O_3 %	0.11	0.12	0.08	0.11	0.10	0.12	0.11	0.12	0.12	0.12
SiO_2 %	0.02	0.03	0.02	0.03	0.03	0.03	0.03	0.03	0.03	0.04
SO_3 %	2.65	1.97	2.75	1.02	0.80	0.45	0.32	0.07	0.10	0.07
$CaSO_4$ %	4.50	3.35	4.67	1.74	1.36	0.76	0.55	0.13	0.17	0.13
Na_2SO_4 %	4.70	3.50	4.87	1.82	1.42	0.80	0.58	0.13	0.18	0.13
K_2SO_4 %	5.76	4.29	5.98	2.23	1.74	0.98	0.71	0.16	0.22	0.16
Cu	40.00	37.00	29.00	26.00	35.00	26.00	49.00	28.00	33.00	30.00
Sc	24.63	27.50	17.37	25.14	23.73	26.83	26.91	28.15	26.80	32.86
Cr	123.14	150.61	111.15	161.26	154.85	166.30	172.72	183.79	160.30	223.35
Co	26.36	28.96	18.14	25.37	24.57	27.61	27.65	29.16	27.52	32.80
Ni	79.60	89.29	73.19	102.99	80.86	108.61	91.47	130.90	82.25	121.77
Zn	80.59	79.98	47.95	62.06	62.56	65.26	71.72	78.69	66.08	82.06
Ga	45.51	78.63	52.88	68.03	25.87	27.55	17.93	20.10	20.96	98.00
As	<2.4	<2.4	<2.7	<2.7	<2.4	<1.6	<1.9	<1.9	<1.6	<2.7
Se	<2.3	<2.3	3.28	0.33	2.41	0.87	2.09	<2.3	<2.3	<2.6
Br	<1.4	<1.4	<1.5	<1.6	<1.6	<1.0	<1.3	<1.2	<1.1	<1.5
Rb	70.59	60.50	45.45	46.44	53.59	58.28	53.75	58.64	47.17	58.77
Sr	219.55	220.55	171.48	221.50	228.71	217.79	198.28	244.23	207.65	270.35
Zr	180.99	165.28	102.66	134.10	128.88	154.72	130.94	128.59	119.23	181.18
Sb	<0.2	<0.2	<0.2	<0.2	<0.3	<0.2	<0.3	<0.2	<0.2	<0.2
Cs	1.76	1.54	0.99	1.02	1.14	1.17	1.22	1.26	1.17	1.33
Ba	260.20	253.57	197.34	203.68	231.94	253.73	246.68	255.48	235.88	267.05
La	24.00	22.62	14.40	23.69	15.14	18.58	20.98	19.36	19.64	23.77
Ce	44.37	39.49	25.69	43.84	28.36	32.92	37.17	34.43	32.64	39.73

Nd	18.04	14.79	10.66	16.82	11.59	13.87	14.37	13.37	13.16	15.23
Sm	3.67	3.40	2.30	3.33	2.66	3.10	3.09	3.03	2.93	3.44
Eu	0.89	0.86	0.57	0.68	0.69	0.73	0.81	0.84	0.76	0.85
Gd	3.78	3.88	<1.1	3.51	2.62	3.27	3.39	3.31	2.55	3.17
Tb	0.56	0.55	0.35	0.51	0.44	0.51	0.55	0.50	0.45	0.57
Tm	0.31	0.24	0.29	0.27	0.32	0.26	0.37	0.38	0.21	0.41
Yb	1.65	1.69	0.97	1.37	1.33	1.52	1.45	1.55	1.49	1.65
Lu	0.28	0.28	0.17	0.22	0.22	0.25	0.24	0.24	0.24	0.27
Hf	4.00	3.70	2.46	2.79	2.81	2.86	3.12	2.85	2.57	3.47
Ta	0.78	0.59	0.40	0.41	0.48	0.56	0.52	0.50	0.41	0.65
W	<7.1	<7.1	<7.9	<7.9	<6.2	<4.4	<5.0	<5.2	<4.5	<8.3
Ir (ppb)	<2.4	<2.5	<2.2	<2.4	<2.5	<2.6	<2.7	<2.6	<2.6	<3
Au (ppb)	<3.1	<3	<3.2	<3.4	<4.4	<2.6	<3.7	<3.2	<2.8	<3.3
Th	6.15	5.75	3.93	6.13	3.95	4.53	4.85	4.36	4.36	5.26
U	1.50	1.06	1.01	0.75	0.72	0.79	0.66	0.82	0.77	1.20

TABLE 5. ELEMENTAL ABUNDANCES. LAKE FRYXELL.

Data from Bishop et al., 2014.

elements (ppm)	JB650 LFR-A edge	JB651 LFR-1 edge	JB652 LFR-2 edge	JB653 LFR-3 edge	JB654 LFR-4 ss	JB655 LFR-5 ss	JB656 LFR-6 ss	JB657 LFR-7 ss	JB658 LFR-8 ss	JB659 LFR-9 ss	JB660 LFR-10 ss
SiO_2 %	59.67	54.26	55.69	59.43	57.68	57.47	62.56	62.63	61.66	60.91	57.61
Al_2O_3 %	13.24	13.09	13.55	14.19	13.97	12.93	12.61	12.63	13.26	13.31	13.09
Fe_2O_3 %	5.75	8.84	8.12	6.01	7.05	7.81	6.00	6.18	5.74	5.96	7.34
MgO %	4.39	7.21	6.24	4.97	5.45	7.03	5.85	5.81	5.15	5.22	6.32
CaO %	5.44	6.84	6.78	6.1	6.57	6.58	5.94	6.04	5.78	5.94	6.61
Na_2O %	2.76	3.25	2.95	3.18	3.10	2.86	2.51	2.47	2.67	2.63	2.77

K_2O %	2.47	2.20	2.23	2.51	2.34	2.09	2.03	2.06	2.14	2.17	2.16
TiO_2 %	0.76	1.74	1.40	0.97	1.09	1.16	0.57	0.63	0.64	0.69	1.15
P_2O_5 %	0.18	0.41	0.35	0.25	0.26	0.27	0.11	0.12	0.14	0.16	0.27
MnO %	0.09	0.15	0.14	0.10	0.12	0.14	0.11	0.11	0.10	0.10	0.13
Cr_2O_3 %	0.018	0.035	0.033	0.021	0.025	0.034	0.028	0.028	0.023	0.024	0.030
Co	20.0	34.1	31.3	21.2	23.9	32.9	27.4	25.7	24.2	23.6	31.6
Ni	58.27	128.40	90.13	70.57	87.75	102.65	74.13	73.04	59.43	73.58	107.67
Zn	66.6	98.2	95.6	65.5	74.4	92.4	70.9	71	69	70.4	92
Ga	2	9	9	22	3	7	6	3	2	3	10
As	1.32	1.43	1.10	1.09	1.34	0.61	1.72	<0.8	0.53	0.6	1.25
Se	1.27	<0.9	<0.9	0.75	0.98	1.04	0.29	0.89	0.8	1.07	<1.3
Br	1.7	0.6	0.6	0.6	0.6	0.6	0.7	0.6	0.9	1.2	1.0
Rb	84.5	66.6	74.1	85.8	73.5	66.1	70.2	72.7	74.1	76.2	75.8
Sr	342	512	463	451	422	396	312	285	307	322	251
W	18	27	25	19	24	24	18	19	19	20	22
Zr	172	388	312	214	241	297	169	217	176	159	268
Nb	23	55	41	31	29	28	11	11	16	20	35
Sb	0.14	0.15	0.12	0.15	0.13	0.09	0.03	<0.1	<0.1	0.06	<0.3
Cs	1.77	1.39	1.54	1.66	1.48	1.38	1.28	1.28	1.32	1.39	1.38
Ba	341	323	338	373	345	311	315	325	328	345	346
La	25.5	48.4	42.1	30.0	32.2	41.7	23.6	29.1	28.9	31.0	33.5
Ce	47.5	90	79.4	55.4	60.9	76.9	44.2	55.2	54.4	57.1	60.8
Nd	20.3	38.5	35.4	25.3	27.8	33.4	17.2	24.0	19.6	21.3	25.4
Sm	4.30	7.51	6.69	4.95	5.54	6.24	3.85	4.27	4.05	4.81	5.87
Eu	1.17	2.13	1.89	1.40	1.47	1.67	1.10	1.16	1.19	1.23	1.57
Gd	4.26	6.32	5.99	4.06	5.29	4.48	4.01	4.58	3.98	4.78	4.35
Tb	0.59	1.02	0.90	0.67	0.76	0.85	0.60	0.64	0.61	0.69	0.84
Tm	0.22	0.45	0.39	0.28	0.34	0.38	0.28	0.27	0.27	0.26	0.36
Yb	1.46	2.52	2.28	1.60	1.88	2.12	1.78	1.85	1.72	1.69	2.12

Lu	0.23	0.36	0.34	0.24	0.29	0.34	0.27	0.29	0.28	0.27	0.30
Hf	3.04	7.48	6.03	4.29	5.16	6.42	3.41	4.78	4.08	3.12	5.02
Ta	1.6	4.29	3.17	2.47	2.13	2.44	0.98	1.07	1.06	1.35	2.88
Ir (ppb)	<1.2	<1.4	<1.4	<1.2	<1.5	<1.3	<1.4	<1.4	<1.4	<1.4	<1.5
Au (ppb)	4.6	0.3	0.2	0.3	<0.3	0.8	0.9	<0.3	<0.3	<0.3	<2.3
Th	6.40	8.58	7.56	6.40	6.48	7.62	5.52	6.33	7.01	7.47	11.0
U	1.59	1.97	1.79	1.67	1.55	1.51	0.86	1.02	0.76	1.29	1.65

TABLE 6. ELEMENTAL ABUNDANCES. LAKE VANDA.

Data from Bishop et al., 2014.

elements	JB661	JB662	JB663	JB664	JB665	JB666	JB667	JB668	JB669
(ppm)	LVA-1	LVA-2	LVA-3	LVA-4	LVA-5	LVA-6	LVA-7	LVA-8	LVA-9
	edge	edge	edge	edge	ss	ss	ss	ss	edge
SiO_2 %	74.39	62.53	62.53	64.3	72.99	76.45	75.92	76.91	67.12
Al_2O_3 %	8.39	12.01	7.78	7.99	9.22	8.60	8.71	8.74	10.24
Fe_2O_3 %	4.68	6.64	10.83	9.79	4.73	3.80	3.71	3.33	6.31
MgO %	4.06	5.55	7.23	6.85	3.99	3.11	3.10	2.79	4.84
CaO %	4.54	6.36	6.57	6.31	4.96	4.41	4.35	3.97	6.54
Na_2O %	1.60	2.37	1.28	1.34	1.54	1.45	1.54	1.70	1.68
K_2O %	1.29	1.87	0.92	1.05	1.25	1.17	1.26	1.27	1.24
TiO_2 %	0.32	0.58	1.58	1.35	0.33	0.27	0.25	0.24	0.57
P_2O_5 %	0.06	0.08	0.06	0.06	0.05	0.05	0.05	0.05	0.06
MnO %	0.08	0.12	0.19	0.17	0.09	0.07	0.07	0.06	0.11
Cr_2O_3 %	0.021	0.024	0.033	0.033	0.017	0.014	0.014	0.014	0.019
Co	19.3	27.4	40.7	36.6	20.1	18.3	15.6	15.8	28.4
Ni	46.39	64.54	84.25	74.24	50.83	35.14	33.58	32.87	60.43

Zn	58	93	146	132	60	56	42	43	96
Ga	1.8	3	5.3	9.4	1.6	3.4	1.2	1.8	8.8
As	<1.0	<1.4	<1.5	<2.1	<1.2	<1.3	<1.4	<1.1	0.52
Se	<1.1	<1.4	<1.9	<1.6	<1.1	<1.1	<1.3	<0.9	<1.4
Br	0.4	0.4	0.4	0.5	0.3	0.5	0.6	0.5	0.5
Rb	42.5	58.5	43.8	40.0	44.9	48.0	37.5	47.5	53.2
Sr	81	126	83	73	69	80	72	96	88
Y	14	17	24	20	13	11	11	10	16
Zr	100	186	346	201	104	102	85	111	198
Nb	5	6	10	13	8	5	5	6	7
Sb	<0.2	<0.2	<0.2	<0.2	<0.2	<0.2	<0.2	<0.2	<0.2
Cs	1.15	1.26	1.10	1.16	1.14	1.23	0.88	1.24	1.38
Ba	201	306	163	157	179	207	180	226	211
La	14.5	23	35.3	19.1	12.7	14.6	12.4	13.3	21.0
Ce	25.6	40.3	61.4	34.1	23.3	25.2	22	23.8	37.4
Nd	9.03	15.7	21.4	14.4	9.48	9.34	8.50	8.28	13.4
Sm	2.23	3.18	4.80	3.29	2.12	2.25	1.79	2.04	3.26
Eu	0.59	0.79	0.76	0.64	0.59	0.66	0.53	0.66	0.77
Gd	2.24	3.34	3.86	2.86	2.28	2.27	1.54	2.11	3.56
Tb	0.38	0.52	0.77	0.48	0.35	0.36	0.29	0.32	0.54
Tm	0.17	0.24	0.36	0.29	0.17	0.16	0.14	0.15	0.25
Yb	1.25	1.59	2.42	2.07	1.21	1.21	1.01	1.09	1.78
Lu	0.20	0.27	0.40	0.34	0.20	0.20	0.17	0.17	0.31
Hf	2.15	3.71	9.02	5.26	2.30	2.26	2.2	2.10	4.58
Ta	0.39	0.59	1.31	0.92	0.32	0.36	0.24	0.29	0.53
Ir (ppb)	<1.2	<1.4	<2	<1.6	<1.2	<1.1	<1.3	<0.9	<1.4
Au (ppb)	<1.5	<2.0	<2.1	2.0	<1.6	<1.7	<1.9	<1.6	<1.9
Th	5.66	8.85	13.9	7.52	6.49	6.12	5.01	7.37	9.93
U	0.65	0.80	1.33	1.02	0.75	0.92	0.53	0.68	0.97

TABLE 7. ELEMENTAL ABUNDANCES. LAKE BROWNWORTH.

Data from Bishop et al., 2014.

elements (ppm)	JB670 LBR-1 ss	JB671 LBR-2 ss	JB672 LBR-3 ss	JB673 LBR-4 edge
SiO_2 %	69.24	67.4	58.21	57.31
Al_2O_3 %	12.88	11.95	14.14	13.62
Fe_2O_3 %	3.64	5.11	7.63	7.11
MgO %	3.13	4.37	3.34	6.27
CaO %	4.62	5.71	6.39	6.54
Na_2O %	2.67	2.19	3.68	2.81
K_2O %	2.31	1.82	2.13	2.10
TiO_2 %	0.29	0.40	0.69	1.16
P_2O_5 %	0.07	0.08	0.83	0.25
MnO %	0.06	0.09	0.39	0.13
Cr_2O_3 %	0.014	0.024	0.550	0.031
Co	15.6	14.2	15.6	20.6
Ni	39.76	30.26	37.03	50.46
Zn	49	55	45.0	56.3
Ga	4.8	3.9	4	2
As	<1.8	<1.9	<1	<0.6
Se	<1	<1	<0.7	0.98
Br	0.4	0.5	0.5	0.4
Rb	89.2	114	78.8	62.5
Sr	151	170	259	202

Y	13	15	13	17
Zr	131	152	107	105
Nb	6	6	5	8
Sb	0.05	<0.2	<0.1	<0.1
Cs	1.43	1.90	1.33	1.24
Ba	399	485	348	280
La	18.3	20.6	13.7	19.2
Ce	32.9	35.5	25.4	34.5
Nd	12.6	13.8	10.9	13
Sm	2.82	3.18	2.28	3.02
Eu	0.81	0.96	0.82	0.78
Gd	2.81	3.19	2.48	3.6
Tb	0.42	0.46	0.36	0.49
Tm	0.18	0.25	0.19	0.22
Yb	1.14	1.52	1.14	1.48
Lu	0.19	0.22	0.19	0.23
Hf	2.54	3.10	2.37	2.57
Ta	0.50	0.60	0.42	0.60
Ir (ppb)	<1.0	<1.0	<1.1	<1.2
Au (ppb)	6.3	<1.9	0.6	<0.2
Th	8.80	8.88	3.95	5.88
U	0.89	0.96	0.64	0.95

TABLE 8. ELEMENTAL ABUNDANCES. LAKE HOARE, CORE A.

Data from Bishop et al., 1996.

	A-1	A-2	A-3	A-4	A-5	A-5a	A-6
Depth (cm)	0-1	0-3.2	3.2-4.5	4.5-7	7-10	10-12.7	12-12.7

elements (ppm)							
Na %	1.25	1.60	1.75	1.98	1.85	2.10	1.56
K %	1.95	1.89	1.63	1.66	1.66	1.82	1.53
Sc	14.30	14.20	12.70	17.40	12.50	15.00	16.50
Cr	92.00	120.00	110.00	150.00	130.00	130.00	130.00
Mn %	0.09	0.06	0.05	0.06	0.06	0.05	0.07
Fe %	5.81	4.29	3.10	3.68	3.51	3.45	4.07
Co	14.50	11.80	9.10	11.80	10.70	10.60	12.10
Zn	38.00	7.00	3.00	3.00	35.00	8.00	9.00
As	1.09	1.42	0.80	1.59	1.10	1.16	0.74
Rb	123.00	111.00	87.00	83.00	87.00	90.00	88.00
Sr	1400.00	1700.00	1200.00	980.00	1200.00	1200.00	1600.00
Zr	170.00	200.00	89.00	250.00	160.00	150.00	160.00
Sb	0.86	0.50	0.48	0.69	0.69	0.56	0.49
Cs	3.50	2.00	1.30	1.30	1.30	1.40	1.90
Ba	300.00	300.00	280.00	240.00	230.00	260.00	250.00
La	34.00	24.00	18.00	24.00	15.00	23.00	21.00
Ce	71.80	49.80	36.20	46.50	30.20	45.50	40.40
Nd	30.00	20.00	16.00	21.00	19.00	16.00	16.00
Sm	5.18	4.19	2.81	3.11	2.79	3.10	3.58
Eu	1.40	1.30	1.00	1.00	0.90	1.00	1.00
Tb	0.80	0.60	0.50	0.60	0.50	0.50	0.50
Dy	4.40	3.40	2.70	3.60	2.60	3.10	3.20
Yb	1.90	1.80	1.20	1.40	1.40	1.40	1.70
Lu	0.25	0.25	0.18	0.22	0.22	0.20	0.26
Hf	4.32	3.47	2.44	2.35	2.25	2.64	2.79
Ta	2.06	1.22	0.69	0.55	0.63	0.68	0.89

Y	<2	<1	<1	<1.5	<1.5	1.13	<1.5
Au (ppb)	5.00	5.00	0.30	2.00	2.00	1.00	3.00
Th	7.08	5.38	3.82	5.64	3.10	5.78	3.93
U	1.44	1.16	0.57	0.62	0.92	1.01	0.62

TABLE 9. ELEMENTAL ABUNDANCES. LAKE HOARE, CORE B.

Data from Bishop et al., 1996.

	B-1a	B-2a	B-2	B-4	B-5	B-6	B-7	B-8	B-9	B-10	B-11
Depth (cm)	0	2	6	8.5	10	12	13	17	18	20	24
elements (ppm)											
SiO_2 %		52.98	62.68	63.41	61.55	63.64	63.50	63.51	64.00	61.12	64.15
TiO_2 %		0.58	0.48	0.42	0.45	0.44	0.43	0.46	0.48	0.48	0.42
Al_2O_3 %		11.50	12.37	12.12	12.13	12.76	12.99	11.87	13.89	12.46	13.65
Fe_2O_3 %	6.99	5.87	5.66	5.60	5.05	5.31	4.98	5.99	4.99	5.49	4.88
FeO %		5.28	5.09	5.04	4.54	4.78	4.48	5.39	4.49	4.94	4.39
MgO %		5.02	6.31	6.21	5.31	5.33	5.15	6.59	4.81	5.66	4.98
CaO %		9.63	6.33	6.20	6.99	5.39	5.79	5.82	5.27	6.42	5.21
Na_2O %	1.71	2.25	2.63	2.76	2.53	3.02	2.95	2.53	3.04	2.47	3.05
K_2O %	2.16	2.03	1.89	2.02	2.08	2.17	2.24	1.93	2.27	2.07	2.34
P_2O_5 %		0.18	0.15	0.14	0.15	0.15	0.15	0.14	0.16	0.15	0.14
C %	3.5	2.20	0.25	6.74	7.30	6.49	0.48	4.89	8.35	0.09	5.66
Sc	14.9	17.10	20.80	12.80	9.60	16.00	23.40	13.80	8.17	21.50	20.00
Cr	107	138.00	182.00	97.00	82.00	135.00	222.00	104.00	63.00	189.00	141.00
Co	29.1	24.50	26.70	23.30	14.30	27.10	29.50	21.40	13.00	28.10	25.80
Ni	75	71.00	94.00	63.00	21.00	61.00	61.00	51.00	31.00	70.00	159.00
Zn	101	74.00	57.00	82.00	42.00	85.00	72.00	65.00	48.00	69.00	87.00
Ga	10	14.00	21.00	19.00	9.00	22.00	63.00	33.00	9.00	n.d.	16.00
As	2.22	0.75	<0.4	1.07	0.33	1.00	0.30	0.89	0.82	n.d.	1.02

Se	7.8	1.20	0.60	1.80	0.60	1.60	0.80	2.00	1.40	1.00	1.90
Br	41.4	13.40	0.70	60.90	32.60	75.10	1.10	25.00	22.90	<10	41.90
Rb	95.6	71.30	68.20	70.70	42.80	74.70	80.60	81.00	50.70	29.50	82.10
Sr	406	360.00	259.00	318.00	331.00	342.00	367.00	276.00	372.00	380.00	326.00
Zr	102	126.00	76.00	82.00	94.00	71.00	100.00	81.00	101.00	145.00	90.00
Ag	0.122	0.02	0.06	<0.14	0.04	<0.2	0.01	<0.1	0.04	<0.09	0.04
Sb	0.39	0.08	0.09	0.08	0.04	<0.25	0.06	0.07	<0.118	0.14	0.14
Cs	2.51	1.54	0.81	1.85	0.81	2.09	1.02	1.62	1.12	0.99	1.40
Ba	300	271.00	235.00	218.00	151.00	247.00	332.00	238.00	157.00	333.00	268.00
La	31.4	24.50	16.00	22.10	13.70	29.80	22.10	28.50	22.20	25.60	57.60
Ce	64.6	44.30	32.00	49.40	24.20	55.40	41.90	57.30	35.80	42.80	58.10
Nd	27.4	19.70	14.40	22.90	10.30	21.40	17.60	22.30	15.10	18.90	57.60
Sm	4.72	3.73	2.92	4.59	2.11	3.85	3.32	4..07	2.62	3.48	9.74
Eu	1.18	1.00	0.89	0.98	0.52	0.88	0.93	0.87	0.60	1.05	2.01
Tb	0.53	0.54	0.42	0.49	0.30	0.40	0.51	0.44	0.35	0.50	0.95
Tm	0.2	0.20	0.20	0.20	0.10	0.20	0.20	0.20	0.20	0.20	0.40
Yb	1.32	1.37	1.39	1.55	0.89	1.32	1.44	1.25	0.89	1.63	2.33
Lu	0.17	0.20	0.20	0.23	0.13	0.19	0.21	0.19	0.12	0.24	0.32
Hf	2.85	2.40	2.42	2.51	1.36	1.84	2.11	1.97	1.46	2.38	3.21
Ta	1.18	0.74	0.35	0.95	0.32	0.59	0.48	0.85	0.42	0.44	0.56
W	1.5	0.90	1.10	1.80	0.50	2.80	1.30	1.50	0.90	n.d.	0.20
Au (ppb)	2.3	0.10	0.20	0.30	0.10	0.70	0.40	0.70	0.70	n.d.	2.30
Hg	<0.1	0.17	<0.1	0.25	0.51	0.81	<0.1	<0.1	0.62	<0.1	0.86
Th	6.8	4.99	3.58	5.21	5.76	6.50	4.83	4.66	5.45	5.03	4.20
U	1.06	0.79	0.38	0.85	1.06	1.38	0.48	1.20	1.07	0.13	0.42

TABLE 10. ELEMENTAL ABUNDANCES. LAKE HOARE, CORE C.

Data from Bishop et al., 1996.

	C-1	C-2c	C-3	C-4b	C-5	C-6c	C-7a	C-10
Depth (cm)	2	4	7	9	12	15	16	26
elements (ppm)								

SiO_2 %	59.99	62.47	63.22	63.35	63.96	61.43	63.25	60.78
TiO_2 %	0.60	0.45	0.43	0.41	0.45	0.44	0.49	0.52
Al_2O_3 %	12.75	12.08	12.29	12.09	14.00	12.62	11.50	10.97
Fe_2O_3 %	6.17	5.71	5.76	6.01	4.84	5.38	6.38	7.78
FeO %	5.55	5.14	5.18	5.41	4.36	4.84	5.74	7.00
MnO %	0.09	0.09	0.09	0.09	0.08	0.09	0.09	0.10
MgO %	5.49	6.06	5.59	5.94	4.90	5.44	6.99	7.82
CaO %	5.46	5.57	5.41	5.49	4.90	5.33	5.55	6.57
Na_2O %	2.75	2.53	2.69	2.74	3.47	2.97	2.68	2.47
K_2O %	2.12	2.02	2.17	2.01	2.36	2.13	1.98	1.72
P_2O_5 %	0.19	0.14	0.15	0.14	0.16	0.17	0.15	0.13
C %	1.01	0.45	0.23	0.47	0.14	1.13	0.13	0.13
Sc	20.90	21.90	22.60	24.40	16.00	21.90	23.80	31.20
Cr	187.00	208.00	215.00	228.00	161.00	198.00	238.00	289.00
Co	31.20	28.80	29.20	33.50	23.90	29.10	32.20	42.70
Ni	110.00	55.00	120.00	127.00	128.00	64.00	99.00	118.00
Zn	91.00	81.00	77.00	87.00	68.00	86.00	101.00	105.00
Ga	23.00	9.00	9.00	12.00	18.00	12.00	5.00	15.00
As	1.42	0.95	0.64	0.19	0.72	0.38	0.92	0.54
Sc	1.60	1.10	0.60	0.40	0.70	1.00	0.80	0.70
Br	2.50	1.40	1.90	5.10	0.80	11.10	0.90	0.40
Rb	88.10	70.80	75.50	75.10	89.20	108.20	76.80	58.50
Sr	408.00	296.00	307.00	331.00	386.00	402.00	290.00	263.00
Zr	103.00	99.00	66.00	74.00	85.00	85.00	92.00	92.00
Ag	0.14	0.32	0.09	<0.14	0.09	<0.14	0.08	<0.16
Sb	0.08	0.08	0.05	0.03	0.12	0.06	0.07	0.07
Cs	1.35	1.02	0.91	1.01	1.11	1.27	1.01	0.68
Ba	350.00	301.00	312.00	316.00	338.00	358.00	279.00	248.00

La	21.40	22.00	24.20	28.70	21.50	18.60	18.90	22.40
Ce	44.50	42.60	46.00	54.70	39.60	36.90	36.70	43.80
Nd	20.60	16.70	16.80	18.70	16.70	15.20	16.70	17.60
Sm	3.27	2.98	3.11	3.45	2.97	3.51	3.16	3.51
Eu	1.06	0.92	0.92	0.98	1.05	1.02	0.92	0.86
Tb	0.62	0.44	0.47	0.59	0.43	0.51	0.48	0.54
Tm	0.30	0.20	0.20	0.30	0.20	0.30	0.20	0.30
Yb	1.67	1.45	1.59	1.77	1.41	1.66	1.68	1.83
Lu	0.25	0.21	0.22	0.24	0.21	0.25	0.25	0.28
Hf	2.94	1.98	1.91	2.62	2.74	2.53	2.86	3.06
Ta	1.04	0.62	0.56	0.65	0.63	0.69	0.62	0.71
W	0.80	0.70	0.60	0.50	0.90	0.50	0.60	0.80
Au (ppb)	<2	0.90	0.60	<4	<2	0.20	2.00	<2
Hg	1.81	0.09	0.29	0.29	0.04	0.92	0.56	0.39
Th	5.27	5.60	4.94	8.15	4.60	5.41	4.66	5.53
U	1.88	1.02	0.55	0.63	0.84	1.96	1.52	1.33

TABLE 11. ELEMENTAL ABUNDANCES. LAKE HOARE, CORE D.

Data from Bishop et al., 1996.

	Surface	D-1	D-2	D-4	D-5
Depth (cm)	Surface Sand	0-1	5-6	14-16	21-23
elements (ppm)					

SiO_2 %	64.39	58.97	63.92	64.58	62.84
TiO_2 %	0.4	0.69	0.47	0.47	0.44
Al_2O_3 %	13.63	14.05	13.18	15.39	11.66
Fe_2O_3 %	4.78	6.09	5.13	3.82	6.54
FeO %	4.30	5.47	4.61	3.43	5.88
MnO %	0.08	0.09	0.08	0.08	0.09
MgO %	5.1	4.46	5.01	3.2	7.19
CaO %	4.91	6.34	5.32	4.42	6.03
Na_2O %	3.35	2.84	2.89	3.71	2.69
K_2O %	2.35	2.46	2.17	2.69	1.76
P_2O_5 %	0.15	0.17	0.16	0.17	0.13
C %	0.08	0.7	0.25	0.12	0.07
Sc	17.3	16.1	18.4	9.8	27.7
Cr	169	120	174	93	254
Co	24.5	24.8	24.6	16	35.6
Ni	100	45	79	46	117
Zn	68	91	76	52	75
Ga	15	16	16	15	13
As	0.28	0.54	0.56	0.4	0.44
Se	0.8	1.3	0.9	0.9	1.1
Br	0.4	3.8	1.6	0.7	0.6
Rb	92.8	107	74.9	100.7	71.5
Sr	383	392	354	498	334
Zr	81	108	72	113	115
Ag	<0.12	0.07	0.02	<0.09	<0.13
Sb	0.05	0.1	0.12	0.2	0.07
Cs	1.17	1.84	1.11	1.33	0.94
Ba	358	404	338	389	286

La	24.3	34	17.3	18.3	23.8
Ce	46.1	64.7	34.6	30.5	46.3
Nd	19.9	27	13.1	15.2	19.9
Sm	3.03	4.78	2.88	2.77	3.8
Eu	1.05	1.27	0.98	1.14	1.02
Tb	0.47	0.64	0.53	0.38	0.53
Tm	0.2	0.3	0.2	0.2	0.3
Yb	1.3	1.74	1.5	1.19	1.78
Lu	0.2	0.26	0.22	0.17	0.28
Hf	2.8	2.89	2.24	3.06	2.57
Ta	0.52	1.12	0.6	0.68	0.7
W	0.4	1.2	0.7	0.3	0.4
Au (ppb)	1.6	0.3	1	0.4	<2
Hg	0.6	0.19	0.05	<0.1	0.32
Th	6.36	8.04	4.15	3.79	5.24
U	0.72	1.1	0.57	0.94	0.73

TABLE 12. ELEMENTAL ABUNDANCES. LAKE HOARE, CORE E.

Data from Bishop et al., 2001.

	E-2	E-3	E-4	E-5	E-6	E-7	E-8	E-9	E-10
Depth (cm)	1-3	3-5	5-16	16-20	20-24	24-30	30-34	34-38	39-47
elements (ppm)									
SiO_2 %	55.4	26.4	59.4	60.8	64.1	64.4	60	61.5	62.3
TiO_2 %	0.43	0.31	0.55	0.53	0.44	0.58	0.61	0.62	0.5

Al_2O_3 %	13.2	5.5	15.1	15.3	14.1	14.2	15.2	15.3	15.8
Fe_2O_3 %	0.9	1.2	1	0.8	0.8	1	1.1	0.9	1.2
FeO %	3.2	1	3.7	3.9	3.4	3.7	3.8	4.5	3.1
MnO %	0.07	0.03	0.09	0.09	0.08	0.09	0.09	0.10	0.08
MgO %	3.2	1.8	3.9	4.1	3.4	3.9	4.2	3.9	3.4
CaO %	12.3	32.8	7.8	6.4	5.4	4.9	6.4	6	5.5
Na_2O %	2.5	0.9	2.8	3	3.4	3.1	2.9	2.9	3.4
K_2O %	2.4	1.1	2.6	2.6	2.4	2.5	2.7	3	2.7
P_2O_5 %	0.14	0.17	0.15	0.14	0.13	0.16	0.17	0.13	0.15
S %	0.03	0.11	0.04	0.04	0.01	0.02	0.05	0.04	0.05
SO_3 %	0.08	0.28	0.10	0.10	0.03	0.04	0.12	0.10	0.11
CO_2 %	3.81	23.20	1.24	0.43	0.52	0.04	0.72	0.04	0.34
$CaSO_4$ %	0.14	0.48	0.18	0.17	0.05	0.07	0.21	0.17	0.19
K_2SO_4 %	0.17	0.61	0.23	0.22	0.06	0.09	0.27	0.22	0.24
Na_2SO_4 %	0.14	0.50	0.19	0.18	0.05	0.07	0.22	0.18	0.20
$CaCO_3$ %	13.03	49.61	5.00	2.50	0.71		2.50	1.78	0.89
Th	7		10	15	11	13	n.d.	10	11
Zr	112	71	123	121	104	120	134	122	142
Cu	14	22	16	15	14	14	15	14	14
Zn	28	15	31	37	47	51	36	35	30

TABLE 13. ELEMENTAL ABUNDANCES. LAKE HOARE, CORE H.

Data from Bishop et al., 2001.

	H-3	H-4	H-5	H-6	H-7	H-8	H-9	H-10
Depth (cm)	7-13	13-20	20-21	21-25	25-29	29-34	34-36	36-38
elements (ppm)								

SiO_2 %	59.70	60.70	63.90	62.30	58.80	59.40	59.50	60.10
TiO_2 %	0.51	0.61	0.50	0.48	0.75	0.73	0.73	0.68
Al_2O_3 %	14.30	14.90	13.80	14.60	13.00	13.60	12.90	13.10
Fe_2O_3 %	0.90	2.10	0.80	0.70	0.60	3.40	0.80	0.40
FeO %	5.50	3.70	4.20	4.10	6.40	6.20	6.20	6.10
MnO %	0.09	0.10	0.09	0.09	0.13	0.13	0.13	0.12
MgO %	3.80	4.30	4.40	4.00	5.90	5.90	6.40	5.90
CaO %	4.60	5.50	4.90	6.10	7.30	6.70	7.20	6.80
Na_2O %	2.80	2.80	2.60	3.00	2.80	2.50	2.50	2.70
K_2O %	2.40	2.50	2.20	2.40	2.10	2.10	2.00	2.10
P_2O_5 %	0.18	0.17	0.16	0.13	0.18	0.16	0.17	0.18
S_{insol} %	2.56	0.47	0.28	0.13	0.16	0.09	0.07	0.09
SO_3 %	5.04	2.30	2.25	1.30	2.02	1.10	0.65	1.05
$CaSO_4$ %	8.58	3.91	3.82	2.21	3.44	1.87	1.10	1.78
K_2SO_4 %	10.98	5.00	4.89	2.83	4.40	2.39	1.41	2.28
Na_2SO_4 %	8.95	4.08	3.99	2.30	3.59	1.95	1.15	1.86
Th	2.00	11.00	n.d.	6.00	8.00	14.00	6.00	10.00
Zr	90.00	117.00	105.00	111.00	137.00	132.00	140.00	122.00
Cu	26.00	20.00	21.00	16.00	17.00	18.00	13.00	17.00
Zn	27.00	34.00	28.00	30.00	44.00	44.00	44.00	41.00

APPENDIX B, COMPLETE DATASET OF MCMURDO DRY VALLEY SAMPLES: SOLUBLE ANIONS

TABLE 14. SOLUBLE ANIONS. CORE 2074 (JB1124-JB1126) AND CORE 33 (JB1129-1133).

	JB1126	JB1124	JB1125	JB1129	JB1130	JB1131	JB1132	JB1133
Depth (cm)	0	2	10	0-1	3-4	8-10	12-14	16-20
elements (ppm)								
F^-		9.71	9.12	11.16	11.13	20.55	20.96	38.7
Cl^-	71527	27508	10889	29715	8239	5741	5888	12470
SO_4^{2-}	16002	41566	44569	4020	6365	44533	1312	216
NO_3^-	n.d.	n.d.	n.d.	n.d.	n.d.	n.d.	290	229

TABLE 15. SOLUBLE ANIONS. CORE 39 (JB1134-JB1138) AND CORE 42 (JB1100-1105).

	JB1134	JB1135	JB1136	JB1137	JB1138	JB1100	JB1101	JB1102	JB1103	JB1104	JB1105
Depth (cm)	0-1	2-5	6-8	10-12	15-16	0-1	1-4	4-7	8-10	12-15	20-24
elements (ppm)											
F^-	25.67	13.92	13.18	14.99	24.23	16.7	18.56	16.65	50.75	27.74	23.48
Cl^-	9709	39367	17520	1798	1385	17076	11953	n.d.	8680	10462	8673
NO_3^-	274	n.d.	n.d.	n.d.	n.d.	6455	3703	1446	n.d.	4822	3917
SO_4^{2-}	624	7794	9088	650	n.d.	7398	1304	590	44382	19851	5064

TABLE 16. SOLUBLE ANIONS. CORE 52.

	JB1107	JB1108	JB1109	JB1110
Depth (cm)	0-1	2-4	4-8	16-20
elements (ppm)				
F^-	10.58	23.62	80.41	35.46
Cl^-	4716	1779	9.31	1551
NO_3^-	3497	n.d.	n.d.	n.d.
SO_4^{2-}	5002	20728	52114	33055

TABLE 17. SOLUBLE ANIONS. CORE 72.

	JB1087	JB1088	JB1089	JB1090	JB1091	JB1092	JB1093	JB1094	JB1095	JB1096
Depth (cm)	0-1	0-2	2-4	4-6	6-8	8-12	12-16	24-28	32-36	44-48
elements (ppm)										
F^-	54.72	56.09	n.d.	37.73	50.08	28.12	n.d.	44.2	n.d.	n.d.
Cl^-	7328	5808	75342	39087	34347	27108	15407	5096	2399	3332
NO_3^-	n.d.	n.d.	11923	18149	8892	16413	10384	3128	2844	2708
SO_4^{2-}	20258	22621	68412	13890	15124	7184	4266	1141	1164	1324

APPENDIX C, COMPLETE DATASET OF SOURCE ROCKS: ELEMENTAL ABUNDANCES, CIA, AND Al_2O_3/TiO_2.

TABLE 18. ELEMENTAL ABUNDANCES. MCMURDO DRY VALLEY SOURCE ROCKS.

Data from Palmer, 1987; Roser, Korsch, and Pyne, unpubl. data; Grapes et al., 1989; Allibone et al., 1993a.

elements (ppm)	Bsmt Grtd	Beacon SS	Frar Dol	Bon Ptor	Vhal Pton	Bwth Pton
SiO_2 %	65.25	89.73	57.17	65.26	72.17	72.38
TiO_2 %	0.72	0.24	0.83	0.66	0.21	0.25
Al_2O_3 %	16.14	5.70	15.83	16.16	14.88	13.91
Fe_2O_3 %	4.88	1.38	8.46	1.05	0.50	n.d.
FeO %	4.39	1.24	7.61	0.94	0.45	n.d.
MnO %	0.07	0.02	0.11	0.05	0.03	0.02
MgO %	1.56	0.58	4.88	1.54	0.38	0.36
CaO %	3.88	0.68	8.67	3.89	2.20	1.92
Na_2O %	3.63	0.20	2.65	3.26	3.51	2.72
K_2O %	3.69	1.44	1.28	3.83	4.37	4.64
P_2O_5 %	0.17	0.02	0.11	0.17	0.04	0.05
La	174.39	32.70	51.77	133.74	93.55	171.66
Ce	120.17	21.94	31.35	97.00	88.12	127.48
Cr	15	18	96	13.1	4.5	8
Cu	3	17	103	4.8	1.66	1
Th	21	6	5	15.5	6.33	12
Zr	222	142	142	192.75	133.66	324
Zn	73	28	84	68.75	44	73

APPENDIX D, COMPLETE DATA SET OF MCMURDO DRY VALLEY SAMPLES AND SOURCE ROCKS: CIA, MODIFIED CIA, Al_2O_3/TiO_2

TABLE 19. Al_2O_3/TiO_2 (MOLAR), CIA AND SULFATE MODIFIED CIA VALUES. CORE 33 (JB1129-JB1133) AND CORE 39 (JB1134-1138).

	JB1129	JB1130	JB1131	JB1132	JB1133	JB1134	JB1135	JB1136	JB1137	JB1138
Depth (cm)	0-1	3-4	8-10	12-14	16-20	0-1	2-5	6-8	10-12	15-16
Al_2O_3/TiO_2	21.48	20.93	24.24	20.00	22.12	15.41	16.44	22.75	22.09	20.69
CIA	34.96	38.25	35.09	37.63	40.28	39.25	31.02	39.36	43.54	44.49
SO_4^{2-} Mod	37.73	45.23	83.25	58.25	41.47	39.25	36.35	48.20	44.29	44.49

TABLE 20. Al_2O_3/TiO_2 (MOLAR), CIA AND SULFATE MODIFIED CIA VALUES. CORE 42 (JB1100-JB1105) AND CORE 52 (JB1107-1110).

	JB1100	JB1101	JB1102	JB1103	JB1104	JB1105	JB1107	JB1108	JB1109	JB1110
Depth (cm)	0-1	1-4	4-7	8-10	12-15	20-24	0-1	2-4	4-8	16-20
Al_2O_3/TiO_2	22.59	23.35	24.42	18.56	17.49	20.65	18.65	19.45	20.15	20.35
CIA	37.19	38.99	48.20	26.87	33.24	36.46	39.73	37.88	28.00	36.16
SO_4^{2-} Mod	37.20	39.53	50.47	100.00	67.16	57.07	47.13	66.37	100.00	76.29

TABLE 21. Al_2O_3/TiO_2 (MOLAR), CIA AND SULFATE MODIFIED CIA VALUES. CORE 72.

	JB1087	JB1088	JB1089	JB1090	JB1091	JB1092	JB1093	JB1094	JB1095	JB1096
Depth (cm)	0-1	0-2	2-4	4-6	6-8	8-12	12-16	24-28	32-36	44-48
Al_2O_3/TiO_2	18.47	18.82	23.13	21.47	22.26	21.89	21.58	21.53	22.20	23.25
CIA	37.44	37.00	21.26	31.44	32.24	36.09	37.36	40.29	40.86	40.82
SO_4^{2-} Mod	68.24	62.25	36.60	40.56	39.79	40.57	40.69	41.09	41.96	41.61

TABLE 22. Al_2O_3/TiO_2 (MOLAR), CIA AND SULFATE MODIFIED CIA VALUES. LAKE FRYXELL.

	JB650	JB651	JB652	JB653	JB654	JB655	JB656	JB657	JB658	JB659	JB660
	LFR-A	LFR-1	LFR-2	LFR-3	LFR-4	LFR-5	LFR-6	LFR-7	LFR-8	LFR-9	LFR-10
Sample Type	SS	Edge	Edge	Edge	Edge	Edge	SS	SS	SS	SS	SS
Al_2O_3/TiO_2	13.65	5.90	7.59	11.46	10.04	8.74	17.34	15.71	16.24	15.12	8.92
CIA	43.63	39.36	40.88	42.70	41.64	40.58	42.41	42.23	43.51	43.23	40.90
SO_4^{2-} Mod	69.26	40.12	42.21	43.80	42.71	41.40	43.32	42.83	44.11	44.44	42.00

TABLE 23. Al_2O_3/TiO_2 (MOLAR), CIA AND SULFATE MODIFIED CIA VALUES. LAKE VANDA.

	JB661	JB662	JB663	JB664	JB665	JB666	JB667	JB668	JB669
	LVA-1	LVA-2	LVA-3	LVA-4	LVA-5	LVA-6	LVA-7	LVA-8	LVA-9
Sample Type	Edge	Edge	Edge	Edge	SS	SS	SS	SS	Edge
Al_2O_3/TiO_2	20.55	16.23	3.86	4.64	21.90	24.96	27.30	28.54	14.08
CIA	40.58	40.72	34.08	35.04	41.67	42.43	42.45	43.42	39.03
SO_4^{2-} Mod	41.42	43.16	35.04	35.69	42.47	43.32	43.34	43.87	39.34

TABLE 24. Al_2O_3/TiO_2 (MOLAR), CIA AND SULFATE MODIFIED CIA VALUES. LAKE BROWNWORTH.

	JB670	JB671	JB672	JB673
	LBR-1	LBR-2	LBR-3	LBR-4
Sample Type	SS	SS	SS	Edge
Al_2O_3/TiO_2	34.81	23.41	16.06	9.20
CIA	45.72	42.82	41.44	42.03
SO_4^{2-} Mod	46.06	43.15	42.22	43.43

TABLE 25. Al_2O_3/TiO_2 (MOLAR), CIA AND CALCITE MODIFIED CIA VALUES. LAKE HOARE, CORE B.

	B-2a	B-2	B-4	B-5	B-6	B-7	B-8	B-9	B-10	B-11
Depth (cm)	2	6	8.5	10	12	13	17	18	20	24
Al_2O_3/TiO_2	15.54	20.20	22.62	21.13	22.73	23.68	20.22	22.68	20.34	25.47
CIA	32.94	40.89	40.24	38.81	42.71	42.18	41.35	44.91	40.94	44.50
$CaCO_3$ Mod	44.54	58.46	57.64	54.73	61.39	59.85	60.52	63.60	58.37	63.25

TABLE 26. Al_2O_3/TiO_2 (MOLAR), CIA AND CALCITE MODIFIED CIA VALUES. LAKE HOARE, CORE C.

	C-1	C-2c	C-3	C-4b	C-5	C-6c	C-7a	C-10
Depth (cm)	2	4	7	9	12	15	16	26
Al_2O_3/TiO_2	16.65	21.04	22.40	23.11	24.38	22.48	18.39	16.53
CIA	43.23	42.30	42.52	42.04	44.91	42.78	40.86	38.04
$CaCO_3$ Mod	57.69	55.89	56.27	58.03	44.91	55.66	59.08	57.18

TABLE 27. Al_2O_3/TiO_2 (MOLAR), CIA AND CALCITE MODIFIED CIA VALUES. LAKE HOARE, CORE D.

	Surface	D-1	D-2	D-4	D-5
Depth (cm)	Surface Sand	0-1	5-6	14-16	21-23
Al_2O_3/TiO_2	20.77	26.70	15.96	21.98	25.66
CIA	44.52	42.69	44.00	47.44	40.27
$CaCO_3$ Mod	44.52	58.98	63.17	47.44	58.70

TABLE 28. Al_2O_3/TiO_2 (MOLAR), CIA AND SULFATE, CALCITE MODIFIED CIA VALUES. LAKE HOARE, CORE E.

	E-2	E-3	E-4	E-5	E-6	E-7	E-8	E-9	E-10
Depth (cm)	1-3	3-5	5-16	16-20	20-24	24-30	30-34	34-38	39-47
Al_2O_3/TiO_2	24.06	13.90	21.52	22.62	25.11	19.19	19.53	19.34	24.76
CIA	31.22	8.11	41.14	44.11	43.91	45.93	44.02	44.70	46.04
SO_4^{2-} Mod	31.73	8.40	42.15	45.20	44.23	46.43	45.36	45.82	47.34
$CaCO_3$ Mod	40.29	82.14	68.74	67.93	63.67	46.25	68.32	67.13	66.60

TABLE 29. Al_2O_3/TiO_2 (MOLAR), CIA AND SULFATE, CALCITE MODIFIED CIA VALUES. LAKE HOARE, CORE H.

	H-3	H-4	H-5	H-6	H-7	H-8	H-9	H-10
Depth (cm)	7-13	13-20	20-21	21-25	25-29	29-34	34-36	36-38
Al_2O_3/TiO_2	21.97	19.14	21.63	23.84	13.58	14.60	13.85	15.10
CIA	47.88	46.26	46.99	43.94	39.21	42.28	39.98	40.71
SO_4^{2-} Mod	100.00	83.72	87.56	63.97	64.94	58.39	48.07	55.50
$CaCO_3$ Mod	47.88	64.44	46.99	60.50	54.03	58.93	60.93	66.01

TABLE 30. Al_2O_3/TiO_2 (MOLAR), CIA AND SULFATE, CALCITE MODIFIED CIA VALUES. MCMURDO DRY VALLEY SOURCE ROCKS.

	Bsmt Grtd	Beacon SS	Frar Dol	Bon Pton	Vhal Pton	Bwth Pton
CIA	48.67	64.60	42.40	49.36	50.64	51.71
$(Al_2O_3/TiO_2)_{molar}$	17.57	18.61	14.95	19.19	55.53	43.61

APPENDIX E, COMPLETE DATASET OF MARS ROVER ANALOG SAMPLES: ELEMENTAL ABUNDANCES

TABLE 31. ELEMENTAL ABUNDANCES (WT %) OF MARS ANALOG SAMPLES. SPIRIT ROVER.

Data from Planetary Data System Geosciences Node.

Name	Na_2O	MgO	Al_2O_3	SiO_2	P_2O_5	SO_3	K_2O	CaO	TiO_2	Cr_2O_3	MnO	FeO
Adirondack_asis	2.32	9.09	10.93	45.6	0.72	3.47	0.14	7.52	0.71	0.69	0.40	18.0
Adirondack_brush	2.78	9.51	11.35	45.7	0.57	2.16	0.12	7.84	0.49	0.63	0.39	18.0
Adirondack_RAT	2.41	10.83	10.87	45.7	0.52	1.23	0.07	7.75	0.48	0.61	0.41	18.8
Humphrey_Ashley_asis	3.00	8.76	10.66	45.9	0.65	3.53	0.19	7.53	0.48	0.57	0.40	17.7
Humphrey_Heyworth_asis	2.92	8.69	11.13	45.7	0.63	3.24	0.19	7.54	0.53	0.61	0.39	17.9
Humphrey_brush	2.95	8.82	11.20	45.9	0.62	2.63	0.18	7.76	0.54	0.60	0.39	17.9
Humphrey_RAT1	2.76	9.49	10.78	46.3	0.57	1.09	0.13	8.19	0.58	0.68	0.41	18.6
Humphrey_RAT2	2.54	10.41	10.68	45.9	0.56	1.28	0.10	7.84	0.55	0.60	0.41	18.8
Mazatzal_NewYork_RAT1Oregon_Asis	2.74	9.02	9.92	45.7	0.82	3.33	0.29	7.57	0.69	0.45	0.40	18.4
Mazatzal_Brooklyn_RAT2	2.78	9.72	10.70	45.8	0.65	1.48	0.16	8.02	0.59	0.54	0.42	18.9
Route66_brushed	2.88	8.67	10.78	44.8	0.74	4.20	0.23	7.83	0.59	0.53	0.39	17.7
Boroughs_Hellskitchen_side	2.53	10.48	7.85	39.25	0.80	14.06	0.36	5.76	0.85	0.39	0.34	16.50
Mojave_Joshua_Asis	3.07	9.38	10.36	44.8	0.53	3.47	0.20	7.39	0.57	0.53	0.37	18.7
Wishstone_chisel_RAT	4.98	4.50	15.03	43.8	5.19	2.20	0.57	8.89	2.59	0.00	0.22	11.6
champagne_brush	5.30	4.56	15.75	45.8	2.64	2.50	0.51	6.59	2.84	0.00	0.22	12.6
champagne_RAT1	5.04	3.94	14.86	43.4	5.07	1.94	0.53	8.78	2.99	0.00	0.24	12.5
champagne_RAT2	5.02	3.98	14.83	43.5	5.05	1.96	0.53	8.75	2.96	0.00	0.25	12.5
Watchtower_Joker_RAT	2.67	10.00	12.33	42.4	4.50	3.43	0.74	7.44	2.21	0.00	0.22	13.2
Backstay_Scuppers	4.15	8.31	13.25	49.5	1.39	1.52	1.07	6.04	0.93	0.15	0.24	13.0
Backstay_Scurvy	3.83	8.28	12.89	49.4	1.29	2.12	0.96	6.04	0.92	0.17	0.25	13.4
Independence_Penn2_Scuffed	3.18	3.38	18.69	54.9	3.48	2.20	0.52	7.28	1.88	0.04	0.08	3.9

Bourgeosie_Chic.	3.92	5.44	12.26	48.4	3.24	3.50	1.47	8.01	2.38	0.05	0.21	10.2
Irvine	2.68	10.63	8.29	47.0	0.97	2.37	0.68	6.03	1.06	0.20	0.36	19.2
Berkner Island 1	1.98	7.09	6.21	36.93	0.88	22.10	0.28	7.62	0.50	0.43	0.25	15.22
Esperanza_Palma	3.40	8.45	8.40	47.9	0.91	2.36	0.52	5.57	1.05	0.20	0.38	20.2
Home Plate_Humbolt Peak	4.25	9.18	10.11	46.6	1.12	2.13	1.21	6.39	0.84	0.41	0.39	16.7
Home Plate_Humbolt Peak	4.27	9.27	10.16	46.5	1.09	2.12	1.22	6.37	0.83	0.40	0.38	16.7

TABLE 32. ELEMENTAL ABUNDANCES (PPM) OF MARS ANALOG SAMPLES. SPIRIT ROVER.
Data from Planetary Data System Geosciences Node.

Name	Ni	Zn	Br	Cl %
Adirondack_asis	241	242	6	0.43
Adirondack_brush	149	80	16	0.36
Adirondack_RAT	165	81	14	0.20
Humphrey_Ashley_asis	151	159	49	0.58
Humphrey_Heyworth_asis	105	72	39	0.54
Humphrey_brush	158	95	37	0.49
Humphrey_RAT1	202	117	49	0.32
Humphrey_RAT2	164	112	52	0.26
Mazatzal_NewYork_RAT1Oregon_Asis	342	222	144	0.54
Mazatzal_Brooklyn_RAT2	132	75	161	0.23
Route66_brushed	181	125	46	0.55
Boroughs_Hellskitchen_side	438.25	253.35	204.80	0.73
Mojave_Joshua_Asis	97	159	89	0.57
Wishstone_chisel_RAT	67	64	22	0.35
champagne_brush	41	71	38	0.62
champagne_RAT1	24	81	72	0.60
champagne_RAT2	45	58	68	0.60

Watchtower_Joker_RAT	67	140	251	0.80
Backstay_Scuppers	191	269	26	0.35
Backstay_Scurvy	228	274	17	0.44
Independence_Penn2_Scuffed	444	667	24	0.30
Bourgeosie_Chic.	239	132	61	0.83
Irvine	289	230	6	0.45
Berkner Island 1	746.56	191.36	81.66	0.39
Esperanza_Palma	395	368	181	0.47
Home Plate_Humbolt Peak	360	385	29	0.55
Home Plate_Humbolt Peak	333	380	28	0.54

TABLE 33. ELEMENTAL ABUNDANCES (WT %) OF MARS ANALOG SAMPLES. OPPORTUNITY ROVER.
Data from Planetary Data System Geosciences Node.

Name	Na_2O	MgO	Al_2O_3	SiO_2	P_2O_5	SO_3	K_2O	CaO	TiO_2	Cr_2O_3	MnO	FeO
Robert.E	1.56	8.29	7.46	39.6	0.97	19.42	0.57	5.03	0.74	0.19	0.28	15
Guadalupe_asis	1.88	7.95	7.26	40.3	1.01	18.75	0.58	4.92	0.84	0.17	0.3	15.1
McKittrick_RAT	1.67	8	6.2	38.3	0.99	21.31	0.56	4.42	0.81	0.19	0.3	16.5
Last_Chance_Makar_asis	2.09	7.65	7.06	38.4	1	18.91	0.56	4.84	0.7	0.16	0.3	17.4
Mojo2_asis	2.26	7.82	8.39	43	0.98	12.97	0.56	5.98	0.88	0.23	0.29	15.6
Mojo2_RAT	1.64	8.38	6.18	36.3	1.01	23.61	0.59	5.19	0.74	0.2	0.26	15.3
BerryBowl_Empty	2.11	7.86	8.12	42.7	0.97	14.08	0.56	5.51	0.84	0.2	0.34	15.6
RasperryNewton	2.29	8.41	8.34	41.4	1.01	15.19	0.61	5.29	0.84	0.16	0.27	15.1
RealSharksTooth_enamel1_asis	2.16	8.16	6.99	38.3	0.99	18.7	0.52	4.37	0.67	0.17	0.24	17.7
BounceRock_Glanz	1.97	6.56	9.68	48.5	0.99	3.66	0.27	10.93	0.83	0.1	0.42	15.5
BounceRock_Case_Rat	1.66	6.84	10.48	51.6	0.92	0.56	0.11	12.09	0.74	0.11	0.4	14.4
BounceRock_Maggie	2.16	7.65	10.74	47.5	0.88	4.63	0.27	9.83	0.69	0.12	0.37	14.2

LionStone_Leo_asis	1.98	8.03	7.21	39.7	0.98	18.8	0.57	5.11	0.78	0.19	0.29	15.3
LionStone_Numa_RAT	1.72	8.8	6.22	37.2	1.01	22.84	0.58	5.03	0.77	0.18	0.29	14.3
Tenessee_RAT	1.36	8.38	5.87	35	1.03	24.94	0.58	5.03	0.79	0.2	0.32	15.7
Kentucky_asis	0.88	8.04	7.89	43.2	0.8	13.41	0.53	6.34	0.92	0.24	0.24	16.5
Kentucky_Cubble_Hill2_RAT	1.54	9.2	5.9	35.9	1.05	24.38	0.57	4.72	0.71	0.18	0.33	14.7
Virginia_RAT	1.83	9	6.32	36.9	1.07	22.09	0.6	4.43	0.84	0.21	0.39	15.5
Ontario_London_RAT	1.64	9.14	5.99	36.4	1.11	23.71	0.57	4.85	0.74	0.2	0.31	14.5
Grindstone_RAT	1.7	8.38	6.36	38	1.07	21.5	0.58	4.64	0.83	0.19	0.33	14.8
Kettlestone_RAT	1.45	8.63	5.85	36.2	1.03	23.03	0.55	4.85	0.8	0.2	0.33	15.2
millstone_Dramensfjord_RAT	1.58	7.41	6.2	37.6	1.17	21.11	0.59	5.11	0.75	0.21	0.31	15.8
Hoghead_ArnoldZiffel_Asis	2.11	8.29	7.89	41.5	0.99	14.76	0.56	5.45	0.83	0.22	0.25	15.7
Diamon_Jenness_Holman3_RAT1	1.72	6.47	6.71	40.6	1.05	19.62	0.63	5.09	0.79	0.17	0.33	15.4
Diamon_Jenness_Holman3_RAT2	1.71	6.49	6.7	40.1	1.06	19.64	0.63	5.03	0.81	0.22	0.31	15.5
MacKenzie_Campell_RAT	1.93	5.43	7.27	43	1.15	17.01	0.69	4.6	0.86	0.2	0.32	15.6
Inuvik_Toruyuktuk_RAT	1.79	5.45	7.17	39.9	1.11	18.17	0.67	5.48	0.86	0.22	0.36	17.1
Bylot_RAT	1.86	6.81	6.52	37.9	1.01	19.33	0.6	5.01	0.77	0.23	0.37	17.7
Sermilik_vein_asis	2.11	7.87	7.83	42.2	0.96	14.03	0.55	5.84	0.91	0.29	0.34	16
Escher_Kirchner_RAT	1.63	8.37	6.06	36.5	1.01	23.03	0.57	5	0.75	0.18	0.24	15.7
Ellesmere_NoCoating	1.85	8.03	7.27	40.4	1	18.01	0.6	5.26	0.76	0.2	0.25	15
Wopmay_Otter	1.92	7.67	7.31	40.4	1.04	18.29	0.62	5.22	0.81	0.19	0.2	15.1
Wopmay_Otter_b	2.01	7.67	7.27	40.5	1.06	18.32	0.6	5.25	0.69	0.18	0.2	15.1
Paikia_brushed	1.74	8.08	6.45	38.7	1.09	21.47	0.54	4.49	0.76	0.18	0.27	14.9
Paikia_RAT	1.84	7.86	6.36	37.7	1.13	21.35	0.57	4.59	0.77	0.16	0.33	15.7
Wharenhui_RAT_stalled	1.68	9.38	6.28	37	1.02	21.55	0.54	4.27	0.76	0.21	0.29	15.8
Wharenhui_RAT	1.83	9.11	6.43	37.5	1.08	21.33	0.56	4.1	0.81	0.2	0.32	15.1
Russett_Cobble	1.84	7.15	6.81	38.5	1.05	20.82	0.57	5.47	0.8	0.2	0.3	15.4
Omaha as is	2	7.39	7.1	39.4	1.01	19.81	0.56	5.16	0.83	0.2	0.3	15.3
Gagarin_asis	2	7.19	7.54	41	1.04	16.51	0.56	5.46	0.89	0.2	0.34	16.2
Gagarin_brush	1.79	7.25	6.71	38.3	1.03	21.46	0.57	5.36	0.78	0.17	0.31	15.2

IceCream_RAT	1.74	7.31	5.91	36.2	1.04	23.81	0.58	5.49	0.78	0.21	0.31	15.8
LemonRind	2.22	7.07	7.49	40.2	1.07	15.3	0.55	6.07	0.89	0.24	0.37	17
LemonRind_RAT	2.02	7.83	6.17	35.1	1.05	23.12	0.54	5.2	0.75	0.19	0.38	16
Elephant	1.84	7.37	6.84	38.8	1.08	19.53	0.61	5.49	0.79	0.22	0.28	16.1
Desception	1.79	7.45	6.63	38.5	1.05	19.83	0.58	5.06	0.8	0.19	0.23	17
Olympia_Kalavrita	1.78	7.39	6.52	37.5	0.98	20.72	0.55	5.84	0.79	0.25	0.33	16.6
Olympia_Ziakas	1.73	7.36	6.26	36.9	1.02	23	0.55	5.12	0.76	0.18	0.31	15.8
Williams_asis_long	1.88	7.5	6.93	39.1	1.01	19.62	0.57	5.45	0.83	0.19	0.25	15.8
Ted	2.04	7.27	7.29	40.1	1.03	17.51	0.57	5.61	0.85	0.21	0.32	16.2
Ted_Brushed	1.93	7.23	6.69	38.2	1.03	20.62	0.58	5.45	0.78	0.19	0.31	16
Hunt	2	7.48	7	39.2	1.01	19.06	0.55	5.23	0.8	0.2	0.29	16.3
Roosevelt_RoughRider	1.94	6.75	7.29	39.9	1.04	16.02	0.59	5.71	0.84	0.22	0.31	18.4
Brookeville	1.56	8.44	5.96	34.7	1	25.19	0.49	5.01	0.72	0.17	0.29	15.7
Cheyenne	1.67	7.99	6.18	35.6	0.98	24.18	0.5	5.26	0.75	0.18	0.3	15.6
Baltra	1.67	7.36	5.54	35	1.02	25.79	0.54	5.12	0.66	0.17	0.34	15.9
Cha_brushed	1.92	5.48	6.87	41.2	1.15	18.13	0.66	5.24	0.88	0.23	0.36	16.9
Cha_RAT	1.94	5.14	6.66	41.1	1.17	18.89	0.7	5.24	0.86	0.22	0.37	16.7
Rio_de_Janeiro	1.81	6.68	6.34	38.9	1.09	21.09	0.6	5.47	0.8	0.19	0.3	15.6
VivaLaRata	1.93	7.64	7.15	39.8	1.02	17.45	0.54	5.81	0.84	0.24	0.28	16.2
Cercedilla	1.97	7.04	7.31	40.8	1.07	18.42	0.64	5.73	0.86	0.21	0.2	14.8
Cercedilla_brush	1.95	7.09	7.25	40.6	1.06	18.52	0.62	5.74	0.85	0.2	0.2	15
Cercedilla_RAT	2.03	7.14	6.97	39.1	1.04	19.1	0.66	5.88	0.84	0.23	0.21	16.1
StenoAsis	1.88	7.51	7	39.4	1.03	18.36	0.54	5.26	0.79	0.19	0.29	16.7
StenoBrush	1.63	7.4	6.04	36.3	1.01	23.22	0.49	5.35	0.74	0.17	0.31	16.4
StenoRAT	1.46	7.23	5.32	34.4	1	26.38	0.52	5.62	0.71	0.18	0.33	16.1
HallAsis	2.05	7.21	7.33	40	1.02	17.2	0.53	5.44	0.85	0.2	0.32	16.9
SmithAsis	2.16	7.47	8.11	42.5	1.01	12.72	0.52	6.17	0.95	0.23	0.26	16.8
SmithBrushed	1.71	7.65	5.84	36.1	1.07	23.24	0.58	4.34	0.81	0.22	0.29	17.2
SmithBrushed2	1.7	7.63	5.85	36.1	1.04	23.21	0.57	4.37	0.83	0.19	0.26	17.2

Smith2RAT	1.7	7.27	6.1	37.2	1.03	22.02	0.58	4.47	0.83	0.19	0.29	17.3
Lyell1_asis	2	7.53	7.13	39.2	1.03	17.96	0.55	5.49	0.88	0.2	0.26	16.5
Lyell1_RAT	1.47	7.82	5.8	35.7	1.04	23.41	0.58	4.28	0.84	0.19	0.29	17
Lyell2_asis	2.13	7.31	7.6	40.7	1.03	15.59	0.57	5.76	0.89	0.21	0.28	16.7
Lyell3_asis	2.07	7.36	7.54	40.8	1.02	15.79	0.55	5.64	0.89	0.18	0.27	16.6
Smith3_Asis	1.93	7.42	7.3	39.9	1.05	16.69	0.56	5.75	0.81	0.23	0.32	16.8
Smith3_Asis_Second	1.99	7.36	7.37	40	1.01	16.67	0.56	5.71	0.84	0.19	0.35	16.7
Lyell4_asis	2.03	7.45	7.25	39.6	1.04	17.29	0.56	5.51	0.82	0.18	0.33	16.6
Lyell4_asis_second	2.01	7.41	7.18	39.6	1.02	17.45	0.56	5.46	0.81	0.23	0.32	16.7
Lyell4_asis_third	2.01	7.4	7.29	39.5	1	17.32	0.57	5.55	0.82	0.22	0.33	16.7
Lyell5_Smith_Side	2.12	7.24	7.86	41.6	0.99	13.81	0.54	6.08	0.88	0.23	0.34	17.2
Lyell5_Smith_Side_second	2.17	7.3	7.95	41.6	1.02	13.65	0.54	6.01	0.86	0.21	0.36	17.2
Lyell_Buckland_asis	2.15	7.3	7.77	40.9	1	14.58	0.53	6.3	0.89	0.22	0.37	16.8
Lyell_Buckland_RAT	1.6	7.49	5.64	35.1	0.99	22.95	0.55	4.71	0.78	0.18	0.36	17.8
Lyell_Exeter_asis	2.09	7.13	7.92	41.6	0.96	13.49	0.53	6.36	0.93	0.21	0.33	17.2
Lyell_Exeter_asis_Second	2.16	7.22	8.01	41.4	1	13.48	0.55	6.33	0.91	0.21	0.34	17.2
Gilbert_RAT	1.94	5.99	6.68	40.7	1.07	17.38	0.63	4.46	0.9	0.22	0.34	18.2
Candia_Crete	2.12	7.39	8.1	42.2	1.03	13.64	0.53	6.06	0.89	0.23	0.29	16.5
CookIsland	2.11	6.96	8.1	42.2	1	12.42	0.53	6	0.87	0.21	0.28	18.2
Penrhyn	2.01	7.14	7.4	40.2	1.01	16.5	0.57	5.88	0.86	0.26	0.29	16.9
Penrhyn_RAT	1.76	6.92	5.71	33.8	0.97	21.44	0.5	4.96	0.7	0.26	0.25	22
TinosAsis	2.22	7.11	7.74	41	1.06	15.48	0.55	5.45	0.85	0.22	0.3	16.9
TinosAsis2	2.17	7.25	7.78	41.2	1.04	15.36	0.57	5.45	0.87	0.2	0.3	16.7
Absecon_asis	2.2	7.25	8.11	42.2	0.97	12.64	0.56	5.82	0.92	0.25	0.33	17.6
Marquette_PeckBay1	2.48	11.98	11.48	46.1	1	2.33	0.36	5.72	0.59	0.51	0.36	16.6
Marquette_PeckBay2	2.5	11.98	11.45	46.2	1.01	2.36	0.37	5.71	0.48	0.46	0.35	16.6
Marquette_LoonLake	2.71	11.11	12.48	47.3	0.67	1.92	0.51	5.13	0.63	0.56	0.35	16.2
VailBeach	2.7	10.99	12.45	47.3	0.7	1.91	0.51	5.18	0.65	0.56	0.33	16.3
Marquette_PB2_RAT	2.32	14.88	9.82	45	0.71	0.8	0.33	5.44	0.64	0.6	0.38	18.8

Marquette_PB2_RB_0	2.41	14.21	10.76	45.2	0.97	0.91	0.38	5.55	0.57	0.6	0.38	17.7
Marquette_PB2_RB_1	2.35	14.07	10.24	45.1	0.8	1.04	0.38	5.39	0.65	0.63	0.39	18.6
Marquette_PB2_RB_2_TG	3.01	15.83	9.88	43.7	0.48	0.88	0.33	5.15	0.55	0.55	0.38	18.8
Marquette_PB2_RB_2	2.43	15.19	9.45	44.2	0.83	1.05	0.31	5.06	0.6	0.61	0.41	19.5
ChocolateHills_Arogo	1.89	6.93	6.98	38	0.98	18.38	0.55	5.35	0.81	0.19	0.32	18.7
ChocolateHills_Tears	1.95	6.5	7.14	39.5	1	17.12	0.54	5.53	0.88	0.21	0.33	18.4
ClarinBeach	2.13	7.32	8.21	42.2	1.01	12.9	0.52	6.12	0.94	0.24	0.33	17.1
DueroBeach	2.11	7.31	7.85	42.1	1.05	13.58	0.56	5.74	0.85	0.23	0.3	17.1
CerveraShoal	2.09	6.94	7.68	40.8	0.98	12.76	0.49	5.54	0.89	0.21	0.33	20.3
PuertoJiminez	2.15	7	7.87	41.5	1.02	13.51	0.58	5.79	0.87	0.21	0.29	18
LuisDeTorres_Brush	1.86	7.14	6.89	39.3	1.04	19.11	0.54	5.72	0.78	0.21	0.3	16.2
LuisDeTorres_RAT	1.67	7.89	5.81	36.1	1.06	23.79	0.59	4.63	0.82	0.2	0.32	16.4
RuizGarcia	1.83	7.18	6.6	38.6	1.03	20.36	0.61	5.02	0.81	0.17	0.29	16
Valdivia	2.04	7.56	7.31	40.2	1.03	16.92	0.56	5.22	0.76	0.2	0.28	16.7
Gibraltar	2.13	7.41	7.77	41.8	1.03	13.7	0.57	6.19	0.84	0.22	0.3	16.9
Salisbury1_Rat1	2.74	8.81	8.82	45.52	1	3.09	0.41	6.77	1.09	0.25	0.48	20.05
Salisbury1_RatBrush	2.47	8.89	8.51	45.41	0.99	3.48	0.38	6.78	1.04	0.25	0.49	20.18
Rushall	2.03	6.97	7.69	40.77	0.95	13.91	0.49	7.51	0.86	0.25	0.28	17.24
Azilda2_RAT1	2.75	7.67	10.84	50.59	1.44	2.35	0.28	6.06	0.91	0.24	0.37	15.8
Azilda2_RATbrush	2.55	7.91	10.6	51.18	1.5	2.47	0.28	5.98	0.87	0.24	0.36	15.38
Ortiz2B	2.09	6.28	8.57	41.98	1.17	13.51	0.27	10.35	0.78	0.22	0.47	13.24
Tawny	1.83	6.8	7.58	40.68	0.96	11.93	0.54	6.54	0.82	0.27	0.27	20.87
BlackShoulder	1.81	8.35	6.81	38.43	1.03	19.72	0.6	4.66	0.81	0.2	0.25	16.02
BlackShoulder2	1.79	7.73	7.16	39.32	1.03	17.65	0.55	5.59	0.84	0.22	0.3	16.54
BlackShoulder3	1.96	7.96	6.69	37.62	1	19.86	0.53	6	0.82	0.22	0.21	15.6
BlackShoulder_RAT	1.78	8.15	5.95	36.47	1.02	22.36	0.64	4.28	0.79	0.18	0.23	16.45
RedPoker	2.07	7.14	7.5	40.62	1.04	15.53	0.57	6.16	0.85	0.2	0.29	16.77
Callitris	1.54	5.52	6.71	39.45	1.06	18.77	0.49	7.46	0.82	0.21	0.15	16.93
PinnacleIsland4	1.57	9.43	7.57	36.19	1.33	16.44	0.41	5.69	0.91	0.22	1.3	17.94

AnchorPoint1	1.74	8.14	7	37.77	1.82	15.09	0.33	7.28	0.95	0.35	0.75	18.23
CapeFairweather1	1.86	7.31	7.15	39.56	1.02	17.88	0.51	6.38	0.78	0.19	0.18	16.22
CapeFairweather2	2.01	7.39	7.71	42.31	0.98	12.66	0.55	6.29	0.94	0.32	0.34	17.54
Victory2	2.72	6.09	12.3	47.79	1.31	3.73	0.38	7.46	1.31	0.17	0.3	15.79
Margarete_Brush	2.75	6.23	12.56	48.37	1.2	3.72	0.36	7.35	1.23	0.18	0.36	15.23
Cottondale1	1.88	6.03	7.18	36.09	1.02	19.15	0.39	13.24	0.72	0.25	0.27	12.87
Cottondale2	1.9	6.27	7.87	39.31	1.11	15.17	0.44	10.7	0.91	0.2	0.34	14.86
JeanBaptisteCharbonneau	3.27	4.04	16.16	52.7	0.92	3.19	0.44	7.25	0.91	0.01	0.18	10.35
SgtCFloyd_Brush	2.39	10.96	12.55	48.85	0.97	2.8	0.28	5.71	0.73	0.27	0.28	13.65
SgtNathanielPryor	2.74	4.27	18.39	51.65	0.85	2.88	0.29	8.47	0.63	0.03	0.16	9.07
SgtNathanielPryor2	2.88	4.61	18.22	51.1	0.81	2.81	0.25	8.43	0.53	0.05	0.17	9.57
Athens_Brush	1.82	7.88	8.31	44.03	0.97	15.81	0.38	5.87	0.96	0.2	0.18	12.82
Thessaloniki	1.86	7.54	8.34	43.76	0.75	15.21	0.4	5.09	0.95	0.19	0.2	14.74
Thessaloniki2	1.82	7.43	8.74	45.07	0.65	14.78	0.39	4.66	1.01	0.17	0.19	14.3
Thessaloniki3	1.77	7.63	8.49	44.06	0.7	14.63	0.42	5.11	0.97	0.22	0.21	14.83

TABLE 34. ELEMENTAL ABUNDANCES (PPM) OF MARS ANALOG SAMPLES. OPPORTUNITY ROVER.
Data from Planetary Data System Geosciences Node.

Name	Ni	Zn	Br	Cl %
Robert.E	597	569	7	0.81
Guadalupe_asis	657	373	43	0.87
McKittrick_RAT	735	279	342	0.6
Last_Chance_Makar_asis	686	397	32	0.9
Mojo2_asis	633	414	90	0.86
Mojo2_RAT	656	427	105	0.54
BerryBowl_Empty	607	426	103	0.99
RasperryNewton	553	460	177	0.93
RealSharksTooth_enamel1_asis	653	388	100	0.85
BounceRock_Glanz	153	110	41	0.57
BounceRock_Case_Rat	81	38	39	0.1
BounceRock_Maggie	162	145	33	0.94
LionStone_Leo_asis	573	389	76	1
LionStone_Numa_RAT	572	415	268	0.91
Tenessee_RAT	679	533	35	0.65
Kentucky_asis	652	439	139	0.83
Kentucky_Cubble_Hill2_RAT	618	371	54	0.65
Virginia_RAT	664	381	74	0.6
Ontario_London_RAT	638	357	27	0.72
Grindstone_RAT	604	319	39	1.45
Kettlestone_RAT	644	346	19	1.75
millstone_Dramensfjord_RAT	616	437	11	1.98
Hoghead_ArnoldZiffel_Asis	465	388	108	1.26
Diamon_Jenness_Holman3_RAT1	531	444	23	1.37
Diamon_Jenness_Holman3_RAT2	611	486	14	1.64

MacKenzie_Campell_RAT	546	447	9	1.9
Inuvik_Toruyuktuk_RAT	606	489	13	1.67
Bylot_RAT	933	499	10	1.69
Sermilik_vein_asis	540	380	187	0.94
Escher_Kirchner_RAT	564	314	425	0.78
Ellesmere_NoCoating	509	380	395	1.26
Wopmay_Otter	519	394	368	1.07
Wopmay_Otter_b	510	363	424	1.03
Paikia_brushed	564	624	147	1.1
Paikia_RAT	571	628	10	1.42
Wharenhui_RAT_stalled	804	301	103	1.07
Wharenhui_RAT	605	259	38	1.49
Russett_Cobble	628	585	60	0.94
Omaha as is	634	441	53	0.89
Gagarin_asis	543	450	73	0.98
Gagarin_brush	574	405	67	0.92
IceCream_RAT	449	480	109	0.64
LemonRind	525	474	67	1.49
LemonRind_RAT	508	457	67	1.54
Elephant	576	450	294	0.9
Desception	515	423	103	0.74
Olympia_Kalavrita	496	394	67	0.56
Olympia_Ziakas	544	559	74	0.84
Williams_asis_long	549	470	65	0.75
Ted	571	541	161	0.9
Ted_Brushed	548	536	177	0.8
Hunt	561	634	157	0.76
Roosevelt_RoughRider	572	495	73	0.81
Brookeville	553	375	164	0.67

Cheyenne	524	550	123	0.69
Baltra	568	488	303	0.73
Cha_brushed	506	455	463	0.92
Cha_RAT	476	476	471	0.9
Rio_de_Janeiro	483	435	234	1.04
VivaLaRata	497	413	247	1
Cercedilla	319	291	264	0.85
Cercedilla_brush	340	261	274	0.85
Cercedilla_RAT	371	273	297	0.57
StenoAsis	563	506	34	0.87
StenoBrush	580	567	47	0.8
StenoRAT	523	507	22	0.68
HallAsis	583	483	72	0.89
SmithAsis	579	705	170	0.98
SmithBrushed	637	859	122	0.81
SmithBrushed2	598	835	122	0.78
Smith2RAT	624	777	113	0.84
Lyell1_asis	544	434	131	1.11
Lyell1_RAT	603	455	57	1.43
Lyell2_asis	566	392	196	1.1
Lyell3_asis	579	427	248	1.12
Smith3_Asis	628	460	206	1.08
Smith3_Asis_Second	540	437	214	1.07
Lyell4_asis	601	405	162	1.15
Lyell4_asis_second	553	442	165	1.14
Lyell4_asis_third	542	439	169	1.16
Lyell5_Smith_Side	597	467	151	1.02
Lyell5_Smith_Side_second	614	499	153	1.02
Lyell_Buckland_asis	543	499	58	1.07

Lyell_Buckland_RAT	632	549	35	1.7
Lyell_Exeter_asis	537	488	61	1.12
Lyell_Exeter_asis_Second	544	495	54	1.1
Gilbert_RAT	520	553	23	1.41
Candia_Crete	520	496	97	0.88
CookIsland	541	527	63	0.96
Penrhyn	436	514	50	0.88
Penrhyn_RAT	730	391	79	0.69
TinosAsis	487	523	71	0.98
TinosAsis2	487	508	61	0.97
Absecon_asis	484	544	134	0.97
Marquette_PeckBay1	319	182	26	0.43
Marquette_PeckBay2	234	184	16	0.44
Marquette_LoonLake	147	152	12	0.34
VailBeach	201	174	24	0.33
Marquette_PB2_RAT	371	261	29	0.23
Marquette_PB2_RB_0	255	200	25	0.29
Marquette_PB2_RB_1	409	289	32	0.25
Marquette_PB2_RB_2_TG	377	326	0	0.31
Marquette_PB2_RB_2	395	253	30	0.25
ChocolateHills_Arogo	403	550	92	0.8
ChocolateHills_Tears	438	478	66	0.82
ClarinBeach	466	481	122	0.83
DueroBeach	485	488	407	1.03
CerveraShoal	580	511	242	0.83
PuertoJiminez	462	510	93	1.09
LuisDeTorres_Brush	570	464	176	0.82
LuisDeTorres_RAT	644	480	232	0.54
RuizGarcia	509	440	432	1.27

Valdivia	512	359	331	1.09
Gibraltar	426	414	498	1.01
Salisbury1_Rat1	482	246	124	0.87
Salisbury1_RatBrush	488	245	108	1.03
Rushall	379	390	210	0.95
Azilda2_RAT1	951	128	43	0.52
Azilda2_RATbrush	922	134	48	0.53
Ortiz2B	670	144	208	0.95
Tawny	339	322	348	0.81
BlackShoulder	677	275	46	1.18
BlackShoulder2	616	319	77	1.17
BlackShoulder3	660	252	60	1.4
BlackShoulder_RAT	612	294	40	1.6
RedPoker	545	538	632	1.05
Callitris	275	330	65	0.84
PinnacleIsland4	354	204	144	0.91
AnchorPoint1	372	218	117	0.43
CapeFairweather1	311	276	114	0.88
CapeFairweather2	318	477	297	0.83
Victory2	152	124	31	0.61
Margarete_Brush	289	111	20	0.42
Cottondale1	199	192	102	0.85
Cottondale2	254	171	98	0.87
JeanBaptisteCharbonneau	0	50	86	0.51
SgtCFloyd_Brush	21	74	27	0.53
SgtNathanielPryor	0	111	32	0.48
SgtNathanielPryor2	0	63	26	0.47
Athens_Brush	737	100	55	0.65
Thessaloniki	562	163	33	0.88

Thessaloniki2	533	103	19	0.69
Thessaloniki3	457	187	39	0.86

TABLE 35. ELEMENTAL ABUNDANCES (WT %) OF MARS ANALOG SAMPLES. CURIOSITY ROVER.
Data from Planetary Data System Geosciences Node.

Name	Na_2O	MgO	Al_2O_3	SiO_2	P_2O_5	SO_3	K_2O	CaO	TiO_2	Cr_2O_3	MnO	FeO
Jake_Matijevic	7.11	3.61	16.09	50.7	0.49	2.48	2.23	6.07	0.49	0.04	0.14	9.47
JM2_APXS_RP2	6.61	4.57	14.59	49.3	0.6	3.05	2.01	6.54	0.65	0.09	0.17	10.61
JM2_APXS_RP2_OVERNIGHT	6.59	4.6	14.65	48.9	0.85	2.81	1.89	6.78	0.73	0.04	0.21	10.94
Bathurst_Inlet_RP_For_Real	2.21	8.56	7.85	43.7	0.82	3.05	2.18	6.28	1.09	0.42	0.8	22.07
Bathurst_Inlet_Top_RP	2.06	8.68	7.92	44	0.88	3.31	2.88	6.45	1.06	0.36	0.43	21
Gillespie_Lake_1	2.58	9.18	9.11	45.6	0.88	2.88	0.51	6.45	1.12	0.52	0.32	19.59
Ekwir_1_postbrush	2.78	9.66	8.28	45.3	1.07	2.59	0.62	5.9	0.88	0.45	0.21	20.29
Sayunei_RP_a	2.41	9.05	7.43	36.8	0.94	13.5	0.42	9.41	0.67	0.33	0.23	17.12
Sayunei_RP_center	2.33	8.01	7.45	38.4	0.88	12.49	0.35	9.54	0.83	0.39	0.24	17.67
Wernecke_Brushed	3.04	9.8	8.88	46.9	1.02	0.89	0.62	5.4	0.91	0.41	0.28	20.5
Wernecke_3_Brushed	2.98	9.76	8.9	47.6	1.02	1.04	0.69	5.32	0.91	0.42	0.26	19.69
Cumberland_A_adjusted_Target1	2.57	9.27	8.39	43.8	0.79	2.63	0.47	6.26	0.89	0.39	0.21	22.57
Cumberland_A_adjusted_Target2	3.01	9.2	8.75	44.6	0.8	2.07	0.55	6.27	1	0.37	0.3	21.38
Cumberland_A_adjusted_Target1	2.98	9.36	8.47	42.9	0.92	2.61	0.5	6.36	0.98	0.43	0.29	22.55

Cumberland_DRT_RP_twk_postBrush	3.14	9.15	9.34	46.8	0.92	1.57	0.66	5.44	0.91	0.42	0.27	19.82
Dismal_Lakes	4.39	6.31	11.63	49	0.89	2.67	1.65	6.22	0.77	0.38	0.3	14.71
Matthew	4.84	4.66	13.76	49.41	0.73	3.9	1.67	7.23	0.76	0.06	0.27	11.96
Oswego	2.7	8.71	7.98	43.01	0.75	3.29	1.96	6.13	0.89	0.54	0.47	22.35
Morehouse_RP	6.78	3.41	15.37	49.93	0.93	2.32	2.94	5.76	0.72	0.05	0.25	10.27
Lowerre_RP	5.42	3.08	16.22	51.22	0.62	2.13	2.23	5.71	0.54	0.07	0.18	11.48
Monkey_Yard	6.22	2.92	16.93	53.13	0.82	2.58	2.16	5.54	0.36	0.04	0.18	7.84
Windjana_Drillfines_Raster1	0.27	12.77	5.7	39.42	0.72	2.6	3.59	4.98	1.18	0.44	0.49	26.37
Windjana_Drillfines_Raster3	0.4	12.67	5.69	39.3	0.73	2.58	3.65	4.91	1.15	0.44	0.56	26.5
DumpPile_Windjana	4.97	6.37	12	47.32	0.7	2.15	2.16	5.23	0.66	0.21	0.14	16.93
Thimble_1	4.97	6.37	12	47.32	0.7	2.15	2.16	5.23	0.66	0.21	0.14	16.93
Stirling_RP	4.72	6.96	11.37	46.83	0.76	2.81	1.94	5.99	0.76	0.3	0.29	16.38
Tecoya_DRT	3.02	6.66	9.52	42.84	1.06	4.58	0.46	8.75	1.04	0.17	0.38	19.17
Sierra_Nevada_raster1	2.59	6.35	10.45	43.36	0.74	5.17	0.36	12.19	0.61	0.23	0.38	15.6
Sierra_Nevada_raster2	2.46	7.04	9.52	42.49	0.93	4.86	0.45	9.04	1.01	0.41	0.44	19.83
Telegraph_Peak_DT	3.56	3.04	11.06	51.87	1.27	1.85	0.97	4.03	1.28	0.4	0.22	19.85
Alvord_Mountain_raster1	1.52	5.78	5.01	28.99	0.71	10.95	0.12	28.7	0.5	0.19	1	14.28
Alvord_Mountain_raster2	1.51	5.44	5.18	32.2	0.87	12.35	0.1	25.15	0.45	0.26	0.89	13.66
Little_Devil	4.03	3.95	11.21	49.78	0.76	2.29	2.83	5.71	0.99	0.28	0.25	16.99
Buckskin_mini_start_hole	3.43	7.8	10.44	45.65	0.78	2.62	1.36	7.08	0.85	0.5	0.34	18.47
Ravalli	3.43	7.8	10.44	45.65	0.78	2.62	1.36	7.08	0.85	0.5	0.34	18.47
Warsaw	2.55	9.85	8.46	44.48	0.86	3.61	0.39	6.81	0.96	0.3	0.38	20.61
Weissrand	2.74	8.98	9.83	45.69	0.77	3.19	0.43	7.29	0.89	0.43	0.41	18.83

Kibnas_APXS	2.27	9.97	8.49	44.56	0.76	3.28	0.35	7.04	0.9	0.53	0.4	20.76
Greenhorn_post_dump_offs-et	2.43	11.46	8.46	45.85	0.7	2.29	0.35	6.55	0.71	0.3	0.42	20.08
Greenhorn_postsieve_dump	2.27	11.24	8.33	45.53	0.75	2.57	0.38	7	0.75	0.28	0.38	20.02
Gobabeb_Scoop2_RP	2.35	9.32	9.16	45.74	0.73	2.87	0.39	7.13	0.84	0.47	0.39	19.97
Gobabeb_DumpC_corrected	2.73	7.79	10.21	48.31	0.82	3.18	0.51	7.27	0.81	0.38	0.34	16.92
Bergsig	2.73	7.79	10.21	48.31	0.82	3.18	0.51	7.27	0.81	0.38	0.34	16.92
Gobabeb_DumpF	2.29	10.31	7.98	46.13	0.74	3.3	0.44	6.19	0.78	0.3	0.35	20.46

TABLE 36. ELEMENTAL ABUNDANCES (PPM) OF MARS ANALOG SAMPLES. CURIOSITY ROVER.
Data from Planetary Data System Geosciences Node.

Name	Ni	Zn	Br	Cl %
Jake_Matijevic	30	222	92	0.87
JM2_APXS_RP2	0	341	94	1.03
JM2_APXS_RP2_OVERNIGHT	61	319	94	0.95
Bathurst_Inlet_RP_For_Real	399	1359	13	0.73
Bathurst_Inlet_Top_RP	327	1222	40	0.81
Gillespie_Lake_1	320	591	93	1.1
Ekwir_1_postbrush	480	786	325	1.78

Sayunei_RP_a	645	650	192	1.44
Sayunei_RP_center	617	596	156	1.26
Wernecke_Brushed	694	794	401	1.13
Wernecke_3_Brushed	649	764	352	1.2
Cumberland_A_adjusted_Target1	886	876	110	1.39
Cumberland_A_adjusted_Target2	752	799	152	1.38
Cumberland_A_adjusted_Target1	877	865	127	1.42
Cumberland_DRT_RP_twk_postBrush	698	777	122	1.33
Dismal_Lakes	213	480	103	0.92
Matthew	69	300	15	0.65
Oswego	360	1214	176	0.95
Morehouse_RP	41	924	82	1.11
Lowerre_RP	97	617	33	0.89
Monkey_Yard	43	1409	89	0.97
Windjana_Drillfines_Raster1	444	4681	186	0.72
Windjana_Drillfines_Raster3	383	4347	348	0.8
DumpPile_Windjana	316	680	40	0.71
Thimble_1	316	680	40	0.71
Stirling_RP	398	550	79	0.75
Tecoya_DRT	494	925	654	2.01
Sierra_Nevada_raster1	673	940	220	1.73
Sierra_Nevada_raster2	544	776	265	1.17
Telegraph_Peak_DT	423	1212	93	0.34
Alvord_Mountain_raster1	483	2253	112	1.69
Alvord_Mountain_raster2	504	1991	223	1.56
Little_Devil	629	609	77	0.7
Buckskin_mini_start_hole	351	546	24	0.52
Ravalli	351	546	24	0.52
Warsaw	822	209	60	0.64
Weissrand	496	197	32	0.51
Kibnas_APXS	490	228	20	0.51

Greenhorn_post_dump_offset	795	129	37	0.4
Greenhorn_postsieve_dump	753	141	54	0.44
Gobabeb_Scoop2_RP	528	202	28	0.49
Gobabeb_DumpC_corrected	407	192	32	0.55
Bergsig	407	192	32	0.55
Gobabeb_DumpF	822	274	97	0.62

APPENDIX F, COMPLETE DATASET OF MARS ROVER ANALOG SAMPLES: CIA, MODIFIED CIA, AL_2O_3/TIO_2

TABLE 37. AL_2O_3/TIO_2 (MOLAR), CIA AND SULFATE MODIFIED CIA VALUES. OPPORTUNITY ROVER.

Name	$Al_2O_3TiO_2$	CIA	CIA Modified
Robert.E	12.80	37.70	100
Guadalupe_asis	10.98	36.43	100
McKittrick_RAT	9.72	35.25	100
Last_Chance_Makar_asis	12.81	35.47	100
Mojo2_asis	12.11	35.57	100
Mojo2_RAT	10.61	32.61	100
BerryBowl_Empty	12.28	36.55	100
RasperryNewton	12.61	37.26	100
RealSharksTooth_enamel1_asis	13.25	36.69	100
BounceRock_Glanz	14.81	29.26	53.08
BounceRock_Case_Rat	17.99	29.68	32.93
BounceRock_Maggie	19.77	33.09	75.12

LionStone_Leo_asis	11.74	35.39	100
LionStone_Numa_RAT	10.26	33.04	100
Tenessee_RAT	9.44	32.83	100
Kentucky_asis	10.89	36.80	100
Kentucky_Cubble_Hill2_RAT	10.55	33.46	100
Virginia_RAT	9.56	35.04	100
Ontario_London_RAT	10.28	33.05	100
Grindstone_RAT	9.73	34.90	100
Kettlestone_RAT	9.29	33.15	100
millstone_Dramensfjord_RAT	10.50	33.10	100
Hoghead_ArnoldZiffel_Asis	12.07	36.07	100
Diamon_Jenness_Holman3_RAT1	10.79	34.45	100
Diamon_Jenness_Holman3_RAT2	10.50	34.64	100
MacKenzie_Campell_RAT	10.74	37.18	100
Inuvik_Toruyuktuk_RAT	10.59	34.46	100
Bylot_RAT	10.75	33.71	100
Sermilik_vein_asis	10.93	34.78	100
Escher_Kirchner_RAT	10.26	32.85	100
Ellesmere_NoCoating	12.15	35.42	100
Wopmay_Otter	11.46	35.43	100
Wopmay_Otter_b	13.38	35.00	100
Paikia_brushed	10.78	35.71	100
Paikia_RAT	10.49	34.66	100
Wharenhui_RAT_stalled	10.49	36.11	100
Wharenhui_RAT	10.08	36.74	100
Russett_Cobble	10.81	33.38	100
Omaha as is	10.86	34.84	100
Gagarin_asis	10.76	35.29	100
Gagarin_brush	10.93	33.52	100

IceCream_RAT	9.62	30.49	100
LemonRind	10.69	32.89	100
LemonRind_RAT	10.45	31.59	100
Elephant	11.00	33.35	100
Desception	10.53	34.17	100
Olympia_Kalavrita	10.48	31.56	100
Olympia_Ziakas	10.46	32.93	100
Williams_asis_long	10.60	33.72	100
Ted	10.89	33.97	100
Ted_Brushed	10.89	32.79	100
Hunt	11.11	34.32	100
Roosevelt_RoughRider	11.02	33.90	100
Brookeville	10.51	32.81	100
Cheyenne	10.46	32.47	100
Baltra	10.66	30.47	100
Cha_brushed	9.91	33.89	100
Cha_RAT	9.84	33.07	100
Rio_de_Janeiro	10.06	31.84	100
VivaLaRata	10.81	33.30	100
Cercedilla	10.80	33.75	100
Cercedilla_brush	10.83	33.62	100
Cercedilla_RAT	10.54	32.10	100
StenoAsis	11.25	34.58	100
StenoBrush	10.37	31.82	100
StenoRAT	9.52	28.75	100
HallAsis	10.95	34.63	100
SmithAsis	10.84	34.59	100
SmithBrushed	9.16	34.01	100
SmithBrushed2	8.95	33.99	100

Smith2RAT	9.33	34.56	100
Lyell1_asis	10.29	33.96	100
Lyell1_RAT	8.77	34.88	100
Lyell2_asis	10.84	34.24	100
Lyell3_asis	10.76	34.59	100
Smith3_Asis	11.45	33.90	100
Smith3_Asis_Second	11.14	34.07	100
Lyell4_asis	11.23	34.18	100
Lyell4_asis_second	11.26	34.16	100
Lyell4_asis_third	11.29	34.22	100
Lyell5_Smith_Side	11.34	34.19	100
Lyell5_Smith_Side_second	11.74	34.52	100
Lyell_Buckland_asis	11.09	33.30	100
Lyell_Buckland_RAT	9.18	32.36	100
Lyell_Exeter_asis	10.82	33.71	100
Lyell_Exeter_asis_Second	11.18	33.84	100
Gilbert_RAT	9.43	35.79	100
Candia_Crete	11.56	34.94	100
CookIsland	11.82	35.13	100
Penrhyn	10.93	33.61	100
Penrhyn_RAT	10.36	31.43	100
TinosAsis	11.56	35.35	100
TinosAsis2	11.36	35.56	100
Absecon_asis	11.20	35.39	100
Marquette_PeckBay1	24.71	43.57	78.22
Marquette_PeckBay2	30.29	43.46	78.77
Marquette_LoonLake	25.16	46.54	78.63
VailBeach	24.33	46.35	77.99
Marquette_PB2_RAT	19.49	41.11	52.46

Marquette_PB2_RB_0	23.97	42.65	55.62
Marquette_PB2_RB_1	20.01	42.11	58.00
Marquette_PB2_RB_2_TG	22.81	40.24	52.26
Marquette_PB2_RB_2	20.00	41.12	57.85
ChocolateHills_Arogo	10.94	34.20	100
ChocolateHills_Tears	10.30	34.02	100
ClarinBeach	11.09	35.08	100
DueroBeach	11.73	35.10	100
CerveraShoal	10.96	35.36	100
PuertoJiminez	11.49	34.88	100
LuisDeTorres_Brush	11.22	32.91	100
LuisDeTorres_RAT	9.00	32.98	100
RuizGarcia	10.35	34.02	100
Valdivia	12.22	35.21	100
Gibraltar	11.75	33.57	100
Salisbury1_Rat1	10.28	33.82	76.19
Salisbury1_RatBrush	10.39	33.62	84.44
Rushall	11.36	30.50	100
Azilda2_RAT1	15.13	40.62	74.28
Azilda2_RATbrush	15.47	40.81	76.61
Ortiz2B	13.95	27.54	100
Tawny	11.74	32.86	100
BlackShoulder	10.68	36.01	100
BlackShoulder2	10.83	34.32	100
BlackShoulder3	10.36	31.27	100
BlackShoulder_RAT	9.57	34.29	100
RedPoker	11.21	33.01	100
Callitris	10.39	28.75	100
PinnacleIsland4	10.56	36.15	100

AnchorPoint1	9.36	29.84	100
CapeFairweather1	11.64	31.97	100
CapeFairweather2	10.42	33.45	100
Victory2	11.92	40.00	85.83
Margarete_Brush	12.97	40.73	87.09
Cottondale1	12.66	20.65	100
Cottondale2	10.98	25.45	100
JeanBaptisteCharbonneau	22.55	45.91	82.96
SgtCFloyd_Brush	21.83	46.20	87.92
SgtNathanielPryor	37.07	47.63	73.90
SgtNathanielPryor2	43.66	47.26	73.29
Athens_Brush	10.99	37.12	100
Thessaloniki	11.15	39.55	100
Thessaloniki2	10.99	42.37	100
Thessaloniki3	11.12	40.15	100

TABLE 38. Al_2O_3/TiO_2 (MOLAR), CIA AND SULFATE MODIFIED CIA VALUES. SPIRIT ROVER.

Name	Al_2O_3/TiO_2	CIA	CIA Modified
Adirondack_asis	19.64	38.26	78.78
Adirondack_brush	29.52	37.46	59.97
Adirondack_RAT	28.63	37.46	50.44
Humphrey_Ashley_asis	28.32	36.16	79.42
Humphrey_Heyworth_asis	26.81	37.31	75.10
Humphrey_brush	26.41	36.89	65.20
Humphrey_RAT1	23.44	35.52	45.56
Humphrey_RAT2	24.68	36.55	49.82
Mazatzal_NewYork_RAT1Oregon_Asis	18.27	34.78	74.09

Mazatzal_Brooklyn_RAT2	23.06	35.63	51.02
Route66_brushed	23.23	35.91	89.59
Boroughs_Hellskitchen_side	11.76	34.30	100.00
Mojave_Joshua_Asis	23.28	35.63	79.21
Wishstone_chisel_RAT	7.36	37.56	57.39
champagne_brush	7.05	42.57	73.61
champagne_RAT1	6.32	37.45	54.12
champagne_RAT2	6.36	37.48	54.56
Watchtower_Joker_RAT	7.08	39.71	80.87
Backstay_Scuppers	18.02	41.15	60.41
Backstay_Scurvy	17.82	41.29	74.01
Independence_Penn2_Scuffed	12.63	49.56	74.35
Bourgeosie_Chic.	6.55	35.16	76.61
Irvine	9.93	34.00	69.50
Berkner Island 1	15.70	26.30	100.00
Esperanza_Palma	10.13	34.01	74.85
Home Plate_Humbolt Peak	15.26	33.68	63.59
Home Plate_Humbolt Peak	15.59	33.77	63.29

TABLE 39. Al_2O_3/TiO_2 (MOLAR), CIA AND SULFATE MODIFIED CIA VALUES. CURIOSITY ROVER.

Name	Al_2O_3/TiO_2	CIA	CIA Modified
Jake_Matijevic	25.73	39.02	67.27
JM2_APXS_RP2	17.59	36.91	76.70
JM2_APXS_RP2_OVERNIGHT	15.73	36.75	70.00
Bathurst_Inlet_RP_For_Real	5.64	31.07	79.79
Bathurst_Inlet_Top_RP	5.86	30.28	84.13
Gillespie_Lake_1	6.37	35.54	76.34

Ekwir_1_postbrush	7.37	34.14	75.28
Sayunei_RP_a	14.08	25.66	100.00
Sayunei_RP_center	11.40	25.68	100.00
Wernecke_Brushed	7.65	36.44	48.39
Wernecke_3_Brushed	7.66	36.74	51.67
Cumberland_A_adjusted_Target1	7.39	34.23	72.08
Cumberland_A_adjusted_Target2	6.86	34.05	63.64
Cumberland_A_adjusted_Target1	6.77	33.25	70.79
Cumberland_DRT_RP_twk_postBrush	8.04	37.19	62.43
Dismal_Lakes	11.84	36.40	79.20
Matthew	14.19	37.52	92.68
Oswego	7.03	31.06	89.13
Morehouse_RP	16.73	38.25	66.67
Lowerre_RP	23.54	42.76	71.40
Monkey_Yard	36.86	42.78	77.92
Windjana_Drillfines_Raster1	3.79	29.87	84.87
Windjana_Drillfines_Raster3	3.88	29.59	85.69
DumpPile_Windjana	14.25	37.47	71.59
Thimble_1	14.25	37.47	71.59
Stirling_RP	11.72	35.39	83.77
Tecoya_DRT	7.17	30.81	84.48
Sierra_Nevada_raster1	13.43	28.04	62.84
Sierra_Nevada_raster2	7.39	31.22	87.10
Telegraph_Peak_DT	6.77	43.73	84.27
Alvord_Mountain_raster1	7.85	8.37	21.47
Alvord_Mountain_raster2	9.02	9.68	40.71
Little_Devil	8.87	35.83	77.25
Buckskin_mini_start_hole	9.63	34.31	68.63
Ravalli	9.63	34.31	68.63

Warsaw	6.91	33.23	87.39
Weissrand	8.66	35.03	74.35
Kibnas_APXS	7.39	33.42	76.15
Greenhorn_post_dump_offset	9.34	34.19	63.66
Greenhorn_postsieve_dump	8.70	33.05	63.53
Gobabeb_Scoop2_RP	8.55	34.68	69.13
Gobabeb_DumpC_corrected	9.88	35.86	75.09
Bergsig	9.88	35.86	75.09
Gobabeb_DumpF	8.02	33.99	88.36

APPENDIX G, AVAILABLE DATA FOR UNDISCUSSED MCMURDO DRY VALLEYS MICROENVIRONMENTS

TABLE 40. ELEMENTAL ABUNDANCES. POND #3.

elements (ppm)	JB1139
Na (wt%)	1.57
K (wt%)	1.42
Sc	18.3
Cr	133
Fe (wt%)	3.55
Co	19.7
Ni	53
Zn	61
Ga	6
As	0.63
Se	<1.7

Br	<1.0
Rb	64.2
Sr	126
Zr	174
Sb	0.11
Cs	1.83
Ba	270
La	19.3
Ce	35.8
Nd	13.6
Sm	3.05
Eu	0.74
Gd	2.62
Tb	0.40
Tm	0.19
Yb	1.36
Lu	0.23
Hf	4.12
Ta	0.64
W	0.0
Ir (ppb)	<2
Au (ppb)	0.3
Th	6.42
U	1.07

TABLE 41. SOLUBLE ANIONS. CORE 41 (JB1152) AND CORE 20 (JB1153-1154).

elements (ppm)	JB1152	JB1153	JB1154
F^-	45.79	48.43	31.49
Cl^-	8731	17499	3073
NO_3^-	5693	8642	2538

SO_4^{2-}	3044	2152	1341